CHEMICAL SPECIATION OF
FLUE GAS DESULFURIZATION SLUDGE
CONSTITUENTS

SCS ENGINEERS

STEARNS, CONRAD AND SCHMIDT
CONSULTING ENGINEERS, INC.

FINAL REPORT

CHEMICAL SPECIATION OF
FLUE GAS DESULFURIZATION SLUDGE
CONSTITUENTS

Phase I
Contract No. 68-03-2471

Prepared by:

Jasenka Vuceta, Ph.D.
John P. Woodyard, P.E.
SCS Engineers
4014 Long Beach Boulevard
Long Beach, California 90807

James C. S. Lu, Ph.D.
Cal Science Research, Inc.
7261 Murdy Circle
Huntington Beach, California 92647

Prepared for:

Solid and Hazardous Waste Research Division
Municipal Environmental Research Laboratory
U.S. Environmental Protection Agency
Cincinnati, Ohio 45268

Donald E. Sanning, Project Officer

January 1981

ABSTRACT

This project addresses the problem of flue gas desulfuriza-
tion (FGD) sludge disposal to land. Specifically, the chemical
species of FGD sludge constituents are thermodynamically modeled
using the equilibrium constant approach, in an attempt to predict
the constituent concentrations in fresh and aged FGD wastewater
and sludge. This method involves solving the stoichiometric
equations of various chemical species, which are subject to con-
straints imposed by the equilibrium constants as well as mass
balance and charge balance relations. Diagrams, such as Eh-pH
plots, ion-ratio plots, concentrations pH figures, and species
distribution figures, are then used to display the stability
field and speciation results.

The thermodynamic model used in this study was verified for
suitability and accuracy by the analytical results of various FGD
sludge samples taken from the Kansas City Power and Light La
Cygne Power Station. The model is also operated over a wide
range of operational and chemical changes to determine their im-
pacts on the concentration and speciation of various solid and
soluble species. The impacts of (1) changes in pH and ionic
strength; (2) addition of lime, silicates, hydrogen sulfide, and
phosphates to the sludge; (3) variation of chloride, sulfate, and
borate levels; (4) addition of magnesium to the sorbent; and (5)
sulfite oxidation, are all estimated using the model.

The report was submitted in fulfillment of Contract No. 68-
03-2471 by SCS Engineers, Long Beach, California. The work was
completed January 27, 1981.

CONTENTS

CONTENTS (continued)

FIGURES

FIGURES (continued)

FIGURES (continued)

TABLES

TABLES (continued)

ACKNOWLEDGEMENTS

SECTION 1

INTRODUCTION

DESCRIPTION OF PROBLEM

The removal of sulfur oxides from power plant exhaust
gases to meet air quality standards (flue gas desulfurization,
or FGD) is usually accomplished by wet scrubbing. These scrub-
ber systems are classified by the type of sorbent employed:
lime, limestone, or sodium salts (double alkali). Lime and
limestone sorbents are both effective and inexpensive relative
to other FGD alternatives, and as a result are currently the
most popular types of sorbents. These sorbents are also non-
regenerable; the sorbents are removed from the system after a
certain contact period. Because the ultimate disposal of the
spent sorbent sludges is usually accomplished on land, by pond-
ing or landfilling, a potential for detrimental environmental
effects exists from groundwater or surface water contamination
near the disposal site.

An important consideration when assessing the potential
environmental impact of FGD sludge disposal is the chemical
forms of major and minor constituents in the sludge and leachate.
The mobility or attenuation of these impurities as they pass
through underlying soils depends upon their chemical forms
and is not necessarily a function of total concentration.
This is particularly true for metals, which may be transported
in soluble or particulate form. Conventional chemical
analysis only provides information on the total concentration,
not on the speciation of the elements present.

The only feasible means of obtaining species information in
a complex system (such as FGD sludge) lies in thermodynamic
modeling. This approach is not entirely successful when complex
organic materials exist along with inorganic materials. However,
FGD sludge may be an ideal subject for this approach because the
material is dominated by well-defined crystal phases and contains
no significant organic materials.

A wide variety of elements exist in FGD sludge, as either
dominant or trace species. The equations governing interactions
between all the species and phases present can be solved on a
computer, where it is also possible to explore the effects of

1

various FGD operating changes on sludge chemistry without conducting expensive field testing.

The scrubber operating mode may create nonequilibrium conditions, which manifest themselves in the growth rate of the crystals during sludge formation. The crystal nucleation and growth rate is controlled by operating parameters such as liquid flow rates, sulfur dioxide removal efficiencies, hold tank design, and point of reagent addition. Impurities absorbed on the surfaces may be buried in the crystals. Whether these nonequilibrium impurities buried in the crystal phases will achieve equilibrium in a reasonable time during storage depends upon solid state diffusion kinetics.

Even without fully accounting for the above effects, a thermodynamic model will show the migration trends of the constituents. If the soluble level of trace metals in the FGD wastewater is below the equilibrium level, it can be predicted that the constituents will be released from the solid phase(s). Conversely, when the analyzed soluble level exceeds the equilibrium level, the dissolved forms will decrease in concentration with age. A combined liquid and solid phase thermodynamic model could therefore serve as a useful prediction of both chemical species and their concentrations in FGD sludge leachate.

FGD WASTE CHARACTERISTICS

The application of large-scale wet scrubbing technology for FGD is gaining favor in the United States. The most popular of the wet FGD systems are the lime/limestone processes. More than half of the systems currently being considered or implemented are of this variety. By the early 1980's these systems may account for over 20,000 megawatts of generating capacity.

The physical and chemical properties of the wastes from wet FGD processes are influenced by many interrelated factors, such as fuel type and composition; boiler type, design and operation; fly ash and bottom ash removal systems and their relation to sludge generation; FGD system type, design, and operation; and FGD reagent and input water quality. Because of the numerous variables involved, the composition and quantity of FGD wastes can vary over extremely wide ranges (Ref. 1). The general concentration ranges of constituents in FGD sludges and leachates are listed in Tables 1 to 3.

Table 1 shows that the by-products on nonregenerable FGD systems are typically composed of four major solid constituents: calcium sulfate dihydrate ($CaSO_4.2H_2O$), calcium sulfite hemihydrate ($CaSO_3.1/2H_2O$), calcium carbonate ($CaCO_3$), and fly ash. The solid phase of FGD sludge also contains significant amounts of magnesium, barium, iron, sodium, and potassium. There is

TABLE 1. MAJOR COMPOSITION OF SLUDGE FROM OPERATING SO_2 SCRUBBERS[*]

| Facility | Scrubber Sorbent | Sludge composition (dry basis), wt percent[†] | | | | Comments |
		$CaSO_3 \cdot 1/2H_2O$	$CaSO_4 \cdot 2H_2O$	$CaCO_3$	Fly Ash	
Lawrence	Limestone	10	40	5	45	
Hawthorn 3	Limestone	20	25	5	50	
Hawthorn 4	Limestone	17	23	15	45	
Will County 1	Limestone	50	15	20	15	
Stock Island	Limestone	20	5	74	1	Oil fired
La Cygne	Limestone	40	15	30	15	
Cholla	Limestone	15	20	0	65	14% $CaS_2O_3 \cdot 6H_2O$
Paddy's Run 6	Lime	94	2	0	4	
Mohave 2	Limestone	2	95	0	3	
Shawnee 1	Limestone	19-23	15-32	4-14	20-43	
Shawnee 2	Lime	50	6	3	41	
Phillips	Lime	13	19	0.2	60	9.8% CaS_3O_{10}
Parma	Dual alkali	14	72	8	7	
Scholz 1A	Dual alkali	65-90	5-25	2-10	0	
Utah	Dual alkali	0.2	82	11	9	
Colstrip	Lime/alkaline ash	0.5	5-20	0	40-70	5-30% $MgSO_4$

* Reference 2, 3.

† By-products on nonregenerable FGD systems are typically composed of four major solid constituents.

3

TABLE 2. CONCENTRATIONS OF TRACE ELEMENTS IN FGD SLUDGES[*]

Element	Concentration Ranges (ppm)	Median Concentration (ppm)	Number of Observations	Range of Trace Elements Measured in Coal (ppm)
Arsenic	3.4 - 63	33	9	3 - 60
Beryllium	0.62 - 11	3.2	8	0.08 - 20
Cadmium	0.7 - 350	4.0	9	-
Chromium	3.5 - 34	16	8	2.5 - 100
Copper	1.5 - 47	14	9	1 - 100
Lead	1.0 - 55	14	9	3 - 35
Manganese	11 - 120	63	5	-
Mercury	0.02 - 6.0	1	9	0.01 - 30
Nickel	6.7 - 27	17	5	-
Selenium	<0.2 - 19	7	9	0.5 - 30
Zinc	9.8 - 118	57	5	0.9 - 600

* Reference 5.

TABLE 3. CONCENTRATION OF CONSTITUENTS IN FGD SCRUBBER LIQUORS[*]

Constituents	Range of Constituent Concentrations at Potential Discharge Points	
	mg/l (Except pH)	M
Aluminum	0.03 - 0.3	$10^{-5.95}-10^{-4.95}$
Antimony	0.09 - 2.3	$10^{-6.13}-10^{-4.72}$
Arsenic	<0.004 - 0.3	$<10^{-7.27}-10^{-5.40}$
Beryllium	<0.002 - 0.14	$<10^{-6.65}-10^{-4.81}$
Boron	8.0 - 46	$10^{-3.13}-10^{-2.37}$
Cadmium	0.004 - 0.11	$10^{-7.44}-10^{-6.01}$
Calcium	520 - 3,000	$10^{-1.89}-10^{-1.12}$
Chromium (total)	0.01 - 0.5	$10^{-6.72}-10^{-5.02}$
Cobalt	0.10 - 0.7	$10^{-5.77}-10^{-4.92}$
Copper	<0.002 - 0.2	$<10^{-7.50}-10^{-5.50}$
Iron	0.02 - 8.1	$10^{-6.45}-10^{-3.84}$
Lead	0.01 - 0.4	$10^{-7.32}-10^{-5.71}$
Magnesium	3.0 - 2,750	$10^{-3.91}-10^{-0.95}$
Manganese	0.09 - 2.5	$10^{-5.79}-10^{-4.34}$
Mercury	0.0004 - 0.07	$10^{-8.70}-10^{-6.46}$
Molybdenum	0.91 - 6.3	$10^{-4.71}-10^{-4.18}$
Nickel	0.05 - 1.5	$10^{-6.07}-10^{-4.59}$
Potassium	5.9 - 32	$10^{-3.82}-10^{-3.09}$
Selenium	<0.001 - 2.2	$<10^{-7.90}-10^{-4.56}$
Silicon	0.2 - 3.3	$10^{-5.15}-10^{-3.93}$
Silver	0.005 - 0.6	$10^{-7.33}-10^{-5.25}$
Sodium	14 - 2,400	$10^{-3.21}-10^{-0.98}$

TABLE 3 (continued)

Constituents	Range of Constituent Concentrations at Potential Discharge Points	
	mg/l (Except pH)	M
Tin	3.1 - 3.5	$10^{-4.58}-10^{-4.53}$
Vanadium	<0.001 - 0.67	$<10^{-7.71}-10^{-4.88}$
Zinc	0.01 - 0.35	$10^{-6.82}-10^{-5.27}$
Carbonate	41 - 150 (as $CaCO_3$)	$10^{-3.39}-10^{-2.82}$
Chloride	420 - 4,800	$10^{-1.93}-10^{-0.87}$
Fluoride	0.07 - 10	$10^{-5.43}-10^{-3.28}$
Sulfite	0.8 - 3,500	$10^{-5.00}-10^{-1.36}$
Sulfate	720 - 10,000	$10^{-2.12}-10^{-0.98}$
Phosphate	0.03 - 0.41	$10^{-6.50}-10^{-5.36}$
pH	3.04 - 10.7	$10^{-3.04}-10^{-10.7}$
Ionic strength		0.05 - 0.80

* Reference 4.

also a wide variety of trace metals contained in the solid phase as shown in Table 2. These solid constituents in raw FGD sludges can originate in the fly ash, sorbent, or makeup water.

The liquid phase of FGD wastes is important due to its potential as leachate. As can be seen in Table 3, the FGD liquors typically contain high soluble levels of sulfate, sulfite, calcium, magnesium, sodium, potassium, chloride, carbonate, and also various trace chemical species. The concentrations of these constituents range from trace amounts (e.g., trace metals) to as high as 10,000 ppm (e.g., sulfate). However, these constituents are usually in a nonequilibrium condition. In fact, most of the major chemical species are oversaturated. After a certain time period, the effects of precipitation, dissolution, redox reaction, complexation, or adsorption could affect the redistribution of the chemical species. Chemical analysis data is usually available only for fresh FGD sludge. Concentration data for constituents in aged FGD sludge are less available.

FGD processes employ inorganic reagents and caustic solutions, and are subject to high temperature exhaust gases. These factors do not create an environment conducive to biological activity. The organic species in the FGD wastes therefore exist at nondetectable levels, which will increase the accuracy of any inorganic equilibrium model.

AVAILABLE THERMODYNAMIC MODELS

Comparing the sludge equilibrium chemical composition derived from a thermodynamic model with that of the actual solid-aqueous system can provide a clearer understanding of the chemical behavior of the system. An FGD process can be represented by an array of chemical reactions, including the transfer of mass from reactant species (either solid or soluble species) to other species in the system. Due to the oversaturation of the species in most FGD systems and the high reactivity between the constituents in flue gas and in scrubber liquor, the components in the scrubber are commonly in a state of nonequilibrium or partial equilibrium during the scrubbing process. The partial equilibrium may occur among species in the liquid phase, due to the relatively high rate of complexation reactions. However, the equilibrium between the solid phase and soluble phase (in FGD liquor) may not be reached so quickly due to kinetic constraints (Ref. 6, 7, 8).

Many techniques can be used for constructing and interpreting a chemical thermodynamic model for the calculation of the equilibrium condition of a complex system. The first step in the equilibrium calculations is to identify the components and phases in the system. The next step is to identify the maximum number of unknown activities with the number of independent

relationships that describe the system, such as the equilibrium constant for each reaction, stoichiometric conditions, and electroneutrality conditions in the solution phase. With the phase-composition requirements identified and with adequate thermodynamic data (free energies, equilibrium constants) available, chemical equilibrium in the closed system is then assumed. The composition variables (activities, partial pressures, mole fractions) of the system are then computed.

The actual calculation of chemical equilibrium may be performed using the following methods:

- The equilibrium constant approach (or K approach)

- The Gibbs free energy of reaction and reaction quotient approach (or ΔG and Q approach)

- The total Gibbs function minimization approach (or G and ξ approach)

- The mass transfer approach (or M approach)

- The nongeneralized approach.

In the <u>equilibrium constant approach</u>, stoichiometric equations involving all possible chemical species are set up and solved subject to constraints imposed by the equilibrium constants, mass balance and charge balance relations. This method was pioneered by Brinkley (Ref. 9, 10) and further developed by Feldman, et al. (Ref. 11), Morel and Morgan (Ref. 12) and Crerar (Ref. 13).

In the <u>Gibbs free energy and reaction quotient approach</u>, the free energy for each reaction, ΔG, is computed from

$$\Delta G = G^O + RT \ln Q \tag{1}$$

or

$$\Delta G = RT \ln \frac{Q}{K} \tag{2}$$

subject to the stoichiometric constraints. At equilibrium, $\Delta G = 0$ and the composition is then the equilibrium composition (Ref. 6).

In the <u>total Gibbs function minimization approach</u>, the optimization techniques are used to minimize the total Gibbs free energy function. This method, again, is subject to mass and charge balance constraints. This method was first proposed by White, et al. (Ref. 14), then modified and extended by many researchers, including Naphtali (Ref. 15) and Karpov and Kazmin (Ref. 16).

The concentrations of these two species at varying pH levels are shown in Figure 18. Note that the soluble levels are relatively unchanged throughout the entire pH range.

Sodium

The results of the speciation of sodium in fresh FGD wastewater at I = 0.05 is presented in Figure 19. The distribution of soluble species for sodium is quite similar to that of potassium, with the exception of the presence of $NaCO_3^-$.

Cadmium

Figure 20 displays the speciation of cadmium in fresh FGD wastewater at I = 0.05. Cadmium can form strong soluble complexes with Cl^- and SO_4^{2-}. At high pH levels (pH >8) the $Cd-CO_3$ species will also become significant. When the pH is below 8, the relative concentrations of soluble cadmium species in FGD wastewaters are as follows:

$$Cd^{2+} > Cd-Cl \text{ complexes (mainly } CdCl^+) > CdSO_4(aq)$$

$$Cd-CO_3 \text{ complexes (mainly } CdHCO_3^+) > Cd-OH \text{ complexes}$$

$$(\text{mainly } CdOH^+).$$
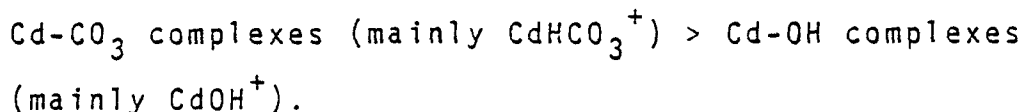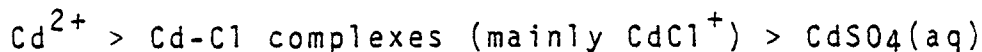
When the pH is above 8, the concentrations of the $Cd-CO_3$ complex (primarily $CdCO_3(aq)$ and $Cd-OH$ complexes (primarily $Cd(OH)_2(aq)$) increase significantly; free metal ion, Cd^{2+}, and $CdSO_4(aq)$ concentrations show a corresponding decrease.

Chromium

Figure 21 shows that the Cr-OH complexes (including $CrOH^{2+}$, $Cr(OH)_2^+$, and $Cr(OH)_4^-$ are the predominant soluble chromium species in fresh FGD wastewater when the pH is greater than 4. The speciation calculation shows that $CrOH^{2+}$ is predominant (50 to 79 percent of the total soluble chromium) between pH levels of 4 and 5. Between pH levels of 5 and 7, $Cr(OH)_2^+$ will predominate (50 to 90 percent). At a pH greater than 7, the $Cr(OH)_4^-$ species can account for almost all soluble chromium. This is consistent with the stability field calculation in Section 3 (see Figure 6).

Aside from the OH^- complexes, free Cr^{3+} is the next most common species when the pH is below 4. Other complexes such as $CrSO_4^+$, $CrHPO_4^+$, Cr-Cl complexes (mainly $CrCl^{2+}$), and Cr-F complexes (mainly CrF^{2+}) can also exist in the FGD wastewater at very low concentrations.

9

The mass transfer approach was developed by Helgeson (Ref. 17-19). Differential equations providing for simultaneous dissolution of multiple reactant minerals, precipitation of mineral assemblages, variable activity of H_2O, oxidation reduction reactions, binary solid solution, and changes in activity coefficients in both open and closed systems are incorporated in a grand matrix equation for describing mass transfer. Computer and thermodynamic data permit mass transfer calculations to be carried out for a complex system under a variation of temperature and pressure.

The nongeneralized approach entails specific, as opposed to generalized, calculations. Here, a set of equations describing a given system is reduced to one or more equations amenable to simple numerical solution. Typical examples are Butler (Ref. 20), Helgeson (Ref. 21), Stumm and Morgan (Ref. 6), Crerar and Anderson (Ref. 22), and Lu (Ref. 23).

PROJECT OBJECTIVES

As discussed previously, constituents in FGD wastes (both sludges and leachates) can exist in various chemical forms with substantial differences in mobility and pollution potential. However, documentation of constituent speciation in FGD wastes is still lacking. A thermodynamic model that can be used to characterize the distributions, migration trends, stability fields, concentration levels, and environmental effects of the constituents is therefore desirable.

In this study, a thermodynamic equilibrium model suitable for evaluating the chemical speciation of FGD waste constituents is evaluated. The Eh-pH plot and ion-ratio methods are also used to construct the stability field of the species.

In order to perform the stability field and speciation calculation, collection, and evaluation of existing FGD waste data and thermodynamic data was necessary. The FGD waste data includes concentrations of various constituents in solid and solution phases. The thermodynamic data including available information on liquid phase interactions between all species present in the FGD wastes, together with the information on possible solid species, interactions between the soluble species and solid surfaces, as well as the solid-solution effects.

After stability field and speciation models were constructed, verification of the calculated results with actual chemical analyses was performed. It is impossible to verify the models directly by chemical analysis data since both the distribution of solid and soluble species of a constituent in the FGD system cannot be determined experimentally. However, the models can be verified by the migration trends of the constituents as well as the ultimate concentration levels in the aged FGD wastes.

The models were then used to determine the effects of various changes in the FGD system or sludge treatment system on the concentration and chemical form of the impurities of interest. Eleven specific investigations were conducted:

- Effects of pH on speciation

- Effects of ionic strength on speciation

- Effects of chloride concentrations on the solubilities of metals

- Effects of sulfate concentrations on the solubilities of metals

- Effects of borate concentrations on the solubilities of metals

- Effects of lime addition on FGD wastes

- Effects of silicate addition on FGD wastes

- Effects of hydrogen sulfide addition on FGD wastes

- Effects of phosphate addition on FGD wastes

- Effects of magnesium addition on FGD sorbent

- Effects of sulfite oxidation.

SECTION 2

PRINCIPLES AND METHODOLOGIES FOR
INVESTIGATIONS INTO CHEMICAL SPECIATION OF FGD SLUDGE

THE STABILITY FIELD OF CONSTITUENT SPECIES

Two principal graphical treatments have been used to
describe the stability relationships of the distribution of the
various soluble and insoluble forms of constituents in the
aqueous solution: Eh-pH plots and the ion-ratio method (Ref. 6,
23). The Eh-pH stability field diagram shows the simultaneous
effect of protons and electrons on the equilibria under various
Eh and pH conditions, and can thus indicate which species pre-
dominate under any given condition of Eh and pH. This method is
useful for constituents such as iron, manganese, mercury,
arsenic, and selenium, which appear in nature in different oxi-
dation states. However, for other constituents with only one
oxidation state, the Eh-pH approach becomes unsuitable. In the
latter case, the ion-ratio method can be used. The ion-ratio
method shows the most stable solid phase by comparing the relevant
reaction constants and ion ratios. Details are given in the
following pages.

Eh-pH Stability Diagrams

The Eh-pH stability diagram of a specific constituent can
be constructed using mass laws and concentration conditions for
that constituent. The general procedures are as follows:

- Identify all the species present in the system

- Identify all the possible reactions among the species
  in the system

- Set up the mass equations by relating the stability
  constants and the molar concentrations of the possible
  reactions

- Plot the resulting equations on a graph with Eh and pH
  axes

12

The following is an example of the calculated stability field for selenium in the FGD system using the Eh-pH approach. Possible species of selenium include:

Solid ———— Se^0

Soluble ——— H_2SeO_3, $HSeO_4^-$, $HSeO_3^-$, SeO_3^{2-}, SeO_4^{2-}

The associated equilibrium conditions are as follows:

$$Se^0 + 3H_2O \rightleftharpoons HSeO_3^- + 5H^+ + 4e^- \qquad K = 10^{-52.3} \qquad (3)$$

$$Se^0 + 3H_2O \rightleftharpoons SeO_3^{2-} + 6H^+ + 4e^- \qquad K = 10^{-58.8} \qquad (4)$$

$$Se^0 + 3H_2O \rightleftharpoons H_2SeO_3 + 4H^+ + 4e^- \qquad K = 10^{-49.8} \qquad (5)$$

$$HSeO_3^- \rightleftharpoons SeO_3^{2-} + H^+ \qquad K = 10^{-6.53} \qquad (6)$$

$$H_2SeO_3 \rightleftharpoons HSeO_3^- + H^+ \qquad K = 10^{-2.55} \qquad (7)$$

$$HSeO_3^- + H_2O \rightleftharpoons SeO_4^{2-} + 3H^+ + 2e^- \qquad K = 10^{-36.1} \qquad (8)$$

$$SeO_3^{2-} + H_2O \rightleftharpoons SeO_4^{2-} + 2H^+ + 2e^- \qquad K = 10^{-29.6} \qquad (9)$$
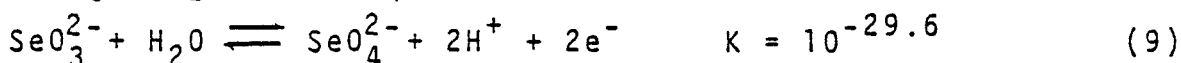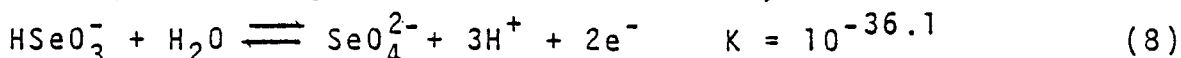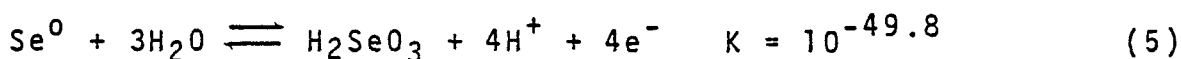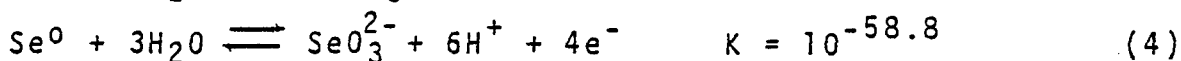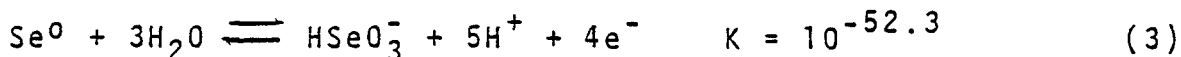
The concentration condition is as follows:

$$[Se_T] = 1.4 \times 10^{-5} M \text{ (total selenium concentration)}$$

The resulting mass equations corresponding to Equations 3 through 9 are as follows:

Redox Couple	Equation (at I=0, T=25°C)	
$Se^0 - HSeO_3^-$	$5\ pH + 0.24\ Eh = 47.5$	(10)
$Se^0 - SeO_3^{2-}$	$6\ pH + 0.24\ Eh = 54.5$	(11)
$Se^0 - H_2SeO_3$	$4\ pH + 0.24\ Eh = 44.9$	(12)
$HSeO_3^- - SeO_3^{2-}$	$pH = 6.53$	(13)
$H_2SeO_3 - HSeO_3^-$	$pH = 2.55$	(14)
$HSeO_3^- - SeO_4^{2-}$	$3\ pH + 0.12\ Eh = 36.1$	(15)
$SeO_3^{2-} - SeO_4^{2-}$	$2\ pH + 0.12\ Eh = 29.6$	(16)

Equations 10 through 16 can then be plotted on the Eh-pH diagram, as shown in Figure 13 (see Section 3).

Due to the wide variety of constituents in the FGD system, the construction of Eh-pH diagrams first requires that the speciation model identify the important soluble species. In the construction of the Eh-pH diagram for mercury, for example, the $HgCl_2$ (aq) complex may become one of the predominant species. Therefore, for FGD systems, mercury should be considered in an $Hg-H_2O-Cl$ system instead of an $Hg-H_2O$ system.

Ion-Ratio Method

The ion-ratio method can be used to identify the most abundant or the most stable solid of a constituent by comparing all the concentrations of anions which comprise the possible solid species of that constituent. For example, if comparing two solid compounds of metal M, M_mX_n and M_pY_q, the reactions are:

$$M_mX_n(s) = m\ M_f^{+z} + n\ X_f^{-r} \tag{17}$$

$$M_pY_q(s) = p\ M_f^{+z} + q\ Y_f^{-s} \tag{18}$$

where m, n, p, q, z, r, and s are positive integers and,

M_f^{+z} = free metal ion with +z valence

X_f^{-r} = free anion with -r valence

Y_f^{-s} = free anion with -s valence

The mass equations become

$$K_{sp,M_mX_n} = (\gamma_{M_f^{+z}})^m\ (\gamma_{X_f^{-r}})^n\ [M_f^{+z}]^m\ [X_f^{-r}]^n \tag{19}$$

$$K_{sp,M_pY_q} = (\gamma_{M_f^{+z}})^p\ (\gamma_{Y_f^{-s}})^q\ [M_f^{+z}]^p\ [Y_f^{-s}]^q \tag{20}$$

where γ is the activity coefficient.

The free metal ion concentrations, controlled by solids M_mX_n and M_pY_q, can be solved by equations 19 and 20, respectively, as shown below:

$$[M_f^{+z}]_{M_mX_n} = \frac{(K_{sp,M_mX_n})^{1/m}}{(\gamma_{M_f^{+z}})\ (\gamma_{X_f^{-r}})^{n/m}\ [X_f^{-r}]^{n/m}} \tag{21}$$

$$[M_f^{+z}]_{M_pY_q} = \frac{(K_{sp,M_pY_q})^{1/p}}{(\gamma_{M_f^{+z}})\ (\gamma_{Y_f^{-s}})^{q/p}\ [Y_f^{-s}]^{q/p}} \tag{22}$$

From equations 21 and 22, the ratio of the free metal ion concentrations can be calculated as follows:

$$\frac{[M_f^{+z}]_{M_mX_n}}{[M_f^{+z}]_{M_pY_q}} = \frac{(K_{sp,M_mX_n})^{1/m} (\gamma_{Y_f^{-s}})^{q/p}}{(K_{sp,M_pY_q})^{1/p} (\gamma_{X_f^{-r}})^{n/m}} \cdot \frac{[Y_f^{-s}]^{q/p}}{[X_f^{-r}]^{n/m}} \qquad (23)$$

If the result of equation 23 is >1, then the solid MpYq will become the solubility controlling solid; that is MpYq is more stable than M_mX_n. If the result is <1, the situation will be reversed. Therefore, the right-hand side of equation 23 can exist under three conditions:

$$\frac{[Y_f^{-s}]^{q/p}}{[X_f^{-r}]^{n/m}} - \frac{(\gamma_{X_f^{-r}})^{n/m} (K_{sp,M_pY_q})^{1/p}}{(\gamma_{Y_f^{-s}})^{q/p} (K_{sp,M_mX_n})^{1/m}} \qquad (24)$$

The value of the right-hand side of equation 24 is constant if the conditions of the system are known. Assuming this constant value is R, then

$$\frac{[Y_f^{-s}]^{q/p}}{[X_f^{-r}]^{n/m}} > R \qquad (25)$$

means M_pY_q is more stable than M_mX_n. If

$$\frac{[Y_f^{-s}]^{q/p}}{[X_f^{-r}]^{n/m}} < R, \qquad (26)$$

this means MmXn is more stable than MpYq. If more than two solid compounds of a constituent can exist in the system, then the comparison should be made among all the possible ion ratios of the anions to obtain the corresponding R values. In this way, the most stable solid will be identified and the remainder screened out.

THE SPECIATION MODEL

Soluble cations (such as trace metals) in a complex system will not exist as a bare ion (i.e., free ion) alone. These cations will instead combine with molecules or anions containing free paris of electrons (bases) in the solution phase. This phenomenon is called complex formation or coordination.

In general, the metal cation (i.e., central atom) will be surrounded by the anions or molecules; these surrounding species

are called ligands. The nearest neighbor atoms to the central atom constitute the first or inner coordination sphere, and the number of atoms in this first coordination sphere is the coordination number of the central atom. Complexes with coordination numbers from two to nine are known, but most exhibit two-, four-, of six-fold coordination. Complexes with different coordination numbers will exhibit different properties even when they have the same metal cation. Therefore, it is important to know the species (coordination number and metal cation) of a complex in order to evaluate its mobility. In a complex system, the thermodynamic model approach is the only way to obtain this information.

Case 1: No Solids Present

In a system where there is no solid present or no migration of constituents between solid and liquid phases, equilibrium among soluble species is easily reached. The relative distribution of all soluble species can be characterized by one of the five methods described previously. In this study, the equilibrium constant approach will be used.

The actual mathematical equilibrium model solves a series of simultaneous equations which describes the interactions among components of the system. For any given metal $M(i)$ and ligand $L(j)$, these equations can be expressed as follows:

$$[M(i)_m L(j)_n] = \beta(i,j)_{nm} [M(i)_f]^m [L(j)_f]^n \cdot \frac{\gamma_{M(i)}^m \; \gamma_{L(j)}^n}{\gamma_{M(i)L(j)}} \quad (27)$$

$$[M(i)_T] = [M(i)_f] + \sum_{M=1}^{k} \sum_{n=1}^{l} \sum_{j=1}^{h} m \, [M(i)_m L(j)_n] \quad (28)$$

$$[L(j)_T] = [L(j)_f] + \sum_{m=1}^{k} \sum_{n=1}^{l} \sum_{i=1}^{g} n \, [M(i)_m L(j)_n] \quad (29)$$

where:

$[M(i)_T]$ = total soluble metal concentration of ith metal (in moles/liter)

$[L(j)_T]$ = total soluble ligand concentration of jth ligand (in moles/liter)

$[M(i)_f]$ = free concentration of ith metal

$[L(j)_f]$ = free concentration of jth ligand

i = metal species
j = ligand species

$[M(i)_m L(j)_n]$ = concentration of complex $M(i)_m L(j)_n$

k = maximum number of metals $M(i)$ coordinating ligands $L(j)$

l = maximum number of ligands $L(j)$ coordinating metals $M(i)$

g = total number of metals

h = total number of ligands

$(i,j)_{nm}$ = overall formation constant of complexes $M(i)_m L(j)_n$, and

γ_x = thermodynamic activity coefficient of species x.

(In general, multi-salt ligands are negligible and therefore are omitted in the above equations.)

In order to solve the above three equations, data are needed for overall formation constants, activity coefficients and total concentrations of metals and ligands in the system. In an FGD system, the major metal species considered are calcium, magnesium, potassium, sodium, iron, manganese, copper, cadmium, zinc, nickel, mercury, lead, cobalt, silver, chromium, aluminum, beryllium, tin, and hydrogen. The major ligands are carbonate (CO_3^{2-}), sulfate (SO_4^{2-}), chloride (Cl^-), fluoride (F^-), phosphate (PO_4^{3-}), silicate (SiO_3^{2-}), borate $(B(OH)_4^-)$, sulfite (SO_3^{2-}), hydroxide (OH^-), molybdate (MoO_4^{2-}), arsenate (AsO_4^{3-}), bivanadate (HVO_4^{2-}), and selenite (SeO_3^{2-}).

The overall formation constants used in this study are compiled from the work of Sillen and Martell (Ref. 24, 25), Ringbom (Ref. 26), and Garrels and Christ (Ref. 27). Individual activity coefficients for the soluble species are calculated from the Davies modification of the Debye-Hückel expression by using A = 0.52 (Ref. 28):

$$\log \gamma_z = 0.51 \ z^2 \left(\frac{\sqrt{I}}{1 + \sqrt{I}} - 0.3I \right), \tag{30}$$

where:

z = valence of the soluble species, and

I = ionic strength of the solution.

A computer is necessary for solving equations 27, 28, and 29 simultaneously, as the expanded equations number in the hundreds. The resultant nonlinear equations are solved by

Newton-Raphson iteration. A detailed description of the computer model is contained in Morel and Morgan (Ref. 12) and McDuff and Morel (Ref. 29).

Case 2: Solid and Gas are Present

If a system contains liquid, solid, and gas phases, the distribution of a constituent is also affected by the solubility products and Henry's constants of its constituent species. For metals under equilibrium conditions, the concentration levels of various soluble species are controlled by the solubilities of the solids. For volatile constituents, both solid and gas species can control the soluble levels of these constituents in the solution phase.

If there is only one solid species, M_pX_q, for a given metal M, then the free metal ion concentration can be regulated at the following level under the equilibrium condition:

$$[M_f] = \left(\frac{(K_{sp})_{M_pX_q}}{\gamma_M^p \, \gamma_x^q \, [X_f]^q} \right)^{1/p} \qquad (31)$$

where:

$[X_f]$ = concentration of free anion (in moles/liter)

K_{sp} = solubility product of solid M_pX_q.

This free metal ion can react further with ligands in the system and form complex species. The concentration of the metal complex can be solved as follows:

$$[M_mL(i)_n] = m \, \beta(i)_{nm} [M_f]^m \, [L(i)_f]^n \cdot \frac{\gamma_M^m \, \gamma_{L(i)}^n}{\gamma_{M_m L(i)_n}} \qquad (32)$$

By combining equations 31 and 32, the total soluble concentration of the metal can thus be solved as shown below:

$$[M_T] \stackrel{=}{\downarrow} [M_f] + \sum_{m=1}^{k} \sum_{n=1}^{l} \sum_{j=1}^{h} m \, [M_m L(j)_n] = [M_f] +$$

$$\sum_{m=1}^{k} \sum_{n=1}^{l} \sum_{j=1}^{h} m \, \beta(i)_{nm} [M_f]^m \, [L(j)_f]^n \cdot \frac{\gamma_M^m \, \gamma_{L(j)}^n}{\gamma_{M_m L(j)_n}} \qquad (33)$$

18

In order to solve equation 33, the data on solubility products, ligand species and concentrations, overall formation constants ($\beta(i)_{nm}$), and activity coefficients are needed. If the solubility controlling solids of each ligand are known, the same procedure (equations 31, 32, and 33) also can be used to solve for the free ligand concentrations. If the total concentrations of ligands are known, then solving for the free ligand concentrations should follow the same procedures as mentioned in the previous section (using the simultaneous solution of equations 27 through 29).

The solids occurring in nature are seldom pure solid phases, i.e., more than one solid species controls the solubility of a constituent. Isomorphous replacement by a foreign component in the crystalline lattice is an important factor by which the concentration of the constituent may be decreased. This phenomenon is called the solid-solution effect.

To characterize the solid-solution effect on the solubility of a given metal, M, consider a heterogeneous system where solid $M_uX_v(s)$ as solute become dissolved in another solid M_pY_q as the solvent. The reaction may be characterized by the equilibrium

$$uM_pY_q(s) + pvX_f^{-r} = pM_uX_v(s) + uqY_f^{-s} \qquad (34)$$
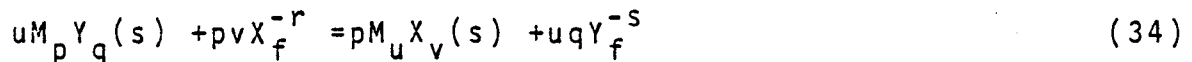
The equilibrium constant for equation 34 (the distribution constant D) corresponds to the quotient of the solubility product constants of $M_pY_q(s)$ and $M_uX_v(s)$

$$\frac{\gamma_M^{pu}[M_f]^{pu}\gamma_x^{pv}[X_f]^{pv}}{\{M_uX_v(s)\}^p} = K_{sp,pM_uX_v} \qquad (35)$$

$$\frac{\gamma_M^{up}[M_f]^{up}\gamma_y^{uq}[Y_f]^{uq}}{\{M_pY_q(s)\}^u} = K_{sp,uM_pY_q} \qquad (36)$$

$$D = \frac{\gamma_Y^{uq}[Y_f]^{uq}\{M_uX_v(s)\}^p}{\gamma_x^{pv}[X_f]^{pv}\{M_pY_q(s)\}^u} = \frac{K_{sp,\ uM_pY_q}}{K_{sp,pM_uX_v}} \qquad (37)$$

The activity ratio of the solids may be replaced by the mole fractions multiplied by activity coefficients:

$$\{M_uX_v(s)\} = R_{M_uX_v} \cdot f_{M_uX_v} \qquad (38)$$

$$\{M_pY_q(s)\} = R_{M_pY_q} \cdot f_{M_pY_q} \qquad (39)$$

19

where:

$$R_{M_u X_v} = \frac{N_{M_u X_v}}{N_{M_u X_v} + N_{M_p Y_q}} \qquad (40)$$

$$R_{M_p Y_q} = \frac{N_{M_p Y_q}}{N_{M_u X_v} + N_{M_p Y_q}} \qquad (41)$$

The total amount of M in the system will become

$$[M_T] = [M_f] + \sum_{m=1}^{k} \sum_{n=1}^{l} \sum_{j=1}^{h} m[M_m L(j)_n] + \sum_{u=1}^{c} \sum_{v=1}^{d} u[M_u X_v(s)]$$

$$+ \sum_{p=1}^{a} \sum_{q=1}^{b} p[M_p Y_q(s)], \qquad (42)$$

where $[M_u X_v(s)]$ and $[M_p Y_q(s)]$ are the molar concentration of solids based on the solution volume. Limits a, b, c, and d represent the maximum numbers of metals or ligands in the solids. In equation 42, $[M_f]$ should be solved simultaneously using equations 35 and 36. If there are more than two solids of M involved, $[M_f]$ should be calculated by solving all the mass equations (similar to equations 35 and 36) simultaneously. The same procedures can be used to solve for $[L(i)_f]$ if $L(i)$ is controlled by more than one solid species. If a gas phase is involved, the same type of equations also can be derived by substituting solubility products for Henry's constants.

Therefore, in order to characterize a system which includes solid, gas, and liquid phases, the following general equations should be solved simultaneously:

$$[M(i)_m L(j)_n] = \beta(i,j)_{nm} [M(i)_f]^m [L(j)_f]^n \cdot \frac{\gamma_{M(i)}^m \gamma_{L(j)}^n}{\gamma_{M(i)_m L(j)_n}} \qquad (43)$$

$$[M(i)_f] = \frac{K_{M(i)_p L(j)_q} \cdot R_{M(i)_p L(j)_q} \cdot f_{M(i)_p L(j)_q}}{\gamma_{M(i)}^p \cdot \gamma_{L(j)}^q \cdot [L(j)_f]^q} \qquad (44)$$

$$[L(j)_f] = \frac{K_{M(i)_u L(j)_v} \cdot R_{M(i)_u L(j)_v} \cdot f_{M(i)_u L(j)_v}}{\gamma_{M(i)}^u \cdot \gamma_{L(j)}^v \cdot [M(i)_f]^v} \qquad (45)$$

$$\sum_{j=1}^{h} \sum_{p=1}^{a} \sum_{q=1}^{b} R_{M(i)_p L(j)_q} = 1 \qquad (46)$$

$$\sum_{i=1}^{g} \sum_{u=1}^{c} \sum_{v=1}^{d} R_{M(i)_u L(j)_v} = 1 \qquad (47)$$

$$[M(i)_T] = [M(i)_f] + \sum_{m=1}^{k} \sum_{n=1}^{l} \sum_{j=1}^{h} m[M(i)_m L(j)_n]$$

$$+ \sum_{j=1}^{h} \sum_{p=1}^{a} \sum_{q=1}^{b} p[M(i)_p L(j)_q]$$

$$+ \sum_{j=1}^{h} \sum_{u=1}^{c} \sum_{v=1}^{d} n[M(i)_m L(j)_n] \qquad (48)$$

$$[L(j)_T] = [L(j)_f] + \sum_{m=1}^{k} \sum_{n=1}^{l} \sum_{i=1}^{g} n[M(i)_m L(j)_n]$$

$$+ \sum_{i=1}^{g} \sum_{p=1}^{a} \sum_{q=1}^{b} q[M(i)_p L(j)_q]$$

$$+ \sum_{i=1}^{g} \sum_{u=1}^{c} \sum_{v-1}^{d} [M(i)_u L(j)_v] \qquad (49)$$

where:

$[M(i)_m L(j)_n]$ = concentration of complex $M(i)_m L(j)_n$ (in moles/liter)

$[M(i)_f]$ = free metal ion concentration of ith metal (in moles/liter)

$[L(j)_f]$ = free concentration of jth ligand (in moles/liter)

$[M(i)_T]$ = total concentration of ith metal in the system (in moles/liter)

$$R_{M(i)_p L(j)_q}$$

and
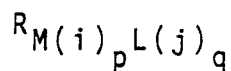
$R_{M(i)_u L(j)_v}$ = mole fraction of solid or gas species for metal or ligand solids

i = metal species

j = ligand species

g = total number of metals

h = total number of ligands

k = maximum number of metals $M(i)$ coordinating ligands $L(j)$

l = maximum number of ligands $L(j)$ coordinating metals $M(i)$

$a, b, c,$ and d = positive integer showing maximum number of the composition of metals or ligands in the solids or gases

$\beta(i,j)_{nm}$ = overall formation constant of complex $M(i)_m L(j)_n$

γ_x = thermodynamic activity coefficient of soluble species x, and

f_x = thermodynamic activity coefficient of solid (or gas) species x (in this study, assume $x \simeq 1$).

K = solubility products or Henry's constants.

In order to solve the above equations simultaneously, the information on metal and ligand species, overall formation constants, solubility products (or Henry's constants), and activity coefficients must be known.

The computer model used in this study follows the simultaneous solution methodology used by Morel and Morgan (Ref. 12) and McDuff and Morel (Ref. 29) with some minor modifications. The major metals and ligands present in FGD sludge were noted previously. The overall formation constants, solubility products, and Henry's constants were compiled from the literature (Ref. 24-27). The activity coefficients for soluble species are followed by Davies modification of the Debye-Huckel expression.

22

SECTION 3

STABILITY FIELD OF SOLID SPECIES
IN FGD SLUDGE

COMMON SOLID SPECIES AND THERMODYNAMIC DATA

Knowledge of the solid species in FGD sludge is important to evaluate both the migration trends and levels of contaminants. The solid species in the raw FGD wastes originate mainly in fly ash, undissolved sorbent, bottom ash, and new precipitates. Due to the nonequilibrium conditions of the raw FGD wastes, the original solid species in the FGD system may be gradually transformed to another species and subsequently affect contaminant mobility as the wastes are aging. Stability field analyses can be used to derive these transformation trends. In order to perform these stability field analyses, information on common solid species and their thermodynamic data are required.

The common solid species of metals in nature are compiled in Table 4. This table follows the information compiled by Lu (Ref. 23). Additional information in this table is from Wedepohl (Ref. 30), Energlyn and Brealey (Ref. 31), Garrels and Christ (Ref. 27), Garrels (Ref. 32), Latimer (Ref. 33, Stumm and Morgan (Ref. 6), Krauskopf (Ref. 34), Leckie and James (Ref. 7), and Weber and Posselt (Ref. 35). The important solubility products of these metallic solids are compiled in Table 5. These data are mainly from Latimer (Ref. 33), Sillen and Martell (Ref. 24, 25), and Ringbom (Ref. 8).

In the stability field analyses performed in this study, the solids considered are limited to simple metallic solids. This is because simple solids are usually more active than complex solids. Such active solids may persist in metastable equilibrium with the solution and may convert ("age") slowly into inactive forms (Ref. 6). As can be seem from Tables 4 and 5, most of the simple metallic solids in the FGD system are oxides, hydroxides, carbonates, sulfites, sulfates, phosphates, and simple silicates. Due to the slow nucleation rates and dissolution rates of the complex solids (especially complex silicates), it is not likely that they will play important roles in the regulation of soluble species; they will therefore be omitted in the stability field analysis.

TABLE 4. COMMON SOLID SPECIES OF METALS IN NATURE[*]

Aluminum

Oxides:	Al_2O_3 (corundum)
Hydroxides:	$Al(OH)_3$ (gibbsite)
Phosphates:	$AlPO_4$, $Al(H_2PO_4)(OH)_2$
Silicates:	$Al_2Si_2O_5$ (kaolinite), $NaAlSi_3O_8$ (albite)
	$CaAl_2Si_2O_8$ (anorthite), $KAl_3Si_3O_{10}(OH)_2$(K-mica)
	$KAlSi_3O_8$ (K-feldspar), $Na_{0.33}Al_{2.33}Si_{3.67}O_{10}(OH)_2$
	(Na-montmorillonite)
	$Ca_{0.33}Al_{4.67}Si_{7.33}O_{20}(OH)_4$ (Ca-montmorillonite)

Antimony

Native:	Sb^0
Oxides:	Sb_2O_3, Sb_2O_5, $Sb_2O_3 \cdot Sb_2O_5$ (cervanite)
Hydroxides:	$Sb(OH)_3$, $Sb(OH)_3Cl_2$
Simple Sulfides:	Sb_2S_3, Sb_2S_5
Complex Sulfides:	$AgSbS_2$, Ag_3SbS_3 (pyrargyrite), $Cu_{12}Sb_4S_{13}$ (tetrabedrite)
	$2PbS \cdot Sb_2S_3$ (jamesonite), $3Cu_2S \cdot Sb_2S_5$ (famatinite)
	$3(PbCu_2)S \cdot Sb_2S_3$ (bournonite)

Arsenic

Native:	As^0
Oxides:	As_2O_3, $Ca_3(AsO_4)_2$
Complex Oxides:	Ag_3AsO_3, Ag_3AsO_4, $Ca_3(AsO_4)_2$
Simple Sulfides:	As_2S_3, As_2S_5, As_4S_3, AsS (realgar)
Complex Sulfides:	$FeAsS$ (mispickel), $CoAsS$ (cobaltite), Ag_3AsS_3 (proustite)
	Cu_3AsS_4 (enargite), $AgAsS_2$
Halides:	$AsBr_3$, AsI_3

TABLE 4 (continued)

Beryllium

Oxides:	BeO (bromellite)
Complex Oxides:	$BeO \cdot Al_2O_3$ (chrysoberyl)
Hydroxides:	$Be(OH)_2$ amorphous, $\propto$-$Be(OH)_2$, β-$Be(OH)_2$, $BeO \cdot Be(OH)_2$
Simple Sulfides:	BeS
Sulfates:	$BeSO_4$
Halides:	$BeCl_2$, $BeBr_2$, BeI_2, Na_2BeCl_4, K_2BeCl_4
Silicates:	$3BeO \cdot Al_2O_3 \cdot 6SiO_2$ (beryl), $(Zn,Fe)_2(Fe_2S)Be(SiO_4)_3$ (helvite)
	$NaCaBeF(SiO_3)_2$ (leucophane), $Be_2Fe(YO)_2(SiO_4)_2$ (gadolinite)
Other:	$Be(VO_3)_2$, $BeMoO_4$

Cadmium

Oxides:	CdO (monteporrite)
Hydroxides:	$Cd(OH)_2$
Carbonates:	$CdCO_3$ (otavite)
Sulfides:	CdS (greenockite)

Calcium

Hydroxides:	$Ca(OH)_2$
Carbonates:	$CaCO_3$ (calcite), $CaCO_3$ (aragonite), $CaMg(CO_3)_2$ (dolomite)
Simple Sulfides:	CaS (oldhamite)
Sulfates:	$CaSO_4$, $CaSO_3$, $CaSO_4 \cdot 2H_2O$, $CaSO_3 \cdot 1/2H_2O$
Phosphates:	$Ca_2P_2O_7$, $CaHPO_4$, $Ca_3(PO_4)_2$, $CaH_2(PO_4)_2$, $Ca_5OH(PO_4)_3$

TABLE 4 (continued)

Silicates:	$NaCaFBe(SiO_3)_2$ (leucophane), $CaAl_2Si_4O_{12} \cdot 4H_2O$ (laumontite)
	$CaSiO_3$ (wollastonite), $CaO \cdot MgO \cdot 2SiO_2$ (diopside)
	$Ca_{10}Mg_2Al_4(Si_2O_7)_2(SiO_4)_5(OH)_4$ (idocrase)
	$CaAl_2Si_2O_8$ (anorthite), $Ca_{0.33}Al_{4.67}Si_{2.33}O_{20}(OH)_4$ (Ca-montmorillonite)
Halides:	CaF_2, $CaBr_2$, CaI_2

Chromium

Oxides:	$FeO \cdot Cr_2O_3$ (chromite), $PbCrO_4$ (crocoisite), Cr_2O_3
Hydroxides:	$Cr(OH)_3$

Cobalt

Oxides:	CoO, Co_2O_3, Co_3O_4
Hydroxides:	$Co(OH)_3$, $Co(OH)_2$
Carbonates:	$CoCO_3$ (spherocobaltite)
Simple Sulfides:	CoS, $Co(HS)_2$
Complex Sulfides:	$CoAsS$
Sulfates:	$Co(SO_4)_2 \cdot H_2O$, $Co(OH)_{1.5}(SO_4)_{0.25}$
Phosphates:	$Co_3(PO_4)_2$, $CoHPO_4$
Silicates:	Co_2SiO_4

Copper

Native:	Cu^0
Oxides:	Cu_2O (cuprite), CuO (tenorite)
Hydroxides:	$CuCl_2 \cdot 3Cu(OH)_2$ (ataramite), $Cu(OH)_2$
Carbonates:	$Cu_2(OH)_2CO_3$ (malachite), $Cu_3(OH)_2(CO_3)_2$ (azurite)
Simple Sulfides:	Cu_2S (chalcocite), CuS (covellite)

TABLE 4 (continued)

	Complex
Sulfides:	$CuFeS_2$ (chalcopyrite), Cu_5FeS_4 (bornite)
	Cu_3AsS_4 (enargite), $(Cu,Fe)_{12}Sb_4S_{13}$ (tetrahedrite)
Sulfates:	$Cu_4(OH)_6SO_4$ (brochantite), $CuSO_4 \cdot 5H_2O$ (chalcanthite)
Silicates:	$CuSiO_3 \cdot nH_2O$ (chrysocolla), $CuO \cdot SiO_2 \cdot H_2O$ (dioptase)

Iron

Oxides:	Fe_2O_3 (hematite), $FeOOH$ (geothite), Fe_3O_4 (magnetite)
	$FeOOH \cdot nH_2O$ (limonite)
Hydroxides:	$Fe(OH)_3$, $Fe_3(OH)_8$ (ferrosofferric hydroxide)
Carbonates:	$FeCO_3$ (siderite)
Sulfides:	FeS_2 (pyrite), $Fe_{1-x}S$ (pyrrhotite), FeS (machinawite)
	Fe_3S_4 (greigite)
Sulfates:	$KFe_3(OH)_6(SO_4)_4$ (jarosite)
Phosphates:	$FePO_4$
Silicates:	$FeSiO_3$ (glauconite), $(Fe(II), Fe(III), Mg,Al)$
	$(Si,Al)O_{7.3-5}(OH)_{4-1}$ (chamosite)

Lead

Native:	Pb^O
Oxides:	PbO (massicot), PbO_2 (plattnerite), Pb_3O_4 (minimum)
	$PbCrO_4$ (crocoite), $PbMoO_4$ (wulfenite)
Hydroxides:	$Pb(OH)_2$
Carbonates:	$PbCO_3$ (cerussite), $Pb_3(OH)_2(CO_3)_2$ (hydrocerussite)
Sulfides:	PbS (galena)
Sulfate:	$PbSO_4$ (anglesite)
Halides:	$3Pb_3As_2O_8 \cdot PbCl_2$ (mimetite), $3Pb_3V_2O_8 \cdot PbCl_2$
	(vanadinite)

TABLE 4 (continued)

Magnesium

Oxides:	MgO (periclase), $Mg_7Cl_2B_{16}O_{30}$ (boracite)
	$MgAl_2O_4$ (spinel)
Hydroxides:	$Mg(OH)_2$ (brucite)
Carbonates:	$MgCa(CO_3)_2$ (dolomite), $MgCO_3$ (magnesite), $MgCO_3$ (nesquehonite)
	$3MgCO_3 \cdot Mg(OH)_2 \cdot 3H_2O$ (hydromagnesite)
Simple Sulfides:	MgS
Sulfates:	$MgSO_4$
Phosphates:	$MgNH_4(PO_4)$, $Mg_3(PO_4)_2$, $MgNH_4(PO_4)(H_2O)_6$, $MgK(PO_4)(H_2O)_6$
	$MgHPO_4(H_2O)_3$
Halides:	MgF_2, $KMgCl_3(H_2O)_3$, $MgCl_2(H_2O)_6$, $MgCl_2$
Silicates:	$MgSiO_3$ (clinoenstatite), Mg_2SiO_4 (forsterite)
	$Mg_3Si_4O_{10}(OH)_2 \cdot nH_2O$ (vermiculite), $Mg_3Si_4O_{10}(OH)_2$ (talc)

Manganese

Simple Oxides:	MnO_2 (pyrolusite), Mn_3O_4 (hausmannite), MnOOH or Mn_2O_3 (manganite)
	$MnO_{1.2}$ to MnO_2 (nonstoichiometric oxides)
Complex Oxides:	$(Mn,Si)_2O_3$ (braunite), $Mn_3O_4 \cdot Fe_3O_4$ (vrendenburgite)
	$(Mn,Fe)_2O_3$ (bixbyrite), $(Mn(II)Fe)(Mn(III)Fe)_2O_4$ (jacobsite)
	$BaMn(II)Mn(IV)_8O_{16}(OH)_4$ (psilomelane)
Hydroxides:	$Mn(OH)_2$ (pyrochroite), $Mn(OH)_3$
Carbonates:	$MnCO_3$ (rhodochrosite)
Sulfides:	MnS (alabandite)
Silicates:	$MnSiO_3$ (rhodonite), $Mn_3Al_2(SiO_4)_3$ (spessartite)

TABLE 4 (continued)

Mercury

    Native: Hg^0

    Oxides: HgO, $HgSb_4O_7$ (livingstonite)

    Hydroxides: $Hg(OH)_2$

    Sulfides: HgS (cinnabar)

    Sulfates: $HgSO_4 \cdot 2HgO$

    Halides: $HgCl_2$, Hg_2OCl, Hg_4OCl_2, Hg_2Cl_2 (calomel)

Molybdenum

    Oxides: MoO_3 (molybdine), MoO_2, H_2MoO_4, $PbMoO_4$ (mulfenite)

    Simple
    Sulfides: MoS_2 (molybdenite), MoS_3, MoS_4

    Phosphates: $Mo(PO_3)_6$

Nickel

    Oxides: NiO_2, Ni_2O_3, Ni_3O_4, Ni_3O_4, $Ni_3As_2O_8 \cdot 8H_2O$ (annabergite)

    Hydroxides: $Ni(OH)_2$

    Carbonates: $NiCO_3$, $NiCO_3 \cdot 2Ni(OH)_2 \cdot 4H_2O$ (emerald nickel)

    Sulfides: NiS (millerite)

    Sulfates: $NiSO_4 \cdot 7H_2O$ (nickel vitroil)

    Silicates: $(Ni,Mn)_3Si_2O_5(OH)_4$ (garnierite), Nepouite (nickelferrous chlorite)

Potassium

    Complex
    Oxides: $K_2(UO_2)_2(VO_4)_2(VO_4)_2 \cdot 3H_2O$ (carnotite)

    Phosphates: $K_3PO_4(MoO_3)_{11}$, $K_3PO_4(WO_3)_{12}$

    Halides: K_2SiF_6

    Silicates: $KAl_3(SO_4)_2(OH)_6$ (alunite), $KAl_3(AlSi_3O_{10})(OH)_2$ (muscovite)

                $KAlSi_3O_8$ (orthoclase), $K(Mg,Fe)_3(AlSi_3O_{10})(OH)_2$ (biotite)

TABLE 4 (continued)

<u>Selenium</u>

Native: Se^0

Oxide: SeO_2

Sulfides: SeS

<u>Silicon</u>

Oxides: SiO_2 (quartz), SiO_2 (amorphous), Al_2SiO_5 (kaolinite)
$NaAlSi_3O_8$ (albite), $3BeO \cdot Al_2O_3 \cdot 6SiO_2$ (beryl),
$(ZnFe)_2 \cdot (Fe_2S)Be(SiO_4)_3$ (helvite)
$NaCaBeF(SiO_3)_2$ (leucophane), $Na_2Al_2Si_3O_{10} \cdot 2H_2O$
   (natrolite)
$CaAl_2Si_4O_{12} \cdot 4H_2O$ (laumontite), $(Ca_1Na_2)Al_2Si_7O_{18} \cdot 6H_2O$
   (heulandite)
$Na(Li,Mg,Fe^{+2},Al)_6Al_6B_3Si_6(OH)_4$ (tourmaline), Fe_2SiO_4
   (olivine)
$Fe_2Al_9O_6(SiO_4)_4(O,OH)_2$ (staurolite), $Zn_4Si_2O_7(OH)_2 \cdot H_2O$
   (hemimorphite)
$Ca_{10}Mg_2Al_4(Si_2O_7)_2 \cdot (SiO_4)_5(OH)_4$ (idocrase)
$NaCa_2(MgFeAl)_5(SiAl)_8O_{22}(OH)_2$ (hornblende)
$Al_4Si_4O_{10}(OH)_8$, $Al_2Si_4O_{10}(OH_2) \cdot nH_2O$, $Mg_3Si_4O_{10}(OH)_2$
   (talc)
$KAl_3(AlSi_3O_{10})(OH)_2$ (muscovite), $K(Mg,Fe)_3(AlSi_3O_{10})(OH)_2$
   (biotite)

Halides: K_2SiF_6

<u>Silver</u>

Native: Ag^0

Oxides: AgO, Ag_2O

Complex
Oxides: $Ag_2Cr_2O_7$, $Ag_6V_4O_{13}$, Ag_2CrO_4, $AgIO_3$, $AgBrO_3$, Ag_3AsO_4

Hydroxides: $AgOH$

Carbonates: Ag_2CO_3

TABLE 4 (continued)

Simple Sulfides:	Ag_2S
Complex Sulfides:	Ag_3AsS_3, Ag_3SbS_3, $AgAsS_2$, $AgSbS_2$
Sulfates:	Ag_2SO_4, Ag_2SO_3
Phosphates:	Ag_3PO_4, $AgPO_3$, AgP_2O_7
Halides:	$AgCl$, $AgBr$, AgI, $Ag(NH_3)_2Br$

Sodium

Oxides:	Na_2VO_4, $Na_2O \cdot 2CaO \cdot 2B_2O_3 \cdot IOH_2O$ (kramite)
	$NaCaB_5O_9 \cdot 8H_2O$ (ulexite), $Na_2O \cdot 2B_2O_3 \cdot 5H_2O$
Sulfates:	$NaHSO_4$
Halides:	Na_2SiF_6
Silicates:	$NaAlSi_3O_8$ (albite), Na-montmorillonite, $NaCaBeF(SiO_3)_2$ (leucophane)
	$Na_2Al_2Si_3O_{10} \cdot 2H_2O$ (natrolite), $Na_2O \cdot Al_2O_3 \cdot 4SiO_2$ (jadeite)
	$NaCa_2(Mg,Fe,Al)_5(Si,Al)_8O_{22}(OH)_2$ (hornblende)

Tin

Native:	Sn^0
Oxides:	SnO_2, SnO, $Sn_2As_2O_7$
Hydroxides:	$Sn(OH)_2$, $Sn(OH)_4$
Sulfides:	SnS, SnS_2, Sn_2S_3, $Cu_2S \cdot FeS \cdot SnS_2$ (stannine)
Phosphates:	$SnHPO_4$, $Sn_3(PO_4)_2$

Vanadium

Oxides:	V_2O_5, V_2O_3, V_2O_2, VO_2, $Be(VO_3)_2$, $Ag_6V_4O_{13}$
	$K_2(UO_2)_2(VO_4)_2 \cdot 3H_2O$ (carnotite), $(PbCl)Pb_4(VO_4)_3$ (randinite)
Hydroxides:	$V(OH)_2$, $V(OH)_3$, $VO(OH)_2$
Sulfides:	V_2S_5

TABLE 4 (continued)

Zinc

Oxides:	ZnO (zincite)
Hydroxides:	$Zn(OH)_2$
Carbonates:	$ZnCO_3$ (smithsonite)
Sulfides:	ZnS (sphalerite)
Sulfates:	$ZnSO_4 \cdot 7H_2O$ (goslarite)
Silicates:	$ZnSiO_3$, $2ZnO \cdot SiO_2$ (willemite), $Zn2SiO_4 \cdot nH_2O$ (calamine)
	$Zn_4(OH)_2Si_2O_7 \cdot H_2O$ (hemimorphite)

---

* Main Ref. 6, 23, 27, 30, 31, 32, 33, 34, 35, and 36.

TABLE 5.   IMPORTANT SOLUBILITY PRODUCTS OF METALS* (IN pKsp)

Metal	Oxide	Hydroxide	Carbonate	Sulfide	Sulfite	Sulfate	Chloride	Phosphate	Silicate
AL(III)	34 (Gibbsite)	31.7						21 (AlPO$_4$) 30.5 (Al(H$_2$PO$_4$)(OH)$_2$)	38.7[†] (Kaolinite) 40.6[†] (Albite) 52.3[†] (Anorthite) 76.4[†] (K-Feldspar) 123.6[†] (K-Mica) 294[†] (Na-Montmorillonite) 585.2[†] (Ca-Montmorillonite)
Sb(III)	41.4[†] (Sb$_2$O$_3$)	70.5 (Sb(OH)$_3$Cl$_2$)		-0.45[†]					
As(III)									
Be(II)	26.9[†] (BeO) 54.1[†] BeO·Be(OH)$_2$	20.0 (Amorphous) 21.1 (γ-Be(OH)$_2$) 21.5 (β-Be(OH)$_2$)		-5.25		-1.71	-26.4		
Cd(II)		13.6	13.6	26.1					

TABLE 5 (continued)

Metal	Oxide	Hydroxide	Carbonate	Sulfide	Sulfite	Sulfate	Chloride	Phosphate	Silicate
Ca(II)	-4.6†	5.26	8.32 (Calcite) 8.22 (Aragonite) 16.7† (Dolomite)	2.94	6.5, 6.88 (CaSO$_3$·½H$_2$O)	4.6 (CaSO$_4$· 2H$_2$O)		6.25 (CaHPO$_4$) 26 (Ca$_3$(PO$_4$)$_2$) 1.14 (CaH$_2$(PO$_4$)$_2$) 6.4 (CaHPO$_4$·(H$_2$O)$_2$) 40.92 (Ca$_4$H(PO$_4$)$_3$) 55.6 (Ca$_5$OH(PO$_4$)$_3$) 120.86 (Ca$_{10}$(PO$_4$)$_6$ F$_2$)	3.7 (CaSiO$_3$) 52.3† (Anorthite) 585.2† (Ca-Montmorillonite)
Cr(III)		31.0							
Co(II)	84.3†	14.2 (blue) 14.0 (pink, fresh) 15.7 (pink, aged)	12.84	21.3(γ) 26.6(β)		12.7† (Co(OH)$_{1.6}$ (SO$_4$)$_{0.25}$)	-7.32	34.7 (Co$_3$(PO$_4$)$_2$) 6.7 (CoHPO$_4$)	

TABLE 5 (continued)

Metal	Oxide	Hydroxide	Carbonate	Sulfide	Sulfite	Sulfate	Chloride	Phosphate	Silicate
Co(III)		40.5							
Cu(II)	20.35	18.59	9.63 ($CuCO_3$) 33.16 ($Cu_2CO_3(OH)_2$)	35.2				37.7	
Fe(II)		16.3	10.2	16.9 (FeS)				33.3	18.9[†]
Fe(III)	80.1[†] (Fe_2O_3)	39.3		10.2 (Fe_3S_4)				25.8	
Pb(II)	15.35[†] (PbO)	16.09 18.8[†] ($Pb_3(OH)_2(CO_3)_2$)	13.1	26.6		7.78	4.79	43.5 12.6[†] ($PbHPO_4$)	
Mg(II)		9.2 (active) 11.6 (Brucite)	4.9 (Magnesite) 5.4 (Nesquehonite) 16.7[†] ($MgCa(CO_3)_2$)	-2.41	-2.85	-4.27	4.44[†] ($MgCl_2 \cdot (H_2O)_6$) 4.00[†] ($KMgCl_3(H_2O)_3$)	28.4 ($Mg_3(PO_4)_2$) 12.6[†] ($MgNH_4(PO_4)$) 13.15[†] ($MgNH_4PO_4(H_2O)_6$) 5.02[†] ($MgHPO_4(H_2O)_3$)	

TABLE 5 (continued)

Metal	Oxide	Hydroxide	Carbonate	Sulfide	Sulfite	Sulfate	Chloride	Phosphate	Silicate
Mn(II)	0.92†	12.72	9.30	12.9 (Crystalline) 15.7 (Precipitated)				22	13.2†
Hg(I)		23.7	16.05	45.0		6.13	17.88 (Hg_2Cl_2)	2.4 ($Hg_2(HPO_4)$)	
Hg(II)	25.7†	26.4		52.2 (Metacinnabar) 53.6 (Cinnabar)			13.8		
Ni(II)		14.7 (fresh) 17.2 (aged)	6.9	18.5 (X) 24.0 (β) 25.7 (ə)		-2.91 ($NiSO_4$) 1.46 ($NiSO_4 \cdot 6H_2O$)			
K(I)			-4.11	-11.02	-4.53	1.72	-0.93		76.4† (K-Feldspar) 123.6† (K-Mica)
Se									
Ag(I)	7.71		11.1	49.2	13.82	4.8	9.75	15.84	

TABLE 5 (continued)

Metal	Oxide	Hydroxide	Carbonate	Sulfide	Sulfite	Sulfate	Chloride	Phosphate	Silicate
Na(I)						6.6 (Na_aHSO_4)	-1.55		40.6[†] (Albite) 294 (Na-Montmorillonite)
Sn(II)	1.76[†]	28.1		26.0					
V(II)		15.4							
V(III)		34.4							
Zn(II)		15.60 (Amorphous) 16.95 (Amorphous, aged) 16.92 (Cryst. aged)	10.78	25.15 (Sphalerite) 22.80 (Wurzite) 22.05 (Precipitated)				36.7	21.03[†]

TABLE 5 (continued)

* Values in pKsp at $I = 0$, $T = 25^0C$; main Ref. 8, 24, 25, 33.

† $\frac{1}{2}Al_2O_3 \cdot 3H_2O$ (S,Gibbsite) $= Al^{3+} + 3OH^-$

$\frac{1}{2}Al_2Si_2O_5(OH)_4$ (S,Kaolinite) $+ 2\frac{1}{2}H_2O = Al^{3+} + H_4SiO_4 + 3OH^-$

$NaAlSi_3O_8$ (S,Albite or Na-Feldspar) $+ 7H_2O + H^+ = Al^{3+} + Na^+ + 3H_4SiO_4 - 3OH^-$

$CaAl_2Si_2O_8$ (S,Anoythite or Ca-Feldspar) $+ 8H_2O = 2Al^{3+} + 2H_4SiO_4 + 8OH^- + Ca^{2+}$

$1\frac{1}{2}KAlSi_3O_8$ (S,K-Feldspar or Orthoclase) $+ 12H_2O = 1\frac{1}{2}Al^{3+} + 1\frac{1}{2}K^+ + 4\frac{1}{2}H_4SiO_4 + 6OH^-$

$KAl_3Si_3O_{10}(OH)_2$ (S,K-Mica or Muscovite) $+ 10H_2O = 3Al^{3+} + K^+ + 3H_4SiO_4 + 10 OH^-$

$3Na_{0.33}Al_{2.33}Si_{3.67}O_{10}(OH)_2$ (S,Na-Montmorillonite) $+ 30H_2O = 7Al^{3+} + 11H_4SiO_4 + 22OH^- + Na^+$

$3Ca_{0.33}Al_{4.67}Si_{7.33}O_{20}(OH)_4$ (S,Ca-Montmorillonite) $+ 60H_2O = 14Al^{3+} + 22H_4SiO_4 + 44OH^- + Ca^{2+}$

$\frac{1}{2}Sb_2O_3(s) + 1\frac{1}{2}H_2O = Sb^{3+} + 3OH^-$

$\frac{1}{2}Sb_2S_3(s) + \frac{1}{2}S^= = SbS_2^-$

$CaMg(CO_3)_2$ (S,Dolomite) $= Ca^{2+} + Mg^{2+} + 2CO_3^{2-}$

$Fe_2O_3(s) + 3H_2O = 2Fe^{3+} + 6OH^-$

$FeSiO_3(s) + H_2O = Fe^{2+} + 2OH^- + SiO_2(s)$

$BeO(s) + H_2O = Be^{2+} + 2OH^-$

$CaO(s) + H_2O = Ca^{2+} + 2OH^-$

$CoO(s) + H_2O = Co^{2+} = 2OH^-$

$Co(OH)_{1.5}(SO_4)_{0.25}(s) = Co^{2+} + 1.5OH^- + 0.25SO_4^=$

$Pb_3(OH)_2(CO_3)_2(s) = 3Pb^{2+} + 2OH^- = 2CO_3^=$

$PbO(s) + H_2O = Pb^{2+} + 2OH^-$

$PbHPO_4(s) = Pb^{2+} + HPO_4^{2-}$

$MgNH_4(PO_4)(s) = Mg^{2+} + NH_4^+ + PO_4^{3-}$

$MgNH_4(PO_4)(H_2O)_6(s) = Mg^{2+} + NH_4^+ + PO_4^{3-} + 6H_2O$

$MgHPO_4(H_2O)_3(s) = Mg^{2+} + HPO_4^{2-} + 3H_2O$

$MgCl_2(H_2O)_6$ (S,bischofite) $= Mg^{2+} + Cl^- + 6H_2O$

TABLE 5 (continued)

$$KMgCl_3(H_2O)_3 \text{ (S.Carnallite)} = K^+ + Mg^{2+} + Cl^- + 3H_2O$$

$$MnO_2(s) + 2H^+ = Mn^{2+} + \tfrac{1}{2}O_2 + H_2O$$

$$MnSiO_3(s) + H_2O = Mn^{2+} + 2OH^- + SiO_2(s)$$

$$HgO(s) + H_2O = Hg^{2+} + 2OH^-$$

$$2Hg^0 = Hg^{2+} + 2e^-, E^0 = -0.789$$

$$Se^0 + 6OH^- = SeO_3^{2-} + 3H_2O + 4e^-, E^0 = 0.366$$

$$SnO(s) + 2H^+ = Sn^{2+} + H_2O$$

$$ZnSiO_3(s) + H_2O = Zn^{2+} + 2OH^- + SiO_2(s)$$

$$As^0 + 3H_2O = H_3AsO_3 + 3H^+ + 3e^-$$

RESULTS OF STABILITY FIELD ANALYSIS

The stability field of solids can be described as either
(1) a function of Eh and pH or (2) a function of associated ions
and corresponding activity coefficients. Results are reported
in Eh-pH diagrams or ionic ratio (in log scale) and ionic
strength diagrams. Only the stability field diagrams of alumi-
num, antimony, arsenic, cadmium, calcium, chromium, copper, iron,
lead, mercury, manganese, nickel, selenium, sulfur, and zinc
will be evaluated.

Due to the wide variety of FGD wastes, the data used here
to construct the ion-ratio diagram was chosen from both the
minimum and maximum levels of contaminants in order to cover all
possible conditions (see Table 3). Owing to the complexity of
the calculation and graphing procedures in the Eh-pH diagram,
only median levels of the constituents were used. Results of the
stability field analyses are discussed below.

Aluminum

The stability field of aluminum in the FGD wastes is shown
in Figure 1. There are three possible solid forms of aluminum (Al)
that can exist in the FGD wastes: $Al_2O_3.3H_2O(s)$, $AlPO_4(s)$ and
$Al(H_2PO_4)(OH)_2(s)$. Figure 1 shows that if the equilibrium ratio
of $\{OH^-\}^3$ to $[PO_4^{3-}]$ of the FGD wastewater is greater than about
10^{-14}, the $Al_2O_3.3H_2O(s)$ solid is more stable than the $AlPO_4(s)$
solid. However, if $\{OH^-\}^3/[PO_4^{3-}]$ is less than 10^{-14}, the
$AlPO_4(s)$ species becomes more stable than $Al_2O_3.3H_2O(s)$ species.

From the diagram, it can also be seen that the effect of
ionic strength on the stability field of aluminum is usually
minor. Between species $Al_2O_3.3H_2O(s)$ and $AlPO_4(s)$, the boundary
effects of the ionic ratio upon the ionic strength (0.05 to 0.8
for FGD systems) vary only from 10^{-13} to $10^{-14.2}$. For
$Al_2O_3.3H_2O(s)$ and $Al(H_2PO_4)(OH)_2(s)$, this variation is from
$10^{-3.50}$ to $10^{-3.64}$ and for $Al(H_2PO_4)(OH)_2(s)$ and $AlPO_4(s)$ it is
from $10^{-9.5}$ to $10^{-10.6}$.

In order to illustrate the use of the ion-ratio diagram,
consider the following example: Assume a sample of FGD waste-
water has the following characteristics:

$I = 0.6$

$pH = 8$

$P_T = 10^{-5.5}M$ (total phosphate concentration)

and the dissociations constants of phosphate species at $I = 0$
and $T = 25^oC$ are:

$K_1 = 10^{-2.2}$, $K_2 = 10^{-7.0}$, and $K_3 = 10^{-12.0}$.
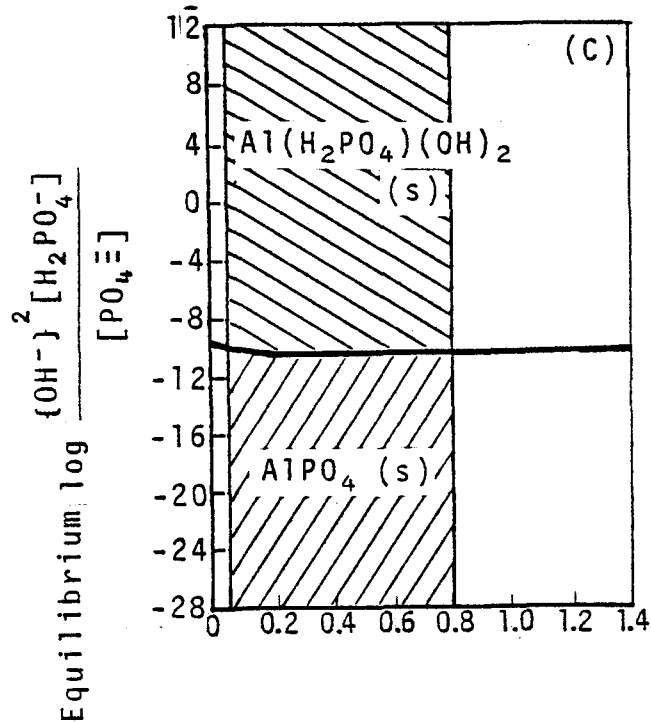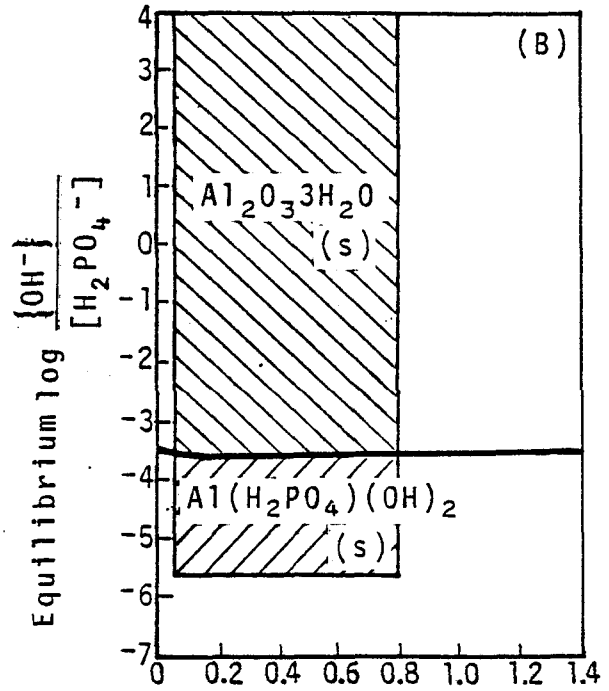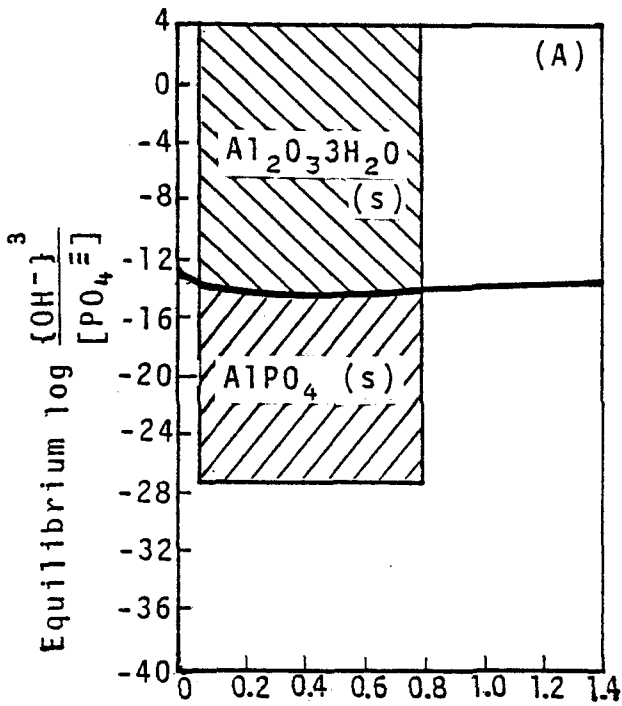
Figure 1.   Stability field of Al in FGD sludge.

From equation 30, the activity of the soluble species can be solved:

Valence	γ
0	1
1	0.74
2	0.3
3	0.066

Therefore:

$$K_1' = \frac{1}{0.74} \times 10^{-2.2} = 10^{-2.1} = \frac{[H_2PO_4^-][H^+]}{[H_3PO_4]} \tag{50}$$

$$K_2' = \frac{0.74}{0.3} \times 10^{-7.0} = 10^{-6.6} = \frac{[HPO_4^{2-}][H^+]}{[H_2PO_4^-]} \tag{51}$$

$$K_3' = \frac{0.3}{0.066} \times 10^{-12.0} = 10^{-11.3} = \frac{[PO_4^{3-}][H^+]}{[HPO_4^{2-}]} \tag{52}$$

Assume:

$$P_T = [H_3PO_4] + [H_2PO_4^-] = [HPO_4^{2-}] + [PO_4^{3-}] \tag{53}$$

From equations 5 to 53 and the given pH value, the free concentrations of the phosphate species can be determined. These equilibrium results are:

$$[H_2PO_4^-] = 10^{-6.9} M \tag{54}$$

$$[PO_4^{3-}] = 10^{-8.8} M \tag{55}$$

Therefore:

$$\frac{\{OH^-\}^3}{[PO_4^{3-}]} = \frac{(10^{-6})^3}{10^{-8.8}} = 10^{-9.2} \tag{56}$$

By using this value and also Figure 1(A), it can be found that $Al_2O_3 \cdot 3H_2O(s)$ is more stable than $AlPO_4(s)$. And following the determination of the ionic ratio:

$$\frac{\{OH^-\}^2}{[H_2PO_4^-]} = \frac{(10^{-6})^2}{10^{-6.9}} = 10^{-5.1}, \tag{57}$$

it can be seen that the more stable solid falls in the stability field of $Al(H_2PO_4)(OH)_2(s)$ (see Figure 1(B)). It can be concluded from the above that $Al(H_2PO_4)(OH)_2(s)$ will become the most stable solid. If there are any other phosphate solids present in this given condition, they will gradually transform to $Al(H_2PO_4)(OH)_2(s)$. Therefore, if the soluble aluminum level is very high in the FGD wastewater in this condition, it can be predicted that the soluble aluminum level will gradually be controlled by the solid $Al(H_2PO_4)(OH)_2(s)$.

Antimony

The stability field for antimony (Sb) solids is given in Figure 2. The main solid species for antimony in nature are oxide and hydroxide-chloride species. However, under most FGD system conditions, the only possible stable solid species of antimony is $Sb(OH)_3Cl_2(s)$. The stability field of this solid is very narrow and is controlled mainly by the chloride concentration (see Figure 2).

Arsenic

The stability diagram for arsenic (As) is given in Figure 3. Native element $As^0(s)$ is the only solid considered in this calculation. Since there are three valances involved in the transformation of arsenic, the Eh-pH plot was used for the stability field analysis. The total arsenic concentration chosen for the calculation is $2 \times 10^{-6}M$.

Results show that in the FGD system the $As^0(s)$ species can exist under reducing conditions. In a strong oxidizing environment, $H_2AsO_4^-$ is the most stable species in the low pH region (<7) and $HAsO_4^{2-}$ will become the most stable species in the high pH region. In a moderate oxidizing environment, $H_3AsO_3(aq)$ will be dominant at a pH of less than about 9. $H_2AsO_3^-$ also has a small predominant field in the high pH levels (see Figure 3).

Cadmium

There are two possible solid stability fields for cadmium (Cd) in the FGD system: $Cd(OH)_2(s)$ and $CdCO_3(s)$ (see Figure 4).
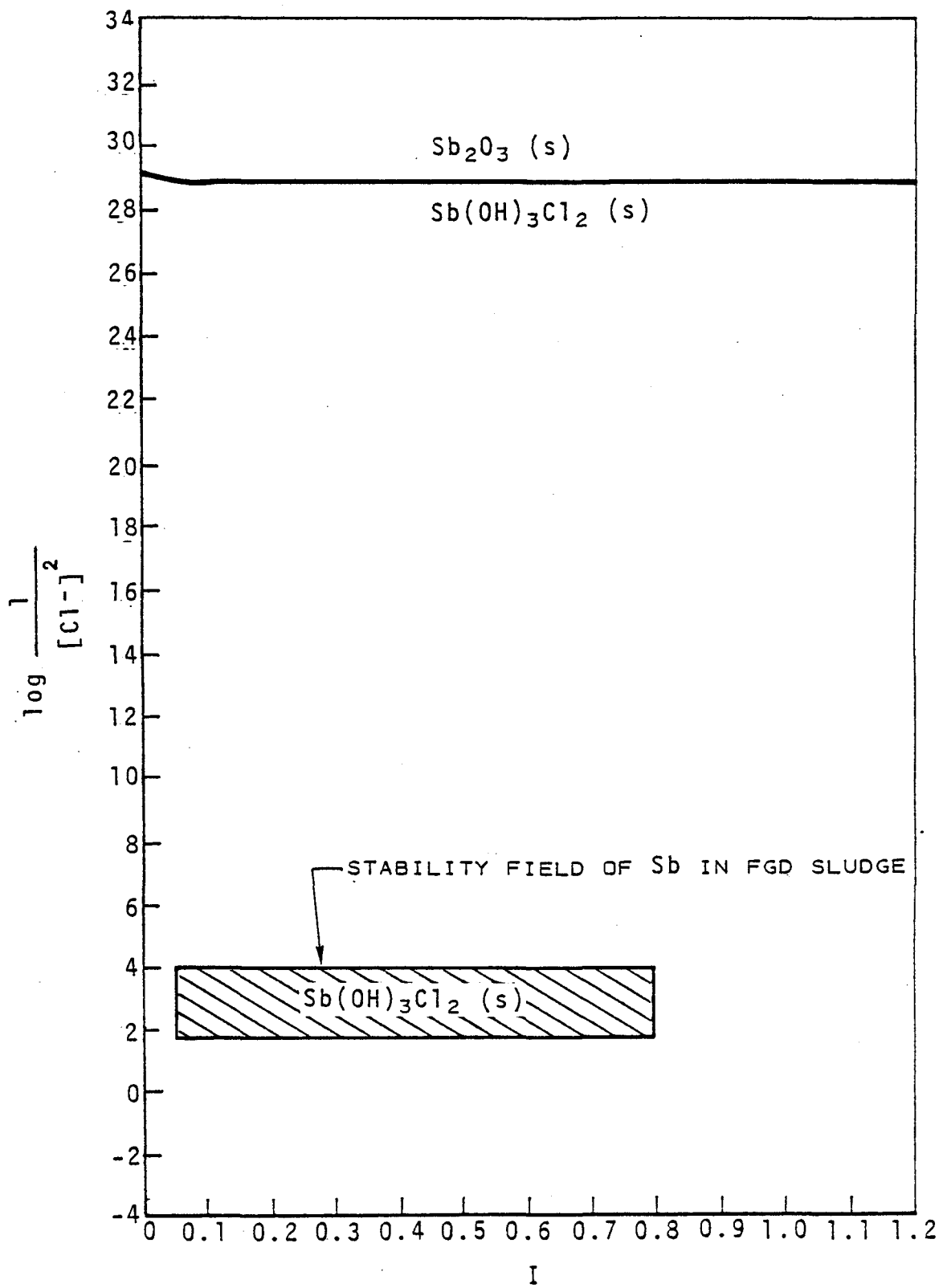
Figure 2. Stability field of Sb in FGD sludge.
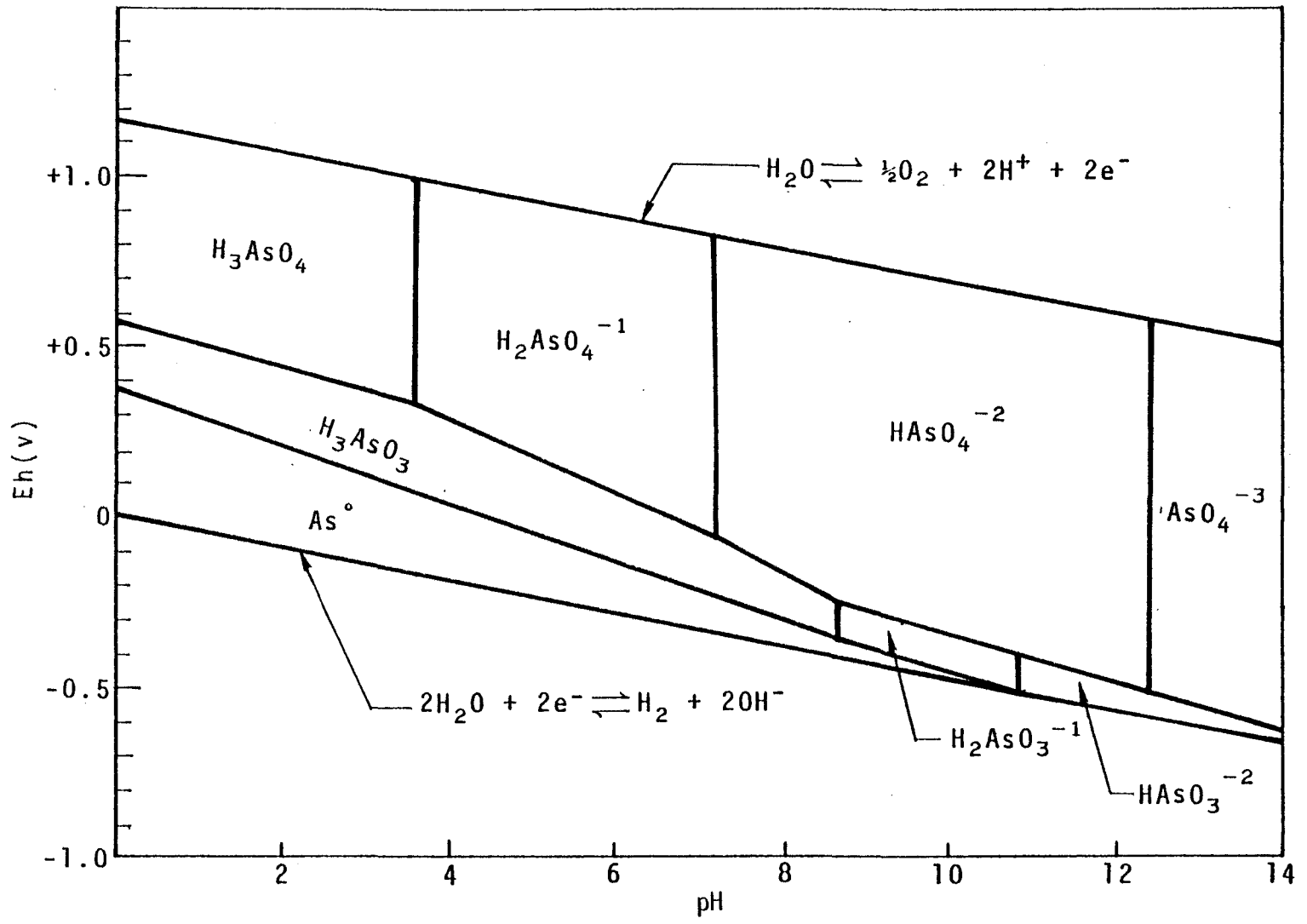
Figure 3. Stability field of As in FGD wastes at $[As_T] = 2 \times 10^{-6}M$.
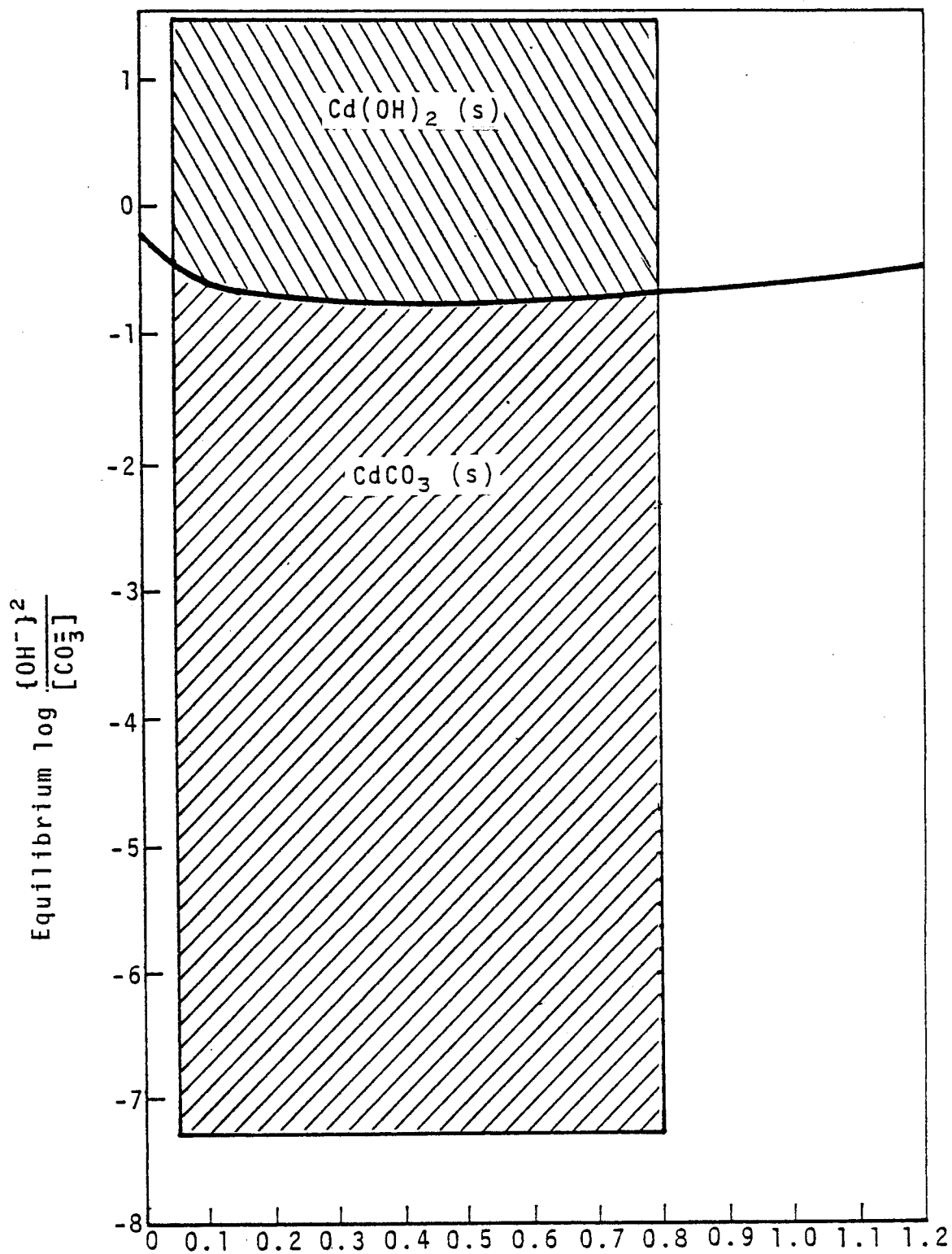
Figure 4. Stability field of Cd in FDG sludge.

The boundary between these two solids under equilibrium conditions lies in the range of the following ionic ratio, depending on the ionic strengths:

$$\frac{\{OH^-\}^2}{[CO_3^{2-}]} = 0.18 \text{ to } 0.23 \tag{58}$$

If the chemical equilibrium ionic ratio of $\{OH^-\}^2/[CO_3^{2-}]$ of a FGD system exceeds this range, then the hydroxide solid, $Cd(OH)_2(s)$, will become the predominant solid. Otherwise, the carbonate solid, $CdCO_3(s)$, will predominate.

Figure 4 shows that $CdCO_3(s)$ has a larger possible stability field than that of $Cd(OH)_2(s)$ in an FGD system. $CdCO_3(s)$ can predominate in the $10^{-7.2}$ to 0.2 $\{OH^-\}^2/[CO_3^{2-}]$ ratio range. The same ratio for the stability field of $Cd(OH)_2(s)$ only ranges from $10^{-1.5}$ to 0.2. Due to the high levels of carbonate (from the flue gas) in the FGD sludge liquid phase, $CdCO_3(s)$ is more likely to be present in most FGD systems. Therefore, the solubility of cadmium in the FGD wastes is more likely controlled by the carbonate concentration and the solubility product of $CdCO_3(s)$.

Calcium

Calcium (Ca) solids which can exist in the FGD system are hydroxide, carbonate, sulfite, sulfate, phosphate, fluoride and silicate. However, stability field calculations show that only carbonate, sulfite or sulfate solids of calcium predominate. The comparison of these three solids is given in Figure 5. The boundaries for these solids exist at the following equilibrium ionic ratios:

$$\frac{[CO_3^{2-}]}{[SO_4^{2-}]} = 10^{-3.72} \tag{59}$$

$$\frac{[SO_3^{2-}]}{[CO_3^{2-}]} = 10^{2.44} \tag{60}$$

$$\frac{[SO_3^{2-}]}{[SO_4^{2-}]} = 10^{-1.28} \tag{61}$$

Results show that $CaCO_3(s)$ has a relatively smaller stability field than that of $CaSO_4.2H_2O(s)$ and $CaSO_3.1/2H_2O(s)$ (see Figure 5). This is due to the extremely high levels of sulfate or sulfite ions in the FGD liquid phase. Results also show that ionic strength is not a very significant factor in the distribution of calcium solids.
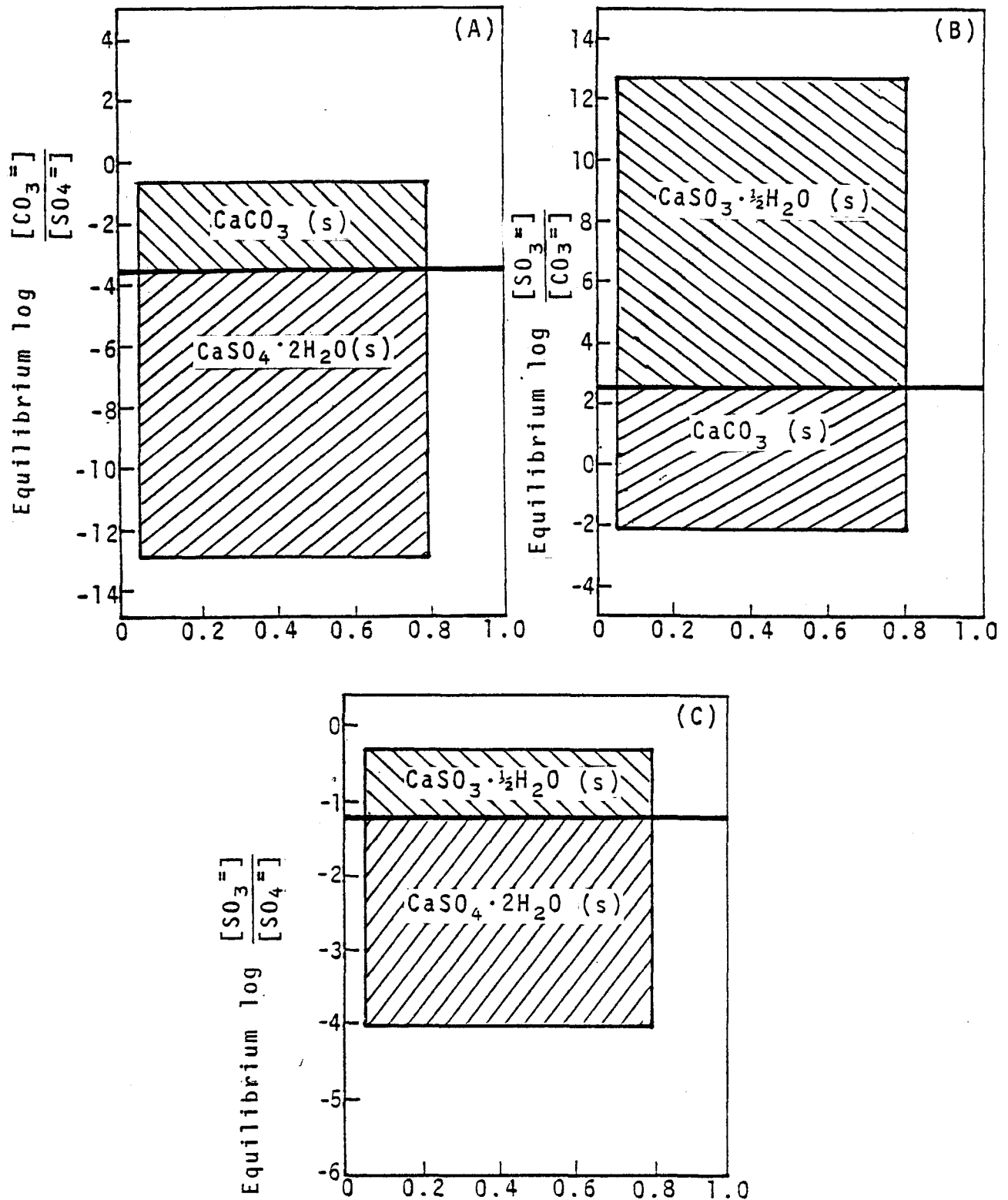
Figure 5.   Stability field of Ca in FGD sludge.

In most FGD systems, the speciation of calcium solids appears to be governed by the stability constants of $CaSO_4 \cdot 2H_2O(s)$ and $CaSO_3 \cdot 1/2H_2O(s)$ as well as the relative concentration of sulfate and sulfite ions. Due to the tremendous amount of Ca and S in the FGD wastewater, the Ca-S-H_2O system also may affect the redox conditions of the entire FGD system. Therefore, the stability field of calcium and the relative levels of sulfate and sulfite ions can become one of the most important factors in determining the characteristics of FGD wastes.

Chromium

The stability field of chromium (III) (Cr) in FGC wastes can be examined in Figure 6. Chromium can exist as a stable hydroxide solid ($Cr(OH)_3(s)$) in the FGD waste system. However, at the median concentration of soluble chromium ($10^{-5.30}$M) (Table 3), the predominant species are hydroxide complexes. As shown in Figure 6, at low pH levels (pH 5), the $Cr(OH)^{2+}$ species is the most predominant. More Cr^{3+} ions can coordinate with available hydroxide ligands when the pH levels increase. This shift of predominant species to $Cr(OH)_2^+$ occurs in the pH range of 5 to 7, and to $Cr(OH)_4^-$ at pH values higher than 7.

Copper

Among the copper (Cu) solids (oxide, hydroxide, carbonate, phosphate, sulfate, etc.), $Cu(OH)_2(s)$ and $Cu_2CO_3(OH)_2(s)$ are the most common in FGD sludge. The stability field of these two solids is shown in Figure 7. The boundary between these two solids under equilibrium conditions ranges from $10^{-14.30}$ to $10^{-14.55}$ for $[CO_3^{2-}]1/2\{OH^-\}$.

As can be seen from the diagram, the soluble concentrations of copper in the FGD liquors are largely regulated by both hydroxide and carbonate concentrations. Higher hydroxide or carbonate concentrations tend to lower the concentration of soluble copper species. At neutral or slightly alkaline conditions $Cu_2CO_3(OH)_2(s)$ is less soluble than $Cu(OH)_2(s)$. Since higher soluble carbonate concentrations favor the formation of $Cu_2CO_3(OH)_2(s)$ (see Figure 7), the soluble carbonate levels in the FGD systems may control copper mobility.

Iron

The stability field of iron (Fe) in FGD sludge is shown in Figure 8. At a pH of less than about 7, and under reducing and moderately oxidizing conditions, the ferrous ion (Fe^{2+}) will become the predominant species. At a pH of less than 5, and under strong oxidizing conditions, the $FeSO_3^+$ species may predominate. Under all other conditions, iron will exist primarily in the solid phase.
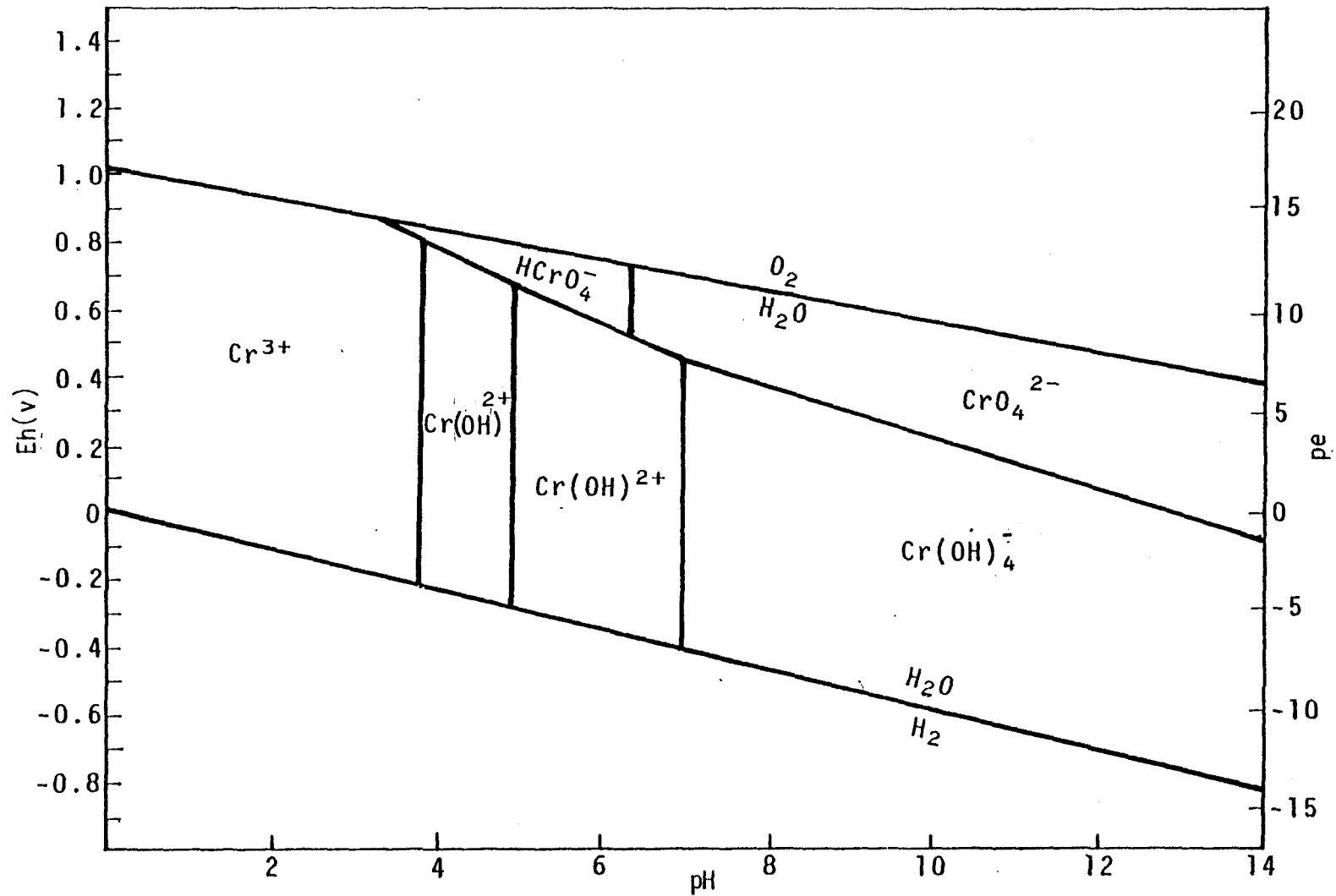
Figure 6.   Stability field of Cr in FGD waste.   (Activity of soluble Cr = $10^{-5.30}$M (I = 0, T = 25°C))
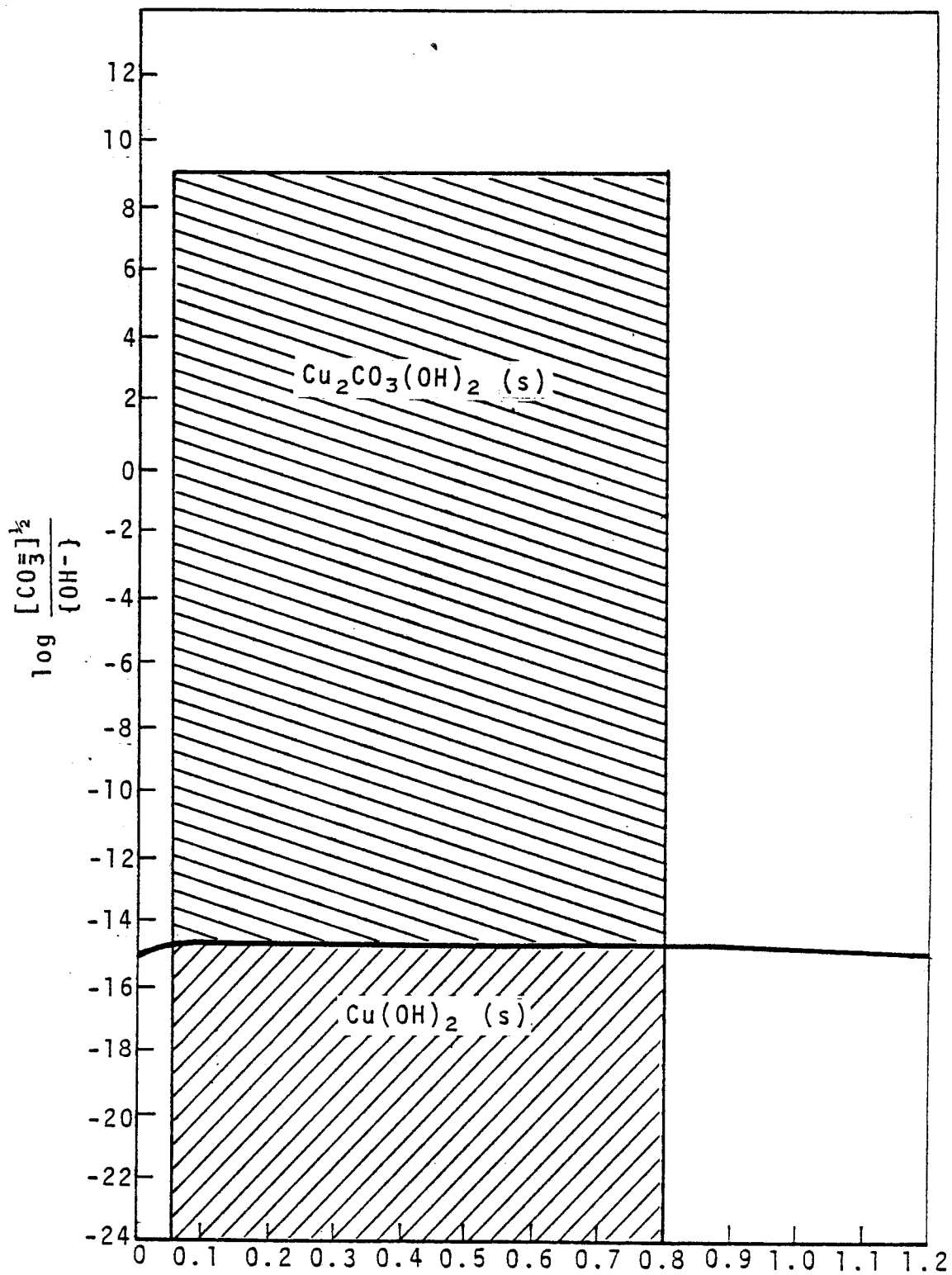
Figure 7. Stability field of Cu in FGD sludge.

51
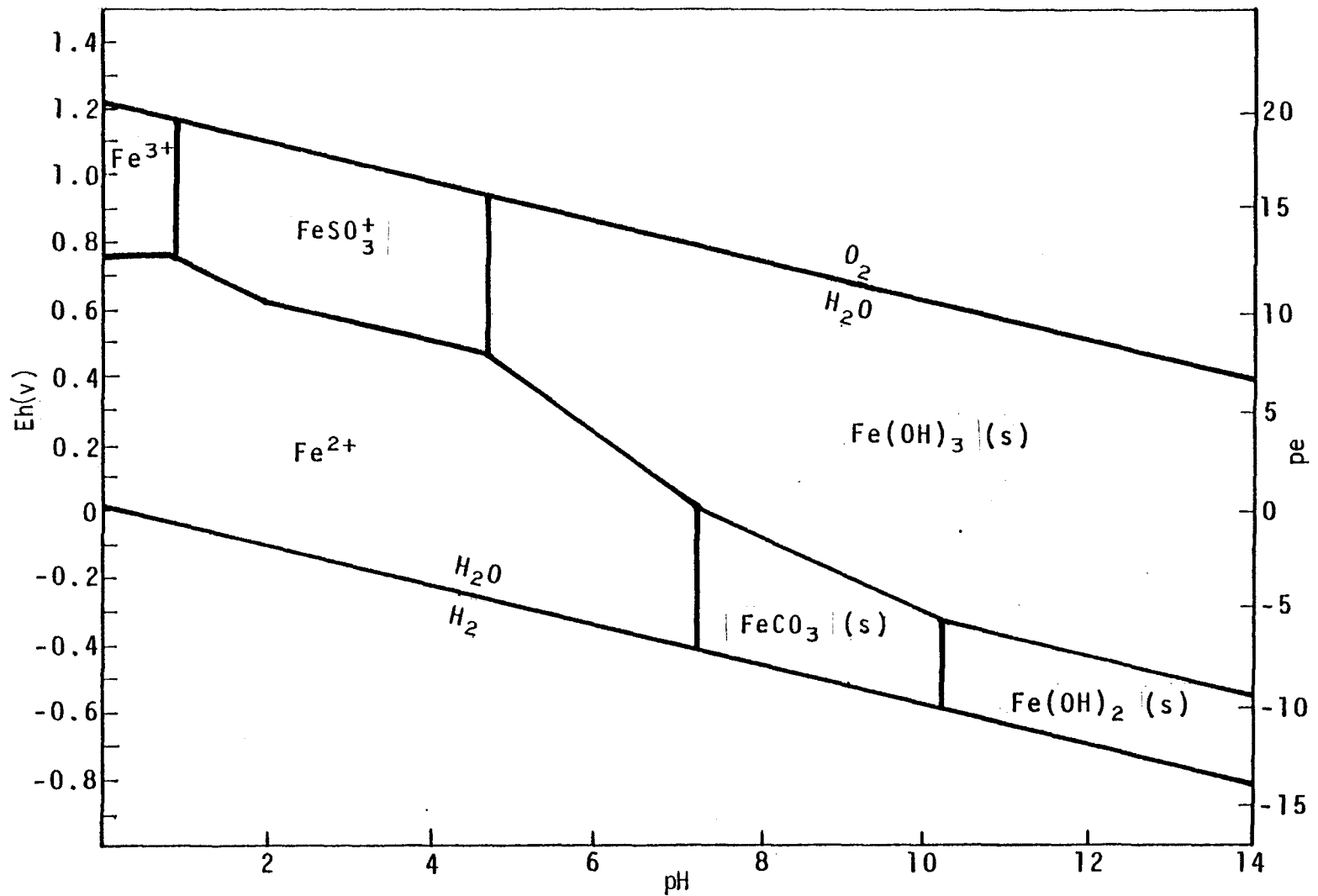
Figure 8.   Stability field of Fe in FGD waste.   ($C_T = 10^{-3}$M; $[SO_3^=]_T = 10^{-1.66}$M; $P_T = 10^{-5.64}$; activity of soluble Fe = $10^{-4.14}$M ($I = 0$, $T = 25°C$, sulfide not included))

The three most common iron solids in FGD sludge are $Fe(OH)_3(s)$, $FeCO_3(s)$, and $Fe(OH)_2(s)$. Among these three solids, $FeCO_3(s)$ and $Fe(OH)_2(s)$ can only exist in relatively small regions of the stability field. As shown in Figure 8, $Fe(OH)_3(s)$ is probably the most important sink for iron in the FGD sludge system. Since $Fe(OH)_3(s)$ has a very low solubility, it is expected that soluble iron will gradually be reduced to trace levels as the sludge ages.

Lead

Fourteen lead solids were considered for the FGD sludge system: $PbO(s)$, $PbCO_3$, $PbO_2(s)$, $Pb^0(s)$, $Pb_3(OH)_2(CO_3)_2(s)$, $Pb(OH)_2(s)$, $PbSO_3$, $PbS(s)$, $PbSO_4(s)$, $PbCl_2(s)$, $Pb_3(PO_4)_2(s)$, $PbHPO_4(s)$, $PbF_2(s)$, and $PbMoO_4(s)$. Among these solids only $Pb(OH)_2(s)$, $PbCO_3(s)$, $Pb_3(OH)_2(CO_3)_2(s)$, and $PbMoO_4(s)$ show a stability field in FGD sludge. The ion-ratios (R's) for these four solids under equilibrium conditions are as follows:

$Pb(OH)_2(s)-PbCO_3(s)$:

$$\frac{\{OH^-\}^2}{[CO_3^{2-}]} \quad : \quad R = \frac{\gamma_{CO_3^{2-}}}{(\gamma_{OH^-})^2} \cdot \frac{K_{sp,Pb(OH)_2}}{K_{sp,PbCO_3}} = 10^{-2.99} \sim 10^{-3.54} \tag{62}$$

(see Figure 9(A))

$Pb_3(OH)_2(CO_3)_2(s)-PbCO_3(s)$:

$$\frac{\{OH^-\}^{2/3}}{[CO_3^{2-}]^{1/3}} \quad : \quad R = \frac{\gamma_{CO_3^{2-}}}{(\gamma_{OH^-})^{2/3}(\gamma_{CO_3^=})^{2/3}} \cdot \frac{K_{sp,Pb_3(OH)_2(CO_3)_2}}{K_{sp,PbCO_3}}$$
$$= 10^{-5.7} \sim 10^{-5.88} \tag{63}$$

(see Figure 9(B))

$Pb(OH)_2(s)-Pb_3(OH)_2(CO_3)_2$:

$$\frac{\{OH^-\}^{4/3}}{[CO_3^{2-}]^{2/3}} \quad : \quad R = \frac{(\gamma_{OH^-})^{2/3}(\gamma_{CO_3^{2-}})^{2/3}}{(\gamma_{OH^-})^2} \cdot \frac{K_{sp,Pb(OH)_2}}{K_{sp,Pb_3(OH)_2(CO_3)_2}}$$
$$= 10^{2.71} \sim 10^{2.34} \tag{64}$$

(see Figure 9(C))
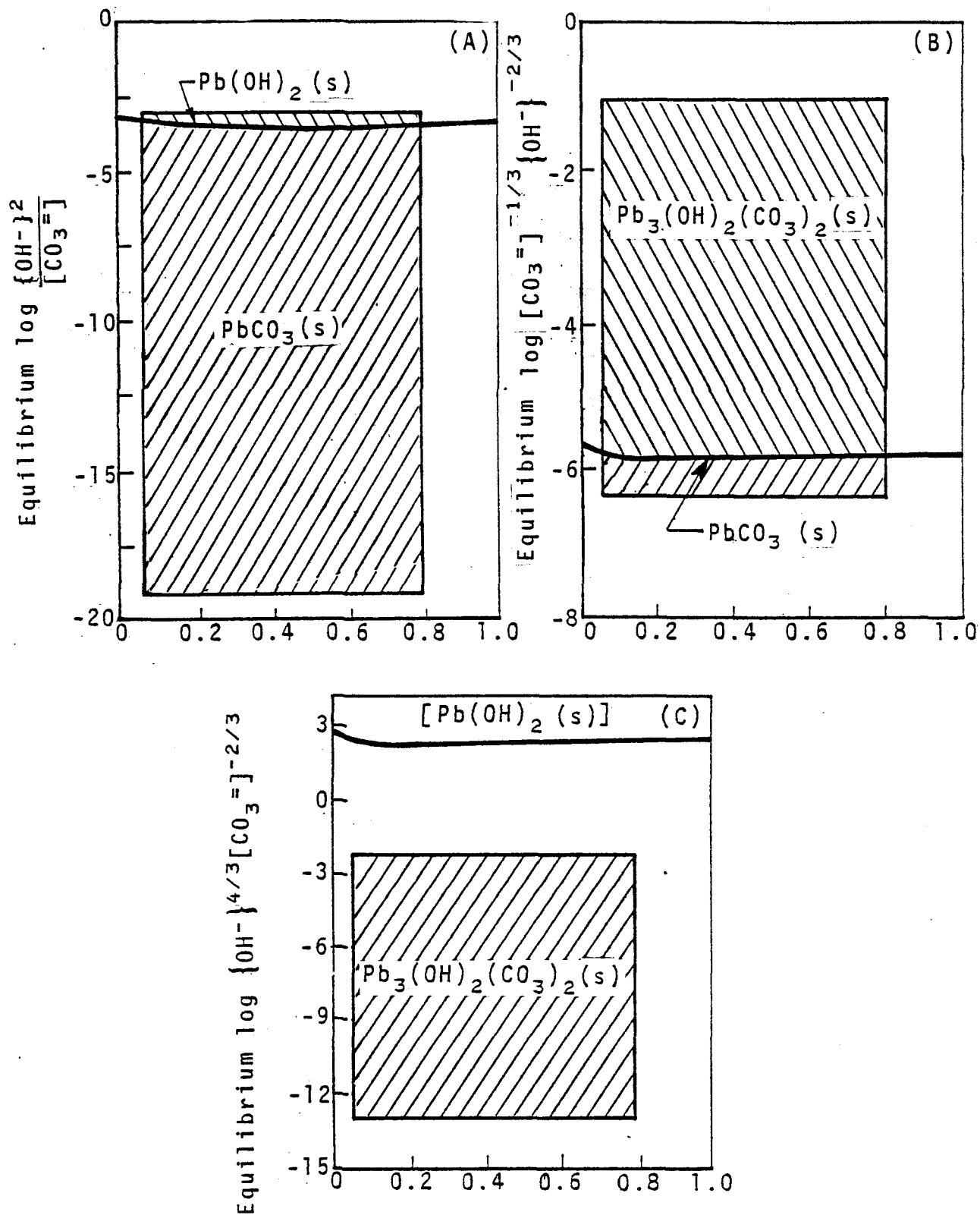
Figure 9. Stability field of Pb in FGD sludge.
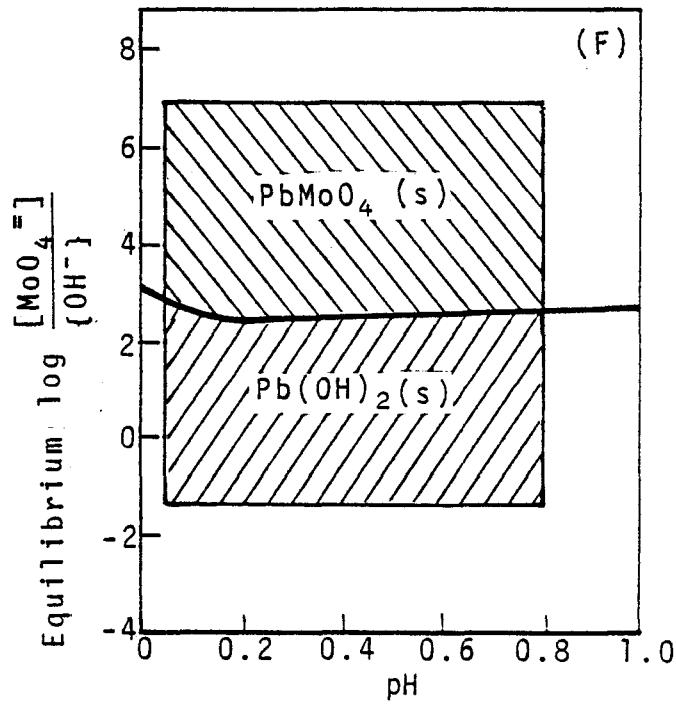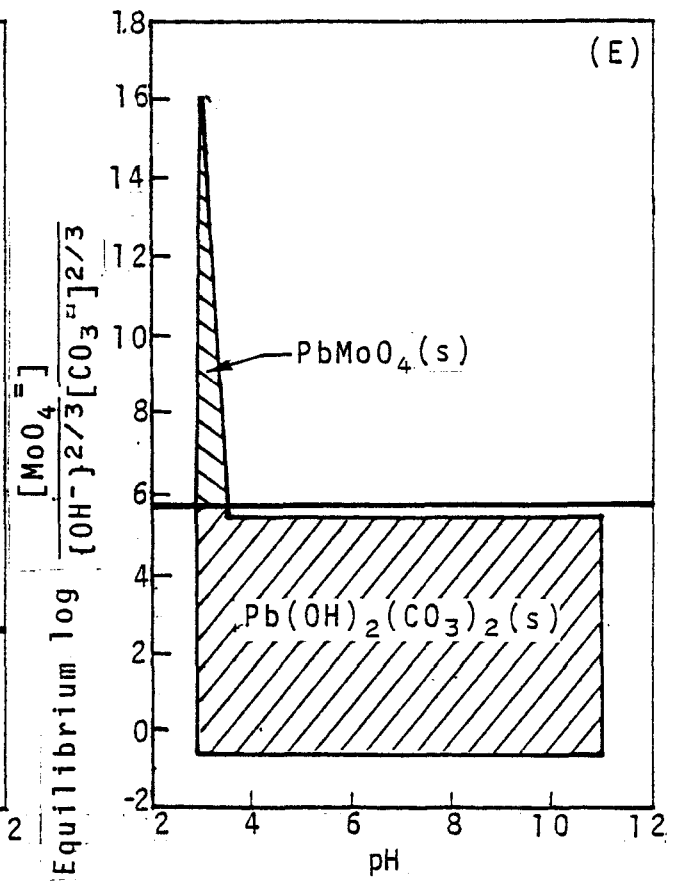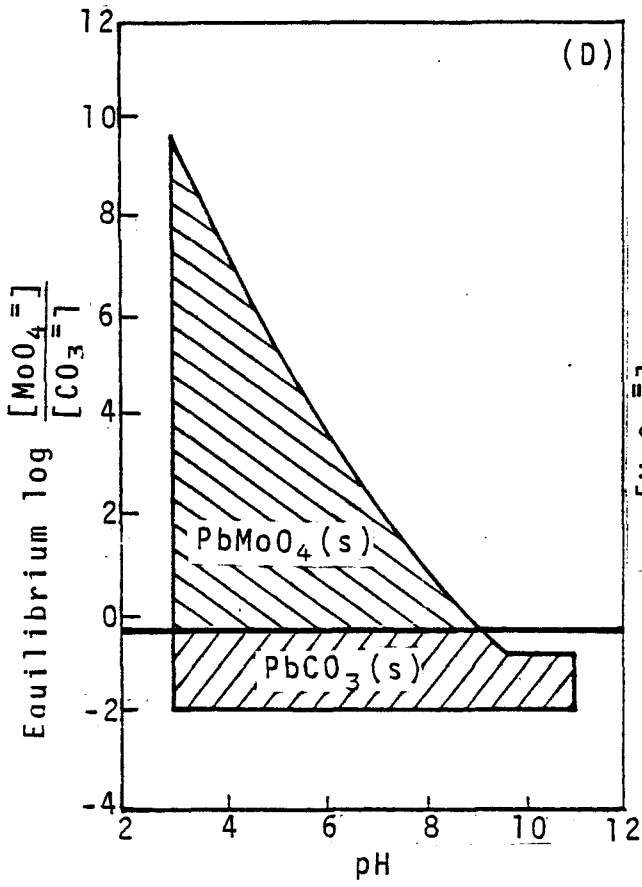
Figure 9 (continued)

$PbMoO_4(s)-PbCO_3(s)$:

$$\frac{[MoO_4^{2-}]}{[CO_3^{2-}]} : R = \frac{\gamma_{CO_3^{2-}}}{\gamma_{MoO_4^{2-}}} \cdot \frac{K_{sp,PbMoO_4}}{K_{sp,PbCO_3}} = 10^{-0.10} \qquad (65)$$

(see Figure 9(D))

$PbMoO_4(s)-Pb(OH)_2(C)_3)_2(s)$:

$$\frac{[MoO_4^{2-}]}{\{OH^-\}^{2/3}[CO_3^{2-}]^{2/3}} : R = \frac{(\gamma_{OH^-})^{2/3}(\gamma_{CO_3^{2-}})^{2/3}}{\gamma_{MoO_4^{2-}}} \cdot$$

$$\frac{K_{sp,PbMoO_4}}{K_{sp,Pb_3(OH)_2(CO)_3)_2}} = 10^{5.80} \quad 10^{5.25} \qquad (66)$$

(see Figure 9(E))

$PbMoO_4(s)-Pb(OH)_2(s)$:

$$\frac{[MoO_4]}{\{OH^-\}} : R = \frac{(\gamma_{OH^-})^2}{\gamma_{MoO_4^{2-}}} \cdot \frac{K_{sp,PbMoO_4}}{K_{sp,Pb(OH)_2}} = 10^{3.09} \sim 10^{2.54} \qquad (67)$$

(see Figure 9(F))

A comparison among $Pb(OH)_2(s)$, $PbCO_3(s)$, and $Pb_3(OH)_2(CO_3)_2(s)$ solids reveals that $Pb(OH)_2(s)$ has a relatively small stability field in FGD sludge. In particular, when $Pb_3(OH)_2(CO_3)_2(s)$ is present, $Pb(OH)_2(s)$ will not exist in FGD sludge.

$PbMoO_4(s)$ solid is stable at low pH levels in the FGD system when MoO_4^{2-} concentrations are high (Figures 9(D) and 9(E)). This solid species may in fact control the soluble lead levels in low pH FGD wastes.

Mercury

The mercury (Hg) stability field includes the eight significant solids species and the six significant soluble species shown below (chosen from the results of the speciation calculation):

Solids: $Hg^0(\ell)$, $HgCl_2(s)$, $HgO(s)$, $HgSO_4(s)$, $Hg(OH)_2(s)$, $Hg_2Cl_2(s)$, $Hg_2OCl(s)$, and $Hg_4OCl(s)$.

Soluble: $HgCl_2(aq)$, $HgCl_3^-$, $Hg(OH)_2(aq)$, $HgCl(OH)(aq)$, $HgCl_4^{2-}$, and Hg^{2+}.

Although mercury can exist as 0, +1, and +2 oxidation states in nature, the +1 oxidation state is quite unstable (Ref. 33) and is therefore excluded from the calculations. The results show that only three mercury species can predominate in FGD systems: $Hg^o(\ell)$, $HgCl_2(aq)$, and $Hg(OH)_2(aq)$ (Figure 10). $HgCl_2(aq)$ will predominate when both the redox potential of the FGD system is above +300 mv and the pH is below 9. $Hg(OH)_2(aq)$ will pre-dominate at levels of similar high pH and redox potential (see Figure 10). The balance of the commonly encountered Eh-pH levels are contained in the stability field of $Hg^o(\ell)$. This region provides moderately oxidizing or reducing conditions. Since most FGD sludges are moderately oxidizing or reducing, the majority of the mercury contained in FGD sludge will exist as $Hg^o(\ell)$. This is favorable for the control of mercury con-tamination from FGD leachates.

Manganese

It has been reported that the most common manganese (Mn) compounds are those in the +2, +3, and +4 oxidation states (Ref. 33). The +3 oxidation state of manganese compounds is relatively unstable, unless stabilized by very strong complexing agents in the aqueous environment (Ref. 6). The +6 oxidation state of manganese can exist in a highly oxidizing and alkaline environment (Ref. 33). The primary species of manganese used for the stability field calculation include the oxide, hydroxide, and carbonate solids, as well as soluble complexes of chloride, hydroxide, sulfate and manganous ions (Mn^{2+}). As suggested by Mandel (Ref. 37), manganese can exist in different oxide solids, such as $MnO(s)$, $MnO_2(s)$, $Mn_2O_3(s)$, and $Mn_3O_4(s)$. Ponnamperuma, et al. (Ref. 38), noted that more than 150 nonstoichiometric oxides of manganese ranging from $MnO_{1.2}(s)$ to $MnO_2(s)$ have been identi-fied in nature. In view of these complicated phenomena, coupled with the lack of reliable thermodynamic data, the construction of a manganese stability field is a difficult task.

In this study, the solid species used follow those employed by Stumm and Morgan (Ref. 6) and Bricker (Ref. 39): $MnCO_3(s)$, $Mn(OH)_2(s)$, $Mn_3O_4(s)$, $MnOOH(s)$, and $MnO_2(s)$. The significant soluble species used in constructing the stability diagram are taken mainly from the results of the speciation model. These species are: Mn^{2+}, $HMnO_2^-$, MnO_4^{2-}, $Mn(OH)_3^-$, $MnOH^+$, $MnSO_4(aq)$, and $MnCl^+$. The manganese stability diagram is presented in Figure 11. It can be seen from the diagram that Mn^{2+} is the predominant species at low pH levels (pH less than about 7). The $MnCO_3(s)$ species can exist in FGD sludge at a pH of about 7 to 11 and at a reducing to moderately oxidizing redox poten-tial. $Mn(OH)_2(s)$ solid can exist when the pH is greater than

57
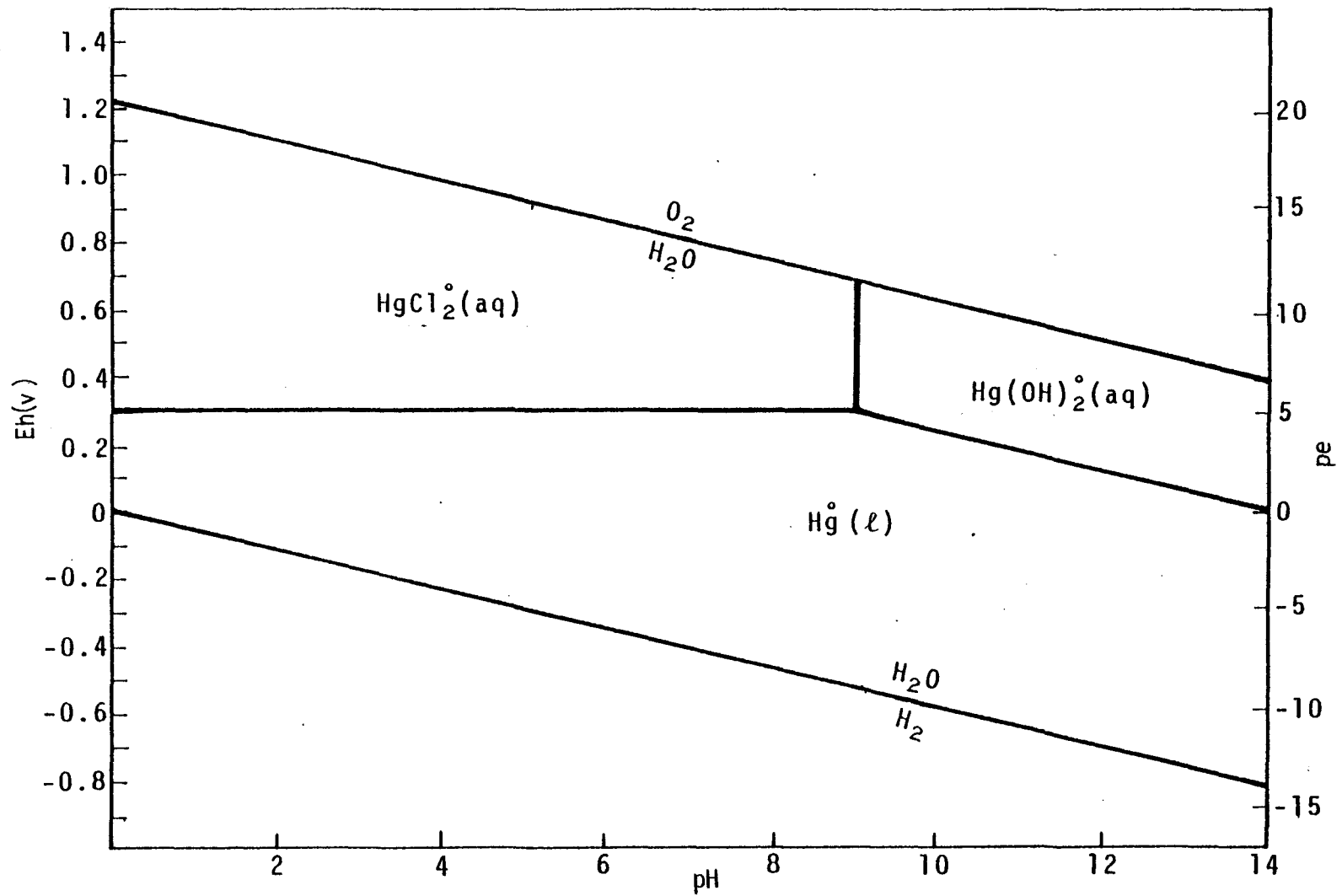
Figure 10. Stability field of Hg in FGD waste. ($Cl = 10^{-1.13}M$; activity of soluble Hg = $10^{-6.70}M$ ($I = 0$, $T = 25°C$, $Hg_T = 10^{-5.78}M$))
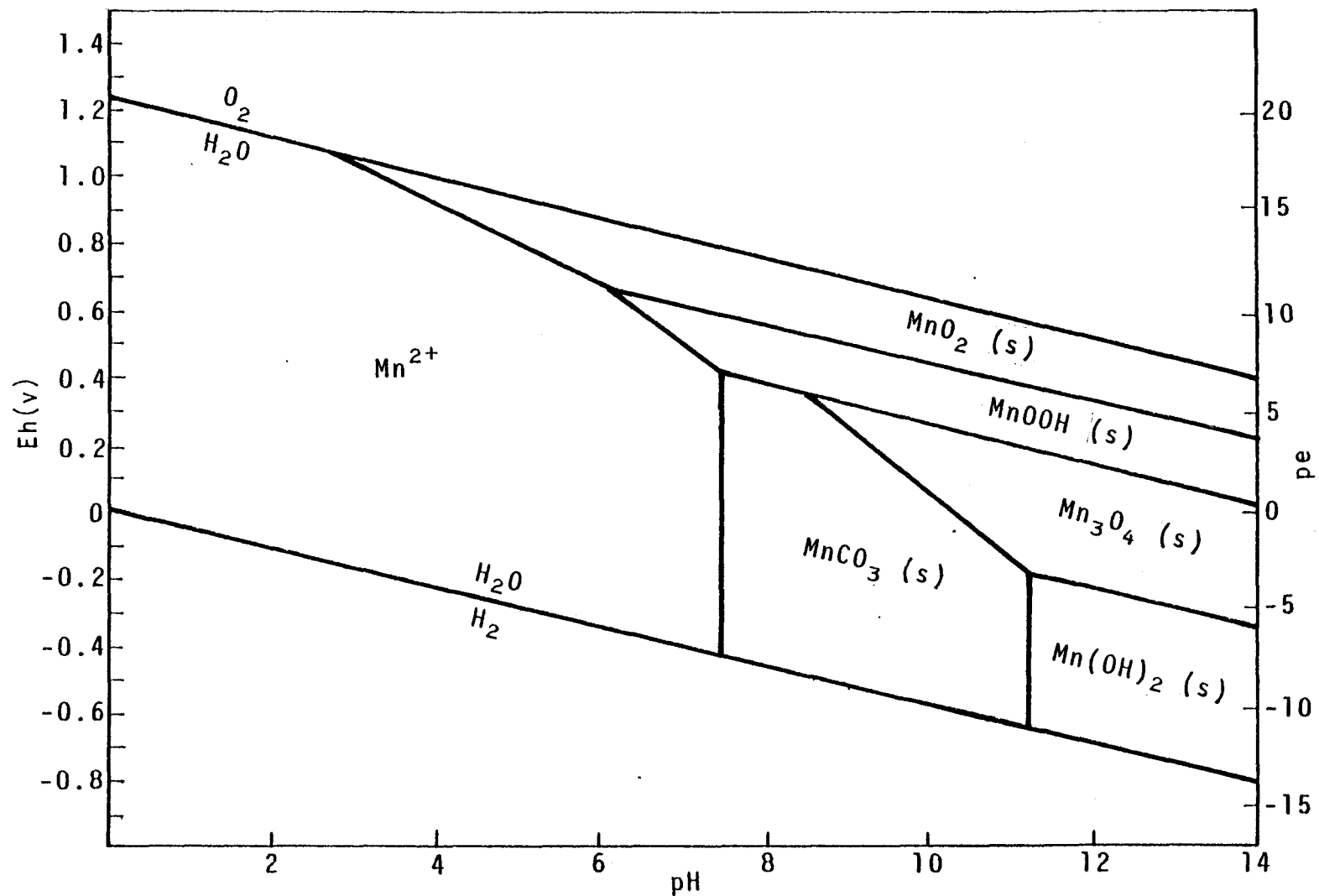
Figure 11. Stability field of Mn in FGD waste. ($C_T = 10^{-3}$M; activity of soluble Mn = $10^{-4.62}$M (I = 0, T = 25°C))

11, which is outside normal FGD conditions. $Mn_3O_4(s)$, $MnOOH(s)$, and $MnO_2(s)$ also have stability fields in the FGD sludge at higher redox potentials (see Figure 11).

Since conditions usually change toward higher redox potential and higher pH levels as FGD sludges age, it can be speculated that the predominant species of manganese will transform as follows during the aging process:

$$Mn^{2+} \rightarrow MnCO_3(s) \rightarrow Mn_3O_4(s) \rightarrow MnOOH(s) \rightarrow MO_2(s)$$
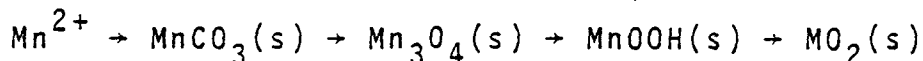
This transformation trend indicates that the soluble manganese concentration will be gradually reduced in the FGD leachates with time.

Nickel

When constructing the stability field for nickel (Ni), the major solids of concern are $Ni(OH)_2$ (s, fresh), $Ni(OH)_2$ (s, aged), $NiCO_3(s)$, $NiSO_4(s)$, $NiSO_4 \cdot 6H_2O(s)$, $NiS(\alpha)$, and $NiS(\gamma)$. Only $Ni(OH)_2$(s, aged) and $NiCO_3(s)$ have a stability field in FGD sludge. The boundary between these two solid species exists at the following ion-ratios (Figure 12):

$$R = \frac{\gamma_{CO_3^{2-}}}{(\gamma_{OH^-})^2} \cdot \frac{K_{sp,Ni(OH)_2, \text{ aged}}}{K_{sp,NiCO_3}} = 10^{-10.30} \quad 10^{-10.85}$$

The $Ni(OH)_2$(s,aged) species will predominate when the ratio of $\{OH^-\}^2/[CO_3^{2-}]$ is higher than the above R values. Otherwise, the $NiCO_3(s)$ species will be the most stable solid in the FGD sludge.

Selenium

Like arsenic, only one solid species is considered for selenium (Se): native selenium ($Se^0(s)$). The transformation of selenium also involves a valence change, so the Eh-pH plot is used. A selenium concentration of 1.4×10^{-5} M was chosen.

The stability field of selenium is presented in Figure 13. Results show that the predominant species of selenium in FGD sludge are $Se^0(s)$, SeO_3^{2-}, $HSeO_3^-$, and SeO_4^{2-}. Among these four species, the former three are the most likely to exist in FGD sludge. $Se^0(s)$ is the most stable selenium species in moderately oxidizing or reducing environments. However, if conditions become more oxidizing, $HSeO_3^-$ will predominate at low pH levels (less than about pH 6.5) and SeO_3^{2-} will predominate at high pH levels. As FGD wastes age, conditions usually change toward higher redox potentials and higher pH levels. Therefore, it

60
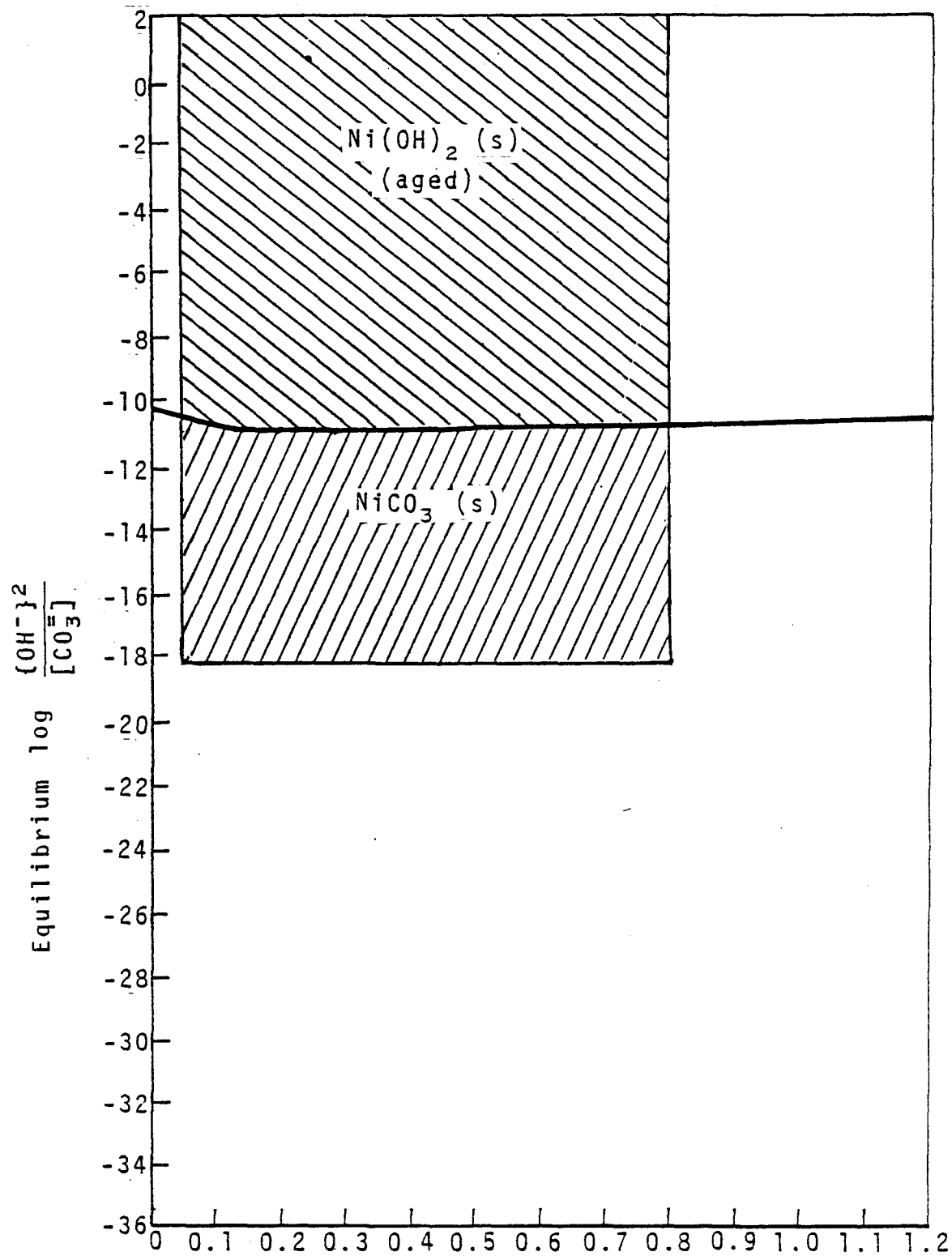
Figure 12.   Stability field of Ni in FGD sludge.
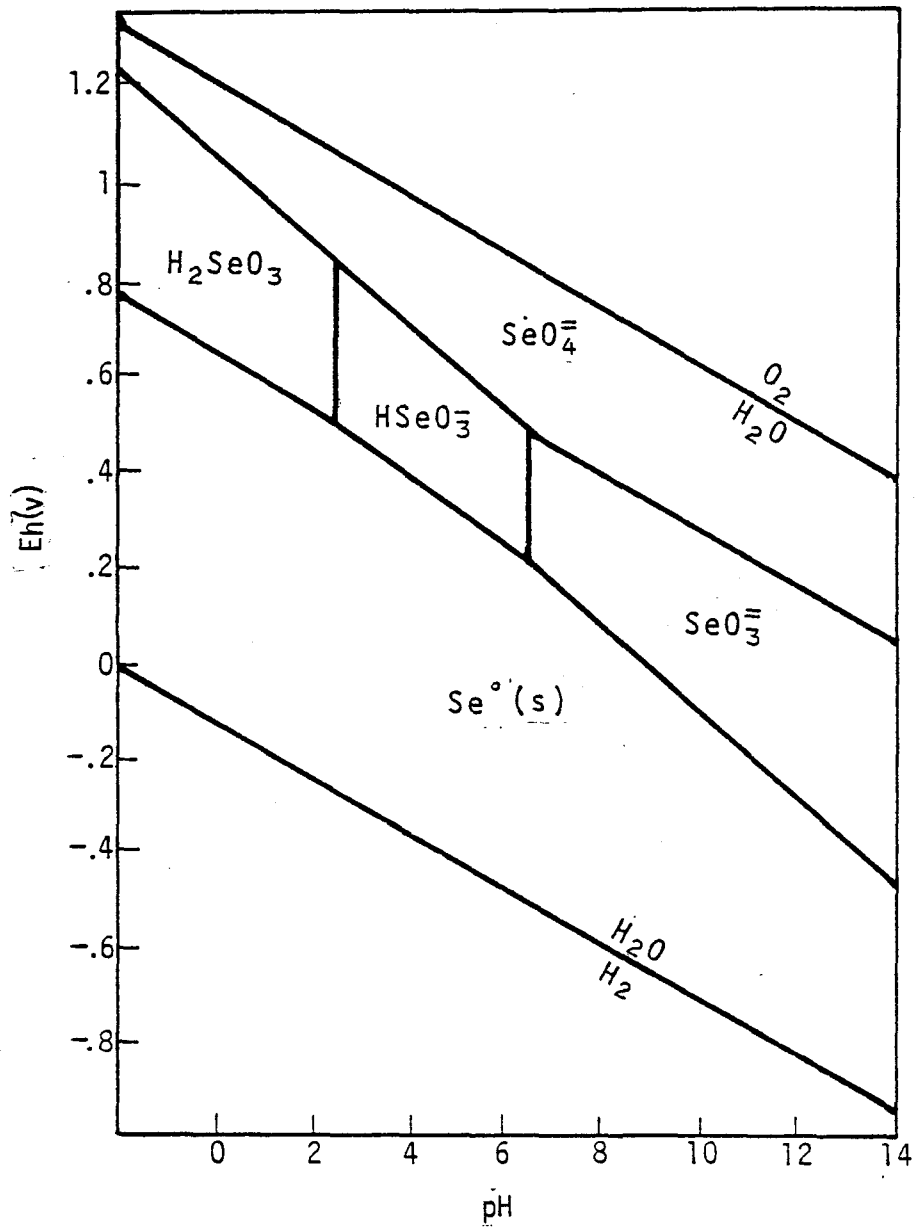
Figure 13. Stability field of Se in FGD waste at $[Se_T] = 1.4 \times 10^{-5} M$.

would appear that selenium would exist as $Se^0(s)$ in the raw
FGD wastes, and transform with time to SeO_3^{2-} and $HSeO_3^-$. There-
fore, the aging of FGD sludge will probably increase the sele-
nium levels in the associated leachate.

Sulfur

The important sulfur (S) species in FGD sludge include the
following:

Solids: $CaSO_4.2H_2O(s)$, $CaSO_3.1/2H_2O(s)$, $S^0(s)$, and
$BaSO_4(s)$.

Soluble: SO_4^{3-}, HSO_4^-, SO_3^{2-}, HSO_3^-, $CaSO_4(aq)$, and $FeSO_3^+$.

Among the listed species, $CaSO_4.2H_2O(s)$, $CaSO_3.1/2H_2O(s)$,
and $S^0(s)$ are the predominant species in FGD sludge. The
stability fields of these three species are shown in Figure 14.
The resulting boundaries among these species are as follows:

Redox couple	Equation (at I = 0, T = 25°C)	
$CaSO_4.2H_2O(s)-CaSO_3.1/2H_2O(s)$	$pH + 16.95\ Eh = -0.93$	(69)
$CaSO_4.2H_2O(s)-S^0(s)$	$pH + 12.71\ Eh = 4.18$	(70)
$CaSO_3.1/2\ H_2O(s)-S^0(s)$	$pH + 11.30\ Eh = 5.89$	(71)

It can be seen in Figure 14 that the $CaSO_4.2H_2O(s)$ species
predominates in FGD sludges at any pH value if redox potential is
positive. The figure also shows that elemental sulfur ($S^0(s)$)
may exist as the major sulfur species in strong reducing environ-
ments. The sulfide species may not be significant in strong
reducing environment due to the extremely low organic contents
of the FGD sludges. $CaSO_3.1/2H_2O(s)$ is thermodynamically un-
stable and will gradually convert to $CaSO_4.2H_2O(s)$.

Zinc

The primary oxidation state of zinc (Zn) in the aqueous
environment is +2 (Ref. 33). Since the transformation of zinc
species occurs without electron transfer, the ion-ratio method is
used for the evaluation of the zinc stability field. Zinc solids
which are stable in FGD sludge may include hydroxide, carbonate,
silicate, and phosphate. The solids used in the stability calcu-
lation are $Zn(OH)_2$ (s, amorphous), $Zn(OH)_2$ (s, amorphous aged),
$ZnCO_3(s)$, $Zn_3(PO_4)_2(s)$, and $ZnSiO_3(s)$. Among these solids,
$Zn(OH)_2$(s, amorphous aged), $ZnCO_3(s)$ and $ZnSiO_3(s)$ are the pos-
sible predominant solids. As shown in Figure 15, the boundary
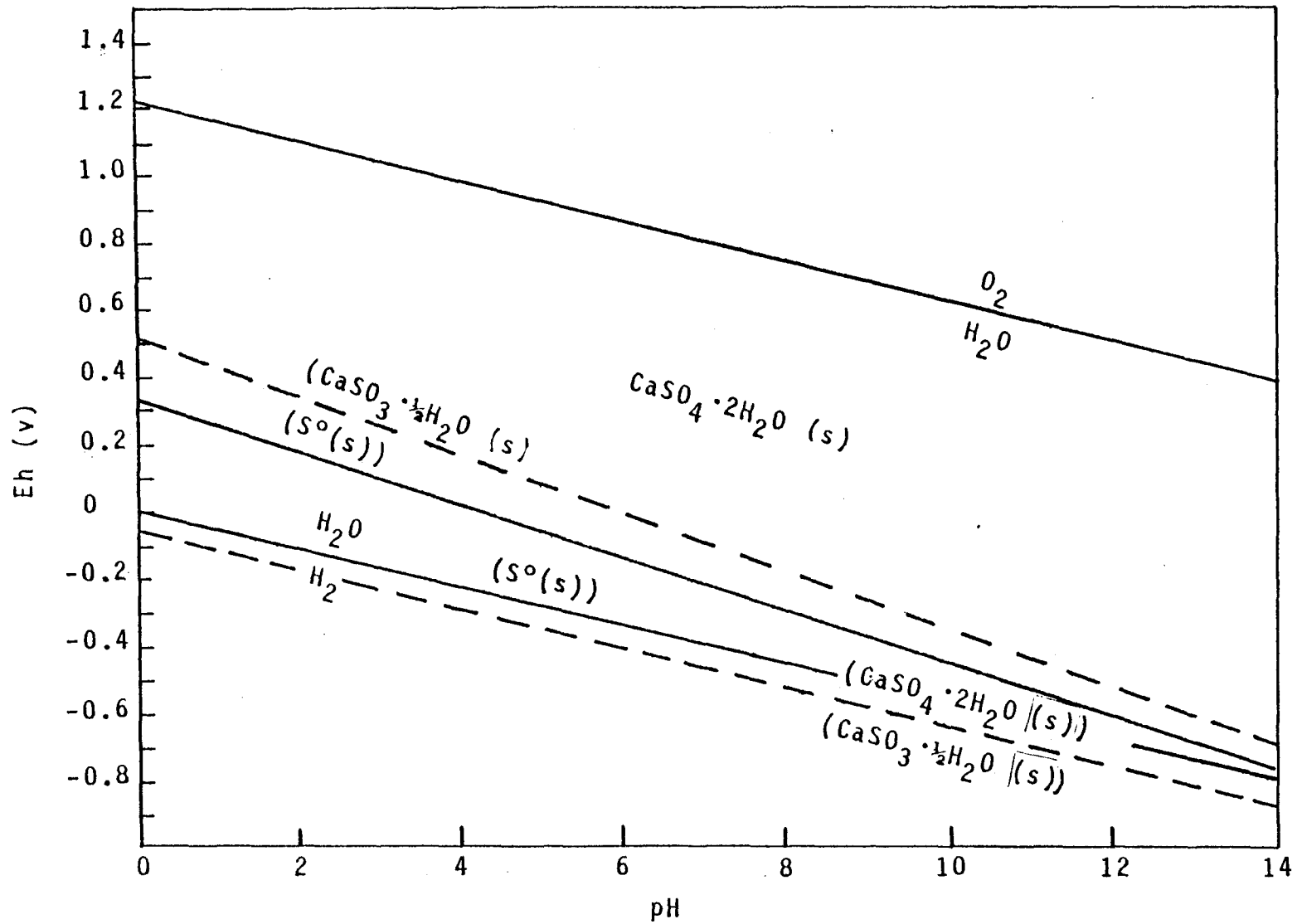
Figure 14.   Stability field of S in FGD waste.   ([S_T] = $10^{-0.001}$M,
[Ca^{2+}] = $10^{-1.35}$M (I = 0, T = 25°C))
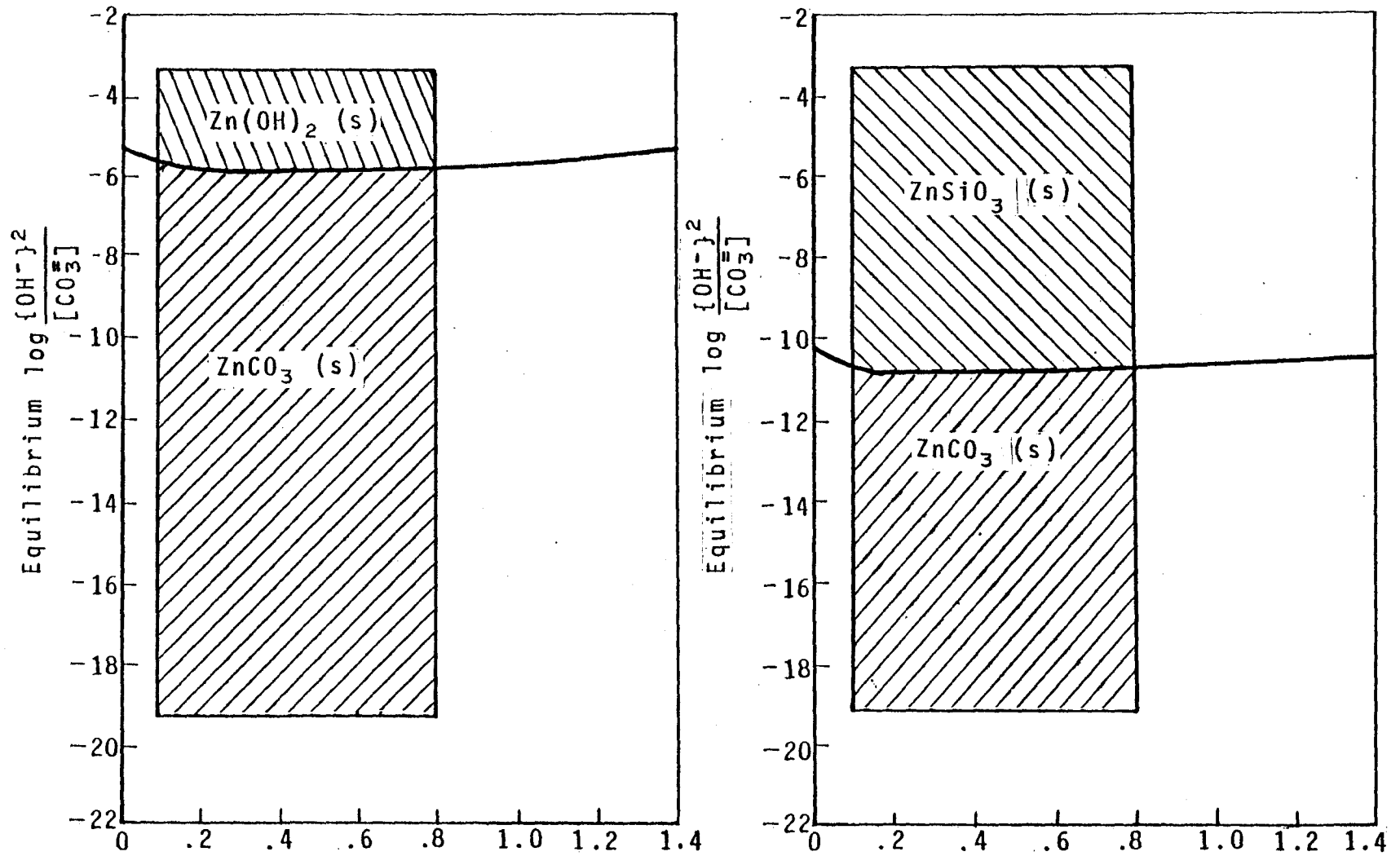
Figure 15. Stability field of Zn in FGD sludge.

between $Zn(OH)_2(s)$ and $ZnCO_3(s)$ is at the $\{OH^-\}^2/[CO_3^{2-}]$ ratio of $10^{-5.17}$ to $10^{-5.72}$. For $ZnSiO_3(s)$ and $ZnCO_3(s)$, the boundary field is a ratio of $10^{-10.25}$ to $10^{-10.80}$. $Zn(OH)_2(s)$ is relatively unstable when $ZnSiO_3(s)$ is present in FGD sludge.

SECTION 4

SOLUBLE CHEMICAL SPECIES IN FRESH
FGD WASTEWATER

The speciation of soluble constituents in FGD wastewater can be modeled as demonstrated in Section 2. The models, which described interactions among solid and soluble species, are inherently complex and subject to inaccuracy if all significant species are not considered.

When modeling speciation in fresh FGD wastewater, however, two simplifying assumptions can be made: (1) the equilibrium conditions among the soluble species can easily be reached, and (2) the rates of nucleation and dissolution of the solid species are very low. The thermodynamic modeling of fresh FGD wastewater can therefore be performed as if no solid species were present. The speciation in this study was performed in such a manner.

Modeling accuracy was assured through the incorporation of all significant species. Included in the model were 20 important metals, 13 important ligands, and 155 possible complexes. These species are listed in Table 6; the corresponding formation constants are listed in Appendix A.

Because the composition of fresh FGD wastewater varies substantially, the speciation modeling was performed only for the extremes of the expected range (shown in Table 3). The minimum concentration of species in FGD wastewater at the scrubber discharge point occurs at an ionic strength (I) of about 0.05. The maximum ionic strength can reach I = 0.80, which is higher than the seawater condition (I = 0.67). It is expected that all other possible distributions of species would fall within this range.

The following discussion presents the modeling results for species concentrations in the low and high ionic strength cases, respectively. In each case, the results were prepared in graphical form (Figures 16-37). The concentrations of each group of complexes are plotted against pH values. With the exception of free ions, each curve on the graph represents the summation of the concentrations of similar ligand complexes. For example, the "Cl^-" curve in the speciation diagram of cadmium (see Figure 20) represents $[CdCl^+] + [CdCl_2(aq)] + [CdCl_3^-] + [CdCl_4^{2-}] + [CdCl_5^{3-}]$.

TABLE 6. POSSIBLE CHEMICAL SPECIES EXISTING IN FGD WASTES[*]

Constituent	Chemical Species	
	Solid	Soluble
Aluminum	$AlPO_4(s)$, $Al_2(SiO_3)_2(OH)_2(s)$, $AlAsO_4(s)$, $Al(OH)_3^-(s)$, $Al(H_2PO_4)(OH)_2(s)$, $Al_2O_3 \cdot 3H_2O(s)$	$AlSO_4^+$, $Al(SO_4)_2^-$, AlF^{2+}, AlF_2^+, $AlF_3(aq)$, AlF_4^-, AlF_5^{2-}, AlF_6^{3-}, $AlOH^{2+}$, $Al(OH)_4^-$
Beryllium	$Be_3(PO_4)_2(s)$, $Be(OH)_2(s)$	$BeSO_4(aq)$, $Be(SO_4)_2^{2-}$, $Be(SO_4)_3^{4-}$, $BeCl^+$, BeF^+, $BeF_2(aq)$, BeF_3^-, $BeOH^+$
Cadmium	$CdCO_3(s)$, $Cd_3(AsO_4)_2(s)$, $CdSeO_3(s)$, $Cd(OH)_2(s)$	$CdCO_3(aq)$, $CdHCO_3^+$, $CdSO_4(aq)$, $CdCl^+$, $CdCl_2(aq)$, $CdCl_3^-$, $CdCl_4^{2-}$, $CdOHCl(aq)$, CdF^+, $CdF_2(aq)$, CdF_3^-, $CdPO_4^-$, $Cd(SO_3)_2^{2-}$, $CdOH^+$; $Cd(OH)_2(aq)$, $Cd(OH)_3^-$, $Cd(OH)_4^{2-}$, Cd_2OH^{3+}, $Cd_4(OH)_4^{4+}$
Calcium	$CaCO_3(s)$, $CaSO_4 \cdot 2H_2O(s)$, $CaF_2(s)$, $Ca(PO_4)_3(OH)(s)$, $Ca_4(PO_4)_3H(s)$, $CaHPO_4(s)$, $CaSiO_3(s)$, $CaSO_3 \cdot 1/2H_2O(s)$, $CaMoO_4(s)$, $Ca_3(AsO_4)_2(s)$, $CaSeO_3(s)$, $Ca(OH)_2(s)$	$CaCO_3(aq)$, $CaHCO_3^+$, $CaSO_4(aq)$, CaF^+, $CaHPO_4(aq)$, $CaOH^+$
Chromium	$CrAsO_4(s)$, $Cr(OH)_3(s)$	$CrSO_4^+$, $CrCl^{2+}$, $CrCl_2^+$, CrF^{2+}, CrF_2^+, $CrF_3(aq)$, $CrHPO_4^+$, $CrOH^{2+}$, $Cr(OH)_2^+$, $Cr(OH)_4^-$
Cobalt	$CoCO_3(s)$, $Co_3(AsO_4)_2(s)$, $CoSeO_3(s)$, $Co(OH)_2(s)$	$CoCO_3(aq)$, $CoHCO_3^+$, $CoSO_4(aq)$, $CoCl^+$, $CoCl_2(aq)$, $CoHPO_4(aq)$, $CoOH^+$, $Co(OH)_2(aq)$, $Co(OH)_3^-$

TABLE 6 (continued)

Constituent	Chemical Species	
	Solid	Soluble
Copper	$CuCO_3(OH)_2(s)$, $Cu_3(PO_4)_2(s)$, $Cu_3(AsO_4)_2(s)$, $CuSeO_3(s)$, $Cu(OH)_2(s)$, $CuCO_3(s)$	$CuCO_3(aq)$, $Cu(CO_3)_2^{2-}$, $CuHCO_3^+$, $CuOHCO_3^-$, $CuSO_4(aq)$, $CuCl^+$, $CuCl_2(aq)$, $CuCl_3^-$, $CuCl_4^{2-}$, $CuOHCl(aq)$, CuF^+, $CuHPO_4(aq)$, $CuH_2PO_4^+$, $CuB(OH)_4^+$, $Cu(B(OH)_4)_2(aq)$, $CuOH^+$, $Cu(OH)_2(aq)$, $Cu(OH)_3^-$, $Cu(OH)_4^{2-}$, $Cu_2(OH)_2^{2+}$
Hydrogen		HCO_3^-, $H_2CO_3(aq)$, HSO_4^-, $HF(aq)$, HPO_4^{2-}, $H_2PO_4^-$, $H_3PO_4(aq)$, $HSiO_3^-$, $H_2SiO_3(aq)$, $HB(OH)_4(aq)$, HSO_3^-, $HMoO_4^-$, $HAsO_4^{2-}$, $H_2AsO_4^-$, $H_2VO_4^-$, $HSeO_3^-$, $H_2SeO_3(aq)$
Iron	$FePO_4(s)$, $FeAsO_4(s)$, $FeSeO_3(s)$, $Fe(OH)_3(s)$, $FeCO_3(s)$, $Fe(OH)_2(s)$	$FeSO_4^+$, $Fe(SO_4)_2^-$, $FeCl^{2+}$, $FeCl_2^+$, $FeCl_3(aq)$, FeF^{2+}, FeF_2^+, FeF_3^+, $FeHPO_4^+$, $FeHSiO_3^{2+}$, $FeB(OH)_4^{2+}$, $Fe(B(OH)_4)_2^+$, $FeSO_3^+$, $FeOH^{2+}$, $Fe(OH)_2^+$, $Fe(OH)_4^-$, $Fe_2(OH)_2^{4+}$
Lead	$PbCO_3(s)$, $Pb_3(CO_3)_2(OH)_2(s)$, $PbF_2(s)$, $PbHPO_4(s)$, $Pb_3(PO_4)_2(s)$, $Pb_5(PO_4)_3(OH)(s)$, $Pb_2SiO_3(OH)_2(s)$, $PbMoO_4(s)$, $Pb_3(AsO_4)_2(s)$, $PbSeO_3(s)$, $Pb(OH)_2(s)$, $PbO(s)$, $PbO_2(s)$, $PbSO_3(s)$, $PbSO_4(s)$, $PbCl_2(s)$	$PbCo_3(aq)$, $Pb(CO_3)_2^{2-}$, $PbHCO_3^+$, $Pb(HCO_3)_2(aq)$, $PbSO_4(aq)$, $PbCl^+$, $PbCl_2(aq)$, $PbCl_3^-$, $PbCl_4^{2-}$, $PbOHCl(aq)$, $PbB(OH)_4^+$, $Pb(B(OH)_4)_2(aq)$, $PbOH^+$, $Pb(OH)_2(aq)$, $PB(OH)_3^-$, $Pb^0(s)$, $Pb_2(OH)^{3+}$, $Pb_3(OH)_4^+$, $Pb_6(OH)_8^{4+}$

TABLE 6 (continued)

Constituent	Chemical Species	
	Solid	Soluble
Magnesium	$MgCO_3(s)$, $MgF_2(s)$, $Mg_3(PO_4)_2(s)$, $Mg_3(AsO_4)_2(s)$, $MgSeO_3(s)$, $Mg(OH)_2(s)$	$MgCO_3$, $MgHCO_3^+$, $MgSO_4(aq)$, MgF^+, $MgHPO_4(aq)$, $MgOH^+$
Manganese	$MnCO_3(s)$, $MnSiO_3(s)$, $Mn_3(AsO_4)_2(s)$, $MnSeO_3(s)$, $Mn(OH)_2(s)$, $Mn_3O_4(s)$	$MnOOH(aq)$, $MnO_2(aq)$, $MnHCO_3^+$, $MnSO_4^0$, $MnCl^+$, $MnCl_2^0$, $MnCl_3^-$, $MnHPO_4^0$, $MnOH^+$, $Mn(OH)_3^-$
Mercury	$Hg(OH)_2(s)$, $Hg^0(l)$	$HgCO_3(aq)$, $HgHCO_3^+$, $HgSO_4(aq)$, $Hg(SO_4)_2^{2-}$, $HgCl^+$, $HgCl_2(aq)$, $HgCl_3^-$, $HgCl_2^{2-}$, $HgOHCl(aq)$, HgF^+, $HgOH^+$, $Hg(OH)_2(aq)$, $Hg(OH)_2(aq)$, $Hg(OH)_3^-$, Hg_2OH^{3+}, $Hg_3(OH)_3^{3+}$
Nickel	$NiCO_3(s)$, $Ni_3(AsO_4)_2(s)$, $NiSeO_3(s)$, $Ni(OH)_2(s)$	$NiCO_3(aq)$, $NiHCO_3^+$, $NiSO_4(aq)$, $NiCl^+$, $NiCl_2(aq)$, NiF^+, $NiHPO_4(aq)$, $NiOH^+$
Potassium		KSO_4^-
Sodium		$NaCO_3^-$, $NaSO_4^-$
Silver	$Ag_2CO_3(s)$, $Ag_2SO_4(s)$, $AgCl(s)$, $Ag_3PO_4(s)$, $Ag_2MoO_4(s)$, $Ag_3AsO_4(s)$, $Ag_2SeO_3(s)$, $AgOH(s)$, $Ag^0(s)$	$AgSO_4^-$, $AgCl(aq)$, $AgCl_2^-$, $AgCl_3^{2-}$, $AgCl_4^{3-}$, $AgSO_3^-$, $Ag(SO_3)^{3-}$, $AgOH(aq)$, $Ag(OH)_2^-$
Tin	$Sn(OH)_2(s)$	SnF^+, $SnF_2(aq)$, SnF_3^-, $SnOH^+$

TABLE 6 (continued)

Constituent	Chemical Species	
	Solid	Soluble
Zinc	$ZnCO_3(s)$, $Zn_3(PO_4)_2(s)$, $ZnSiO_3(s)$, $Zn_3(AsO_4)_2(s)$, $ZnSeO_3(s)$, $Zn(OH)_2(s)$	$ZnCO_3(aq)$, $ZnHCO_3^+$, $ZnSO_4(aq)$, $ZnCl^+$, $ZnCl_2(aq)$, $ZnCl_3^-$, $ZnOHCl(aq)$, $ZnCl_4^{2-}$, ZnF^+, $ZnHPO_4(aq)$, $ZnOH^+$, $Zn(OH)_3^-$, $Zn(OH)_4^{2-}$, $Zn(OH)_2(aq)$, Zn_2OH^{3+}

* Represents those included in the Thermodynamic Model.
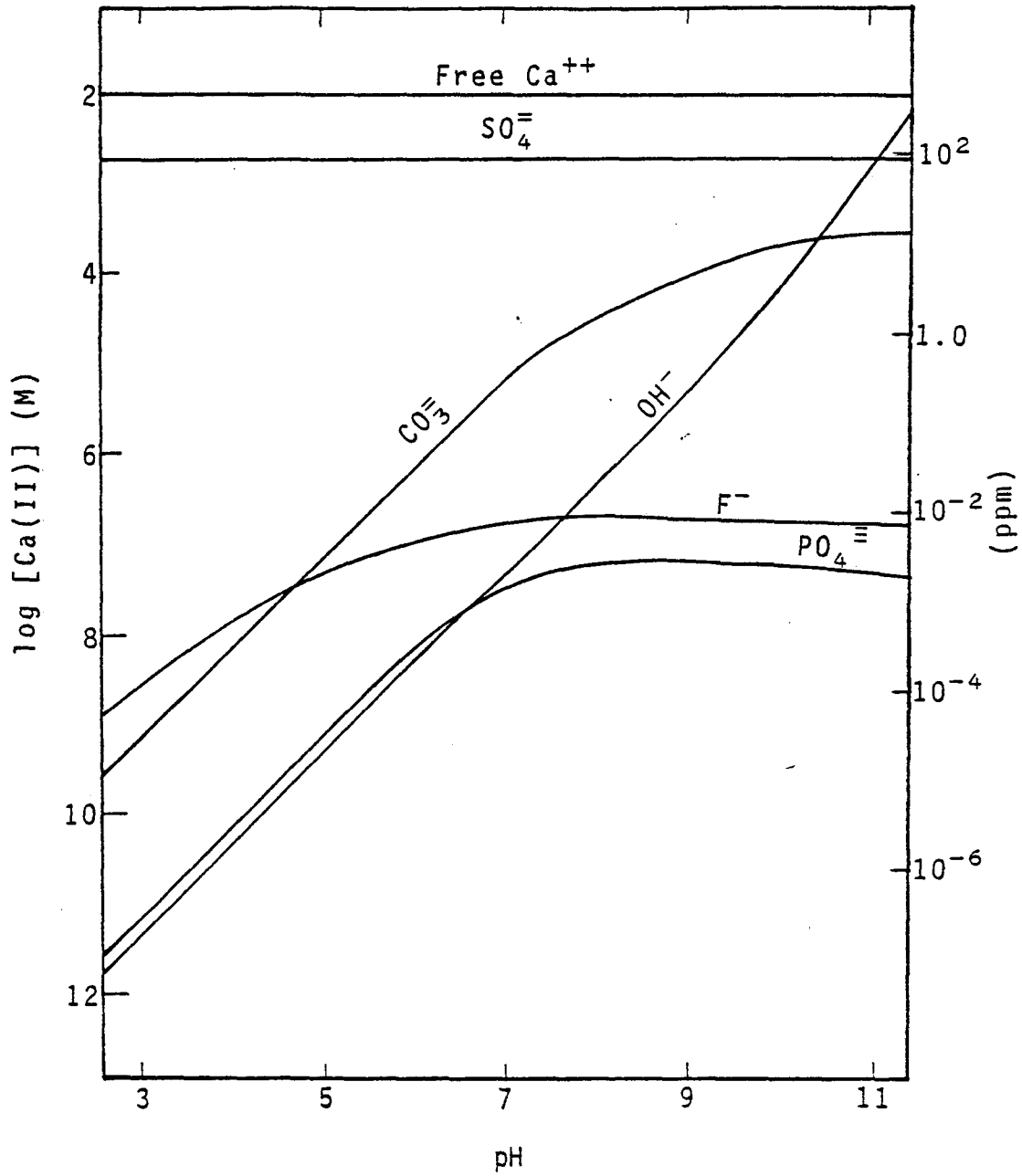
Figure 16. Speciation of Ca in raw FGD wastewater
at $I = 0.05$, $[Ca_T] = 10^{-1.89}M$.
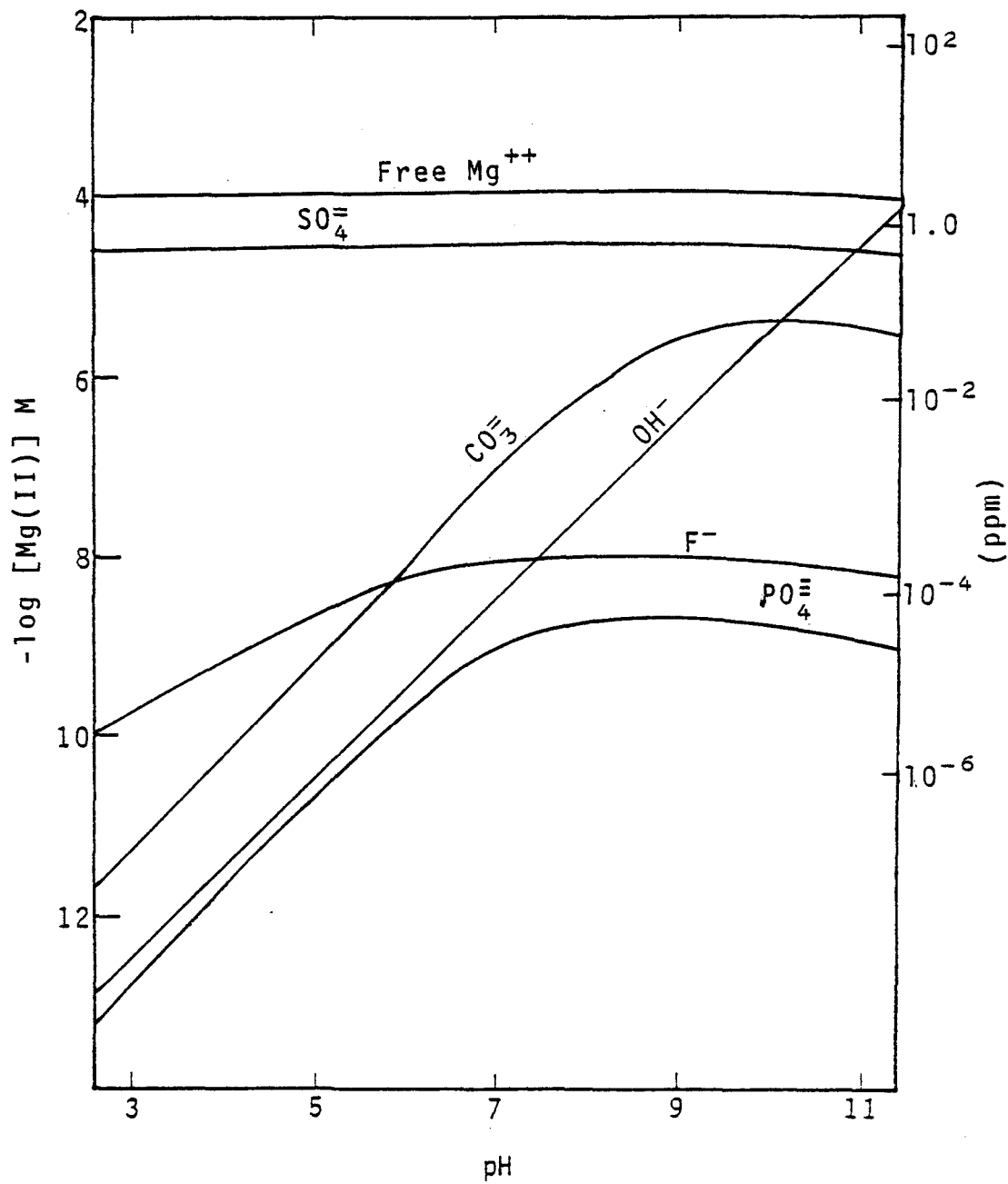
Figure 17. Speciation of Mg in raw FGD wastewater at I = 0.05, $[Mg_T] = 10^{-3.91}$ M.
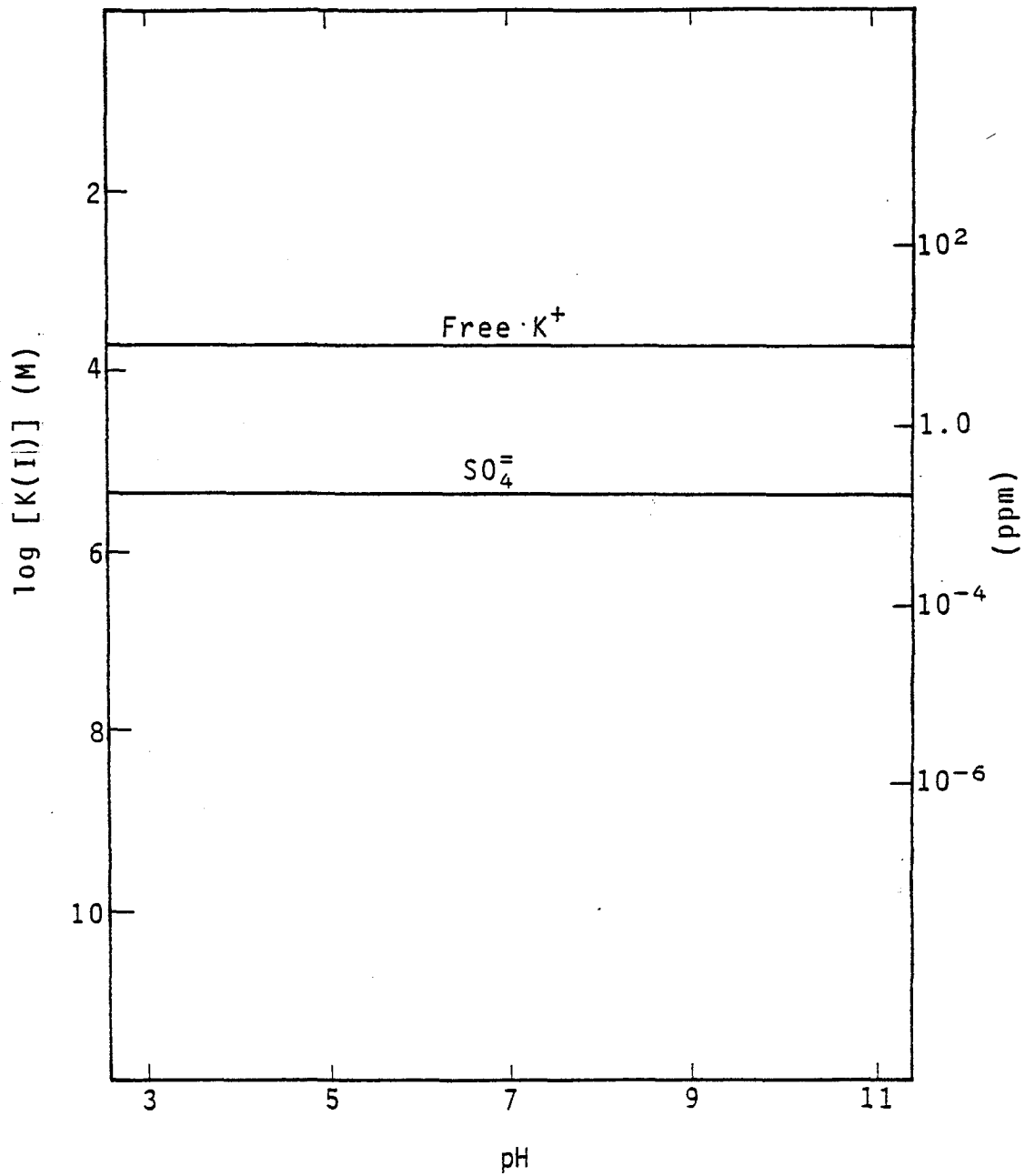
Figure 18. Speciation of K in raw FGD wastewater at I = 0.05, $[K_T]$ = $10^{-3.82}$ M.
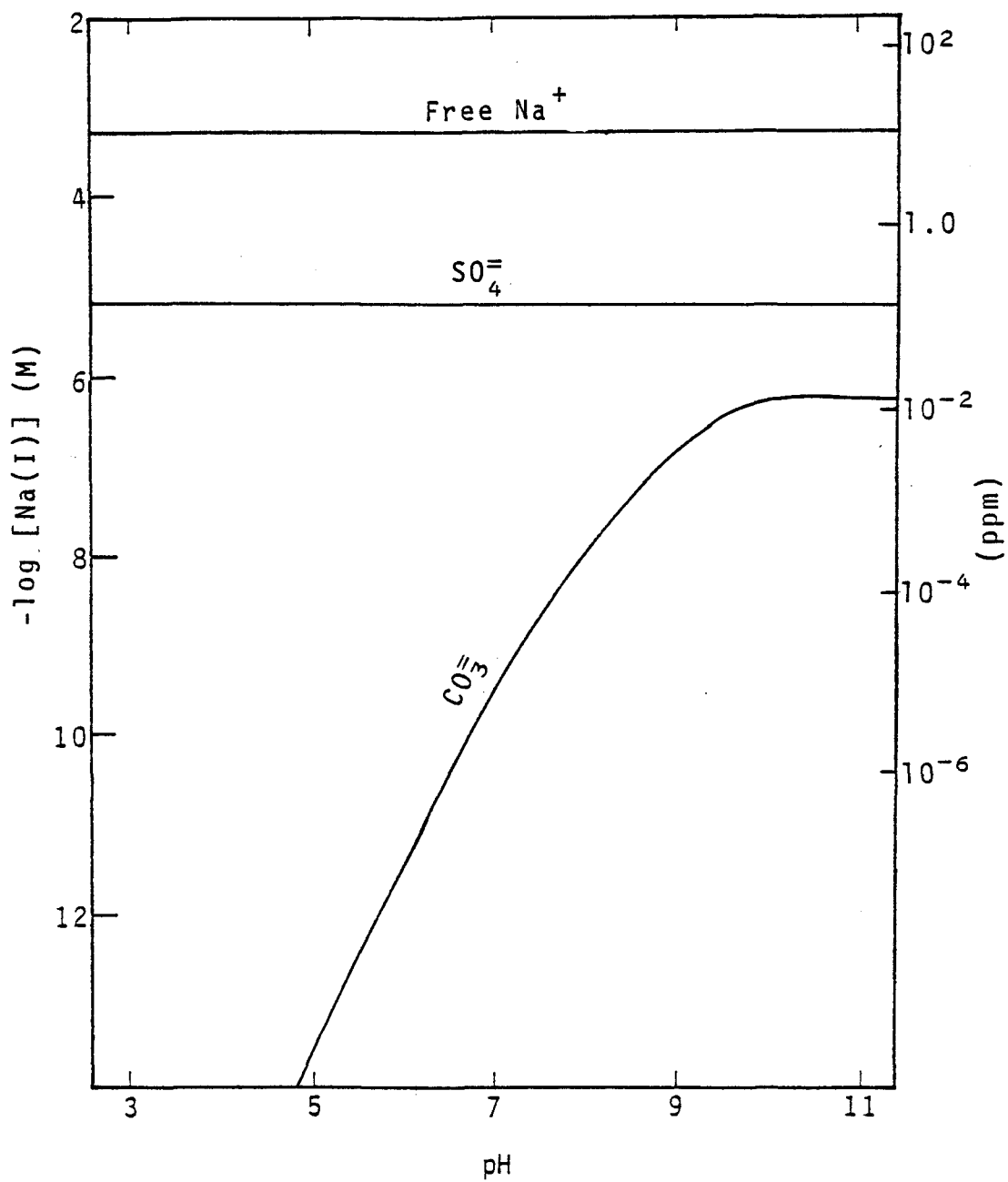
Figure 19. Speciation of Na in raw FGD wastewater
at I = 0.05, $[Na_T]$ = $10^{-3.21}$M.

75
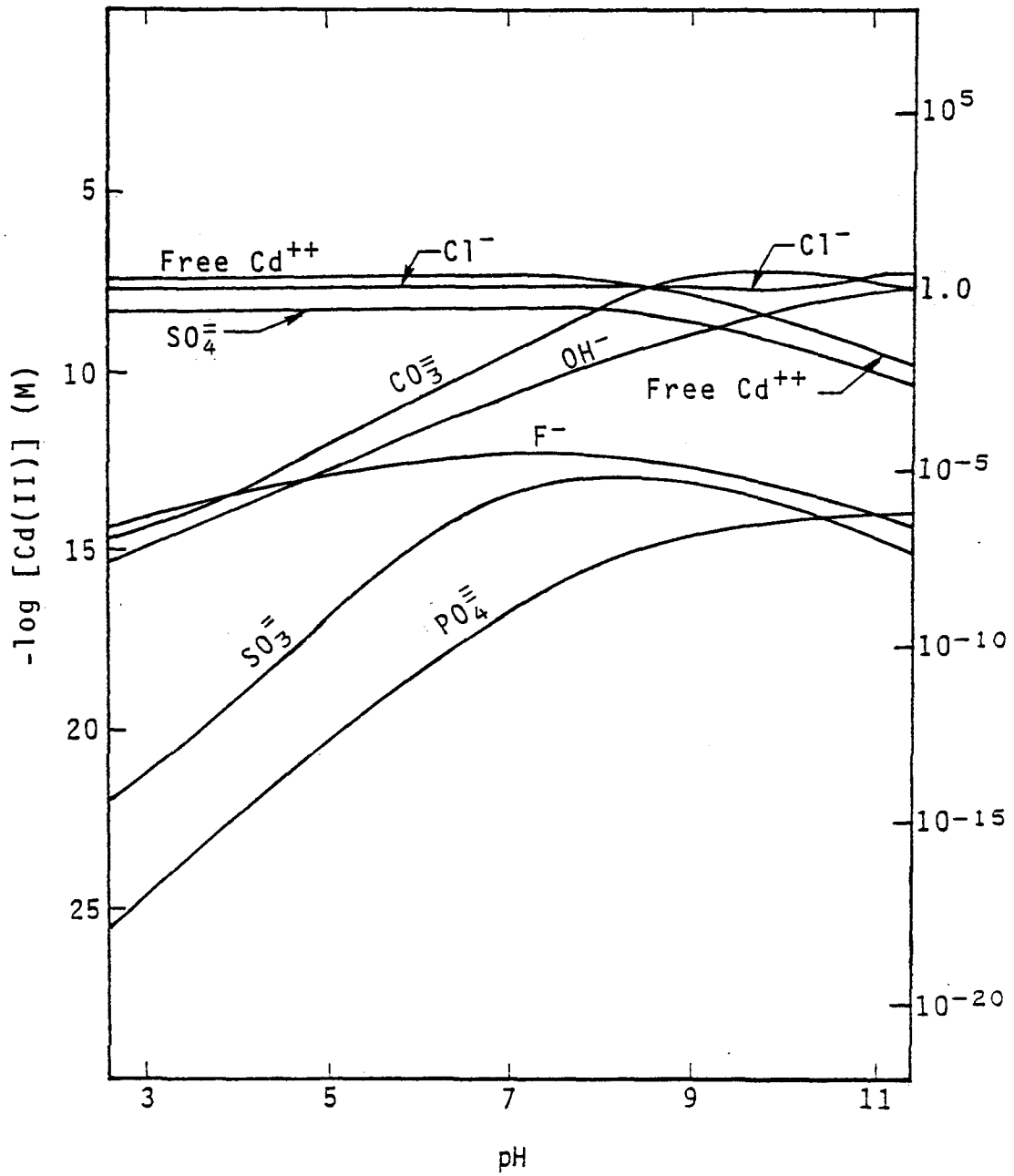
Figure 20.   Speciation of Cd in raw FGD wastewater
at I = 0.05, $[Cd_T]$ = $10^{-7.44}M$.
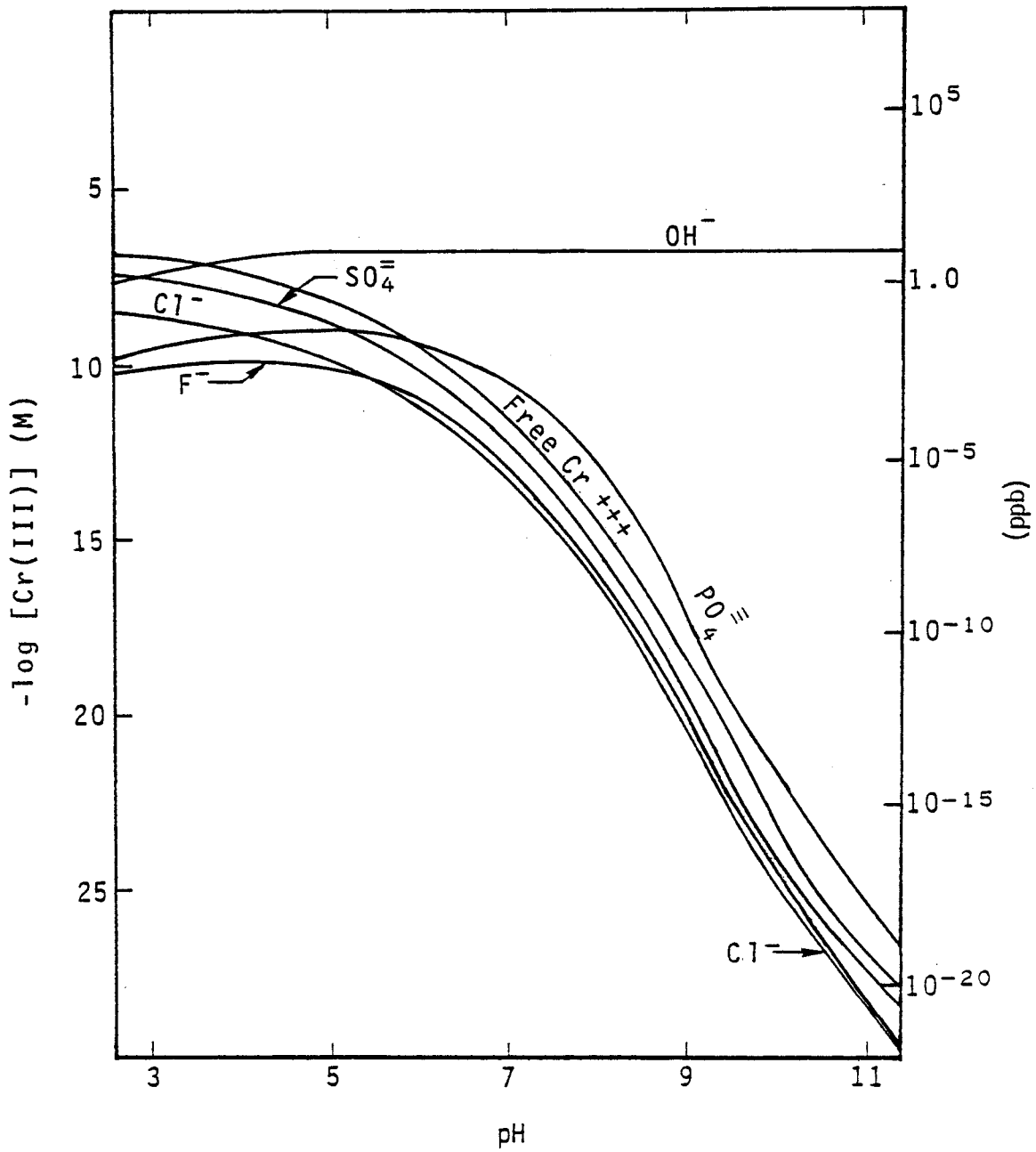
Figure 21. Speciation of Cr in raw FGD wastewater
at I = 0.05, $[Cr_T] = 10^{-6.72}M$.
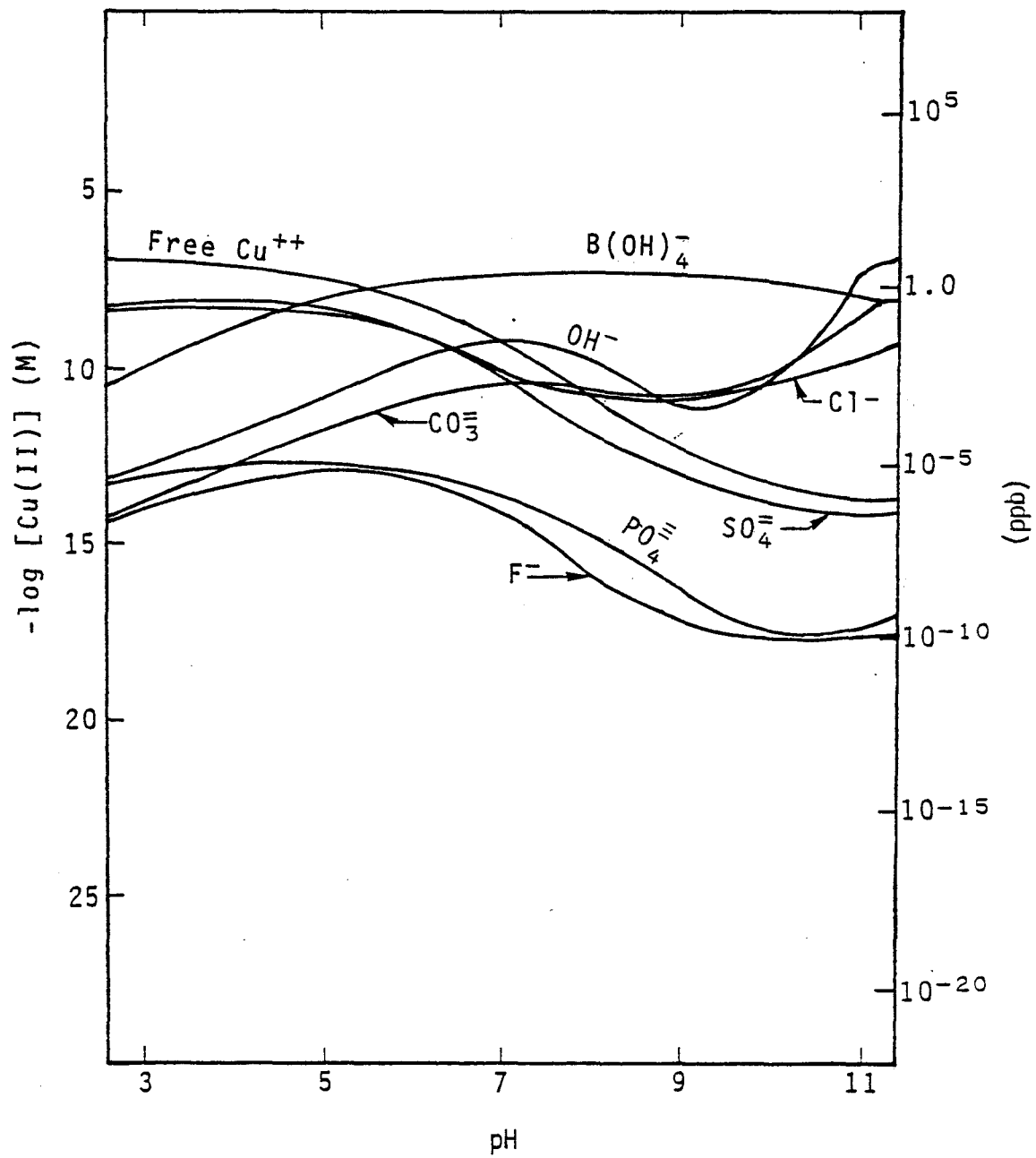
Figure 22. Speciation of Cu in raw FGD wastewater at I = 0.05, $[Cu_T] = 10^{-7.50}M$.
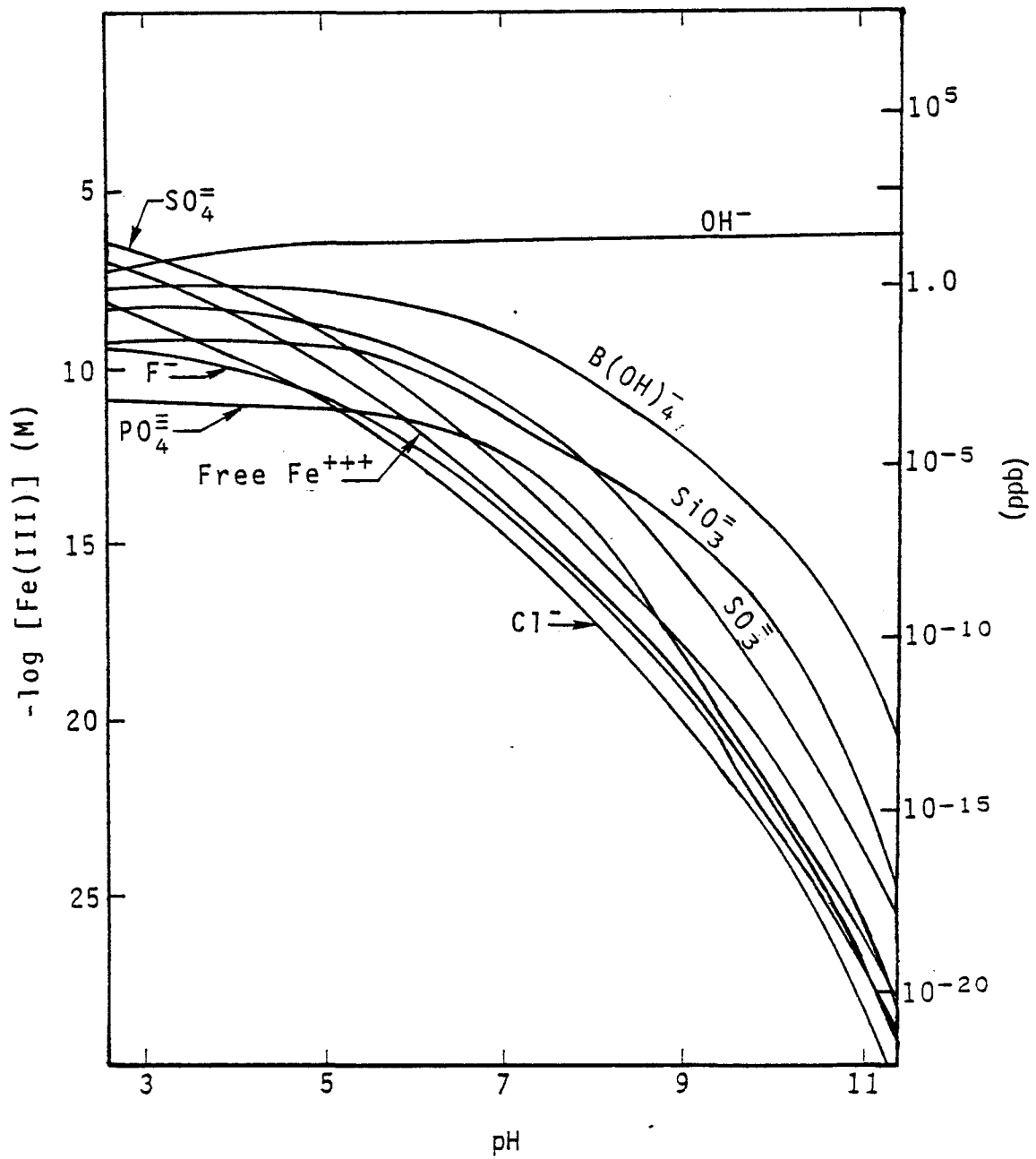
Figure 23. Speciation of Fe in raw FGD wastewater
at I = 0.05, $[Fe_T] = 10^{-6.45}M$.
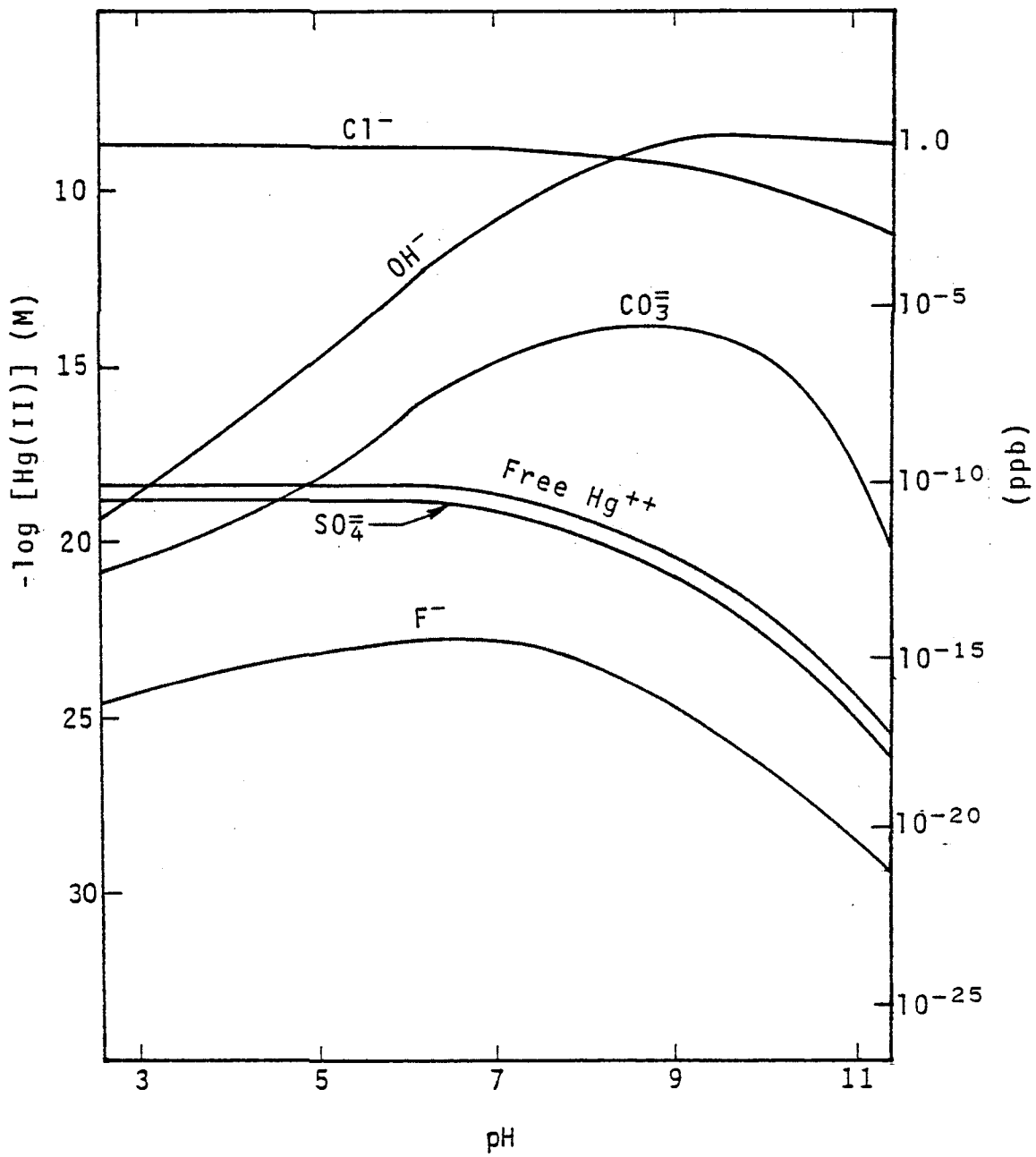
Figure 24.   Speciation of Hg in raw FGD wastewater
at $I = 0.05$, $[Hg_T] = 1.0^{-8.7}M$.
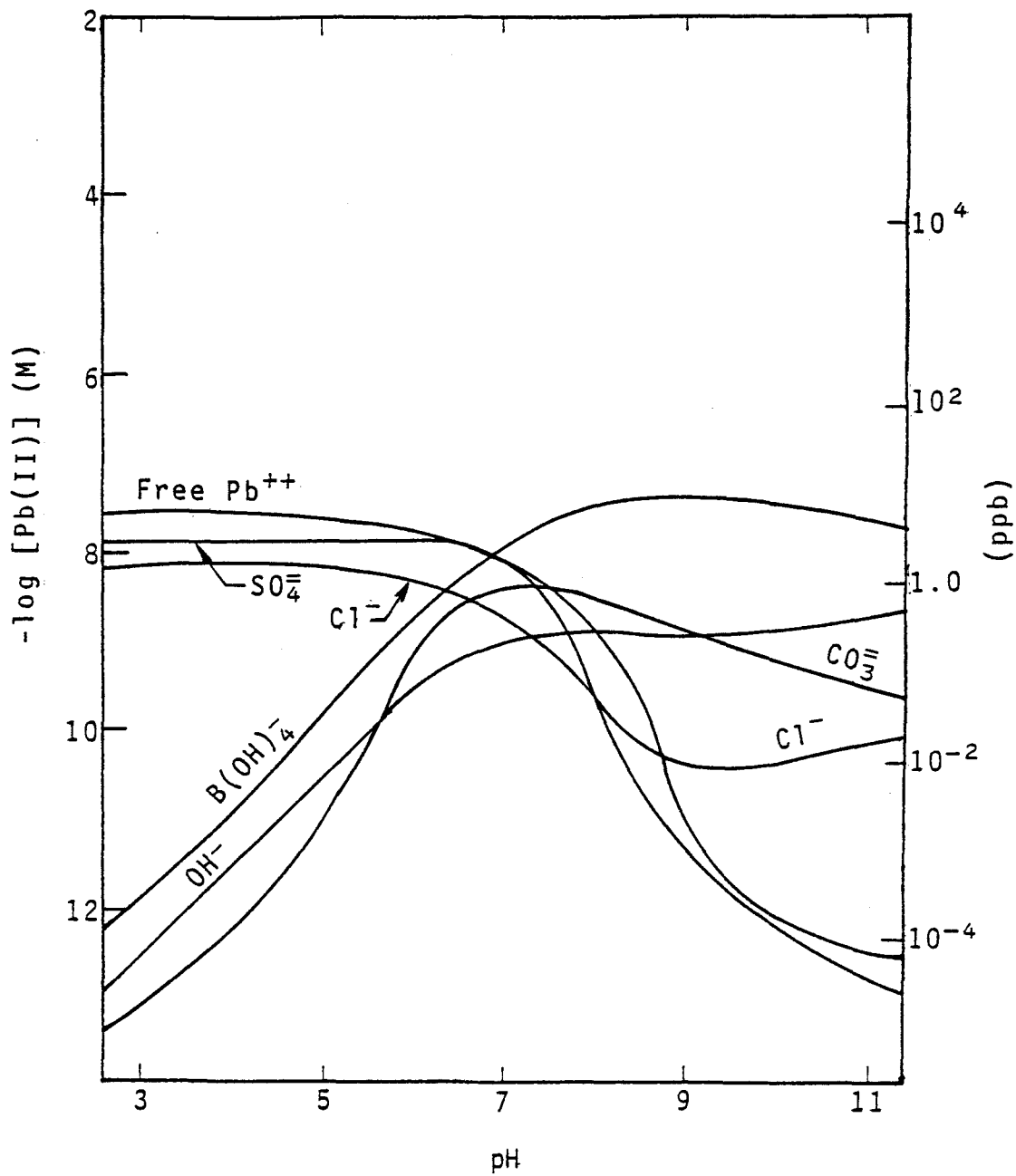
Figure 25.   Speciation of Pb in raw FGD wastewater
at I = 0.05, [Pb_T] = $10^{-7.32}$M.
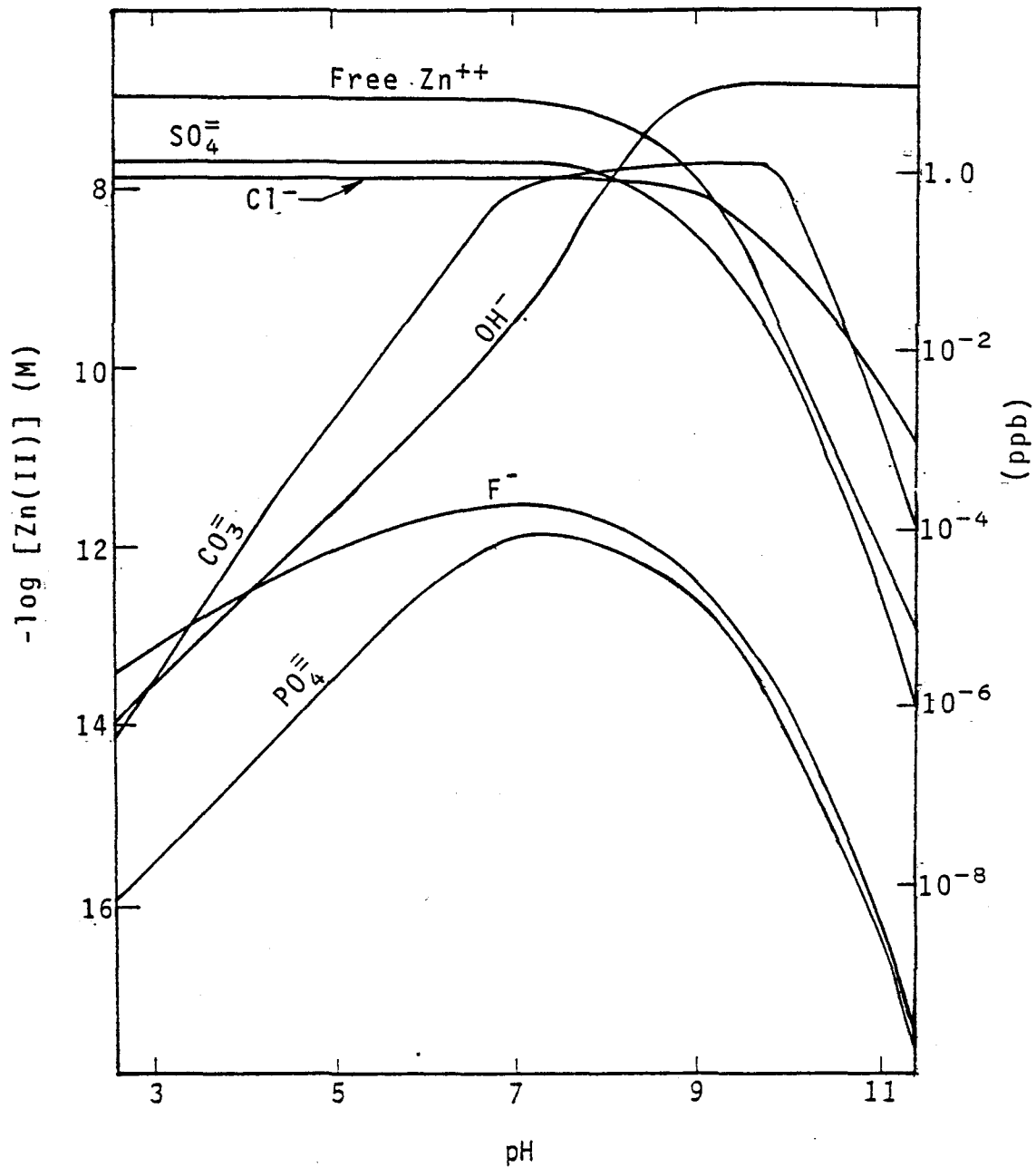
Figure 26.   Speciation of Zn in raw FGD wastewater
at I = 0.05, $[Zn_T] = 10^{-6.82}M$.
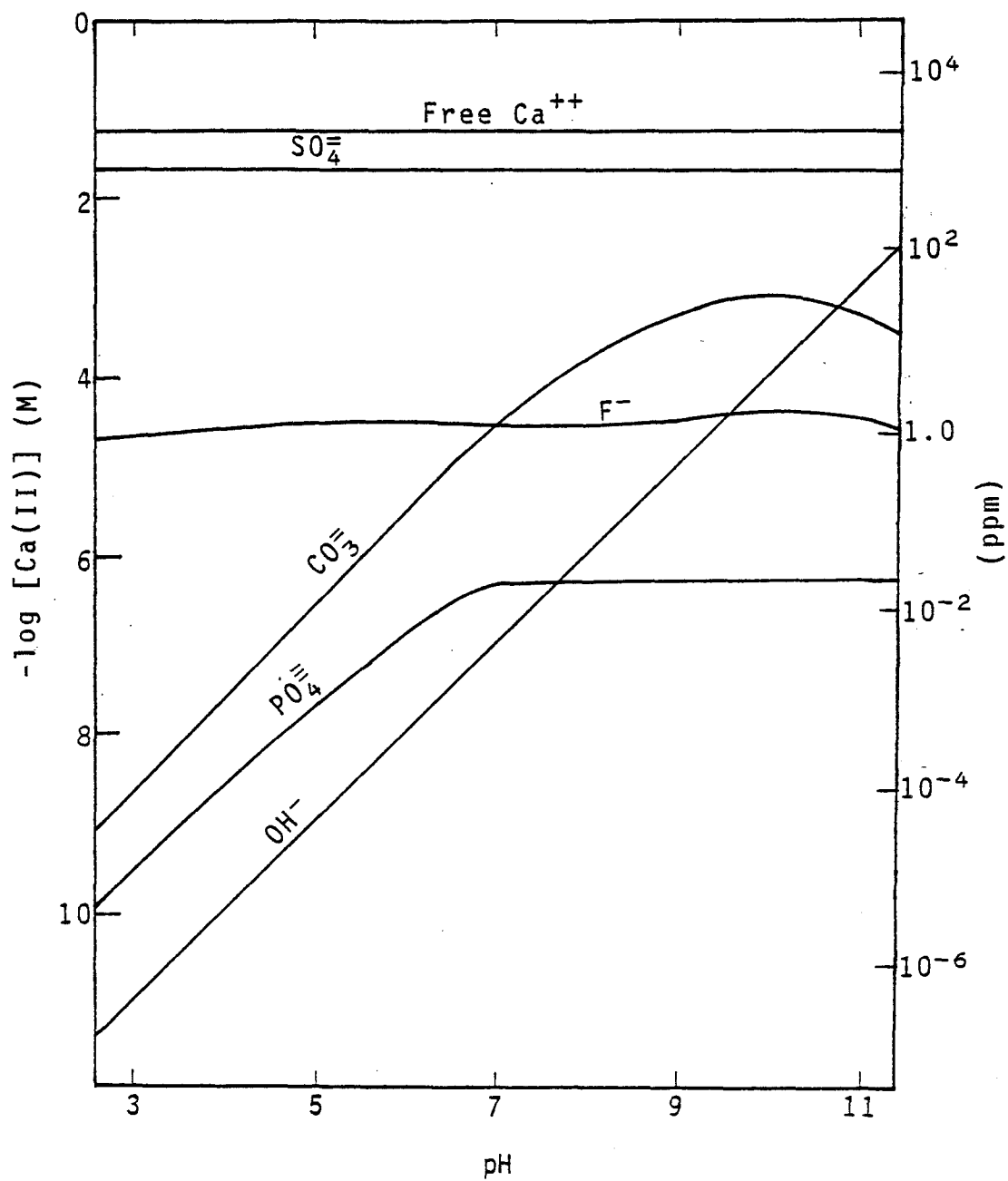
Figure 27. Speciation of Ca in raw FGD wastewater
at I = 0.8, $[Ca_T] = 10^{-1.12}M$.
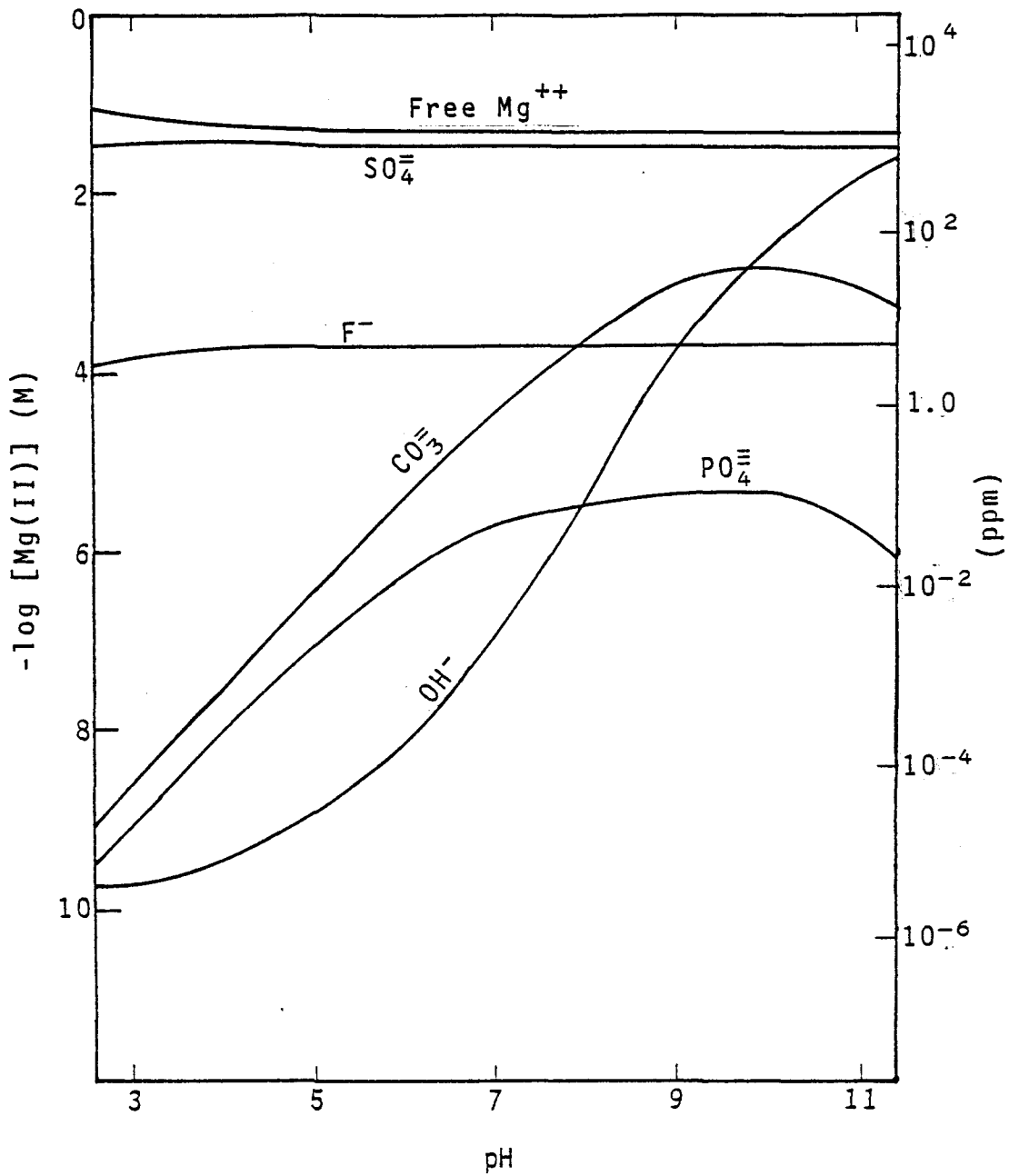
Figure 28. Speciation of Mg in raw FGD wastewater
at I = 0.8, $[Mg_T]$ = $10^{-0.95}$M.
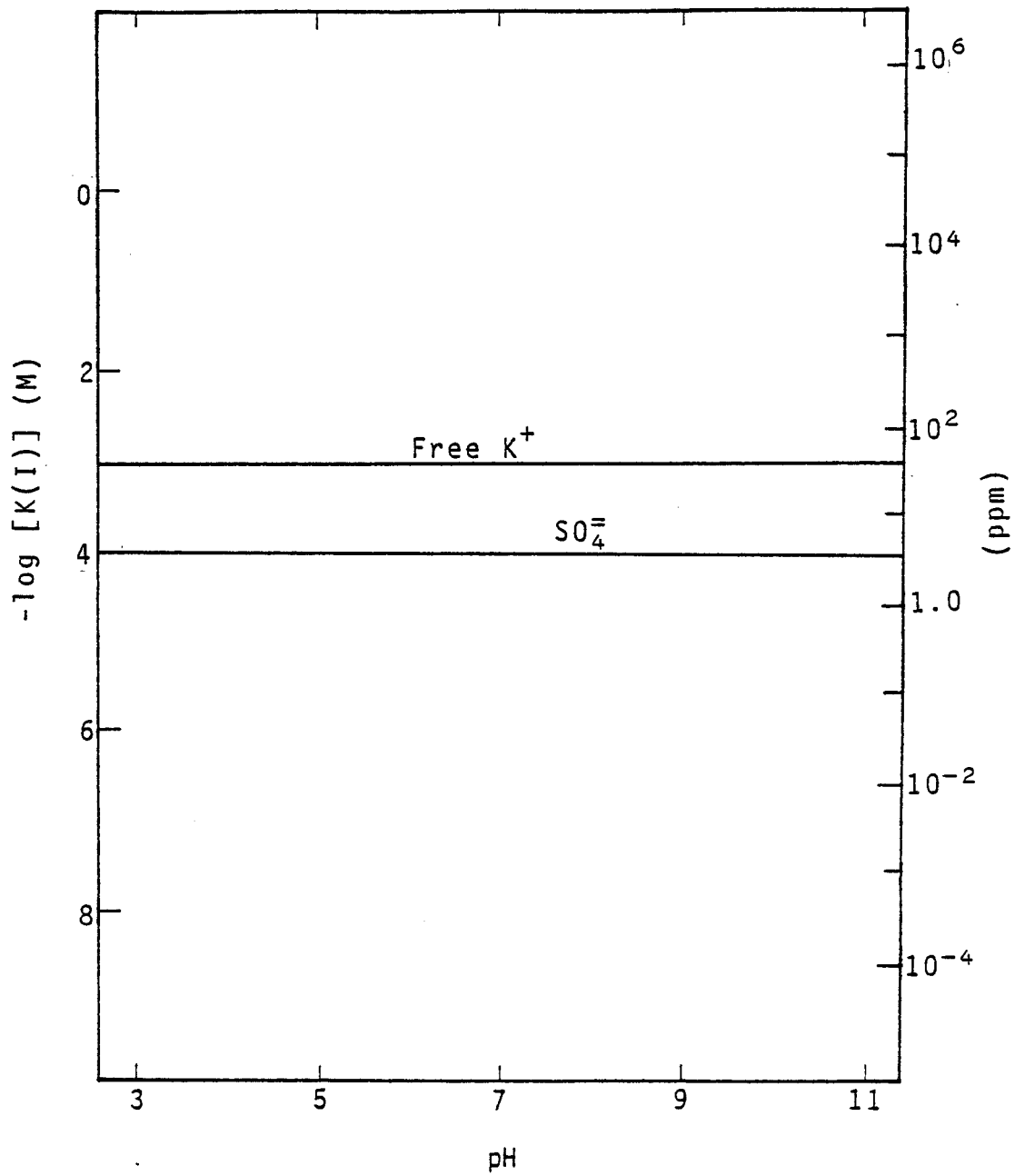
Figure 29. Speciation of K in raw FGD wastewater
at I = 0.8, $[K_T] = 10^{-3.09}$M.
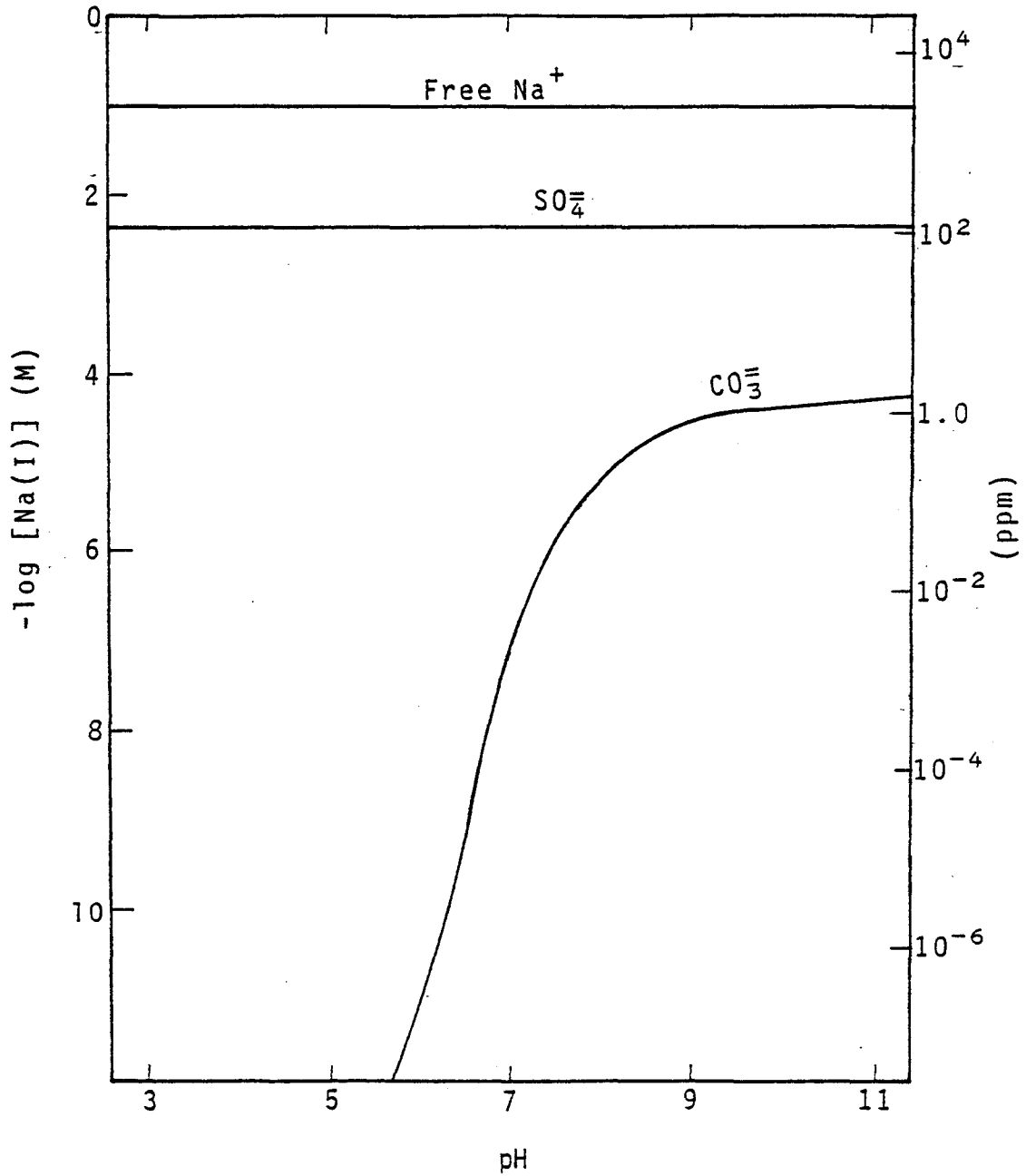
Figure 30.   Speciation of Na in raw FGD wastewater
at $I = 0.8$, $[Na_T] = 10^{-0.98}M$.
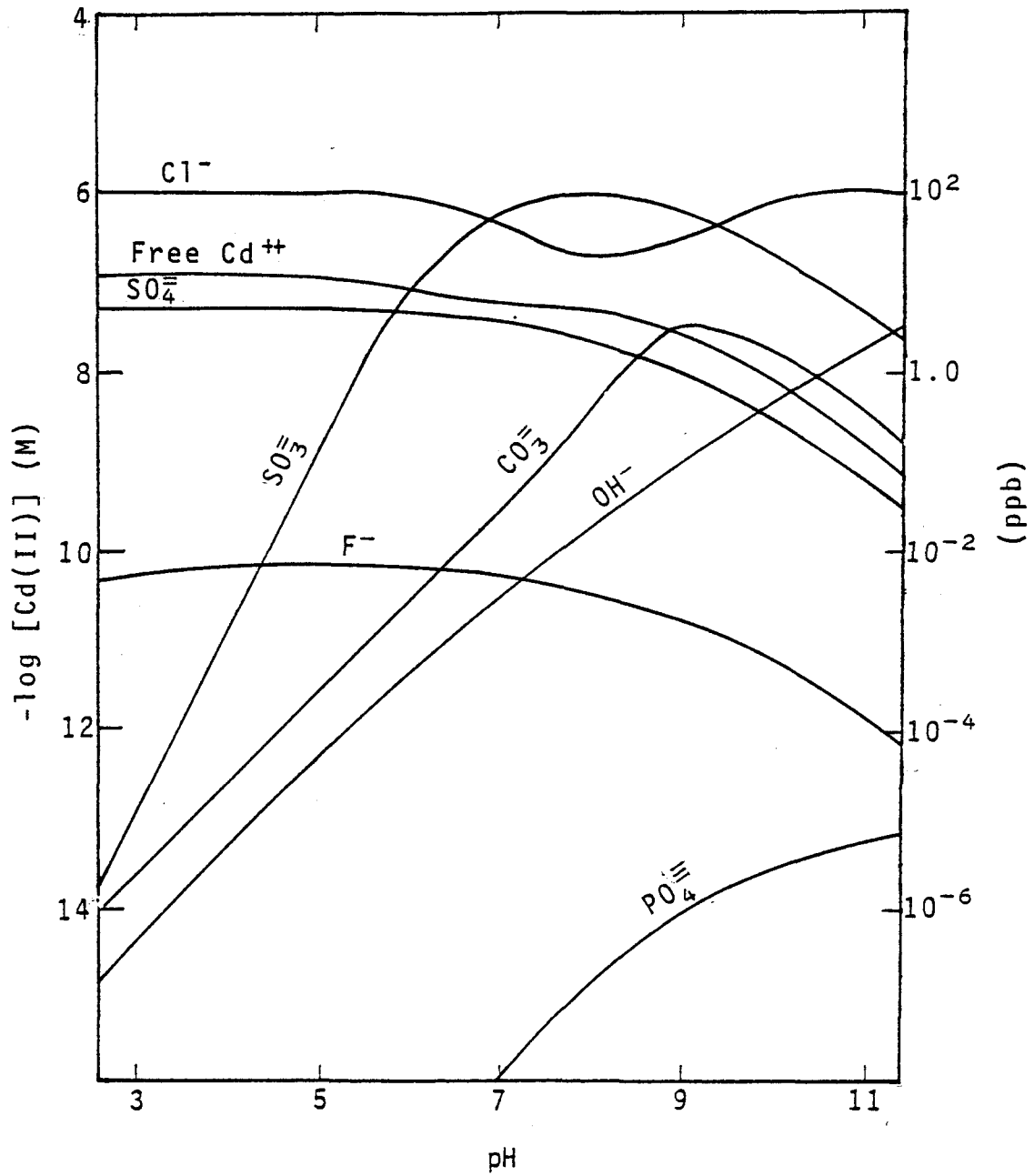
Figure 31. Speciation of Cd in raw FGD wastewater
at $I = 0.8$, $[Cd_T] = 10^{-6.01}M$.
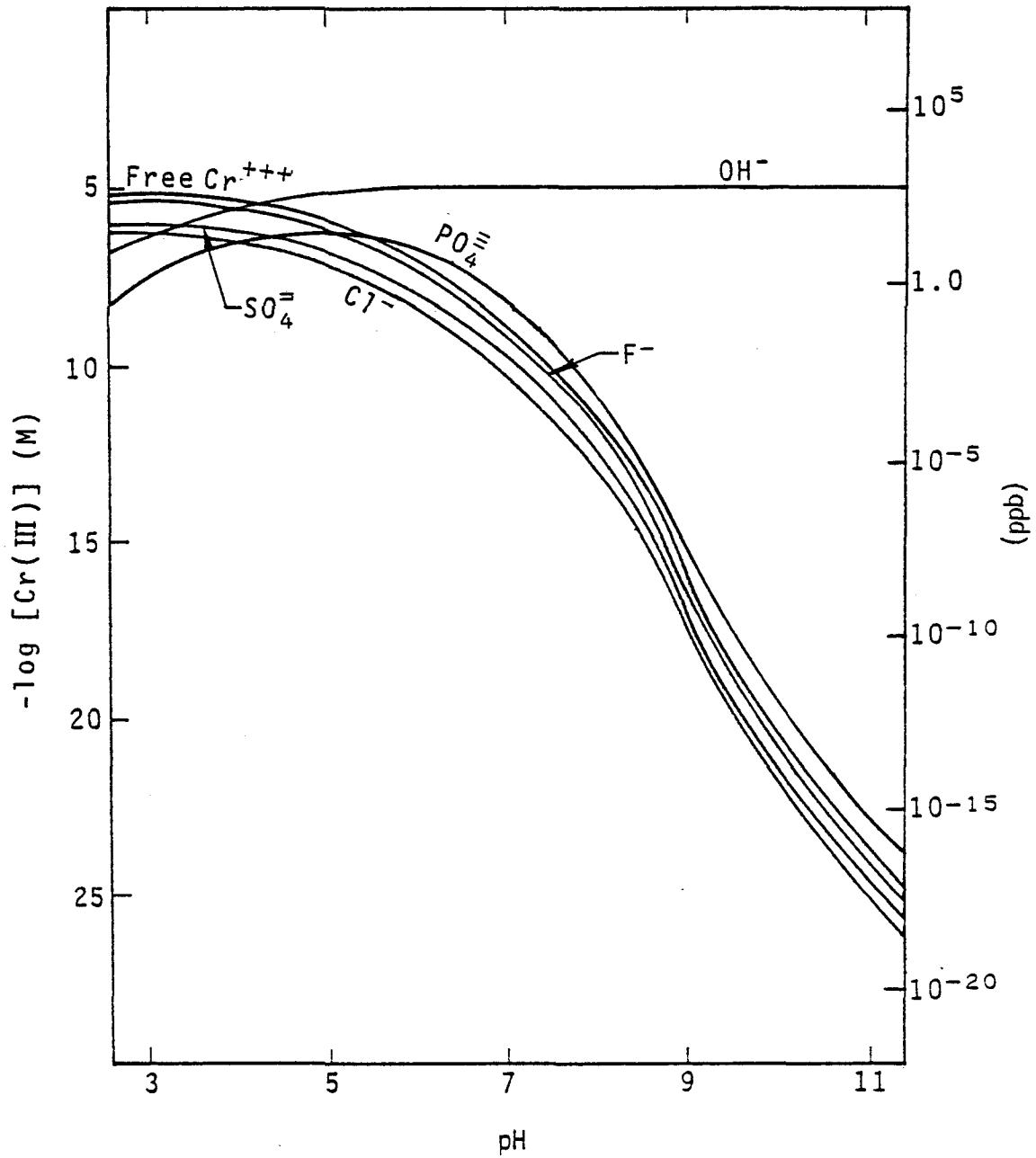
Figure 32.   Speciation of Cr in raw FGD wastewater
at I = 0.8, $[Cr_T]$ = $10^{-5.02}$M.
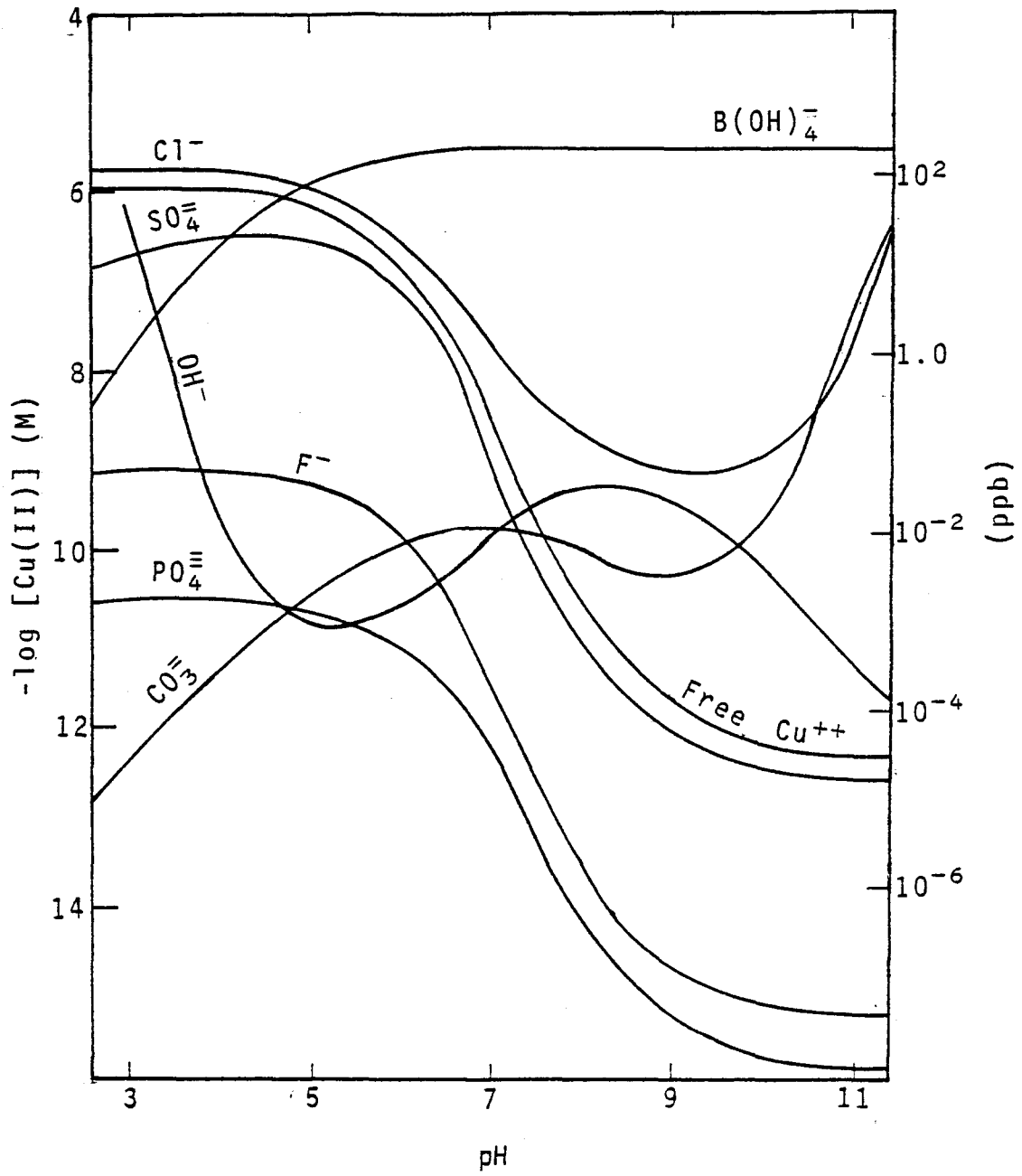
Figure 33. Speciation of Cu(II) in raw wastewater
at $I = 0.8$, $[Cu_T] = 10^{-5.5}M$.
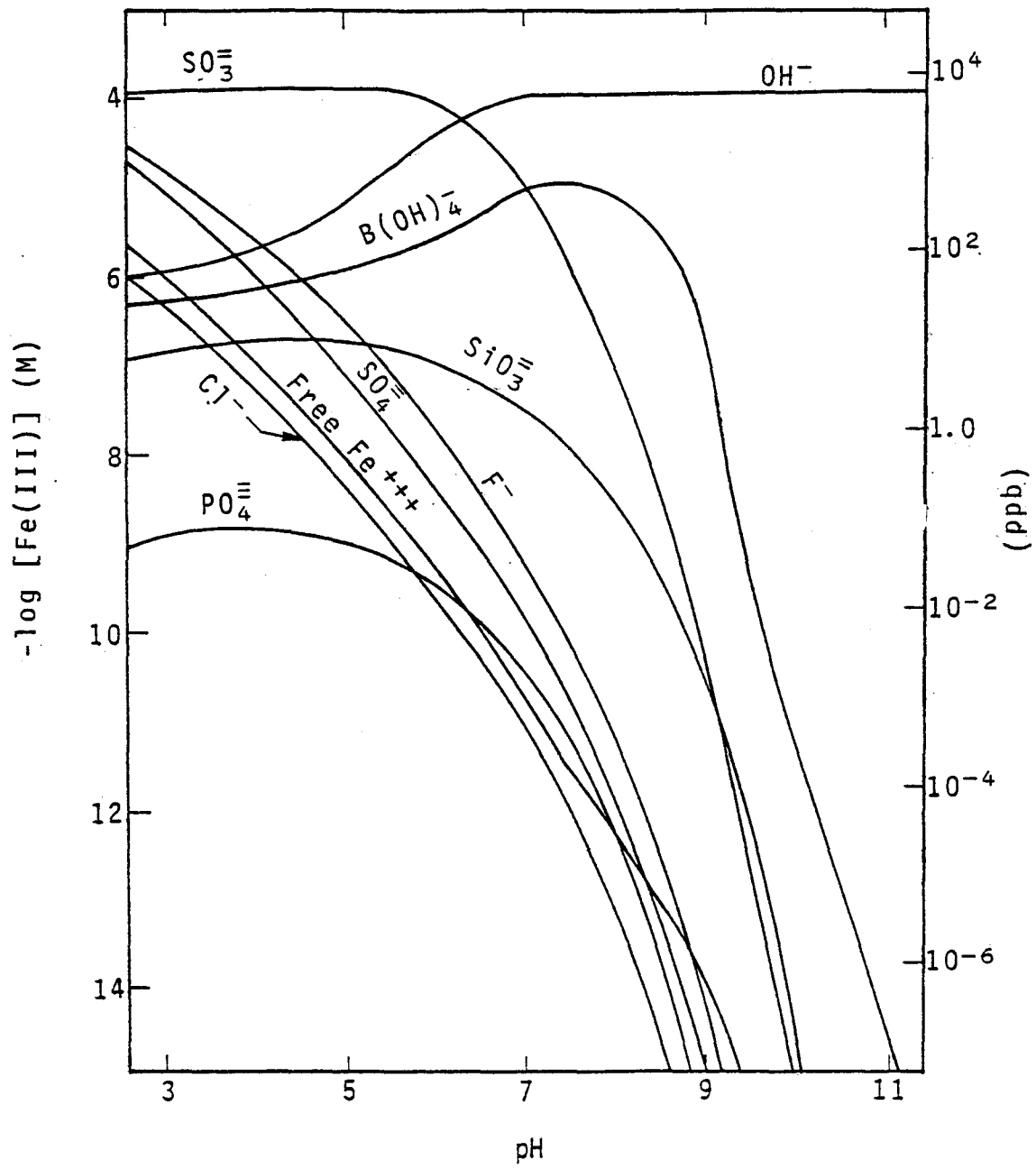
Figure 34.   Speciation of Fe in raw FGD wastewater
at $I = 0.8$, $[Fe_T] = 10^{-3.84}M$.
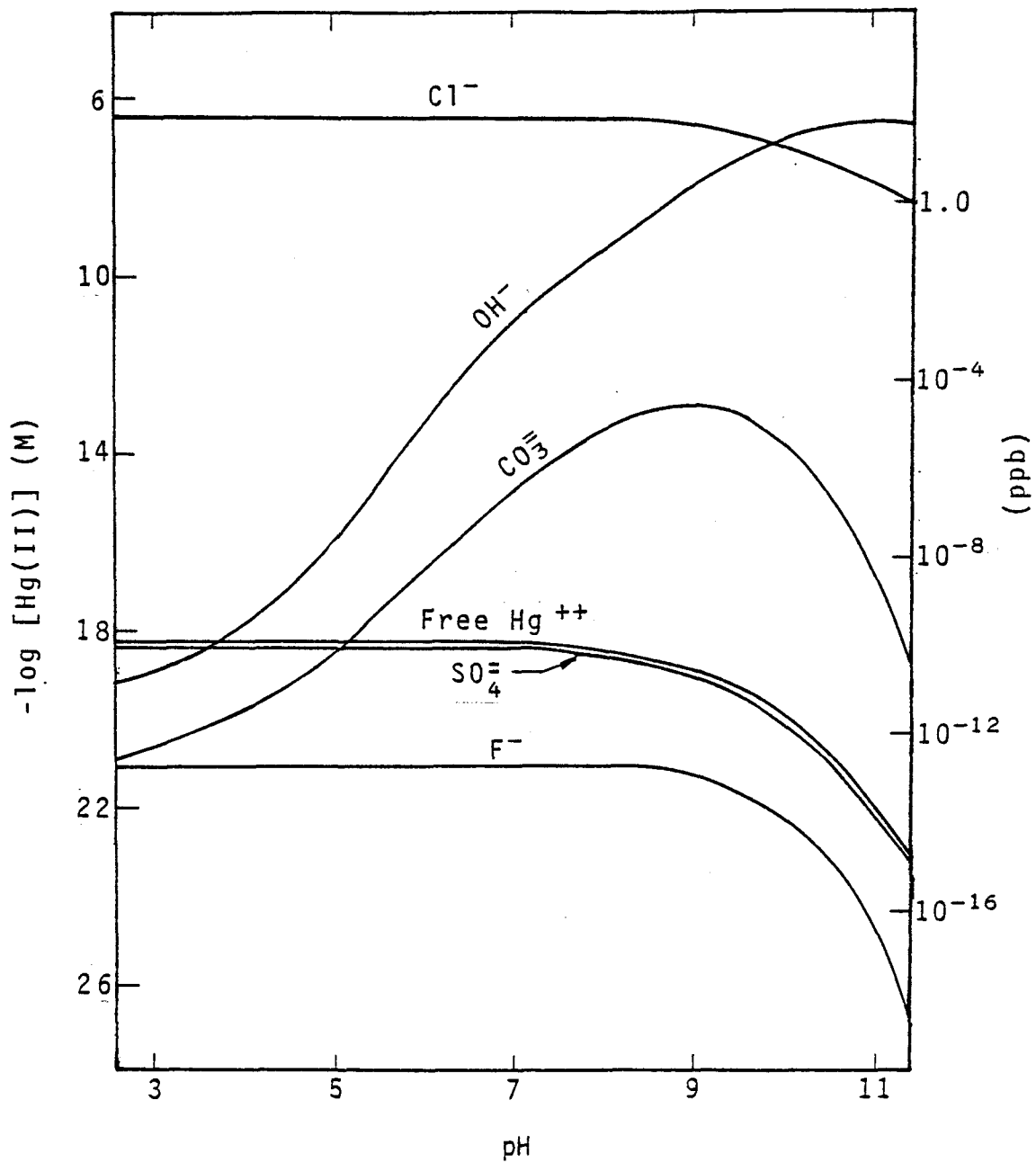
Figure 35. Speciation of Hg in raw FGD wastewater
at $I = 0.8$, $[Hg_T] = 10^{-6.47}M$.
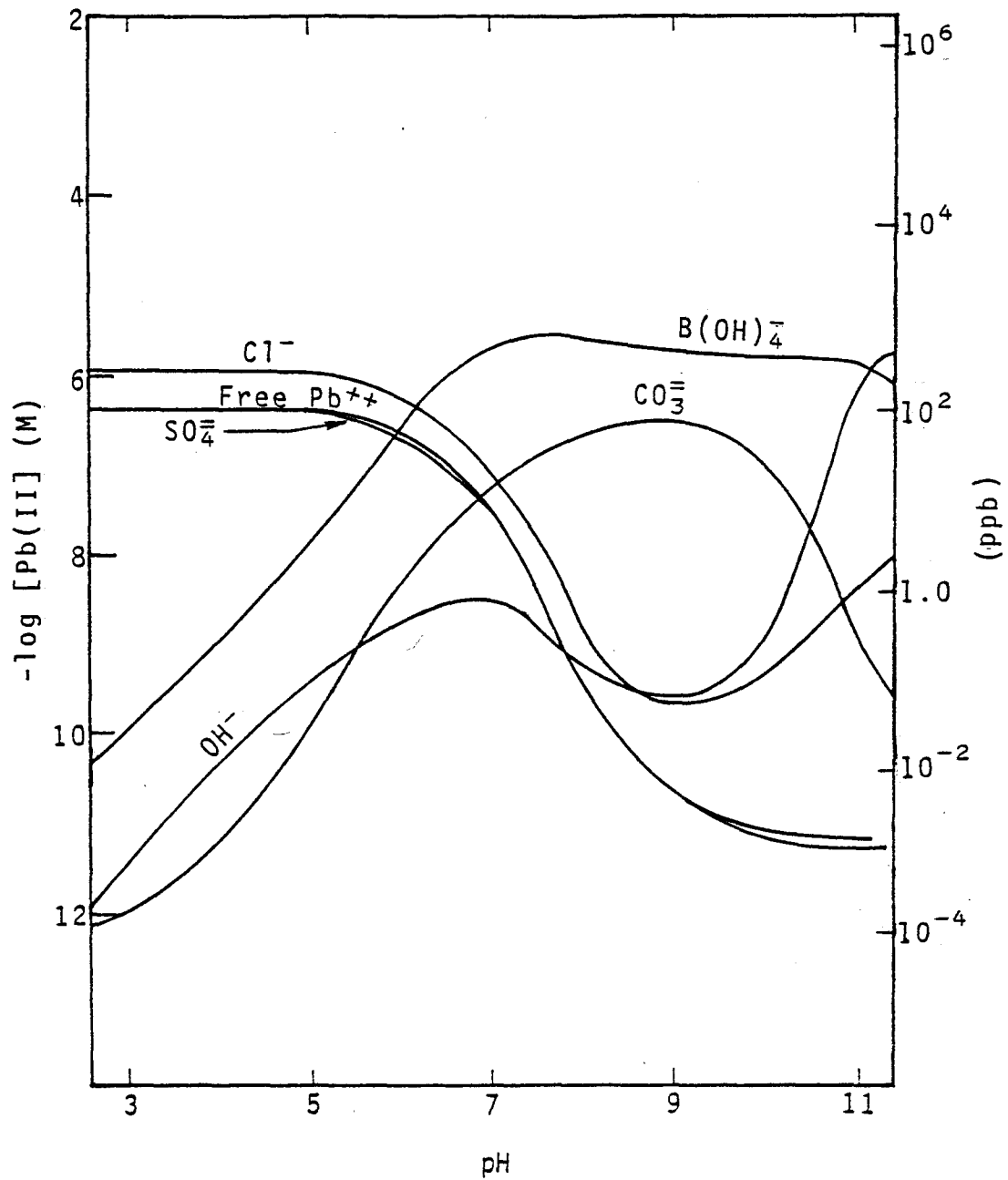
Figure 36. Speciation of Pb in raw FGD wastewater
at $I = 0.8$, $[Pb_T] = 10^{-5.71}M$.
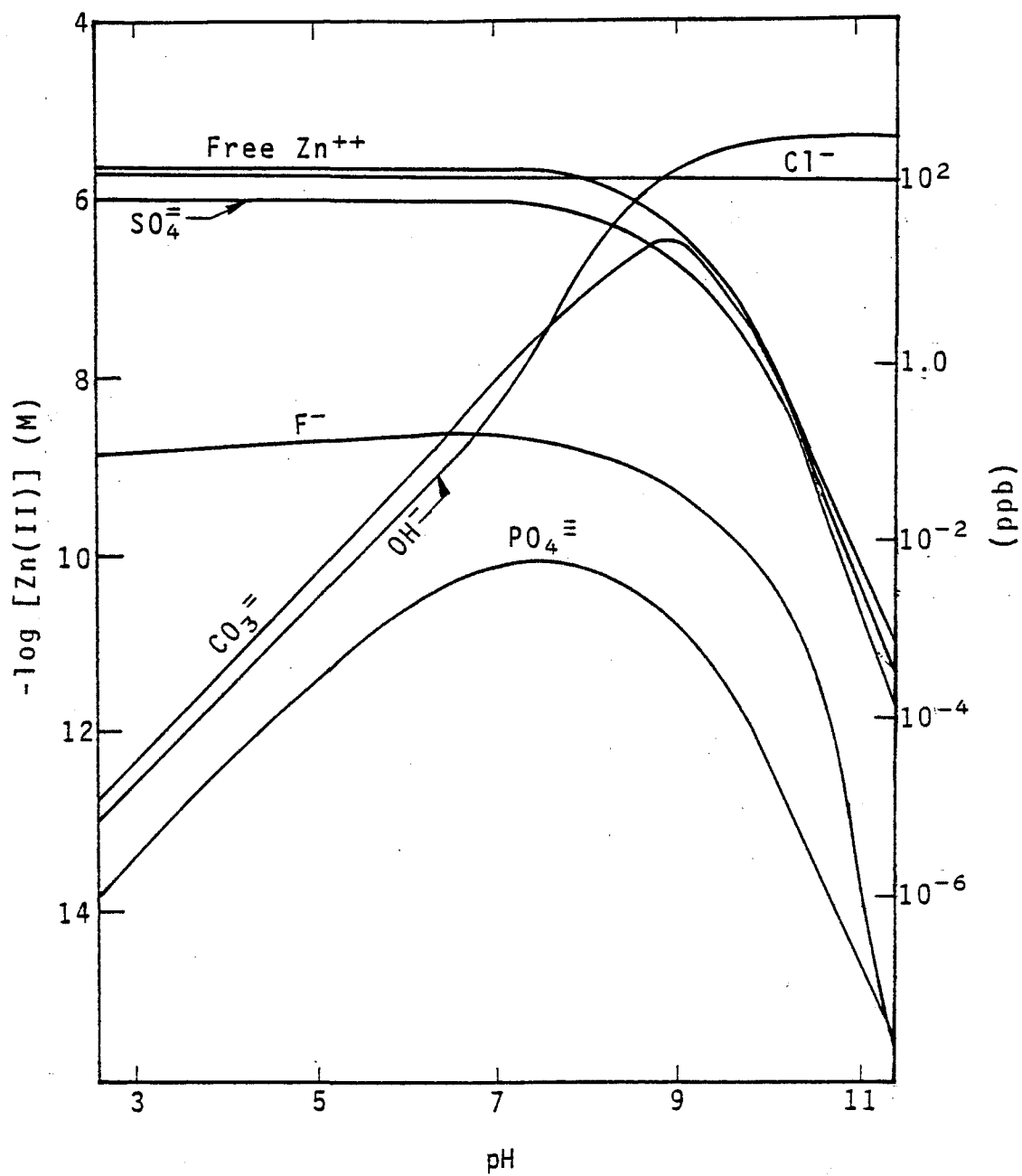
Figure 37. Speciation of Zn in raw FGD wastewater
at I = 0.8, $[Zn_T]$ = $10^{-5.67}$M.

From these diagrams, it can be seen that the major ions exist mainly as free ions. However, trace metals are complexed considerably in fresh FGD wastewater.

CONSTITUENT SPECIATION: LOW IONIC STRENGTH

In this section, the speciation of four major ions, Ca, Mg, K, and Na, and eleven minor ions, Cd, Cr, Cu, Fe, Hg, Pb, Zn, As, B, F, and Se will be discussed. The discussion will also cover the possible soluble complexes with the following important ligands: Cl^-, OH^-, SO_4^{2-}, CO_3^{2-}, $B(OH)_4^-$, SO_3^{2-}, F^-, PO_4^{3-}, $S_2O_3^{2-}$, MoO_4^{2-}, AsO_4^{3-}, HVO_4^{2-}, and SeO_3^{2-}. The major species and their percentage of the total concentrations for the constituents studied are listed in Table 7.

Calcium

The speciation of calcium in fresh FGD wastewater at low ionic strength (I = 0.05) is shown in Figure 16. This figure shows that the most significant soluble calcium species in this condition is the free calcium ion. This ion alone can account for from 78.4 percent (at pH 11) to 83.6 percent (at pH 3) of the total soluble calcium in fresh FGD wastewater. The second significant species is $CaSO_4(aq)$, which may account for 16.4 percent to 16.5 percent of the total calcium concentration. The calcium-carbonate and calcium-hydroxide complexes are significant only in the high pH region. At pH 11, for example, $CaCO_3(aq)$ and $CaHCO_3^+(aq)$ constitute about 2 percent of the total soluble calcium content. At lower pH levels, the carbonate complex concentration becomes negligible. Other less significant species (e.g., fluoride and phosphate complexes) may also exist. Other ligands considered (Cl^-, $B(OH)_4^-$, SO_3^{2-}), cannot form stable complexes with calcium.

Magnesium

The speciation of magnesium in fresh FGD wastewater at I = 0.05 is presented in Figure 17. The relative importance of ligands in magnesium complexation is similar to that of calcium. The majority of soluble magnesium also exists as a free ion, ranging from 59.0 percent (at pH 11) to 80.2 percent (at pH 3). $MgSO_4(aq)$ is the second important soluble species of magnesium, and can range from 15.7 percent (at pH 11) to 19.8 percent (at pH 3). The relatively minor concentrations of other magnesium complexes are shown in Figure 17.

Potassium

Thermodynamic calculations show that there are only two significant soluble species for potassium in FGD wastewaters: free K^+, and KSO_4^- (97.2 percent and 2.8 percent, respectively).

94

TABLE 7. DISTRIBUTIONS OF CHEMICAL SPECIES IN LOW-IONIC-STRENGTH FRESH FGD WASTEWATER (AT pH 7)

Major Ions	Major Species	Percentage
Calcium	Ca^{2+}	82.8
	$CaSO_4(aq)$	17.2
Magnesium	Mg^{2+}	79.2
	$MgSO_4(aq)$	20.7
Potassium	K^+	97.2
	KSO_4^-	2.8
Sodium	Na^+	98.8
	$NaSO_4^-$	1.2
Minor Ions		
Cadmium	Cd^{2+}	48.6
	$CdSO_4(aq)$	10.1
	$CdCl_1^+ + CdCl_2(aq) + CdCl_3^-$ $+ CdCl_4^{2-} + CdCl_5^{3-}$	40.9
Chromium	$CrOH^{2+} + Cr(OH)_2^+ + Cr(OH)_4^-$	100
Copper	Cu^{2+}	1.1
	$CuCl_1^+ + CuCl_2(aq) + CuCl_3^-$ $+ CuCl_4^{2-} + CuOHCl(aq)$	0.9
	$CuB(OH)_4^+ + Cu(B(OH)_4)_2(aq)$	97.9
Iron (III)	$FeOH^{2+} + Fe(OH)_2^+ + Fe(OH)_4^-$ $+ Fe_2(OH)_2^{4+}$	99.6
	$FeB(OH)_4^{2+} + Fe(B(OH)_4)_2^+$	0.3
Mercury	$HgCl^+ + HgCl_2(aq) + HgCl_3^-$ $+ HcGl_4^{2-} + HgOHCl(aq)$	99.5
	$HgOH^+ + Hg(OH)_2(aq) + Hg(OH)_3^-$ $+ Hg_2OH^{3+}$	0.5

TABLE 7 (continued)

Minor Ions	Major Species	Percentage
Lead	Pb^{2+}	18.7
	$PbCO_3(aq) + Pb(CO_3)_2^{2-} + PbHCO_3^+$ $+ Pb(HCO_3)_2(aq)$	8.6
	$PbSO_4(aq)$	9.8
	$PbCl_1^+ + PbCl_2(aq) + PbCl_3^-$ $+ PbCl_4^{2-} + PbOHCl(aq)$	5.3
	$PbB(OH)_4^+ + Pb(B(OH)_4)_2(aq)$	55.3
	$PbOH^+ + Pb(OH)_2(aq) + Pb(OH)_3^-$	2.3
Zinc	Zn^{2+}	
	$ZnSO_4(aq)$	
	$ZnCl^+ + ZnCl_2(aq) + ZnCl_3^-$ $+ ZnOHCl(aq) + ZnCl_4^{2-}$	10.0
Arsenic	$HAsO_4^{2-} + H_2AsO_4^-$	100
Boron	$B(OH)_4^-$	1.1
	$HB(OH)_4(aq)$	98.9
Fluorine	F^-	91.4
	CaF^+	5.4
	$BeF^+ + BeF_2(aq) + BeF_3^-$	0.8
	$SnF^+ + SnF_2(aq) + SnF_3^-$	2.1
Selenium	SeO_3^{2-}	6.1
	$HSeO_3^- + H_2SeO_3(aq)$	93.9

Copper

Copper can form complex species with $B(OH)_4^-$, OH^-, Cl^-, CO_3^{2-}, SO_4^{2-}, PO_4^{3-}, and F^- ligands. However, at low pH levels (pH 5), these complexes account for only 29 to 45 percent of the total soluble copper; free Cu^{2+} is the predominant species here. When the pH is greater than 5, $B(OH)_4^-$ can account for 24 percent to 99.9 percent of the total soluble copper (depending on pH).

At pH 7, the relative distribution of copper in fresh FGD wastewater was shown in Table 7. At this pH level, the Cu^{2+}-$B(OH)_4^-$ complexes comprise about 97.7 percent of the total soluble copper. The two borate complexes, $CuB(OH)_4^+$ and $Cu(B(OH)4)_2(aq)$ exist at approximately equal concentrations at pH 7. When the pH is higher than 7, $Cu(B(OH)4)_2(aq)$ will predominate (see Figure 22).

Iron

The calculated concentrations of soluble iron(III) species are presented in Figure 23. As is the case with chromium, hydroxide complexes are the most important soluble species for Fe(III). Their existence can account for 27 to almost 100 percent of the total soluble Fe(III), depending on pH. Other species such as free Fe^{3+}, $FeSO_4^+$, and Fe-$B(OH)_4^-$ complexes (mainly $FeB(OH)_4^{2+}$) may become significant at a pH below 4.

Mercury

The speciation of mercury in fresh FGD wastewater is presented in Figure 24. Results of thermodynamic calculations show that when the pH is less than about 8.5, Hg^{2+}-Cl^- complexes (primarily $HgCl_2(aq)$) are the predominant soluble mercury species. These species can account for 50 to almost 100 percent of the total soluble mercury. When the pH exceeds 8.5, Hg-OH complexes (primarily $Hg(OH)_2(aq)$ become the principal soluble mercury species. Other soluble mercury species, such as Hg-CO_3 complexes (including $HgCO_3(aq)$ and $HgHCO_3^+$), free metal ions, Hg^{2+}, Hg-SO_4 complexes (including $HgSO_3(aq)$ and $Hg(SO_4)_2^{2-}$), and HgF^+ will also exist in low concentrations.

Lead

The distribution of soluble lead species is shown in Figure 25. Soluble lead speciation shows two distinct trends: concentrations of free metal ions, Pb^{2+}, Pb-SO_4 complexes, and Pb-Cl complexes decrease when pH increases; concentrations of Pb-$B(OH)_4$ complexes, Pb-OH complexes, and Pb-CO_3 complexes increase when pH increases. The division occurs at about pH 7. As can be seen in the diagram, free Pb^{2+} is the dominant lead species below pH 7. When the pH is higher than 7, borate complexes dominate; $Pb(B(OH)_4)_2(aq)$ is the most important species under this condition. The relative distribution of the primary species at pH 7 is

listed in Table 7. Examination of this table shows almost all the possible lead-ligand complexes to comprise at least two percent of the total soluble lead. This distribution phenomenon is quite different from the other elements studied.

Zinc

Thermodynamic calculations showing that zinc forms predominantly hydroxide complexes (primarily $Zn(OH)_2(aq)$) in fresh FGD wastewaters when the pH is higher than 8.5. In this pH region, carbonate, sulfate, chloride, fluoride, and phosphate complexes also may be formed but in trace amounts only (see Figure 26). When the pH is below 8.5, free zinc ion is the predominant species and accounts for 50 to 75 percent of the total soluble zinc (depending on the pH level). In this pH region, $ZnSO_4(aq)$ and Zn-Cl complexes can account for about 15 percent and 10 percent, respectively, of the total soluble zinc. Other zinc complexes occur at insignificant levels.

Arsenic, Boron, Fluorine, and Selenium

Arsenic (As), boron (B), fluorine (F), and selenium (Se) in FGD wastewater exist as ligands. Among these four elements, boron (existing as borate, $B(OH)_4^-$) and fluorine (existing as fluoride, F^-) serve as important ligands for certain trace metals, $B(OH)_4^-$ for Cu and Pb, and F^- for Sn. Arsenic and selenium exist either alone as free ligands, or in association with hydrogen ions.

Although borate forms predominant complexes with certain trace metals, the relatively low metal concentrations and high borate concentrations will force the majority of borate ions to exist either as free ions ($B(OH)_4^-$) or as $HB(OH)_4(aq)$. The fluoride species, however, will complex with a variety of metals under different pH levels. The following calculated results show the complexing trends of soluble fluoride species in low ionic strength in fresh FGD wastewater:

pH	Species	Distribution (% of available fluoride)
3	SnF^+	94.5
	AlF^{2+}	2.4
	F^-	1.7
	$HF(aq)$	1.2

pH	Species	Distribution (% of available fluoride)
5	SnF^+	52.2
	F^-	24.6
	$AlF^{2+} + AlF_2^+$	20.8
5	CaF^+	1.4
	BeF^+	0.7
7	F^-	91.4
	CaF^+	5.4
	SnF^+	2.1
	BeF^+	0.8
9	F^-	94.2
	CaF^+	5.5
11	F^-	94.6
	CaF^+	5.2

In the low ionic strength, fresh FGD wastewater, arsenic exists primarily as $HAsO_4^{2-}$, $H_2AsO_4^-$ and AsO_3^{3-}. These three species comprise almost 100 percent of the total soluble arsenic. The calculated distribution of these three species is as follows:

pH	Species	Distribution (% of available arsenic)
5	$H_2AsO_4^-$	97.7
	$HAsO_4^{2-}$	2.3
7	$HAsO_4^{2-}$	66.9
	$H_2AsO_4^-$	33.1

pH	Species	Distribution (% of available arsenic)
9	$HAsO_4^{2-}$	99.0
	$H_2AsO_4^{-}$	0.5
	AsO_4^{3-}	0.5
11	$HAsO_4^{2-}$	67.1
	AsO_4^{3-}	32.9

Two selenium species predominate in fresh FGD wastewater: free $SeO_3^{=}$, and either $HSeO_3^{-}$ or $SeO_3^{=}$. The relative distribution of these species is shown below:

pH	Species	Distribution (% of available selenium
3	$HSeO_3^{-}$	72.4
	$H_2SeO_3(aq)$	26.9
	SeO_3^{2-}	0.7
5	$HSeO_3^{-}$	99.9
7	$HSeO_3^{-}$	93.3
	SeO_3^{2-}	6.1
	$H_2SeO_3(aq)$	0.6
9	SeO_3^{2-}	86.6
	$HSeO_3^{-}$	13.3
11	SeO_3^{2-}	99.8

CONSTITUENT SPECIATION: HIGH IONIC STRENGTH

The relative distribution of the important soluble species in high ionic strength (I = 0.80), fresh FGD wastewater is given in Table 8. In general, the relative distribution of the species

Major Ions	Major Species	Percentage
Calcium	Ca^{2+}	70.7
	$CaSO_4(aq)$	29.3
Magnesium	Mg^{2+}	65.6
	$MgSO_4(aq)$	34.2
Potassium	K^+	89.8
	KSO_4^-	10.2
Sodium	Na^+	95.7
	$NaSO_4^-$	4.3
Minor Ions		
Cadmium	Cd^{2+}	5.6
	$CdSO_4(aq)$	2.3
	$CdCl_1^+ + CdCl_2(aq) + CdCl_3^- + CdCl_4^{2-} + CdCl_5^{3-}$	33.5
	$Cd(SO_3)_2^{2-}$	58.5
Chromium	$CrOH^{2+} + Cr(OH)_2^+ + Cr(OH)_4^-$	99.9
Copper	$CuB(OH)_4^+ + Cu(B(OH)_4)_2(aq)$	99.4
Iron(III)	$FeOH^{2+} + Fe(OH)_2^+ + Fe(OH)_4^- + Fe_2(OH)_2^{4+}$	83.4
	$FeB(OH)_4^{2+} + Fe(B(OH)_4)_2^+$	9.2
	$FeSO_3^+$	7.4
Mercury	$HgCl^+ + HgCl_2(aq) + HgCl_3^- + HgCl_4^{2-} + HgOHCl(aq)$	100
Lead	Pb^{2+}	1.9
	$PbCO_3(aq) + Pb(CO_3)_2^{2-} + PbHCO_3^+$	0.5
	$PbSO_4(aq)$	2.0
	$PbCl^+ + PbCl_2(aq) + PbCl_3^- + PbCl_4^{2-} + PbOHCl(aq)$	4.9

TABLE 8 (continued)

Minor Ions	Major Species	Percentage
Lead	$PbB(OH)_4^+ + Pb(B(OH)_4)_2(aq)$	90.6
Major Ions		
Arsenic	$HAsO_4^{2-} + H_2AsO_4^-$	100
Boron	$B(OH)_4^-$	1.4
	$HB(OH)_4(aq)$	97.8
	$FeB(OH)_4^{2+}$	0.6
Fluorine	F^-	40.9
	CaF^+	6.3
	MgF^+	43.5
	$AlF^{2+} + AlF_2^+ + AlF_3(aq) + AlF_4^-$ $+ AlF_5^{2-} + AlF_6^{3-}$	3.8
	$BeF^+ + BeF_2(aq) + BeF_3^-$	4.7
	$SnF^+ + SnF_2(aq) + SnF_3^-$	0.8
Selenium	SeO_3^{2-}	10.3
	$HSeO_3^- + H_2SeO_3(aq)$	89.7

of major ions in both high and low ionic strength cases is quite similar. However, due to the tremendous increase in ligand concentrations, the relative distribution of trace metal species in high ionic strength wastewater can differ significantly from the low ionic strength distribution. The important calculated results for some selected elements are discussed below.

Major Ions

The major cations which exist in high ionic strength fresh FGD wastewater are calcium, magnesium, potassium, and sodium. The speciation of these four elements is displayed in Figures 27 through 30. Comparing the results of the high ionic strength and low ionic strength calculations (i.e., comparing Figures 27-30 with Figures 16-19), it can be found that all the soluble species of these four elements display similar concentration vs. pH patterns. The concentrations of calcium, magnesium, potassium, and sodium in the high ionic strength case are about 6, 920, 5, and 170 times higher, respectively, than those calculated for the low ionic strength case. The high ionic strength ligand concentrations are from 4 to 4,380 times higher (see Table 3). The increase in concentration of both the metals and ligands leads to an associated increase in the concentrations of soluble complexes (refer to Equation 27, Section 2). Therefore, the relative distribution of species shifts toward major ion complexes and away from free ions. This phenomenon can be observed by comparing the results shown in Table 8 to those in Table 7. For example, in the low ionic strength case, the ratio of Ca^{2+} to $CaSO_4(aq)$ is 82.8 to 17.2. In the high ionic strength case, the ratio becomes 70.7 to 29.3. Although the concentrations of soluble complexes is higher in high ionic strength fresh FGD wastewater, the majority of major ion soluble species still exist as free metal ions. This is because major ions, in general, have relatively low formation constants for complex species. The lack of variety of possible complex species (as can be seen in Appendix A) also limits the complexation trend.

Minor Ions

Eleven minor ions were considered in the high ionic strength case: cadmium, chromium, copper, iron, mercury, lead, zinc, arsenic, boron, fluorine, and selenium. The total soluble concentrations of these elements are listed in Table 3. The models used for calculation are equations 27-30, described in Section 2. The total soluble levels of the above mentioned elements were found to be from 6 to 2,200 times higher than in the low ionic

strength case. The following table summarizes the approximate ranges of concentration differences for each element:

Concentration ratio of elements (high ionic strength to low ionic strength)	Elements
1-10	B
10-50	Cd, Cr, Pb, Zn
50-100	As, Cu
100-1,000	Fe, Hg, F
1,000	Se

The thermodynamic calculations show that the relative distribution of soluble species for cadmium, copper, iron, lead, zinc, and fluorine are significantly different from the low ionic strength results (comparing Figures 20-26 with Figures 31-37, and Table 7 with Table 8). The distribution patterns of soluble species for chromium, mercury, arsenic, selenium, and boron, however, are similar to those of Case I results.

Figure 31 shows that the Ca-Cl complexes (primarily $CdCl^+$) and the $Cd(SO_3)_2^-$ complex may become the predominant species of cadmium in the high ionic strength case. The free metal ion, Cd^{2+}, and $Cd-CO_3$ complexes (which are among the predominant species in the low ionic strength case) are less significant in relation to total soluble cadmium.

The speciation of chromium in the high ionic strength case is shown in Figure 32. By comparing this diagram with Figure 21, it can be seen that the relative distribution of soluble chromium species is quite similar in both high and low ionic strength cases. The predominant species of chromium at pH greater than 4 are the Cr-OH complexes. For pH lower than 4, Cr^{3+} is the predominant chromium species.

In the high ionic strength case, Cu-Cl complexes (primarily $CuCl^+$), are the predominate copper species when the wastewater pH is less than 5 (Figure 33). At corresponding pH levels, however, free Cu^{2+} is the predominant species for low ionic strength wastewater (Figure 22). When the pH is higher than 5, $Cu-B(OH)_4$ complexes are the major species for both high and low ionic strength wastewaters.

Figure 34 indicates that the predominant species of soluble Fe(III) can shift with increasing ionic strength from hydroxide complexes (Figure 23) to sulfite complex ($FeSO_3^+$) in the low pH

104

regions (pH 6.5). This is due to both the high sulfite level in high ionic strength FGD wastewater, and the relatively high formation constant of $FeSO_3^+$ species.

The speciation pattern of mercury in the fresh high ionic strength wastewater is quite similar to that of the low ionic strength wastewater (see Figures 24 and 35). The only significant difference between these two cases is that the region of Hg-Cl predominance can be extended from pH 8 to about pH 10. This phenomenon is due primarily to the increase in HgOHCl(aq) concentration at high pH.

When the pH exceeds 6, the predominant species for lead in high ionic strength wastewater is the $Pb-B(OH)_4$ complex (Figure 36). The same complex predominates in the low ionic strength case at a pH higher than 7 (Figure 25). However, in the high ionic strength acidic region, the predominant species for soluble lead will be Pb-Cl complexes (mainly $PbCl^+$) rather than free Pb^{2+} ion.

In high ionic strength wastewater, as in the low ionic strength case, free Zn^{2+} is still the predominant soluble zinc species when the pH is lower than 8. However, the second most predominant species changes from $ZnSO_4$(aq) to Zn-Cl complexes (primarily $ZnCl^+$) (Figure 37). A similar situation exists at high pH levels (pH 9), where Zn-OH complexes (primarily $Zn(OH)_2$(aq) are the predominant species, followed in importance by Zn-Cl complexes (primarily (ZnOHCl(aq)). Between pH 8 and 9, the Zn-Cl complexes may become the predominant species. Therefore, chloride concentration will also play an important role in the speciation of zinc in FGD wastewater.

For the speciation of arsenic, selenium, and boron, very little change results from a variation in the ligand concentrations (see Tables 7 and 8). The major factor affecting the distribution of species for these elements is the pH value of the wastewater. For fluoride, the percent distribution of free fluoride will be reduced due to the formation of significant complexes with Ca^{2+}, Mg^{2+}, Al^{3+}, and Sn^{2+}. This can be seen by comparing Tables 7 and 8.

105

SECTION 5

CONSTITUENT SPECIATION IN AGED FGD SLUDGE

The speciation of constituents in aged FGD wastes was also evaluated for both low and high ionic strength conditions. It was assumed that the equilibrium condition among all the soluble and solid species in the aged FGD wastes had been reached. The concentrations of constituents used for the speciation computation are compiled in Table 9. These data are derived from Ref. 1, 5, and 36. Only the median levels of constituents in FGD sludge were used for the computation. The models used for calculation are discussed in Section 1. The results are discussed in the following sections.

CONSTITUENT SPECIATION: LOW IONIC STRENGTH

In the low ionic strength speciation computation, twenty important metals and thirteen important ligands in FGD sludge were included. The total concentrations of constituents selected for use are the lowest levels present in FGD sludge. Calculated results can be viewed as the least deleterious situation in terms of leachate quality. Results of the speciation calculation for selected constituents in FGD sludge at low ionic strength ($I = 0.05$) are presented in Figures 38 through 59.

Results show that in the aged FGD wastes, the total soluble levels and species of constituents can be greatly affected by the solid phases. It can also be seen that the distribution of species is pH-dependent.

Calcium

The speciation diagram of calcium (Figure 38) shows that the most predominant soluble calcium species in the aged, low ionic strength FGD wastewater is the free Ca^{2+} ion. $Ca-SO_4$ complex is the second predominant soluble species for calcium; however, its concentration becomes significant only at high pH levels (pH 9).

It is evident from comparing Figures 16 and 38, that the levels of soluble calcium species will increase with aged in FGD wastes for low pH levels (pH 9). This is especially true for the free Ca^{2+} ion.

106

TABLE 9. TOTAL LEVELS OF CONSTITUENTS IN AGED FGD SYSTEMS USED FOR COMPUTATION

Constituent	Total Concentrations in FGD Wastes (Aqueous and Solid Phases)	
	I = 0.05 (M)	I = 0.8 (M)
Ca	$10^{0.19}$	$10^{0.21}$
Mg	$10^{-3.91}$	$10^{-0.95}$
K	$10^{-1.89}$	$10^{-1.87}$
Na	$10^{-1.36}$	$10^{-0.83}$
Fe	$10^{-0.57}$	$10^{-0.57}$
Mn	$10^{-3.46}$	$10^{-3.41}$
Cu	$10^{-4.18}$	$10^{-4.16}$
Cd	$10^{-4.97}$	$10^{-4.97}$
Zn	$10^{-3.58}$	$10^{-3.57}$
Ni	$10^{-4.06}$	$10^{-3.95}$
Hg	$10^{-5.83}$	$10^{-5.74}$
Pb	$10^{-4.69}$	$10^{-4.65}$
Co	$10^{-2.87}$	$10^{-2.86}$
Ag	$10^{-4.56}$	$10^{-4.48}$
Cr	$10^{-4.03}$	$10^{-3.99}$
Al	$10^{-5.95}$	$10^{-4.95}$
Be	$10^{-3.97}$	$10^{-3.91}$
Sn	$10^{-3.06}$	$10^{-3.06}$
Ba	$10^{-2.76}$	$10^{-2.76}$
CO_3	$10^{-0.20}$	$10^{-0.20}$
SO_4	$10^{-0.45}$	$10^{-0.35}$

TABLE 9 (continued)

Constituent	Total Concentrations in FGD Wastes (Aqueous and Solid Phases)	
	$I = 0.05$ (M)	$I = 0.8$ (M)
Cl	$10^{-1.93}$	$10^{-0.87}$
F	$10^{-2.2}$	$10^{-2.17}$
PO_4	$10^{-6.50}$	$10^{-5.36}$
SiO_3	$10^{-5.15}$	$10^{-3.93}$
$B(OH)_4$	$10^{-2.57}$	$10^{-2.21}$
SO_3	$10^{-0.24}$	$10^{-0.21}$
MoO_4	$10^{-3.95}$	$10^{-3.80}$
AsO_4	$10^{-3.88}$	$10^{-3.87}$
HVO_4	$10^{-3.45}$	$10^{-3.43}$
SeO_3	$10^{-4.58}$	$10^{-4.27}$
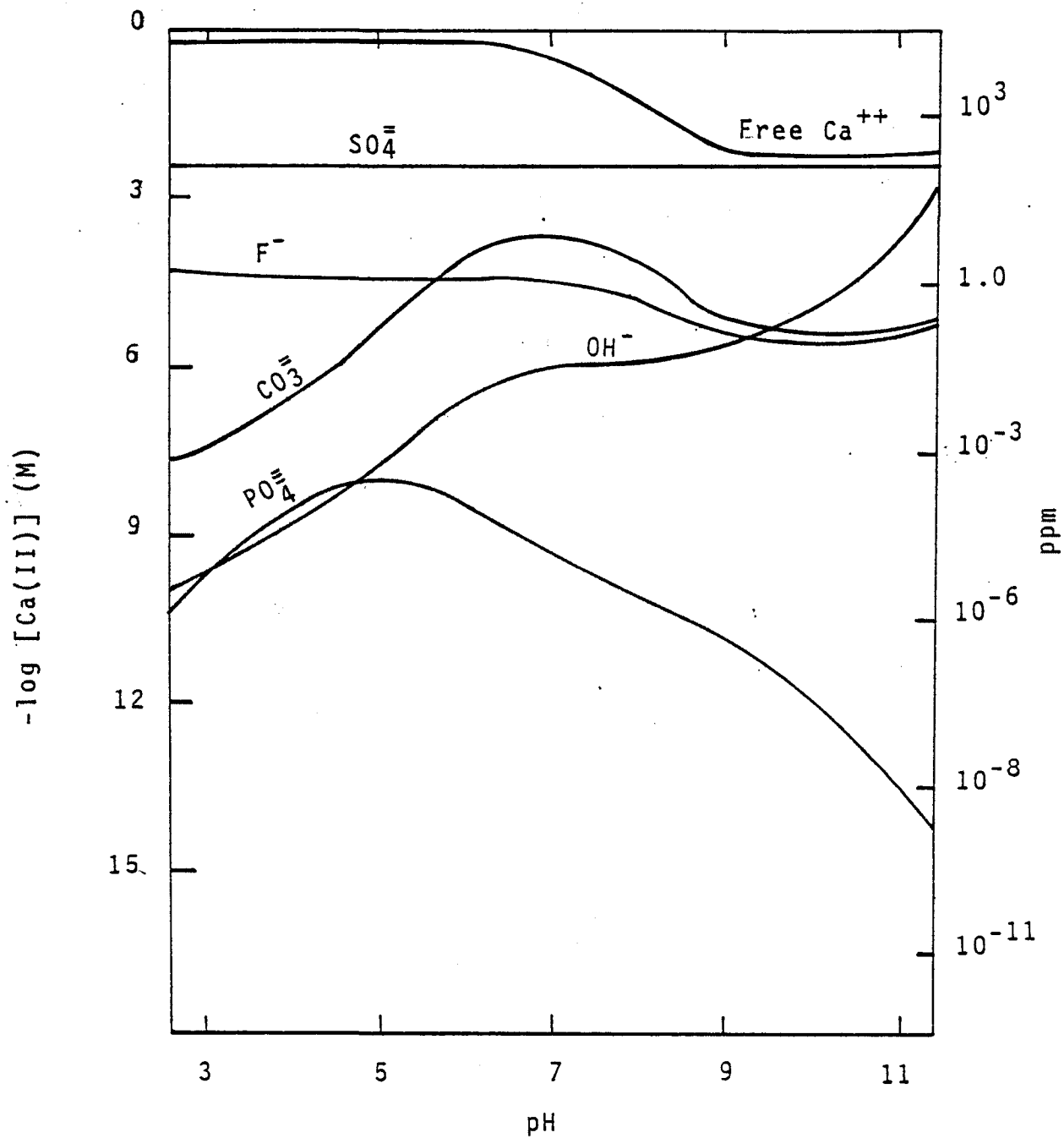
Figure 38. Speciation of soluble Ca in aged FGD wastes
at I = 0.05, original $[Ca_T]$ = $10^{0.19}$M.
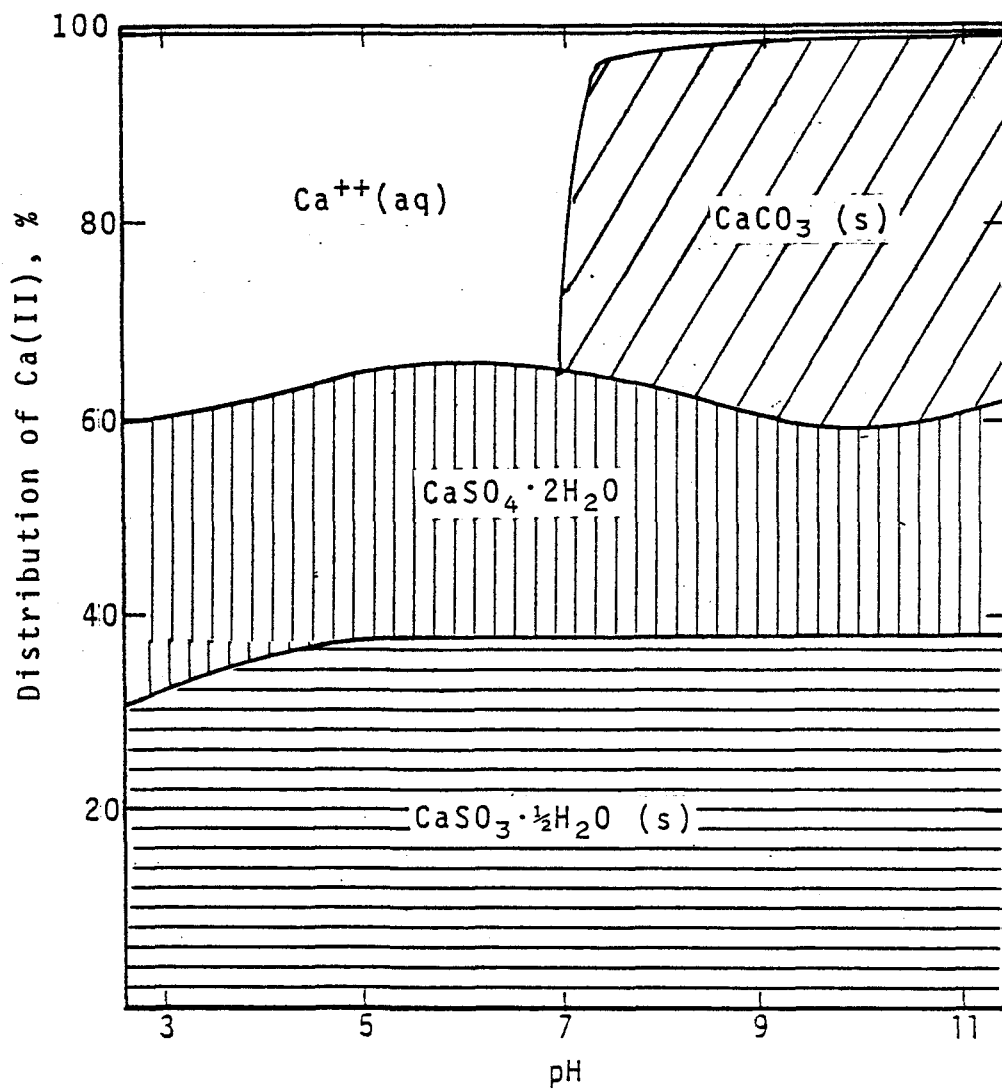
Figure 39. Primary distribution of Ca in aged FGD wastes at I = 0.05, original $[Ca_T] = 10^{0.19} M$.
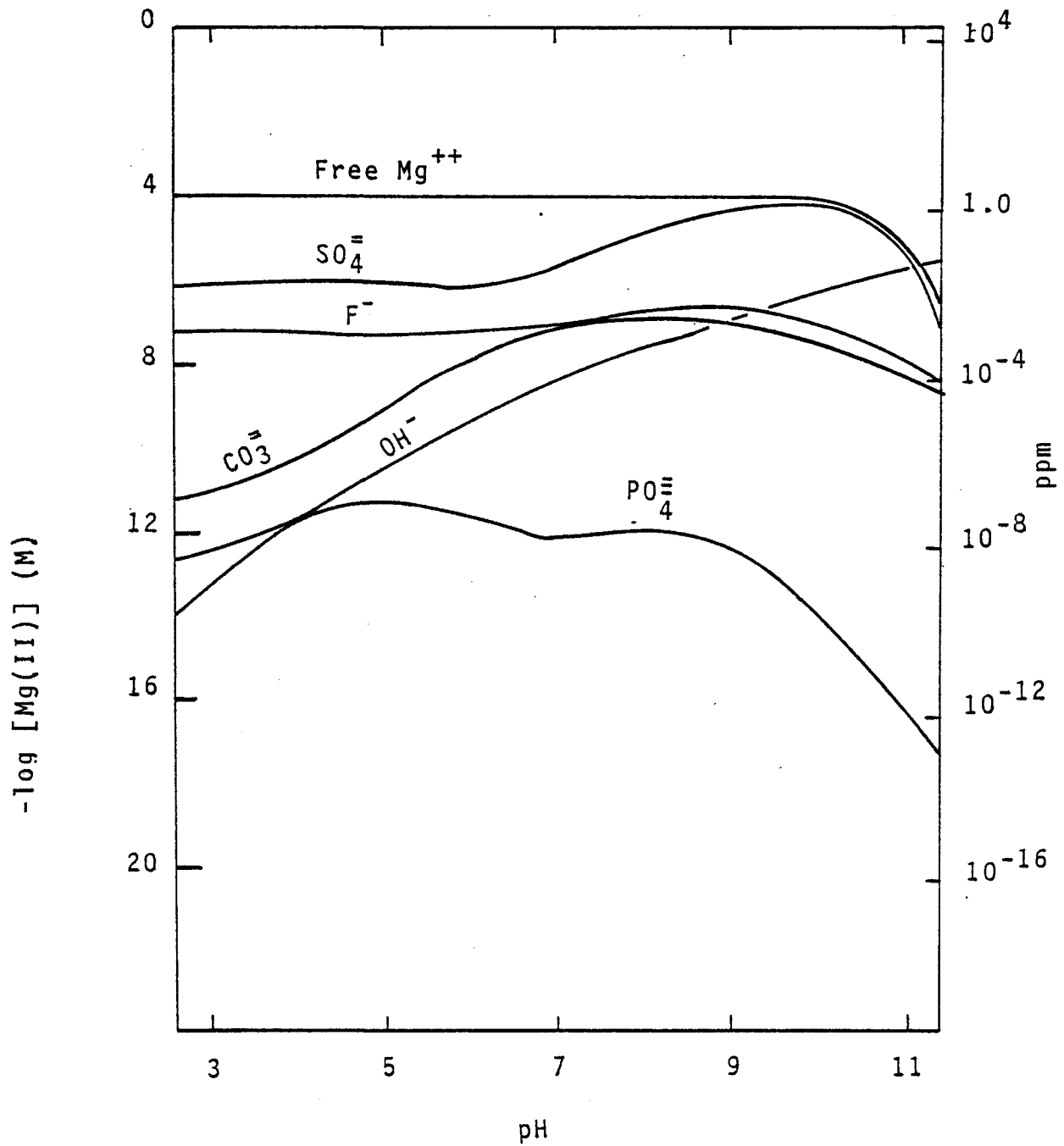
Figure 40. Speciation of soluble Mg in aged FGD wastes at I = 0.05, original $[Mg_T] = 10^{-3.91}M$.
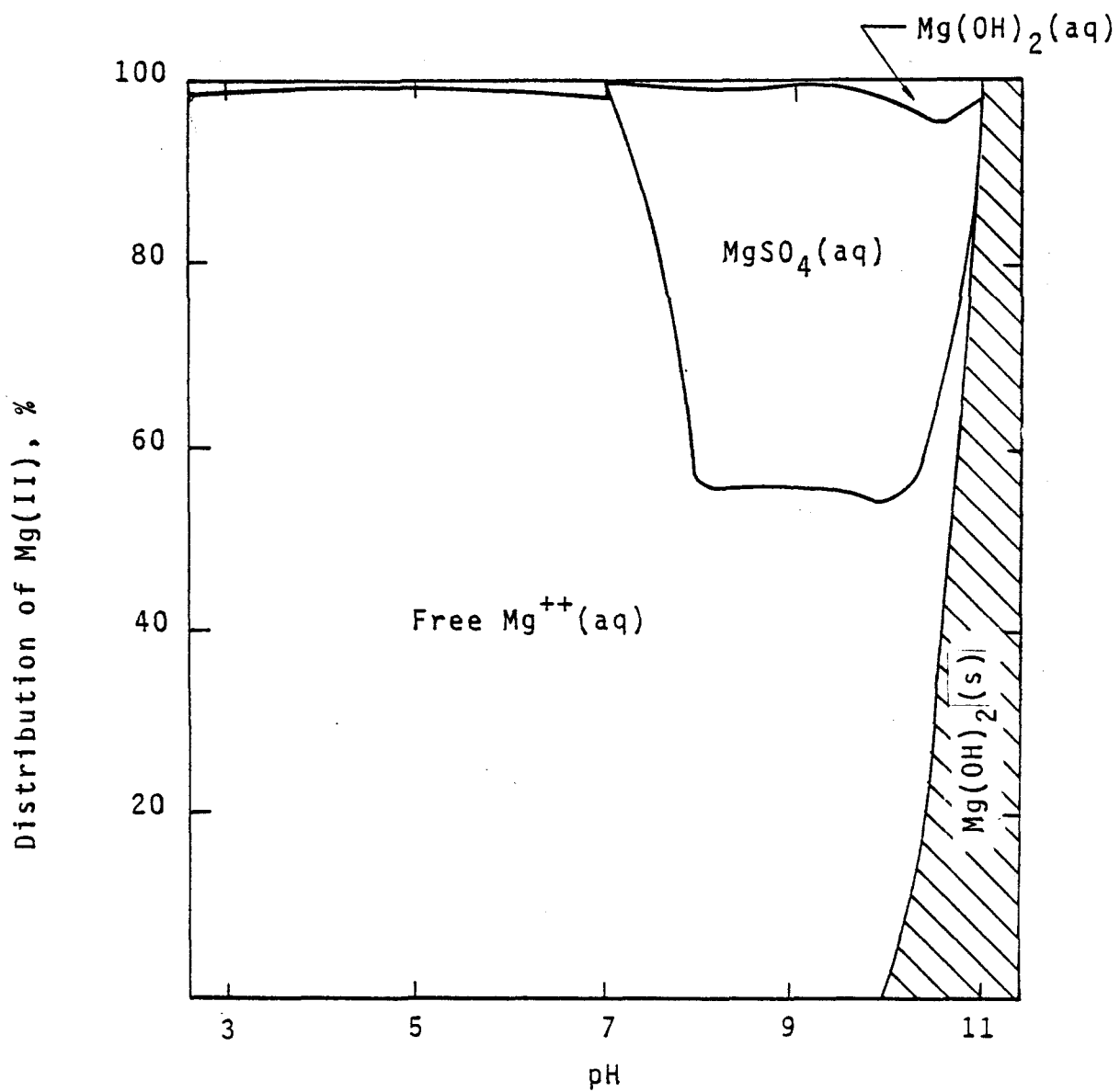
Figure 41.   Primary distribution of Mg in aged FGD wastes
at I = 0.05, original $[Mg_T]$ = $10^{-3.91}$M.
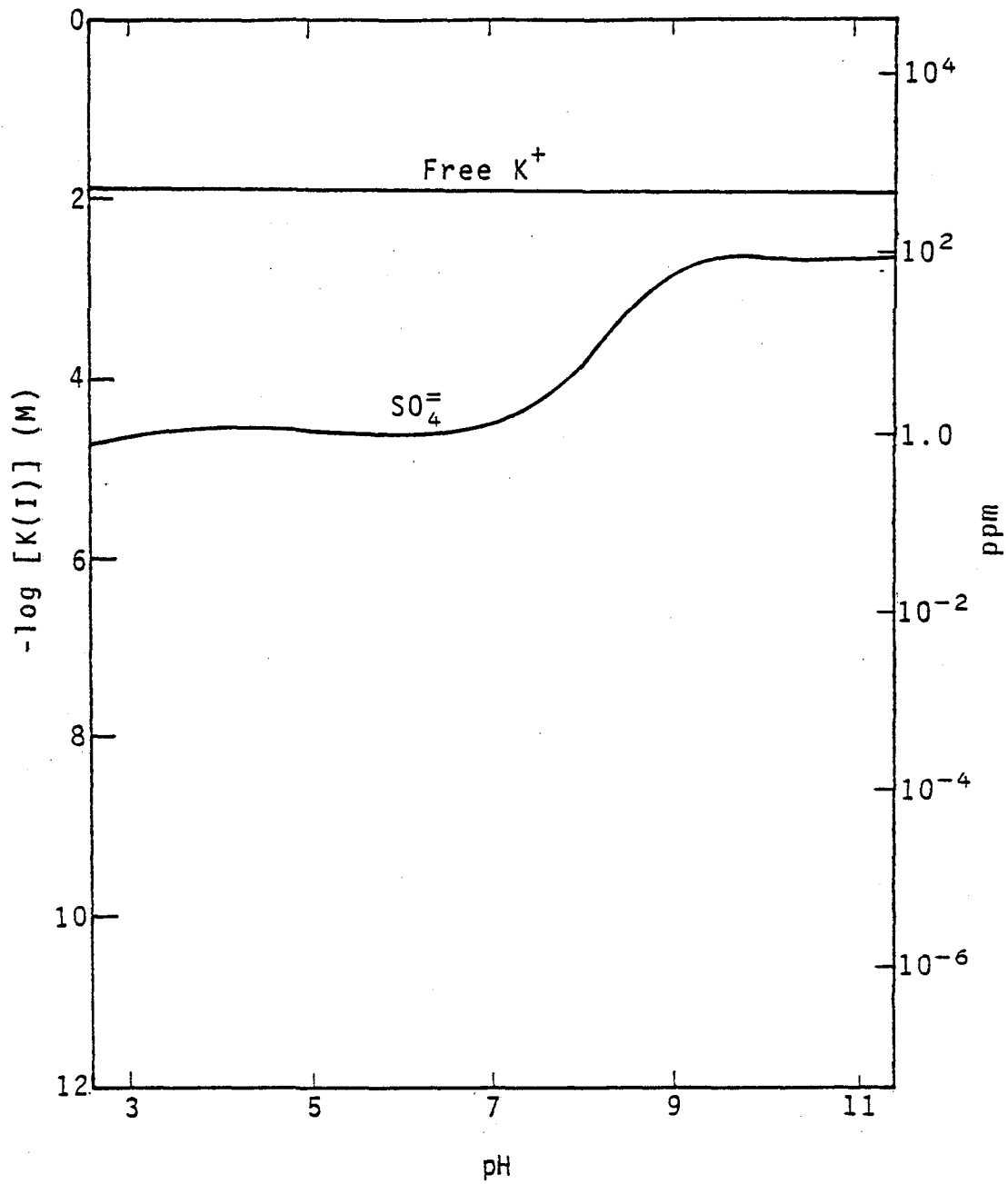
Figure 42. Speciation of soluble K in aged FGD wastes at I = 0.05, original $[K_T] = 10^{-1.89}M$.
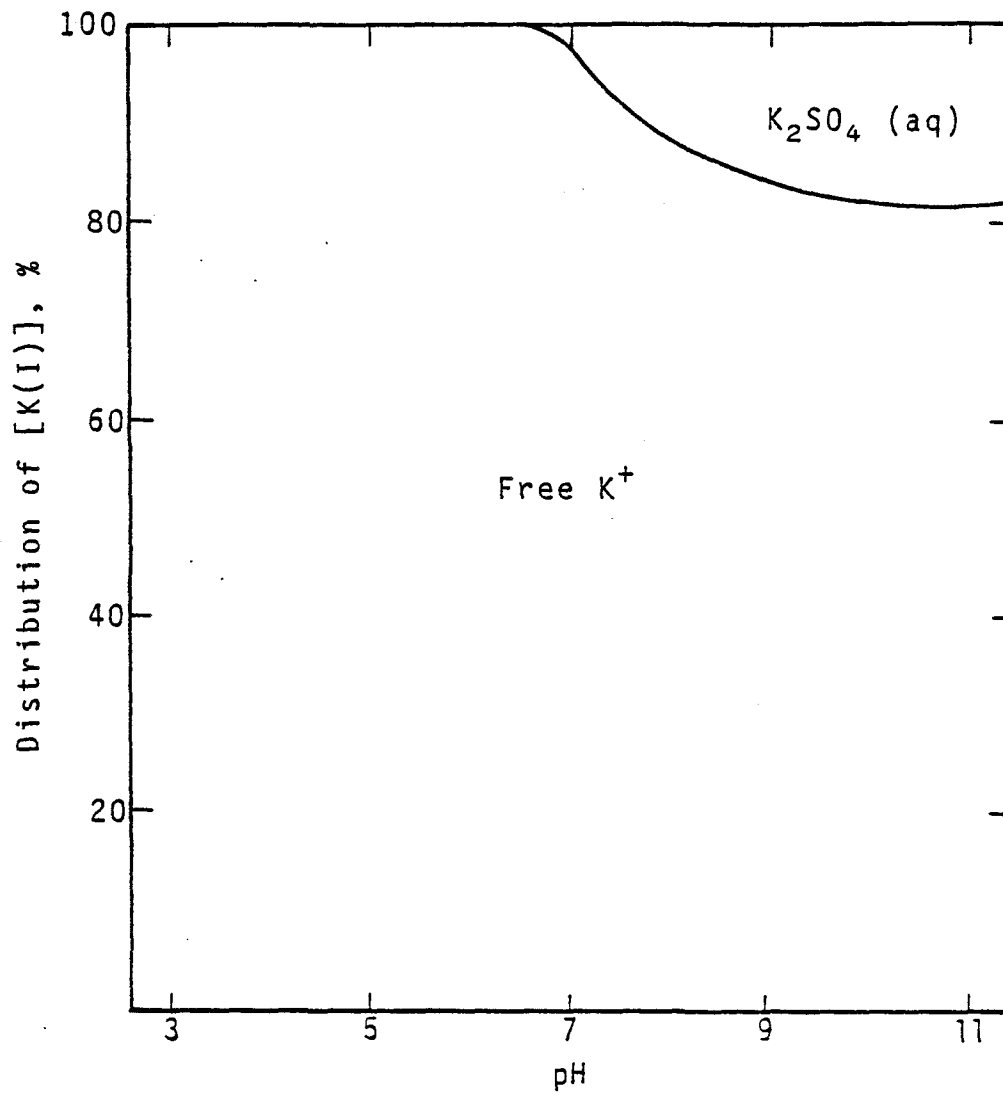
Figure 43. Primary distribution of K in aged FGD wastes
at I = 0.05, original $[K_T] = 10^{-1.89}M$.
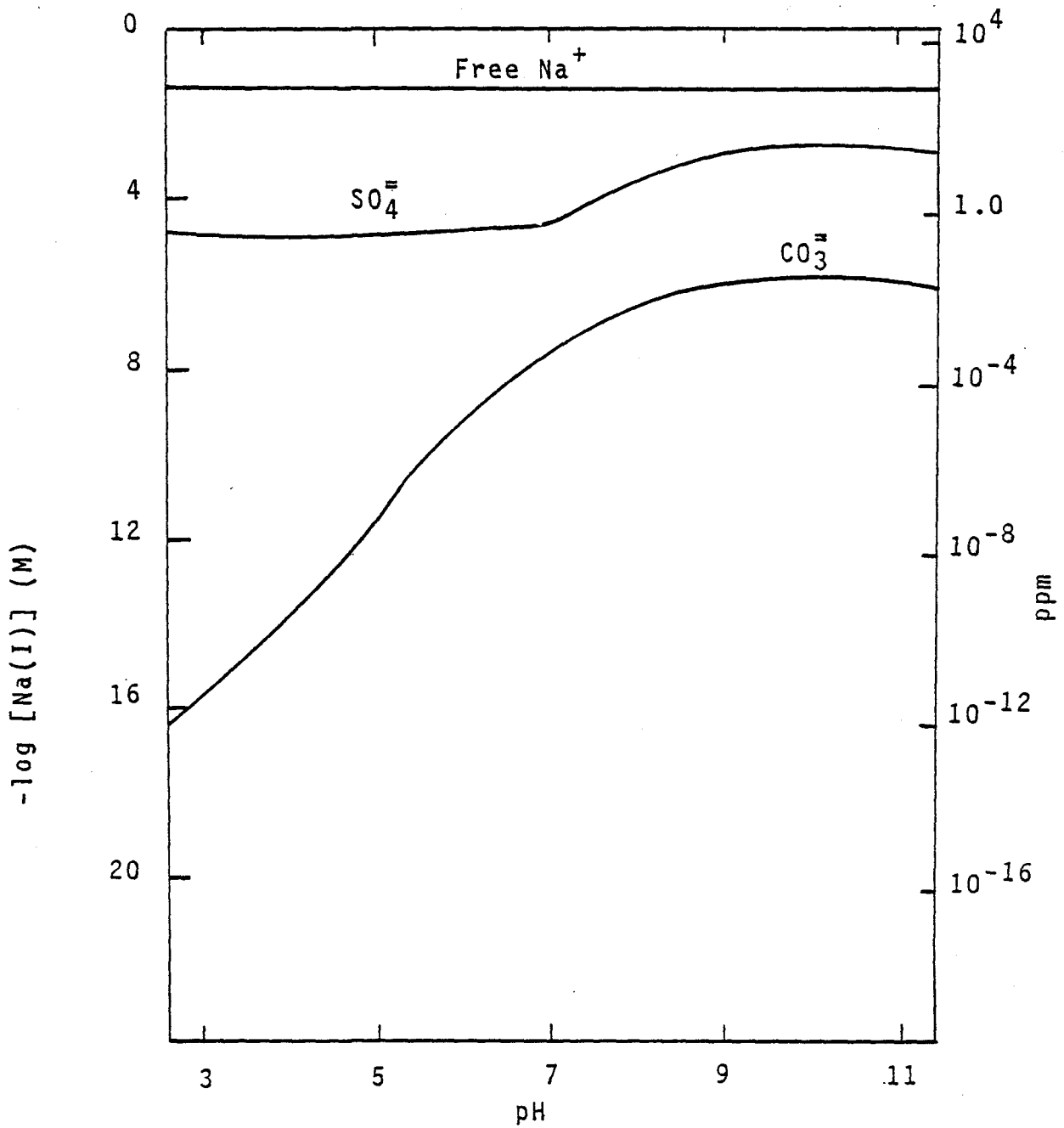
Figure 44. Speciation of soluble Na in aged FGD wastes
at I = 0.05, original $[Na_T]$ = $10^{-1.36}$M.
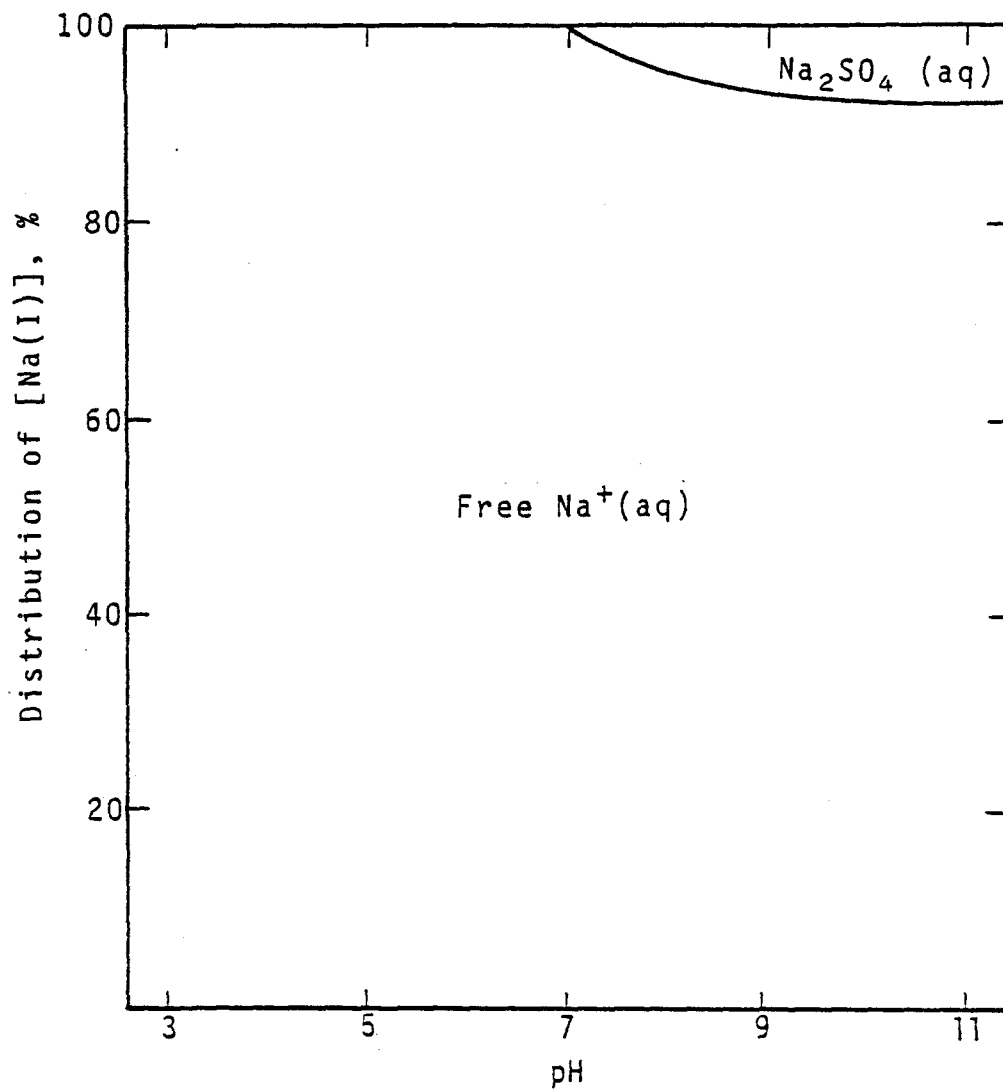
Figure 45.   Primary distribution of Na in aged FGD wastes
at I = 0.05, original $[Na_T] = 10^{-1.36}M$.
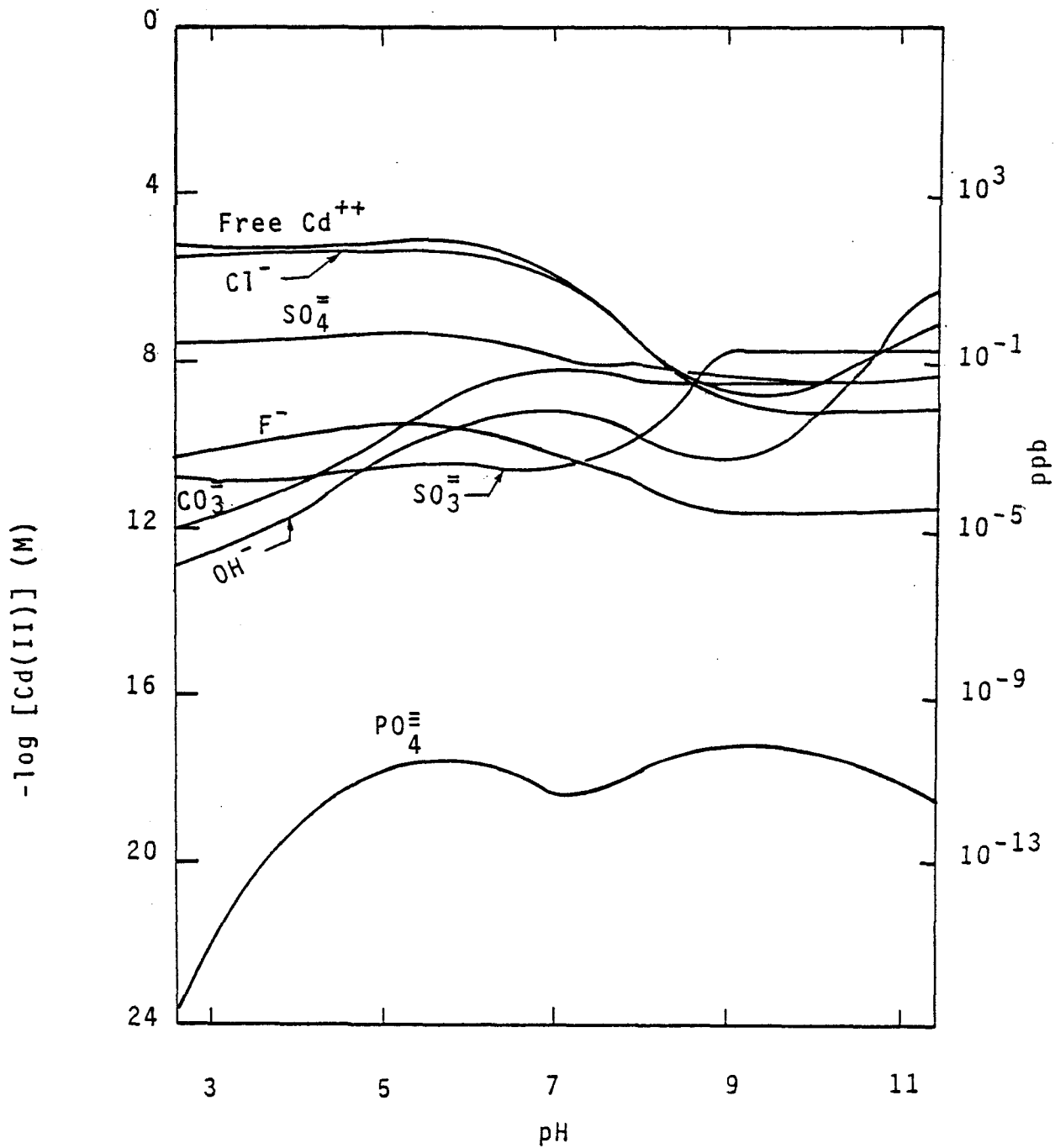
Figure 46. Speciation of soluble Cd in aged FGD wastes at $I = 0.05$, original $[Cd_T] = 10^{-4.97} M$.
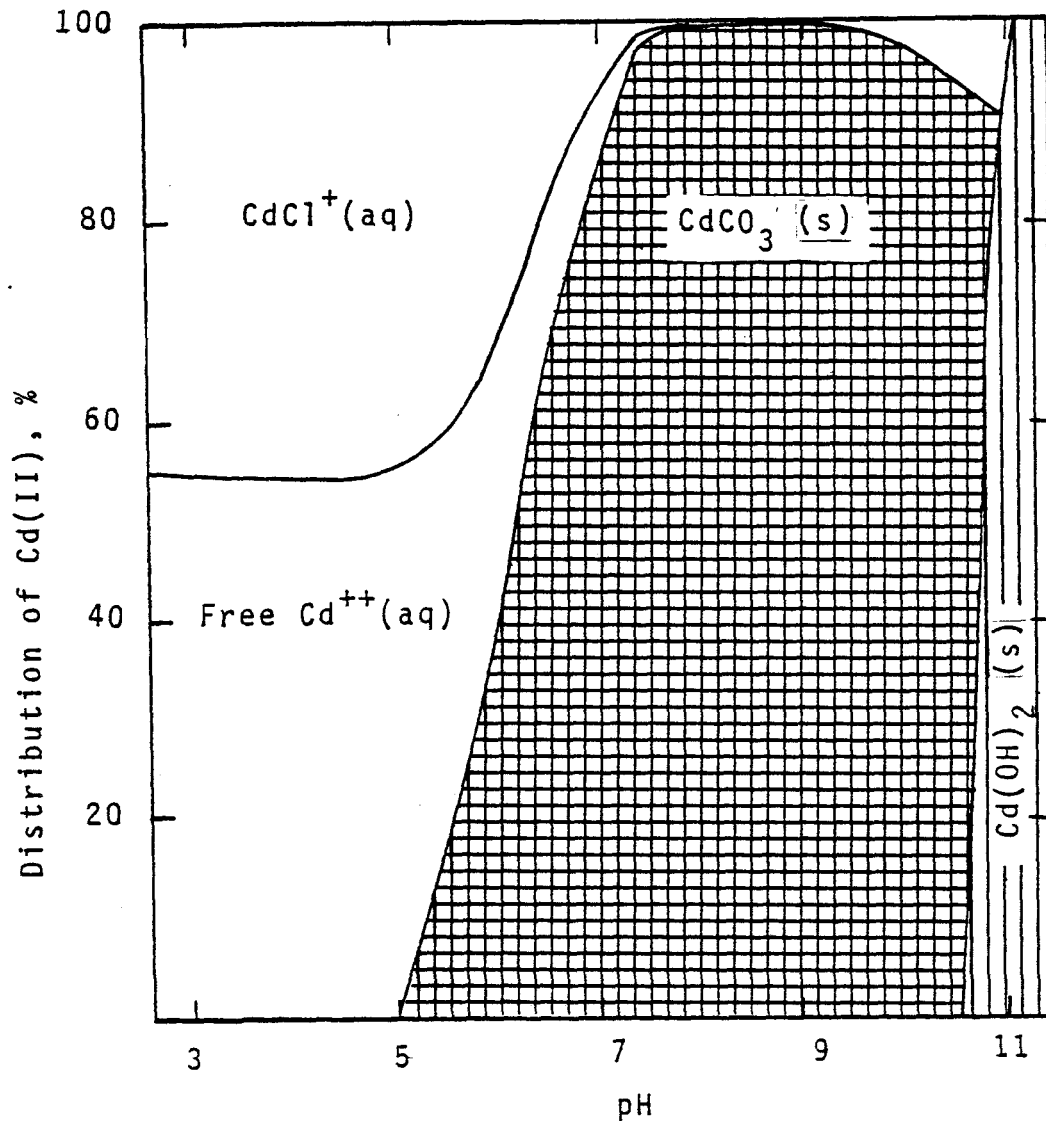
Figure 47. Primary distribution of Cd in aged FGD wastes at I = 0.05, original $[Cd_T] = 10^{-4.97}M$.
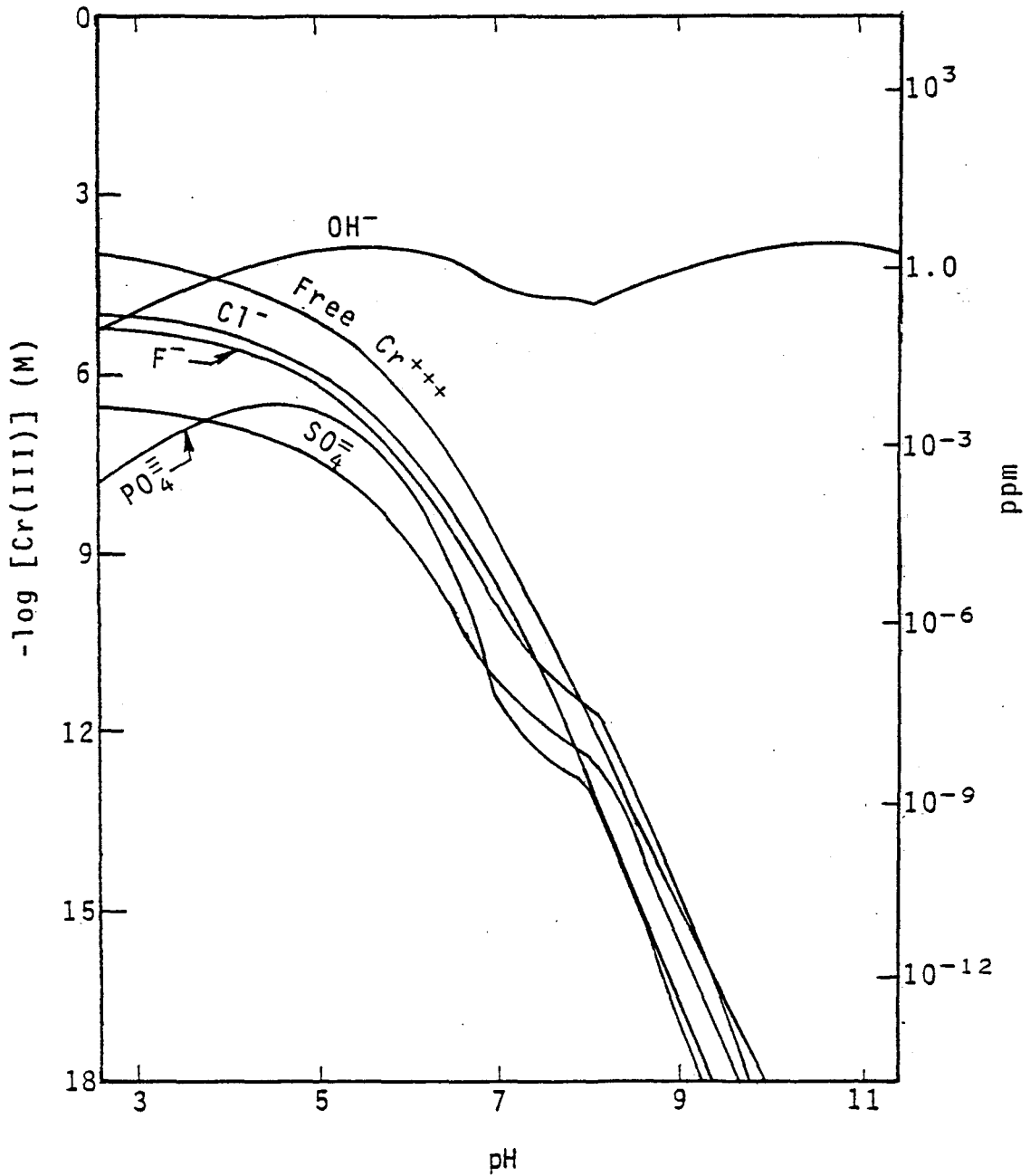
Figure 48. Speciation of soluble Cr in aged FGD wastewater
at I = 0.05, original $[Cr_T] = 10^{-4.03}M$.
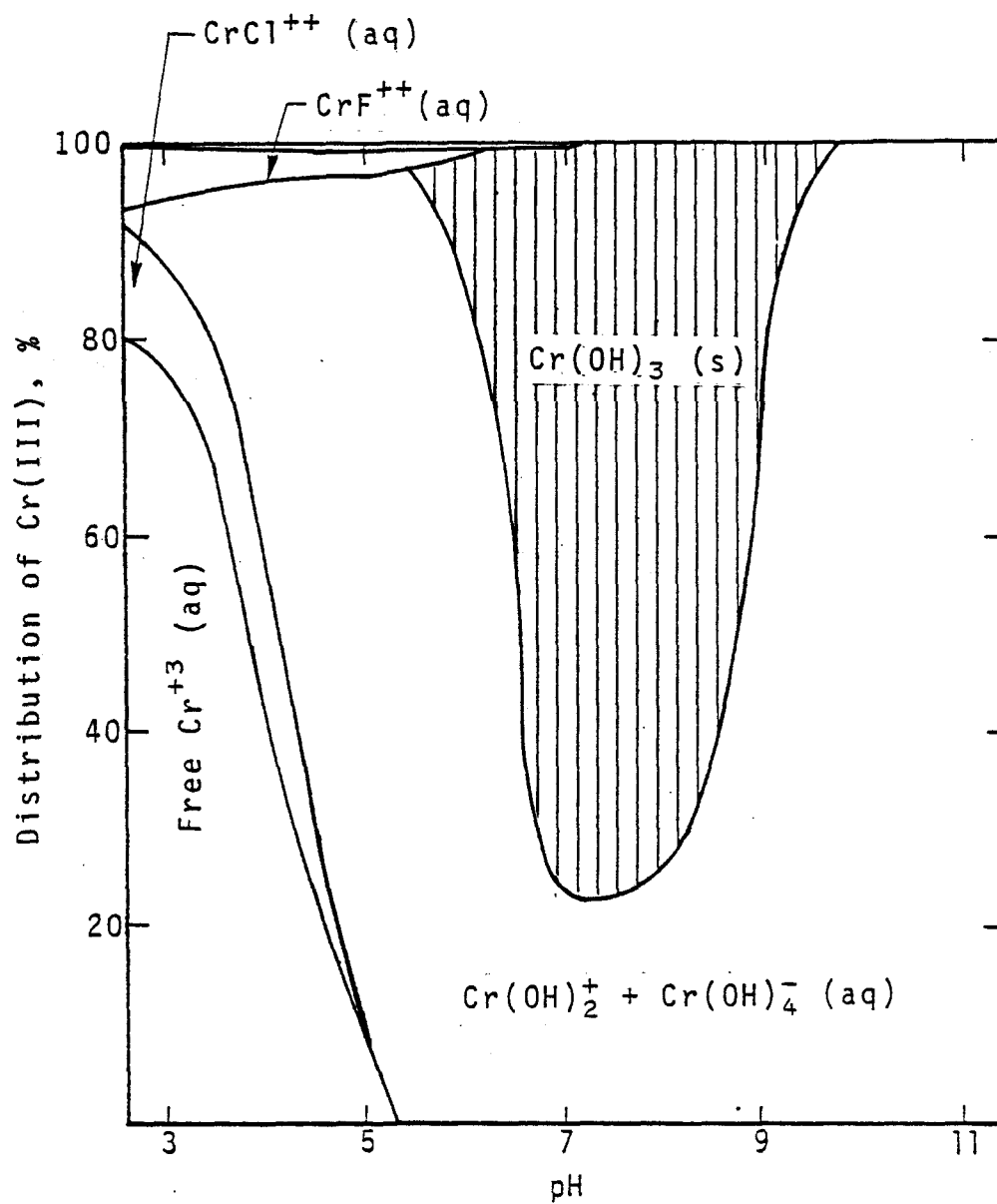
Figure 49. Primary distribution of Cr in aged FGD wastes
at I = 0.05, original $[Cr_T]$ = $10^{-4.03}$M.
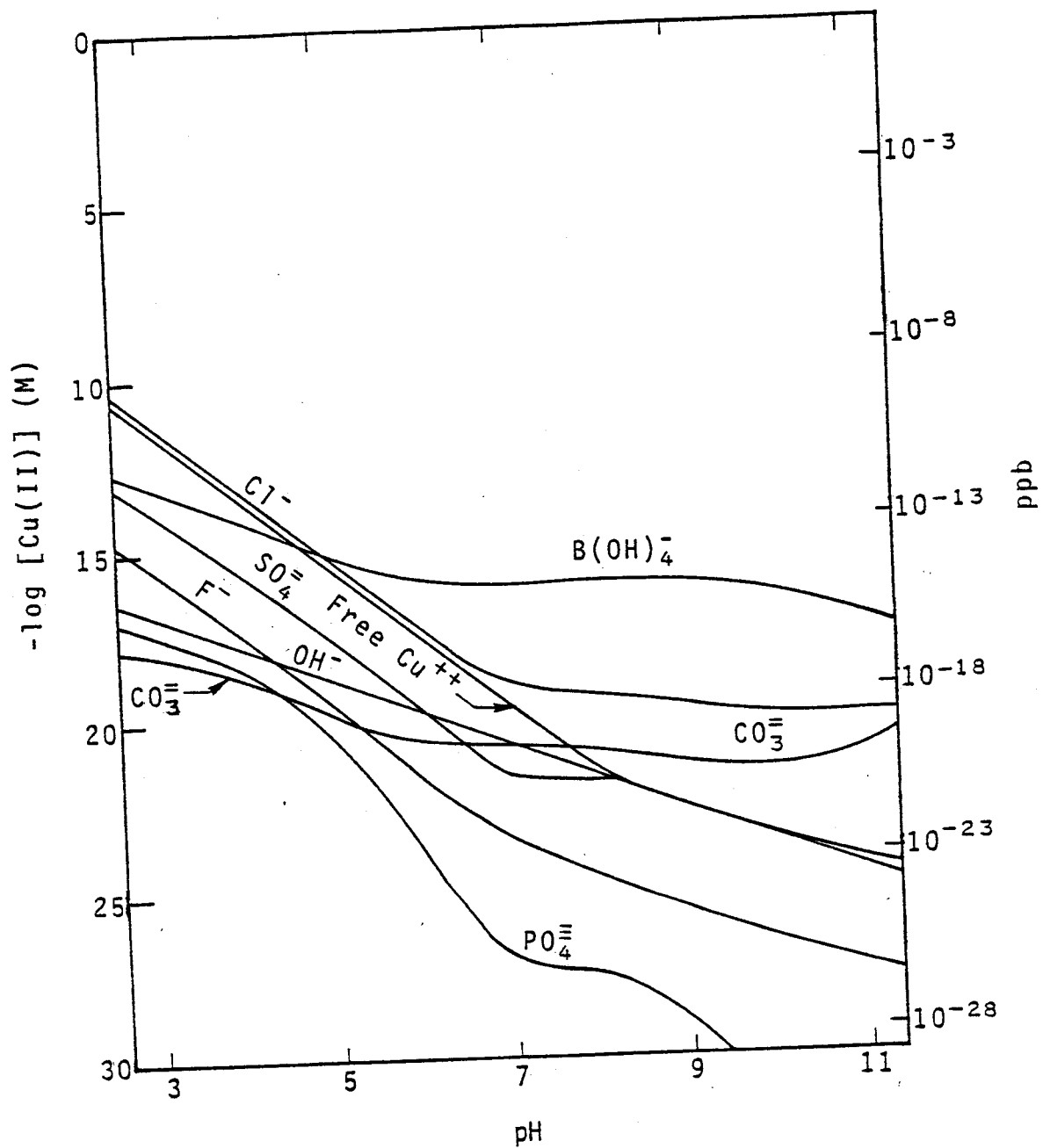
Figure 50. Speciation of soluble Cu in aged FGD wastes at I = 0.05, original $[Cu_T] = 10^{-4.18}$ M.
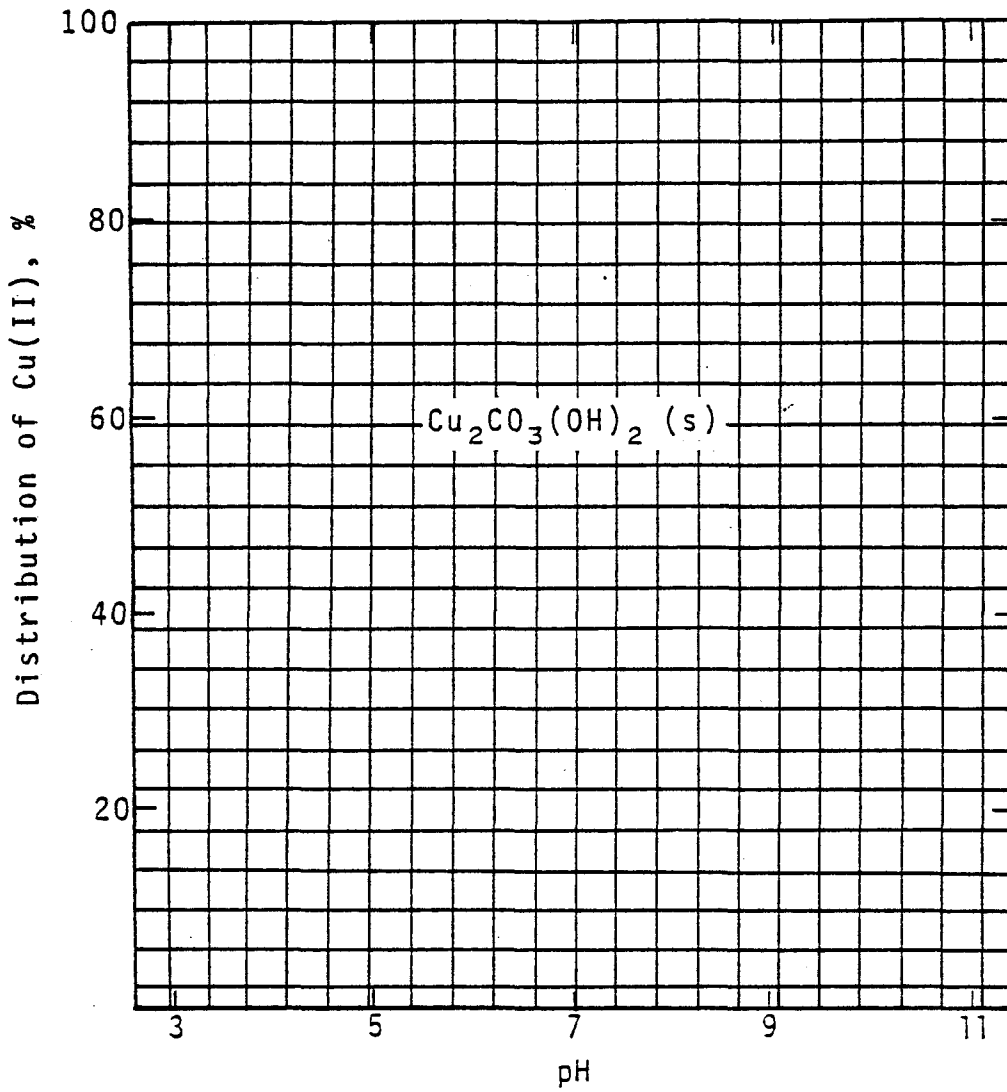
Figure 51. Primary distribution of Cu in aged FGD wastes
at I = 0.05, original $[Cu_T] = 10^{-4.18}M$.
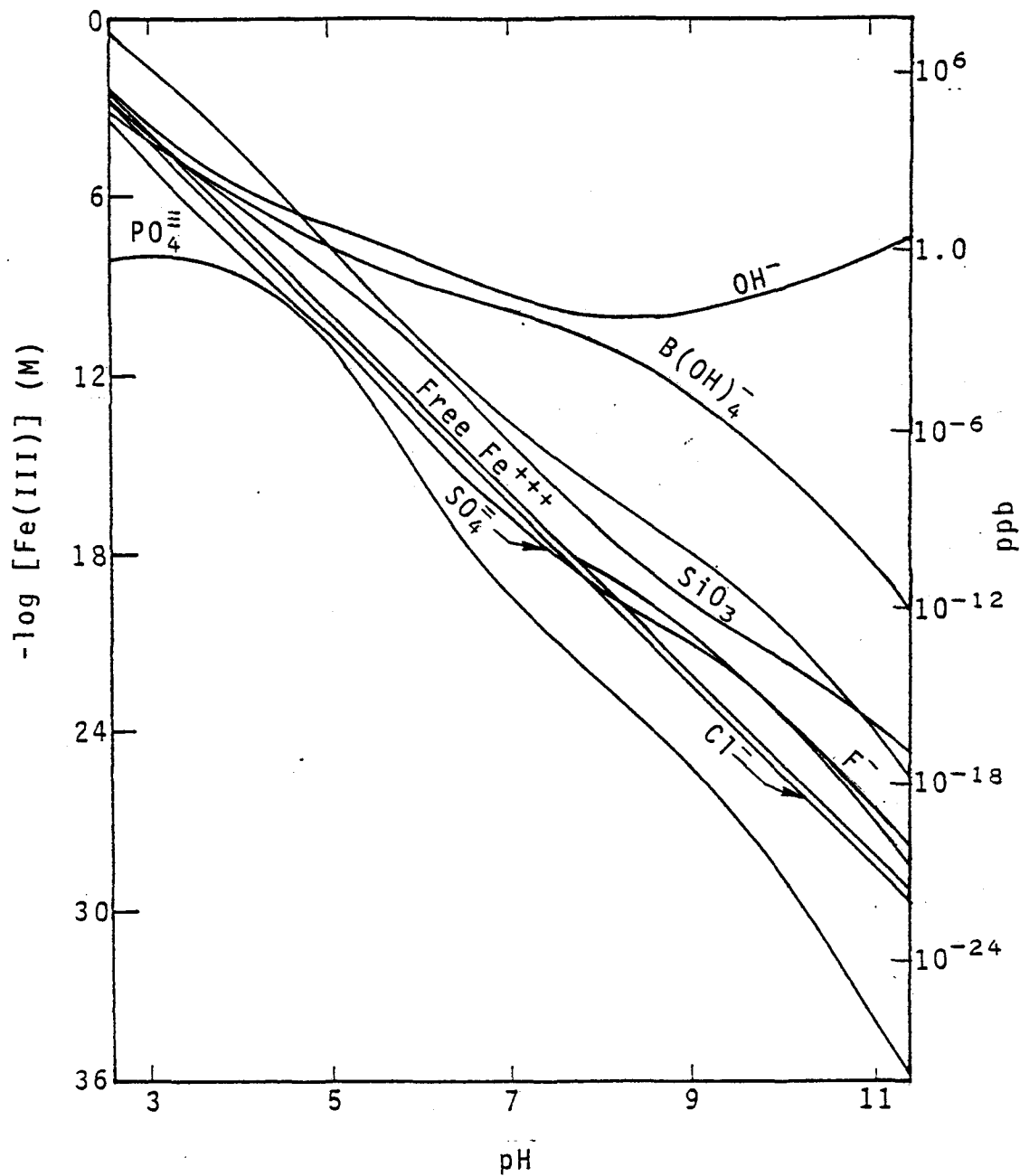
Figure 52. Speciation of Fe(III) in aged FGD wastes at I = 0.05, original $[Fe_T] = 10^{-0.57}M$.
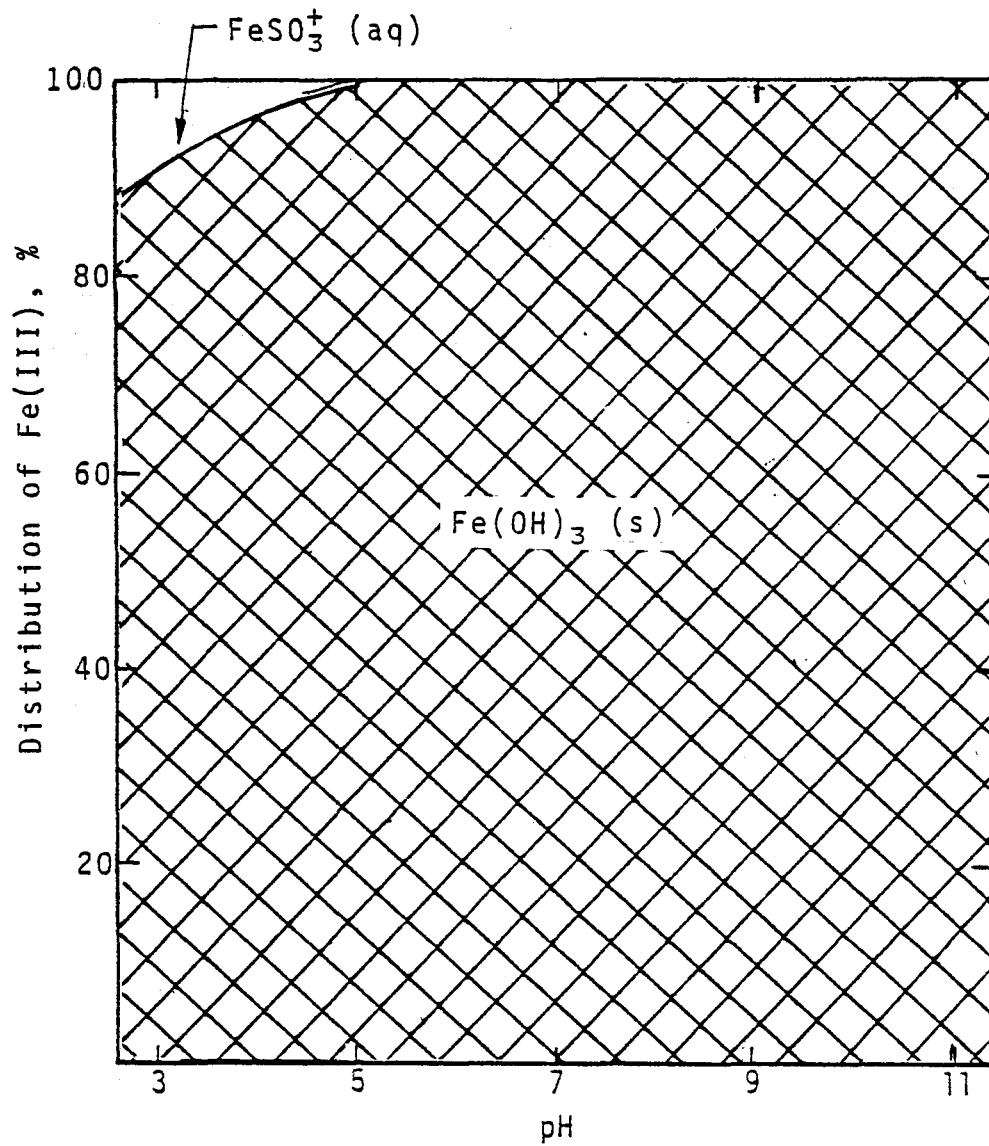
Figure 53.   Primary distribution of Fe(III) in aged FGD wastes
at I = 0.05, original [Fe$_T$] = $10^{-0.57}$M.
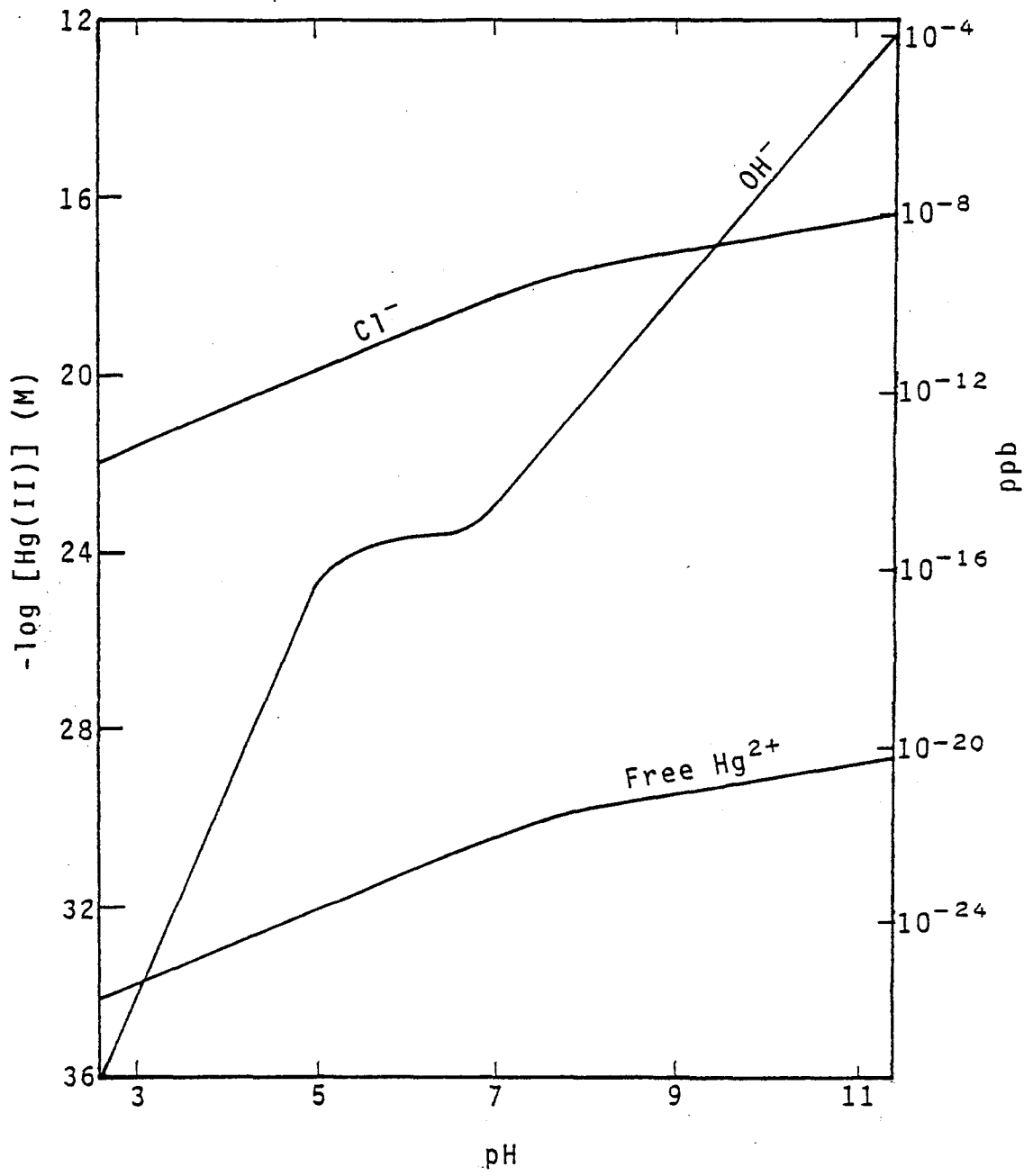
Figure 54.   Speciation of soluble Hg(II) in aged FGD wastes
at I = 0.05, original $[Hg_T] = 10^{-5.83}$M.
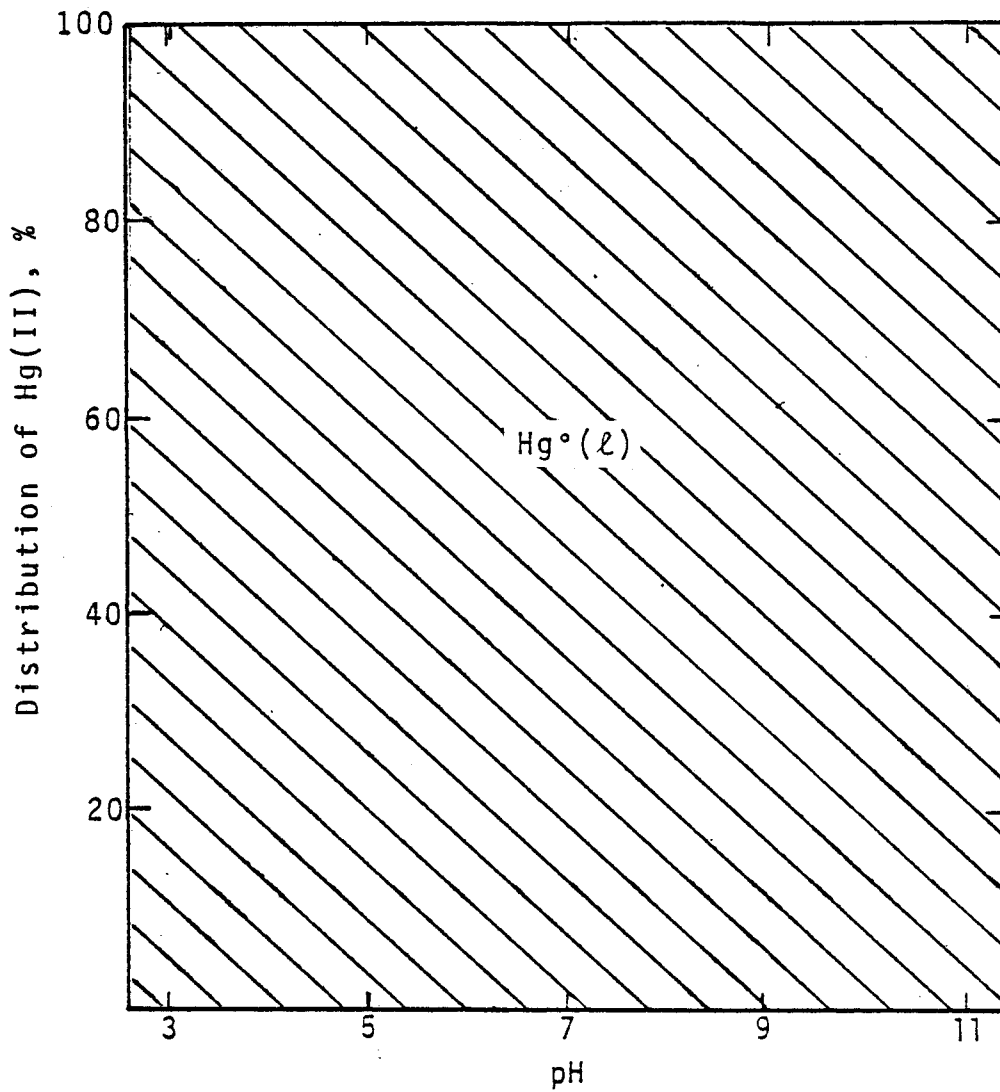
Figure 55. Primary distribution of Hg in FGD wastes at I = 0.05, original $[Hg_T]$ = $10^{-5.83}$M.
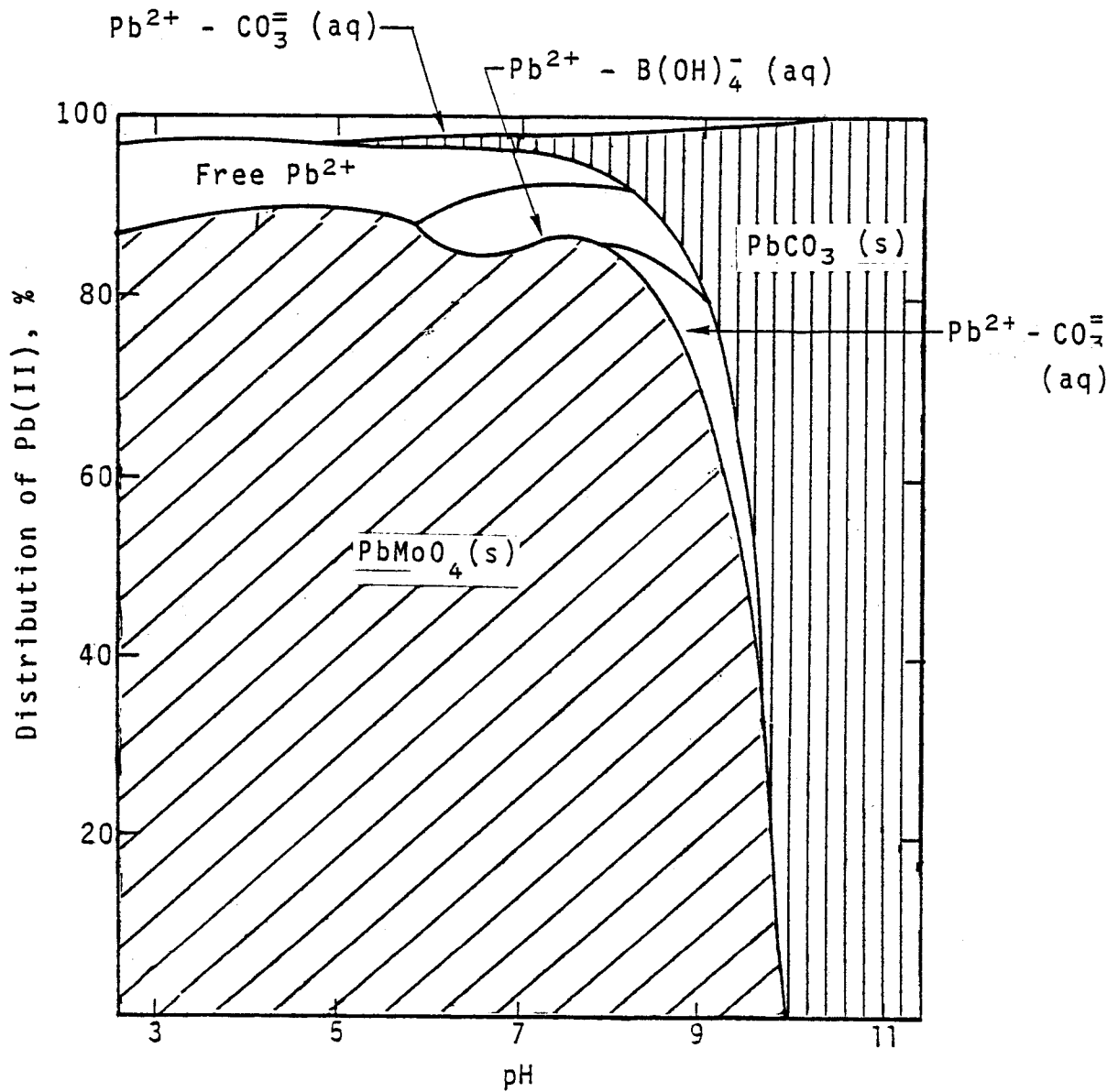
Figure 56.   Speciation of soluble Pb in aged FGD wastes
at I = 0.05, original $[Pb_T] = 10^{-4.69}M$.
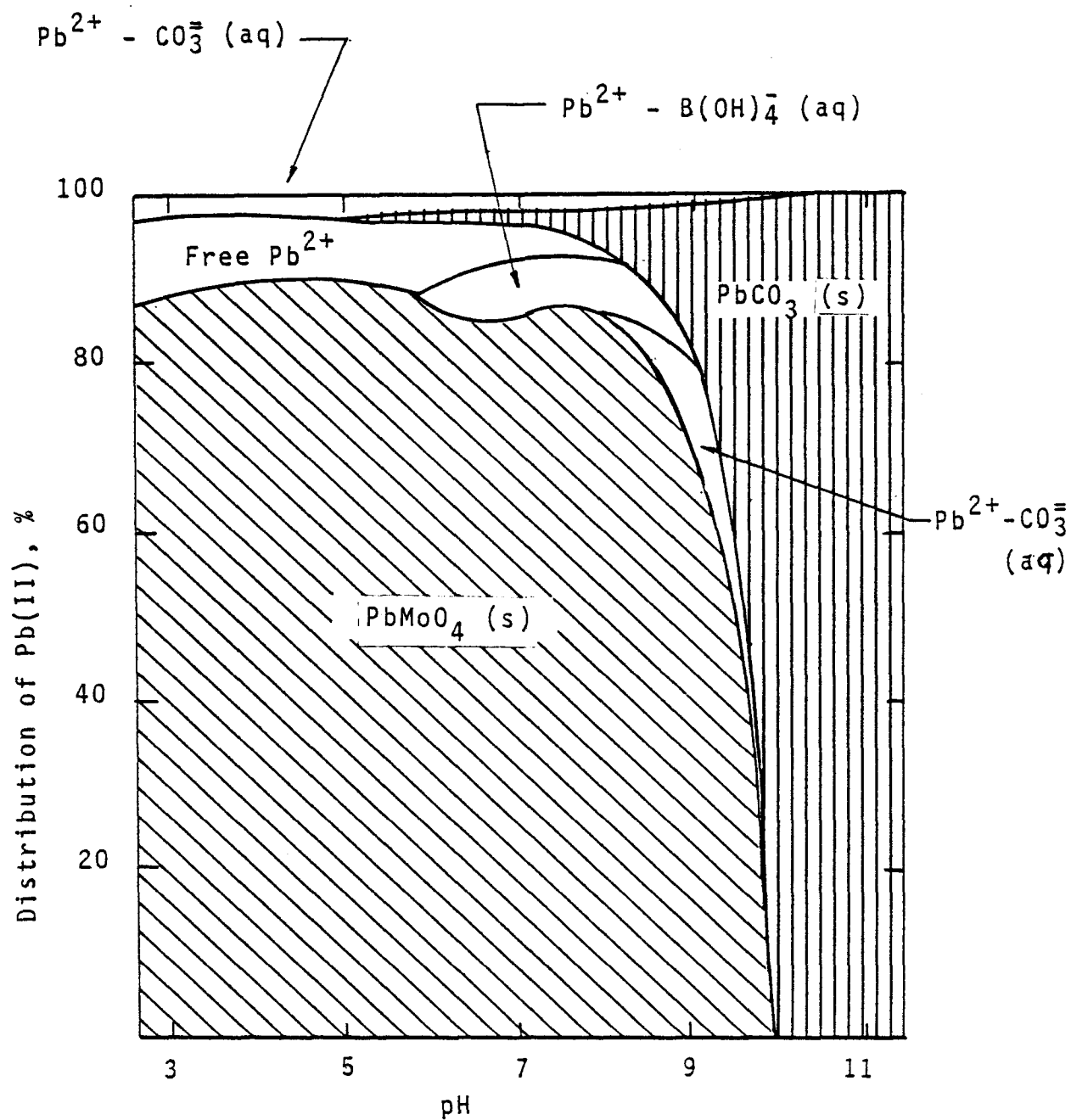
Figure 57. Primary distribution of Pb in aged FGD wastes
at I = 0.05, original $[Pb_T] = 10^{-4.69}M$.
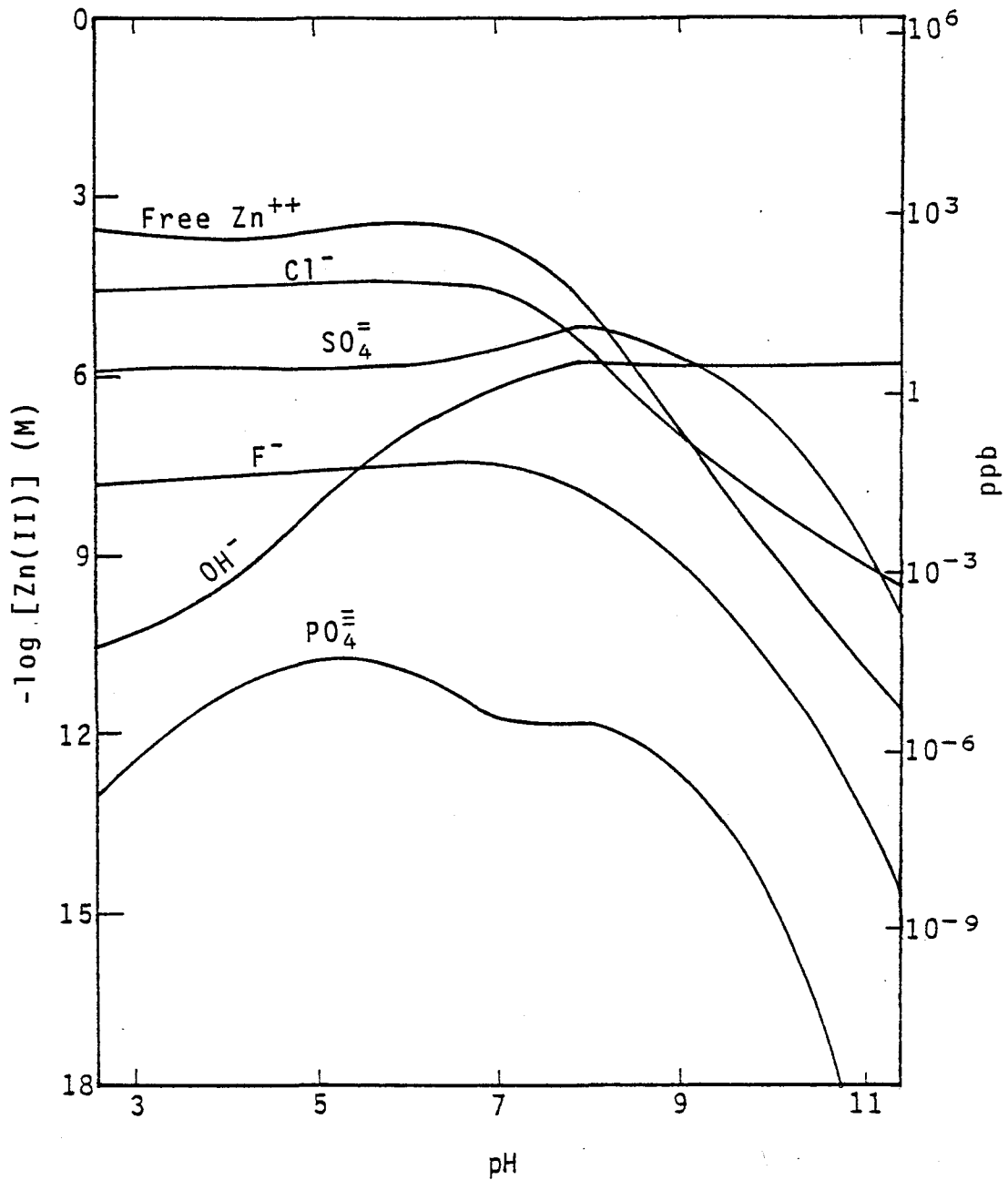
Figure 58. Speciation of soluble Zn in aged FGD wastes at I = 0.05, original $[Zn_T] = 10^{-3.58}M$.
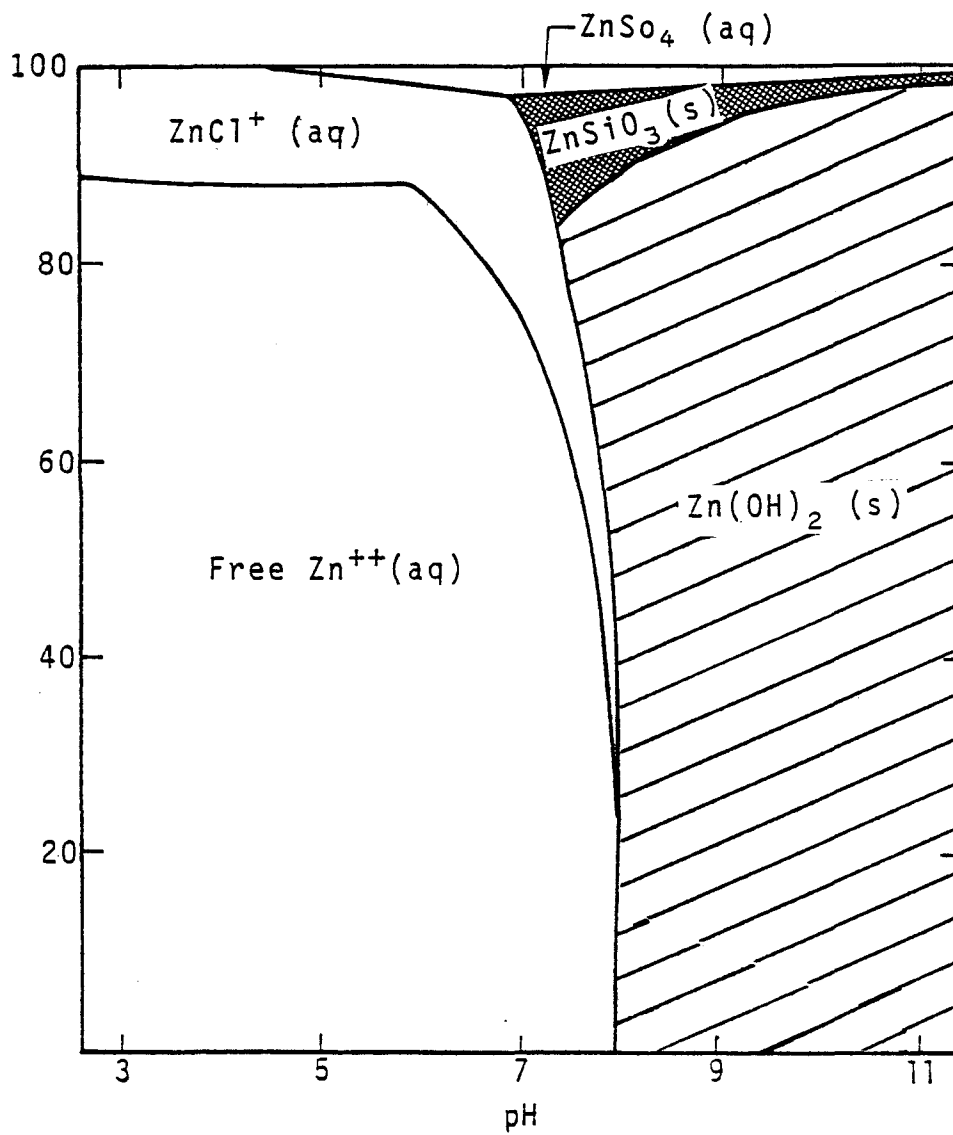
Figure 59. Primary distribution of Zn in aged FGD wastes at I = 0.05, original $[Zn_T]$ = $10^{-3.58}$M.

As shown in Figure 39, the major calcium solids at low pH levels are $CaSO_4.2H_2O(s)$ and $CaSO_3.1/2H_2O(s)$. These two solids have relatively high solubilities compared to that of $CaCO_3(s)$. Therefore, the increase in total soluble calcium levels at low pH is apparently caused by the lack of low solubility calcium solids. At a high pH, the calcium concentrations in the aged FGD wastes are substantially reduced (Figure 38). This is caused by a reduction in the free calcium ion through the formation of $CaCO_3(s)$ (Figure 39). Since the aging of FGD wastes usually results in a higher pH, it is therefore expected that the soluble calcium levels will gradually decrease as FGD wastes are aging.

Magnesium

Figures 40 and 41 show the speciation results of magnesium in the aged FGD wastes. It can be seen that the free magnesium ion is the most predominant soluble species at a pH below 10. The magnesium-sulfate complex will become significant when the pH is between 8 and 10. The levels of free magnesium ion and magnesium-sulfate complexes will decrease at a pH higher than about 10, while the $Mg(OH)_2(s)$ solid will begin to form and reduce the soluble magnesium concentration by two orders of magnitude from its original level.

Comparing fresh and aged FGD wastes at I=0.05, it appears that the concentrations of soluble magnesium species are altered by the aging effect. More free magnesium ion forms in aged wastes than in fresh wastes when the pH is less than 8. At a pH between 8 and 10, an increase in the magnesium-sulfate complex concentration occurs (see both Figures 40 and 41). The distribution diagram (Figure 41) shows that the increase is associated with the loss of free Mg^{2+} ion.

Potassium

Figures 42 and 43 show that the free K^+ ion is the predominant species of soluble potassium in the aged low ionic strength FGD wastes. This species comprises almost 100 percent of the soluble potassium when the pH is below 7. At higher pH (pH 7), small amounts of $K_2SO_4(aq)$ can be formed (about 10 percent, as can be seen from Figure 43. No new potassium solid will be formed during the aging of the FGD wastes due to the slow nucleation of the complex potassium solids and the high solubility of the simple potassium solids.

Sodium

In general, the distribution of soluble sodium in aged FGD wastes at I=0.05 is quite similar to that of potassium. If the sodium speciation in aged (Figures 44 and 45) and fresh (Figure 19) FGD sludge are compared, the distribution of $Na_2SO_4(aq)$

131

appears to increase as the wastes age. As with potassium, how-
ever, no new sodium solid can be formed during aging due to the
slow nucleation of the complex sodium solids and the high solu-
bility of the simple sodium solids.

Cadmium

The thermodynamic model shows that at low pH levels (pH$\leq$6),
the majority of the cadmium species exists as soluble free
Cd^{2+} and $CdCl^+$ (Figure 46 and 47). As the pH increases, cadmium
is removed from solution through the precipitation of $CdCO_3(s)$.
Due to the formation of this solid, cadmium levels in aged FGD
wastewater can be reduced to as low as 1 ppb (see Figure 46).
As the pH rises above 10.7, the soluble cadmium concentration
increases, again owing to the formation of the more soluble
$Cd(OH)_2(s)$.

Comparing the fresh and aged FGD wastes, the predominance
of soluble Cd-SO_4 complex appears to decrease with age at low pH
levels. The relative predominance of this complex in the soluble
phase increases when $CdCO_3(s)$ is formed at high pH, which also
reduces the concentrations of both the free Cd^{2+} and Cd-Cl
complexes. In fresh FGD wastes (see Figure 20) the cadmium-
carbonate complexes will become the predominant soluble species
at a pH of 9 to 11; in the aged FGD wastes, the levels of cad-
mium-carbonate complexes in the same pH range are lower than those
of the free cadmium ion, cadmium-chloride, and cadmium-sulfate
complexes.

Chromium

The calculated results for the speciation of chromium are
given in Figures 48 and 49. By comparing Figure 48 to the specia-
tion results of chromium in fresh FGD wastes (Figure 21), it is
found that the predominant soluble species of chromium (free
Cr^{3+} for pH less than about 4, and Cr-OH complexes for pH
greater than 4) are similar in both cases. However, the concen-
tration of soluble chromium in aged wastes decreases (see Figure
48) when conditions favor $Cr(OH)_3(s)$ formation (see Figure 49).
The $Cr(OH)_3(s)$ can account for as much as 80 percent of the total
chromium in the aged FGD sludge. Neutral pH levels favor the
formation of this solid (pH of 5.5 to 9 appears to be the optimum
range).

Copper

Thermodynamic calculations indicate that at I=0.05, the
predominant soluble species of copper in aged FGD wastes are free
copper ion at pH less than 4.8, and copper-borate complexes
mainly $Cu(B(OH)_4)_2(aq)$, at higher pH. Copper-chloride, copper-
hydroxide, or copper-carbonate complexes are the next most

important soluble species under pH levels as shown in Figure 50. Almost 100 percent of the total available copper exists as $Cu_2CO_3(OH)_2(s)$ precipitate, however (see Figure 51). Due to the formation of this solid, the soluble copper concentration can be reduced to extremely low levels. Therefore, the aging of FGD wastes should control copper migration into the aqueous environment.

Iron

The speciation of Fe(III) is shown in Figures 52 and 53. Under the studied condition, it was found that most of the iron in FGD sludge will precipitate out as $Fe(OH)_3(s)$ (see Figure 53). Soluble iron (as $FeSO_3^+$) may exist in a significant concentration at low pH levels (pH 5). Although Fe-OH complexes are the predominant soluble species when the pH is greater than 5, their concentrations are typically less than 1 ppb. Since the aging process increases both the pH and Eh values, the removal of iron from the FGD wastewaters is favored.

Mercury

The speciation of mercury in the aged FGD wastes is represented in Figures 54 and 55. Note that when the pH is less than about 8.5, the predominant soluble species are Hg-Cl complexes (primarily $HgCl_2(aq)$). At higher pH, Hg-OH complexes (primarily $Hg(OH)_2(aq)$ will predominate in the soluble phase. However, due to the formation of $Hg^0(\ell)$ in aged FGD sludge, most of the mercury in the sludge will precipitate out of the FGD wastewater. This mechanism can regulate the total soluble mercury down to trace levels (less than 10^{-4} ppb, as can be seen in Figure 54). Therefore, the aging process will also remove mercury from the FGD leachates.

Lead

Under the aged, low ionic strength condition, lead can form very strong complexes with the $B(OH)_4$ ion in the pH range of 6.8 to 8.4. Between pH 8.4 and 11, Pb-CO₃ complexes are the principal soluble species (see Figure 56).

The thermodynamic model also shows that under conditions of low pH, $PbMoO_4(s)$ can be formed. This solid will account for about 90 percent of the total lead in the sludge (Figure 57). Through the formation of $PbMoO_4(s)$, the soluble lead concentration can be reduced to about 10 ppb (Figure 56). At a high pH, $PbCO_3(s)$ is more stable than $PbMoO_4(s)$. The soluble lead concentration can therefore be reduced even further The soluble lead concentration in this pH region from pH 7 to 11 is between 10 ppb and 0.1 ppb. Aging would appear to favor the removal of lead from solution.

Zinc

Free zinc ion is the major species in aged FGD waste at pH levels of less than 8.3 (Figures 58 and 59). When pH is above 8.0, most of the zinc precipitates as hydroxide and silicate solids. When the pH is higher than 9.3, the hydroxide solid is still the predominant species, but major soluble species are converted to zinc-hydroxide complexes.

In the low pH region (pH 8), due to the lack of stable zinc solids in the aged FGD sludge, the soluble zinc levels may increase in relation to those of the fresh FGD sludge (see Figure 26). Therefore, if the pH level of aged FGD sludge is less than about 8, the aging process will tend to release zinc into solution.

CONSTITUENT SPECIATION: HIGH IONIC STRENGTH

Speciation of constituents in the aged FGD wastes of high ionic strength (I=0.8) was also evaluated for 20 metals and 13 ligands (155 complexes and 71 possible solids in all). Results of thermodynamic calculations are given in Figures 60 to 81.

Calcium

The distribution pattern and the final total soluble concentrations of calcium in aged FGD waste at I=0.8, is quite similar to that at I=0.05 (see Figures 38, 39, 60, and 61). The principal difference between these two cases is that the high ionic strengh FGD sludge will possess more calcium solids (compare Figures 39 and 61).

In comparing the speciation calculation results for fresh and aged FGD wastes (Figures 60 and 27), the total soluble calcium in aged FGD wastes appears to be higher than that in fresh FGD wastes when the pH is below 8. When the pH is higher than 8, the situation is reversed. Therefore, the aging process can cause the release of calcium into solution if the pH remains below about 8; when the pH is higher than 8, the soluble calcium will gradually be removed from solution.

Magnesium

In general, the distribution of magnesium species at I=0.8 is similar to the distribution at I=0.05 (see Figures 40, 41, 62 and 63). Some differences can still be found. For example, in the high ionic strength case, the hydroxide solid ($Mg(OH)_2(s)$) can be formed from high pH levels down to about pH 8. The same solid for the low ionic strength (I=0.05) case can only be formed above pH 10. The relative percentage of $Mg-SO_4$ complex is smaller in the high ionic strength case. The existence of
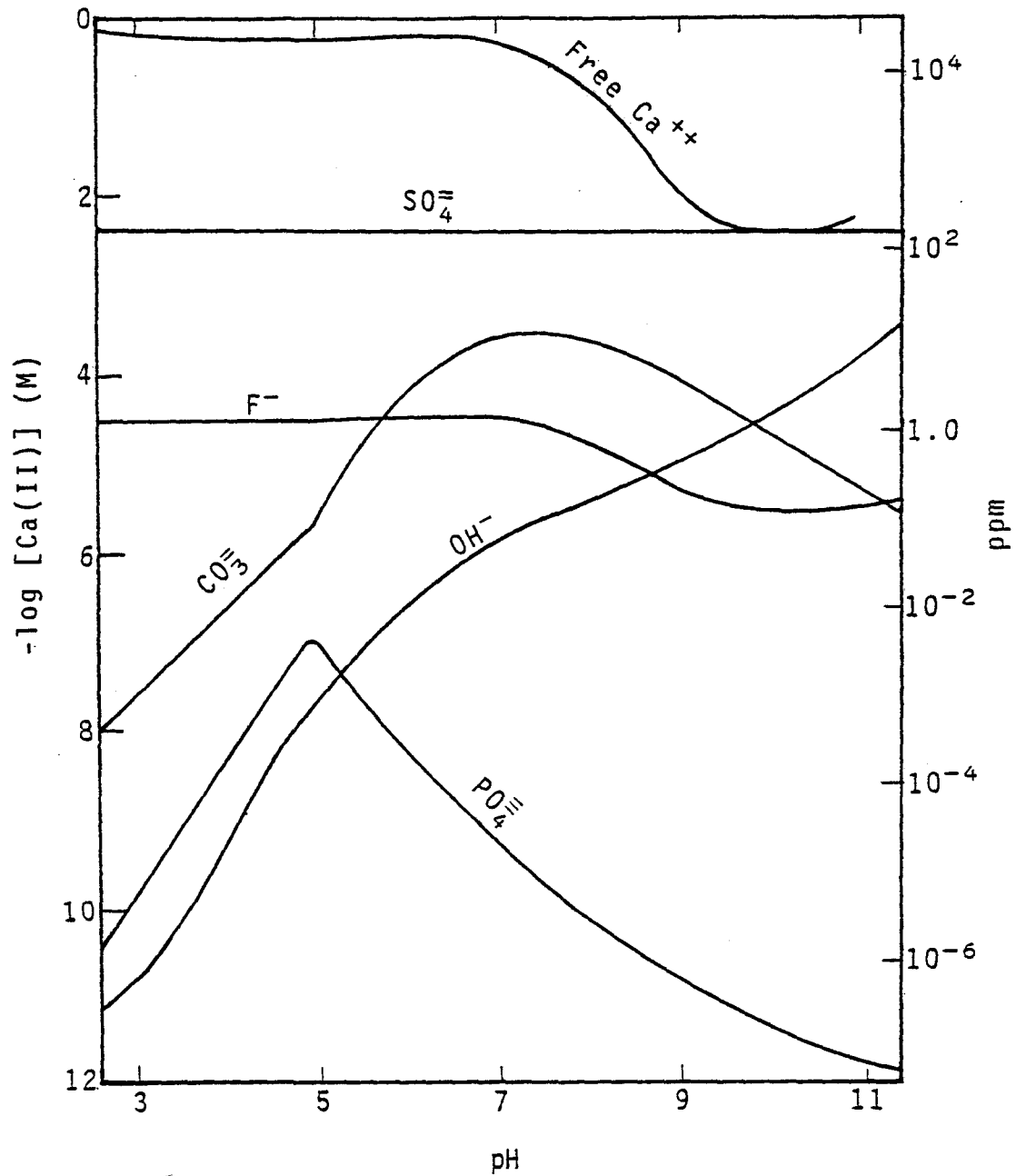
Figure 60. Speciation of soluble Ca in aged FGD wastes at I = 0.8, original $[Ca_T] = 10^{0.21}$M.
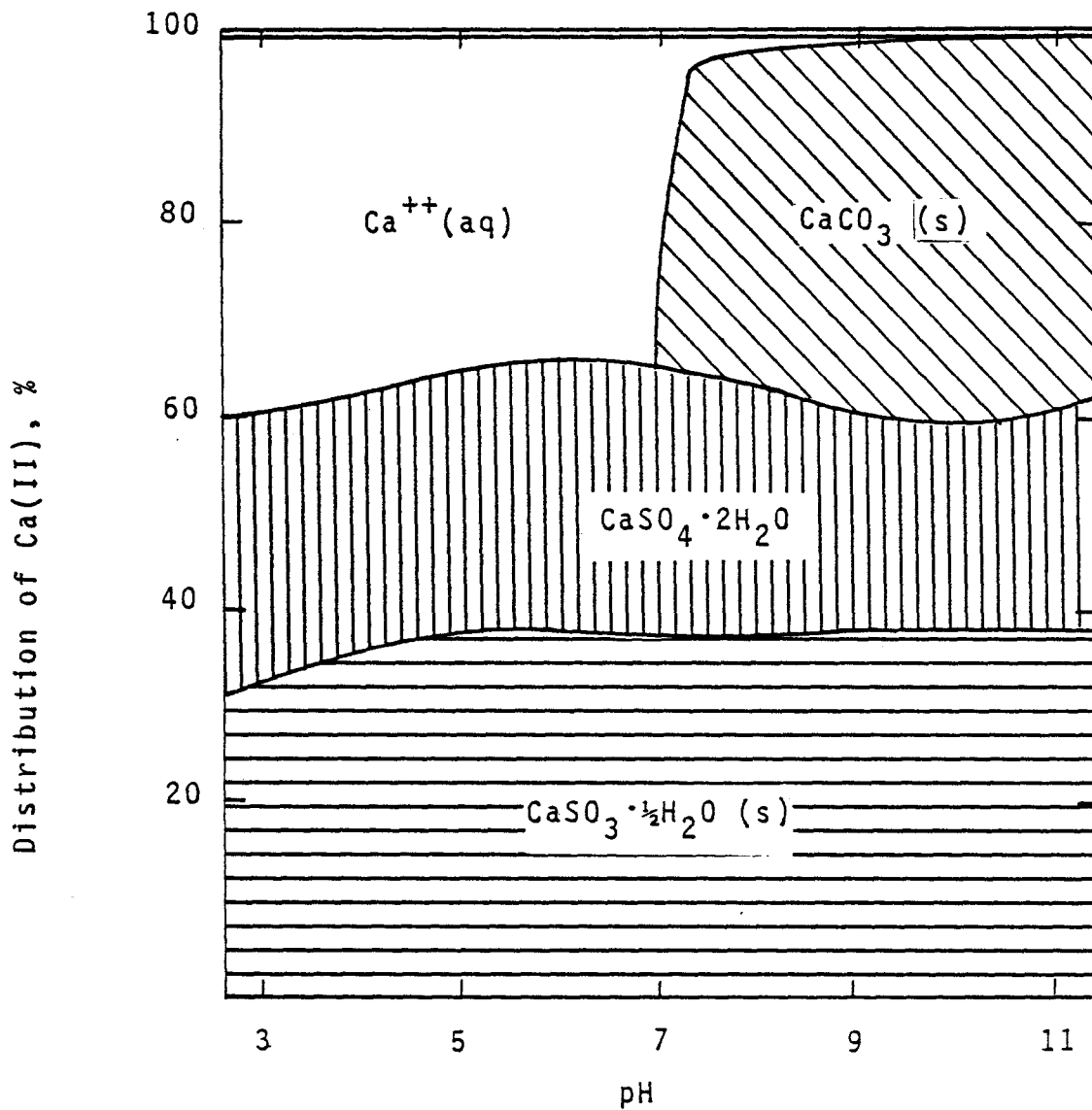
Figure 61. Primary distribution of Ca in aged FGD wastes
at I = 0.8, original $[Ca_T]$ = $10^{0.21}$M.
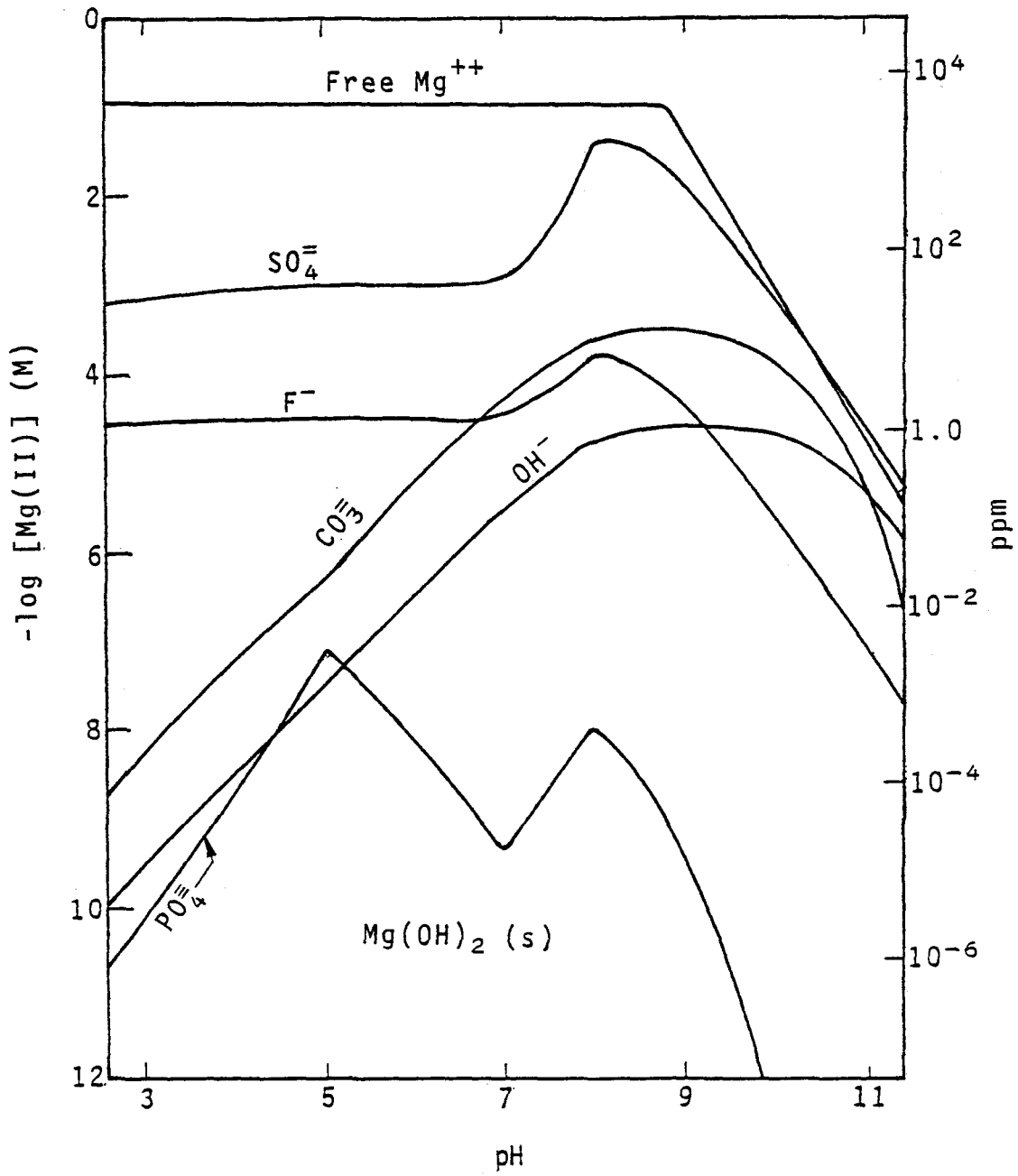
Figure 62.   Speciation of soluble Mg in aged FGD wastes
at I = 0.8, original $[Mg_T]$ = $10^{-0.95}M$.
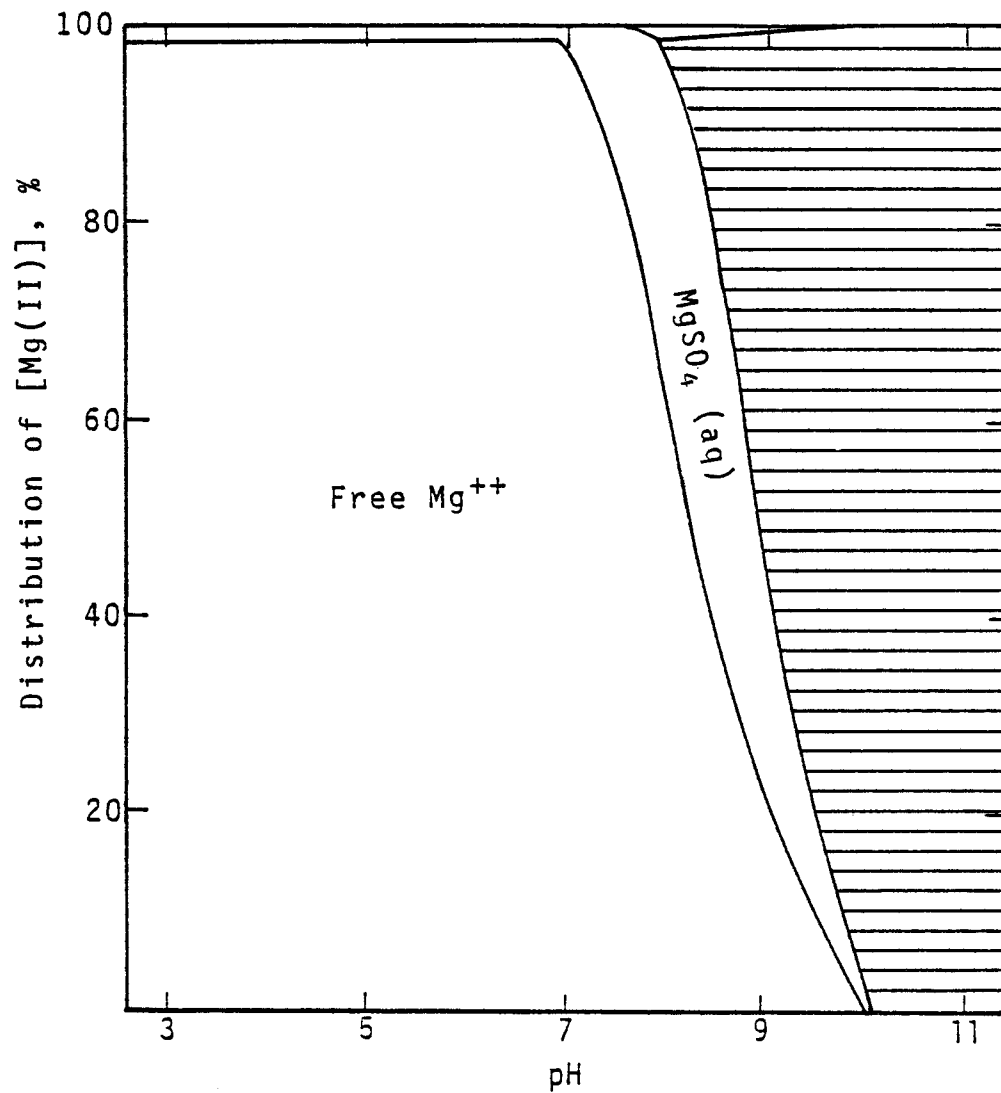
Figure 63. Primary distribution of Mg in aged FGD wastes at I = 0.8, original $[Mg_T] = 10^{-0.95}M$.
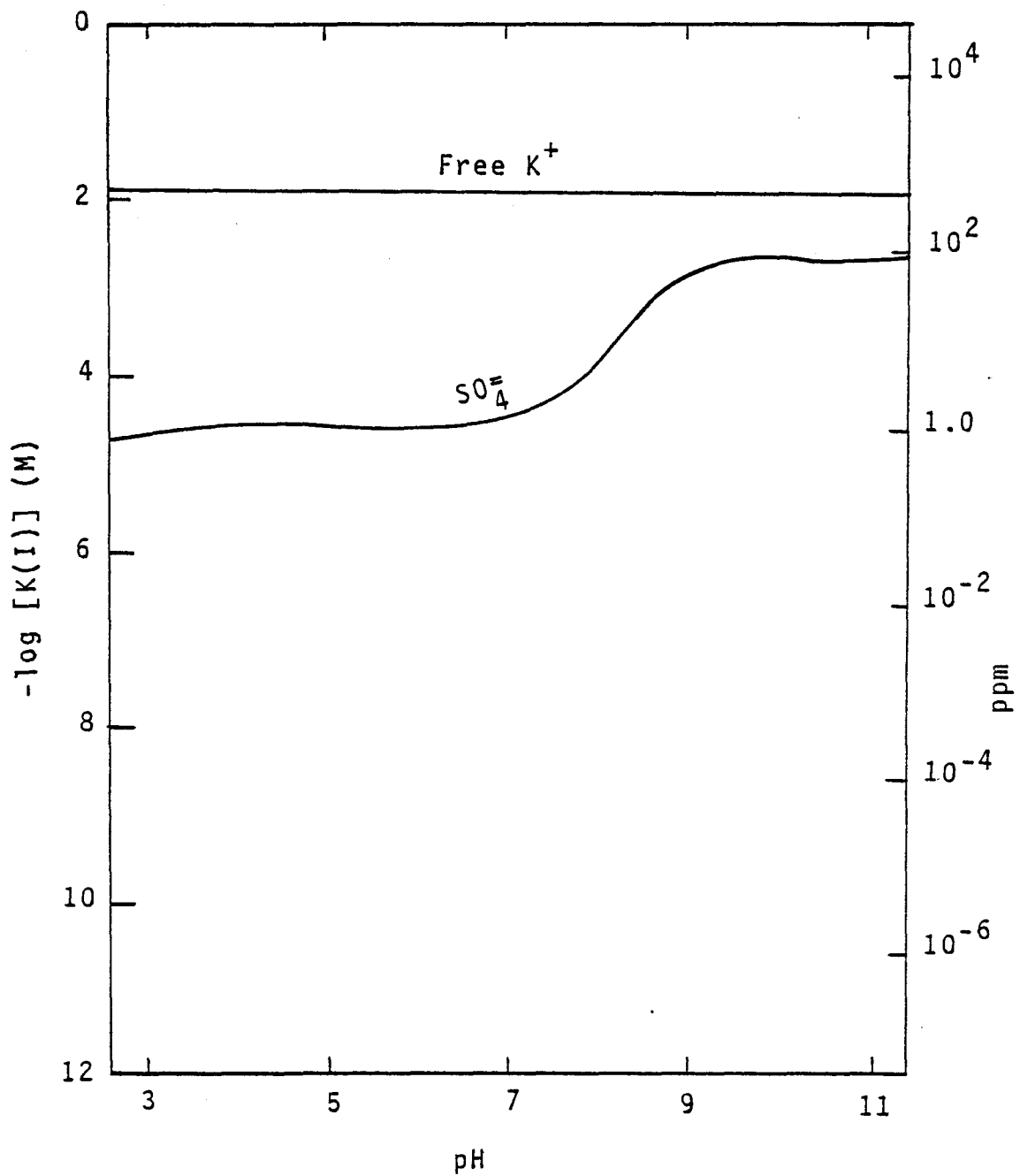
Figure 64.   Speciation of soluble K in aged FGD wastes at I = 0.8, original $[K_T] = 10^{-1.87}M$.

139
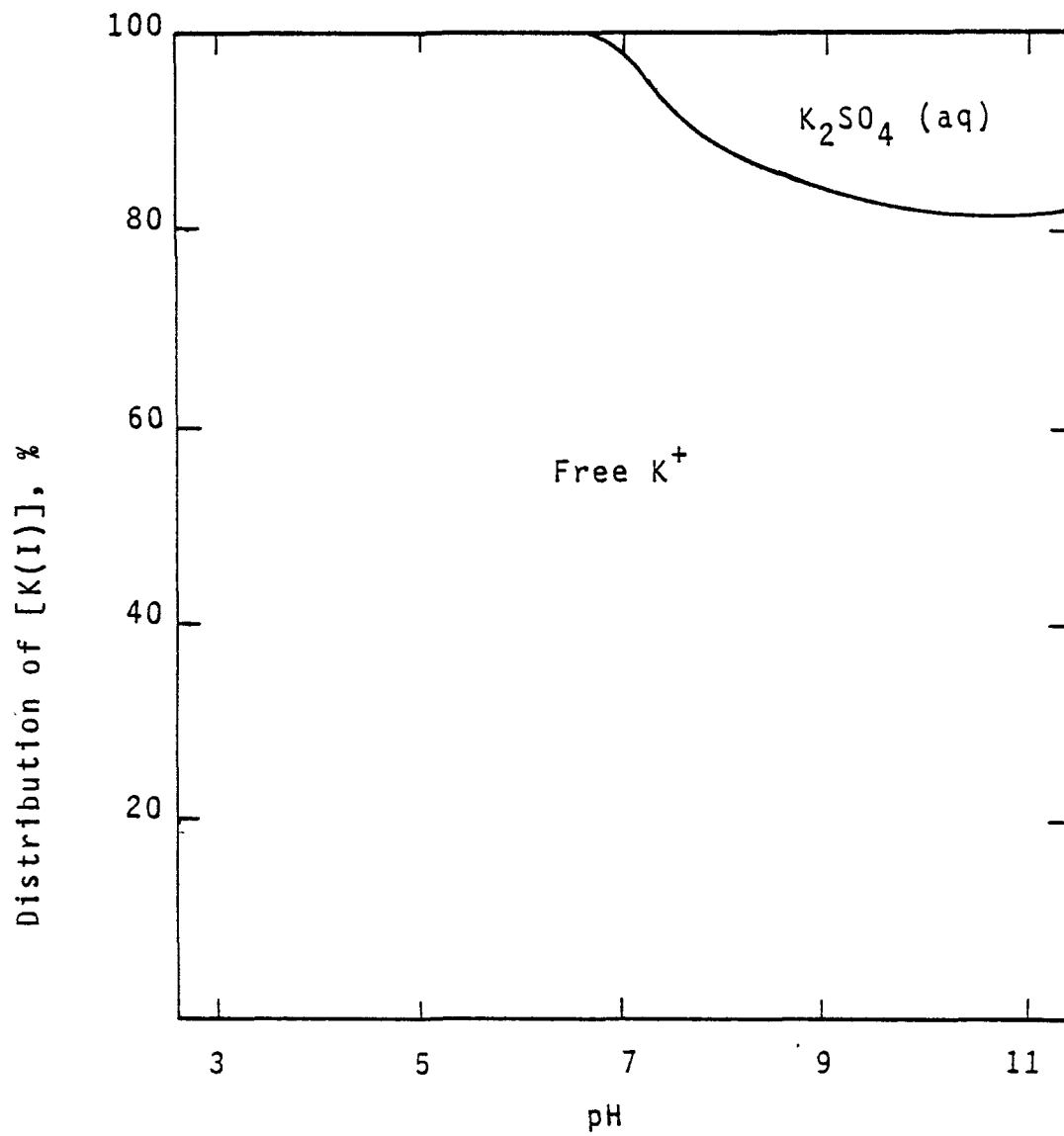
Figure 65.   Primary distribution of K in aged FGD wastes
at I = 0.8, original $[K_T] = 10^{-1.87}$M.
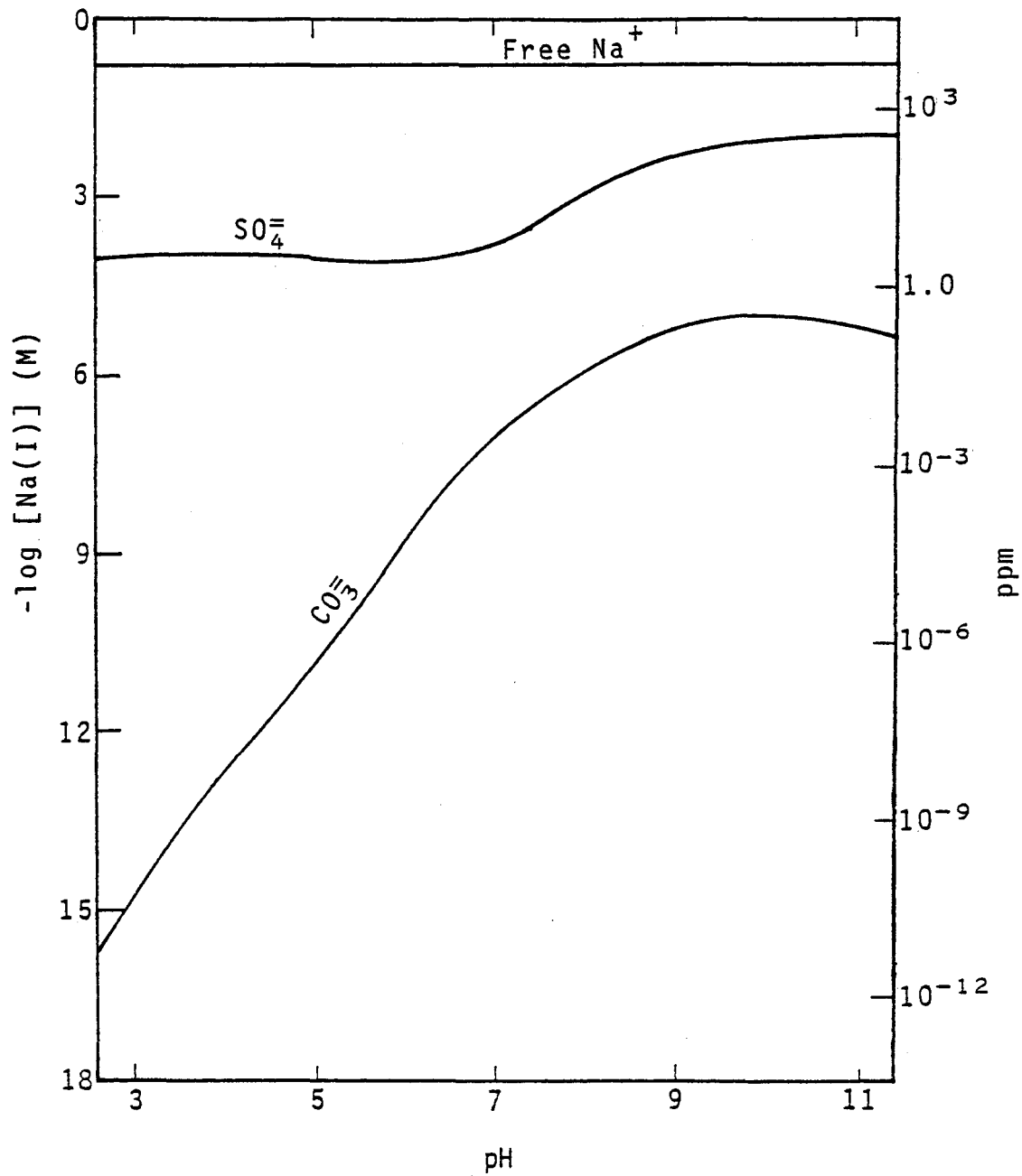
Figure 66.   Speciation of soluble Na in aged FGD wastes
at I = 0.8, original $[Na_T]$ = $10^{-0.83}$M.
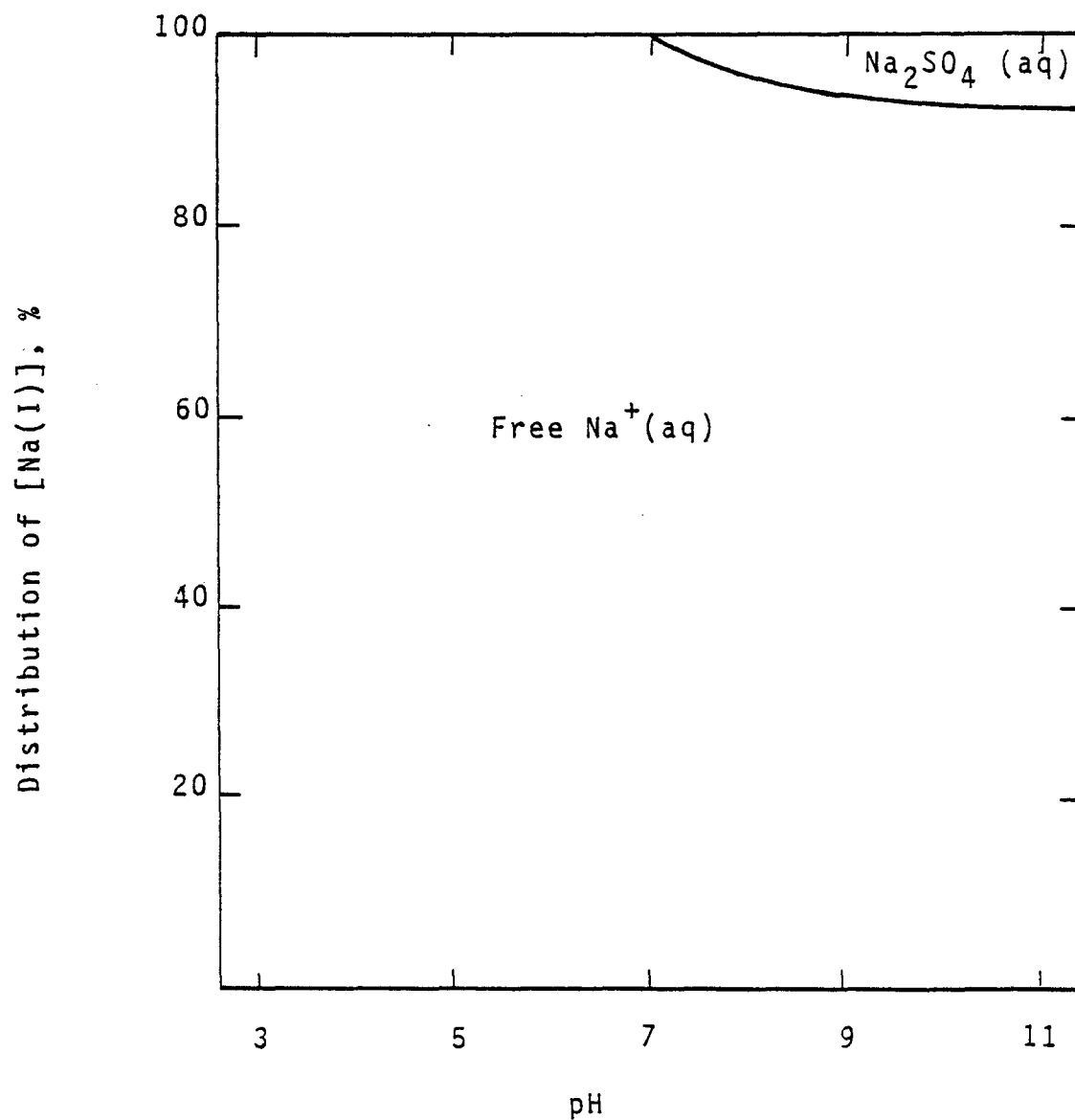
Figure 67. Primary distribution of Na in aged FGD wastes
at I = 0.8, original $[Na_T] = 10^{-0.83}M$.
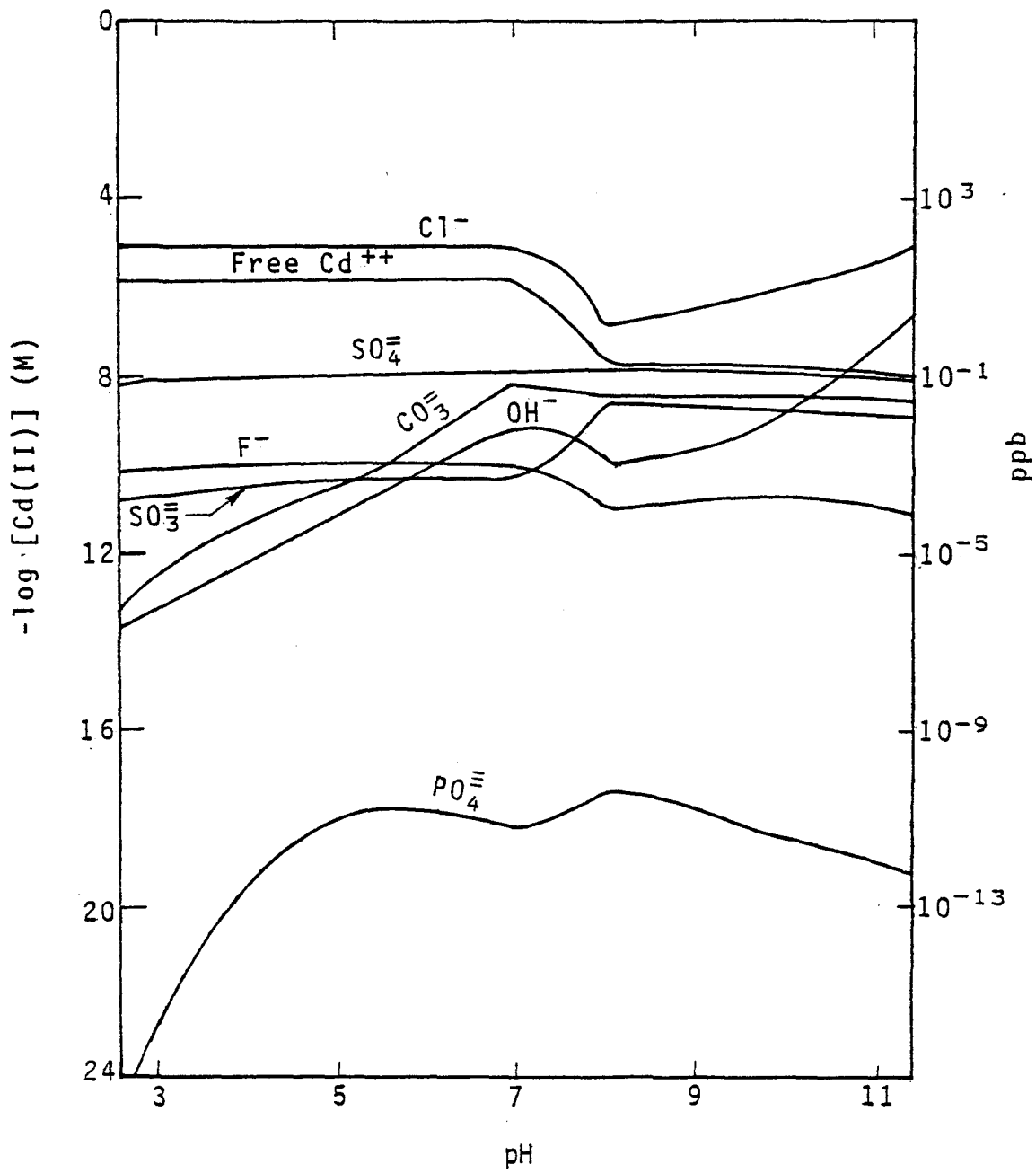
Figure 68. Speciation of soluble Cd in aged FGD wastes at I = 0.8, original $[Cd_T] = 10^{-4.97}M$.
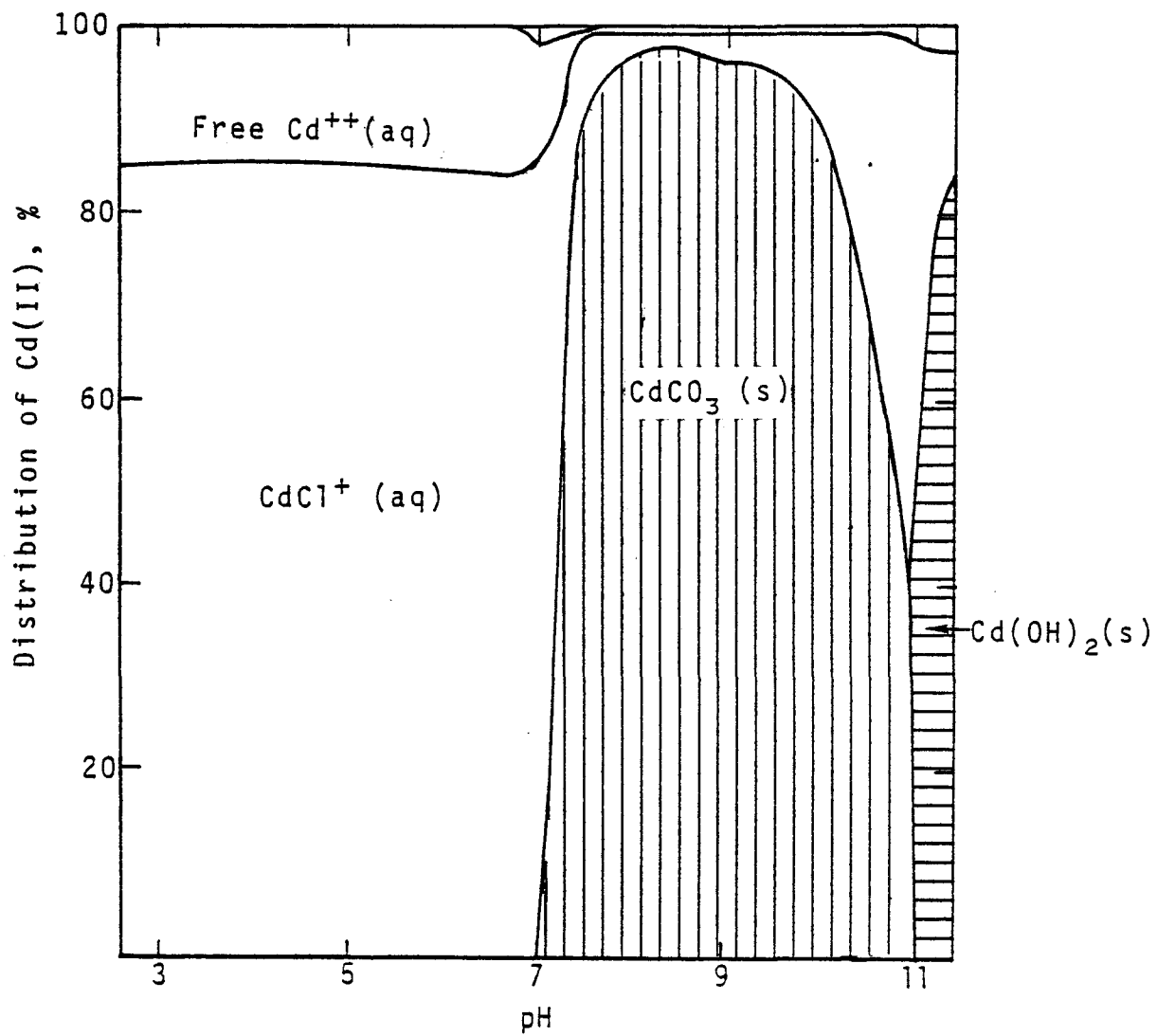
Figure 69. Primary distribution of Cd in aged FGD wastes at I = 0.8, original $[Cd_T] = 10^{-4.97}M$.
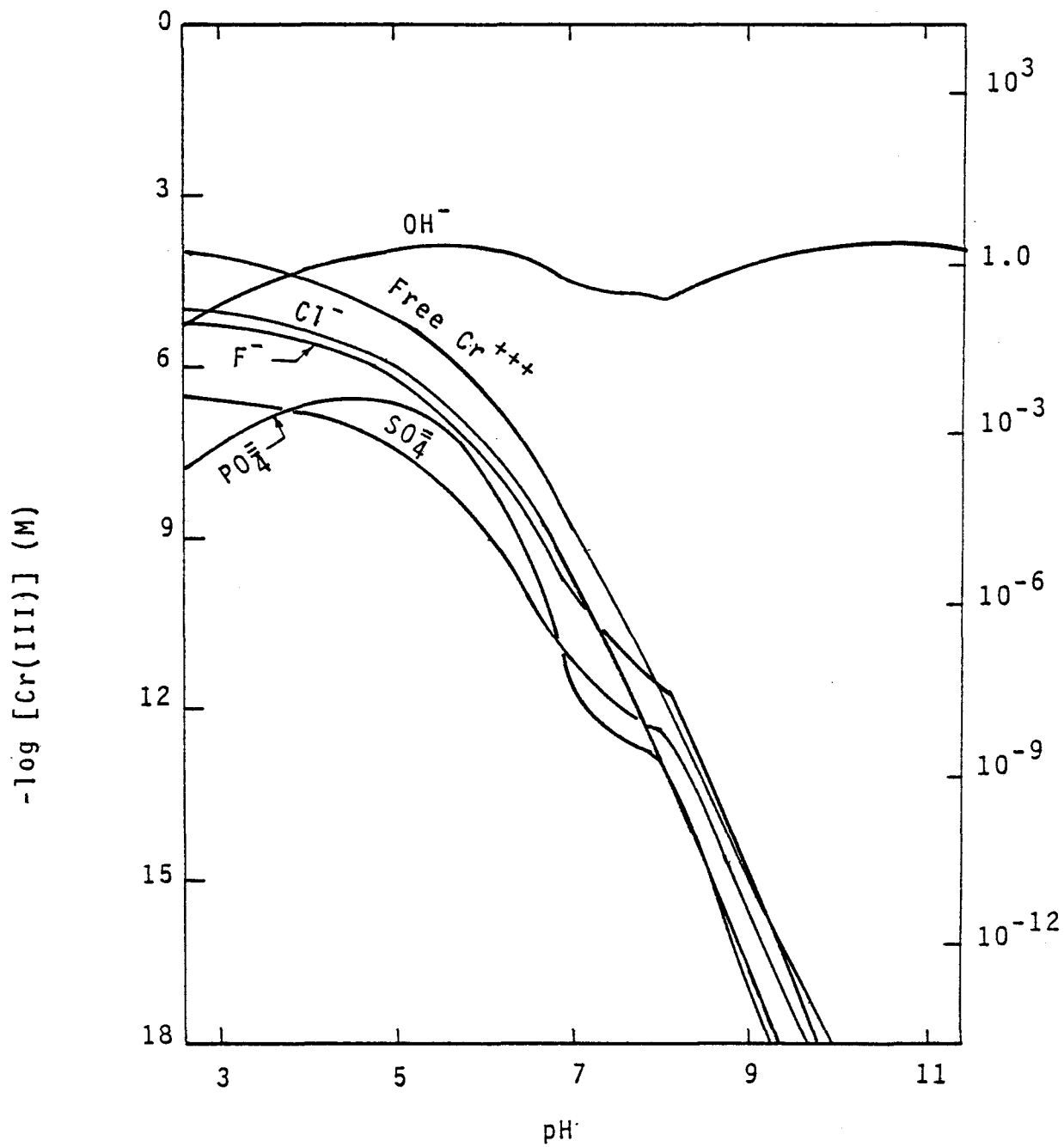
Figure 70. Speciation of soluble Cr in aged FGD wastes
at I = 0.8, original $[Cr_T]$ = $10^{-3.99}$M.
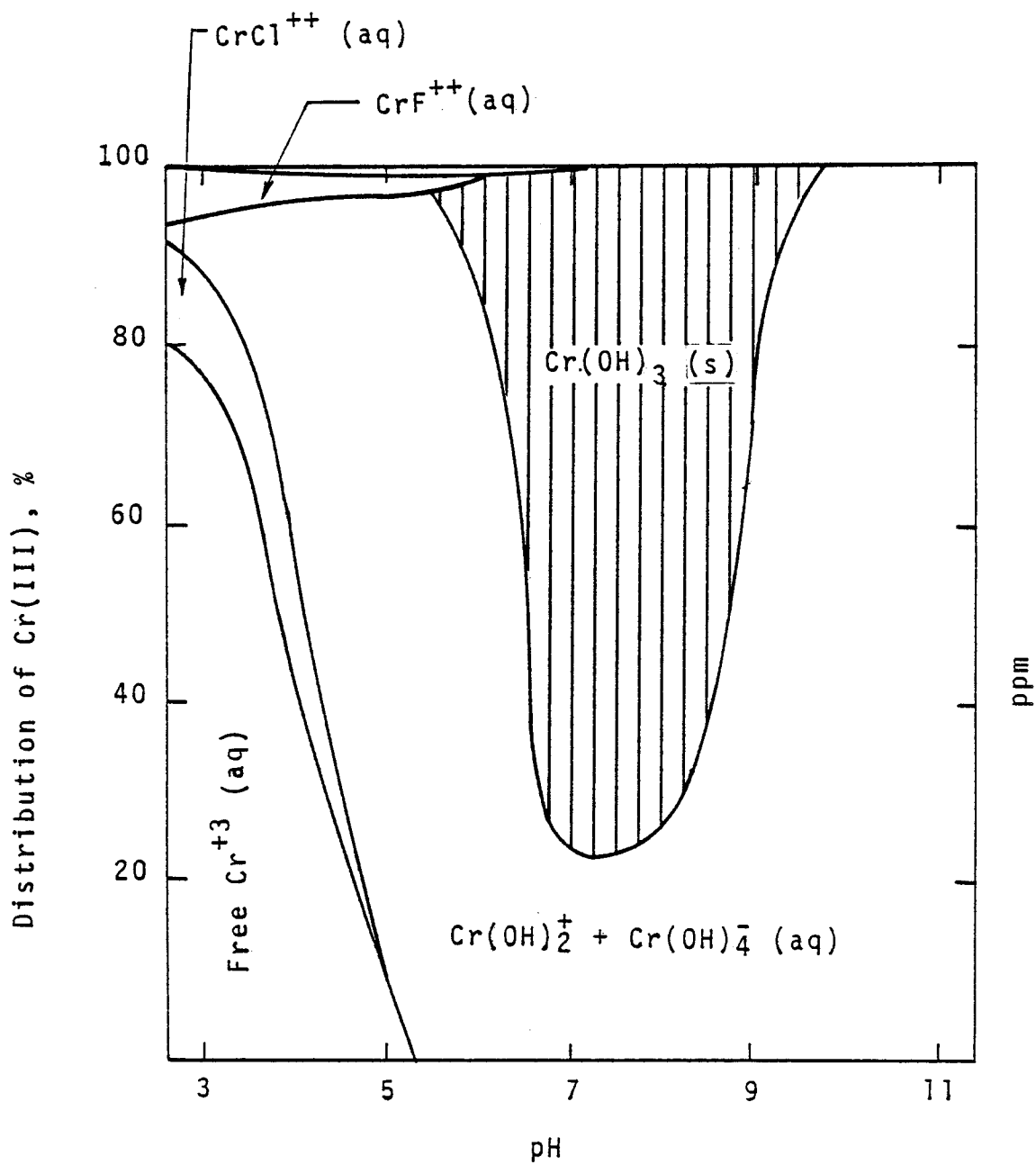
Figure 71. Primary distribution of Cr in aged FGD wastes at I = 0.8, original $[Cr_T] = 10^{-3.99}M$.
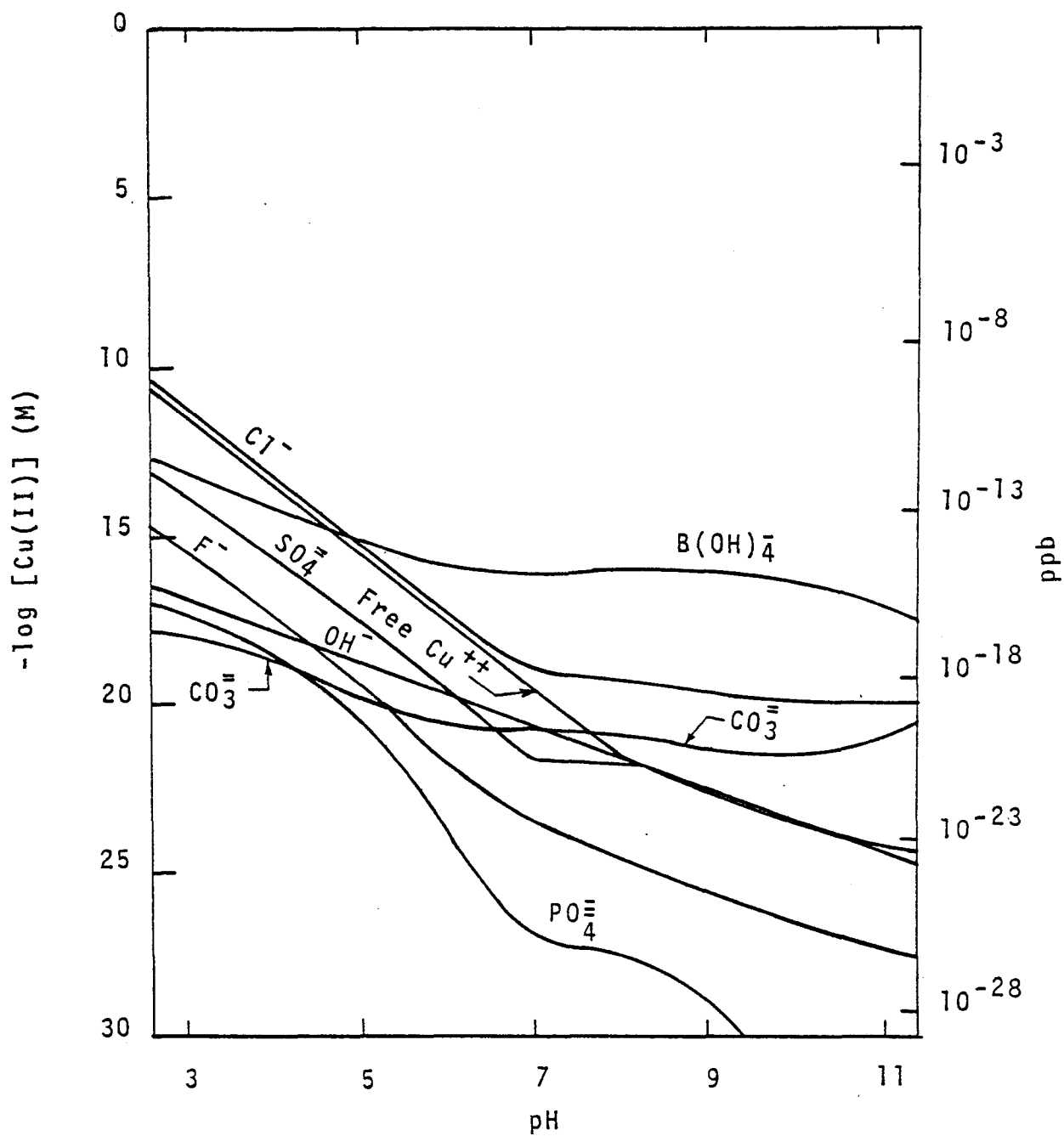
Figure 72. Speciation of soluble Cu in aged FGD wastes at I = 0.8, original $[Cu_T] = 10^{-4.16}M$.
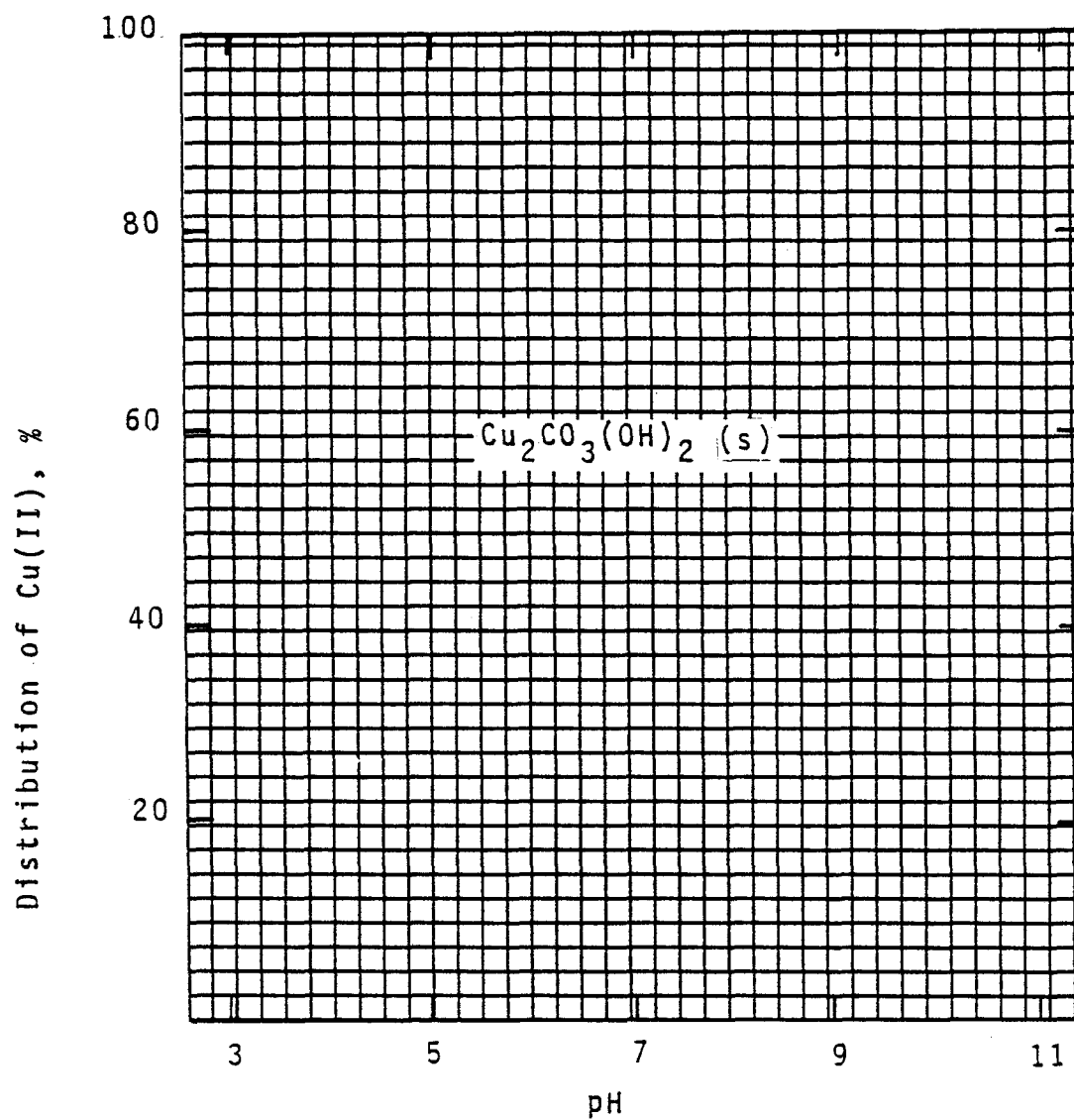
Figure 73.   Primary distribution of Cu in aged FGD wastes
at I = 0.8, original $[Cu_T] = 10^{-4.16}M$.
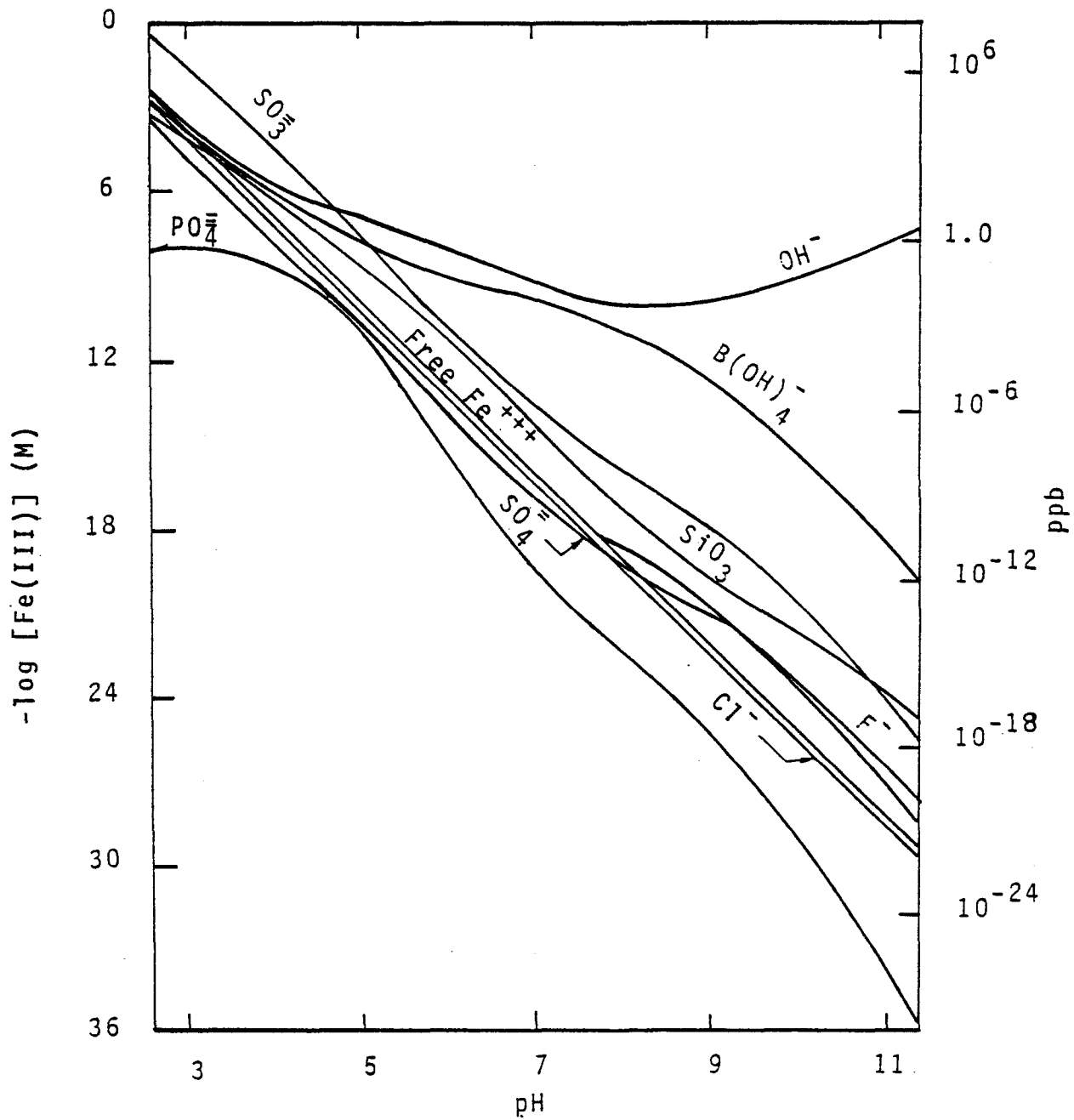
Figure 74. Speciation of soluble Fe(III) in aged FGD wastes
at I = 0.8, original $[Fe_T] = 10^{-0.57}M$.
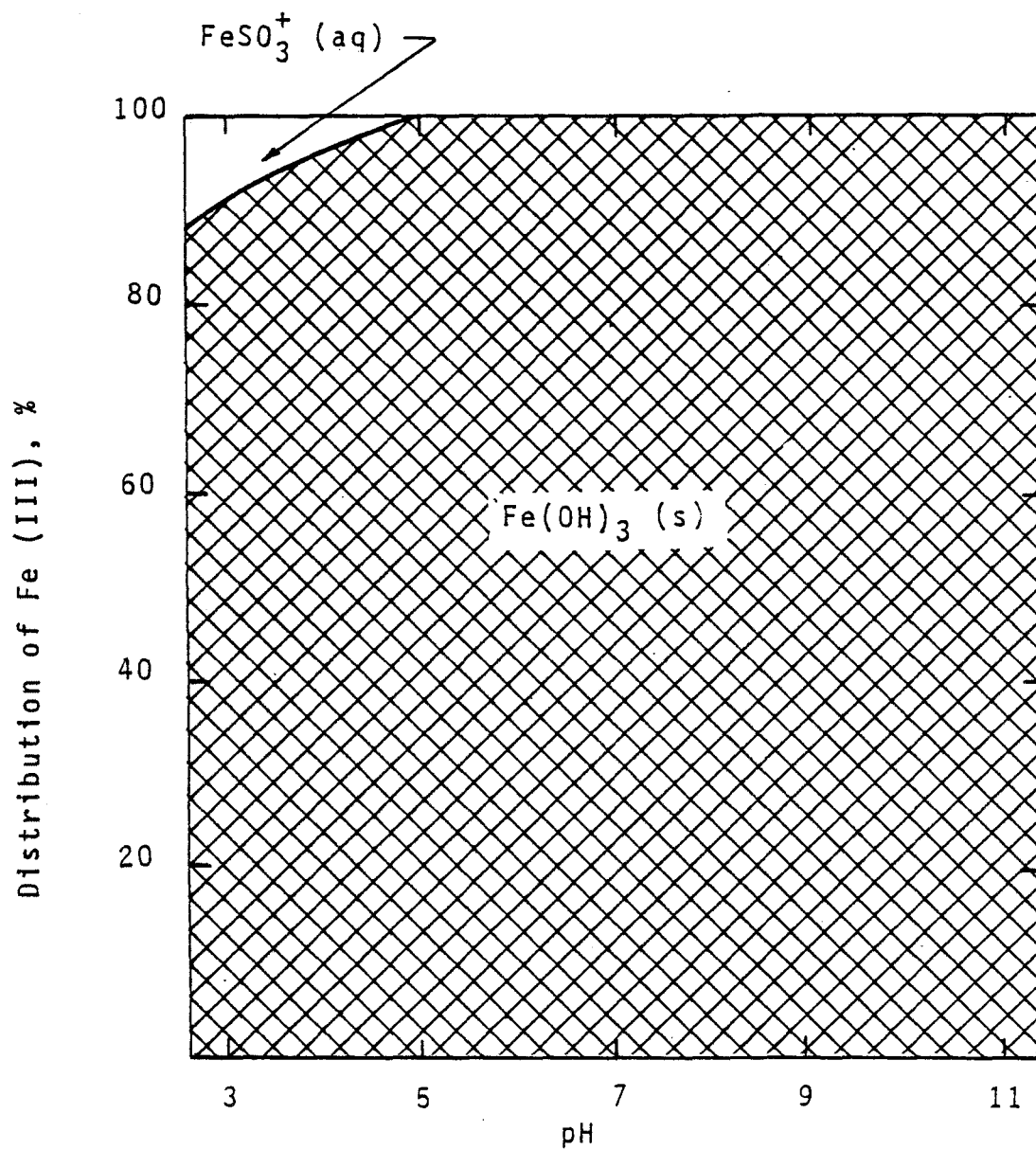
Figure 75. Primary distribution of Fe(III) in FGD wastes at I = 0.8, original $[Fe(III)_T] = 10^{-0.57}M$.
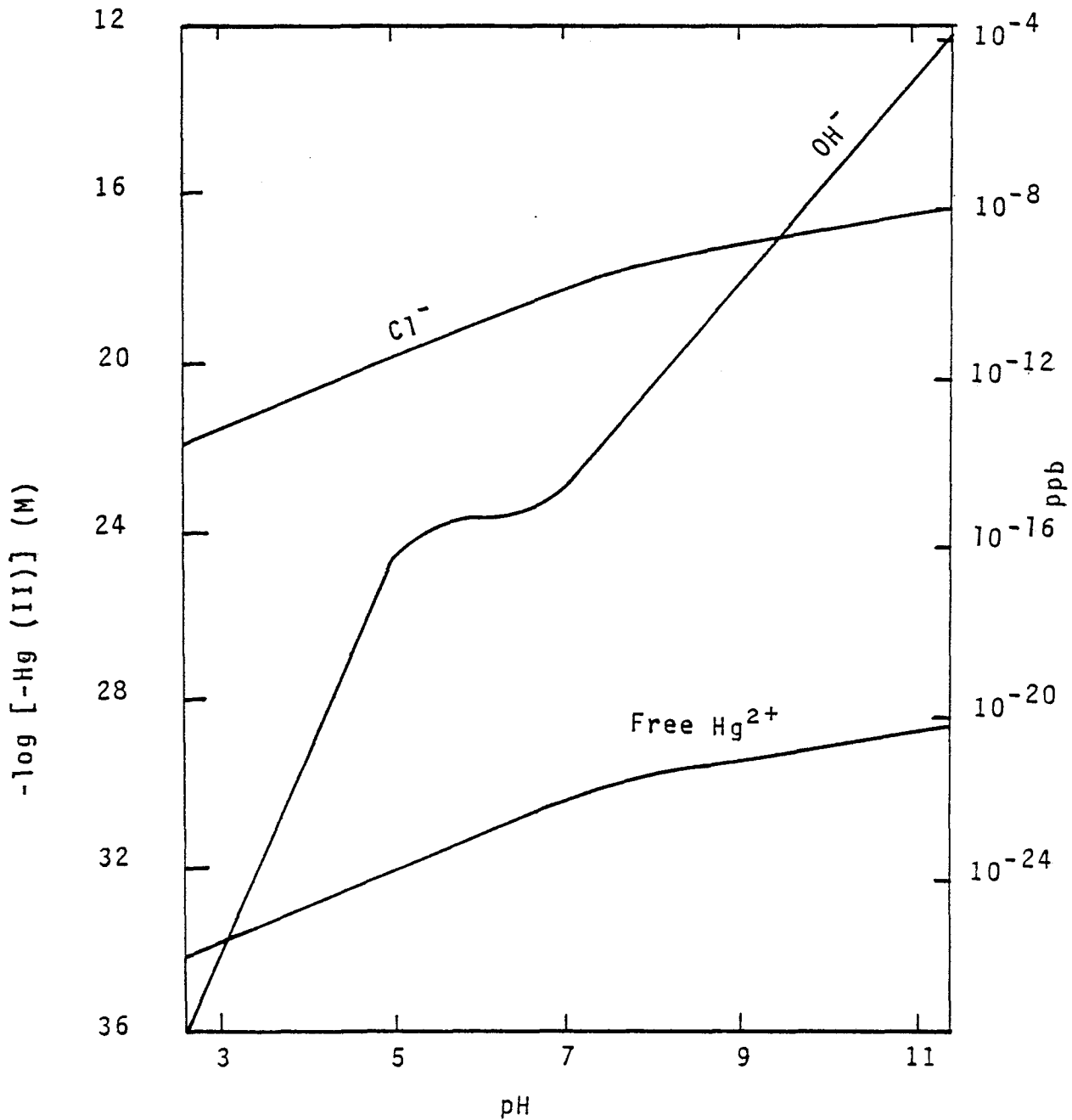
Figure 76.   Speciation of soluble Hg(II) in aged FGD wastes
at I = 0.8, original $[Hg_T] = 10^{-5.74}M$.
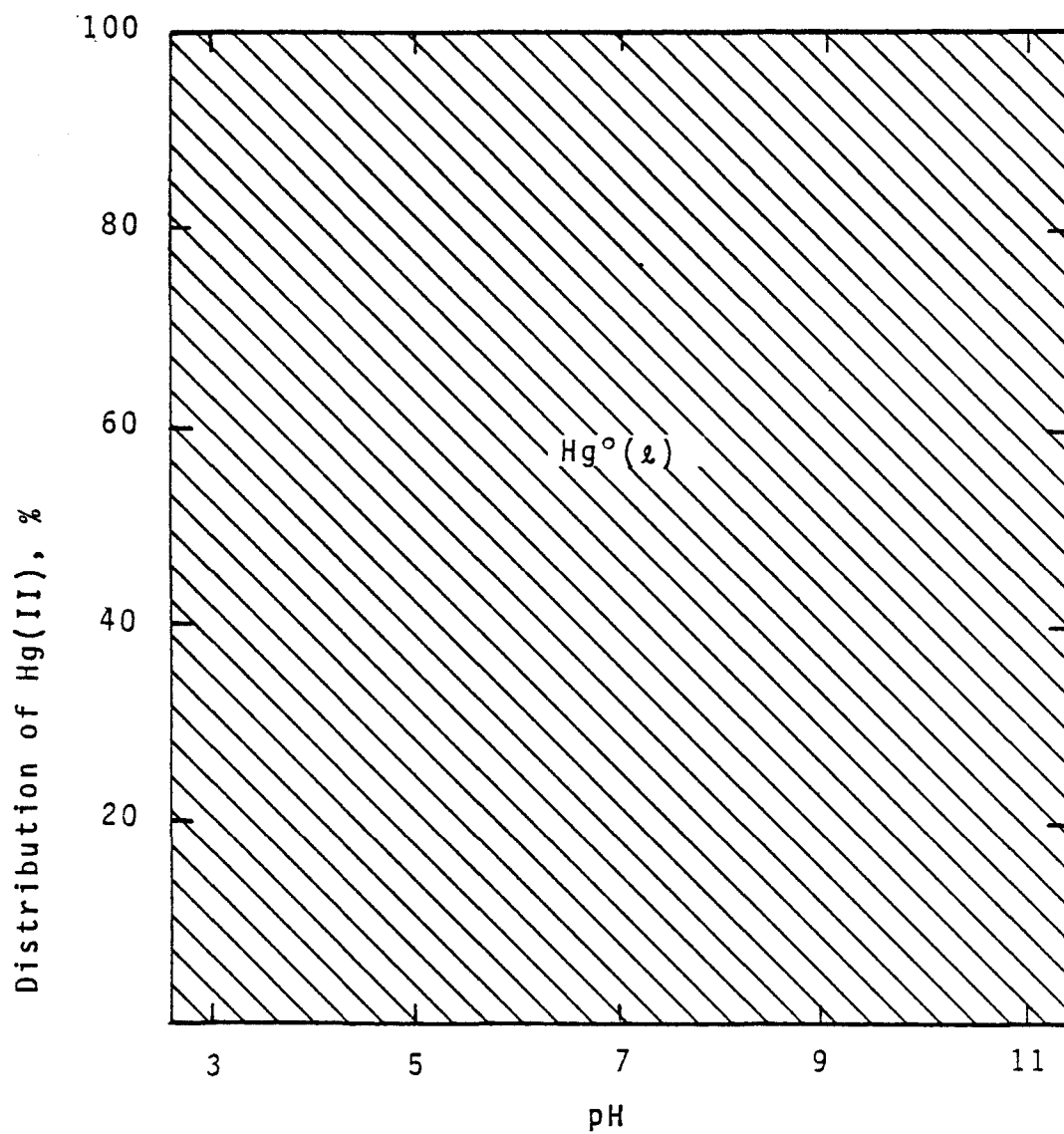
Figure 77. Primary distribution of Hg in FGD wastes at I = 0.8, original $[Hg_T] = 10^{-5.74}M$.
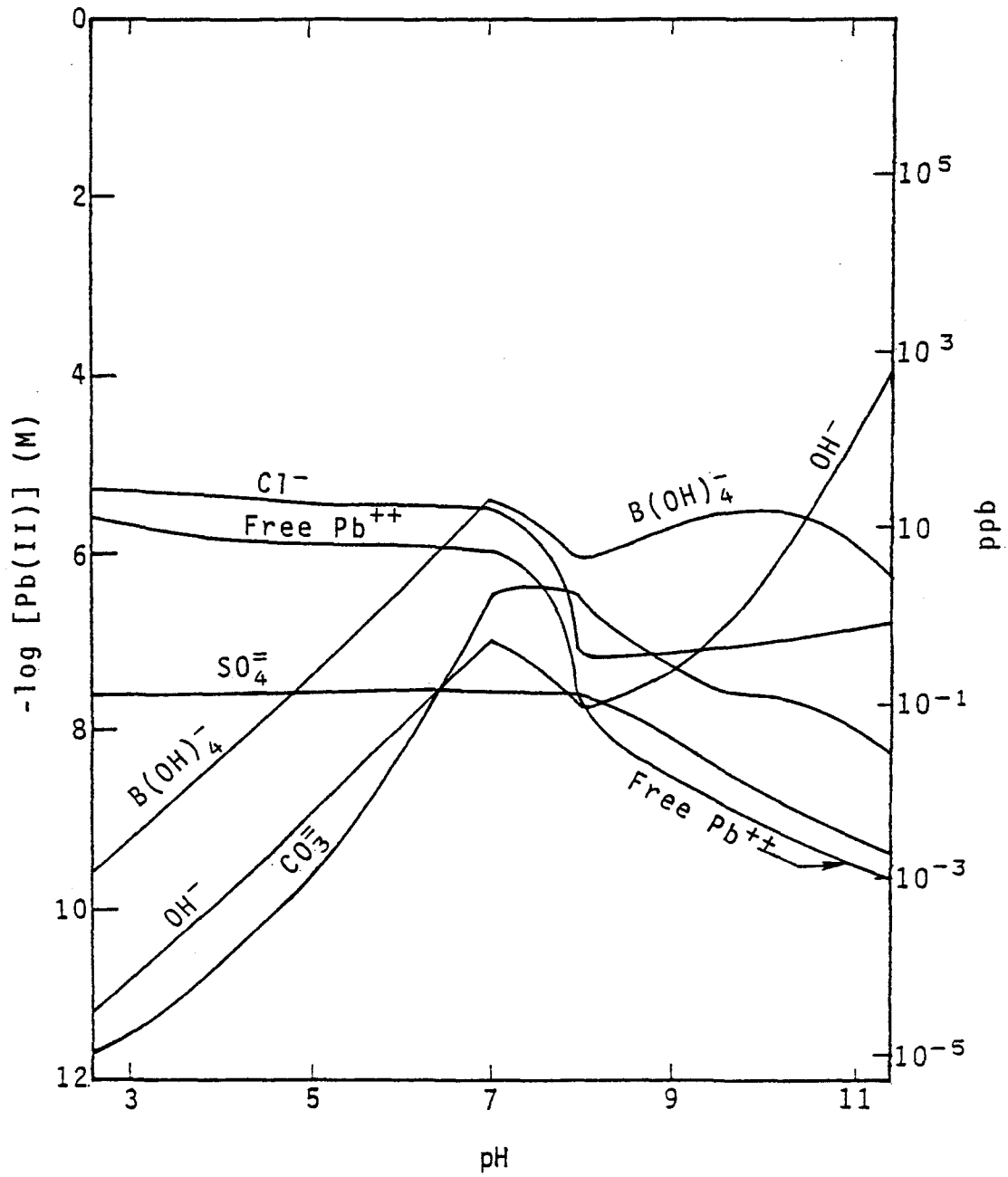
Figure 78.   Speciation of soluble Pb in aged FGD wastes
at I = 0.8, original $[Pb_T] = 10^{-4.65}M$.
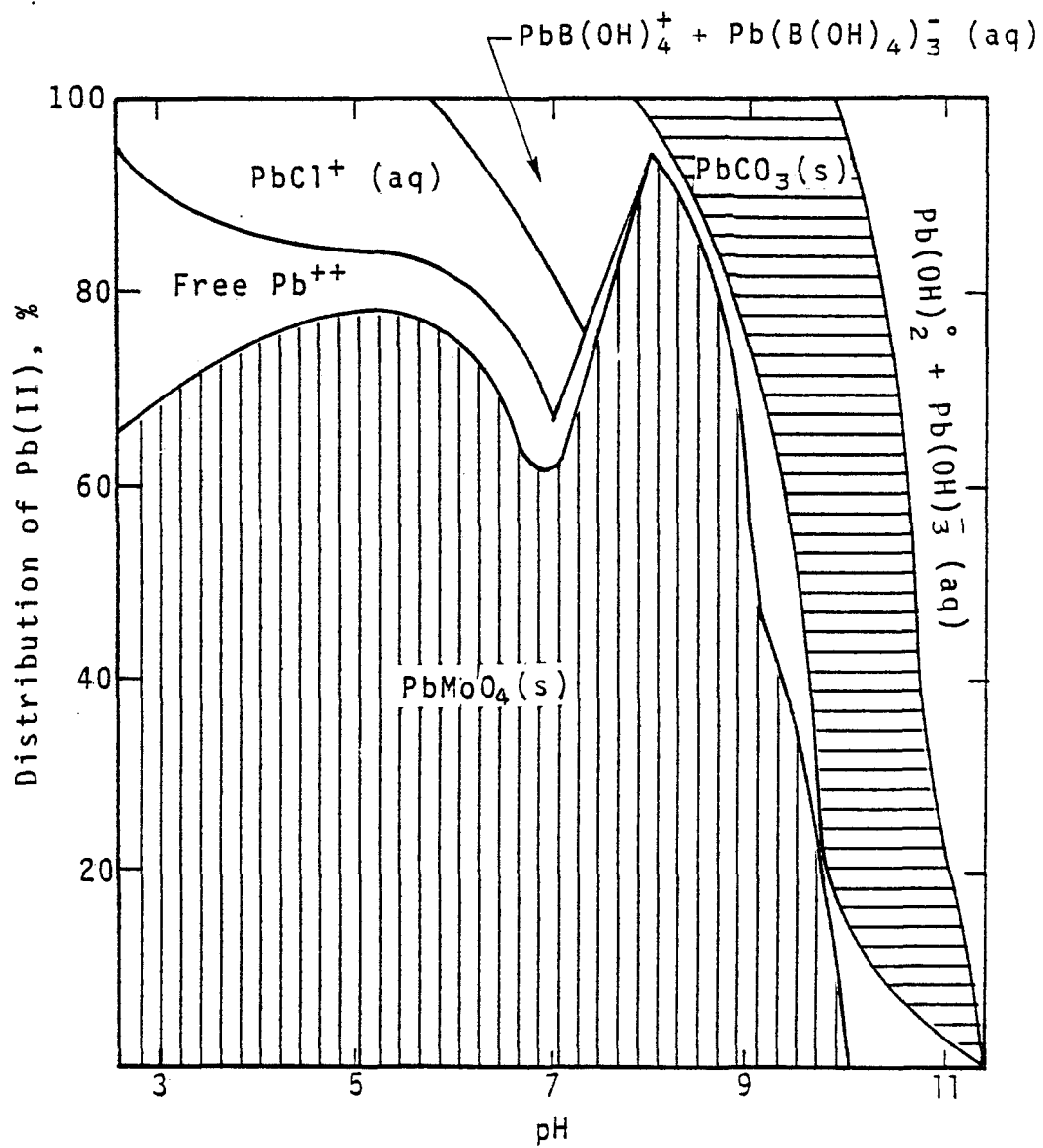
Figure 79. Primary distribution of Pb in aged FGD wastes at I = 0.8, original $[Pb_T] = 10^{-4.65}M$.

154
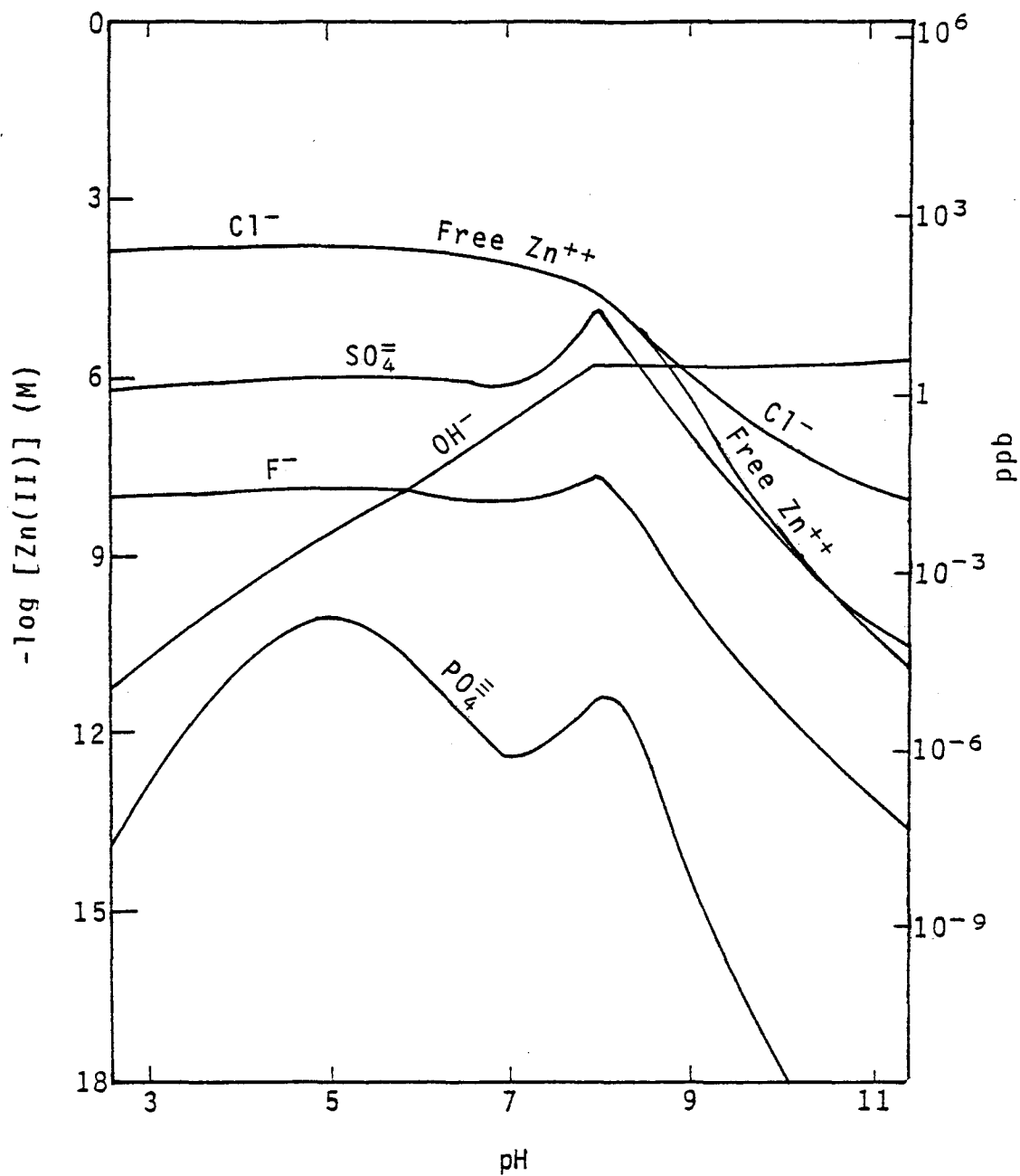
Figure 80.   Speciation of soluble Zn in aged FGD wastes
at I = 0.8, original $[Zn_T] = 10^{-3.57}M$.
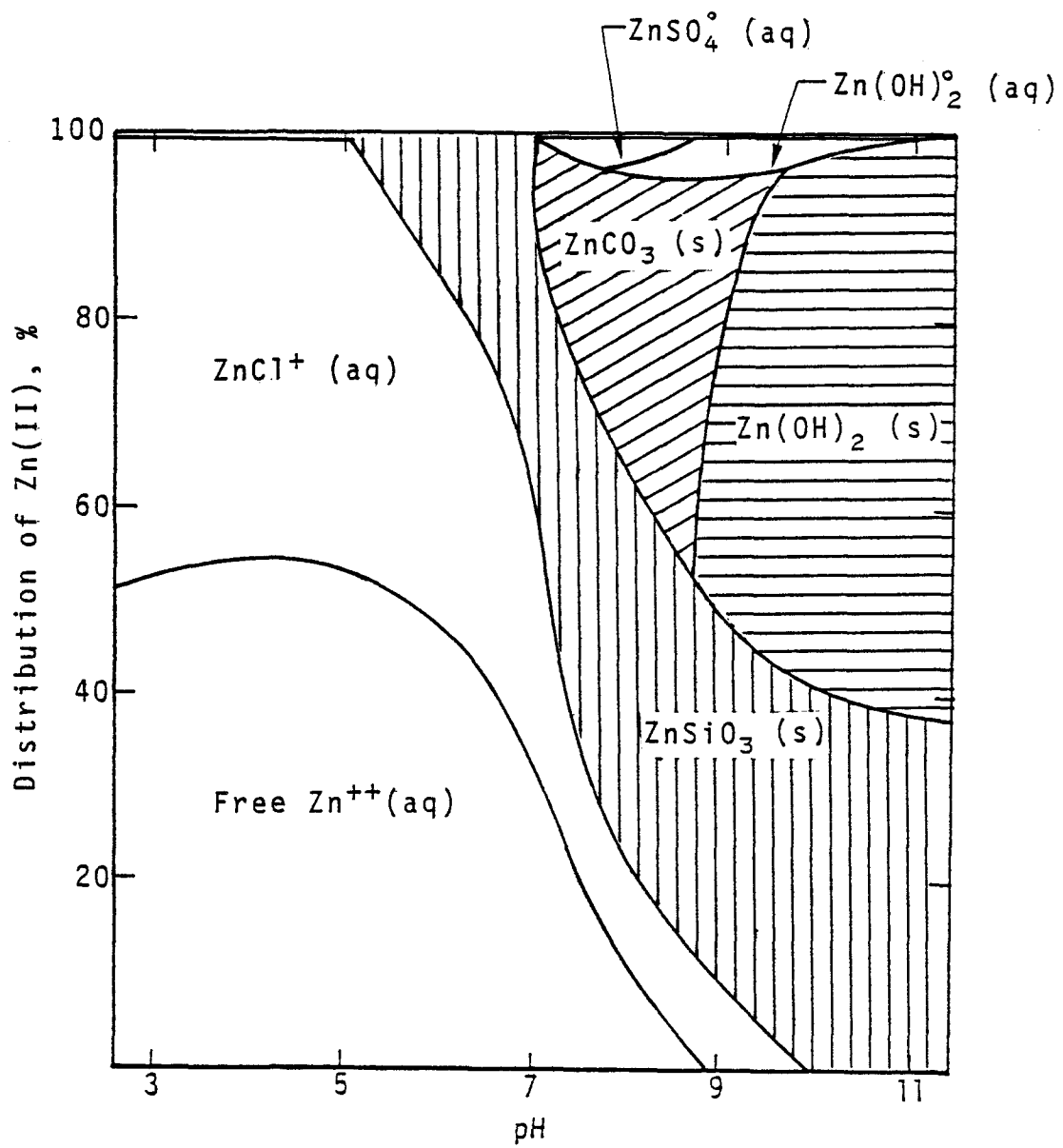
Figure 81. Primary distribution of Zn in aged FGD wastes at I = 0.8, original $[Zn_T]$ = $10^{-3.57}$M.

hydroxide complexes (mainly $Mg(OH)_2(aq)$ also become insignificant in the high ionic strength case.

Due to the formation of hydroxide solids at high pH levels (pH 9), the available soluble magnesium decreases as the wastes are aging. The concentration of soluble magnesium decreases only slightly with age at pH 9, but decreases by a factor of 10^4 at pH 11 (see Figure 62).

Potassium

The distribution of potassium in aged FGD wastes at I=0.8 is also similar to that at I=0.05. But due to the tremendous increase of the soluble sulfate concentration, the concentration of $K-SO_4$ complex is relatively higher in the high ionic strength case. This can be seen by comparing Figures 42 and 43 with Figures 64 and 65.

As mentioned previously, no significant simple potassium solid can be formed in the sludge, so the migration of potassium between solid and liquid phases is negligible. Potassium does exist as complex solids in nature (see Table 4), but with extremely low nucleation and dissolution rates. Therefore, the complex solids of potassium will not play an important role for regulating the soluble potassium levels.

Sodium

The calculated speciation of sodium in aged FGD wastes at I=0.8, is shown in Figures 66 and 67. The pattern of sodium speciation is similar between low and high ionic strength wastes (compare Figures 44 and 45 to Figures 66 and 67). The only difference between these two conditions is the concentration level.

Like potassium, there is no significant simple sodium solid that can regulate the soluble sodium levels in the FGD sludge. Due to kinetic constraints, the complex sodium solid will not play an important role in the transformation of sodium species. Therefore, the sodium concentration in both solid and solution phases of FGD systems will remain at a constant level.

Cadmium

The relative concentrations and percentage distributions of cadmium species in the aged FGD wastes at I=0.8, are shown in Figures 68 and 69. In the high ionic strength case, the cadmium-chloride complexes (mainly $CdCl_2(aq)$ will become the dominant soluble species. Free cadmium ion is the second dominant soluble species; this species is the most common species in the low ionic strength case (I=0.05).

The results also show that cadmium solids are readily formed in aged FGD waste at a pH greater than 7. Two cadmium solids have a stability field in this FGD waste condition: $CdCO_3(s)$ and $Cd(OH)_2(s)$. The former solid is predominant in the pH range from 7 to 10.8. Above pH 10.8, the hydroxide solid can account for more than 40 percent of the total solid cadmium.

Comparing Figures 31 and 68, soluble cadmium concentrations appear to be lower in the aged wastes than in the fresh wastes in the pH range of 7.8 to 10.2 This pH range is in the stability field of $CdCO_3(s)$.

Chromium

The results of the chromium speciation calculation are shown in Figures 70 and 71. Since the amount of soluble chromium is only slightly different between low and high ionic strength cases (Table 9), the speciation patterns of chromium are very similar in both cases (see also Figures 48 and 49.)

In comparing the fresh FGD sludge (Figure 32) to the aged sludge (Figures 70 and 71), it appears that chromium is removed from solution during the aging process.

Copper

The thermodynamic model shows that under the conditions studied, the predominant species of copper are the copper-chloride complexes (mainly $CuCl_2(aq)$) at pH less than 4.8, and the copper-borate complexes (mainly $Cu(B(OH)_4)_2(aq)$) when the pH is between 4.8 and 11 (see Figures 72 and 73).

Results also show that copper is readily removed from solution when $Cu_2CO_3(OH)_2(s)$ is formed under aging conditions. This will decrease the soluble copper concentration to trace levels when FGD wastes are aging.

Iron

There is little difference in the total iron concentration in FGD sludge between high and low ionic strength conditions. Therefore, the distribution pattern of iron is similar in both cases (Figures 52 and 53 versus Figures 74 and 75). Since the high ionic strength sludge has higher ligand concentrations, however, the percentage of $FeSO_3^+$ in the FGD sludge appears to be higher in the high ionic strength case.

Mercury

Since in both high and low ionic strength cases the mercury concentration is controlled by $Hg^0(\ell)$, the distribution patterns are very similar (Figures 54 and 55 versus Figures 76 and 77). Almost 100 percent of the mercury exists in the solid phase.

158

As described previously, the Hg-Cl complexes dominate the soluble levels in the low pH region (less than about 9). Due to the high chloride concentration in the high ionic strength case, the soluble mercury is higher in the high ionic strengh FGD sludge than in the low ionic strength FGD sludge.

Lead

Comparing the aged FGD wastes of low (I=0.05) and high (I=0.8) ionic strengths, the most important soluble lead species at low pH (pH 6.8) will change from free lead ion, Pb^{2+}, to the lead-chloride complexes, Pb-Cl, when ionic strength increases. At high pH, the predominant lead species are the lead-borate complexes, $Pb-B(OH)_4$, in the high ionic strength case. Results also show that in the high ionic strength case, 60 to 90 percent of the lead can be precipitated as $PbMoO_4(s)$ in the low pH region. At high pH (<pH9), the $PbCO_3(s)$ species can also be formed Figures 78 and 79).

Due to the strong complexation effect by chloride and borate ions, the total soluble lead concentration is higher in the high ionic strength case than in the low ionic strength case (Figures 78 and 56). If this soluble lead level is compared to that of fresh FGD wastes, however (Figure 36), it can be seen that soluble lead concentrations may be reduced by a factor of 10 during the aging process.

Zinc

As in the case of cadmium, copper, and lead, the concentration of zinc-chloride complexes, Zn-Cl, increases in the low pH region for increasing ionic strength. This is due to the increased chloride ion level and its strong complexation with these metals. In high pH aged waste, the zinc-hydroxide complexes, Zn-OH, remain the predominant soluble species as ionic strength increases (Figures 80 and 81).

In comparing Figures 81 and 59, it is evident that the amount of zinc silicate solid $(ZnSiO_3)(s)$ increases with age in high pH, high ionic strength sludge. This is due to increase in silicate ion concentration in the system. At a pH greater than 7, the soluble zinc concentration is reduced substantially due to the formation of $ZnSiO_3(s)$, $ZnCO_3(s)$, and $Zn(OH)_2(s)$ solids (Figures 80 and 81). Therefore, the aging process appears to limit the mobility of zinc in the liquid phase.

159

SECTION 6

THERMODYNAMIC MODEL VERIFICATION

In order to verify the suitability and accuracy of the thermodynamic model used in this study, two complementary verification procedures were employed:

- Comparison of modeling results with analytical data

- Evaluation of the model itself in relation to certain scientific considerations.

The comparison of model results with analytical data is limited by the current state of analytical procedures. In recent years, considerable advances in chemical speciation have been made (Ref. 40-45). No sound analytical scheme exists, however, that can accurately define all chemical species which exist in a given natural system. The difficulty is due both to typical system complexity and to the low concentrations of metal species in nature. Therefore, verification of the model using analytical data was limited to (1) comparing <u>total</u> liquid phase concentrations with the total concentrations predicted by the model; and (2) comparison of the solid transformation data to the predicted distribution of stable solids.

Evaluation of the model according to certain scientific considerations provides a general check on model behavior. If a certain variation of input parameters is performed, its perturbation of the model system can be checked for reasonableness against expected trends or results. For example, consider the case in which the model predicts that, for element X, one percen of the total liquid phase concentration of X exists as the chemical species M_mL_n. This cannot be verified by total chemical analysis. However, by increasing the concentration of ligand L to abnormally high levels, the predicted change in M_mL_n concentration can be compared to scientific fact.

COMPARISON OF MODELING RESULTS WITH ANALYTICAL DATA

As mentioned previously, evaluation of the model using analytical data can be approached in two ways:

- Comparison of the total soluble concentrations of constituents in stabilized leachates to the total soluble concentrations of constituents, as predicted by the model

- Comparison of the solid transformation data to the distribution of stable solids as predicted by the model.

Due to the lack of solid transformation data in the published literature, only the first method of comparison will be discussed.

A comparison of the total soluble constituent concentrations with the results of thermodynamic calculation requires analytical data for aged FGD wastes. Unfortunately, almost all available data is for relatively fresh FGD wastes, such as scrubber liquor, discharged slurries, or sludge lagoon supernatant. Data for aged sludge (such as interstitial water from the bottom of the sludge lagoons) is still lacking. Because of this, chemical analysis of raw and aged FGD samples was performed.

The La Cygne Power Station (Kansas City Power and Light) was chosen as a location from which necessary samples could best be obtained. The La Cygne FGD system has been on line for several years without a flue gas bypass, and the limestone and coal used by the plant are mined on the site. The FGD chemistry was therefore expected to approach "steady state" conditions with respect to sludge composition. Four types of FGD sludge/wastewater samples were obtained for analysis:

- Fresh FGD wastewater samples from the scrubber

- Fresh FGD sludge solids samples from the FGD scrubber

- Aged FGD wastewater samples from the far end (away from the discharge point) of the second-stage sludge lagoon

- Aged FGD sludge samples from the far end (the oldest deposition of lime sludge) of the second-stage sludge lagoon, 180 to 270 cm below the surface of the disposed sludge solids.

The sludge samples were further divided into pore water samples and solid sludge samples. The details of sample collection, shipment, preparation, and analytical methods are presented in Appendix B. The results of the analysis of these samples are presented in Table 10.

TABLE 10.   ANALYTICAL RESULTS OF FGD SAMPLES FROM KCP&L LA CYGNE POWER STATION

Constituent	Type of Sample*					
	FW	SW	FSP	SSP	FSS	SSS
Al	0.48	0.43	0.30	0.20	833	856
Sb	0.086	0.034	0.066	0.038	13.9	8.24
As	0.66	0.24	0.20	0.12	32.6	26.7
Be	0.005	0.002	0.003	0.001	0.69	0.34
Cd	0.045	0.045	0.010	0.010	51.4	56.7
Ca	850	663	810	410	3.45×10^5	3.18×10^5
Cr	0.001	0.002	0.001	0.002	42.7	26.6
Co	0.049	0.038	0.022	0.010	12.9	11.7
Cu	Nil	Nil	Nil	Nil	57	54
Fe	1.0	0.55	0.1	0.04	15,220	18,990
Pb	Nil	Nil	Nil	Nil	382	340
Mg	170	88	174	7.0	1,810	2,330
Mn	2.52	2.10	0.55	0.15	306	303
Hg	Nil	Nil	Nil	Nil	0.28	0.23
Mo	3.0	2.1	4.7	5.8	207	203
Ni	0.40	0.38	0.23	0.02	69.0	70.2
K	83	46	74	82	5,340	4,940
Se	0.250	0.235	0.475	0.425	53.4	48.3
Na	73	55	73	75	1,180	1,310
V	0.19	0.26	0.16	0.21	42.2	35.6
Zn	0.71	1.31	0.06	0.06	591	534
Alk. (as $CaCO_3$)	198	44	188	60	--	--
Cl^-	707	605	760	708	--	--
F^-	13.6	9.6	9.4	5.5	1,120	1,093
SO_3^{2-}	19	17	50	93	--	--
SO_4^{2-}	675	1650	925	625	--	--
Eh (mv)	27	130	77	94	--	--
PO_4-P	0.2	0.1	0.1	0.06	185	154
NO_3-N	4.8	1.4	2.3	1.5	--	--

TABLE 10 (continued)

Constituent	FW	SW	FSP	SSP	FSS	SSS
Si	68	30	30	6.5	--	--
B	38.4	20	33	18.4	85	61
TOC	Nil	Nil	Nil	Nil	--	--
TDS	3,700	3,980	3,920	4,160	--	--
pH	6.54	7.14	7.65	9.30	--	--
$CaSO_4 \cdot 2H_2O$(g/kg)	--	--	--	--	452	384
$CaSO_3 \cdot 1/2H_2O$ (g/kg)	--	--	--	--	295	73.4
$CaCO_3$(g/kg)	--	--	--	--	371	515

The column header "Type of Sample*" spans the sample type columns.

* FW   = Fresh wastewater.
  SW   = Stabilized wastewater.
  FSP   = Pore water from 20 days aged fresh sludge.
  SSP   = Pore water from stabilized sludge (about 5 years old).
  FSS   = Fresh sludge solid.
  SSS   = Stabilized sludge solid (about 5 years old).
  Units: Unless specified; for water sample, the unit is mg/l; for solid
         sample, the unit is mg/kg.

163

The analytical results of the total amount of constituents in the La Cygne Plant raw FGD wastes (see Table 11) were entered into the computer model. The total soluble concentrations of constituents in the FGD wastes in aged condition were then predicted by the model at different pH levels, and compared to the field data. The results are shown in Figures 82 through 98.

In these figures, the analytical results are represented by the numbers 0, 1, 2, and 3. Symbol 0 represents the input data (total levels of constituents in the fresh FGD waste). Symbol 1 represents the analytical results for the soluble constituents in the fresh wastewater (0-day data). Symbol 2 represents the analytical results for the soluble constituents in the "relatively" fresh sludge pore water (fresh sludge was aged in the laboratory for 20 days before the pore water was analyzed). The analytical results for the soluble constituents in the fully aged sludge are represented by Symbol 3. According to the La Cygne Plant engineers, the aged sludge had been in the sludge lagoon for about five (5) years. Therefore, it was assumed that the aged pore water data represents potential (stabilized) leachate conditions in the FGD sludge lagoon.

The evaluation of model results in relation to the analytical data can be performed using the migration trends of the constituents represented by Symbols 1, 2, and 3. If the soluble concentrations indicated by the three data points approach the concentrations predicted by the model, then the model can be deemed an accurate prediction of aging phenomena. The results of the evaluation for the 18 selected elements are summarized in Table 12.

It was found that the analytical results for aluminum, arsenic, cadmium, boron, cobalt, copper, iron, manganese, mercury, potassium, selenium, sodium, and zinc are all either very close to or approach the concentration levels predicted by the model. Therefore, it can be concluded that the model serves as a valid predictor for the final (stabilized) concentration or migration trends of the various species of the above-mentioned elements in the FGD wastes. For some other elements (calcium, chromium, fluoride, lead, and magnesium), prediction techniques were not as successful. For calcium, the total soluble concentrations predicted by the model are much lower than the analytical results. The low levels predicted by the model are due primarily to the formation of calcite, as well as the high levels of free carbonate and sulfate (CO_3^{2-} and SO_3^{2-}, respectively) in regions of high pH. For chromium, the high levels of hydroxide complexes calculated by the model lead to the high soluble levels of chromium in the aqueous phase. For lead, the formation of Pb-CO_3 complexes predicted by the model is the primary reason for the discrepancy. For fluoride, the solid phases assumed for the calculation are apparently not suitable. It was also found by this evaluation that the solid phases assumed for magnesium are too soluble.

164

TABLE 11. TOTAL CONCENTRATIONS OF CONSTITUENTS IN
LA CYGNE FGD SYSTEM

Constituent	Total Concentrations in FGD Wastes (Fresh Wastewater and Fresh Sludge) (M)
Ca	$10^{-0.387}$
Mg	$10^{-1.53}$
K	$10^{-2.67}$
Na	$10^{-2.50}$
Fe	$10^{-1.09}$
Mn	$10^{-2.77}$
Cu	$10^{-3.57}$
Cd	$10^{-3.86}$
Zn	$10^{-2.57}$
Ni	$10^{-3.44}$
Hg	$10^{-6.38}$
Pb	$10^{-3.26}$
Co	$10^{-4.17}$
Cr	$10^{-3.61}$
Al	$10^{-2.03}$
Be	$10^{-4.63}$
CO_3^{2-}	$10^{0.048}$
SO_4^{2-}	$10^{-0.096}$
Cl^-	$10^{-1.70}$
F^-	$10^{-1.73}$
PO_4^{3-}	$10^{-2.75}$
SiO_3^{2-}	$10^{-2.61}$
$B(OH)_4$	$10^{-2.23}$
SO_3^{2-}	$10^{-0.16}$
MoO_4^{2-}	$10^{-3.04}$
AsO_4^{3-}	$10^{-3.85}$
HVO_4^{2-}	$10^{-3.59}$
SeO_3^{2-}	$10^{-3.68}$
Ionic Strength	0.1
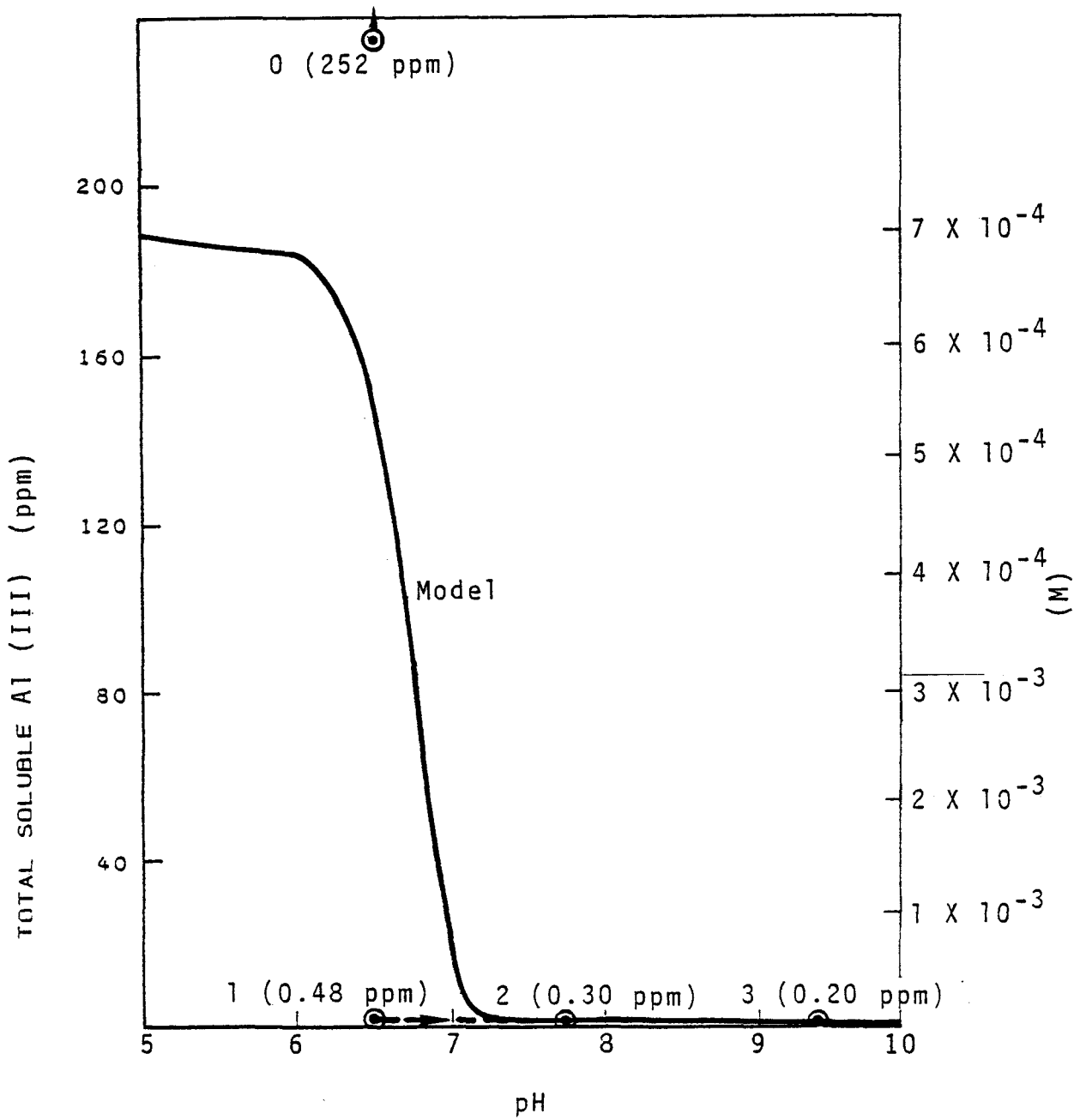
Figure 82. Total soluble Al(III) concentration in La Cygne FGD wastes (see text for explanation).
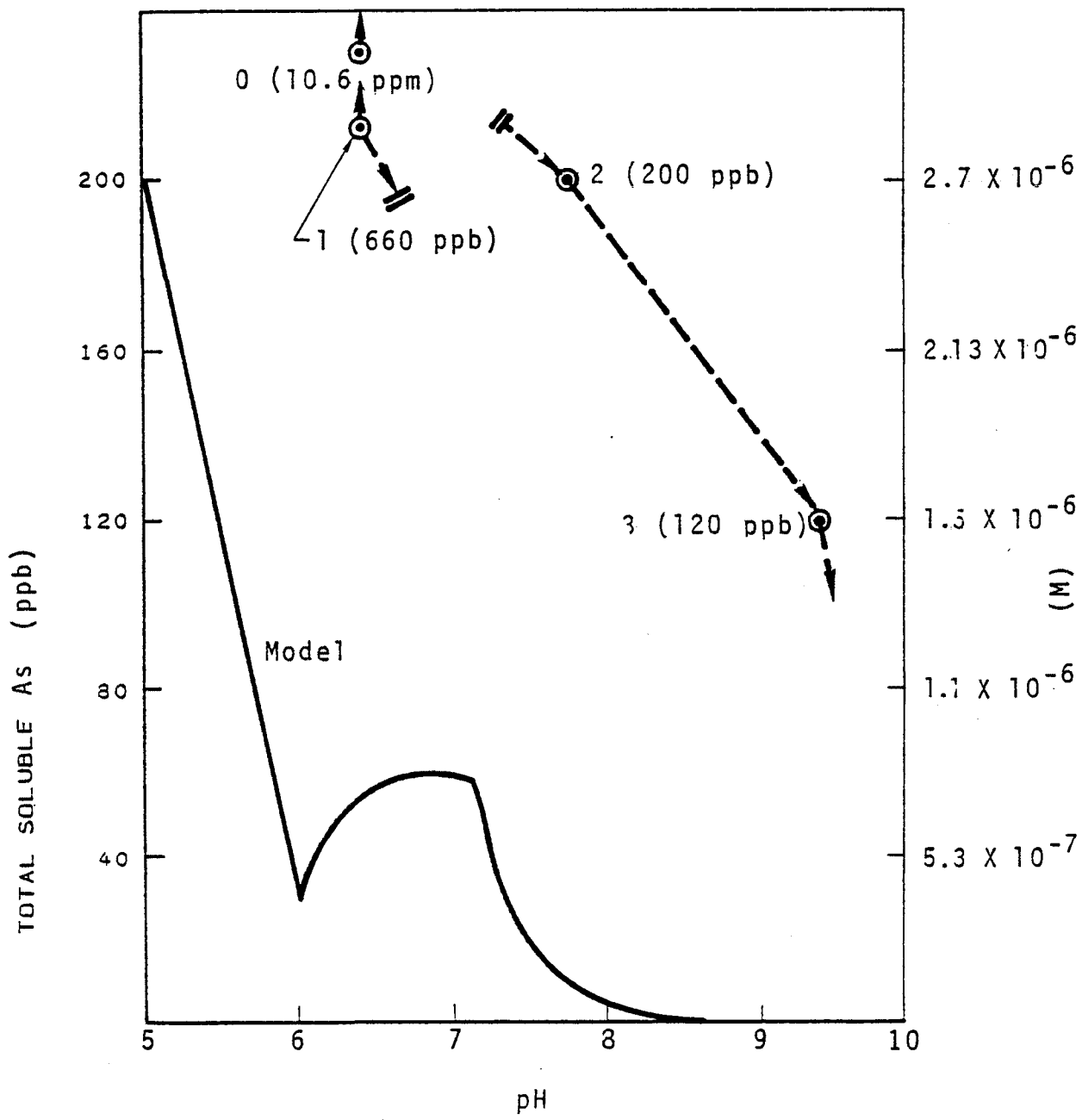
Figure 83. Total soluble As concentration in La Cygne FGD
wastes (see text for explanation).
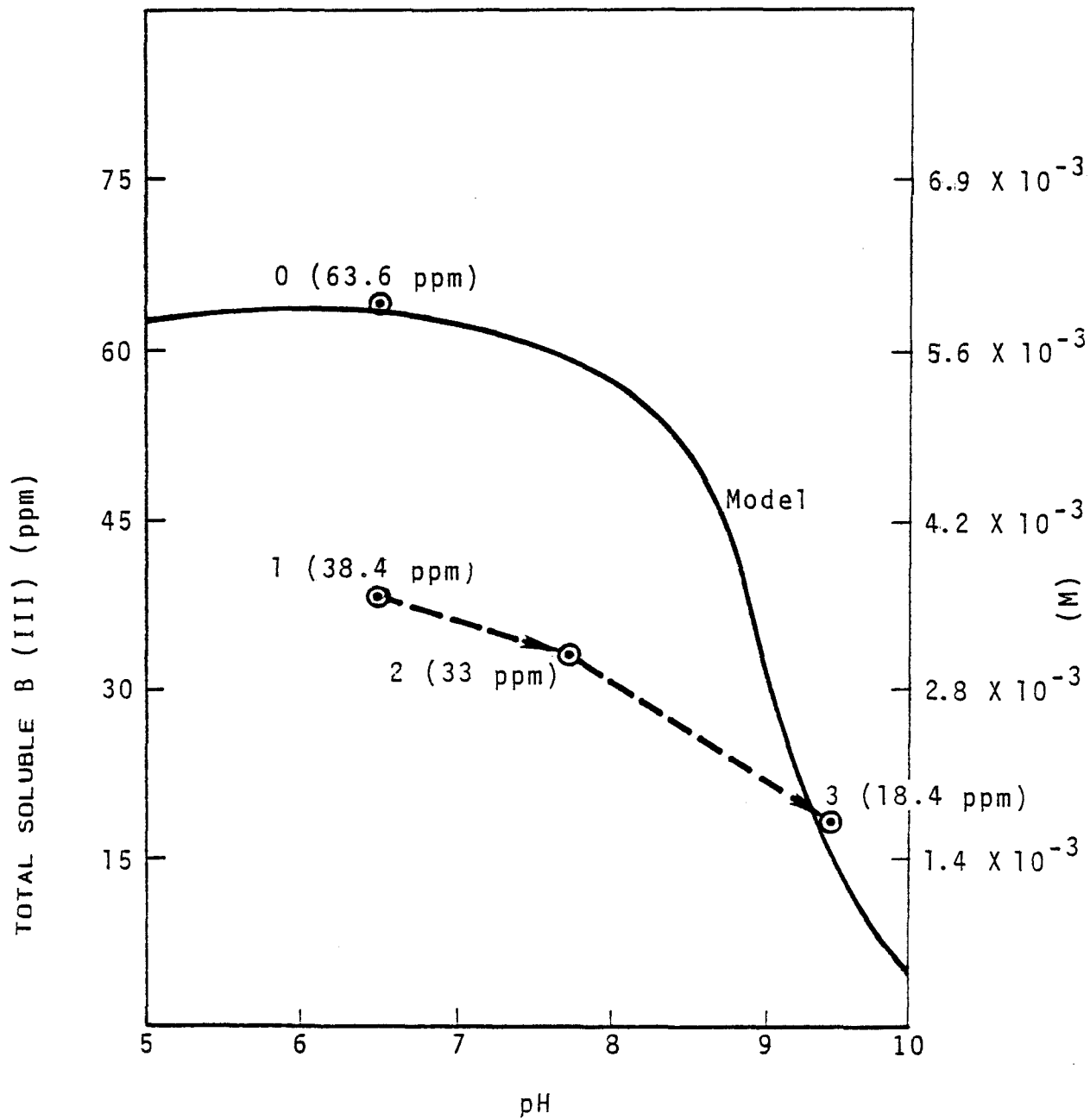
Figure 84.   Total soluble B(III) concentration in La Cygne FGD
wastes (see text for explanation).
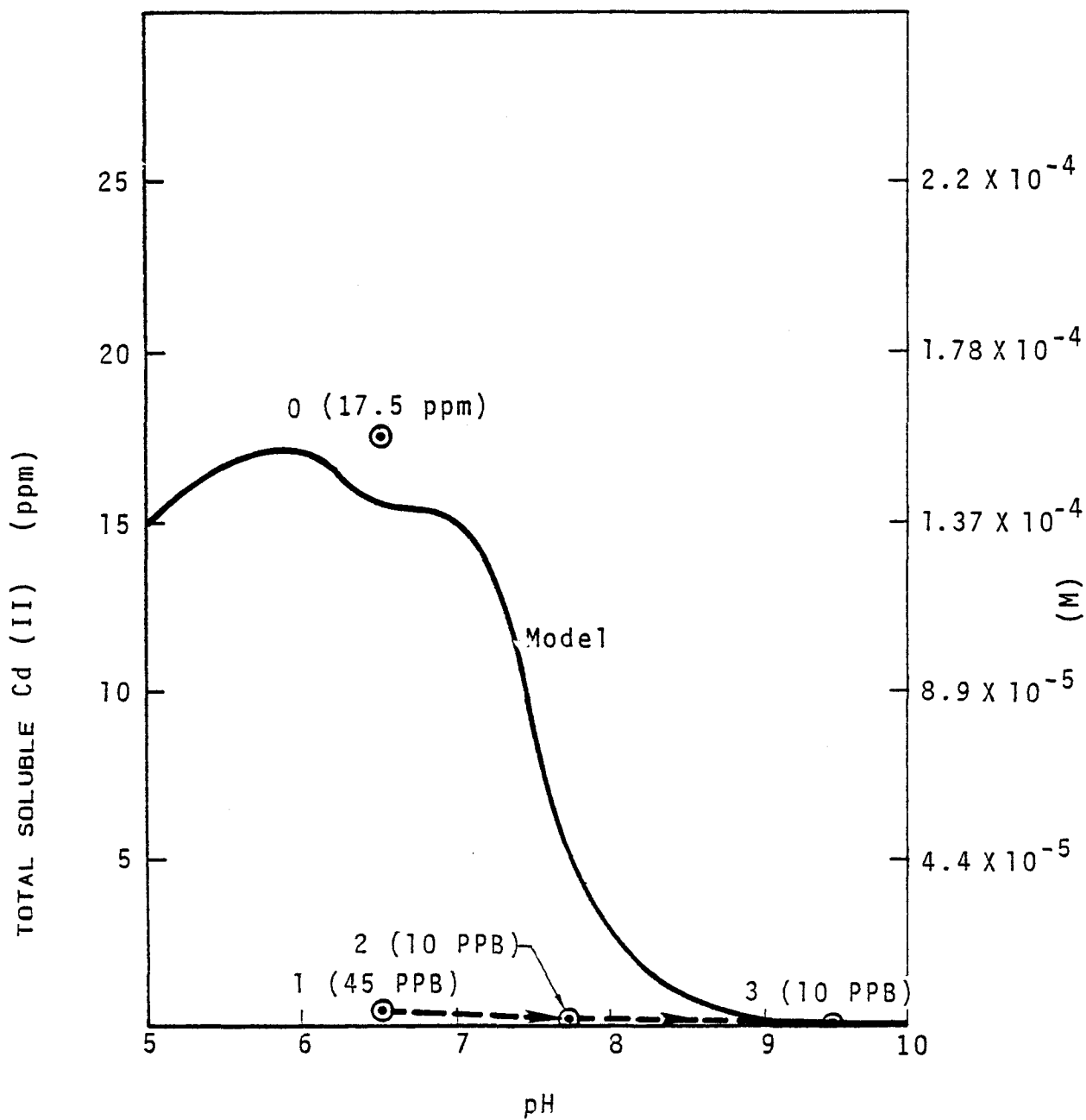
Figure 85. Total soluble Cd(II) concentration in La Cygne FGD wastes (see text for explanation).
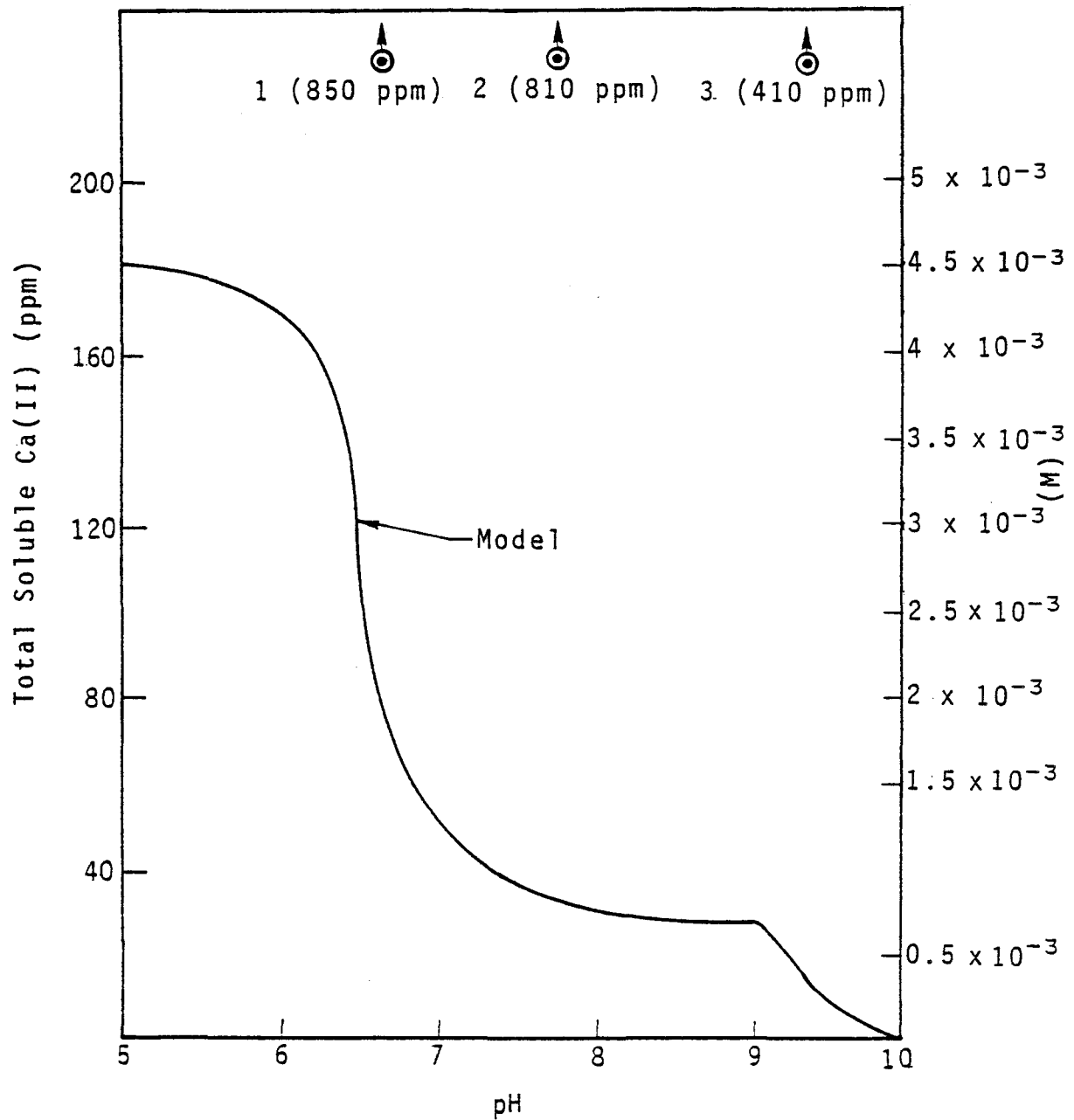
Figure 86.   Total soluble Ca concentration in La Cygne FGD
             wastes (see text for explanation).
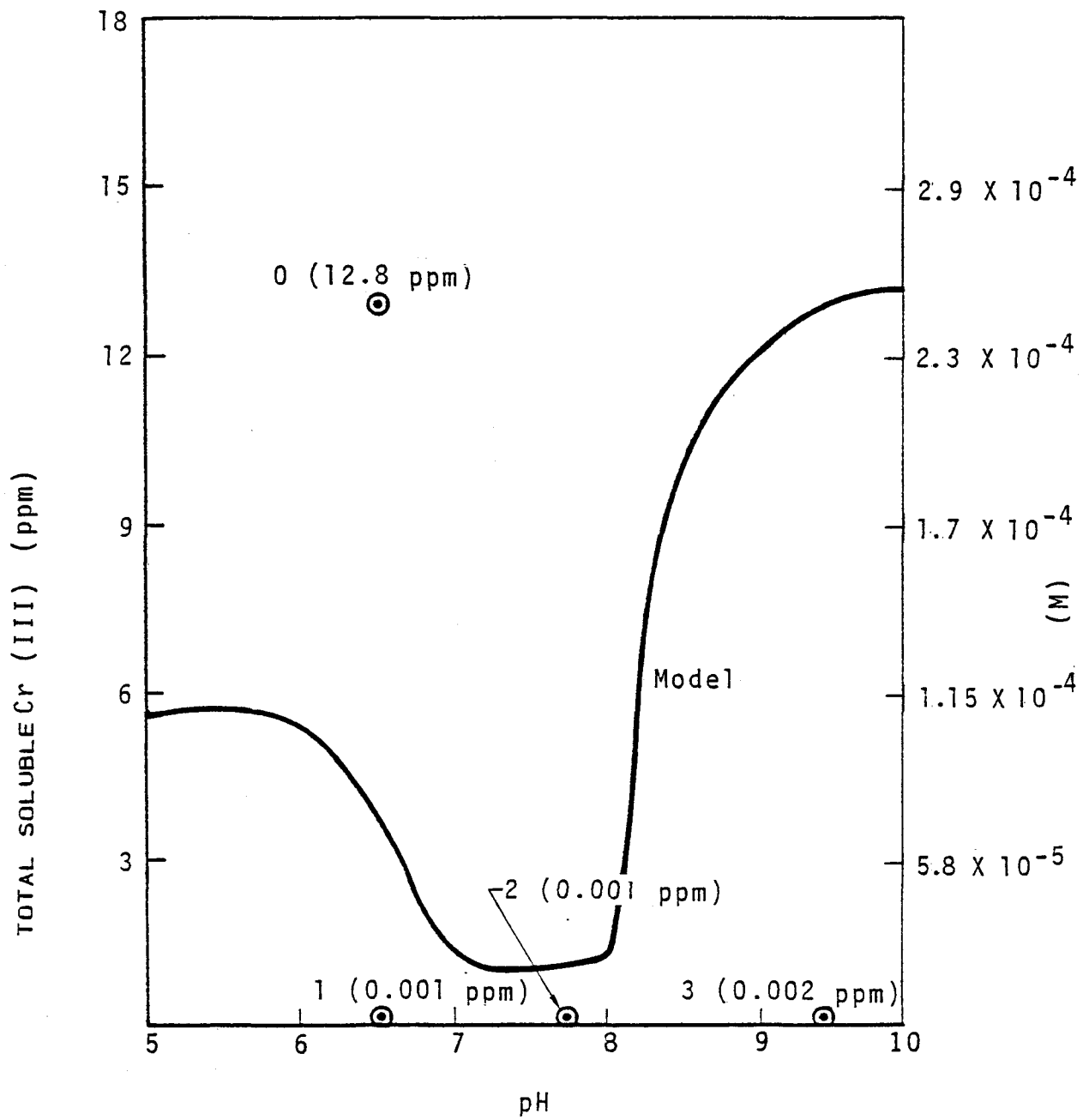
Figure 87. Total soluble Cr(III) concentration in La Cygne FGD
           wastes (see text for explanation).
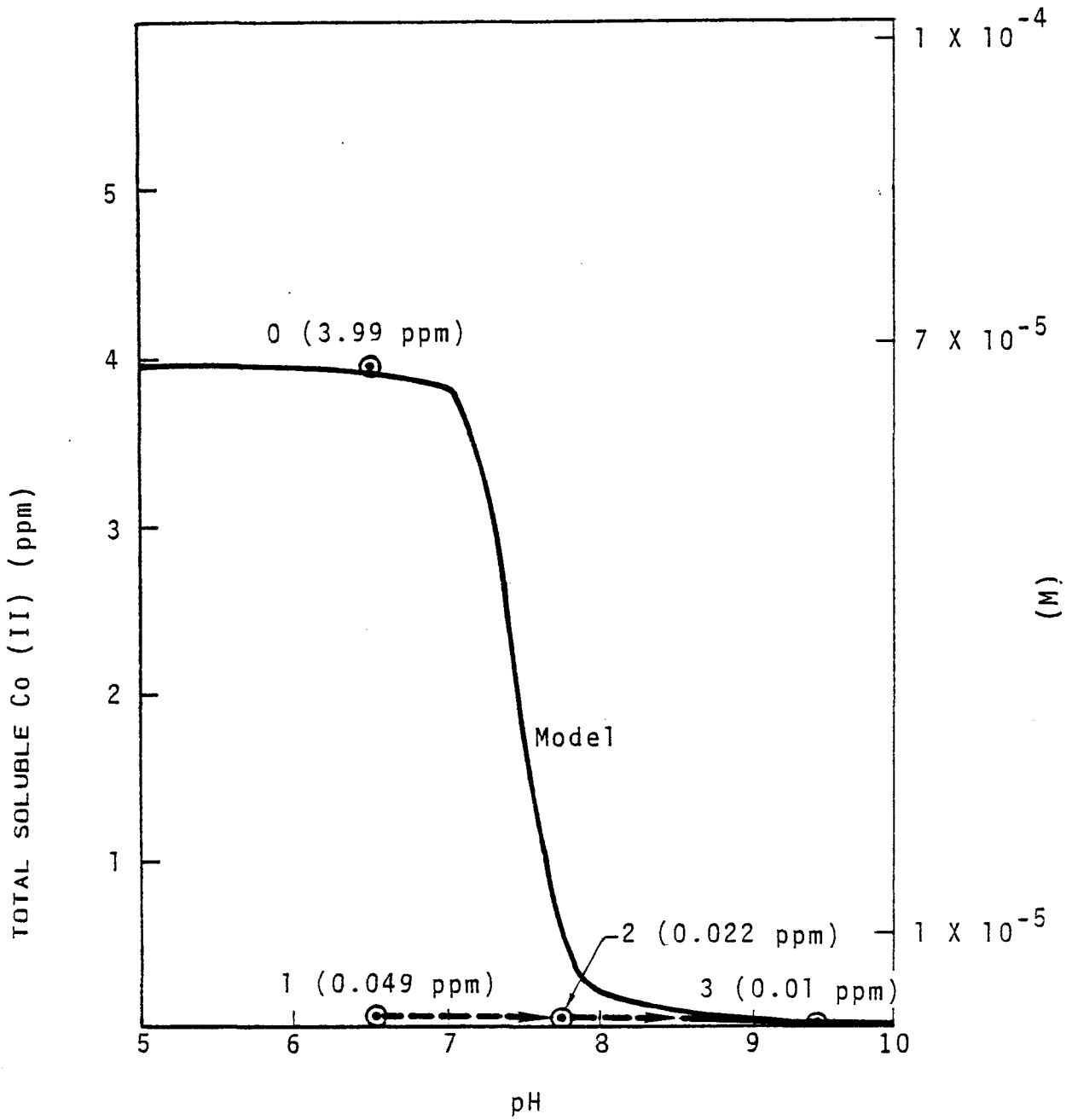
Figure 88.   Total soluble Co(II) concentration in La Cygne FGD
             wastes (see text for explanation).
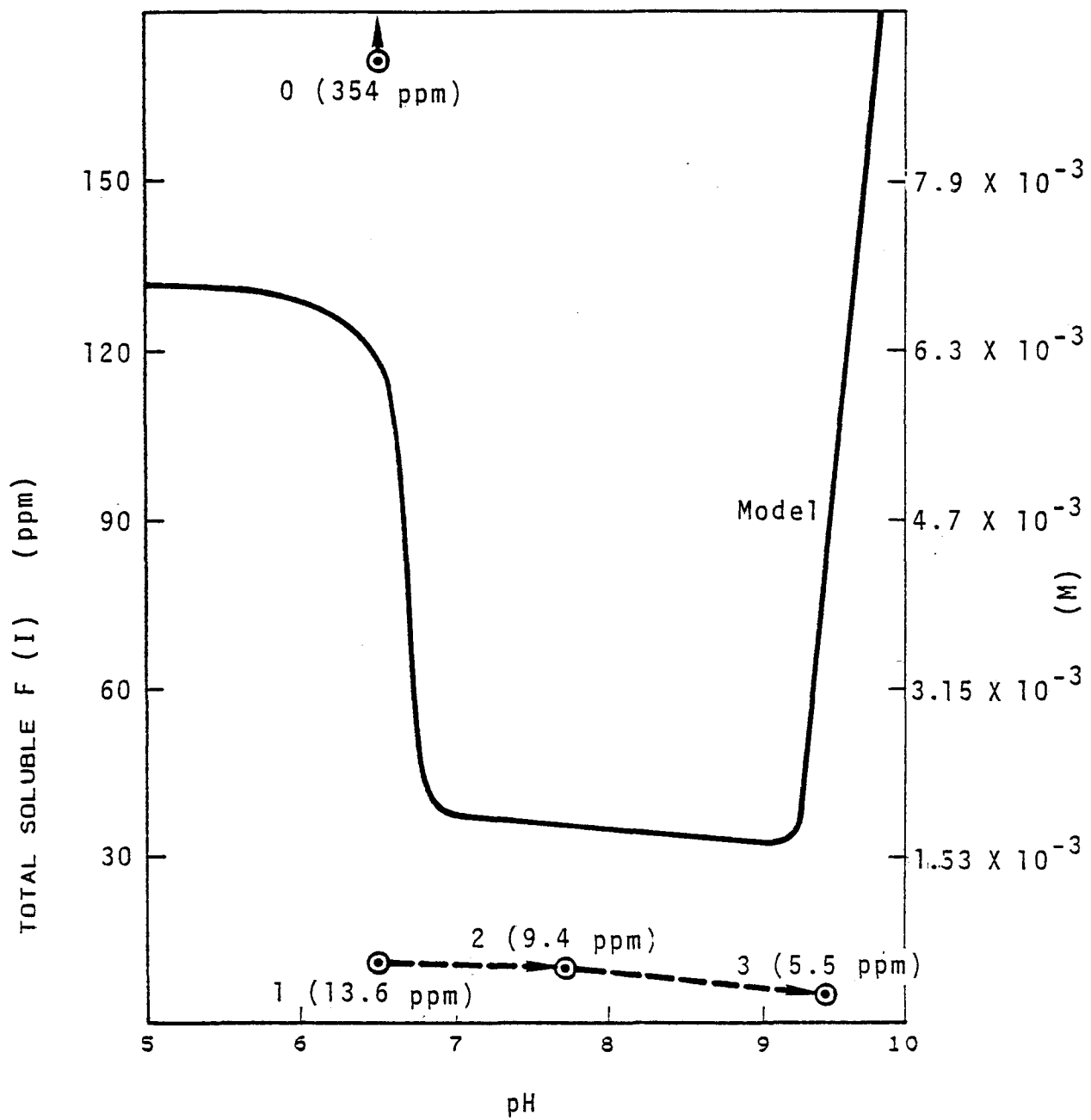
Figure 89. Total soluble F(I) concentration in La Cygne FGD
wastes (see text for explanation).
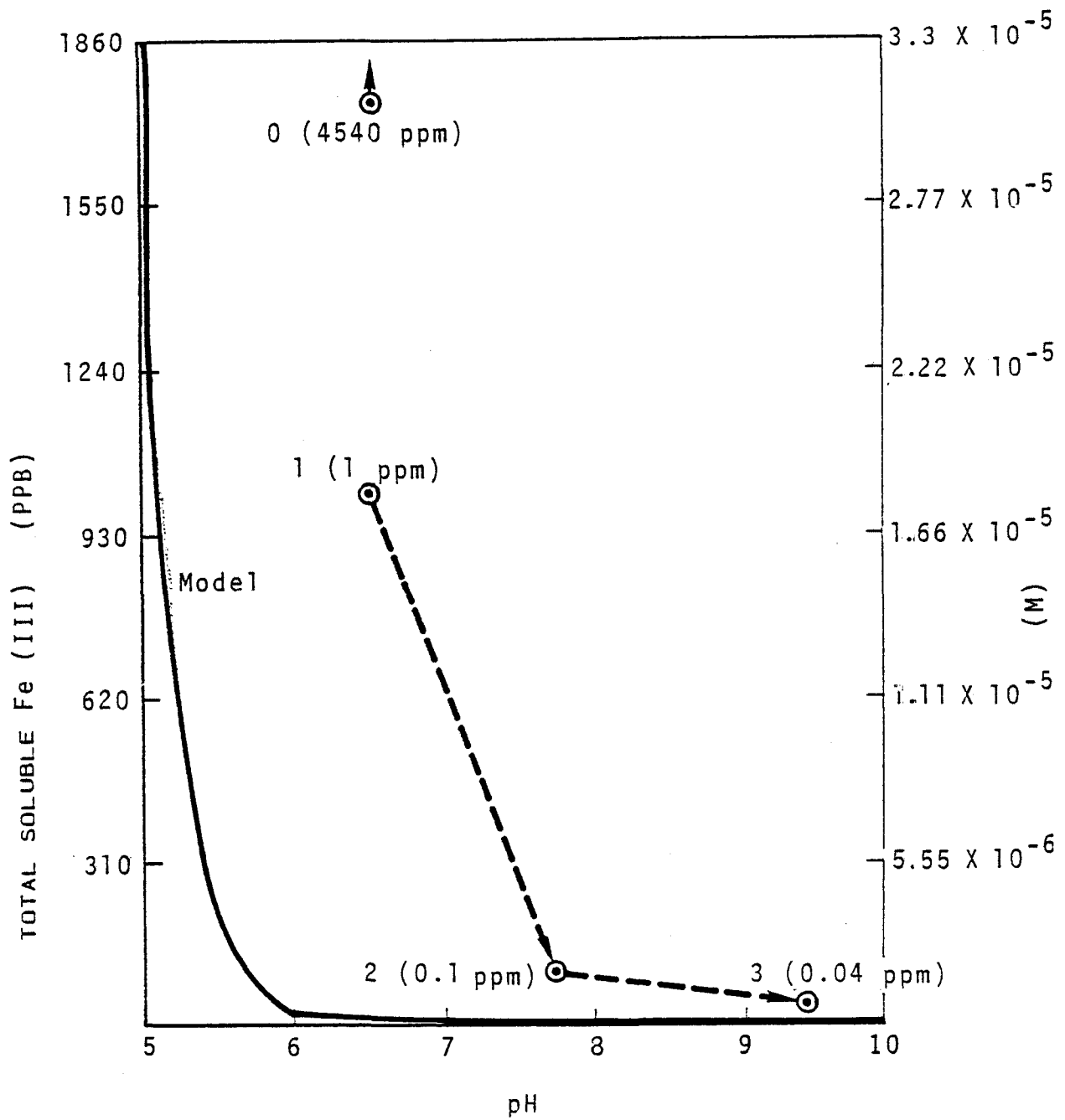
Figure 90.   Total soluble Fe(III) concentration in La Cygne FGD wastes (see text for explanation).
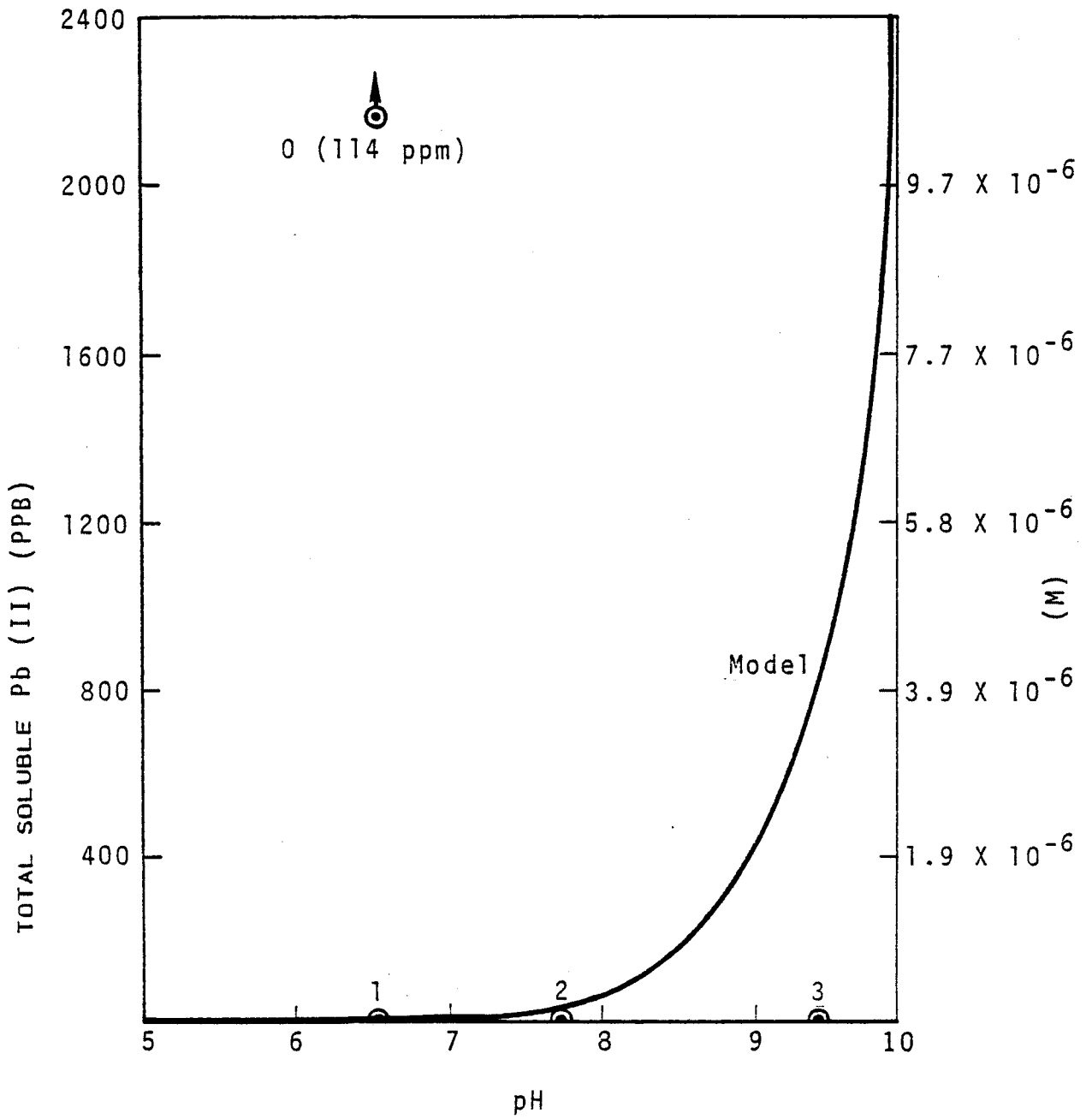
Figure 91.   Total soluble Pb(II) concentration in La Cygne FGD
             wastes (see text for explanation).
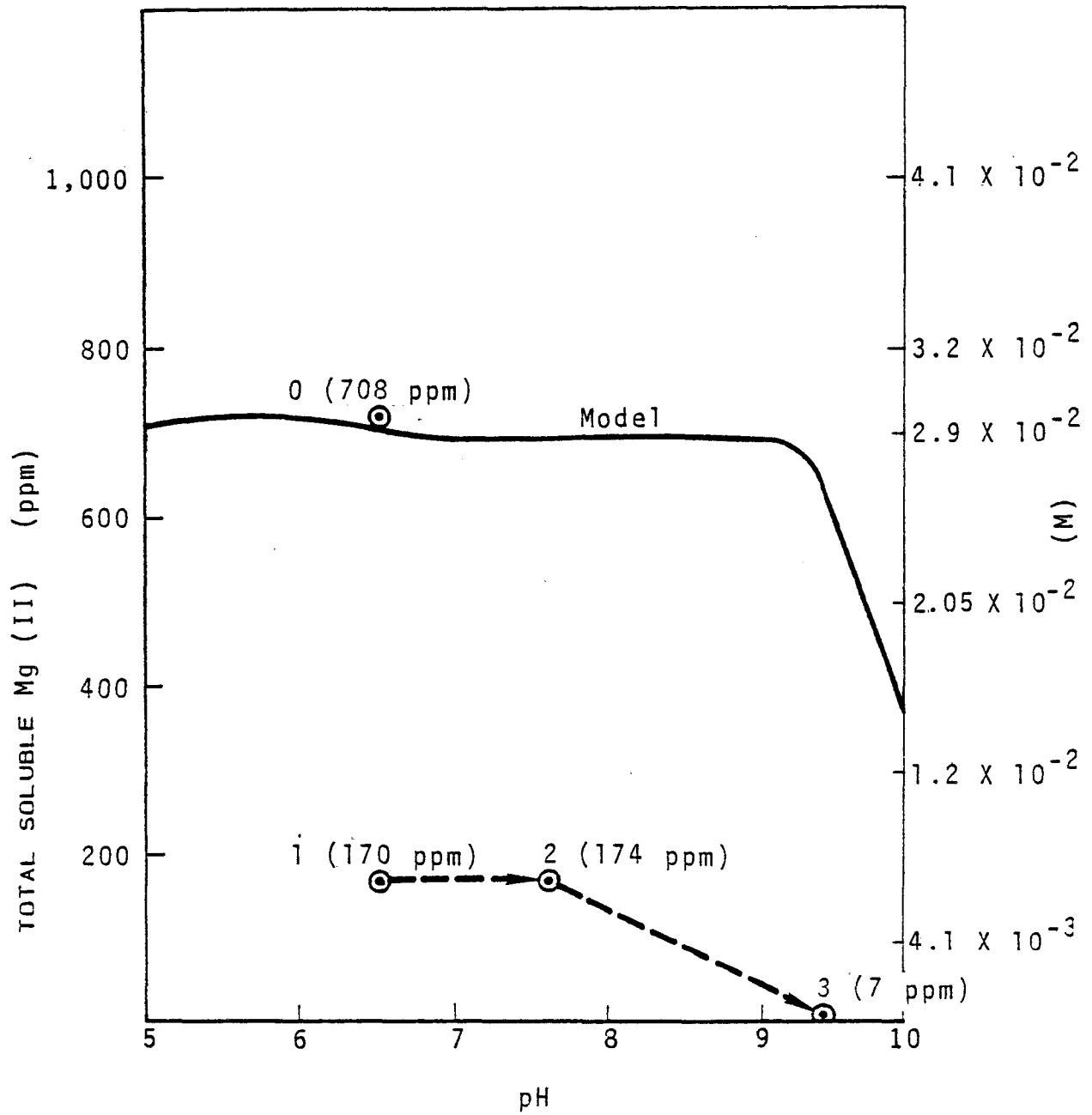
Figure 92. Total soluble Mg(II) concentration in La Cygne FGD
wastes (see text for explanation).
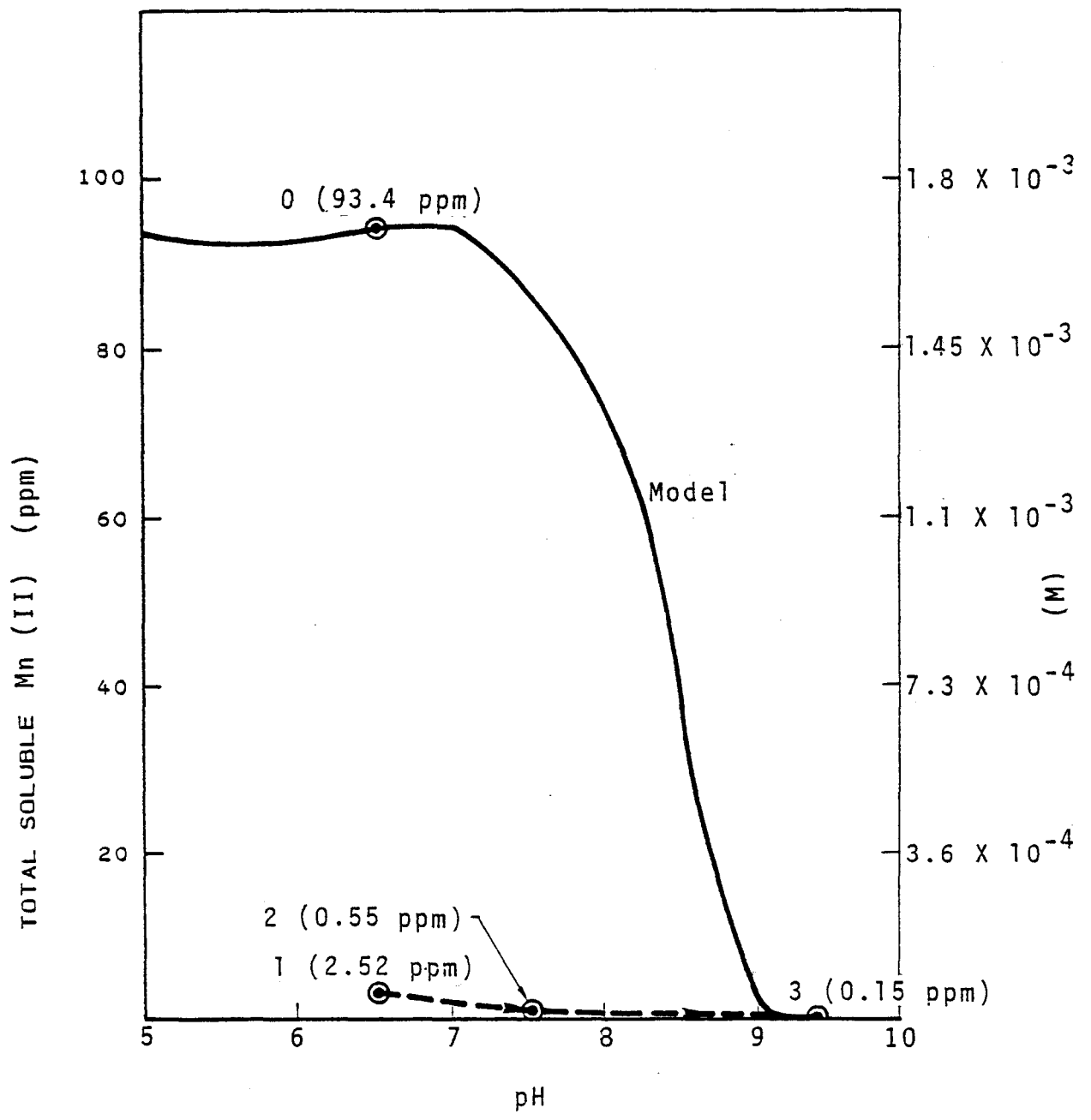
Figure 93. Total soluble Mn(II) concentration in La Cygne FGD
wastes (see text for explanation).
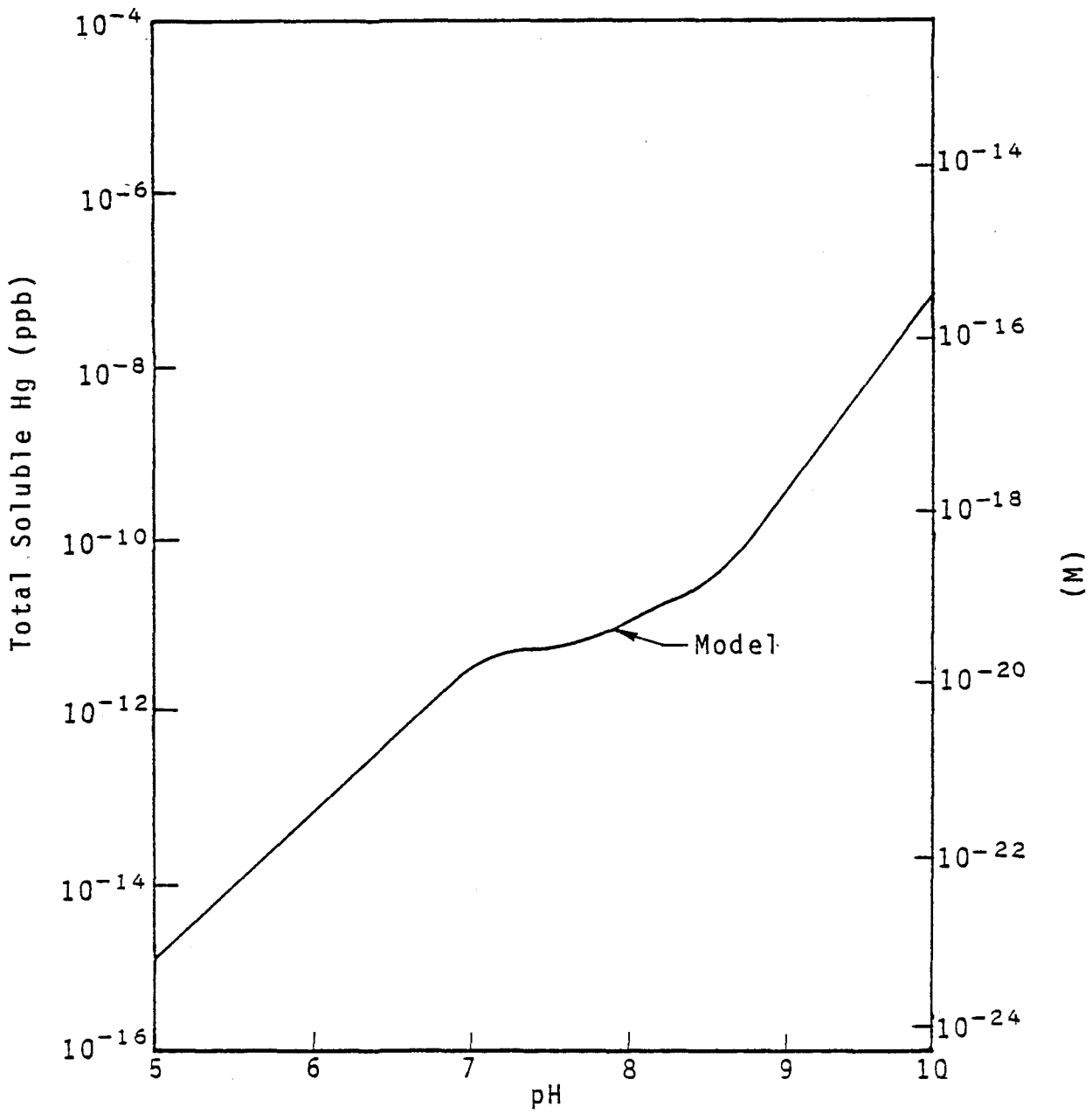
Figure 94. Total soluble Hg concentration in La Cygne FGD
wastes (see text for explanation).
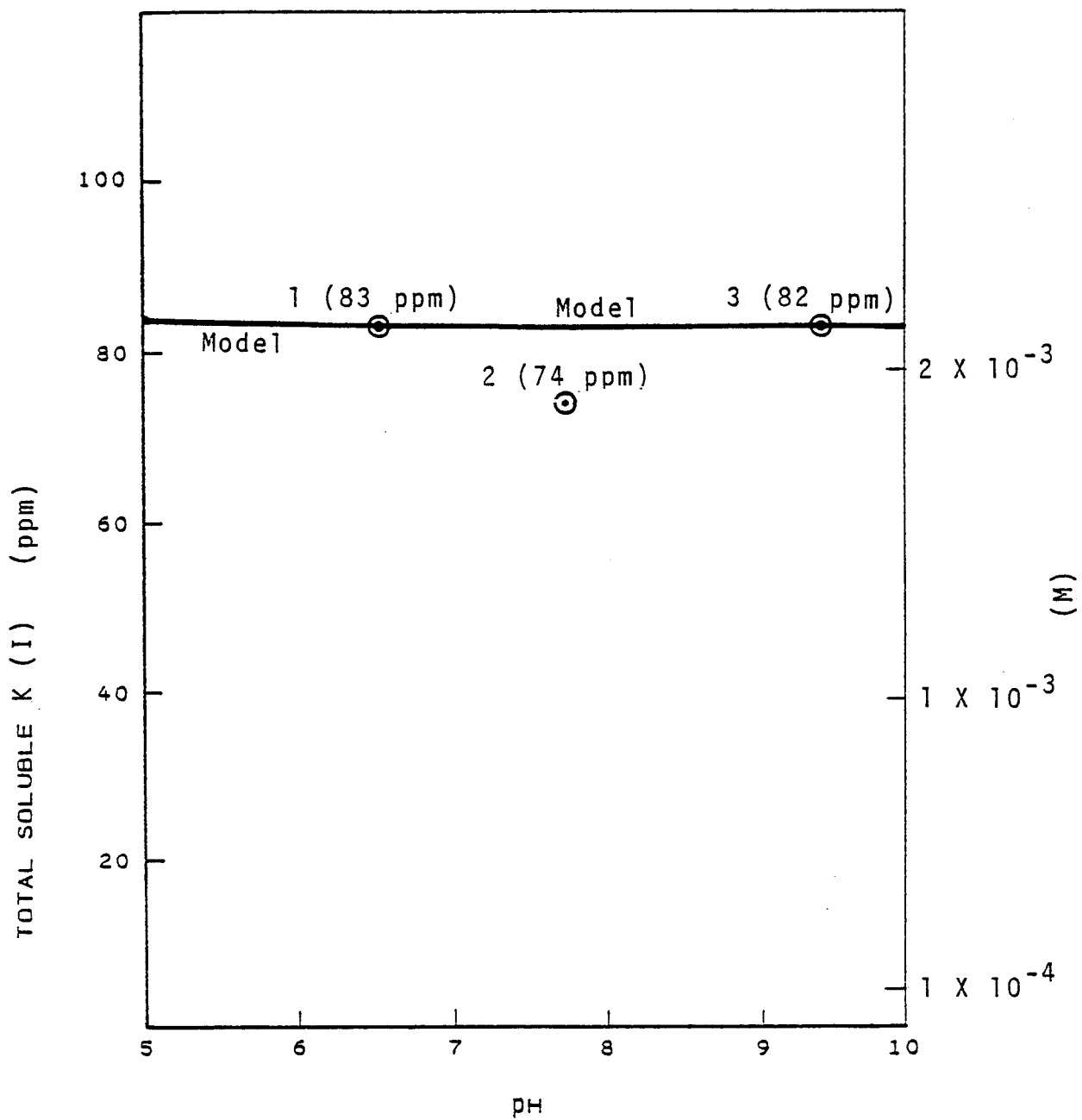
Figure 95. Total soluble K(I) concentration in La Cygne FGD
wastes (see text for explanation).
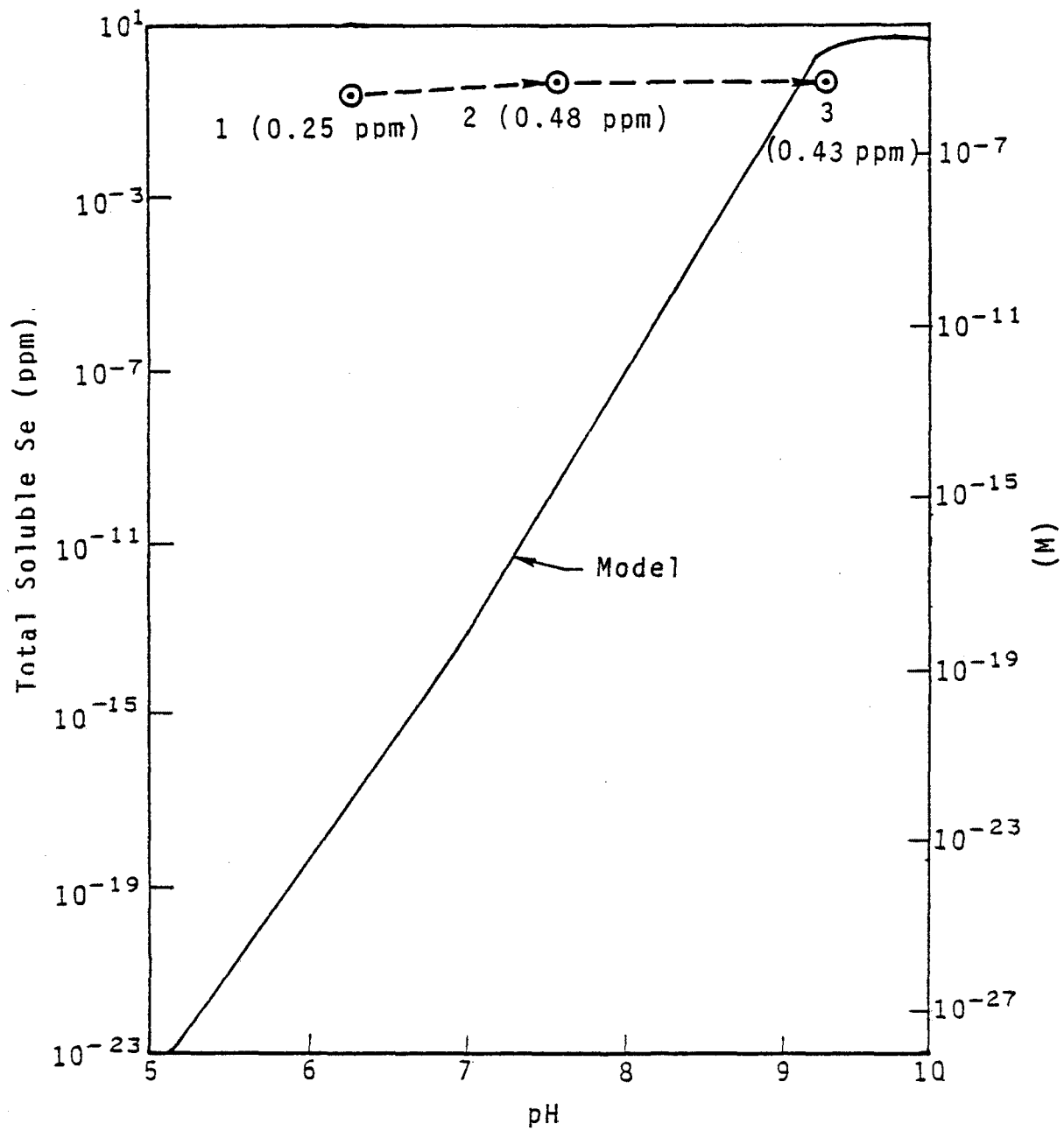
Figure 96. Total soluble Se concentrations in La Cygne FGD wastes (see text for explanation).
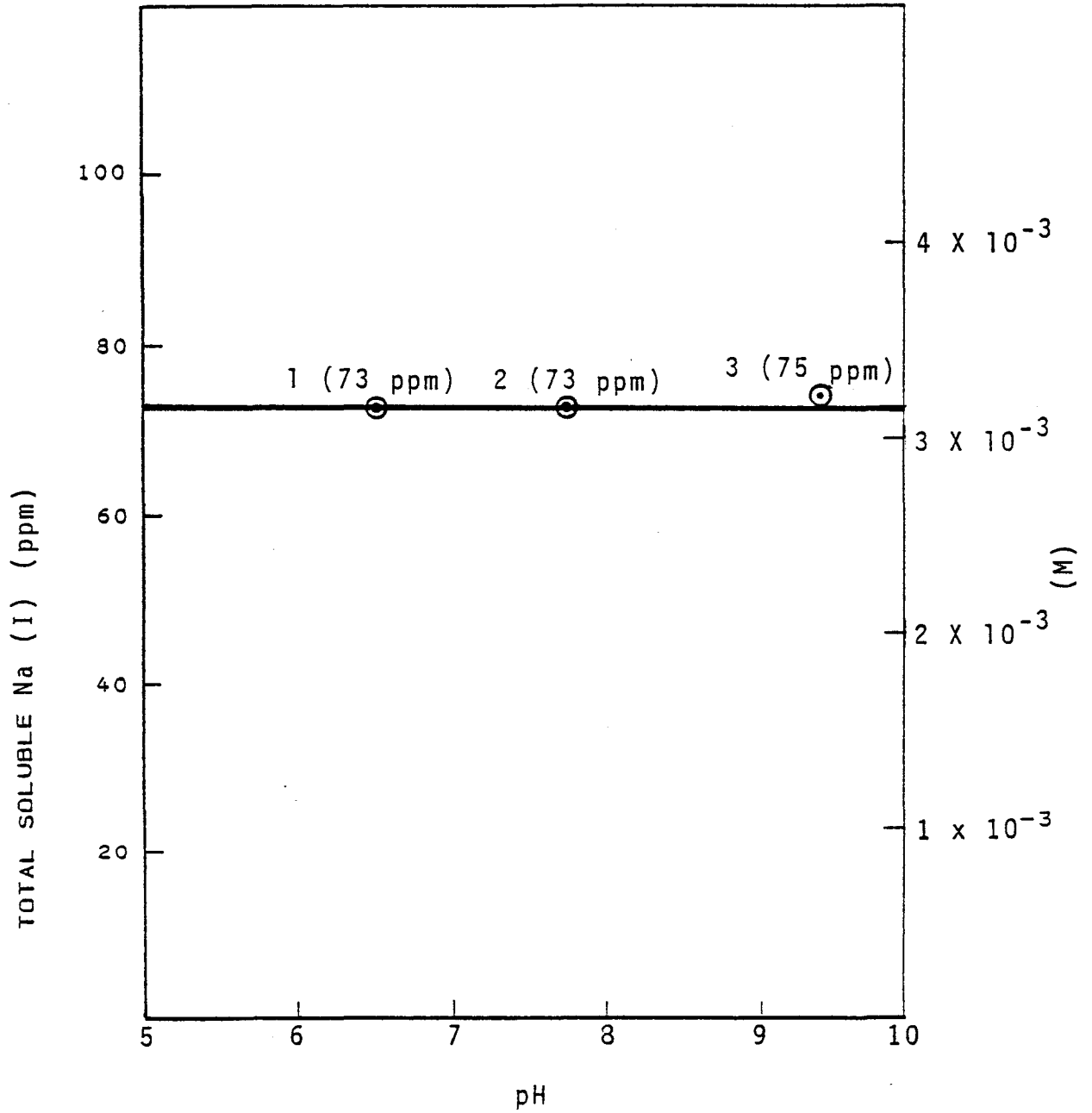
Figure 97.   Total soluble Na(I) concentration in La Cygne FGD
             wastes (see text for explanation).
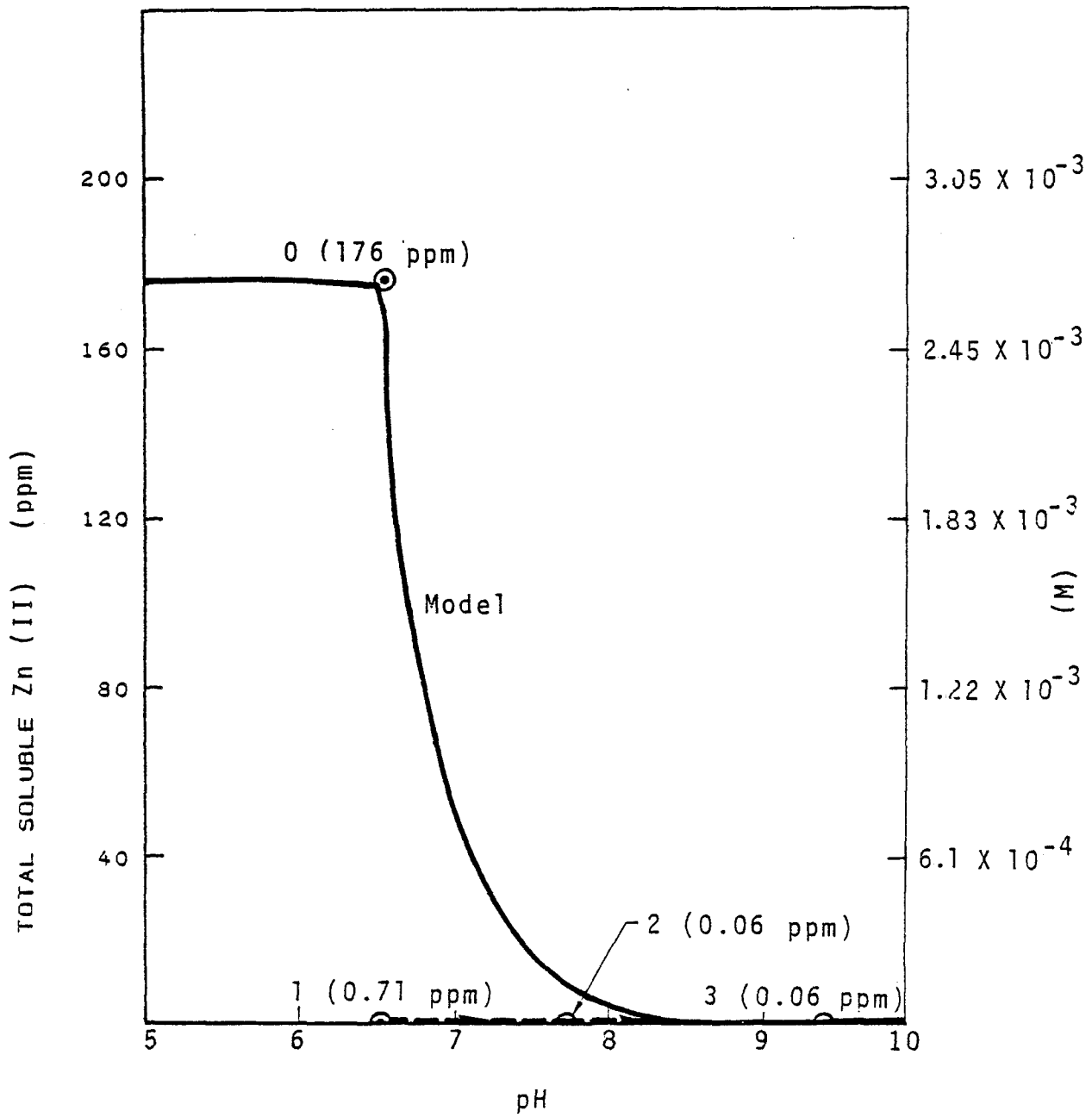
Figure 98.   Total soluble Zn(II) concentration in La Cygne FGD
wastes (see text for explanation).

TABLE 12. COMPARISONS OF THE ANALYTICAL RESULTS OF FGD
WASTEWATER TO THE RESULTS PREDICTED BY COMPUTER MODEL

| Constituent* | Constituent Concentration (ppm - unless otherwise noted) | | | |
	(1) (Fresh Leachate, pH = 6.5)	(2) (20-Day-Aged Leachate, pH = 7.7)	(3) (5-Year-Aged Leachate, pH = 9.3)	Model (Equilibrium Condition, pH = 9.3)
Al	0.48	0.30	0.20	0.14
As	0.66	0.20	0.12	0.0002
Cd	0.045	0.010	0.010	0.011
B	38.4	33.0	18.4	17.5
Ca	850	810	410	20
Cr	0.001	0.001	0.002	12.8
Co	0.049	0.022	0.010	0.003
Cu	Nil	Nil	Nil	4.4×10^{-13}[†]
F	13.6	9.4	5.5	79
Fe	1.0	0.1	0.04	0.012
Pb	Nil	Nil	Nil	1.9
Mg	170	174	7	645
Mn	2.52	0.55	0.15	0.156
Hg	Nil	Nil	Nil	5×10^{-9}[†]
K	83	74	82	83
Se	0.25	0.48	0.43	3.22[#]
Na	73	73	75	73
Zn	0.71	0.06	0.06	0.073

* Refer to Figures 82 through 95.

† ppb.

# pH = 9.15, Se = 0.43 ppm.
  pH = 9.3,   Se = 3.22 ppm.

Many solid phases (such as dolomite, magnesite, nesquehonite, and other sulfate and phosphate species) have been tried for the calculation of the soluble magnesium in the FGD system, but none gave results consistent with the experimental data. Additional study is necessary to improve prediction accuracy for these elements.

EVALUATION OF MODEL IN RELATION TO SCIENTIFIC CONSIDERATIONS

The evaluation of the thermodynamic model in relation to scientific considerations was performed during the phase and speciation calculations (Sections 2-5), as well as during the calculation of the effects of chemical changes on the chemical species (see Section 7). In general, the model results follow the expected behavior patterns. The following are some examples which were used to test the acceptability of the model.

Effects of pH and Eh on the System

The pH of a chemical system can influence the direction of the alternation process (precipitation, dissolution, redox reaction, and sorption), and will affect the speciation of almost all the constituents in the system. Theoretically, low pH conditions tend to dissolve more solids of oxide, hydroxide, carbonate, silicate, sulfate, and thus increase the concentrations of free soluble metal ions. High pH levels tend to precipitate more solids, decrease the free metal ions, and enhance the formation of metal-hydroxide complexes in the system. High pH levels can also increase the concentrations of metal-ligands, if such ligands have a tendency to complex more in the high pH region (e.g., CO_3^{2-}, SO_4^{2-}, PO_4^{3-}, etc.).

The results of thermodynamic calculations show that the constituents of the above-mentioned solids have higher free metal concentrations in the low pH region, and form more solids in the high pH region (refer to Figures 60-81). The predicted levels of metallic hydroxide, and of carbonate, sulfate, and phosphate complexes, also represent tremendous increases in the high pH region (if the decrease of the free metal ions is taken into account).

The Eh (redox potential) of a chemical system will affect the valence and chemical forms of many constituents in the system. Owing to the redox change, the solubility of some solids, as well as the transformation of solids, will be affected. An increase in Eh usually results in a transfer of reduced solids to either higher oxidation state solids (e.g., $CaSO_3 \cdot 1/2H_2O(s)$ transforms to $CaCO_4 \cdot 2H_2O(s)$; $MnCO_3(s)$ transforms to $MnOOH(s)$, or to other Mn oxides), or more elemental solids will be dissolved (e.g., $As^0(s)$, $Hg^0(\ell)$, and $Se^0(s)$)). These transformations can affect the solubility of affected solids.

184

The results derived from the model usually follow the trends mentioned above. For example, as the La Cygne FGD wastes age, the redox potential increases (Table 10). This change should result in a significant increase in soluble mercury and selenium levels in the system (Figures 94 and 96), which agrees with the model results.

Effects of Ligand Concentrations on the Levels of Metallic Complexes

It is known that ligand concentration can affect the soluble level of metallic complexes. Based on previous related studies (Ref. 6-8, 23-25, 27), it is known that the chloride ligand is important to the solubility of cadmium, copper, lead, and zinc. In accounting for soluble copper and lead levels, the borate ligand may also become significant. The hydroxide ligand is important to the dissolution of three-valence metals (e.g., Fe and Cr). The results calculated by the model (see Sections 4 and 5) do follow these general trends. A more detailed discussion of the effects of ligands on the soluble levels of metals is presented in Section 7.

SECTION 7

EFFECTS OF OPERATIONAL (CHEMICAL)
CHANGES ON FGD SLUDGE CHEMICAL SPECIES

The principal goals of FGD sludge disposal are to minimize the concentration of toxic constituents in the liquid phase (leachate), and/or to allow such impurities to exist only in a chemical form which is nontoxic and/or readily adsorbed by soils. In order to assess the potential of contaminant species modification to achieve these goals, the model was operated over a wide range of conditions to determine the impact of various operating changes on the various chemical species. In this study, the effects of 11 operational (chemical) changes were studied. The results are discussed in the following pages.

EFFECTS OF pH ON SPECIATION

As was discussed previously, change in pH level in any chemical system can influence the direction of the alteration process and the speciation of almost all the constituents in both solution and solid phases. In this study, the effects of pH on the speciation of constituents in the FGD sludges have been quantitatively estimated in Eh-pH and ion-ratio diagrams (Figures 1 through 15) and in the primary distribution diagrams (Figures 39 through 81). The effects of pH on the speciation of constituents in the FGD wastewaters (leachates) can be viewed in the resultant speciation diagrams (Figures 16 through 37 and 38 through 80). The effects of pH on soluble constituents can also be seen in Figures 82 through 98.

Effects on Solid Species

The results of thermodynamic calculations show that the pH level can have a significant effect on the stability field of FGD sludge constituents. Figures 3, 10, and 13 indicate that the decrease of pH values favor the formation of elemental $As^0(s)$, $Hg^0(\ell)$, and $Se^0(s)$. However, for constituents which can form hydroxide or carbonate solids such as iron (Figure 8) and manganese (Figure 11), an increase in pH levels instead favors solids formation.

186

The ion-ratio diagrams shown in Section 3 also indicate the significance of pH on the stability field of other constituents in the FGD sludges. In general, high pH levels favor the formation of oxide or hydroxide solids instead of carbonate, phosphate or other solids in FGD sludge. For example, higher pH levels favor the formation of $Al_2O_3 \cdot 3H_2O(s)$, $Cd(OH)_2(s)$, $Cu(OH)_2(s)$, $Pb(OH)_2(s)$, $Ni(OH)_2$ and $Zn(OH)_2(s)$ over $Al(H_2PO_4)(OH)_2(s)$, $CdCO_3(s)$, $Cu_2CO_3(OH)_2(s)$, $PbCO_3(s)$, $NiCO_3(s)$ and $ZnCO_3(s)$, respectively (see Figures 1, 4, 7, 9, 12, and 15).

The effects of pH on relative distribution of primary solids for some selected constituents in the FGD sludges also can be seen in Figures 39 to 81. These results show that the most significant effect of pH on calcium solids is in the formation of $CaCO_3(s)$ in high pH sludges. This phenomenon indicates that, theoretically, the soluble calcium concentration in FGD sludge liquid phase decreases at high pH due to the formation of $CaCO_3(s)$. For magnesium, modeling results indicate that high pH levels favor the formation of $Mg(OH)_2(s)$. The pH effect on the relative distribution of the two most important cadmium solids ($CdCO_3(s)$ and $Cd(OH)_2(s)$ can be seen in Figures 47 and 69. It was found that $Cd(OH)_2(s)$ may become the predominant solid in FGD sludges only in the very high pH region (pH >10.8). In actual practice, few FGD systems will have such a high pH. For chromium, the data show that $Cr(OH)_3(s)$ is the important species only in the neutral pH region, that is, pH 6 to 9 (Figures 49 and 71.

The effects of pH on copper, iron, and mercury is not as obvious due to the tremendous amount of $Cu_2CO_3(OH)_2(s)$, $Fe(OH)_3(s)$, and $Hg^o(\ell)$ in the system (Figures 51, 53, 55, 73, 75, and 77). The most significant effect of pH on the solid distribution of lead is that at a pH below 9, $PbMoO_4(s)$ will become the predominant species. However, high pH levels (pH 9) favor the formation of $PbCO_3(s)$. For zinc, the pH level can also affect the relative distribution of $ZnCO_3(s)$, $Zn(OH)_2(s)$, and $ZnSiO_3(s)$ in the FGD sludges. High pH levels favor the formation of $Zn(OH)_2(s)$. When pH decreases, $ZnSiO_3(s)$ will gradually replace $Zn(OH)_2(s)$ (Figures 59 and 81).

Effects on Soluble Species

The effects of pH on the soluble species were discussed previously in Sections 4 and 5. In general, most species of major ions will be significantly affected by a pH change. Unaffected species include free Ca^{2+}, Mg^{2+}, K^+, and Na^+, and their sulfate complexes.

Typical examples of the pH effects on the total soluble constituent levels were discussed in Section 6. In general, a high pH will reduce the number and concentration of soluble

species. However, due to the complexation effect in the high pH region, the total soluble levels for some species may increase again. Examples are the total soluble levels of chromium (Figure 87), fluoride (Figure 89), lead (Figure 91), mercury (Figure 94), and selenium (Figure 96).

EFFECTS OF IONIC STRENGTH ON SPECIATION

The ionic strength will affect the solubility constants on various reactions in the chemical systems. Through this effect, the concentrations and relative distributions of species may be altered. However, the calculated results show that the effects of ionic strength on FGD systems are relatively small compared to effects such as pH changes or ligands concentration changes.

The quantitative effects of ionic strength on the stability field of constituents have been discussed using ion-ratio diagrams in Section 3. The influence on the stability field of solid phase by ionic strength is usually less than a order of magnitude from $I = 0$ to $I = 1.0$ (see Figures 1, 2, 4, 5, 7, 9, 12, and 15). In FGD systems ($I = 0.05$ to 0.8), the maximum ionic strength variation will expand or reduce the stability field of solids by a factor of no more than four.

The effect of ionic strength variation on the speciation of soluble constituents is also small. Among the constituents studied, only the relative distribution of cadmium between its free metal ion, Cd^{2+}, and its chloro complexes, Cd-Cl, can be altered by a change in ionic strength (Figure 100). Other soluble species, such as sulfate complexes (a typical example is given in Figure 99), may also be affected by as much as one order of magnitude. However, these effects will not significantly change the relative distribution of various soluble species.

EFFECTS OF CHLORIDE CONCENTRATION ON THE SOLUBILITIES OF METALS

The speciation calculations show that chloride complexes may be the predominant soluble species for cadmium, copper, lead, mercury, and zinc. For example, when the chloride concentration is higher than 400 ppm (Figure 101), the Cd-Cl complexes may become the predominant species for cadmium. In general, if the chloride concentration is known, the total soluble levels of chloride-complexing metals can usually be predicted if no other ligands dominate the system.

The results of related calculations are shown in Figures 101 through 105. In this study, the assumed chloride concentrations ranged from 50 to 6,000 ppm. Other parameters used for calculation were based on analysis of the La Cygne FGD wastewater.
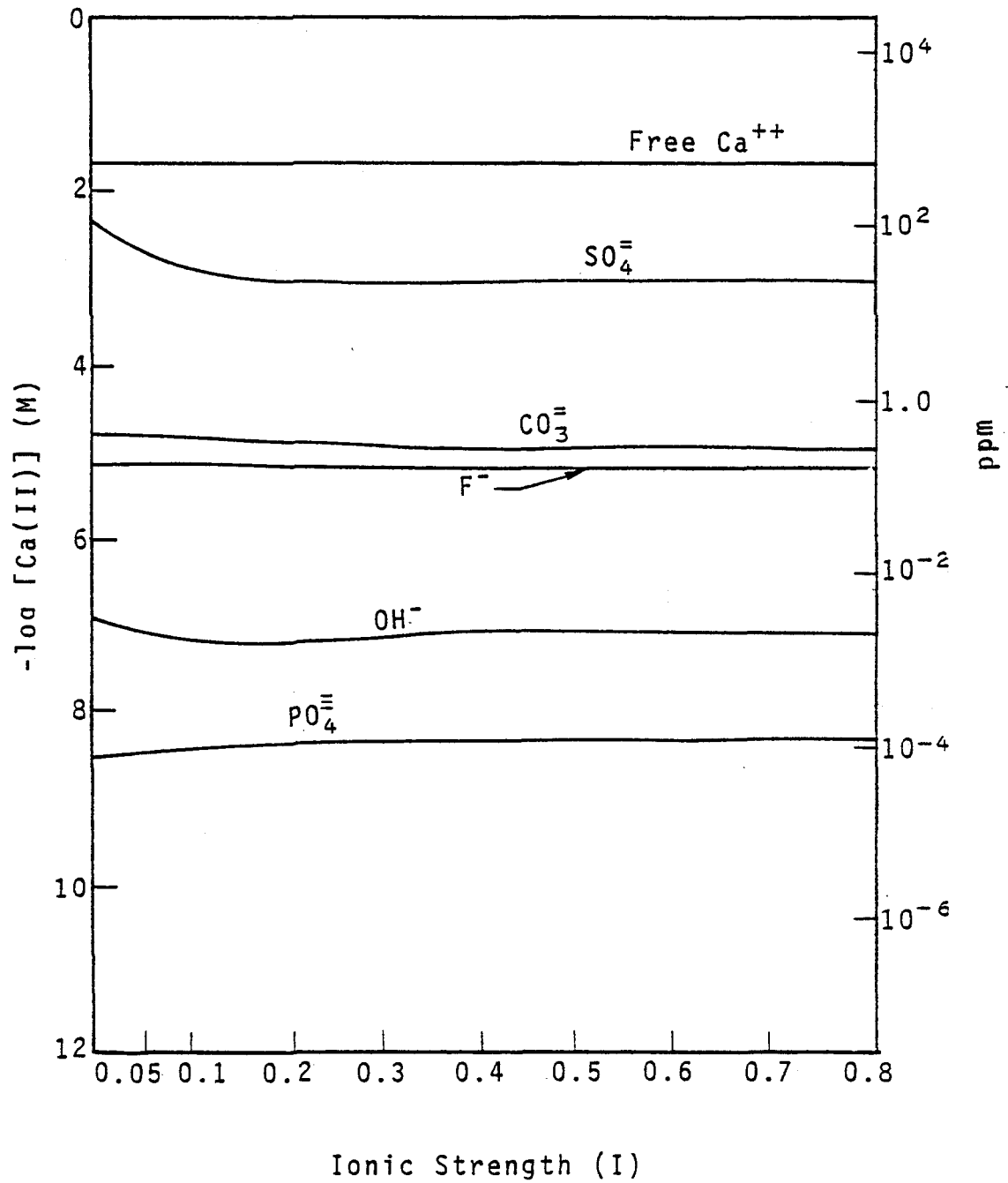
Figure 99. Effects of ionic strength on the speciation of soluble Ca.

189
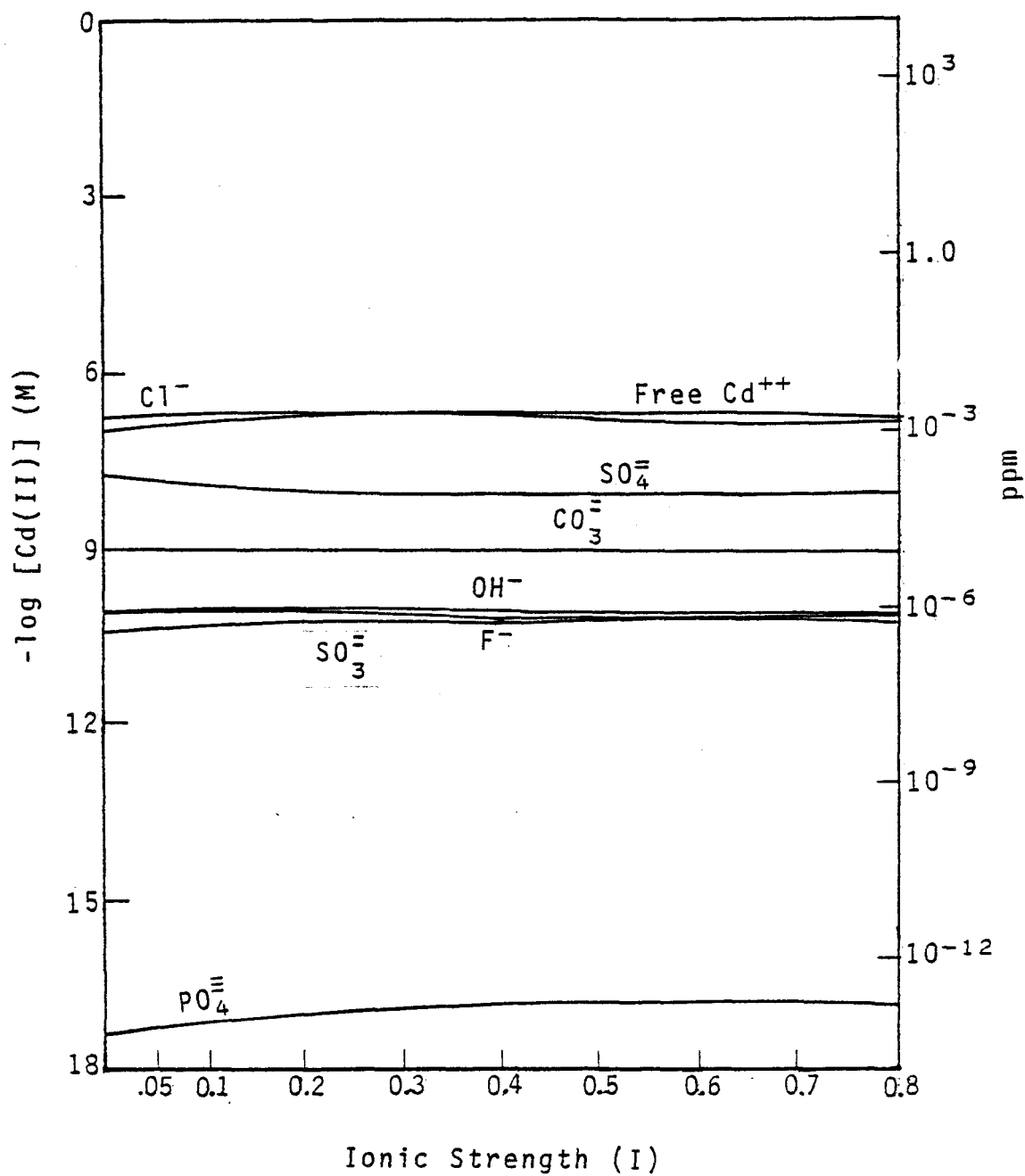
Figure 100. Effects of ionic strength on the speciation of soluble Cd(II).
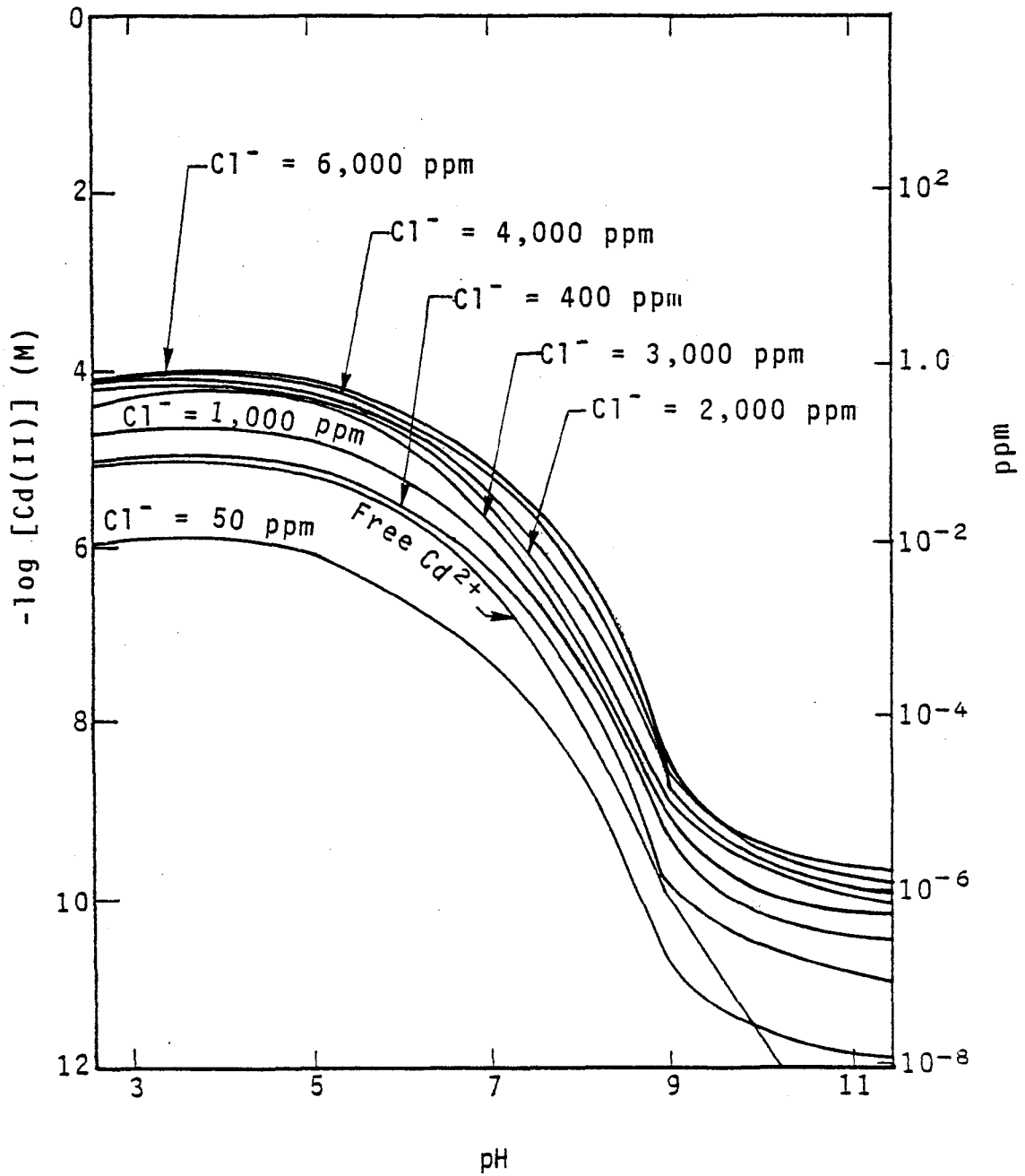
Figure 101. Effects of chloride concentration on soluble Cd concentration.
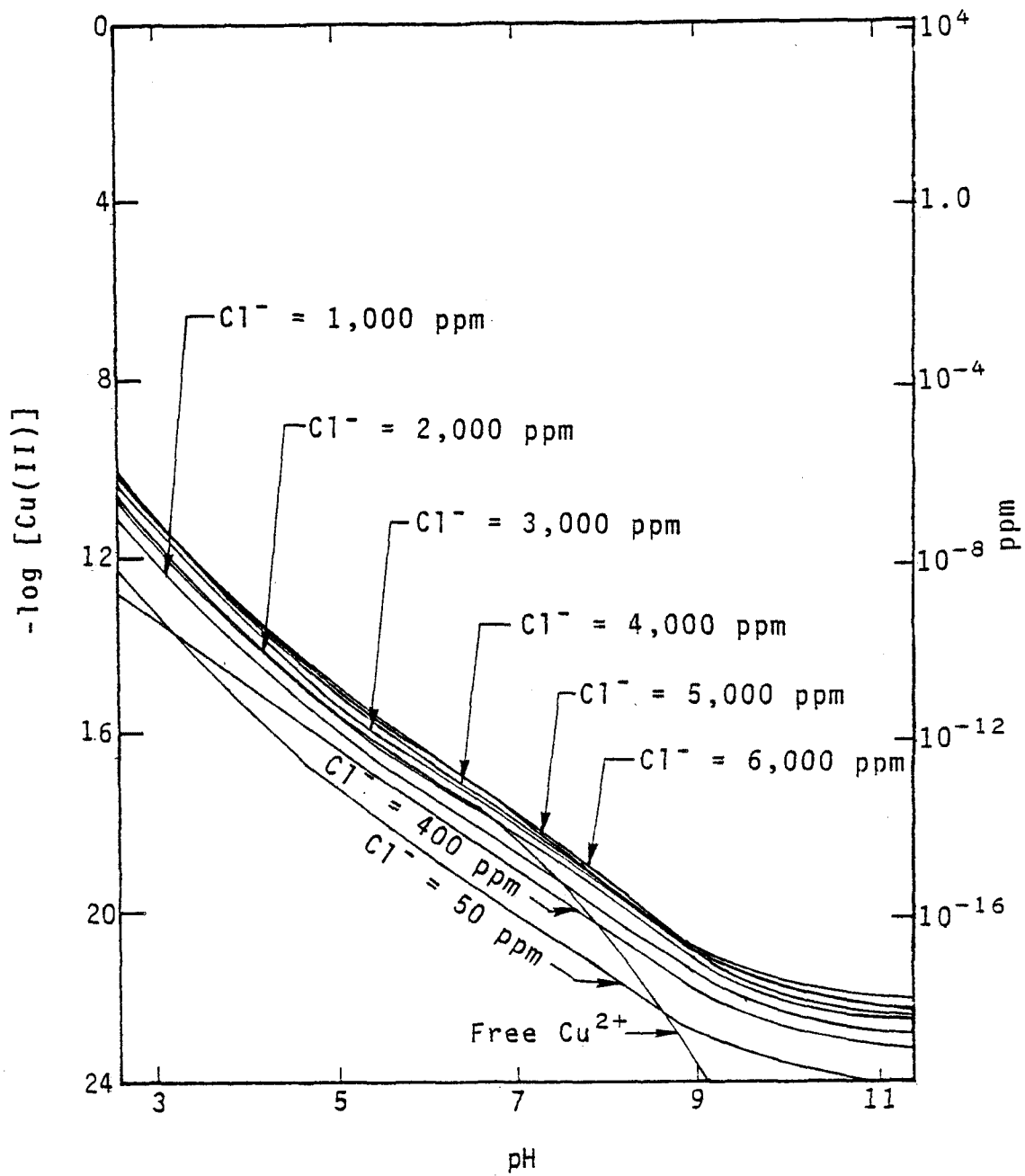
Figure 102. Effects of chloride concentration on soluble Cu concentration.
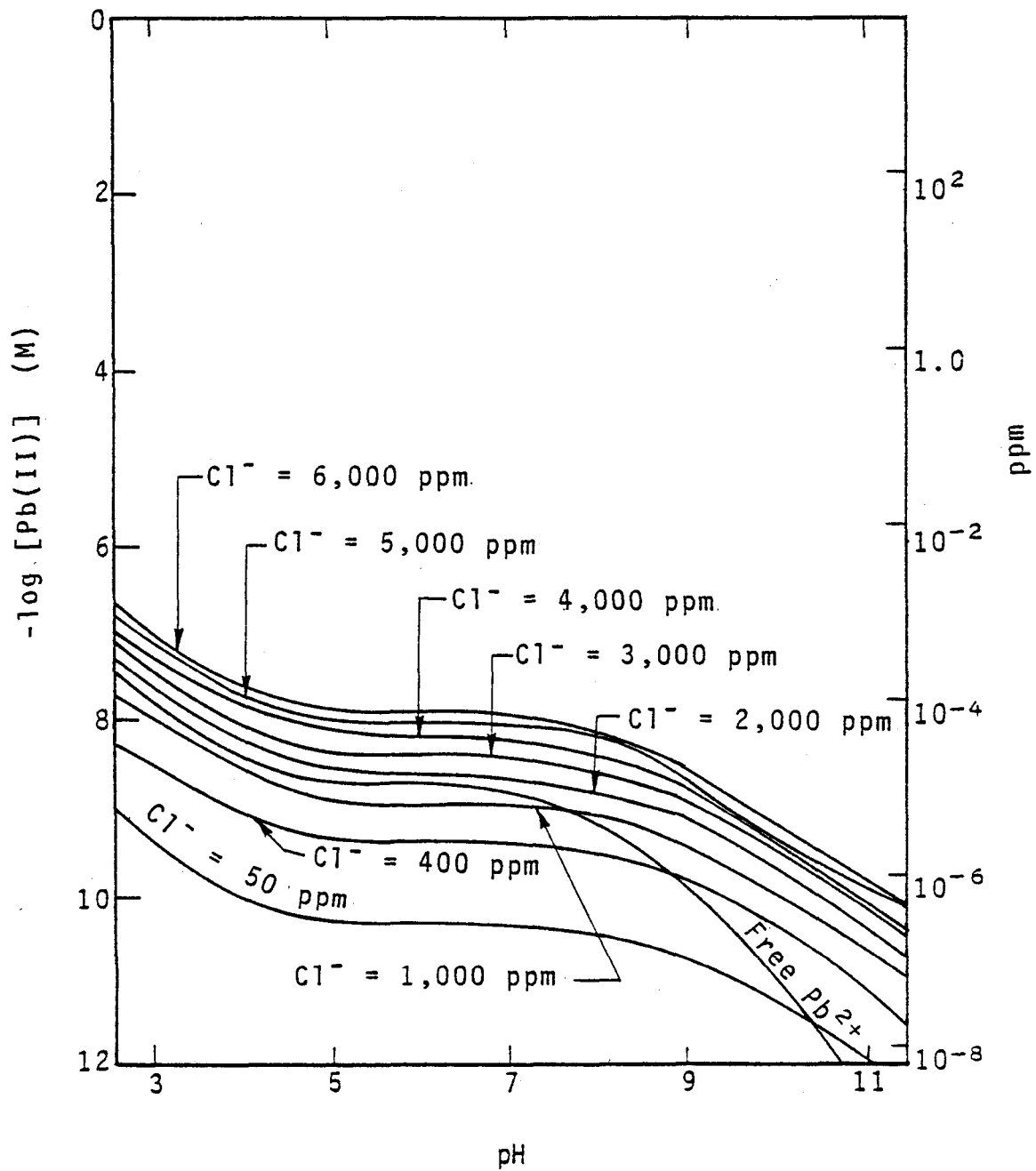
Figure 103.   Effects of chloride concentration on soluble Pb
concentration.
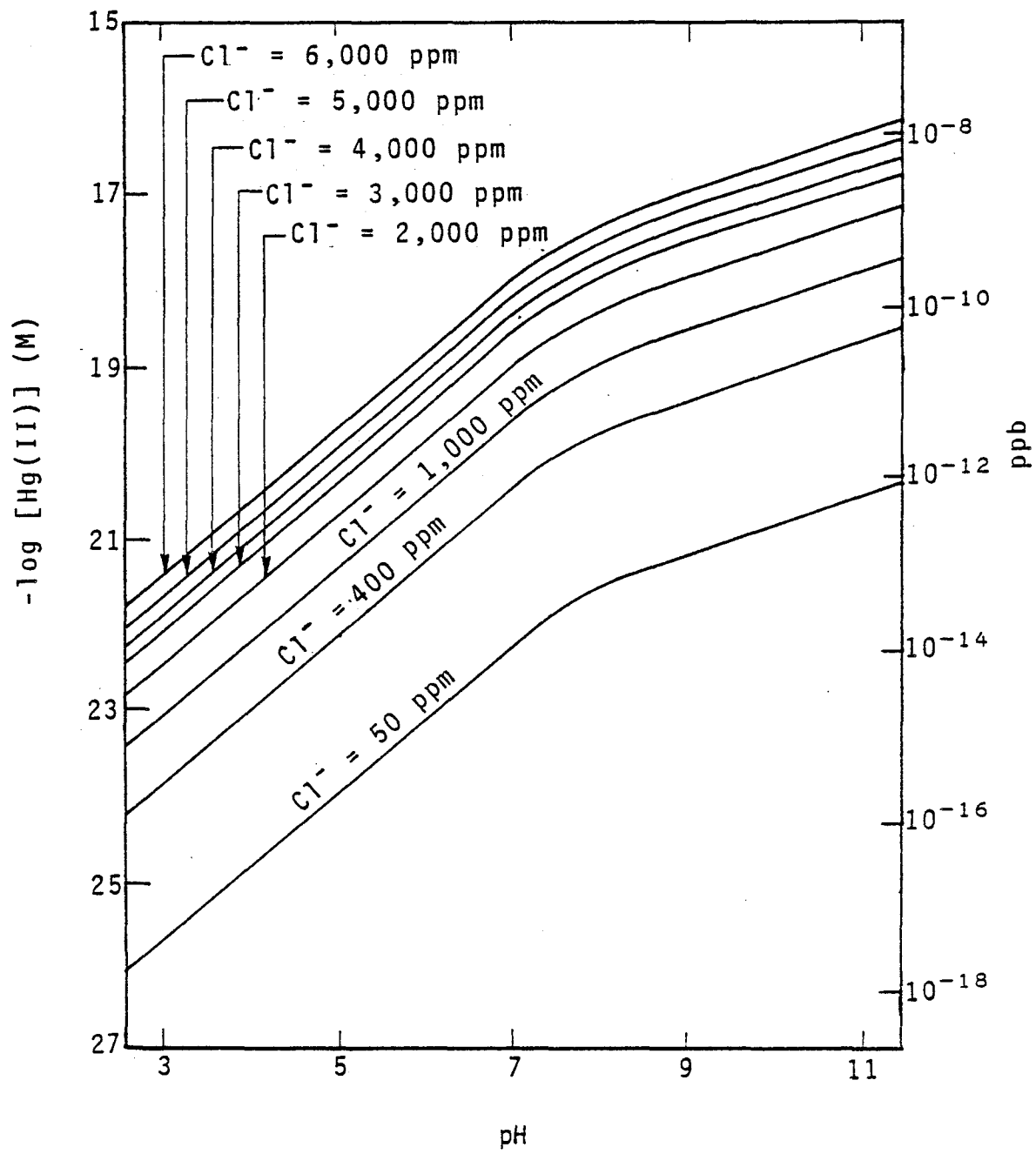
Figure 104. Effects of chloride concentration on soluble Hg concentration.
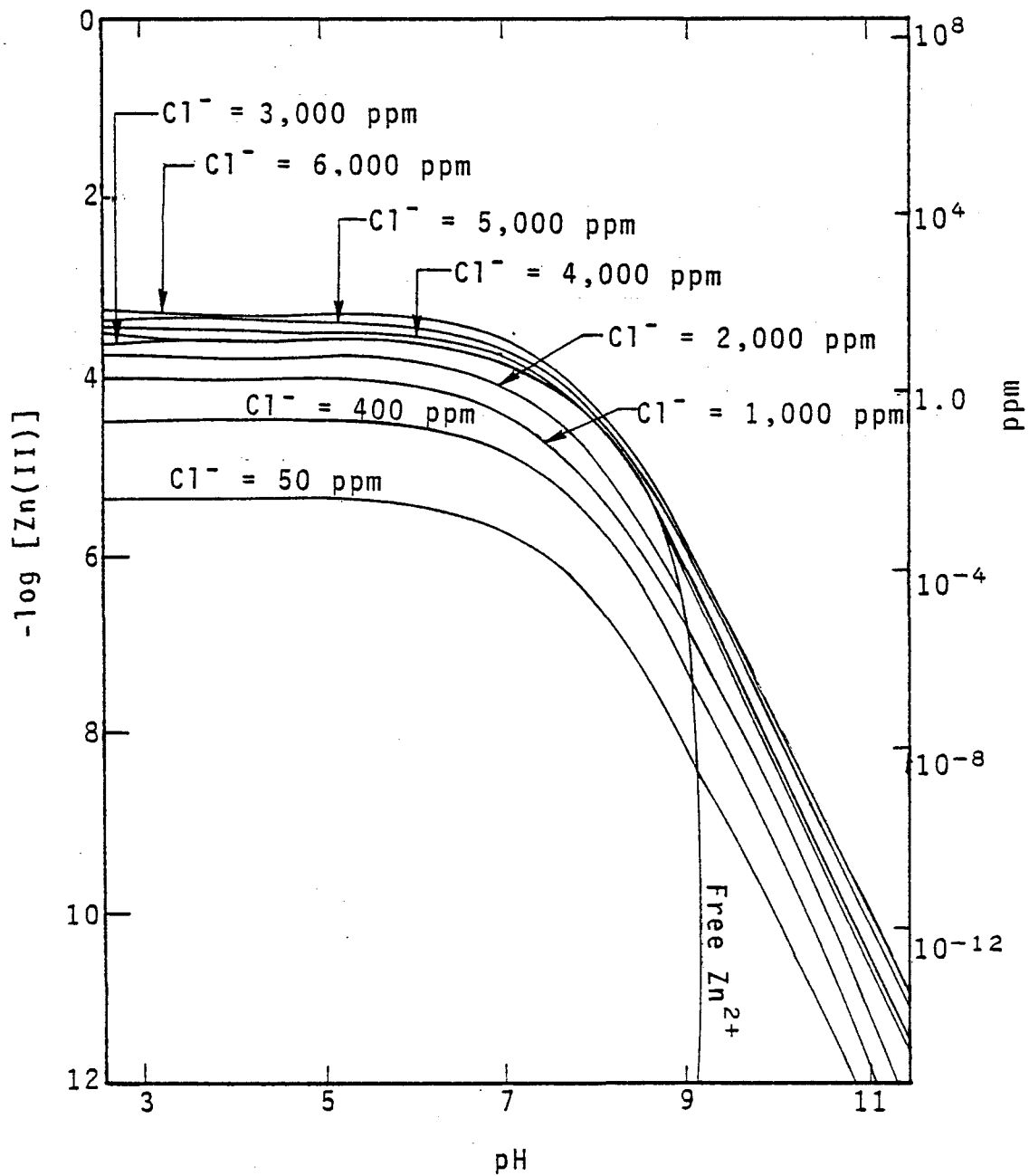
Figure 105.   Effects of chloride concentration on soluble Zn
              concentration.

Effect on Cadmium

It was found that a variation of chloride concentrations from 50 to 6,000 ppm can lead to about a two order of magnitude concentration change for cadmium in FGD wastewaters for any given pH. As shown in Figures 46 and 68, in any FGD sludge free Cd^{2+} is the only species which can exist at a higher concentration than that of the Cd-Cl complexes when the pH is less than 8.7. When the pH exceeds 8.7, species such as cadmium-sulfate, sulfite, or hydroxide complexes may exist in higher concentrations than that of Cd-Cl complexes depending on the ligand concentrations and pH levels.

Therefore, in order to predict cadmium species concentrations in the aged FGD wastewater, the following equations are used:

pH < 8.7

$$[Cd_T] = [Cd^{2+}] + [\text{Cd-Cl complexes}] \tag{73}$$

pH > 8.7

$$[Cd_T] = [\text{Cd-Cl complexes}] + [\text{Cd-SO}_4 \text{ complex}]$$
$$+ [\text{Cd-SO}_3 \text{ complex}] + [\text{Cd-OH complexes}] \tag{74}$$

Generic equations 73 and 74 can be approximated by the following two equations:

pH < 8.7
$$[Cd_T] \approx [Cd^{2+}] + [CdCl^+]$$
$$\approx [Cd^{2+}] + 10^{2.2}[Cd^{2+}][Cl^-] \tag{75}$$

pH > 8.7

$$[Cd_T] \approx [Cd^{2+}] + [CdCl^+] + [CdOHCl(aq)] + [CdSO_4(aq)]$$
$$+ [Cd(SO_3)_2^{2-}] + [CdOH^+]$$
$$\approx [Cd^{2+}] + 10^{2.2}[Cd^{2+}][Cl^-] + 10^{7.3}[Cd^{2+}][OH^-][Cl^-]$$
$$+ 10^{2.3}[Cd^{2+}][SO_4^{2-}] + 10^{5.4}[Cd^{2+}][SO_3^{2-}]$$
$$+ 10^4[Cd^{2+}][OH^-] \tag{76}$$

The value of free cadmium ion concentration, $[Cd^{2+}]$, can be solved using Equation 31 (Section 2) with the aid of the ion-ratio or Eh-pH methods to identify the predominant solid species.

If the Cd-Cl complexes are the most important (predominant) species for soluble cadmium, then Figure 101 can be employed for quick estimation of the total soluble cadmium concentration in aged FGD sludge.

Effect on Copper

Figure 80 indicates that the studied range of chloride concentrations can cause a one order of magnitude variation in concentrations of Cu-Cl complexes, As shown in Figures 50 and 72, free Cu^{2+} ion is the only species whose concentration can exceed the concentration of the Cu-Cl complexes at low pH (pH 4.7). From Figure 102, it can also be seen that this phenomenon occurs when the chloride concentration reaches about 2,000 ppm in the FGD wastewater. At a pH higher than about 4.7, the $Cu-B(OH)_4$ complexes will usually dominate Cu-Cl complex formation.

The same type of equations used previously for the prediction of the total soluble cadmium concentration also can be used for copper:

pH < 4.7

$$[Cu_T] \approx [Cu^{2+}] + [CuCl^+] + [CuOHCl(aq)]$$
$$\approx [Cu^{2+}] + 10^{1.6}[Cu^{2+}][Cl^-] + 10^{9.1}[Cu^{2+}][OH^-][Cl^-] \quad (77)$$

pH > 4.7

$$[Cu_T] \approx [CuB(OH)_4^+] + [Cu(B(OH)_4)_2(aq)]$$
$$\approx 10^{7.1}[Cu^{2+}][B(OH)_4^-] + 10^{12.4}[Cu^{2+}][B(OH)_4^-]^2 \quad (78)$$

From the above discussion, it appears that Figure 102 is a valid predictor of the total soluble copper concentration in aged FGD wastewater when (1) pH is less than 4.7, and (2) the chloride concentration is sufficiently high.

Effect on Lead

The speciation diagrams (Figures 56 and 78 in Section 5) indicate that the Pb-Cl complexes may become the predominant soluble lead species at pH 7 only when chloride is present at a high concentration. (Figure 103 shows this level to be a minimum of 1,500 ppm.) When the pH is higher than 7, the Pb-Cl complexes are insignificant. Therefore, the same types of prediction equations are applicable:

pH < 7

$$[Pb_T] \approx [Pb^{2+}] + [PbCl^+]$$
$$\approx [Pb^{2+}] + 10^{1.7}[Pb^{2+}][Cl^-] \quad (79)$$

197

The model verification indicates that at high pH levels the calculated value for total soluble lead may be higher than the analytical value. Therefore, it is recommended that the thermodynamic model not be used for lead when the pH is higher than about 7.

Effect on Mercury

When the pH is less than about 9, the Hg-Cl complexes alone can account for all soluble mercury. The effect of the soluble chloride level on the soluble mercury level is shown in Figure 104. When the chloride concentration is increased from 50 to 6,000 ppm, the overall soluble mercury concentration will vary by more than four orders of magnitude in the FGD wastewater. Figure 104, which can be used to estimate the total soluble mercury concentration in FGD wastewater when pH is less than about 9, suggests that this estimation is usually unnecessary due to the low concentration.

Effect on Zinc

The effect of soluble chloride on soluble zinc levels is presented graphically in Figure 105. When chloride concentration is increased from 50 to 6,000 ppm, the concentration of soluble zinc increases about two orders of magnitude. The results of the speciation calculation (Figures 58 and 80) show that Zn-Cl complexes may become the predominant soluble zinc species (1) when pH 9, and (2) when the soluble chloride concentration is higher than about 3,000 ppm. Conversely, when the pH is less than about 9 and if soluble chloride concentration is below 3,000 ppm, the free metal ion, Zn^{2+}, can account for all soluble zinc. However, if soluble chloride concentration is higher than 3,000 ppm in the same pH region, the total soluble zinc in the aged FGD sludge will depend on the chloride levels. Therefore, Figure 105 can be used to predict soluble zinc levels within the above mentioned pH range.

The following equation can be used for the estimation of total soluble zinc in the aged FGD wastewater at low pH:

pH < 9

$$[Zn_T] \approx [Zn^{2+}] + 10^{1.4}[Zn^{2+}][Cl^-] \tag{80}$$

EFFECTS OF SULFATE CONCENTRATION ON THE SOLUBILITIES OF METALS

The speciation study thus far has shown that sulfate complexes may become significant at high pH levels for major ions (Ca^{2+}, Mg^{2+}, K^+, and Na^+) and several minor ions such as zinc. Only the effects of sulfate concentration on major ions will be

discussed here, however, due to the less important role of sulfate in the speciation of minor ions. Figures 106 to 109 show the overall sulfate effect.

In this study, the soluble sulfate concentration was varied from 100 up to 40,000 ppm. This variation will result in an increase of four orders of magnitude in the concentration of soluble calcium-sulfate complexes (Figure 106). Since free Ca^{2+} ion and $CaSO_4(aq)$ are the main soluble species for calcium in FGD wastewater, the total soluble level of calcium can thus be approximated as:

$$[Ca_T] \approx [Ca^{2+}] + 10^{2.3}[Ca^{2+}][SO_4^{2-}] \tag{81}$$

Figure 106 indicates that the sulfate concentration will not play an important role in the chemical behavior of calcium in the FGD wastewater when the pH is less than about 5. When the pH is higher than 5, the Ca-SO4 complex, ($CaSO4(aq)$, may become the predominant soluble calcium species in FGD wastewater if $SO4 \leq 5,000$ ppm. As discussed in Section 6, the actual distribution of calcium solids in aged FGD wastewater cannot be accurately estimated by the model. Therefore, it is suggested that Equation 81 receive additional study.

Effect on Magnesium

Figure 107 shows that soluble magnesium levels, ($MgSO_4(aq)$), can vary by almost six orders of magnitude for an increase in soluble sulfate levels from 100 to 40,000 ppm. When the soluble sulfate concentration is raised to as high as 3,000 to 5,000 ppm (depending on the pH level), the level of $MgSO_4(aq)$ may exceed the level of free Mg^{2+}. The following equation best describes the predicted magnesium levels:

$$[Mg_T] \approx [Mg^{2+}] + 10^{2.4}[Mg^{2+}][SO_4^=] \tag{82}$$

In this case, $[Mg^{2+}]$ should be calculated from the solubility controlling solids of magnesium. As was the case with calcium, the actual solid phases of magensium in aged FGD wastes cannot accurately be estimated. Figure 107 is therefore not suggested for the prediction of soluble magnesium levels. It is expected that Equation 82, however, will still be valid for FGD wastewater.

Effects on Potassium and Sodium

The effects of soluble sulfate on the soluble level of potassium and sodium are shown in Figures 108 and 109. Although soluble sulfate levels can affect the formation of potassium or sodium sulfate complexes, the significance of these complex species is far below that of the free ions (K^+ and Na^+). Even when the soluble sulfate level is as high as 40,000 ppm (FGD sludge usually has soluble sulfate less than 10,000 ppm), the
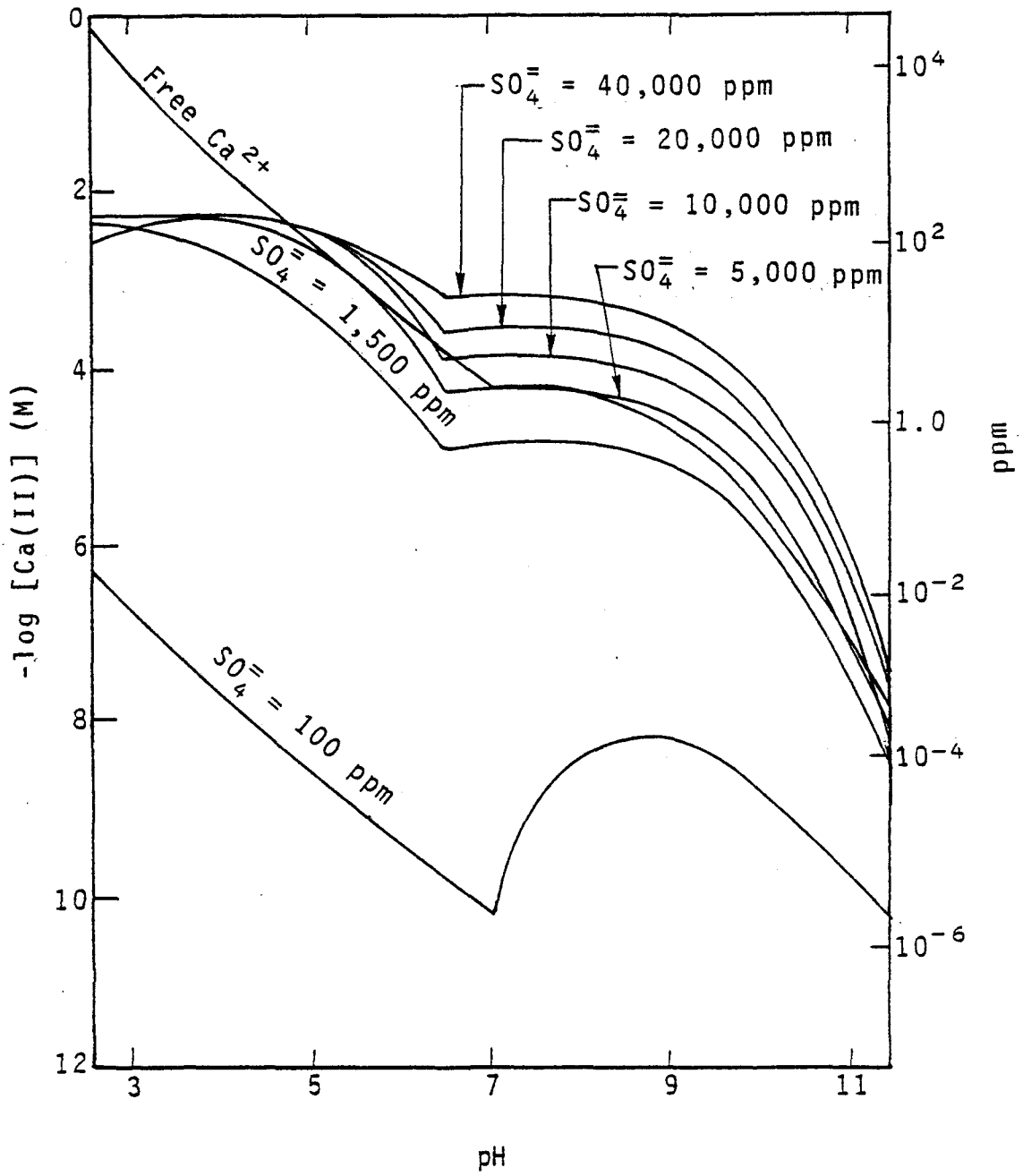
Figure 106. Effects of total sulfate concentration on soluble Ca concentration.
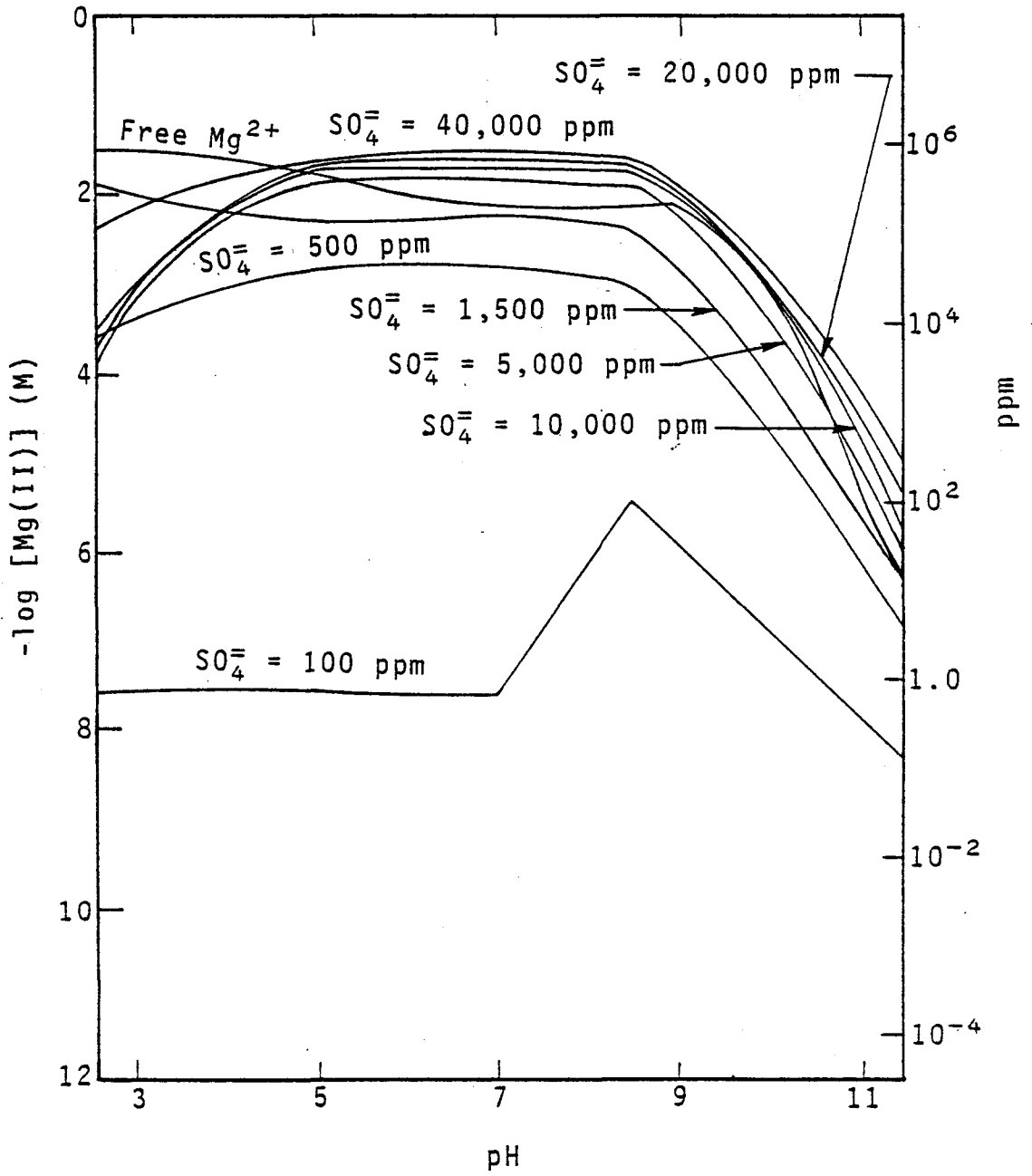
Figure 107. Effects of total sulfate concentration on soluble Mg concentration.
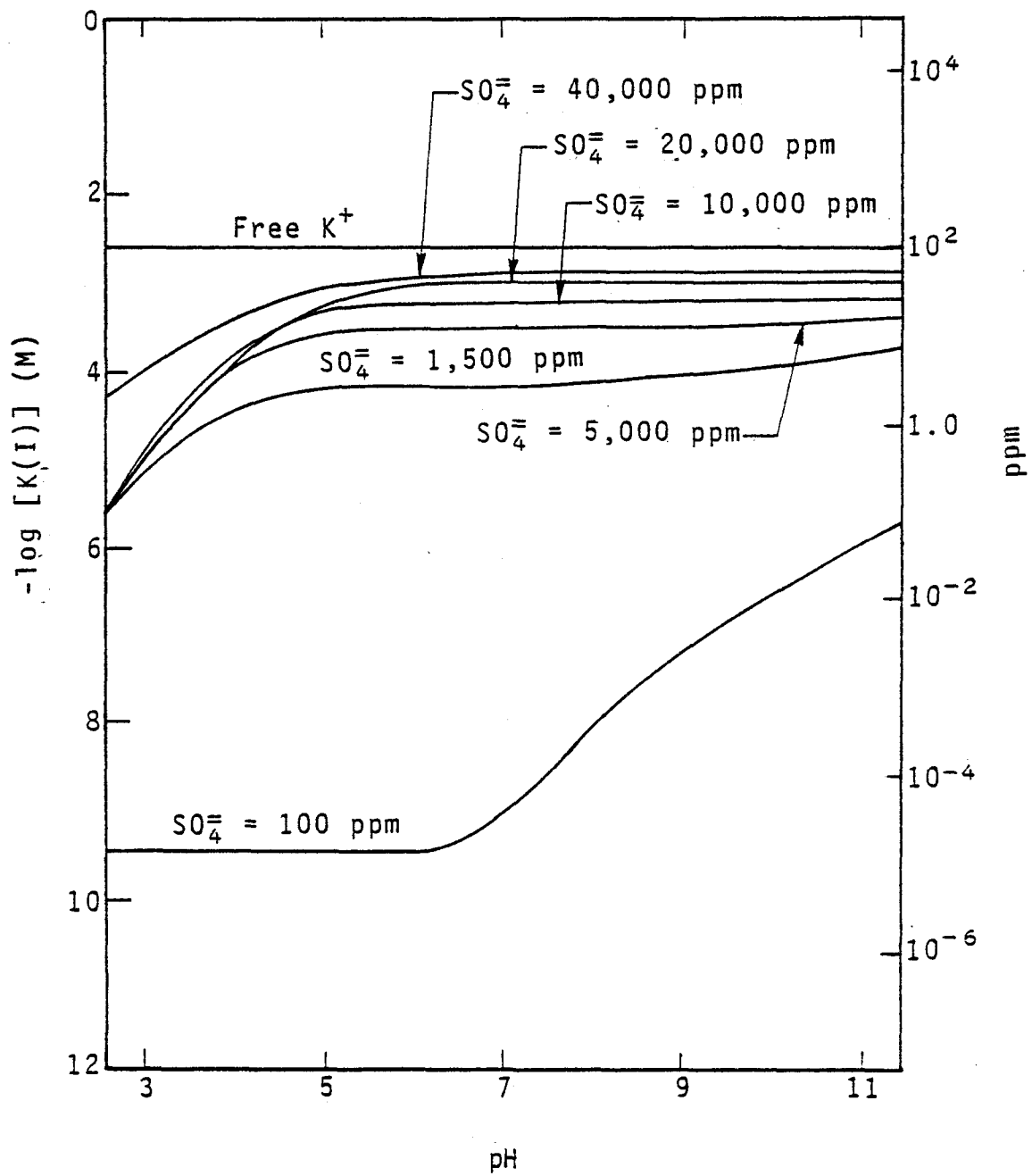
Figure 108. Effects of total sulfate concentration on soluble K concentration.
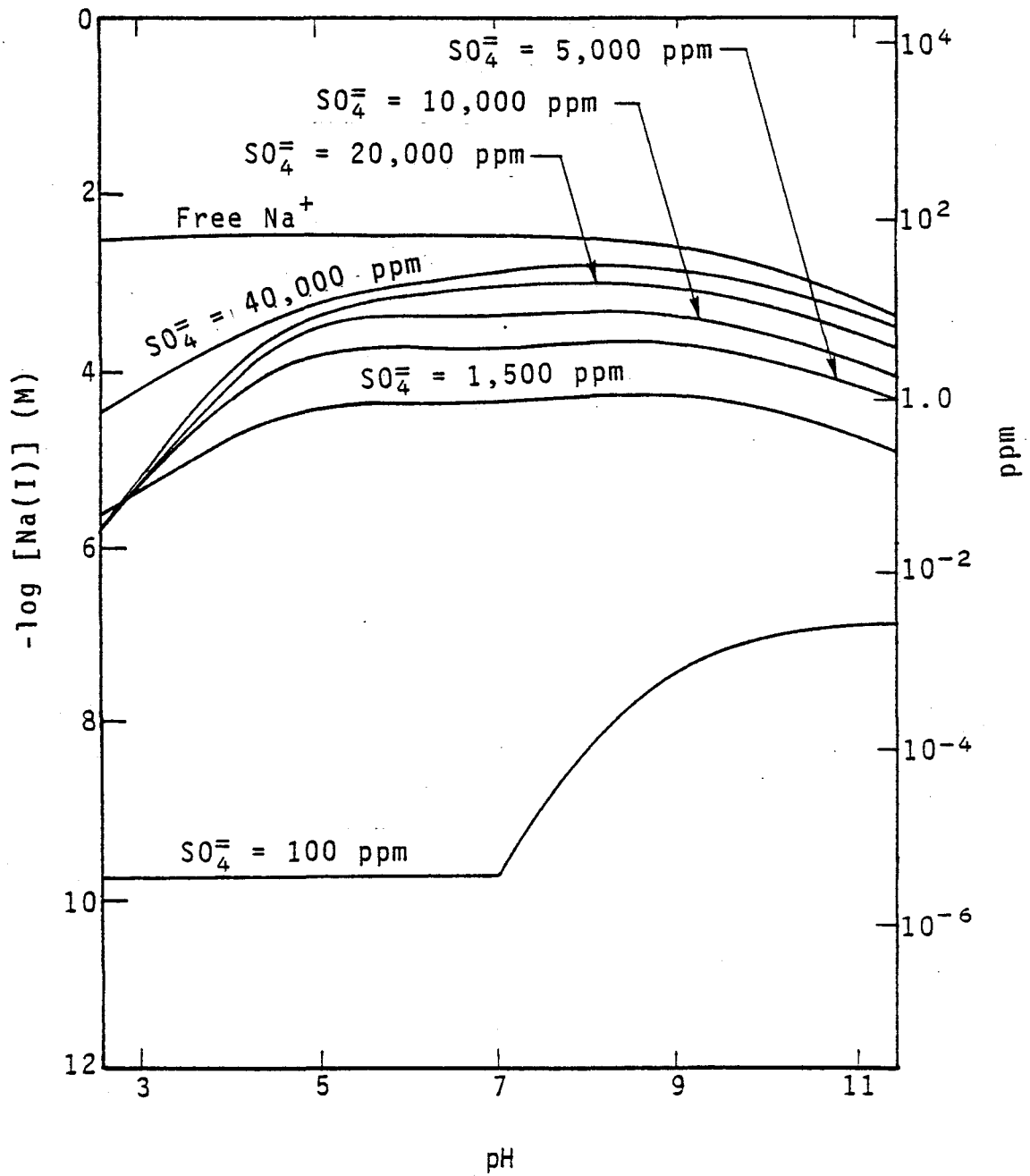
Figure 109. Effects of total sulfate concentration on soluble
Na concentration.

free ion concentrations of potassium and sodium still predominate.

EFFECTS OF BORATE CONCENTRATION ON THE SOLUBILITIES OF METALS

The speciation study has shown that total soluble copper and lead concentrations can be greatly affected by borate concentration of FGD wastewater. These effects are summarized in Figures 110 and 111.

As discussed previously (refer to Equation 78), the Cu-B(OH)$_4$ complex may account for almost 100 percent of the total soluble copper in the FGD wastewater when the pH is higher than about 4.7. In this study, the soluble borate levels were varied from 5 ppm to 200 ppm to observe the effects on copper. Figure 110 shows that a borate concentration increase of this magnitude results in a 2,000-fold increase in the copper-borate concentration.

For lead, an increase from 5 ppm to 200 ppm in borate concentration may produce a 10,000-fold increase in soluble Pb-B(OH)$_4$ (see Figure 111).

Although it is still impossible to verify the presence of various soluble lead species in the FGD wastewater, it can be shown on a theoretical basis that Pb-B(OH)$_4$ complexes can account for a major portion of the total soluble lead concentration. The Pb-CO$_3$ and Pb-OH complexes are the only species which may compete with Pb-B(OH)$_4$ levels when the pH is higher than about 7. If the theoretical evaluation is correct, the soluble lead level can be approximated by the following equation for pH higher than 7 (when pH 7, Equation 79 is followed):

pH > 7

$$[Pb_T] \approx 10^{5.2}[Pb^{2+}][B(OH)_4^-] + 10^{11.1}[Pb^{2+}][B(OH)_4^-]^3$$

$$+ 10^{7.4}[Pb^{2+}][CO_3^=] + 10^{10.8}[Pb^{2+}][CO_3^=]^2$$

$$+ 10^{6.3}[Pb^{2+}][OH^-] + 10^{10.9}[Pb^{2+}][OH^-]^2 \tag{83}$$

EFFECTS OF LIME ADDITION TO FGD SLUDGE AND WASTEWATER

The addition of lime and fly ash to FGD sludge has been employed as a fixative process, primarily to enhance physical properties (permeability, load-bearing strength) through a pozzolanic reaction. However, if lime addition achieves no reduction of the total soluble levels or any toxic complexes of the constituents, or if soluble trace metals constituents
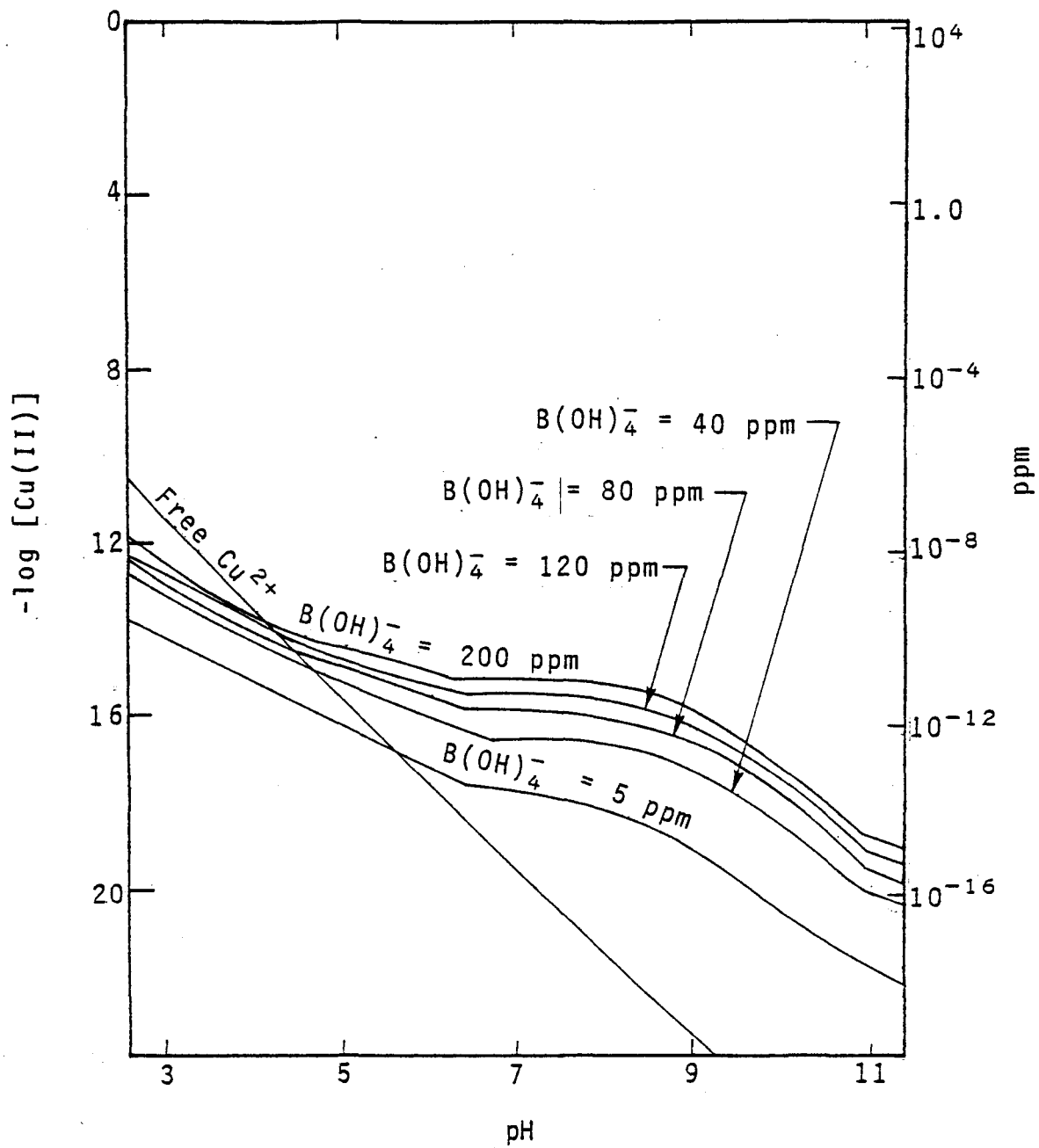
Figure 110.   Effects of borate concentration on soluble Cu
              concentration.
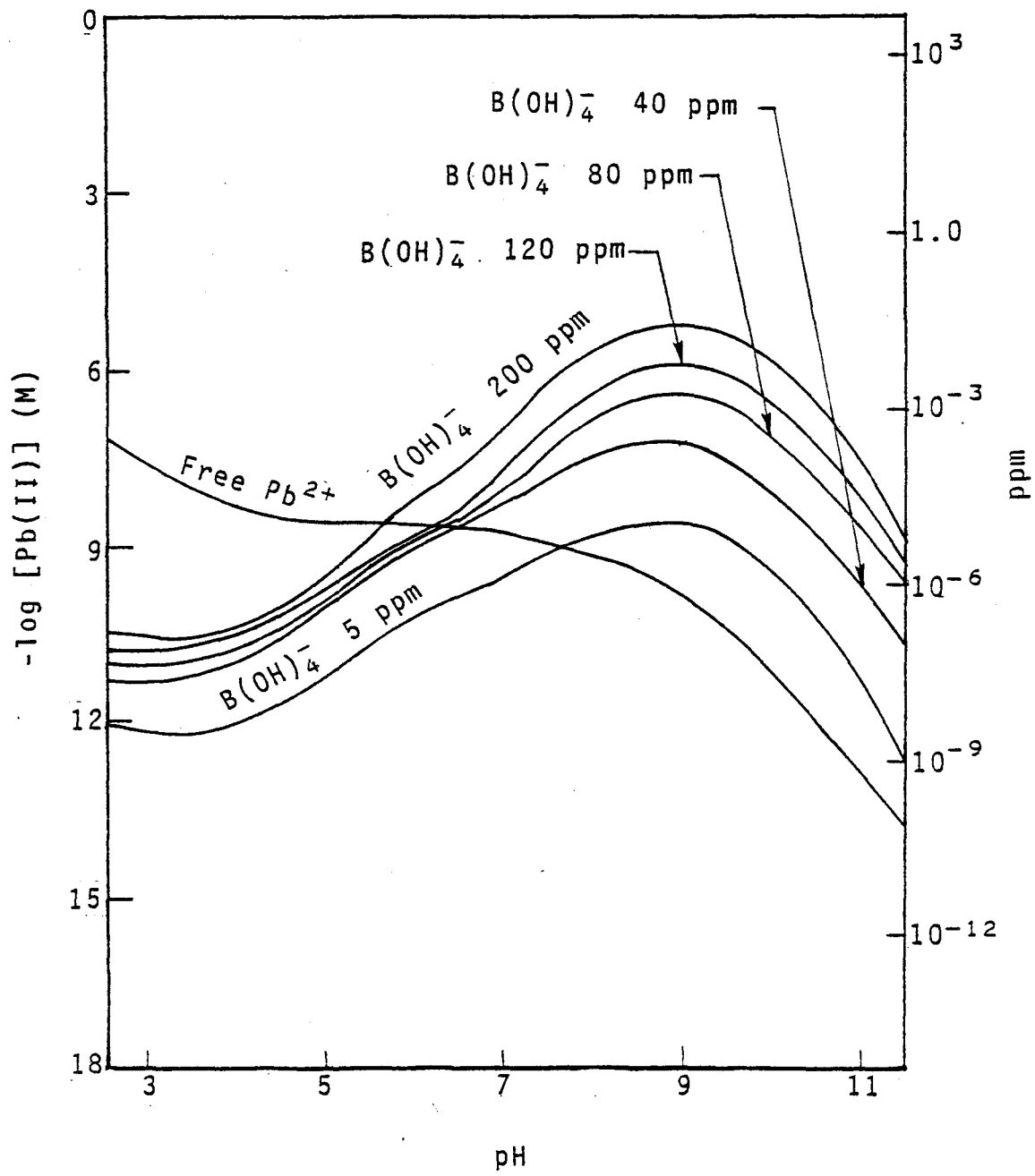
Figure 111. Effects of borate concentration on soluble Pb
concentration.

increase in concentration, there will be little environmental advantage of disposing the sludge with lime addition. Therefore, it would be useful to determine how various kinds of lime additions affect the concentrations of constituents in the sludge liquid phase. Specifically, if lime addition does have beneficial effects, it may be possible to determine how to achieve the optimum lime dosage in order to obtain the minimum concentrations of constituents in the liquid phase.

In this study, the Kansas City Power and Light La Cygne Plant FGD waste was used for the evaluation. The amount of lime addition used for the study ranged from 0 to 10,000 ppm (as $Ca(OH)_2$). Figures 112 through 114 show selected results. As illustrated in Figure 112, the concentrations of free CO_3^{2-}, PO_4^{3-}, SiO_3^{2-}, and OH^- can be increased significantly by lime addition. Free SO_3^{2-} is reduced slightly when lime is added. Other ligands, such as SO_4^{2-}, Cl^-, F^-, $B(OH)_4^-$, MoO_4^{2-}, AsO_4^{3-}, and HVO_4^{2-}, are only slightly, if at all, affected. It is expected that, without any decrease in free metal ion concentrations, the increase in ligand levels will lead to the increase in related metal-ligand complexing.

Figure 113 displays the results of lime addition on the total soluble concentrations of major ions. As can be seen from this diagram, only the total soluble calcium levels may be affected by the lime addition. The total calcium concentration can be increased dramatically by an added 100 ppm of lime. When the dosage of lime is increased from 100 ppm to 10,000 ppm, total soluble calcium will increase steadily from about 200 ppm to 400 ppm.

Most of the minor ions are affected by lime addition. Although lime addition is usually accompanied by a pH increase, the total soluble concentrations of minor ions rather than showing a decreasing trend, usually increase in the FGD sludge liquid phase. This is due to the formation of the strong metallic complexes of hydroxide or carbonate. As shown in Figure 114, total soluble cadmium can be increased from 0.01 ppb to 1.45 ppb if the lime addition exceeds 1,500 ppm. Total soluble Fe(III) also will increase to the level of 22 ppb from its original level of 0.012 ppb for a similar lime dosage. Total soluble manganese is reduced from its original level of 156 ppb to about 20 ppb as the dosage of lime is increased from 0 to about 500 ppm (as $Ca(OH)_2$). When the dosage exceeds 500 ppm, total soluble manganese can reach concentrations as high as 36.5 ppb. Lime addition also may increase the total soluble levels of Cu(II) by a factor of 10. These levels, however, are still in the trace level range (<0.001 ppb).

From the above discussion, it can be seen that thermodynamically, the lime addition has a beneficial effect only for manganese. The liquid phase concentrations of many other soluble

207
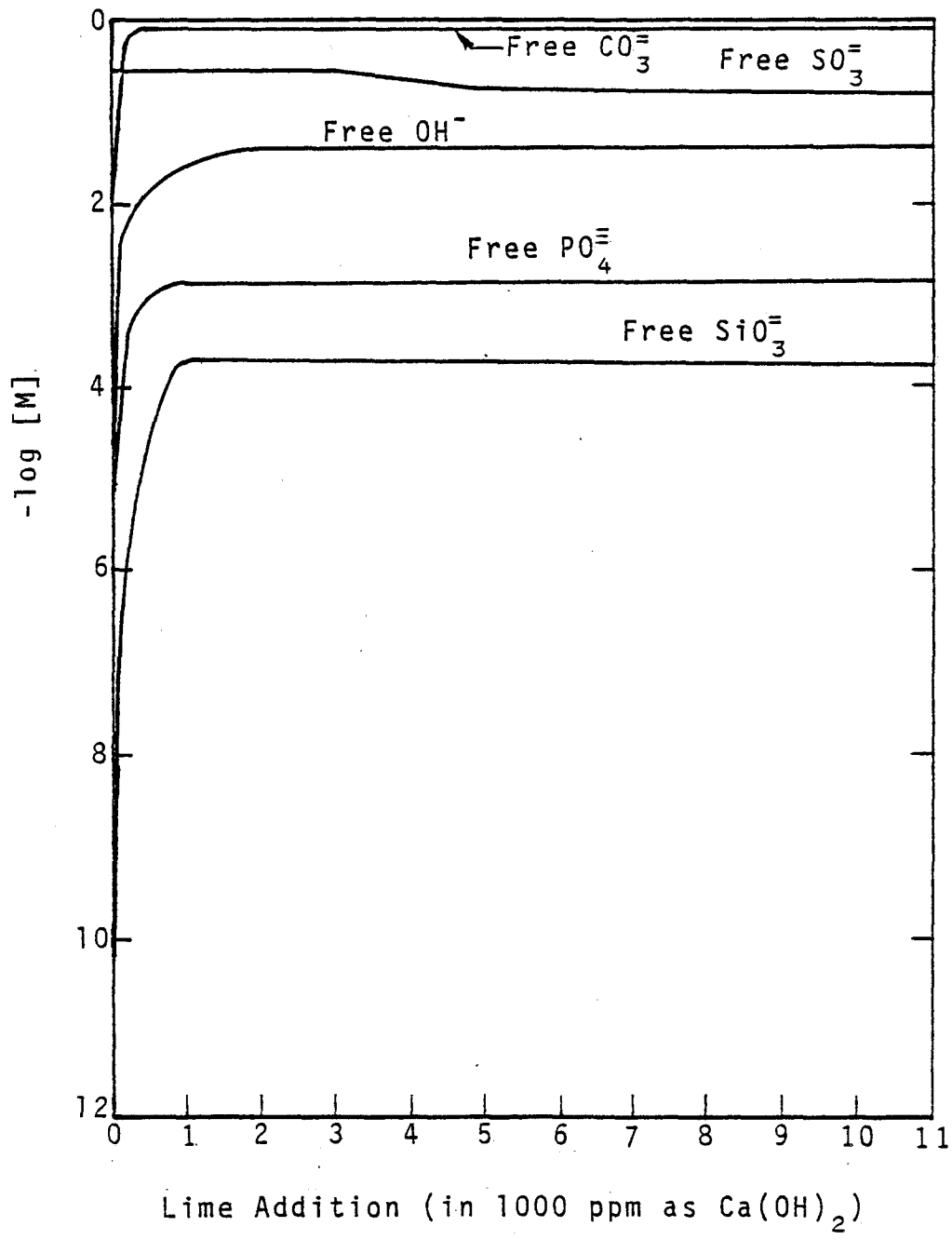
Figure 112.   Effects of lime addition on the concentrations of
free ligands.
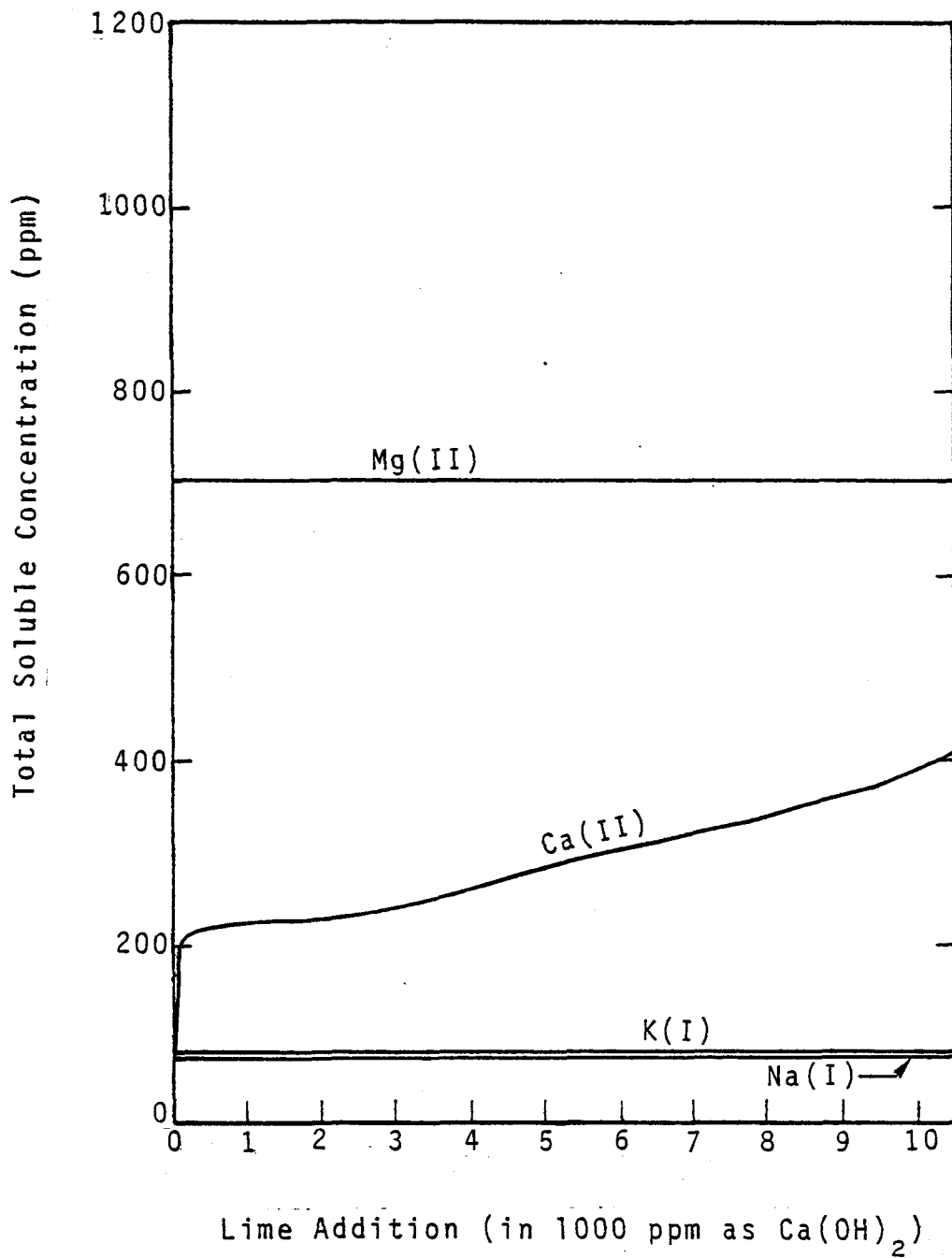
Figure 113. Effects of lime addition on the total soluble
concentrations of major ions.

209
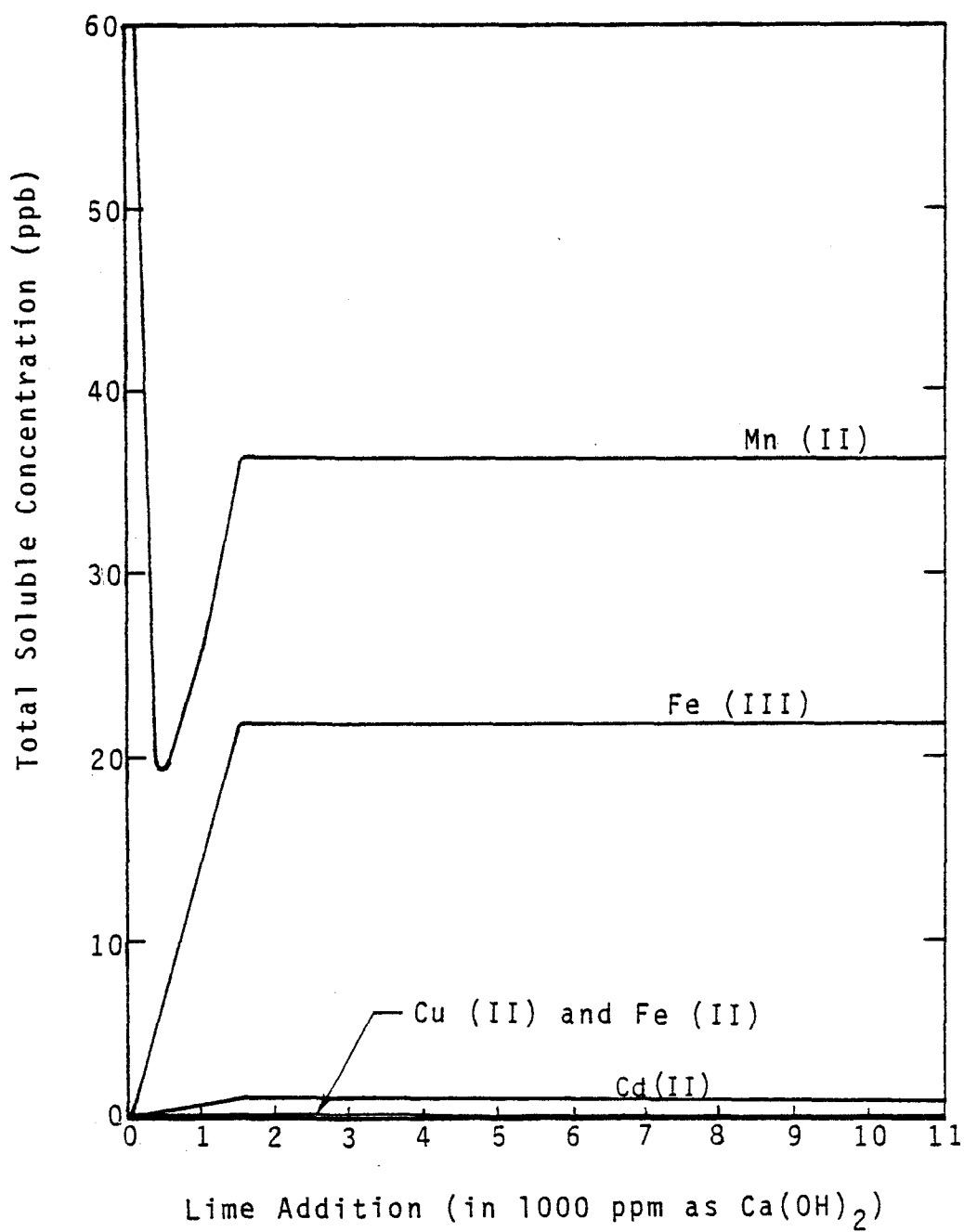
Figure 114.   Effects of lime addition on the total soluble
concentrations of minor ions.

constituents, such as Ca, Fe, Cd, will increase significantly when extra lime is added to the FGD waste, thereby increasing the potential for leaching of these constituents from the sludge disposal site. This phenomenon, however, needs additional field study to verify.

EFFECTS OF SILICATE ADDITION TO FGD SLUDGE

As was the case with lime, the addition of silicate compounds has been employed for the fixation of FGD sludge. How the concentration of metals and other ions in their various forms change as a function of silicate additive concentration was examined in this study. This examination was divided into two sections: (1) to evaluate the overall effects of the silicate addition, and (2) to identify the silicate level where the silicate addition may become significant. The results are given in Figures 115 through 124.

In this study, the effects of silicate addition were observed from $10^{-5}M$ to $10^{0}M$ (0.28 to 28,000 mg/l as Si) of total silicate concentrations in the FGD system. The results of thermodynamic calculations show that silicate addition may have a significant effect on the levels of soluble aluminum (Figure 115) and zinc (Figure 116). However, soluble levels of other elements studied (Figures 117 through 124) were not shown to vary with the silicate addition.

It can be observed in Figure 115 that the level of soluble aluminum species is greatly reduced in the aged FGD sludge liquor when the total silicate level is higher than $10^{-2}M$ (280 mg/l as Si). When silicate levels increase from $10^{-2}M$ to $10^{-1}M$ (280 mg/l to 2,800 mg/l as Si), the total soluble aluminum concentration (about 2.7 ppm) can be reduced by about four orders of magnitude. As silicate levels are further increased ($10^{-1}M$), however, the total soluble aluminum level will remain unchanged. Therefore, if silicate is added for the control of aluminum solubility, the optimum levels of silicate in the FGD system are about $10^{-2}M$ to $10^{-1}M$, depending on the final aluminum levels desired.

Zinc exhibits behavior similar to that of aluminum when silicate is added to the FGD sludge (Figure 116). The total zinc levels will not be affected by silicate until the silicate level reaches as high as $10^{-2}M$ (280 mg/l as Si). Between $10^{-2}M$ and $10^{-1}M$ of silicate, the total soluble zinc level can be reduced 4,000-fold. The same optimum levels of silicate addition for aluminum are suggested for zinc in order to control soluble zinc in the FGD sludge leachate. With the exception of aluminum and zinc, other elements studied (Figures 117 through 124 will not be affected significantly by silicate addition).

211
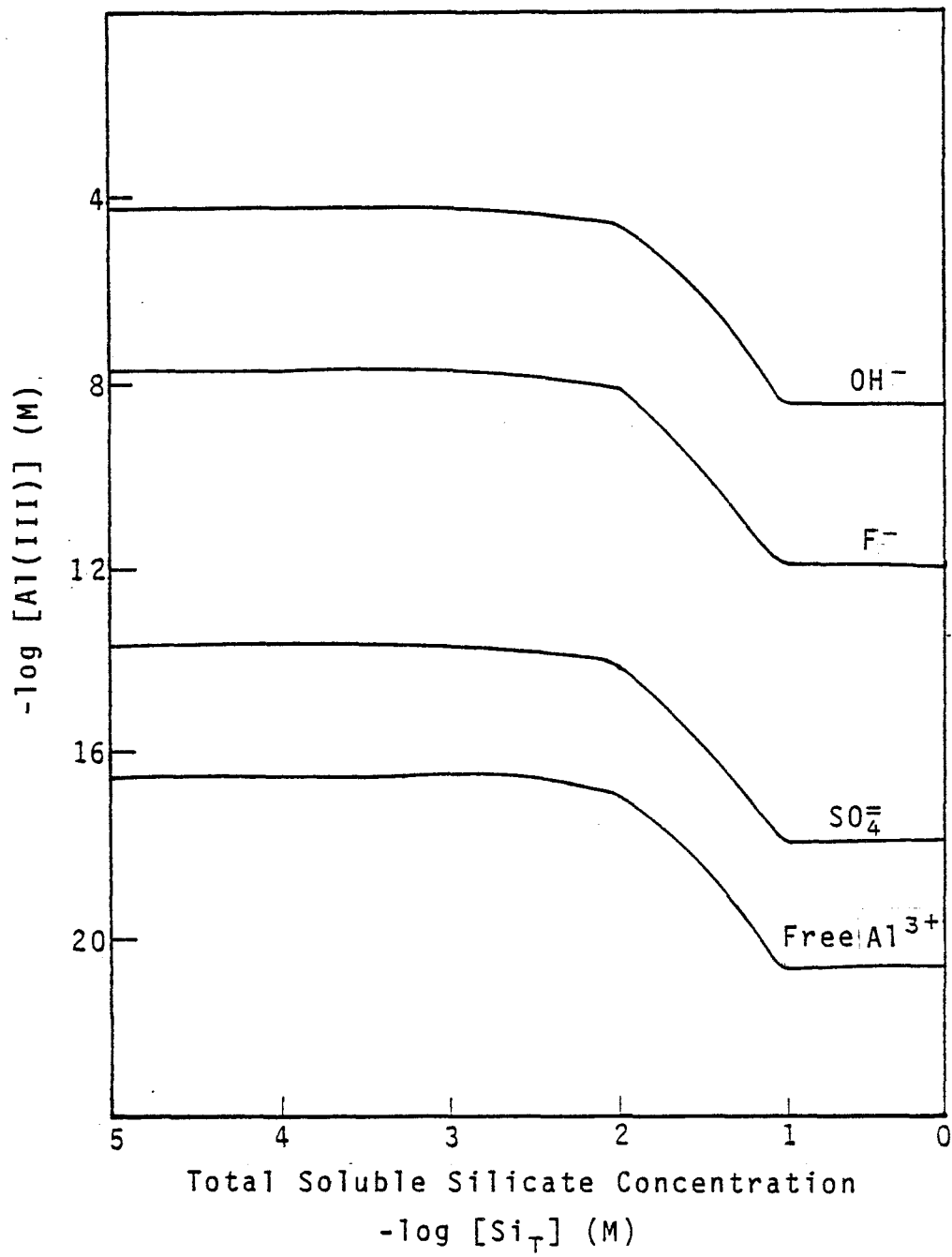
Figure 115. Effects of silicate addition on Al in FGD wastewater.

212
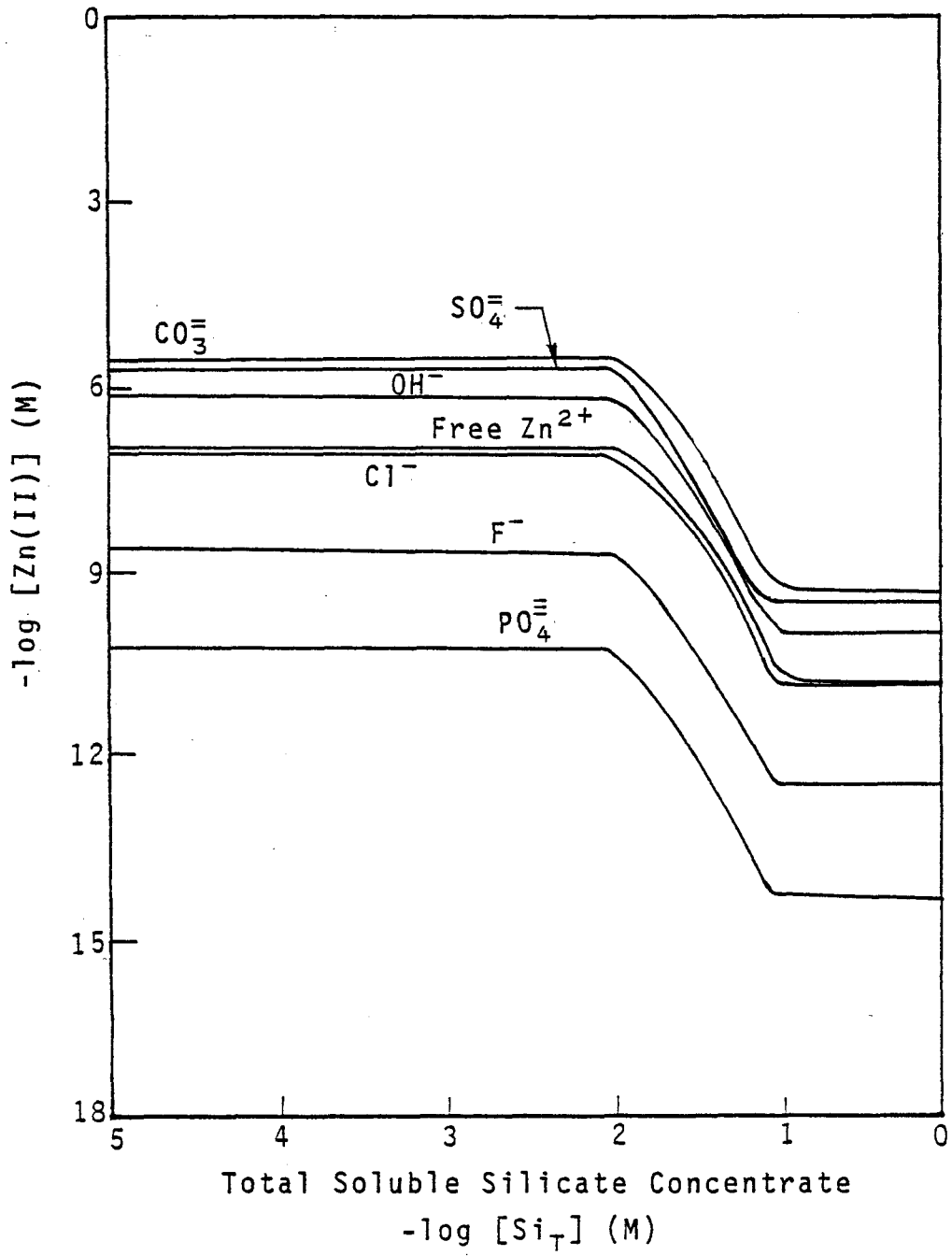
Figure 116.   Effects of silicate addition on Zn in FGD wastewater.
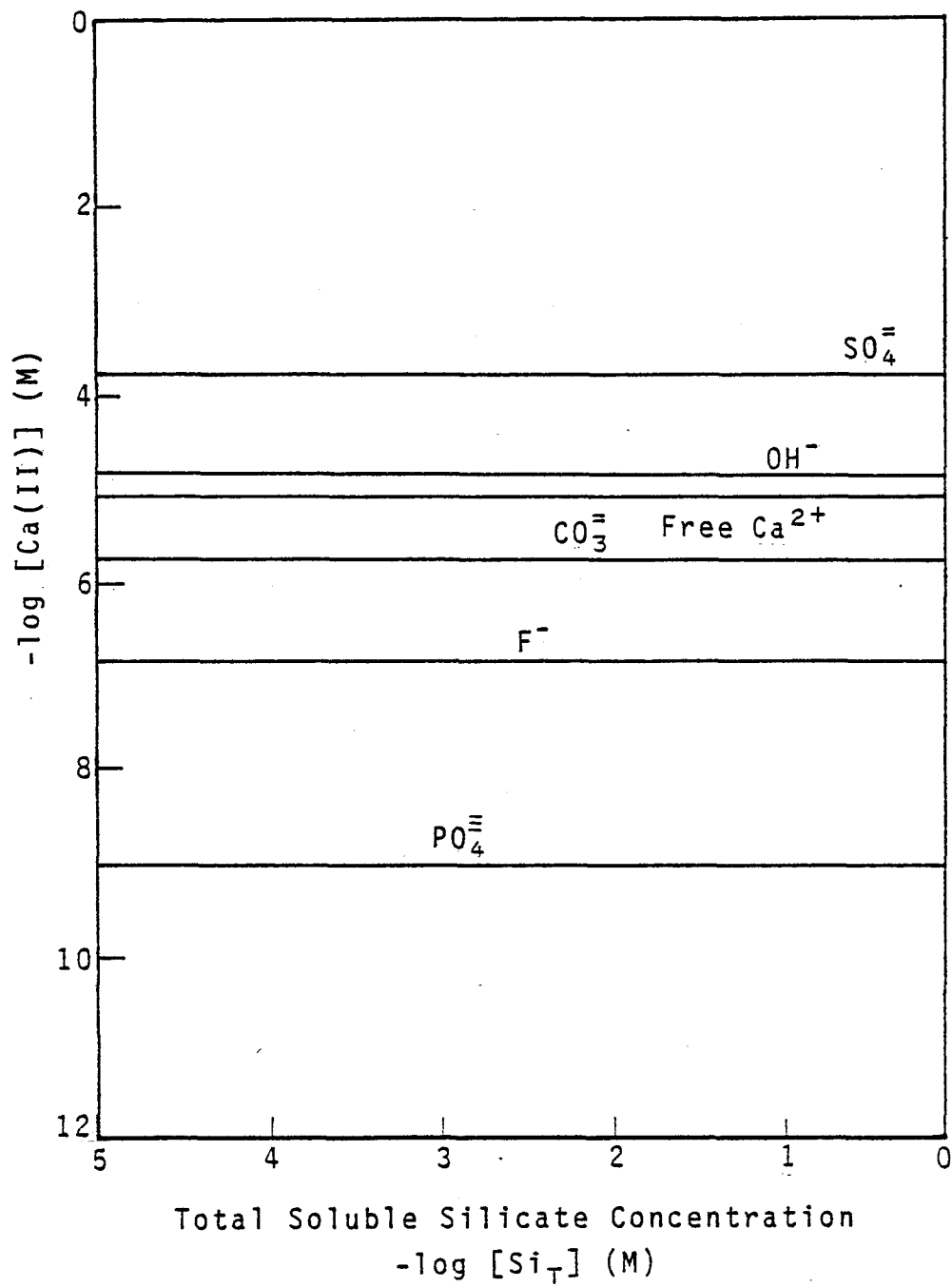
Figure 117. Effects of silicate addition on Ca in FGD wastewater.
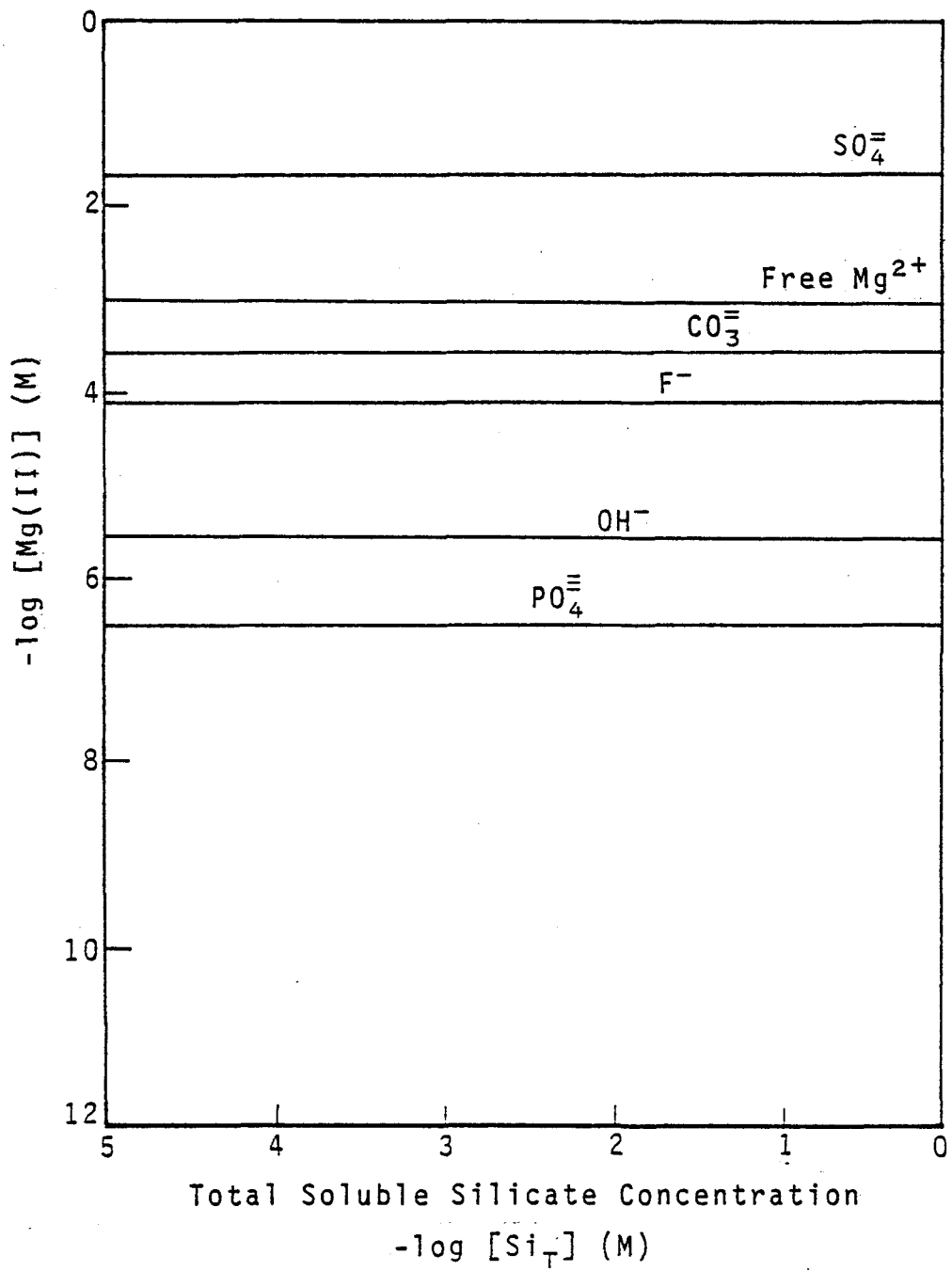
Figure 118.   Effects of silicate addition on magnesium in FGD
             wastewater.
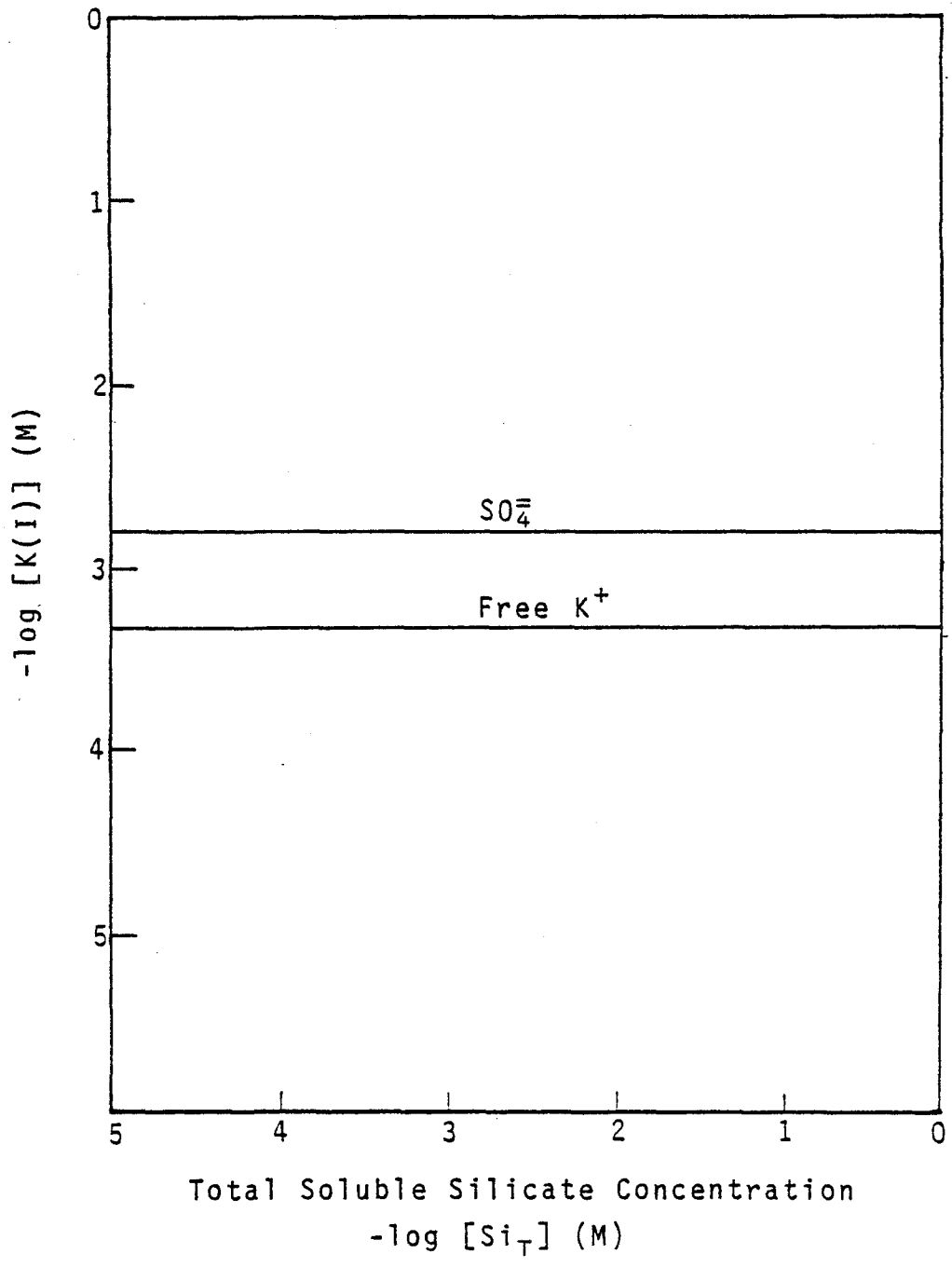
Figure 119.   Effects of silicate addition on K in FGD wastewater.
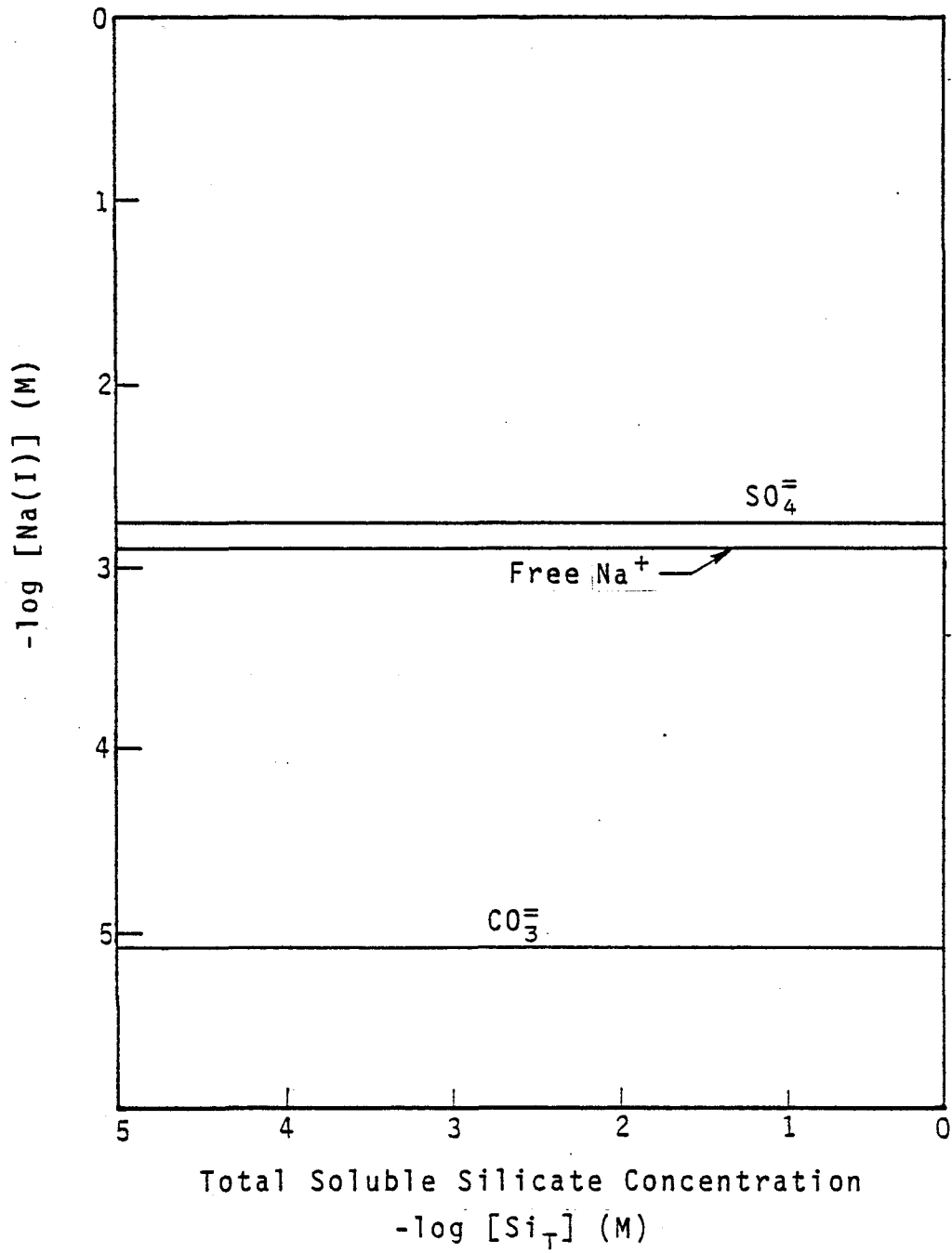
Figure 120. Effects of silicate addition on Na in FGD wastewater.
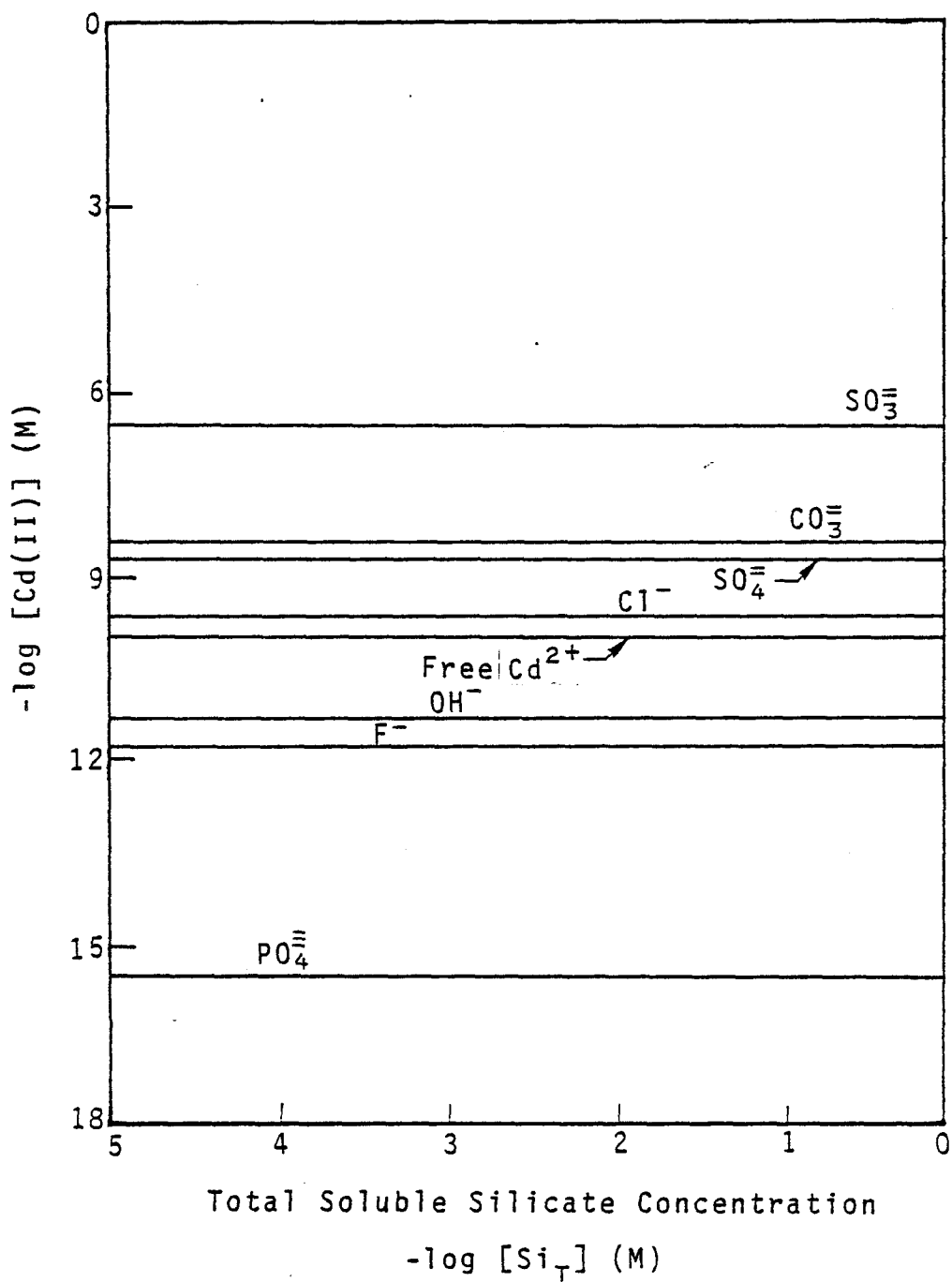
Figure 121.   Effects of silicate addition on Cd in FGD
              wastewater.
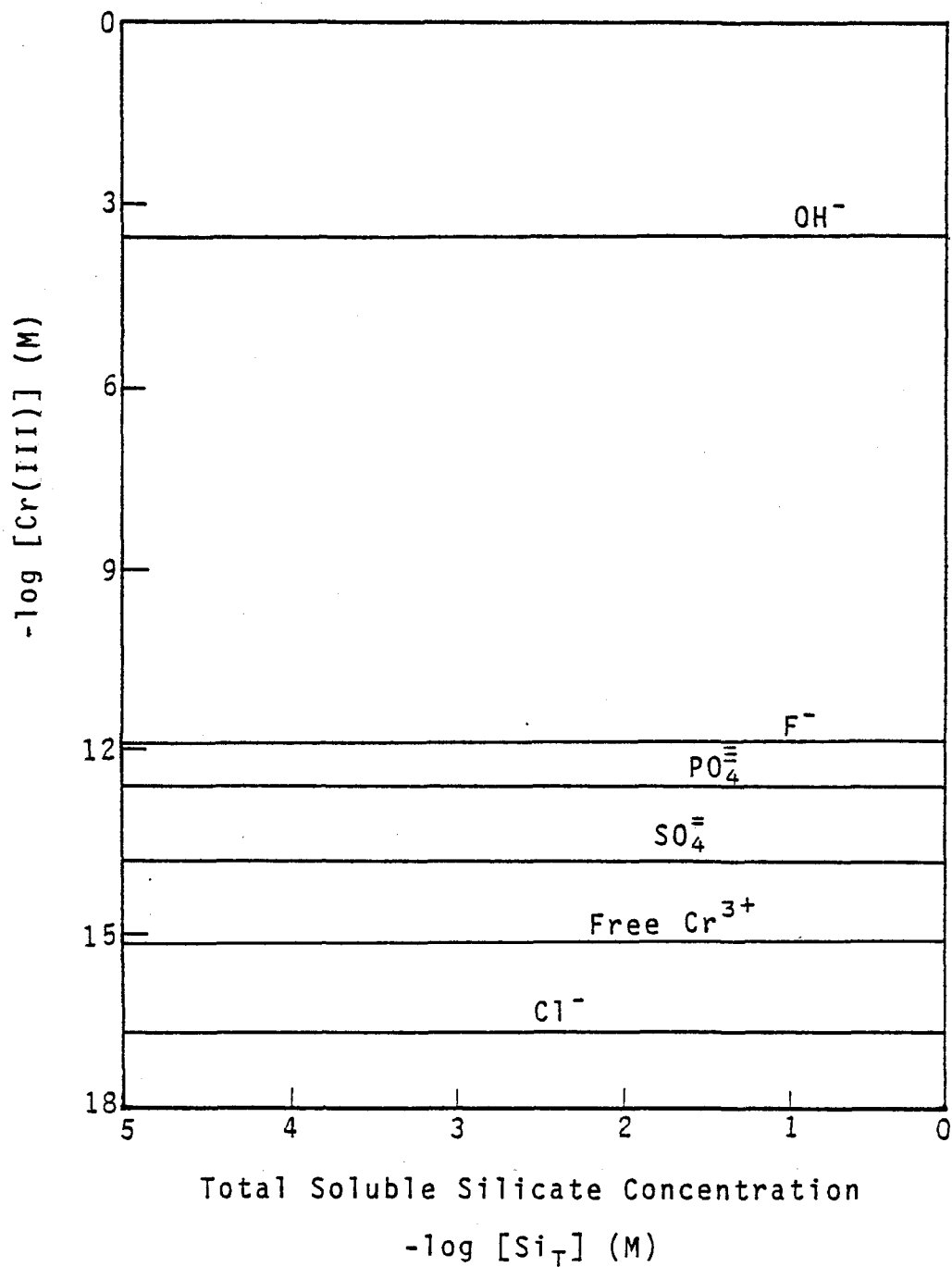
Figure 122.   Effects of silicate addition on Cr in FGD wastewater.
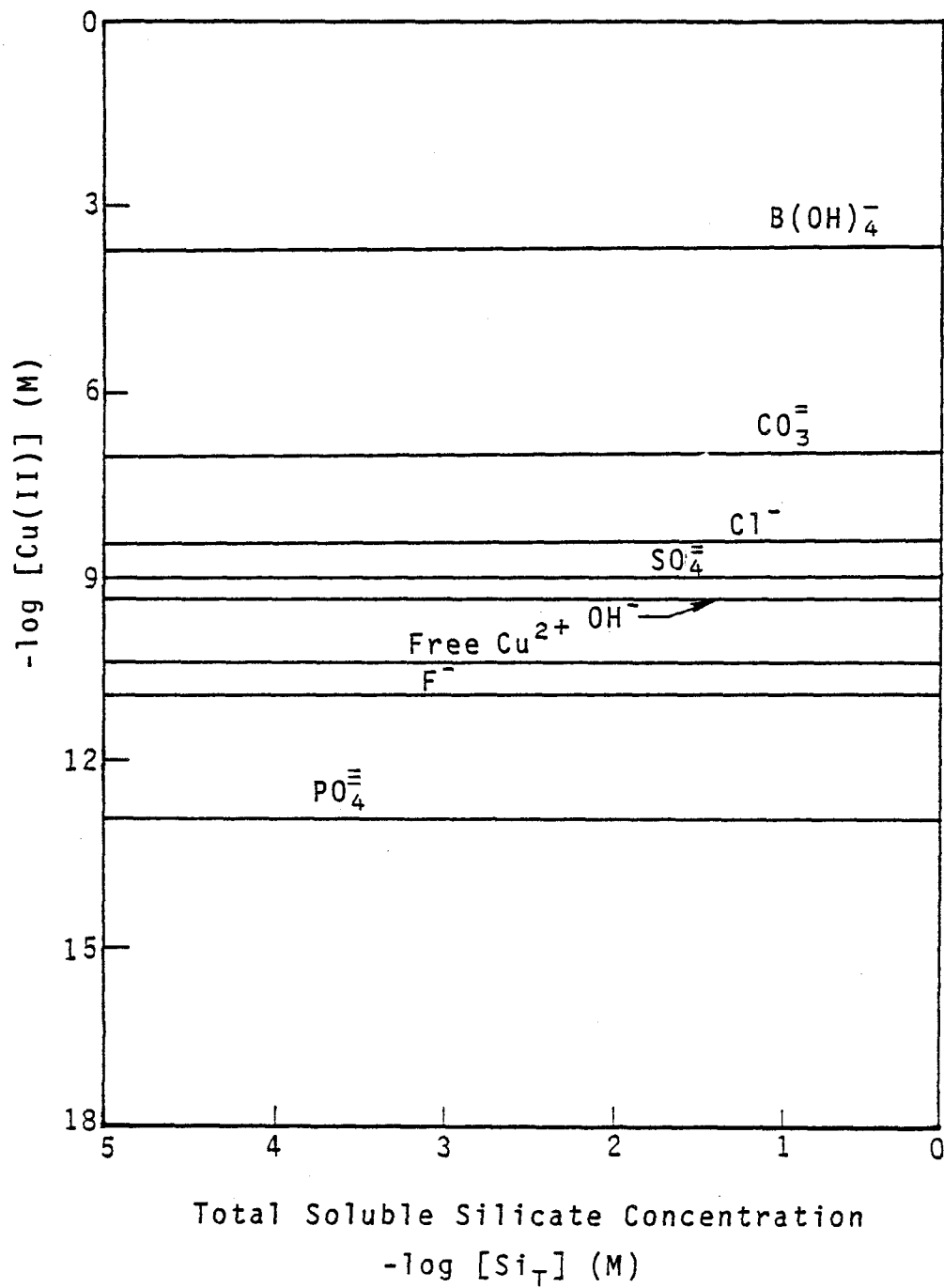
Figure 123.   Effects of silicate addition on Cu in FGD
               wastewater.

220
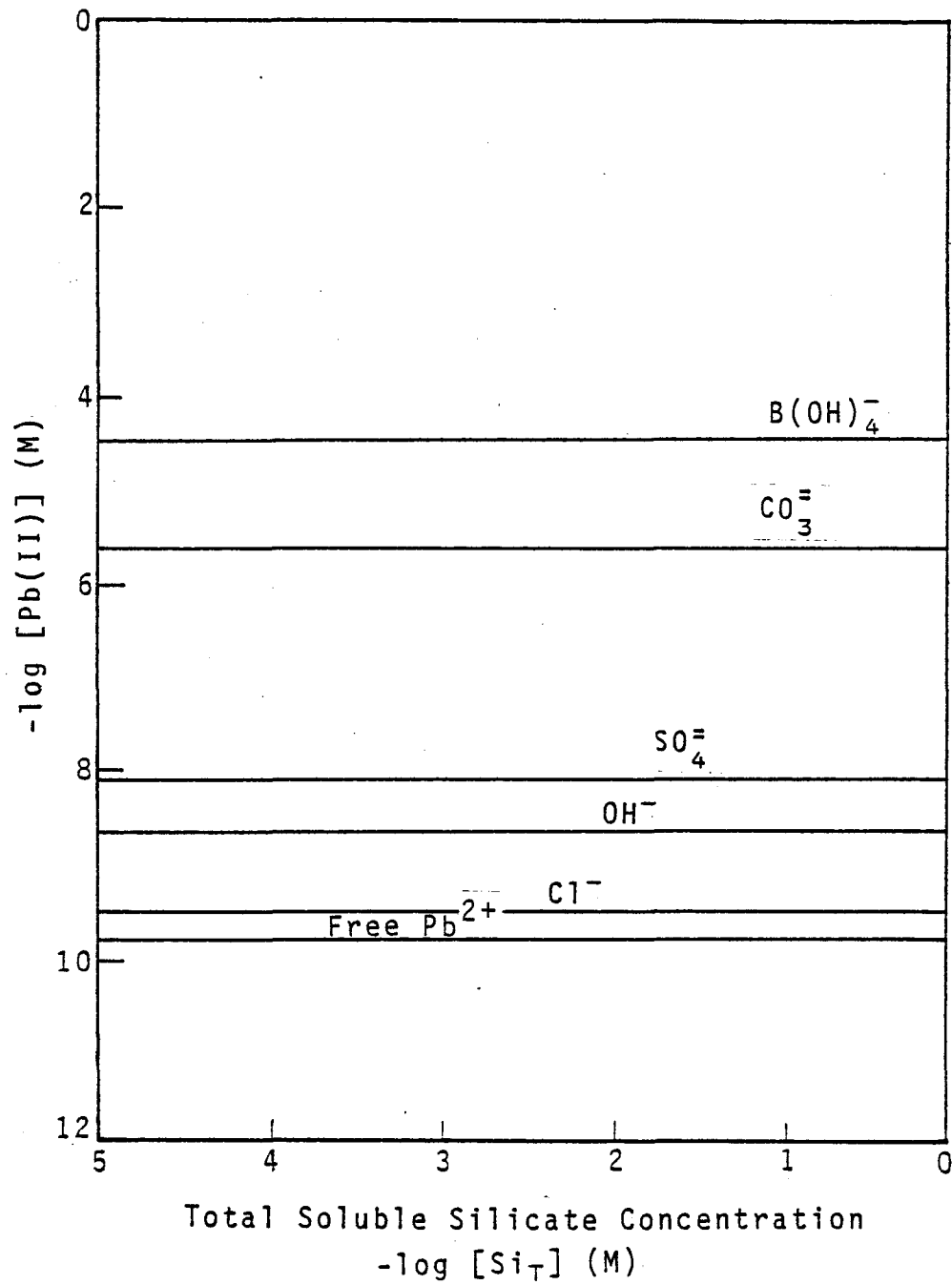
Figure 124.   Effects of silicate addition on Pb in FGD wastewater.

EFFECTS OF HYDROGEN SULFIDE ADDITION TO FGD SLUDGE

Sulfide is known to be an extremely effective scavenger for removing certain trace metals from the aqueous solution. Since hydrogen sulfide may be available at some power plants, the effects of sulfide addition to FGD wastes were investigated.

For modeling purposes, the total sulfide concentration was varied from $10^{-7.51}$M to $10^{-3.20}$M (0.001 ppm to 20 ppm). The results of calculation show that the distributions of copper, lead, cadmium, zinc, mercury, silver, and cobalt species in the FGD waste are significantly affected by sulfide addition. The effect of sulfide addition on other constituents is negligible.

As shown in Figure 125, the total soluble concentrations of both lead and copper can be reduced to trace levels by adding as little as 0.001 ppm ($10^{-7.51}$M) of sulfide to the FGD sludge. The total soluble levels of these two elements will be further reduced when sulfide addition is increased. The effect of sulfide addition on the total soluble cadmium concentration also displays similar behavior (Cd concentration decreases as sulfide addition increases). The total soluble cadmium concentration will not, however, reach trace levels until the sulfide concentration exceeds about 0.2 ppm. The reduction achieved in total soluble zinc concentration is negligible if sulfide addition is less than 0.1 ppm. When the total added sulfide exceeds 0.5 ppm, the soluble zinc can also be reduced to trace levels. The reduction in levels of soluble heavy metals is due to the formation of insoluble metallic sulfide compounds such as $CuS(s)$, $PbS(s)$, $CdS(s)$, and $ZnS(s)$. Figure 126 displays the distribution of metallic sulfides in FGD waste as a function of the sulfide concentration. At low total sulfide levels (e.g., less than 0.001 ppm), sulfide addition will favor the formation of $Ag_2S(s)$ and $CuS(s)$. After sufficient soluble silver and copper are removed from solution, the remaining soluble sulfide can then react with other soluble metals. The order of metallic sulfide formation with increasing sulfide levels is as follows: $Ag_2S(s)$ - $CuS(s)$ - $PbS(s)$ - $CdS(s)$ - $ZnS(s)$ - $CoS(s)$. This sequence can be seen in Figure 126.

Although the trace heavy metals can be removed efficiently by sulfide addition, this treatment may not be desirable for two reasons. First, excess hydrogen sulfide itself is an undesirable contaminant in wastewater (leachate). Second, the FGD sludge lagoon is an open pond, where oxygen can gradually diffuse into the FGD waste and oxidize the metallic sulfide solids. Diffusion and oxidation will eventually convert the sulfide solids into the original predominant solids, and again release the soluble metal species.
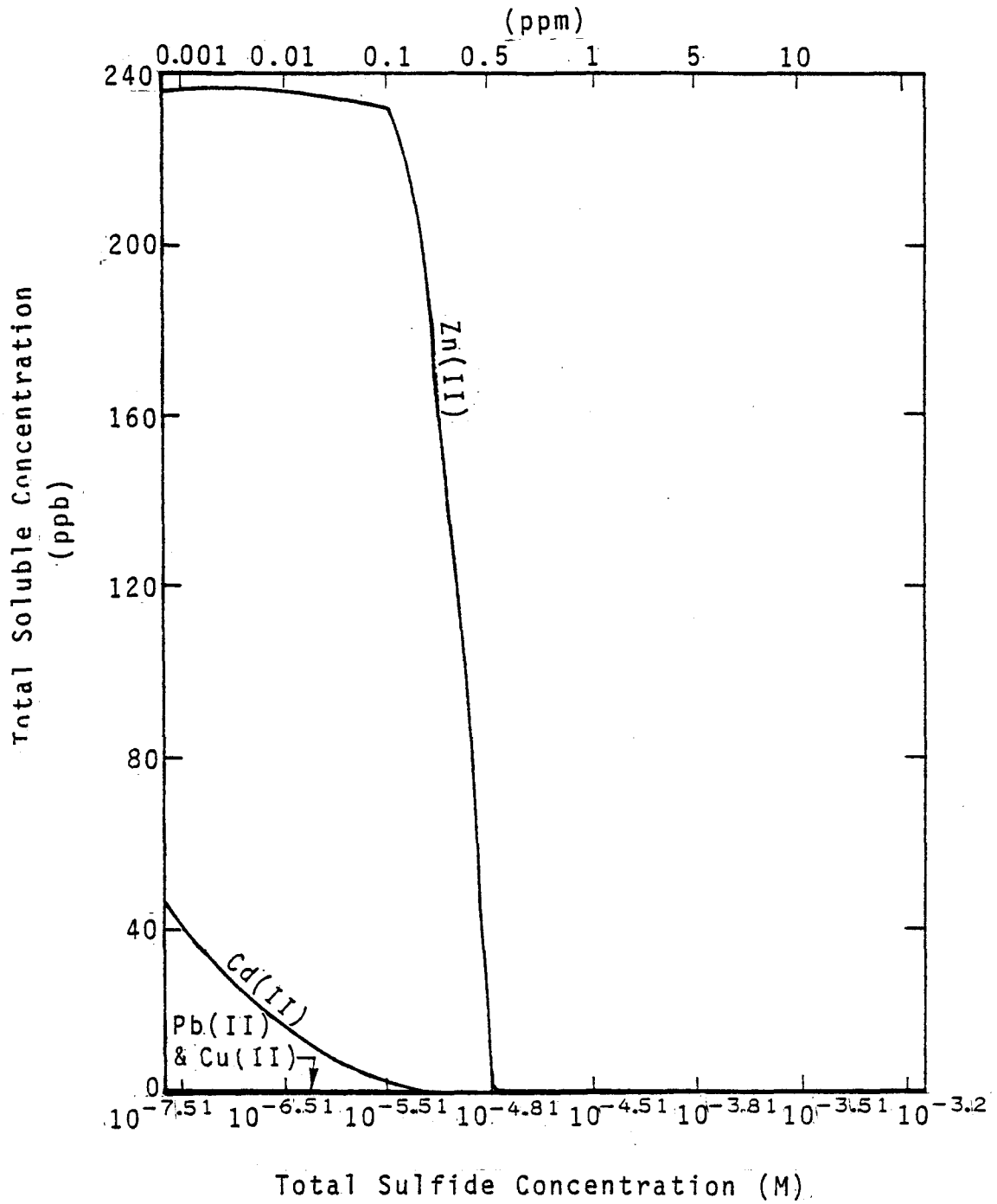
Figure 125. Effects of sulfide addition on the total soluble
levels of metals in the raw FGD waste.
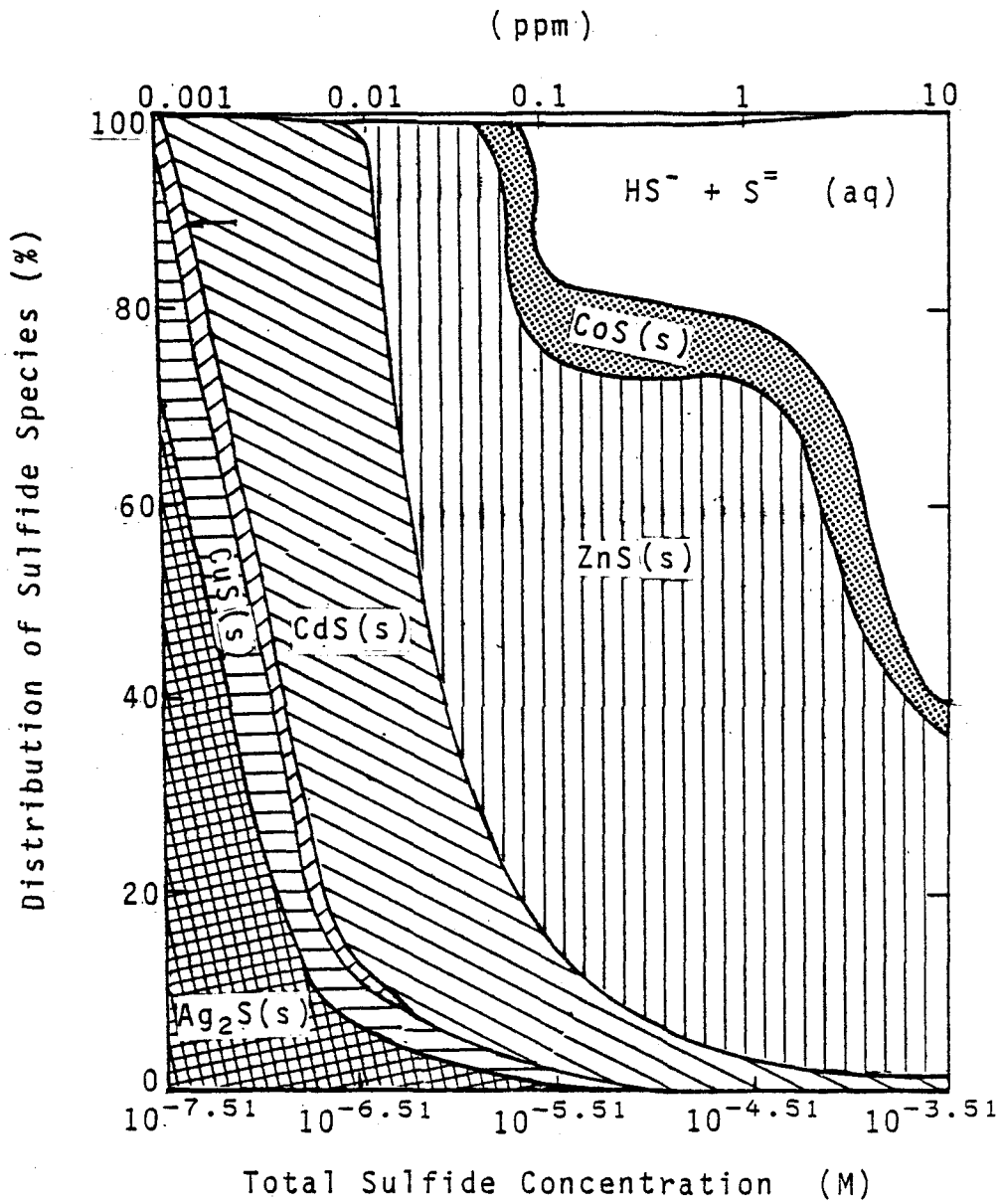
Figure 126. Effects of sulfide addition on the distribution of sulfide species in the FGD waste.

EFFECTS OF PHOSPHATE ADDITION TO FGD SLUDGE

In this study La Cygne Plant data are used for evaluation, total phosphate concentrations in the FGD sludge ranged from 10^{-5} to 10^{-1}M (0.31 to 3,100 mg/l as P). Among the metals studied, it was found that only the total levels of magnesium, calcium, and cadmium can be significantly affected by phosphate addition. Soluble magnesium is reduced by a factor of 2.5 as the phosphate level is increased from 10^{-5} to 10^{-1}M (Figure 127). This change is due primarily to the formation of $Mg_3(PO_4)_2(s)$ solid in the FGD sludge. According to the calculation, the level of $Mg_3(PO_4)_2(s)$ solid in the sludge is increased at the following ratios:

Total phosphate (M) in the FGD system	% of Mg formed as $Mg_3(PO_4)_2(s)$
10^{-5}	≈ 0
10^{-4}	≈ 0
10^{-3}	5
10^{-2}	31.9
10^{-1}	55.5

Due to the formation of $Mg_3(PO_4)_2(s)$, the concentration of free Mg^{2+} ion is significantly reduced. This change also leads to a decrease in the concentration of all soluble magnesium complexes (except the $Mg-PO_4$ complexes, which shows an increase in concentration with the increase of phosphate addition.

The total soluble calcium can also be reduced slightly as the total phosphate level exceeds about 10^{-2}M (310 mg/l as P) (Figure 127). In a manner similar to magnesium, this reduction is due to the formation of calcium phosphate solids in the FGD sludge. Three $Ca-PO_4$ solids may be formed in the FGD sludge: $Ca_5(PO_4)_3OH(s)$, $Ca_4(PO_4)_3H(s)$, and $CaHPO_4(s)$. The following table shows the effect of phosphate variation on $Ca-PO_4$ solids formation:

Total phosphate (M) in the FGD system	% of Ca formed as phosphate solids
10^{-5}	≈ 0
10^{-4}	≈ 0
10^{-3}	≈ 0
10^{-2}	1.5
10^{-1}	36.2

Because of the $Ca-PO_4$ solids formation, the amount of $CaF_2(s)$ solid will decrease slightly (about 0.1 in terms of the total calcium level in the sludge). This effect will lead to an increase in the soluble fluoride level of about 23 percent for a 10^{-1}M addition of phosphate to the sludge.
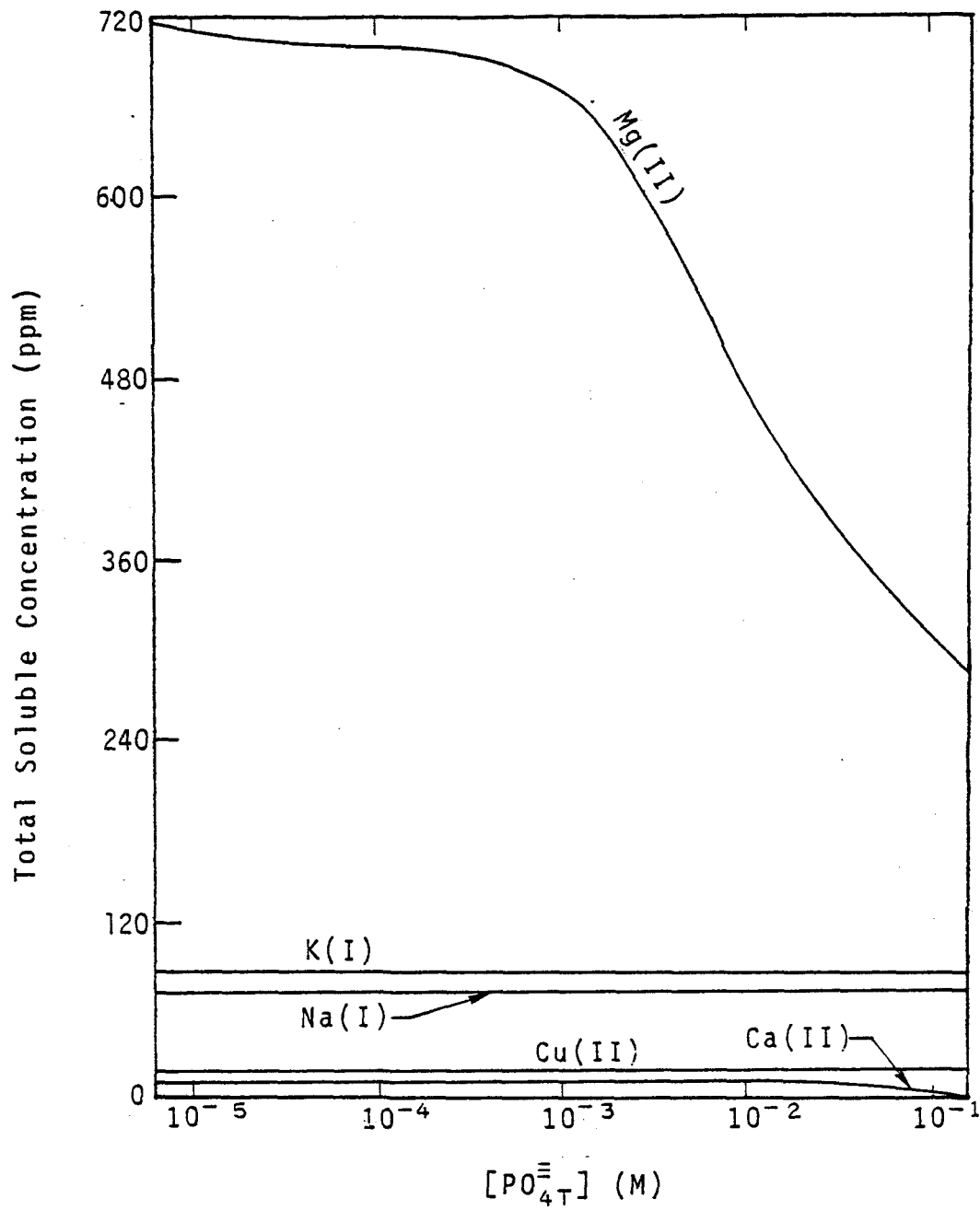
Figure 127. Effects of phosphate concentration on the total soluble concentrations of metals.

The formation of calcium phosphate solids also causes a decrease in the amount of $CaSO_3 \cdot 1/2H_2O(s)$ in the FGD sludge. Due to this change, the free SO_3^{2-} concentration is increased substantially (about 50 percent above its original level). This change leads to a significant increase in $Cd(SO_3)_2^{2-}$ complexes, and in so doing increases the total soluble cadmium concentration by a factor of 2 above its original level (see Figure 128).

EFFECTS OF MAGNESIUM ADDITION TO THE FGD SORBENT

The use of high magnesium scrubbing reagents could become widespread (Ref. 1). This study used the model to identify the effects of various concentrations of magnesium additives on the FGD sludge liquid phase. In this study, the magnesium concentration in the FGD sorbent was varied from 10^{-4} to 10M (2.4 ppm to 0.24 percent as Mg) to observe the effects on the speciation of metals. Results for some selected elements are shown in Figures 129 through 134.

Figure 129 shows that an increase in magnesium concentration in the FGD sorbent will also increase the levels of all soluble species of magnesium. This formation of strong magnesium complexes in the FGD sorbent is due to the increase of soluble free Mg^{2+} ion. This phenomenon leads to the decrease of available free ligands such as SO_4^{2-}, F^-, PO_4^{3-}, and CO_3^{2-}. Therefore, the concentrations of the complexes formed by the above ligands with other metals are usually reduced (see Figures 130 to 134).

The effects of magnesium addition on the speciation of calcium in the FGD system is shown in Figure 130. As can be seen from the diagram, the concentrations of Ca-SO₄, Ca-F, and Ca-PO₄ complexes are greatly reduced in the FGD sorbent when the total magnesium concentration in the system exceeds 10^{-1}M (2,430 ppm as Mg). The Ca-CO₃ complexes appear to be un-affected when magnesium is added to the system. The most important species for calcium in the system is free Ca^{2+} ion, which will not be affected by the addition of magnesium. Therefore, magnesium addition will not alter the total soluble level of calcium in the system.

Similar phenomena also hold true for sodium and potassium. When magnesium is added to the system, the concentrations of sulfate complexes with sodium or potassium are decreased, but total soluble levels of potassium and sodium remain unchanged.

For minor ions, the effects of magnesium addition are also confined to concentration changes of the SO_4^{2-}, F^-, and PO_4^{3-} complexes (Figures 131 through 134). In general, if these complexes comprise the predominant soluble species for a minor element, then magnesium addition may affect the total soluble levels of that element. Otherwise, the effects are confined

227
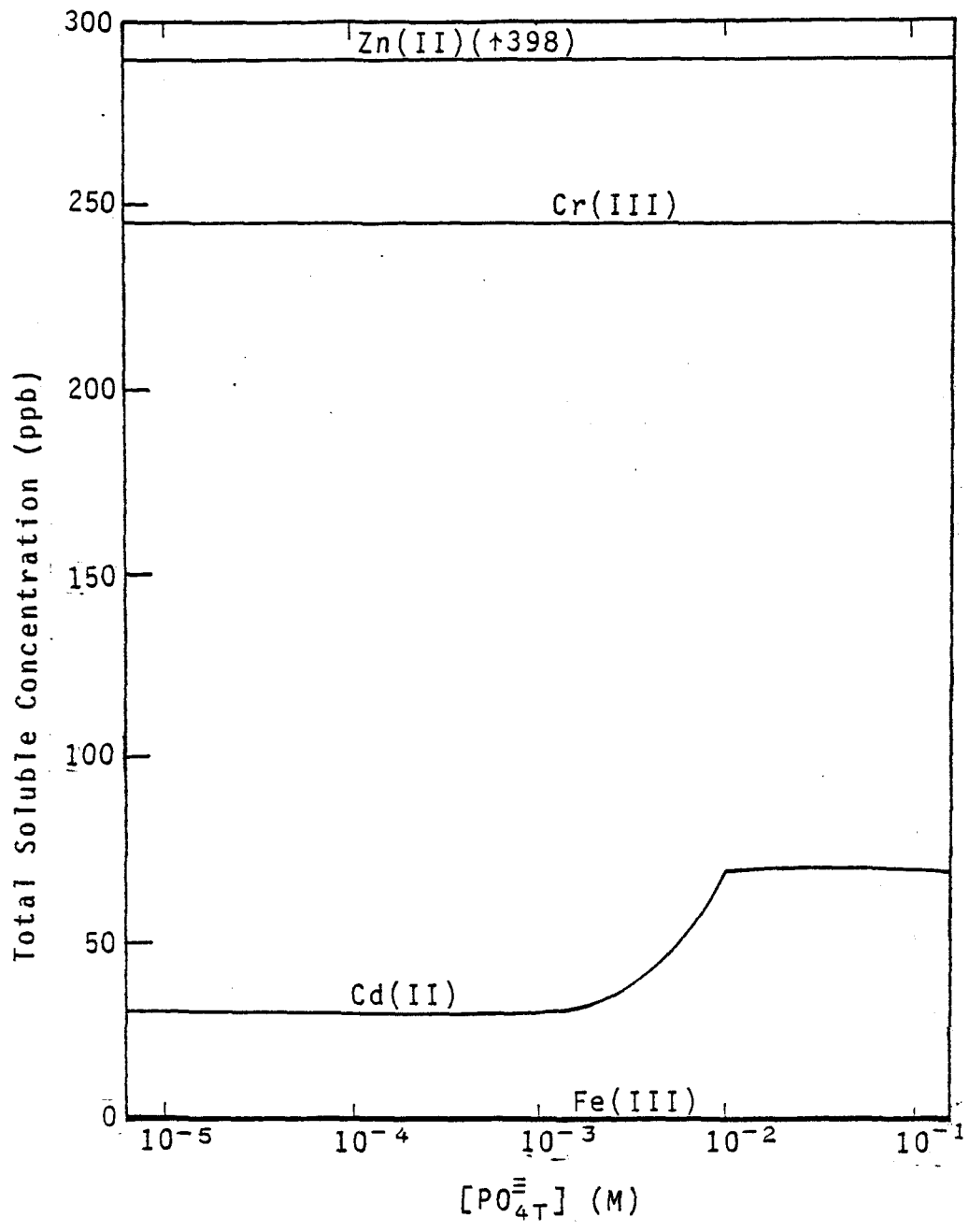
Figure 128. Effects of phosphate concentration on the total soluble concentrations of metals.
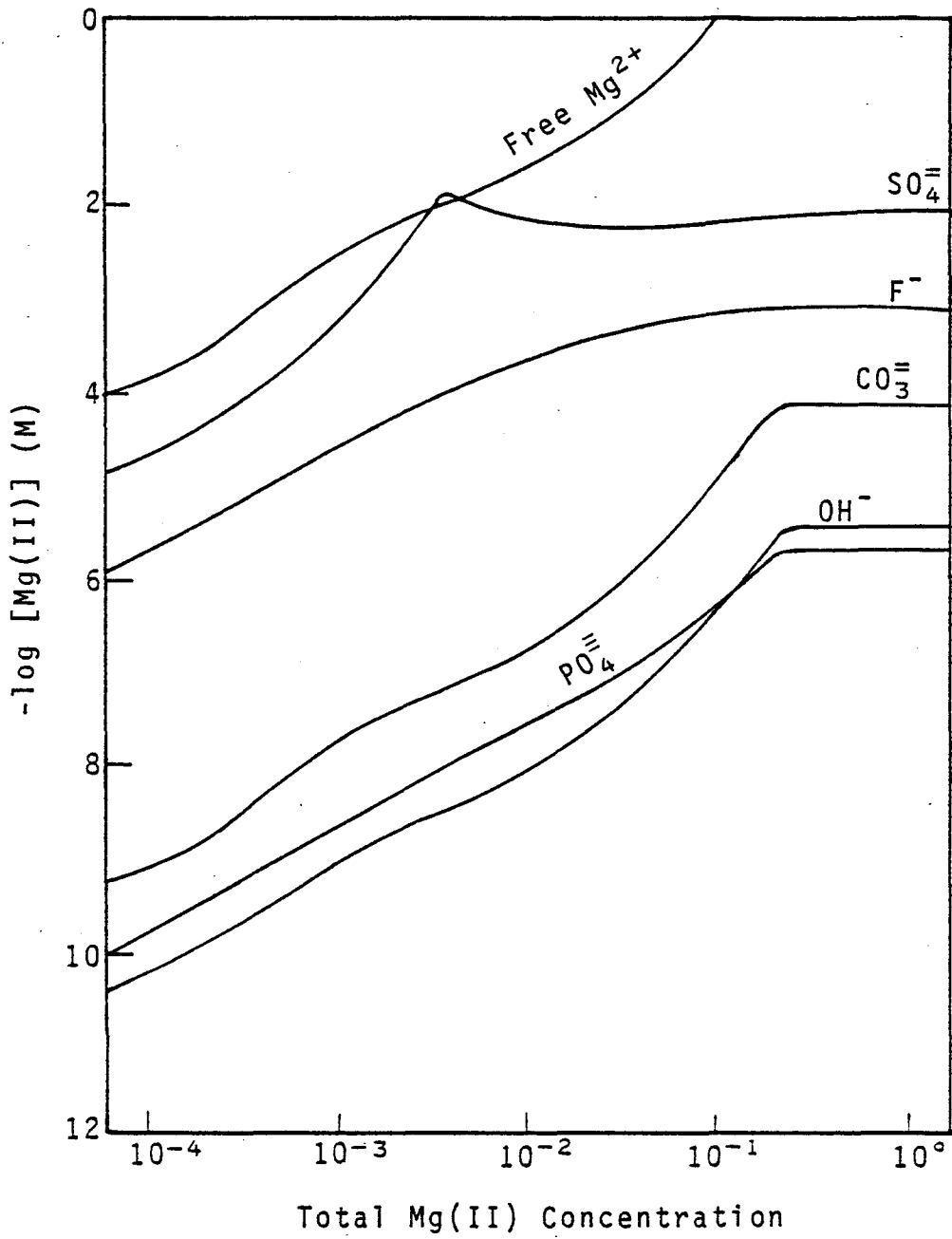
Figure 129. Effects of Mg addition on the distribution of soluble Mg complexes.
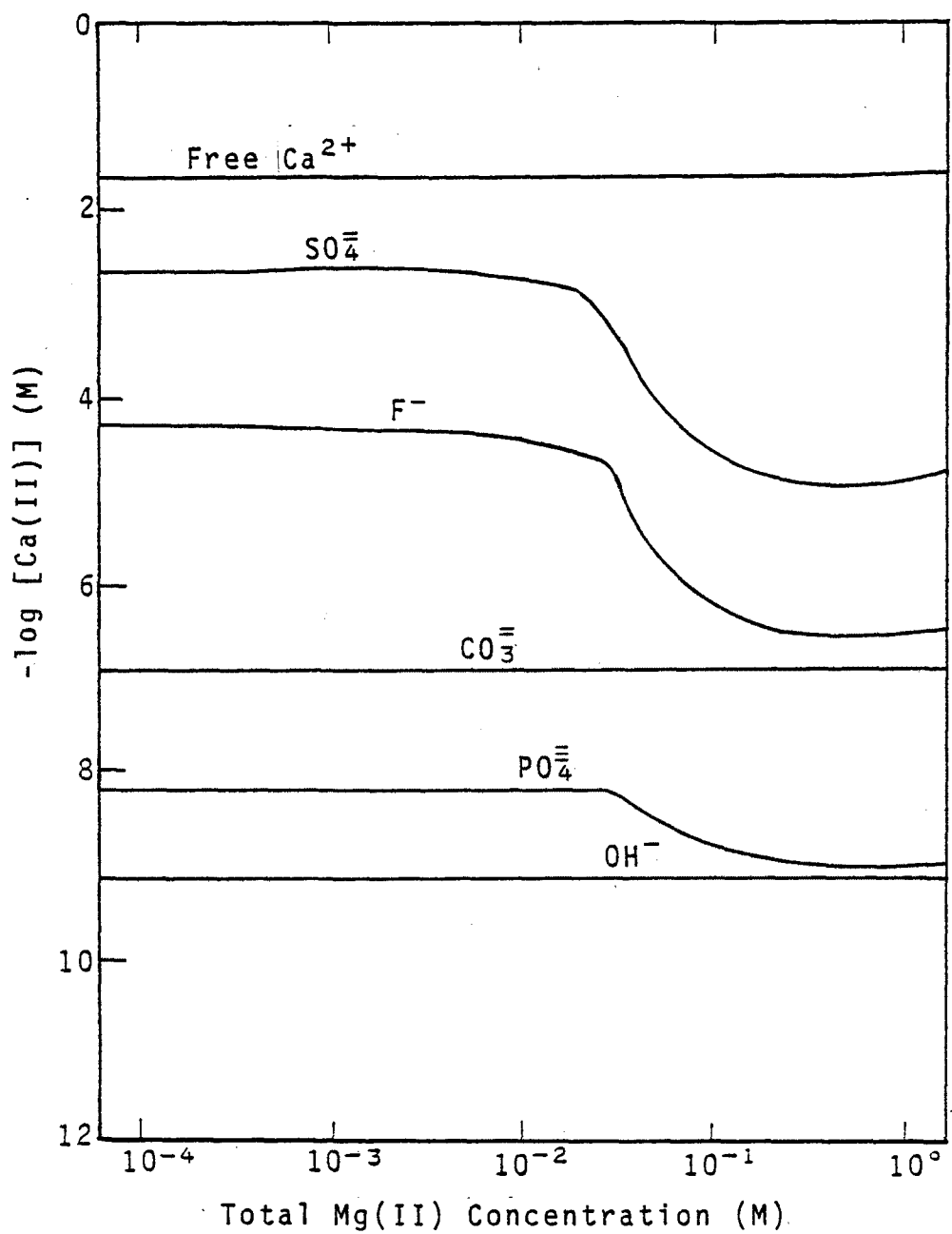
Figure 130. Effects of Mg addition on the speciation of Ca.
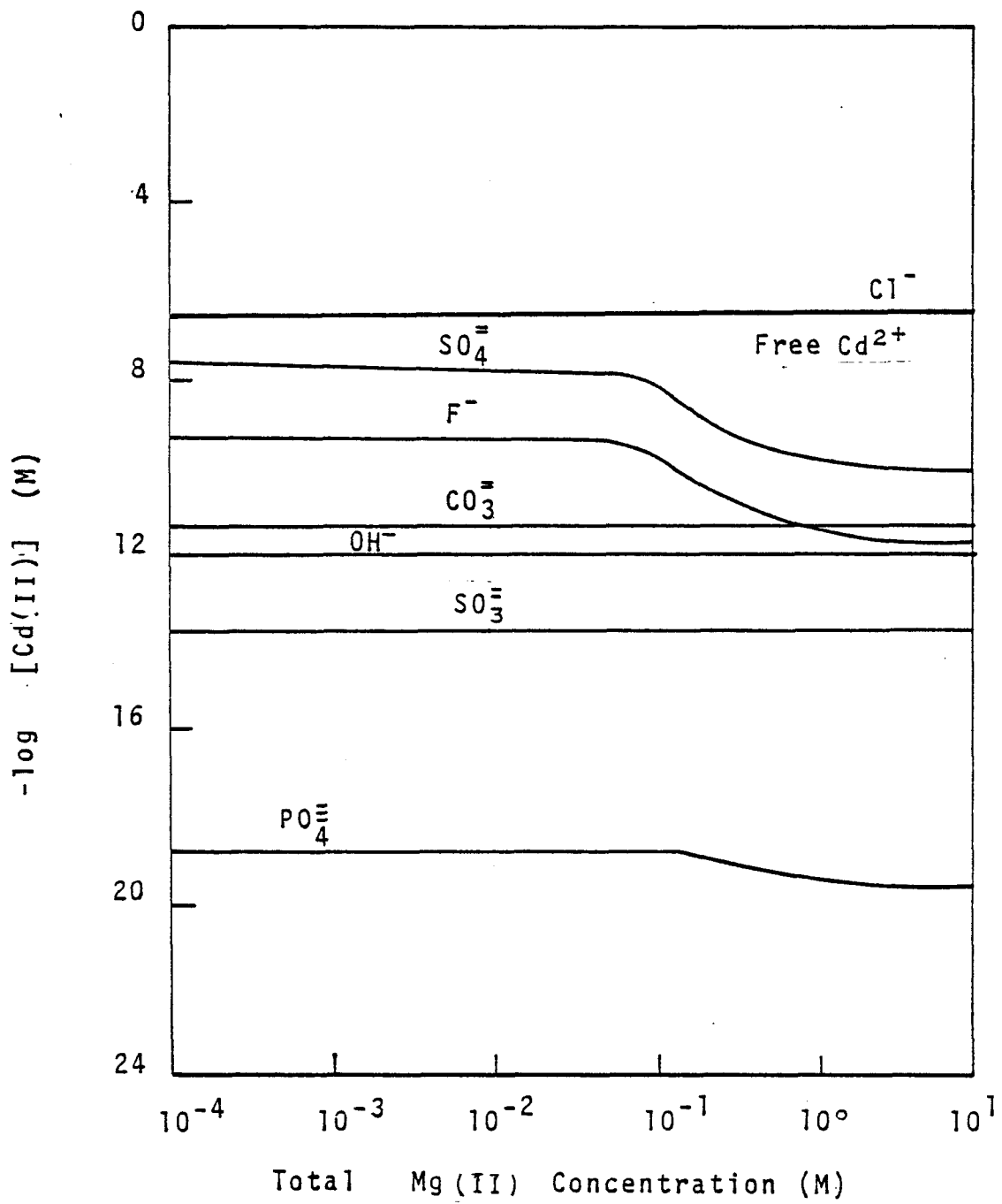
Figure 131. Effects of Mg addition on the speciation of Cd.
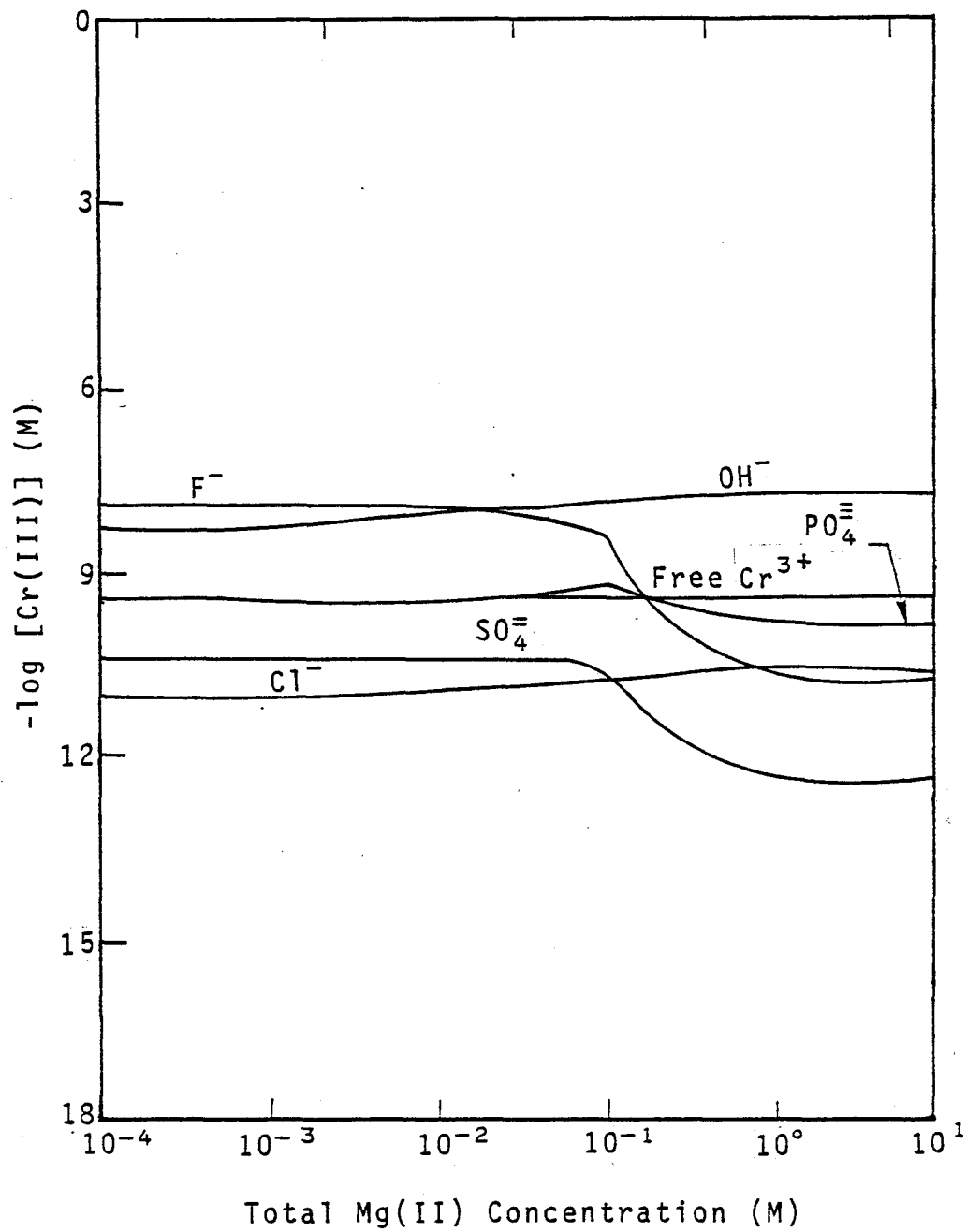
Figure 132.   Effects of Mg addition on the speciation of Cr(III).
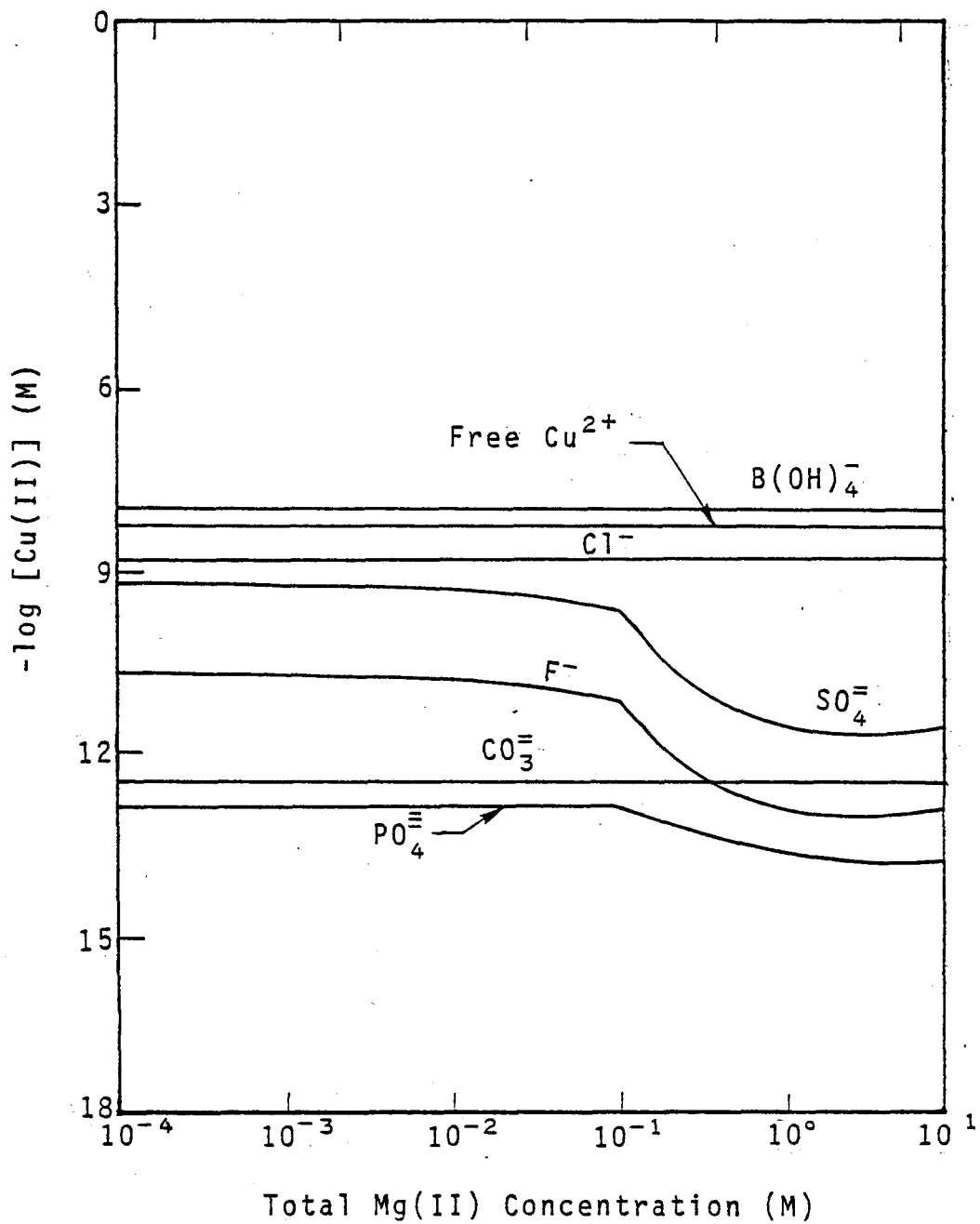
Figure 133. Effects of Mg addition on the speciation of Cu.
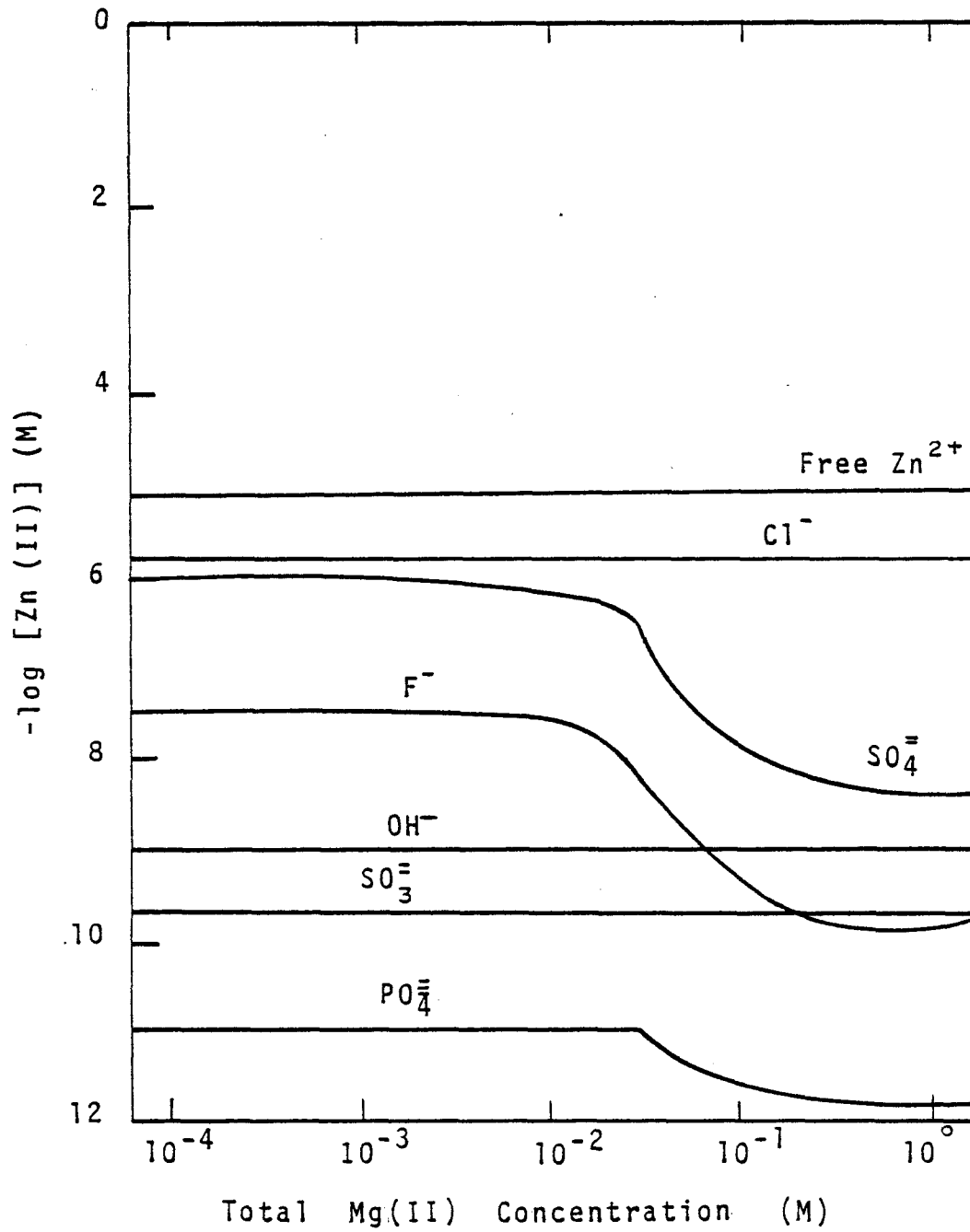
Figure 134. Effects of Mg addition on the speciation of Zn.

only to elements forming the above-mentioned complexes. It is expected that the total soluble levels of most minor elements studied will not be altered by magnesium addition. The principal exception is chromium, which may form strong Cr(III)-F complexes (primarily CrF^{2+}) in the low pH region.

EFFECTS OF SULFITE OXIDATION

As discussed previously, the aging of the FGD wastes usually results in an increase of redox potential and pH. During this aging process, it is expected that the sulfite species will gradually be oxidized to sulfate. Since both sulfite and sulfate species are major components in FGD sludge, the oxidation of sulfite may cause changes in other constituents. In this study, the possible effects of sulfite oxidation on some selected elements were examined. The results are presented in Figures 135 through 156.

In this discussion, total sulfite was assumed to be oxidized from an original concentration of $10^{-0.16}$M to a concentration of $10^{-4.16}$M. The effects on other constituents at the La Cygne Plant were used for the calculation. Only the results of two typical pH values (pH = 6.5 and 9.0) are discussed here.

Figure 135 and 136 show the effects of sulfite oxidation on various sulfite species. Due to the decrease of total sulfite concentrations in the system, various sulfite complexes are also decreased. As can be seen from Figure 135, the decrease of HSO_3^- or free SO_3^{2-} species approximately follow the rate of sulfite oxidation. However, the concentration trends of metallic sulfite complexes are different from that of total sulfite concentration. For example, total sulfite oxidation to 10^{-4} of its original level will result in a factor of 10^{-7} decrease in the Cd-SO_3 complex concentration. Figure 136 indicates that sulfite oxidation will cause a tremendous decrease in the level of $CaSO_3 \cdot 1/2H_2O(s)$ solid in the FGD sludge. For La Cygne Plant FGD wastes, if the total sulfite level is oxidized to one-tenth of its original level (perhaps by aeration), the $CaSO_3 \cdot 1/2H_2O(s)$ solid will disappear as shown in Figure 136.

Sulfite oxidation has only a minor effect on the speciation of soluble calcium (see Figure 137). It may cause a tremendous change, however, in the level of calcium solids in the FGD sludge (see Figure 138). The calculations show that the $CaSO_3 \cdot 1/2H_2O(s)$ solid will be transformed to $CaSO_4 \cdot 2H_2O(s)$ during sulfite oxidation when the pH equals 6.5 and to $CaCO_3(s)$ when the pH equals 9.0.

The magnesium species will not be affected significantly during sulfite oxidation (Figures 139 and 140). For potassium and sodium (Figures 141-144) sulfite oxidation causes an increase
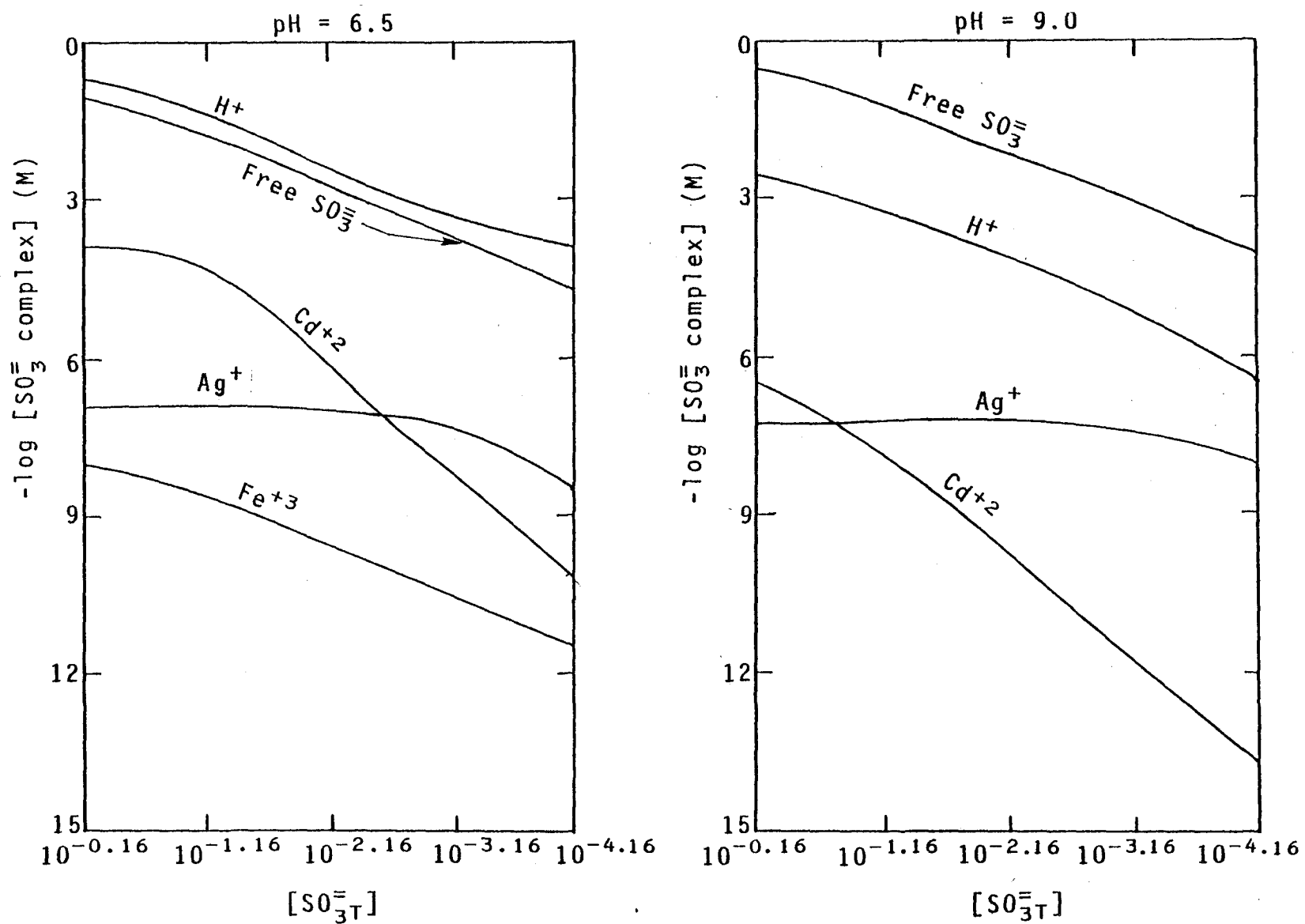
Figure 135.   Effects of sulfite oxidation on the concentrations of sulfite complexes.
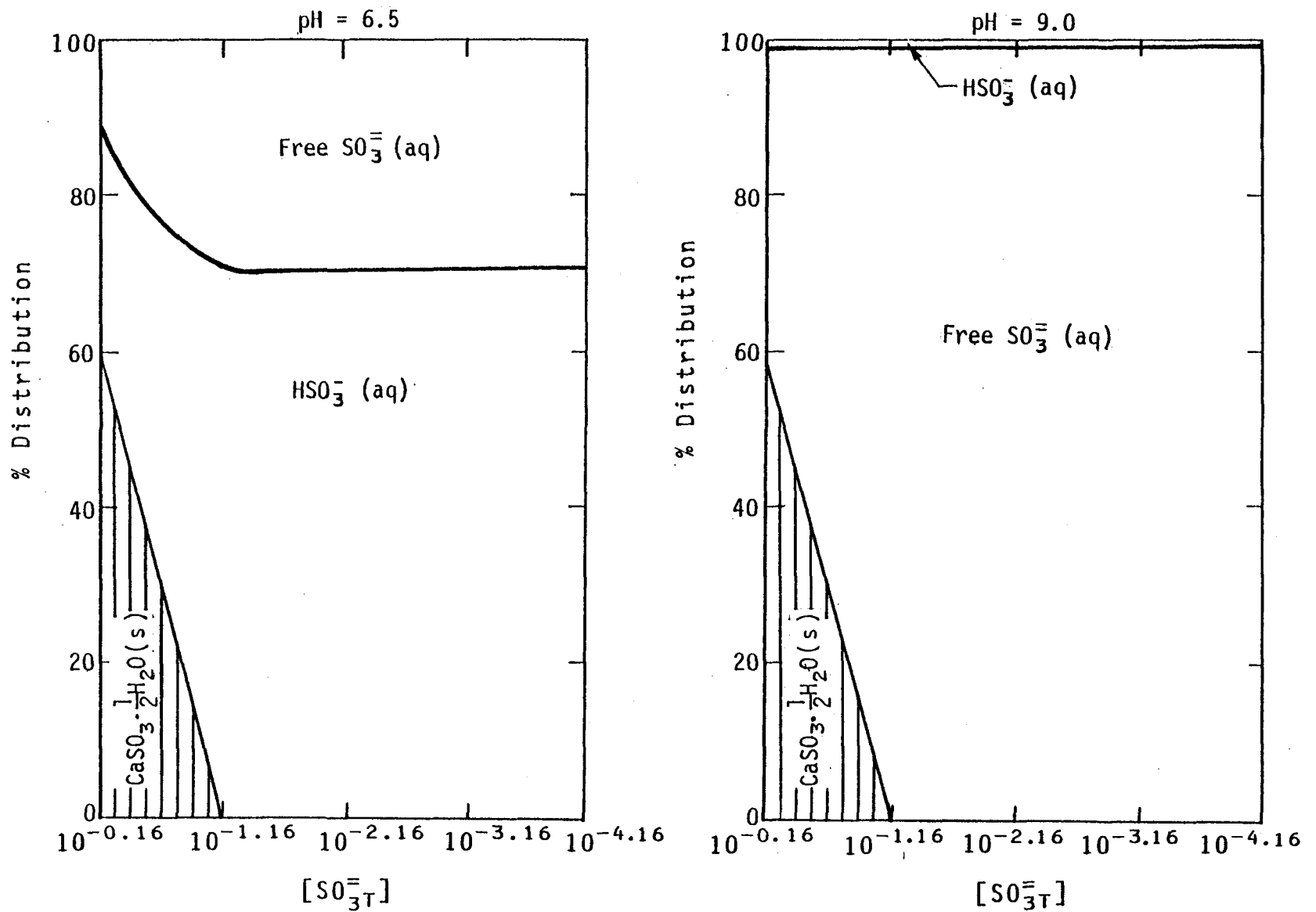
Figure 136.   Effects of sulfite oxidation on the primary distribution of $SO_3^=$ species.
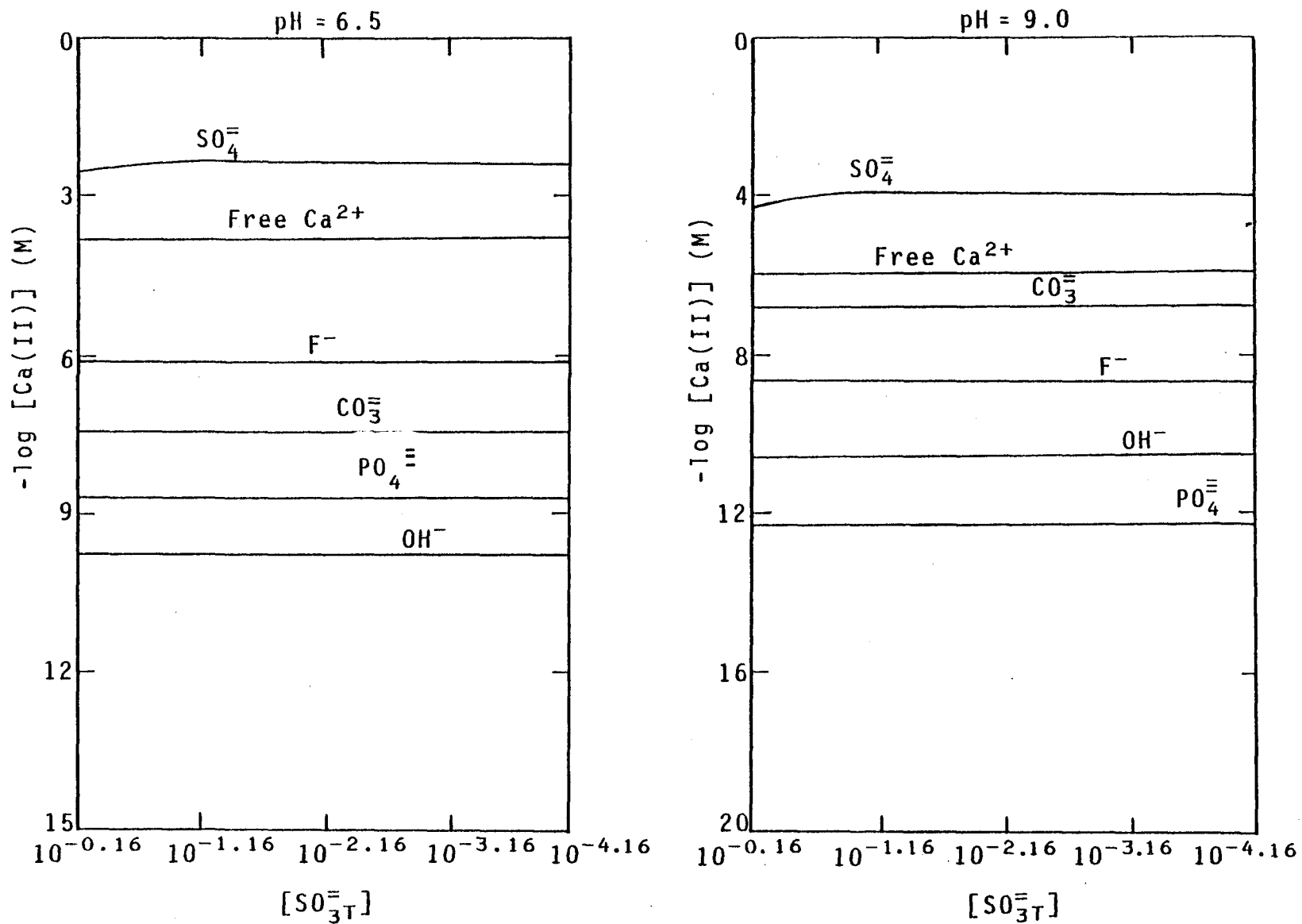
Figure 137. Effects of sulfite oxidation on the speciation of Ca.
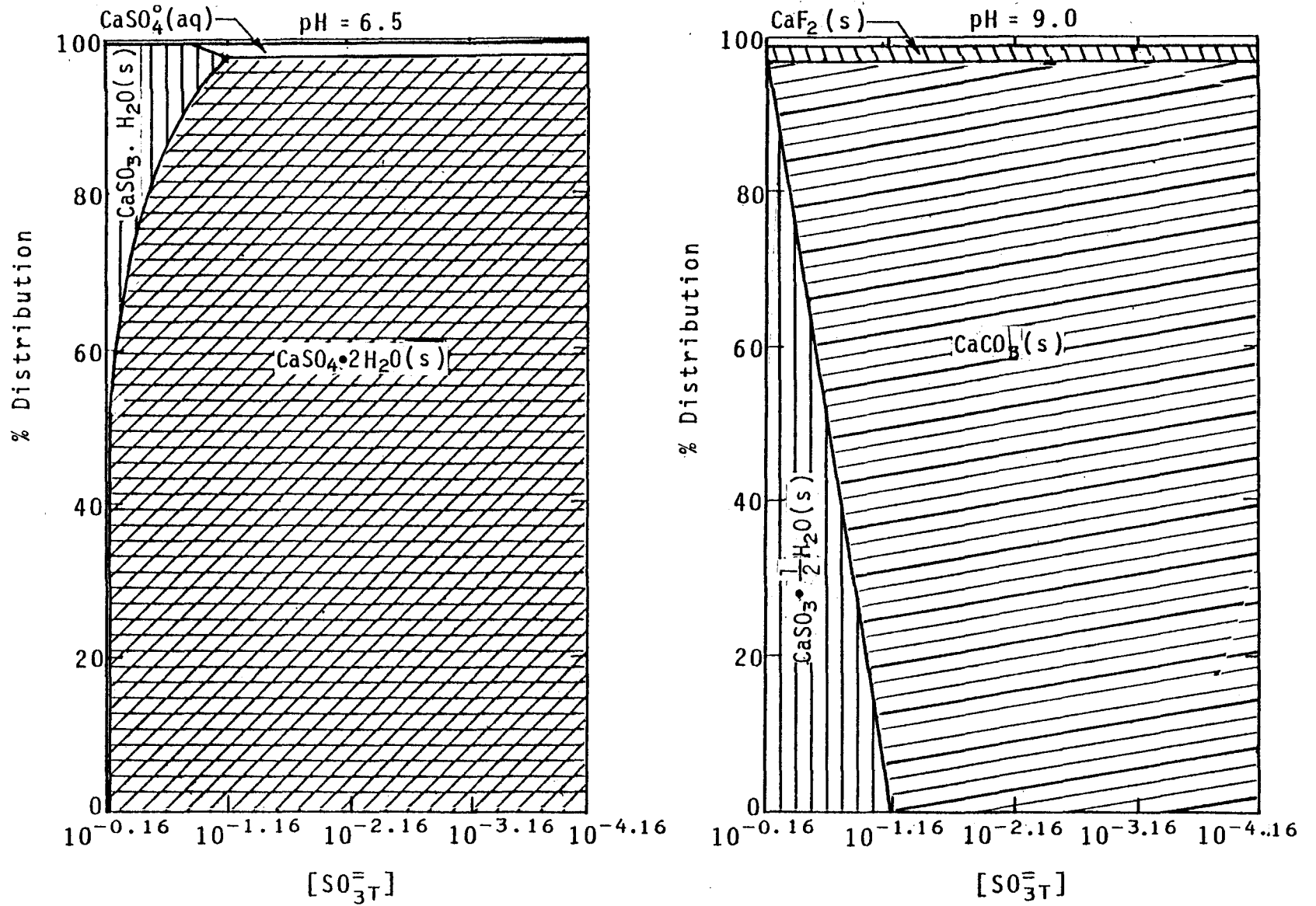
Figure 138. Effects of sulfite oxidation on the primary distribution of Ca species.

239
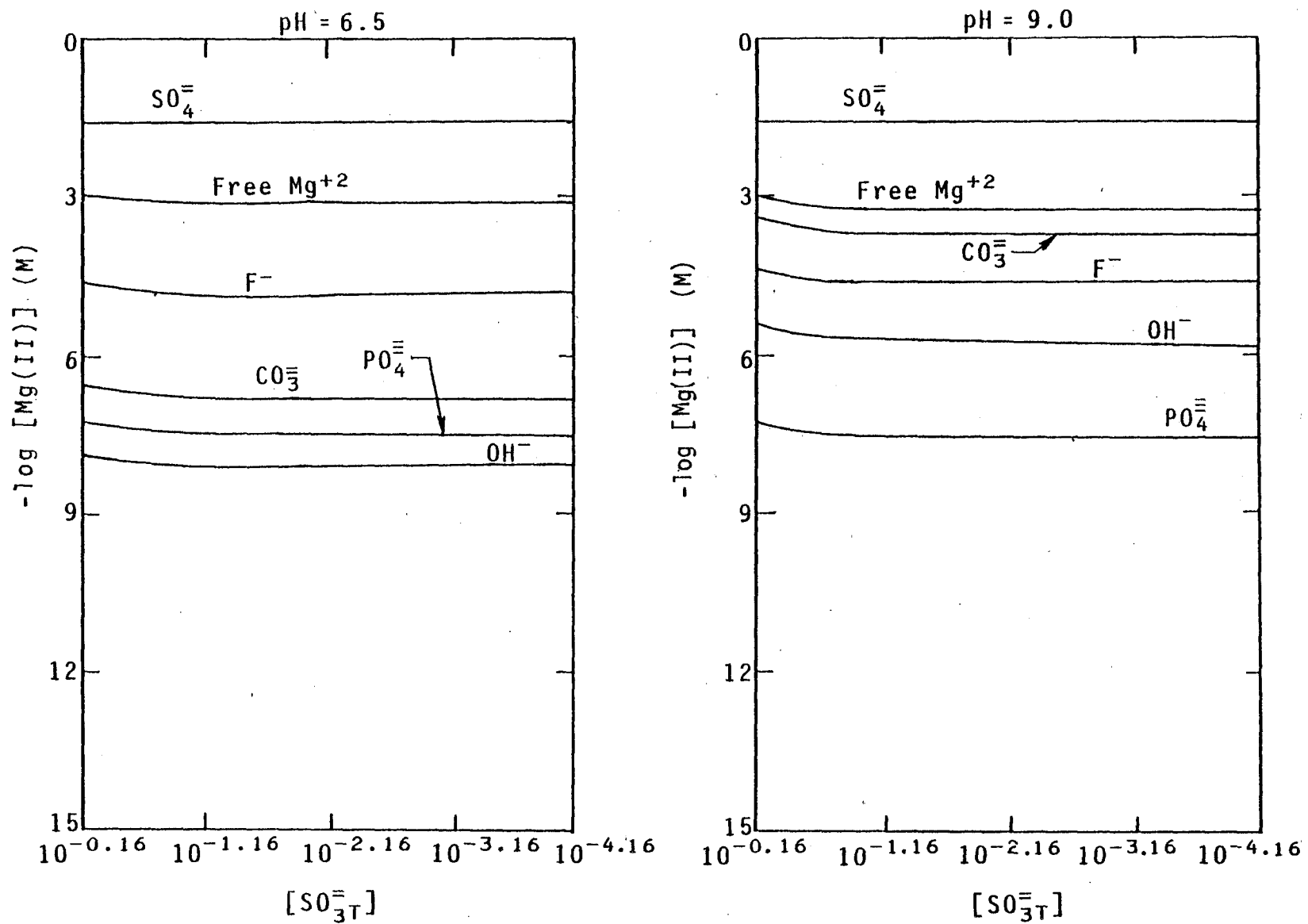
Figure 139. Effects of sulfite oxidation on the speciation of Mg.
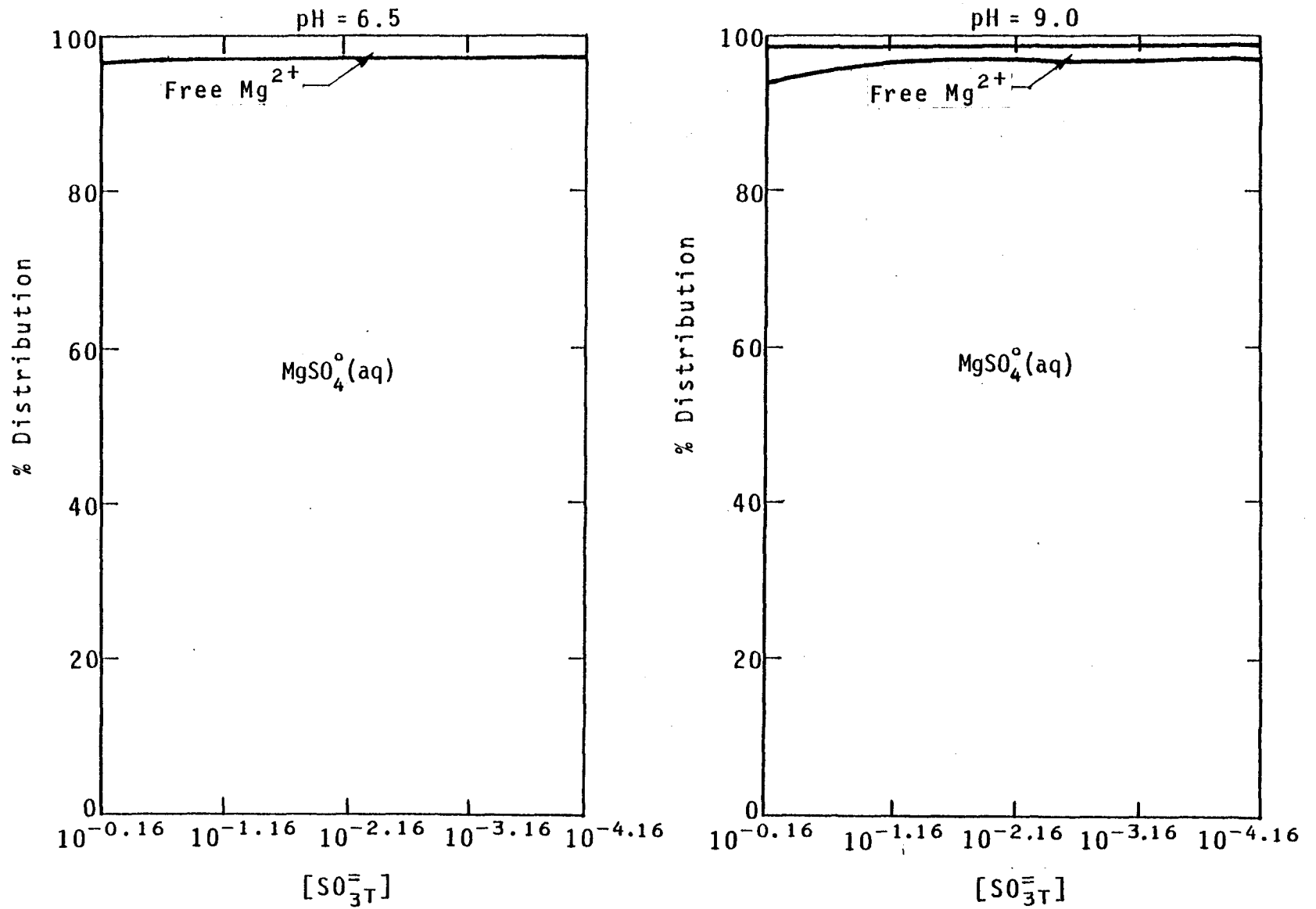
Figure 140. Effects of sulfite oxidation on the primary distribution of Mg species.
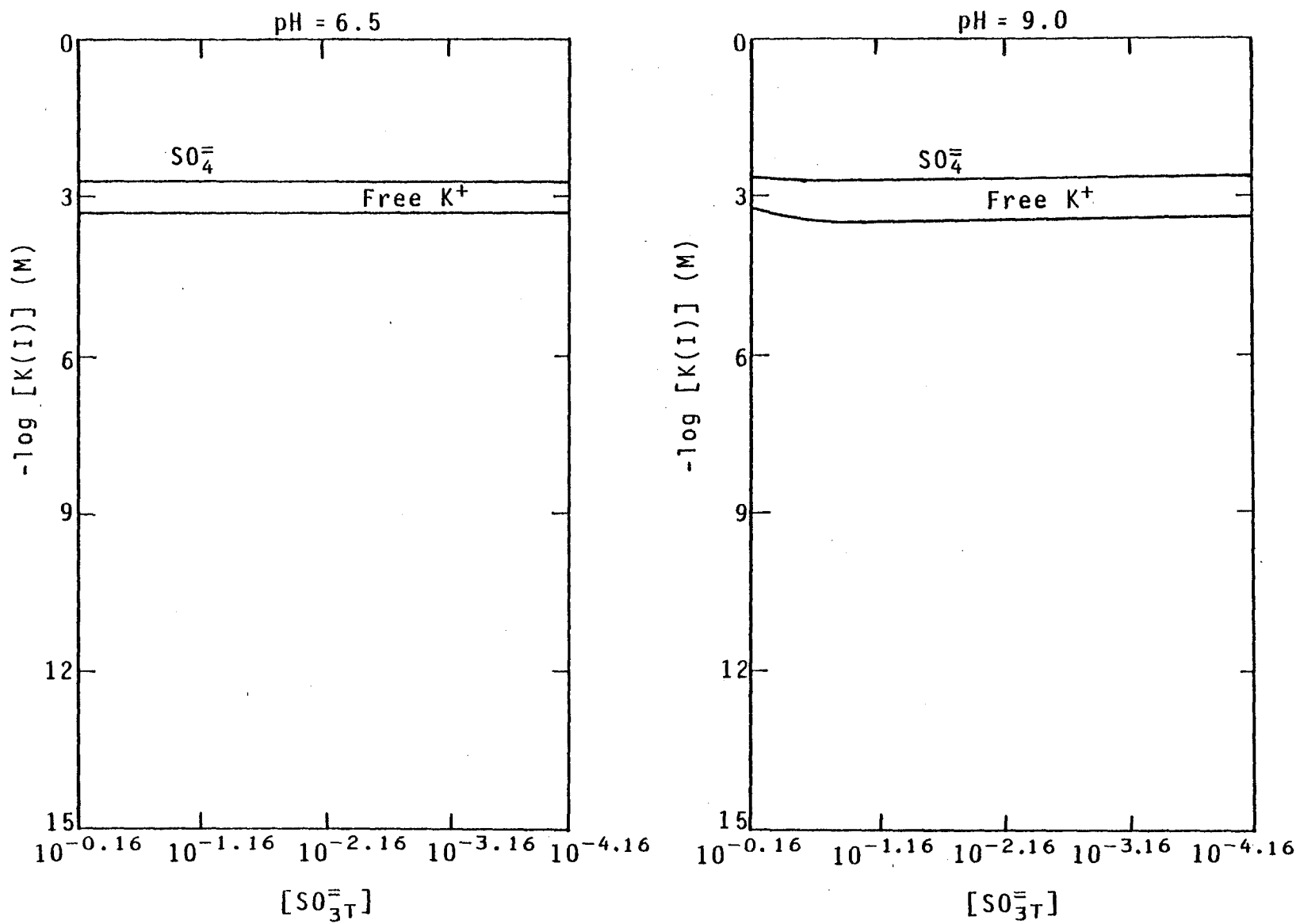
Figure 141. Effects of sulfite oxidation on the speciation of K.
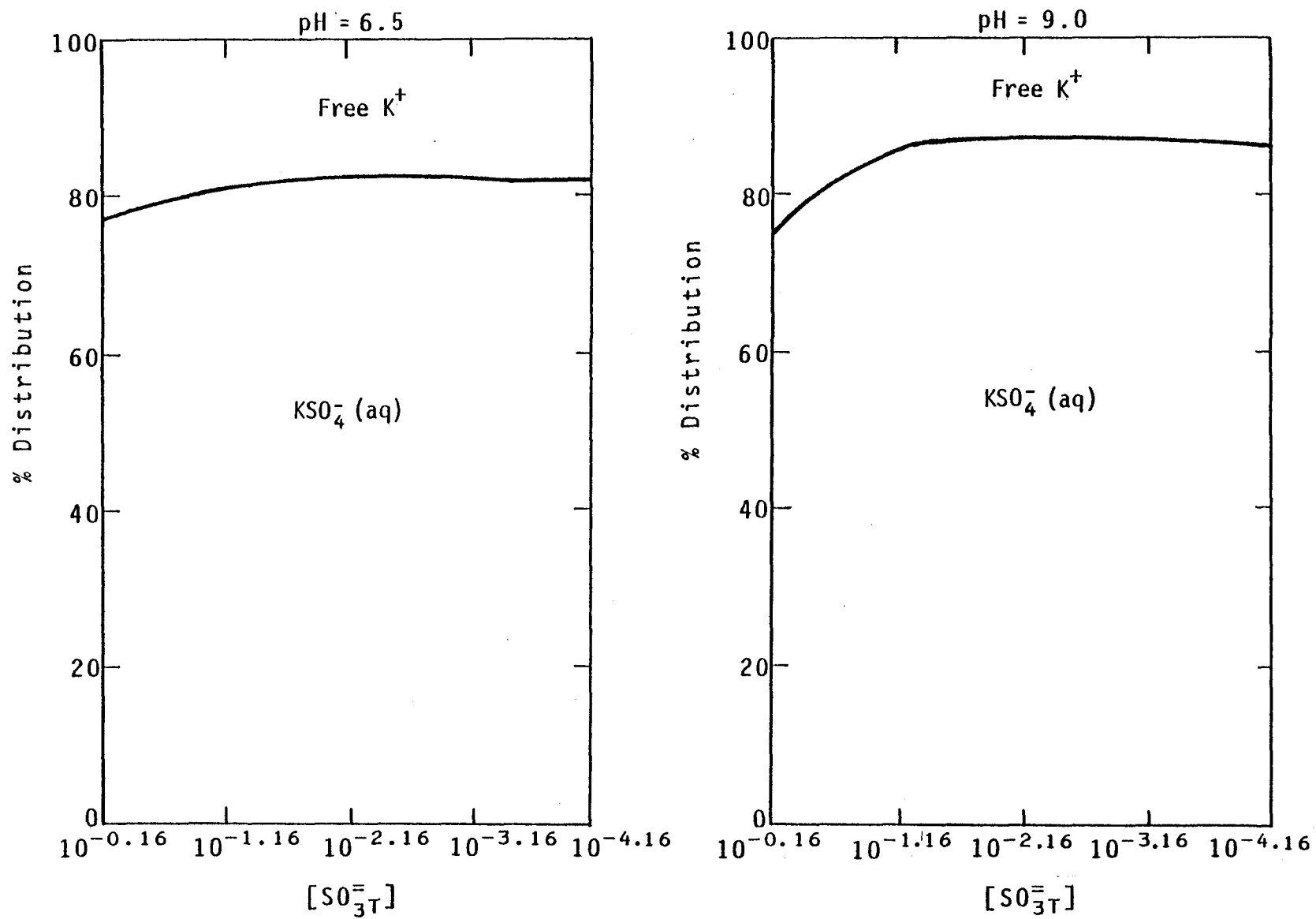
Figure 142. Effects of sulfite oxidation on the primary distribution of K species.

243
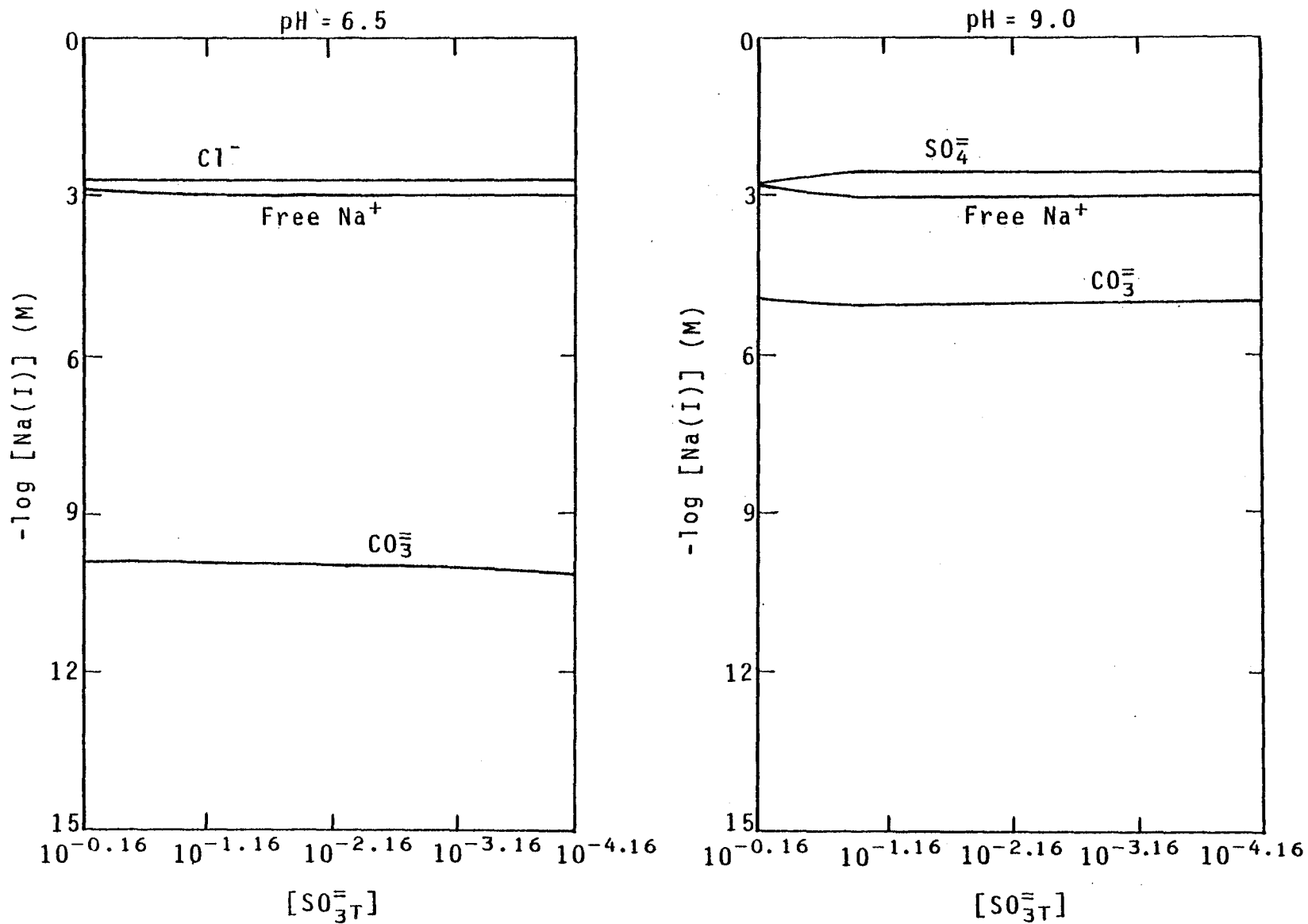
Figure 143. Effects of sulfite oxidation on the speciation of Na.
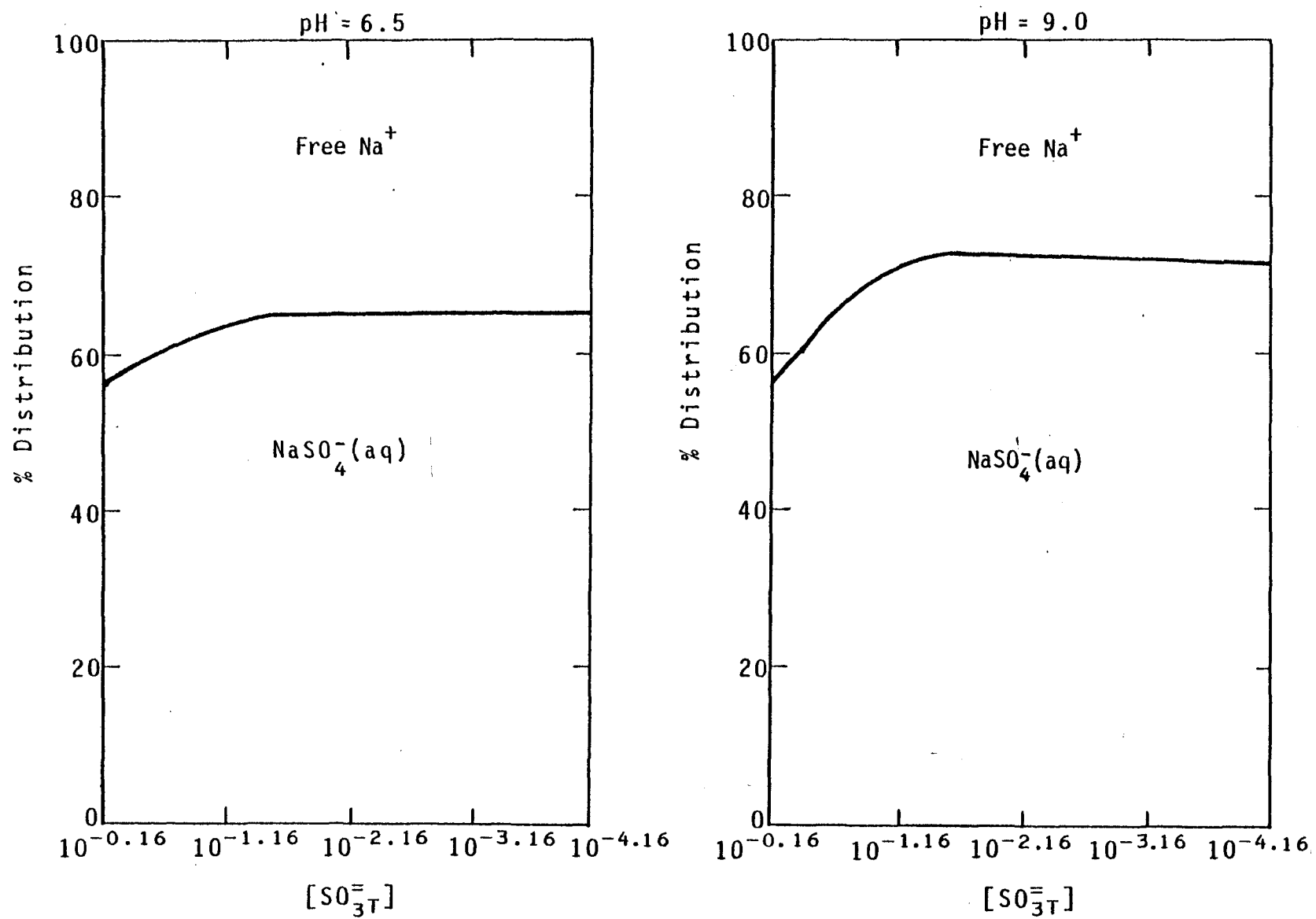
Figure 144. Effects of sulfite oxidation on the primary distribution of Na species.
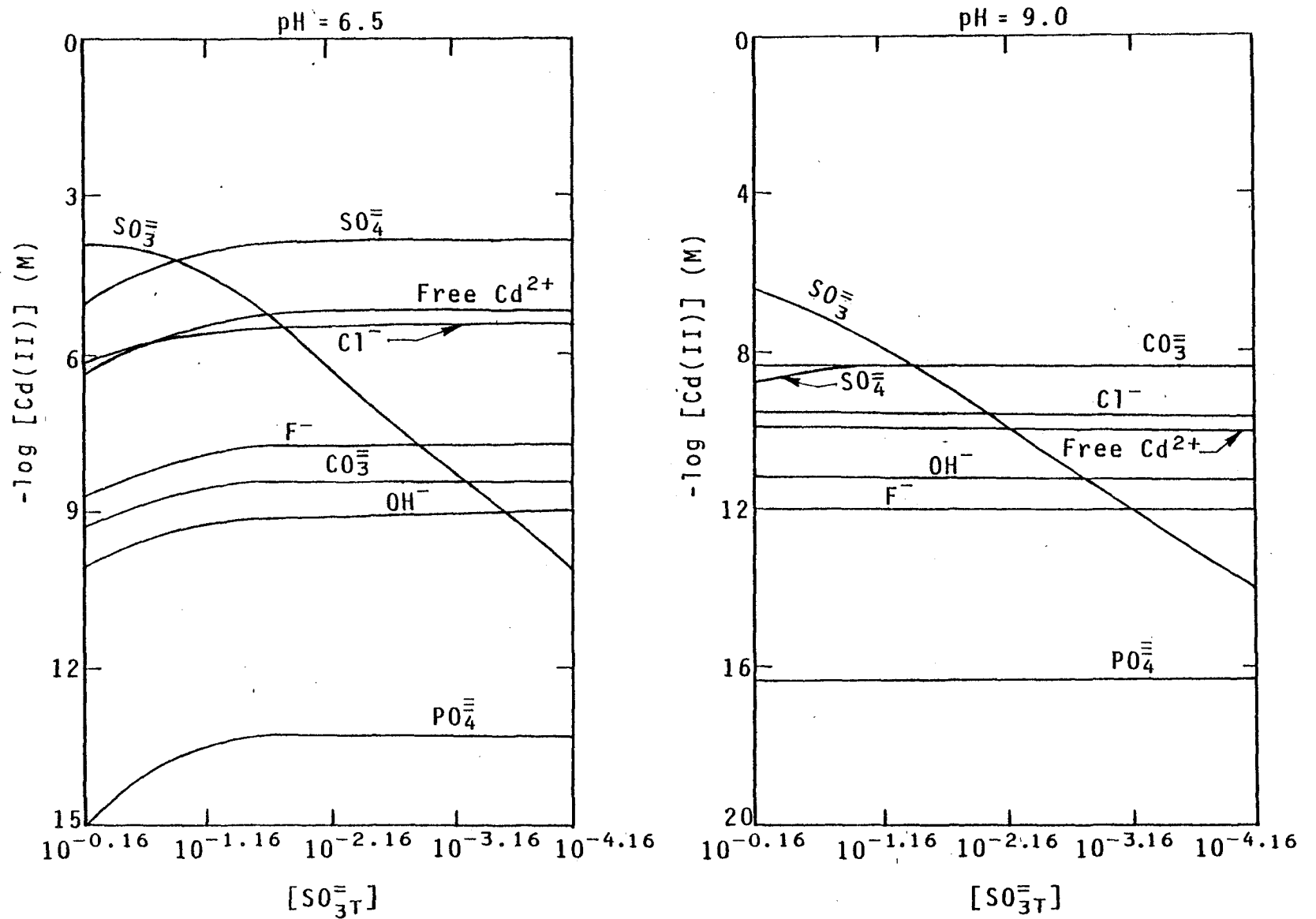
Figure 145. Effects of sulfite oxidation on the speciation of Cd.
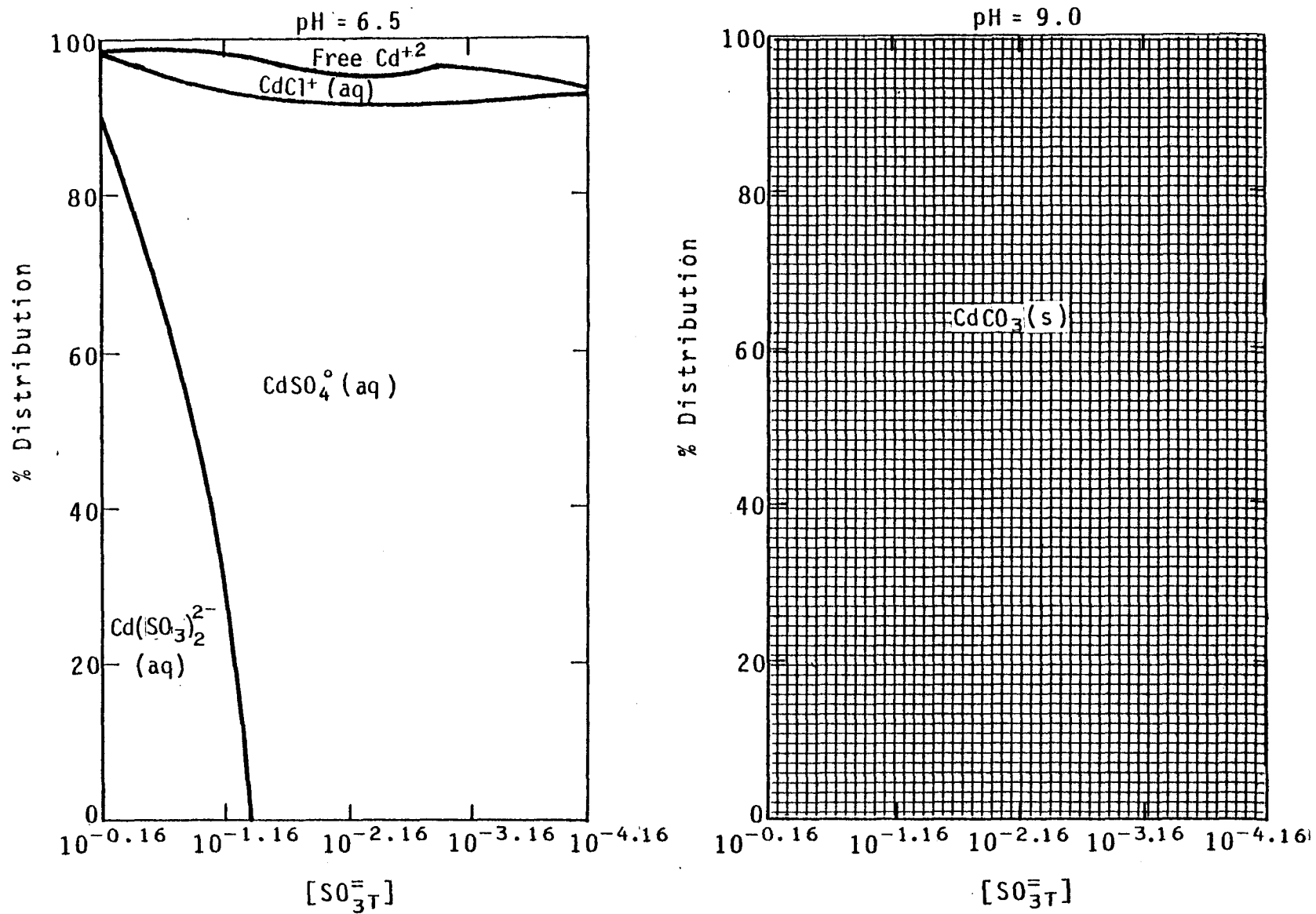
Figure 146. Effects of sulfite oxidation on the primary distribution of Cd species.
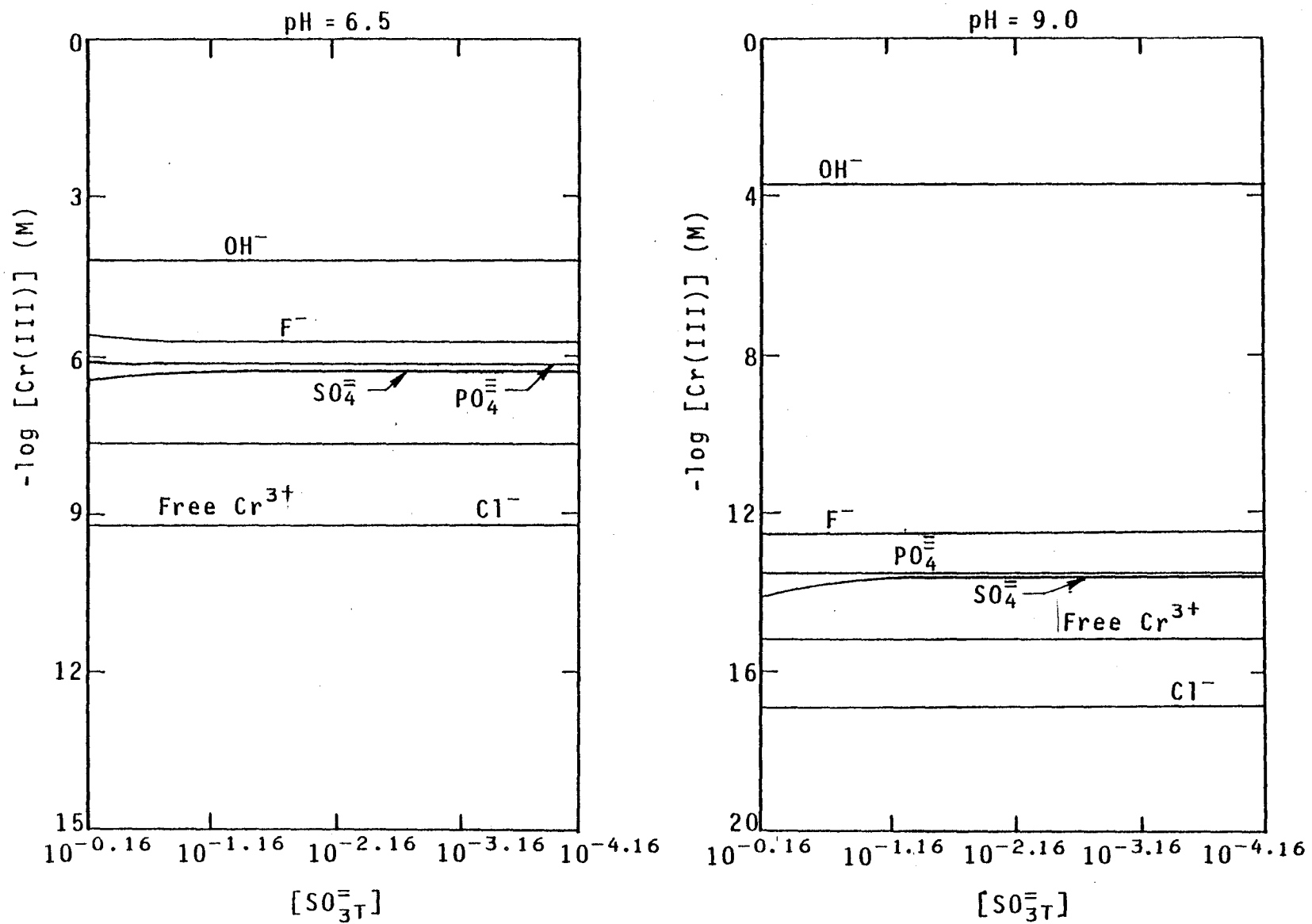
Figure 147. Effects of sulfite oxidation on the speciation of Cr.

248
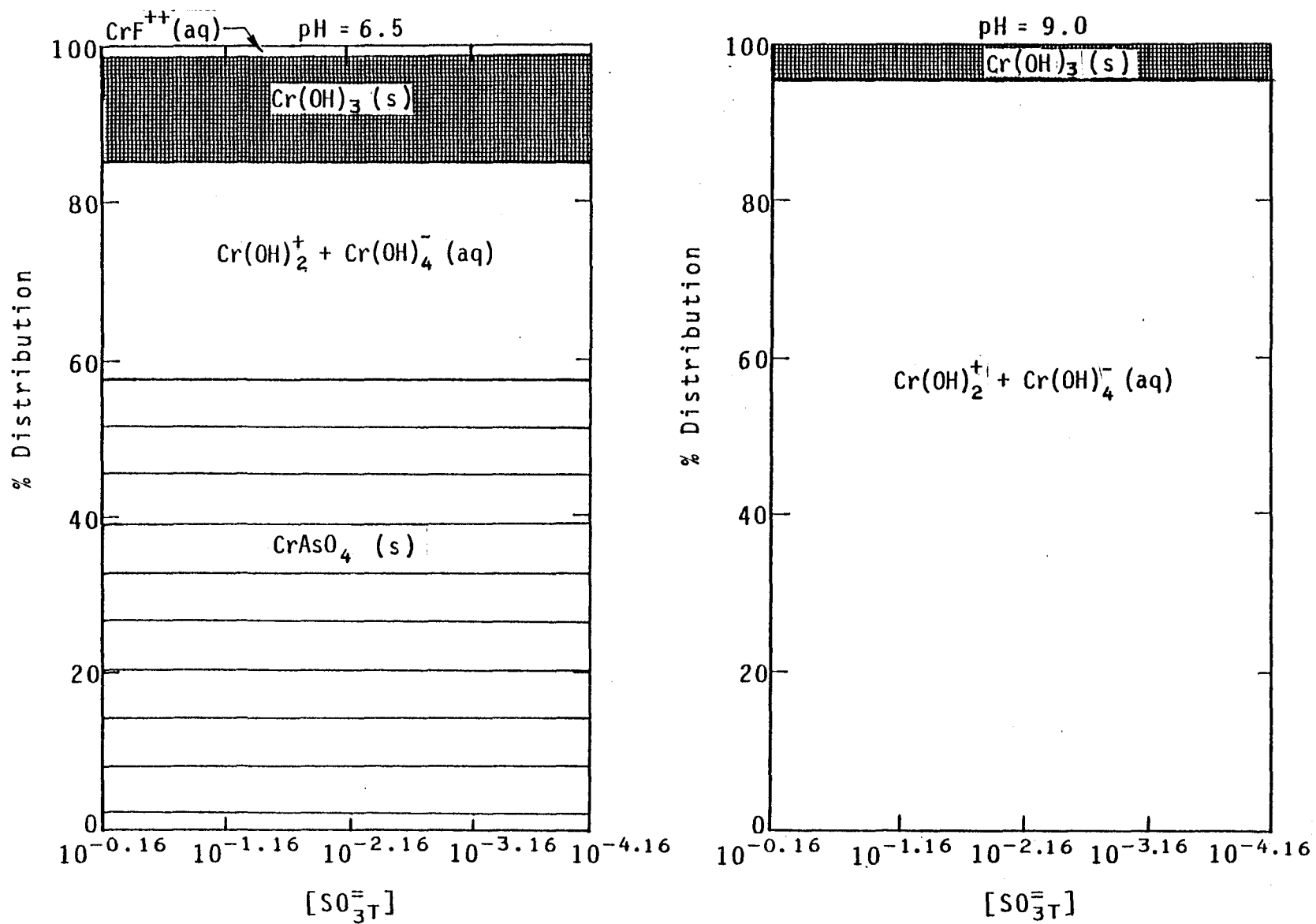
Figure 148.   Effects of sulfite oxidation on the primary distribution of Cr species.

249
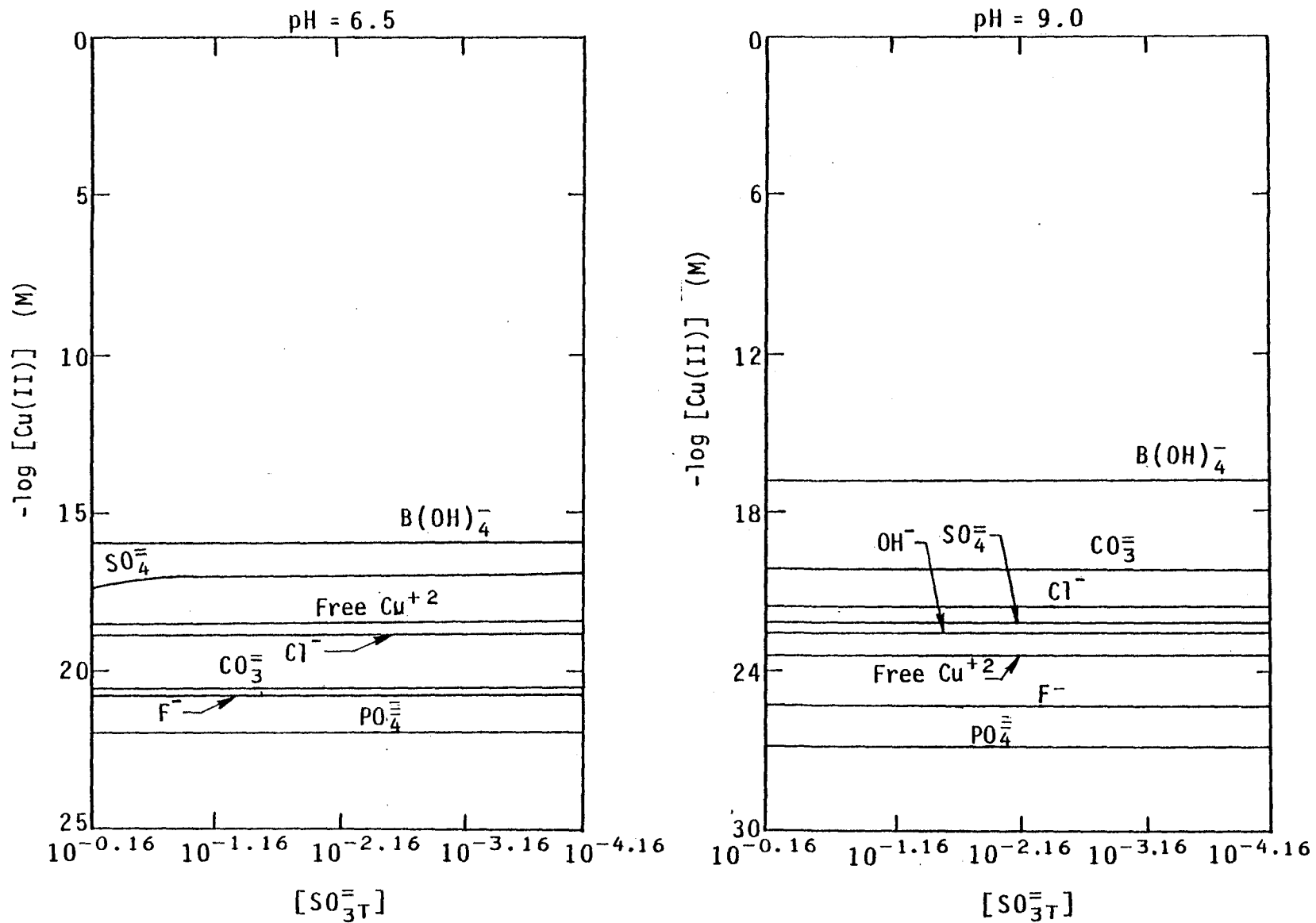
Figure 149. Effects of sulfite oxidation on the speciation of Cu.

250
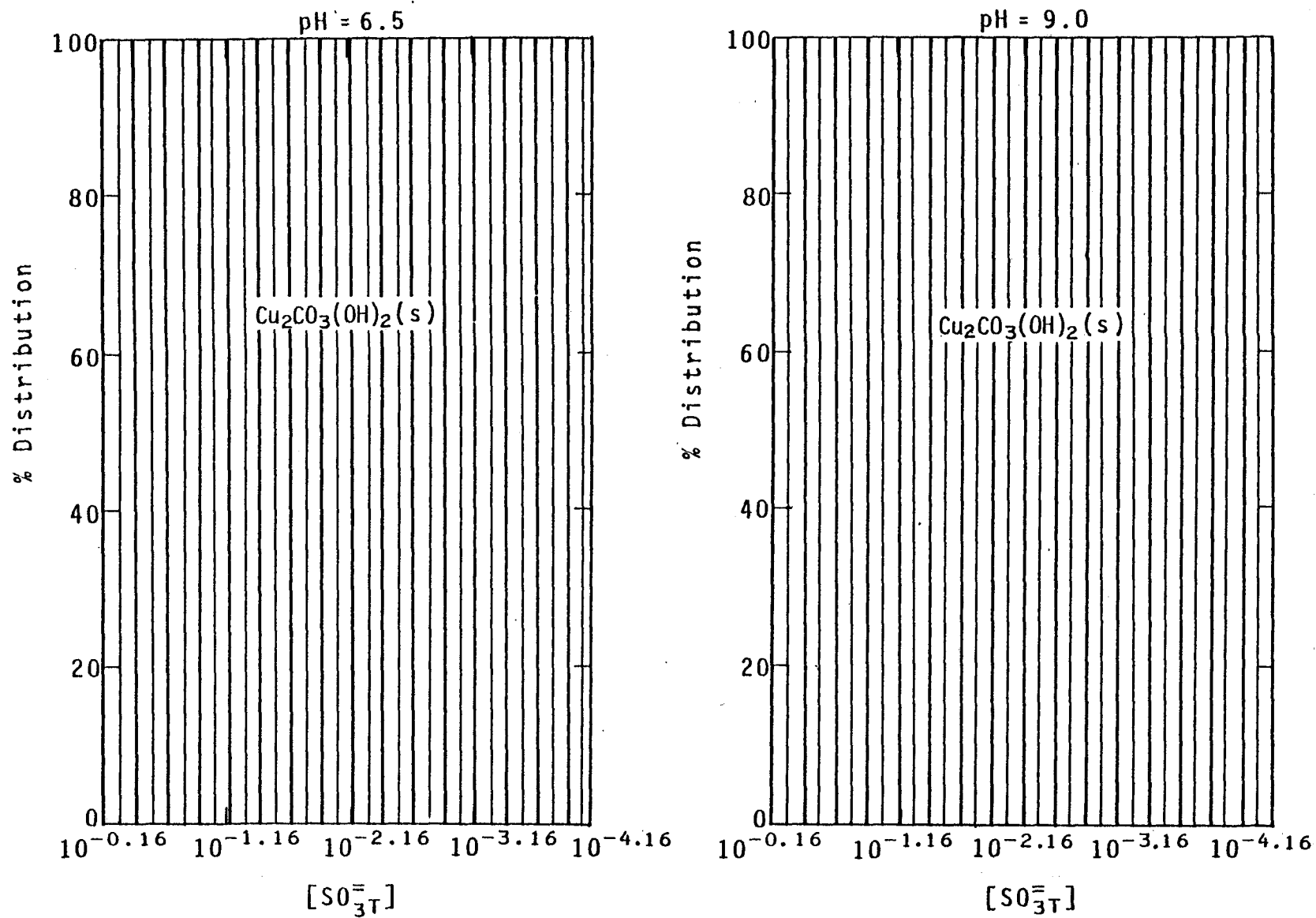
Figure 150. Effects of sulfite oxidation on the primary distribution of Cu species.
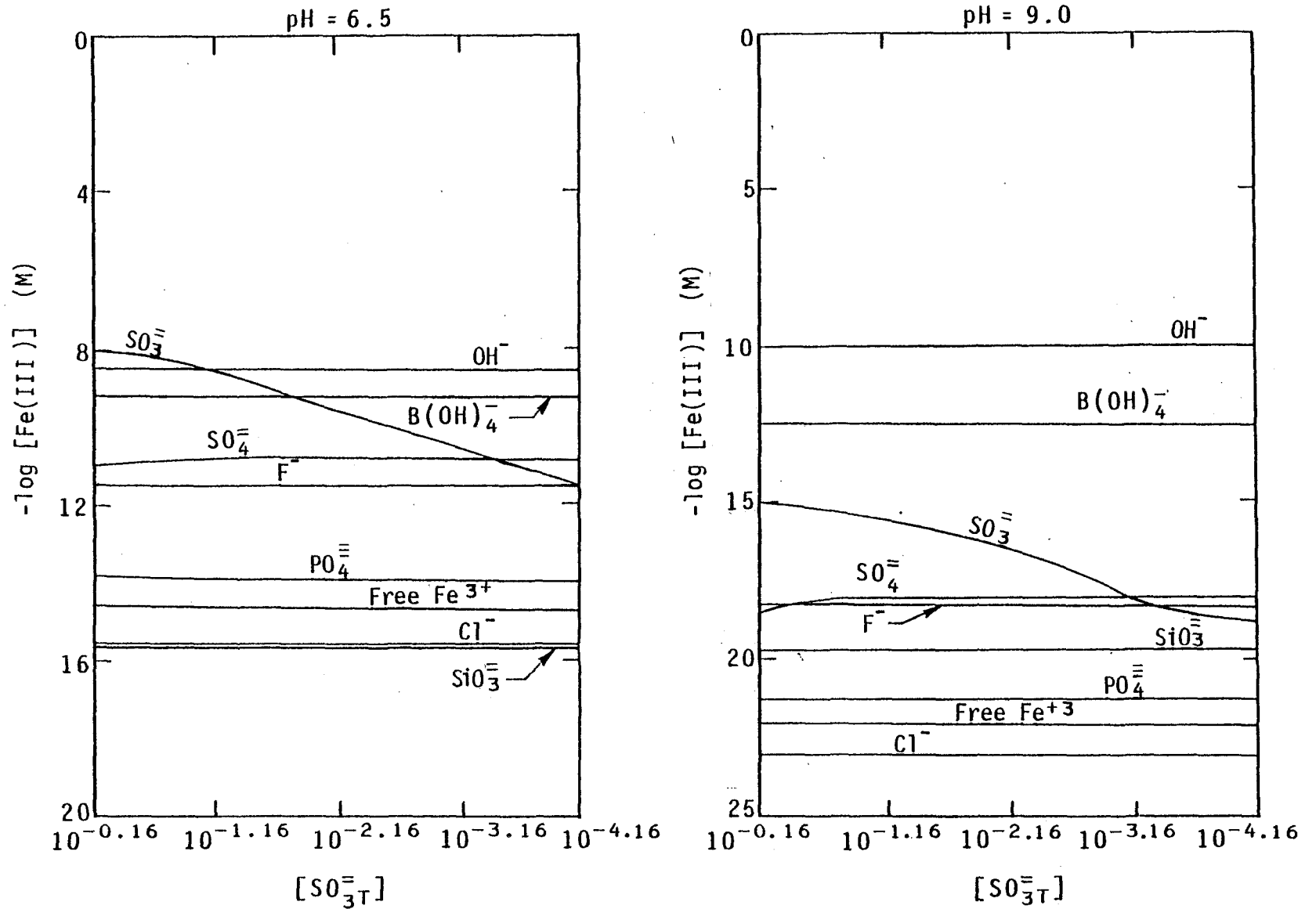
Figure 151. Effects of sulfite oxidation on the speciation of Fe.

252
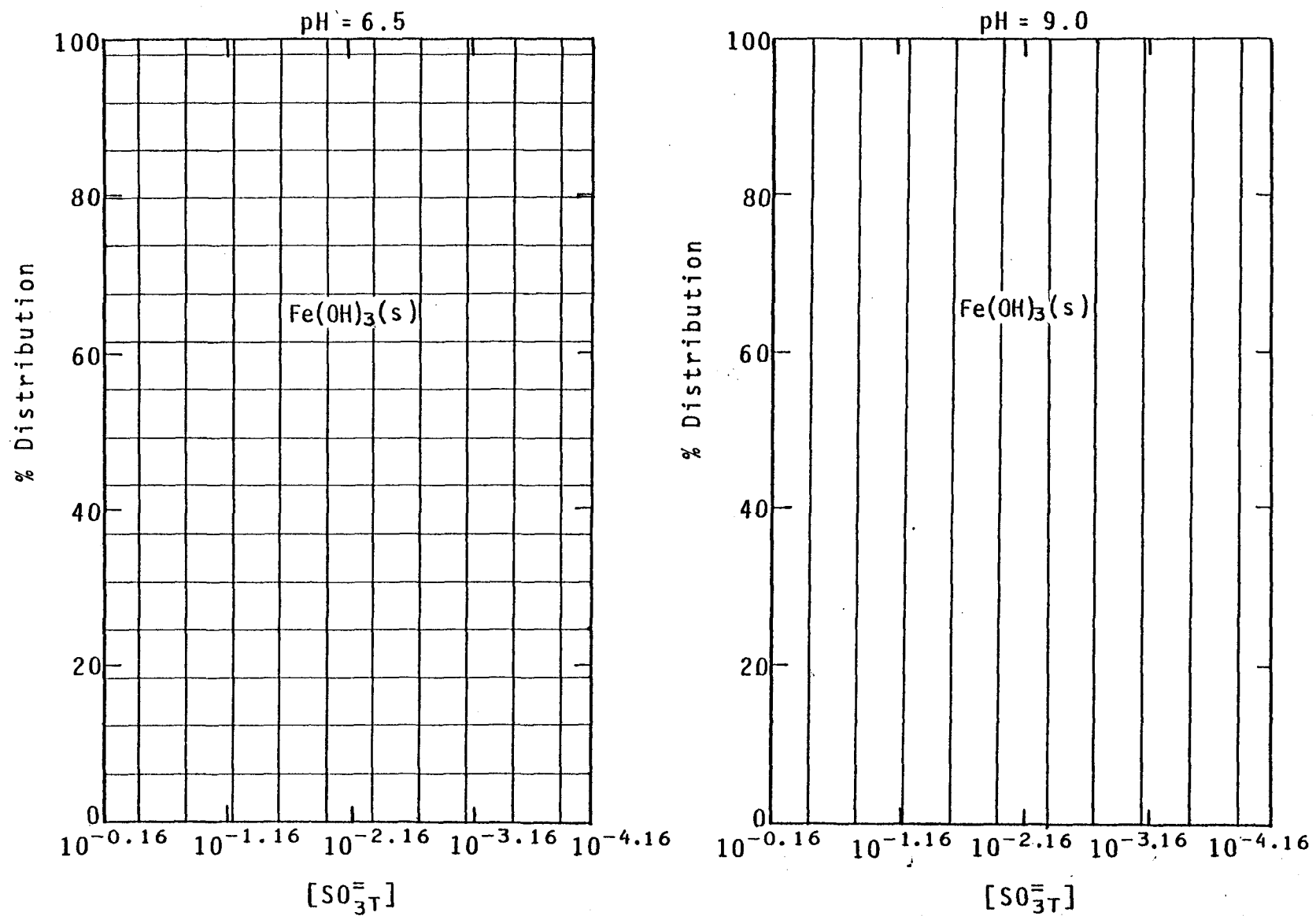
Figure 152. Effects of sulfite oxidation on the primary distribution of Fe species.
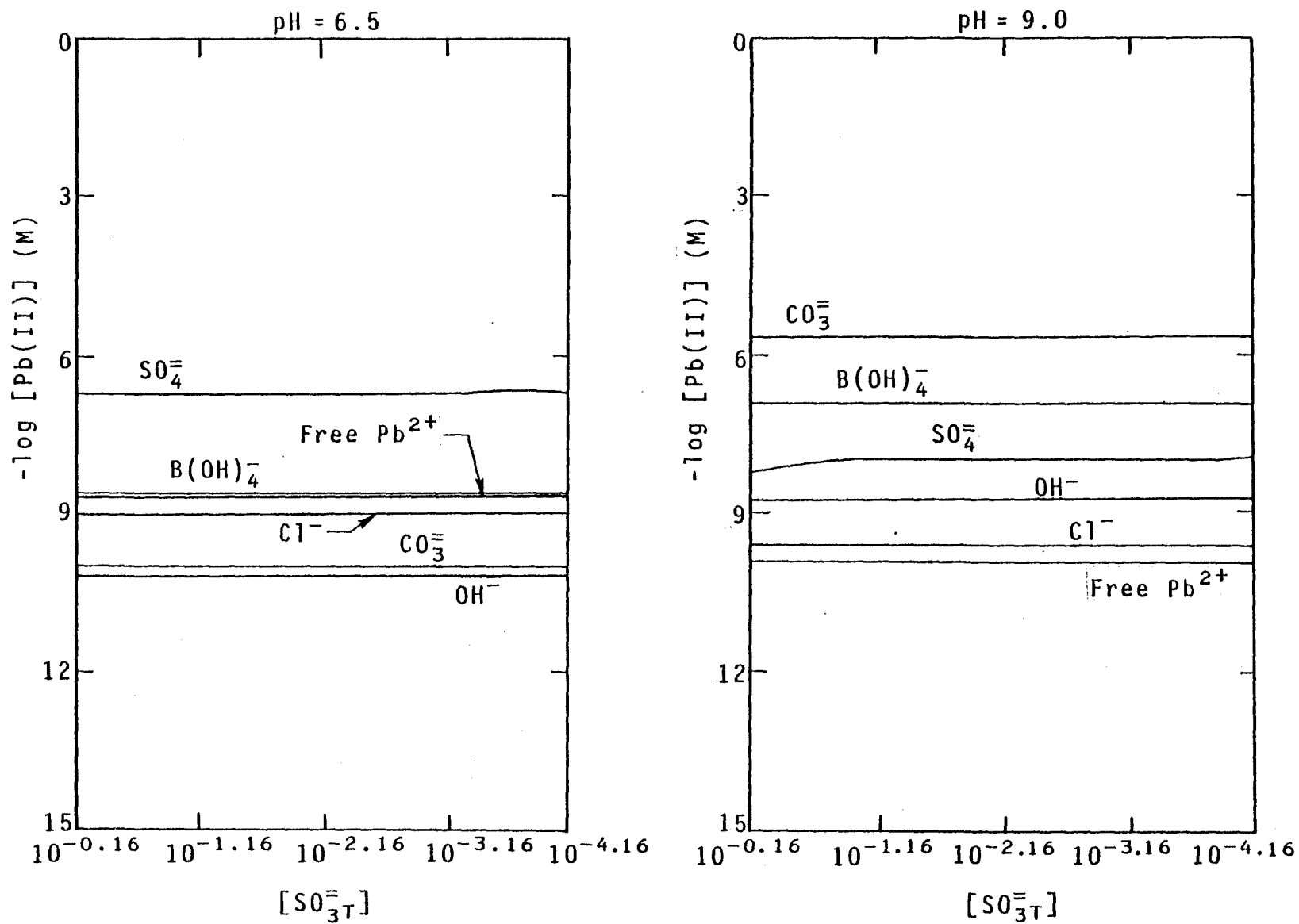
Figure 153. Effects of sulfite oxidation on the speciation of Pb.

254
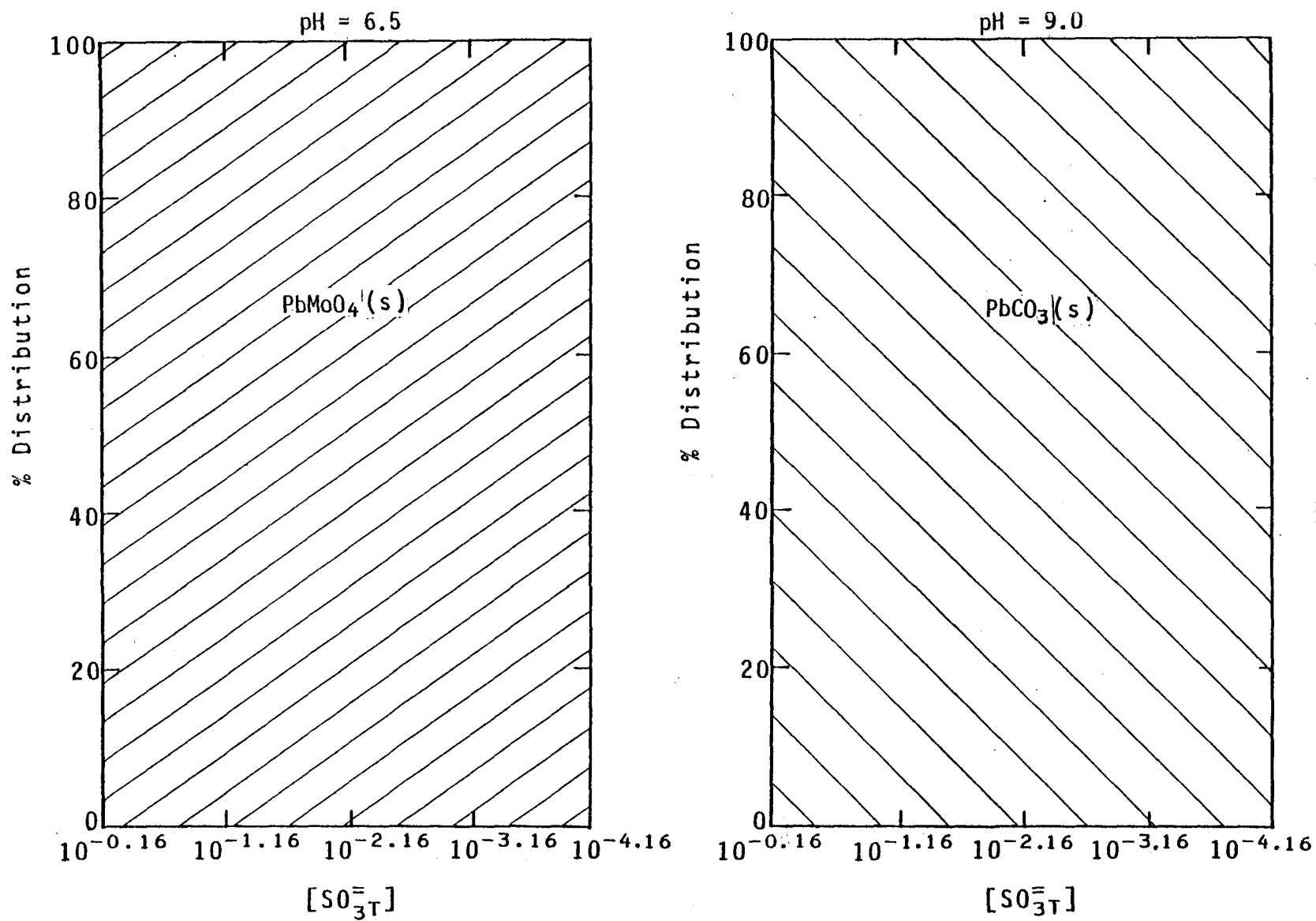
Figure 154.   Effects of sulfite oxidation on the primary distribution of Pb species.
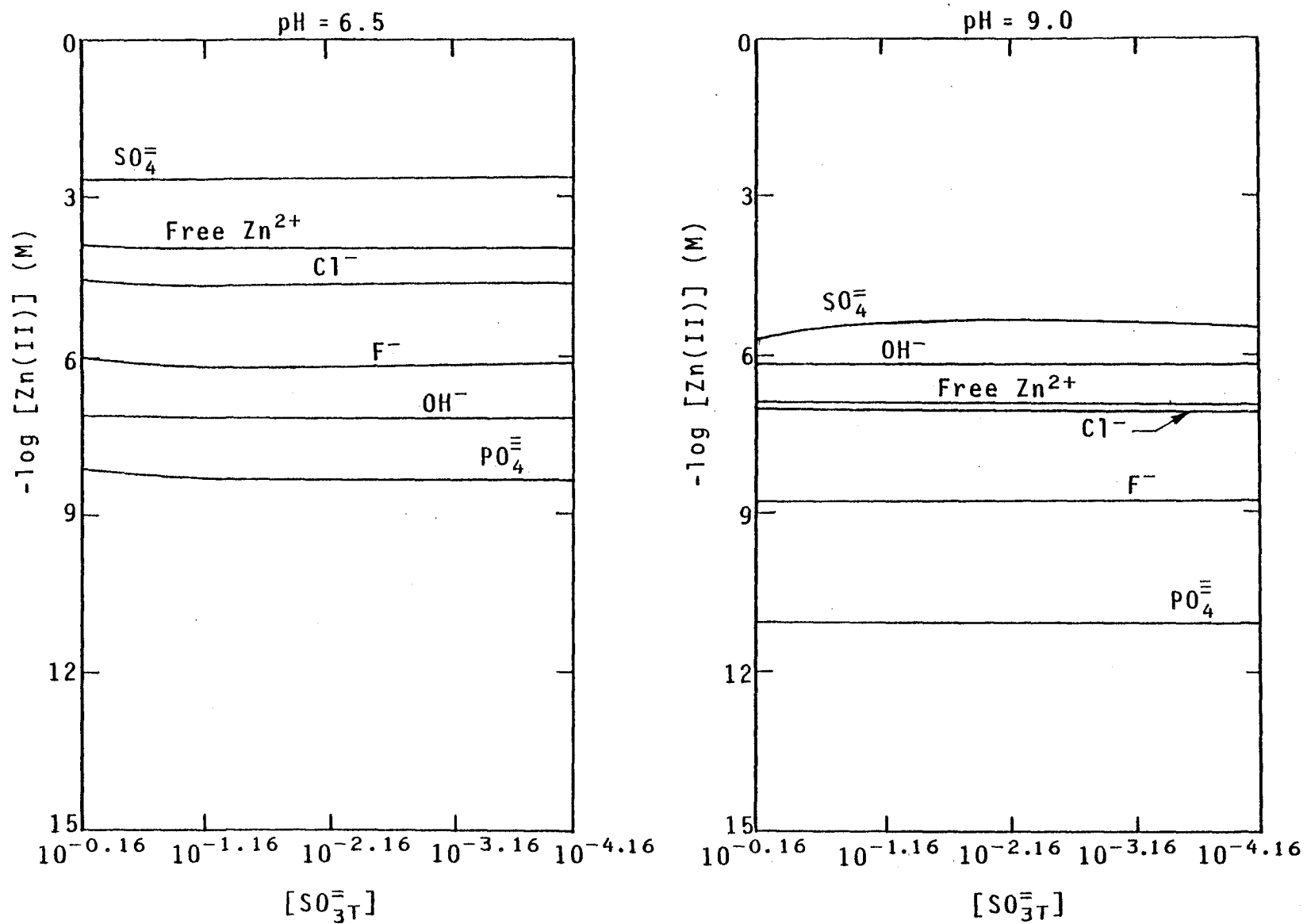
Figure 155. Effects of sulfite oxidation on the speciation of Zn.
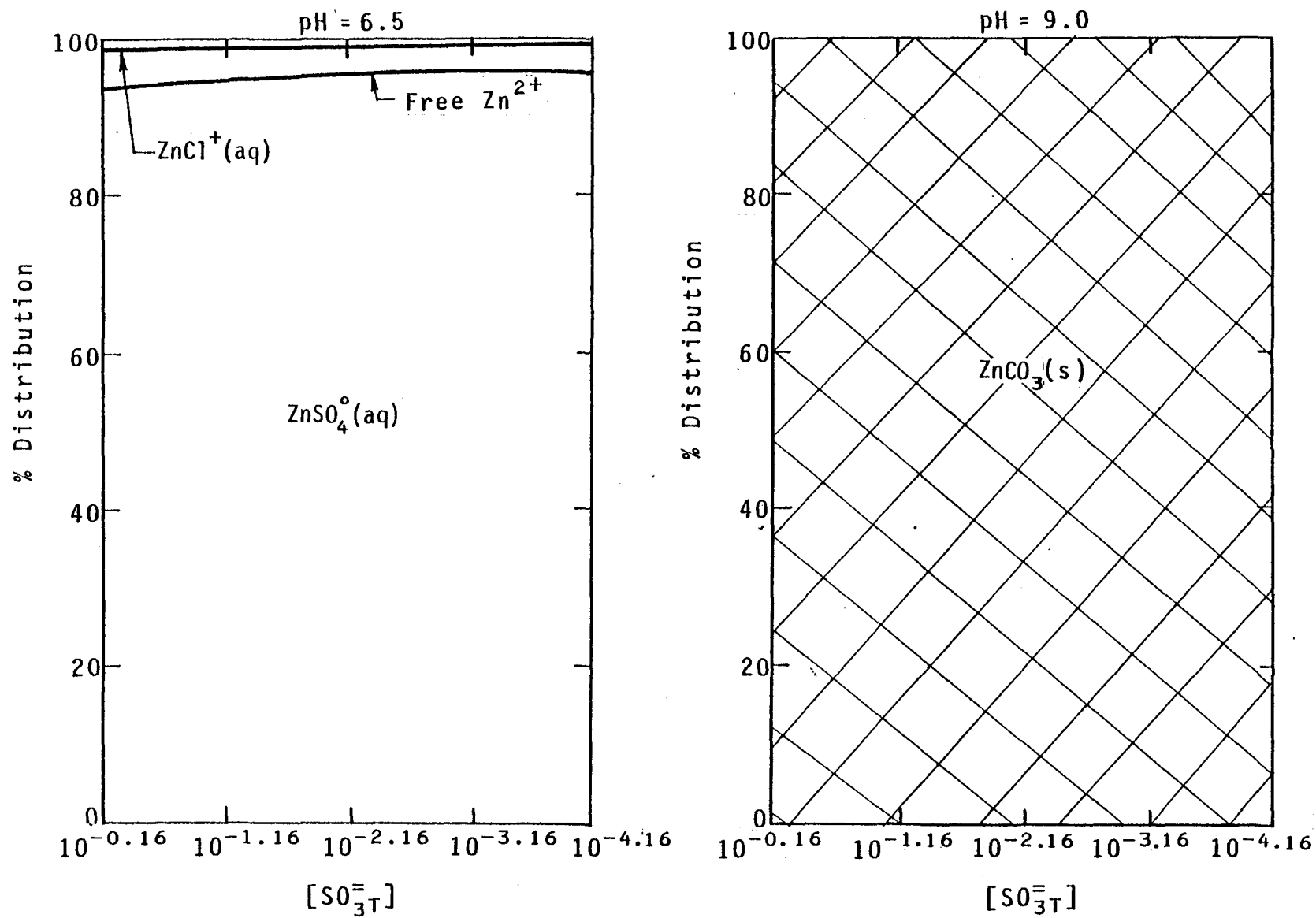
Figure 156. Effects of sulfite oxidation on the primary distribution of Zn species.

in the concentration of sulfate complexes and the decrease of free ions.

Due to the oxidation of sulfite, the $Cd(SO_3)_2^{2-}$ species will be transformed gradually into the $CdSO_4(aq)$ species. As can be seen in Figures 145 and 146, a tenfold decrease in total sulfite concentration will completely transform the $Cd(SO_3)_2^{2-}$ species to $CdSO_4(aq)$. The sulfite oxidation, however, will not affect the cadmium solid phase significantly.

Iron is similar in behavior to cadmium as sulfite oxidation tends to transform the $FeSO_3^+$ complex to $Fe(SO_4)_2^-$ complex. The solid phase of iron, however, again remains unchanged (Figures 151 and 152).

Other minor elements studied, such as chromium, copper, lead, and zinc, appear to be unaffected by sulfite oxidation (Figures 147-150 and 153-156). This is because of the absence of a sulfite complex, as well as the constant oxidation states for these elements in the FGD sludges. Although the concentrations of sulfate complexes of these elements show an increase during sulfite oxidation, the changes are only minor.

SECTION 8

SUMMARY OF FINDINGS

INTRODUCTION

A conventional environmental impact assessment of flue gas desulfurization (FGD) sludge disposal would include chemical analysis and identification of the total concentrations of constituents in the sludge and its leachate. However, public health effects of FGD waste disposal depend on which chemical forms or species of the constituents are released to surrounding waters, and not necessarily on their total concentration.

The only feasible means of obtaining contaminant species information in FGD sludge lies in thermodynamic modeling. A thermodynamic model can also be used to predict the migration trends of the constituents when the FGD wastes age; to estimate the final concentrations of constituents in the FGD leachate (aged wastewater), without conducting expensive field monitoring; and to predict the effects of operational and chemical changes in the FGD wastes.

Many available techniques can be used to construct and interpret a chemical thermodynamic model. In this study, the equilibrium constant approach is employed. This method involves solving the stoichiometric equations of various chemical species, which are subject to constraints imposed by the equilibrium constants as well as mass balance and charge balance relations. Diagrams, such as Eh-pH plots, ion-ratio plots, concentration pH figures, and species distriubtion figures, are then used to display the stability field and speciation results.

The thermodynamic model used in this study was verified for suitability and accuracy by the analytical results of various FGD sludge samples taken from the Kansas City Power and Light La Cygne Power Station. The model is also operated over a wide range of operational and chemical changes to theoretically determine their impacts on the concentration and speciation of various solid and soluble species. The impacts of (1) changes in pH and ionic strength; (2) addition of lime, silicates, hydrogen sulfide, and phosphates to the sludge; (3) variation of chloride, sulfate, and borate levels; (4) addition of magnesium to the sorbent; and (5) sulfite oxidation, were all estimated using the model.

METHODOLOGY OF SPECIES ANALYSES

Two principal graphical treatments, Eh-pH plots and the ion-ratio method, are used to describe the stability fields of constituents in FGD sludge. The Eh-pH plot is employed for constituents with different redox species, such as iron, manganese, mercury, arsenic, and selenium. The ion-ratio method is used for constituents with only one redox state, or for reactions involving no electron transfer.

The speciation model is constructed by the equilibrium constant approach. The actual mathematical equilibrium model involves a series of simultaneous equations which describe the various interactions among components of the system. Seven general equations are involved, as shown in Table 13. In order to solve these equations simultaneously, the information on metal and ligand species, overall formation constants, solubility products (and/or Henry's constants), and activity coefficients must be compiled from the literature. A computer solution is necessary, as the expanded equations number in the hundreds. The resultant nonlinear equations are solved by Newton-Raphson iteration.

Because the chemical composition of FGD sludge can vary over an extremely wide range, this study focused on speciation at the lowest levels (ionic strength (I) = 0.05) and the highest levels (I = 0.8). All possible distributions of species are expected to be within this range.

SPECIATION OF SOLID AND SOLUBLE CHEMICAL SPECIES

Fresh FGD Sludge

The thermodynamic modeling of the fresh FGD wastewater system can be performed as if no solid were formed or dissolved, because (1) the equilibrium conditions among soluble species can easily be reached, and (2) the rates of nucleation and dissolution of the solid species are very low. The predominant soluble species, based upon thermodynamic calculation, are summarized in Table 14. This table shows that the major ions (i.e., calcium, magnesium, potassium, and sodium) and the manganese species exist as free ions, in the fresh FGD wastewaters.

Other trace metals, however, can be complexed considerably in the same wastewaters. As shown in Table 14, chloride complexes may under certain conditions become the predominant species for cadmium, copper, lead, mercury, and zinc; borate complexes may become the predominant species for copper and lead; sulfite complexes may become the predominant species for cadmium and iron; and hydroxide complexes may become the predominant species for mercury, zinc, and the trivalent metals, such as

260

TABLE 13. GENERAL MODELS USED FOR
SPECIATION CALCULATION

$$[M(i)_m L(j)_n] = \beta(i,j)_{nm} [M(i)_f]^m [L(j)_f]^n \cdot \frac{\gamma_{M(i)}^m \gamma_{L(j)}^n}{\gamma_{M(i)_m L(j)_n}}$$

$$[M(i)_f] = \frac{K_{M(i)_p L(j)_q} \cdot R_{M(i)_p L(j)_q} \cdot f_{M(i)_p L(j)_q}}{M(i)^p \cdot L(j)^q \cdot [L(j)_f]^q}$$

$$[L(j)_f] = \frac{K_{M(i)_u L(j)_v} \cdot R_{M(i)_u L(j)_v} \cdot f_{M(i)_u L(j)_v}}{\gamma_{M(i)}^u \cdot L(j)^v \cdot [M(i)_f]^v}$$

$$\sum_{j=1}^{h} \sum_{p=1}^{a} \sum_{q=1}^{b} R_{M(i)_p L(j)_q} = 1$$

$$\sum_{i=1}^{g} \sum_{u=1}^{c} \sum_{v=1}^{d} R_{M(i)_u L(j)_v} = 1$$

$$[M(i)_T] = [M(i)_f] + \sum_{m=1}^{k} \sum_{n=1}^{l} \sum_{j=1}^{h} m[M(i)_m L(j)_n]$$

$$+ \sum_{j=1}^{h} \sum_{p=1}^{a} \sum_{q=1}^{b} p[M(i)_p L(j)_q]$$

$$+ \sum_{j=1}^{h} \sum_{u=1}^{c} \sum_{v=1}^{d} n[M(i)_m L(j)_n]$$

$$[L(j)_T] = [L(j)_f] + \sum_{m=1}^{k} \sum_{n=1}^{l} \sum_{j=1}^{g} n[M(i)_m L(j)_n]$$

$$+ \sum_{i=1}^{g} \sum_{p=1}^{a} \sum_{q=1}^{b} [M(i)_p L(j)_q]$$

$$+ \sum_{i=1}^{g} \sum_{u=1}^{c} \sum_{v=1}^{d} [M(i)_u L(j)_v]$$

TABLE 13 (Continued)

where:

$[M(i)_m L(j)_n]$ = concentration of complex $M(i)_m L(j)_n$ (in moles/liter)

$[M(i)_f]$ = free metal ion concentration of ith metal (in moles/liter)

$[L(j)_f]$ = free concentration of jth ligand (in moles/liter)

$[M(i)_T]$ = total concentration of ith metal in the system (in moles/liter)

$R_{M(i)_p L(j)_q}$

and

$R_{M(i)_u L(j)_v}$ = mole fraction of solid or gas species for metal or ligand solids

i = metal species

j = ligand species

g = total number of metals

h = total number of ligands

k = maximum number of metals ($M(i)$ coordinating ligands $L(j)$

l = maximum number of ligands $L(j)$ coordinating metal $M(i)$

$a, b, c,$ and d = positive integer showing maximum number of metals or ligands in the solids or gases

$\beta(i,j)_{nm}$ = overall formation constant of complex $M(i)_m L(j)_n$

γ_x = thermodynamic activity coefficient of soluble species x.

TABLE 13 (Continued)

f_x = thermodynamic activity coefficient of solid (or gas) species x (in this study, assume $f_x \approx 1$).

K = solubility products or Henry's constants.

TABLE 14. PREDOMINANT SPECIES OF SOLUBLE CONSTITUENTS IN FRESH FGD WASTEWATER

Constituent	Ionic Strength	Predominant Species[*]		
		pH = 5	pH = 7	pH = 9
Al	0.05	$AlF^{2+}(34)$, $Al(OH)^{2+}(20)$, $AlF_2^+(17)$	$Al(OH)_4^-(100)$	$Al(OH)_4^-(100)$
	0.8	$AlF_2^+(55)$	$AlF_2^+(38)$, $AlF_3(31)$	$Al(OH)_4^-(100)$
As	0.05	$H_2AsO_4^-(98)$	$HAsO_4^{2-}(68)$	$HAsO_4^{2-}(100)$
	0.8	$H_2AsO_4^-(95)$	$HAsO_4^{2-}(78)$	$HAsO_4^{2-}(97)$
Cd	0.05	$Cd^{2+}(50)CdCO_3(aq)(40)$	$Cd^{2+}(49)$, $CdCl^+(40)$	$CdCO_3(35)$, $Cd^{2+}(21)$, $CdClOH^{2+}(20)$
	0.8	$CdCl^+(66)$	$Cd(SO_3)_2^{2-}(59)$	$Cd(SO_3)_2^{2-}(65)$
Ca	0.05	$Ca^{2+}(83)$	$Ca^{2+}(89)$	$Ca^{2+}(81)$
	0.8	$Ca^{2+}(71)$	$Ca^{2+}(71)$	$Ca^{2+}(71)$
Cr	0.05	$Cr(OH)^{2+}(79)$	$Cr(OH)_2^+(85)$	$Cr(OH)_4^-(100)$
	0.8	$CrOH^{2+}(65)$	$Cr(OH)_2^+(81)$	$Cr(OH)_4^-(100)$
Co	0.05	$Co^{2+}(69)$	$Co^{2+}(68)$	$CoCO_3(aq)(44)$, $Co^{2+}(26)$
	0.8	$Co^{2+}(40)$, $CoSO_4(aq)(26)$	$Co^{2+}(40)$, $CoSO_4(aq)(26)$	$CoCO_3(aq)(28)$, $Co^{2+}(25)$, $CoCl^+(20)$

TABLE 14 (continued)

Constituent	Ionic Strength	Predominant Species[*]		
		pH = 5	pH = 7	pH = 9
Cu	0.05	$Cu^{2+}(54)$	$Cu(B(OH)_4)_2(aq)(51)$	$Cu(B(OH)_4)_2(aq)(97)$, $Cu(B(OH)_4)_2(aq)$
	0.8	$CuB(OH)_4^+(35)$, $CuCl^+(26)$	$Cu(B(OH)4)_2(aq)(83)$	$Cu(B(OH)_4)_2(aq)(100)$
F	0.05	$F^-(25)$, $SnF^+(52)$	$F^-(91)$	$F^-(93)$
	0.8	$CaF^+(40)$, $F^-(38)$	$F^-(40)$, $MgF^+(44)$	$MgF^+(47)$, $F^-(45)$
Fe	0.05	$Fe(OH)^{2+}(83)$	$Fe(OH)_2^+(100)$	$Fe(OH)_4^-(93)$
	0.8	$FeSO_3^+(97)$	$Fe(OH)_2^+(84)$	$Fe(OH)_2^+(93)$
Pb	0.05	$Pb^{2+}(55)$	$Pb(B(OH)4)_2(aq)(45)$, $Pb^{2+}(19)$	$Pb(B(OH)4)_2(aq)(95)$, $Pb(B(OH)_4)_2(aq)$
	0.8	$PbCl^+(33)$, $PbSO_4(22)$, $Pb^{2+}(21)$	$Pb(B(OH)_4)_2(aq)(87)$	$Pb(B(OH)_4)_2(aq)(100)$
Mg	0.05	$Mg^{2+}(79)$	$Mg^{2+}(79)$	$Mg^{2+}(78)$
	0.8	$Mg^{2+}(66)$	$Mg^{2+}(66)$	$Mg^{2+}(65)$
Mn	0.05	$Mn^{2+}(79)$	$Mn^{2+}(78)$	$Mn^{2+}(76)$
	0.8	$Mn^{2+}(55)$	$Mn^{2+}(55)$	$Mn^{2+}(54)$

TABLE 14 (continued)

Constituent	Ionic Strength	Predominant Species*		
		pH = 5	pH = 7	pH = 9
Hg	0.05	$HgCl_2(aq)(87)$	$HgCl_2(aq)(62)$	$Hg(OH)_2(aq)(65)$
	0.8	$HgCl_3^-(47),HgCl_4^{2-}(26)$ $HgCl_2(aq)(27)$	$HgCl_3^-(46)$,	$HgClOH(aq)(52)$
K	0.05	$K^+(97)$	$K^+(97)$	$K^+(98)$
	0.8	$K^+(89)$	$K^+(89)$	$K^+(89)$
Se	0.05	$HSeO_3^-(97)$	$SeO_3^{2-}(74)$	$SeO_3^{2-}(99)$
	0.8	$HSeO_3^-(97)$	$SeO_3^{2-}(74)$	$SeO_3^{2-}(99)$
Na	0.05	$Na^+(95)$	$Na^+(95)$	$Na^+(97)$
	0.8	$Na^+(95)$	$Na^+(95)$	$Na^+(95)$
Zn	0.05	$Zn^{2+}(74)$	$Zn^{2+}(74)$	$Zn(OH)_2(aq)(68)$
	0.8	$Zn^{2+}(47),ZnCl^+(34)$	$Zn^{2+}(43),ZnCl^+(33)$	$Zn(OH)_2(aq)(42)$, $ZnClOH(aq)(26)$

Note: Values in the parentheses indicate the percent of the total concentration.

* If one species accounts for less than 50 percent of the total concentration, then more than one species will appear.

chromium and iron. In the fresh FGD wastewater, arsenic and selenium exist primarily as arsenate and selenite species. The predominance of a given species can be affected significantly by the pH level of the wastewater. The ionic strength (or, more specifically, the soluble levels of the related ligands) also plays an important role in the speciation of most constituents.

Aged FGD Sludge

The speciation of constituents in the solid and soluble phases of aged FGD sludge was computed with the assumption that the equilibrium condition among all the soluble and solid species had been reached. Due to the long contact period, it is generally quite possible that equilibrium conditions between solid and liquid phases can be reached in the aged FGD wastes. The calculated results are summarized in Table 15.

Results show that sulfur dioxide removed from the flue gas reacts to form $CaSO_4 \cdot 2H_2O(s)$ and $CaSO_3 \cdot 1/2H_2O(s)$ in the FGD sludge. In the aged sludge, carbonate solids may become the predominant species for cadmium, calcium (when pH is greater than 7), copper, lead (at pH greater than about 9), manganese (at pH greater than about 7.5), and zinc (at high ionic strength, and pH around 8). Hydroxide solids are the predominant species for chromium, iron, cadmium (at pH greater than 9), magnesium (at pH greater than 9), manganese (at pH greater than about 9), and zinc (at low ionic strength, and pH greater than about 9) in the aged sludge. Arsenic, mercury, and selenium exist primarily as elemental metals in the aged sludge. Aluminum forms predominantly phosphate solids at low pH, and oxide solids at high pH. In aged sludge, the molybdate and silicate solids are usually the predominant species for lead and zinc, respectively.

The predominant soluble species of constituents in the aged FGD leachates are similar to those found in fresh FGD wastewater. However, the concentrations of these soluble species are generally decreased through aging, due to the nature of solids found. The predominant soluble species, and their concentrations for each individual constituent at two different ionic strengths, are shown in Table 15. In most cases, the predominant species alone will account for a major portion of the concentration of each constituent in FGD wastewater. Therefore, knowing the predominant solid and soluble species, the total soluble concentration of a constituent in FGD leachate can be easily calculated without the aid of the computer.

MODEL VERIFICATION

The thermodynamic model was verified by checking the model results against both analytical data and certain theoretical considerations.

267

TABLE 15. PREDOMINANT SPECIES OF CONSTITUENTS IN AGED FGD SLUDGE

Constituent	Ionic Strength	Predominant Solid Species[*]			Predominant Soluble Species[*]		
		pH = 5	pH = 7	pH = 9	pH = 5	pH = 7	pH = 9
Al	0.05	$Al(H_2PO_4)(OH)_2(s)$	$Al(H_2PO_4)(OH)_2(s)$	$Al_2O_3 \cdot 3H_2O(s)$	$AlF_2^+(6.04)$	$Al(OH)_3(aq)(6.26)$	$Al(OH)_3(aq)(5.95)$
	0.8	$Al(H_2PO_4)(OH)_2(s)$	$Al(H_2PO_4)(OH)_2(s)$	$Al_2O_3 \cdot 3H_2O(s)$	$AlF_2^+(5.05)$	$Al(OH)_3(aq)(6.89)$	$Al(OH)_3(aq)(5.36)$
As	0.05	$As^0(s)$	$As^0(s)$	$As^0(s)$	$H_2AsO_4^-(8.03)$	$HAsO_4^{2-}(11.23)$	$HAsO_4^{2-}(8.82)$
	0.8	$As^0(s)$	$As^0(s)$	$As^0(s)$	$H_2AsO_4^-(7.51)$	$HAsO_4^{2-}(10.87)$	$HAsO_4^{2-}(10.91)$
Cd	0 05	$CdCO_3(s)$	$CdCO_3(s)$	$Cd(OH)_2(s)$	$Cd^{2+}(5.23)$	$Cd^{+2}(6.03)$	$Cd(SO_3)_2^{2-}(7.72)$
	0.8	$CdCO_3(s)$	$CdCO_3(s)$	$Cd(OH)_2(s)$, $CdCO_3(s)$	$CdCl^+(5.12)$	$CdCl^+(5.13)$	$CdClOH(aq)(6.07)$
Ca	0.05	$CaSO_3 \cdot 1/2H_2O(s)$, $CaSO_4 \cdot 2H_2O(s)$	$CaSO_3 \cdot 1/2H_2O(s)$, $CaSO_4 \cdot 2H_2O(s)$	$CaCO_3(s)$, $CaSO_3 \cdot 1/2H_2O(s)$, $CaSO_4 \cdot 2H_2O(s)$	$Ca^{2+}(0.21)$	$Ca^{2+}(0.53)$	$Ca^{2+}(2.19)$
	0.8	$CaSO_3 \cdot H_2O(s)$, $CaSO_4 \cdot 2H_2O(s)$	$CaSO_3 \cdot H_2O(s)$, $CaSO_4 \cdot 2H_2O(s)$	$CaCO_3(s)$, $CaSO_3 \cdot 1/2H_2O(s)$, $CaSO_4 \cdot 2H_2O(s)$	$Ca^{2+}(0.25)$	$Ca^{2+}(0.32)$	$Ca^{2+}(2.0)$
Cr	0.05	$Cr(OH)_3(s)$	$Cr(OH)_3(s)$	$Cr(OH)_3(s)$	$CrOH^{2+}(4.13)$	$Cr(OH)_2^+(4.76)$	$Cr(OH)_4^-(4.03)$
	0.8	$Cr(OH)_3(s)$	$Cr(OH)_3(s)$	$Cr(OH)_3(s)$	$Cr(OH)_2^+(5.0)$	$Cr(OH)_2^+(4.72)$	$Cr(OH)_4^-(3.99)$

TABLE 15 (continued)

Constituent	Ionic Strength	Predominant Solid Species[*]			Predominant Soluble Species[*]		
		pH = 5	pH = 7	pH = 9	pH = 5	pH = 7	pH = 9
Cu	0.05	$Cu_2CO_3(OH)_2(s)$	$Cu_2CO_3(OH)_2(s)$	$Cu_2CO_3(OH)_2(s)$	$CuB(OH)_4^+(15.38)$ (16.78)	$Cu(B(OH)_4)_2(aq)$ (16.9)	$Cu(B(OH)_4)_2(aq)$
	0.8	$Cu_2CO_3(OH)_2(s)$	$Cu_2CO_3(OH)_2(s)$	$Cu_2CO_3(OH)_2(s)$	$CuB(OH)_4^+(14.99)$ (16.09)	$Cu(B(OH)_4)_2(aq)$ (16.4)	$Cu(B(OH)_4)_2(aq)$
Fe	0.05	$Fe(OH)_3(s)$	$Fe(OH)_3(s)$	$Fe(OH)_3(s)$	$Fe(OH)_2^+(7.16)$	$Fe(OH)_2^+(9.16)$	$Fe(OH)_4^-(10.07)$
	0.8	$Fe(OH)_3(s)$	$Fe(OH)_3(s)$	$Fe(OH)_3(s)$	$FeSO_3^+(6.98)$	$Fe(OH)_2^+(9.12)$	$Fe(OH)_4^-(8.96)$
Pb	0.05	$PbMoO_4(s)$	$PbMoO_4(s)$	$PbMoO_4(s)$	$Pb^{2+}(5.80)$	$PbB(OH)_4^+(5.82)$	$Pb(B(OH)_4)_3^-(7.14)$
	0.8	$PbMoO_4(s)$	$PbMoO_4(s)$	$PbMoO_4(s)$, $PbCO_3(s)$	$PbCl^+(5.67)$	$PbB(OH)_4^+(5.44)$	$Pb(B(OH)_4)_3^-(5.55)$
Mg	0.05	--†	--†	$Mg(OH)_2(s)$	$Mg^{2+}(3.91)$	$Mg^{2+}(3.92)$	$Mg^{2+}(4.16)$
	0.8	--†	--†	$Mg(OH)_2(s)$	$Mg^{2+}(0.95)$	$Mg^{2+}(0.95)$	$Mg^{2+}(1.13)$
Mn	0.05	--†	--†	$MnCO_3(s)$	$Mn^{2+}(3.49)$	$Mn^{2+}(3.49)$	$MnSO_4(aq)(4.10)$
	0.8	--†	--†	$Mn(OH)_2(s)$, $MnCO_3(s)$	$Mn^{2+}(3.56)$	$Mn^{2+}(3.56)$	$Mn^{2+}(4.33)$
Hg	0.05	$Hg^0(l)$	$Hg^0(l)$	$Hg^0(l)$	$HgCl_2(aq)(22.1)$	$HgCl_2(aq)(20.4)$	$Hg(OH)_2(aq)(17.9)$
	0.8	$Hg^0(l)$	$Hg^0(l)$	$Hg^0(l)$	$HgCl_3^-(19.9)$	$HgCl_3^-(18.2)$	$HgClOH(aq)(17.0)$

TABLE 15 (continued)

Constituent	Ionic Strength	Predominant Solid Species[*]			Predominant Soluble Species[*]		
		pH = 5	pH = 7	pH = 9	pH = 5	pH = 7	pH = 9
K	0.05	--†	--†	--†	$K^+(1.89)$	$K^+(1.89)$	$K^+(1.93)$
	0.8	--†	--†	--†	$K^+(1.87)$	$K^+(1.87)$	$K^+(1.91)$
Se	0.05	$Se^0(s)$	$Se^0(s)$	$Se^0(s)$	$HSeO_3^-(28.6)$	$SeO_3^{2-}(18.2)$	$SeO_3^{2-}(6.19)$
	0.8	$Se^0(s)$	$Se^0(s)$	$Se^0(s)$	$HSeO_3^-(28.6)$	$SeO_3^{2-}(18.2)$	$SeO_3^{2-}(6.19)$
Na	0.05	--†	--†	--†	$Na^+(1.36)$	$Na^+(1.36)$	$Na^+(1.37)$
	0.8	--†	--†	--†	$Na^+(0.83)$	$Na^+(0.83)$	$Na^+(0.85)$
Zn	0.05	--†	$ZnSiO_3(s)$	$Zn(OH)_2(s)$	$Zn^{2+}(3.63)$	$Zn^{2+}(3.65)$	$ZnSO_4(aq)(5.67)$
	0.8	$ZnSiO_3(s)$	$ZnSiO_3(s)$ $Zn(OH)_2(s)$	$ZnSiO_3(s)$, $ZnCO_3(s)$	$Zn^{2+}(3.84)$	$Zn^{2+}(4.06)$	$Zn(OH)_2(aq)(5.9)$

Note: Values in parentheses indicate the -log molar concentration.

* If one species accounts for less than 50 percent of the total concentration, then more than one species will appear for each condition.

† -- indicates that there is no stable solid or that the stable solid is in complex forms (e.g., complex silicates).

Evaluation of the model in relation to analytical data, was performed by comparing the known soluble concentrations of constituents in aged FGD wastes to those predicted by the model. As summarized in Table 16, the calculated results for aluminum, arsenic, boron, cadmium, cobalt, copper, iron, manganese, mercury, potassium, selenium, sodium, and zinc, either approach or are very close to the concentration levels experienced in the field. For other elements (specifically calcium, chromium, fluoride, lead, and magnesium), the model was not as effective. The low levels of calcium predicted by the model are due primarily to the interaction of calcite with the $Ca-CO_3$ and $Ca-SO_3$ complexes in the model. The high levels of chromium and lead calculated by the model are due to the inclusion of hydroxide and carbonate complexes in the model. For fluoride and magnesium, the discrepancy may be caused by certain unsuitable solids included in the model. The discrepancies also may be due to (1) errors in the stability constants and activity coefficients; (2) the effects of other mechanisms, such as adsorption by hydroxide solids or clay minerals; and (3) the effects of kinetic constraints.

An evaluation of the thermodynamic model was also performed according to scientific considerations. In general, the model results behave in accordance with basic chemical and thermodynamic principles, including the effects of changing pH, Eh, and ligand levels.

EFFECTS OF FGD SYSTEM AND SLUDGE VARIABLES ON CHEMICAL SPECIATION

For the purpose of selecting a sludge treatment or disposal procedure, it is useful to observe the possible beneficial or adverse effects of operational or chemical changes in an FGD system on sludge speciation. The chemical changes studied here include those of pH, ionic strength, chloride concentration, borate concentration, sulfate concentration, and sulfite oxidation. Table 17 summarizes the qualitative results. The operational changes studied were limited to the addition of lime, silicates, hydrogen sulfide, phosphates, and magnesium to the FGD system. The results are summarized in Table 18.

A change in pH can influence the direction of the alteration processes (dissolution, precipitation, adsorption, or complexation), in any chemical system. In general, a pH increase in the FGD sludge system tends to dissolve more elemental constituents, such as $As^0(s)$, $Hg^0(\ell)$, and $Se^0(s)$, and to transform some of the carbonate, phosphate, or other solids into hydroxide solids, thus affecting the concentration of soluble constituents. A pH change may also affect the ligand concentrations, and thereby change the concentration of soluble constituents.

TABLE 16. VALIDITY OF THE THERMODYNAMIC MODEL FOR THE
PREDICTION OF FGD SLUDGE SPECIATION*

Constituent	Validity of Model[†]	Reason for Discrepancy
Al	Excellent	
As	Good	
B	Excellent	
Cd	Excellent	
Ca	Not applicable	Form strong $CaCO_3$(s) when pH >7
Cr	Not applicable	Form strong Cr-OH complexes
Co	Good	
Cu	Excellent	
F	Not applicable	Solubility-controlling solid unknown
Fe	Good	
Pb	Not applicable	Form strong $Pb-CO_3$ and Pb-OH complexes
Mg	Not applicable	Solubility-controlling solid unknown
Mn	Excellent	
Hg	Excellent	
K	Good	
Se	Good	
Na	Good	
Zn	Excellent	

* Based on comparison of modeling results with Kansas City Power and Light FGD sludge analysis.

† "Excellent" means that the migration trends of the constituent follow those predicted by the model, and measured levels in the aged leachate are within 30 percent of those estimated by the model; "Good" means that both estimated and calculated levels of constituents show the same migration trends when FGD waste ages.

TABLE 17. EFFECTS OF CHEMICAL CHANGES ON THE SPECIATION OF CONSTITUENTS IN FGD SLUDGE

Constituent	pH	Ionic Strength	Chloride Concentration	Borate Concentration	Sulfate Concentration	Sulfite Oxidation
Al	Solid: High pH levels favor the formation of $Al_2O_3 \cdot 3H_2O(s)$, low pH levels favor the formation of $Al(H_2PO_4)(OH)_2(s)$	Negligible (when related ligand concentrations are unchanged)	Negligible	Negligible	Negligible	Negligible
	Soluble: When pH is higher than about 6, the predominant species will change from AlF_2^+ to $Al^{3+}-OH^-$ complexes					Negligible
As	High pH levels tend to dissolve $As^0(s)$ and form arsenate species	Negligible	Negligible	Negligible	Negligible	Negligible, if the redox potential is not controlled by sulfate/sulfite species
Cd	Solid: When pH is higher than 10.5, $CdCO_3(s)$ may gradually transform to $Cd(OH)_2(s)$ Soluble: High pH level can lower the total Cd level	The relative distribution of Cd^{2+} and Cd-Cl complexes can be altered by ionic strength changes	Can greatly affect the total soluble Cd levels when chloride is higher than certain levels	Negligible	$Cd-SO_4$ complex may become predominant when Cl^-, SO_3^{2-}, or OH^- complexes are not significant	Will reduce $Cd(SO_3)_2^{2-}$ and increase $CdSO_4(aq)$ levels. However, effects on total soluble Cd and Cd solids are negligible

273

TABLE 17 (continued)

Constituent	pH	Ionic Strength	Chloride Concentration	Borate Concentration	Sulfate Concentration	Sulfite Oxidation
Ca	Solid: $CaCO_3(s)$ may greatly increase in the sludge when pH >7 Soluble: When pH >7, the total Ca and Ca^{2+} are reduced significantly	Negligible	Negligible	Negligible	When pH >5, and the sulfate level is higher than about 5,000 ppm, the $CaSO_4$ (aq) species may become predominant	Will convert the sulfite solid into sulfate or carbonate solids. However, will have very little effect on soluble Ca
Cr	Solid: $Cr(OH)_3(s)$ is significant when pH ranges from 6 to 9 Soluble: When pH is higher than about 4, the predominant species will change from Cr^{3+} to Cr-OH complexes	Negligible	Negligible	Negligible	Negligible	Negligible
Cu	Solid: Negligible Soluble: When pH >4.8, the predominant species will change from Cu^{2+} to Cu-$B(OH)_4$ complexes	Negligible	When pH <4.7, Cu-Cl complexes may become predominant when the chloride level is higher than 2,000 ppm	When the borate level increases from 5 ppm to 200 ppm, the soluble lead level can be increased about 2,000	Negligible	Negligible
Fe	Solid: Negligible Soluble: High pH levels (pH >8.5) tend to increase Fe-OH$^-$ complexes, but reduce the total Fe levels	Negligible	Negligible	Negligible	Negligible	Will transform $FeSO_3^+$ to $Fe(SO)_2^-$, but the solid phase will remain unchanged

TABLE 17 (continued)

Constituent	pH	Ionic Strength	Chloride Concentration	Borate Concentration	Sulfate Concentration	Sulfite Oxidation
Pb	Solid: When pH <9, $PbMoO_4(s)$ is predomi-nant; otherwise, $PbCO_3(s)$ is predominant Soluble: At high pH levels, $Pb-CO_3$ may increase the total Pb levels	Negligible	When pH >7, Pb-Cl complexes may become predominant when the chloride level is higher than 1,500 ppm	When the borate level in-creases from 5 ppm to 200 ppm, the solu-ble lead level can be increased about 10,000 times	Negligible	Negligible
Mg	Solid: High pH levels (pH >9) favor the for-mation of $Mg(OH)_2(s)$ Soluble: When pH is increased, the $MgSO_4$ (aq) species may be-come significant	Negligible	Negligible	Negligible	When the soluble sulfate level is raised to as high as 3,000 to 5,000 ppm, the level of $MgSO_4$(aq) may exceed the Mg^{2+} level	Negligible
Mn	No significant effect on predominant solu-ble species. However, the total soluble level will be decreased at high pH levels due to the formation of more solid	Negligible	May affect the levels of Mn-Cl com-plexes, but will not change the total soluble levels signifi-cantly	Negligible	Negligible	Negligible

TABLE 17 (continued)

Constituent	pH	Ionic Strength	Chloride Concentration	Borate Concentration	Sulfate Concentration	Sulfite Oxidation
Hg	Low pH levels favor the formation of $Hg^0(1)$ in the sludge. High pH levels tend to increase the soluble levels of $HgCl_2$, $HgCl_3^-$, $Hg(OH)_2(aq)$, and $HgClOH(aq)$	Negligible	When the chloride level varies from 50 to 6,000 ppm, the total soluble Hg can be increased for more than four orders of magnitude	Negligible	Negligible	If the redox potential is controlled by sulfate/sulfite species, sulfite oxidation can increase the soluble Mg level
K	Slightly reduces the K^+ levels when pH is increased	Negligible	Negligible	Negligible	Can affect the $K_2SO_4(aq)$ level. Will not, however, affect the total soluble level of K	Will increase the $K_2SO_4(aq)$ level and reduce the K^+ level. But will not have a significant effect on total soluble K
Se	High pH levels tend to dissolve $Se^0(s)$ and form selenate species	Negligible	Negligible	Negligible	Negligible	If the redox potential is controlled by sulfate/sulfite species, sulfite oxidation can increase the soluble Se level
Na	Will slightly reduce the Na^+ levels when pH increases	Negligible	Negligible	Negligible	Can affect the $Na_2SO_4(aq)$ level. Will not, however, affect the total soluble level of Na	Will increase the $Na_2SO_4(aq)$ level and reduce the Na^+ level. But will not have a significant effect on total soluble Na

276

TABLE 17 (continued)

Constituent	pH	Ionic Strength	Chloride Concentration	Borate Concentration	Sulfate Concentration	Sulfite Oxidation
Zn	Solid: High pH levels favor the formation of $Zn(OH)_2(s)$. When pH decreases, $ZnSiO_3(s)$ will replace $Zn(OH)_2(s)$ Soluble: Will reduce total levels when pH increases	Negligible	When pH <9, the total soluble Zn exists predominantly as $ZnCl^+$ if the chloride level is higher than 3,000 ppm	Negligible	$ZnSO_4(aq)$ may become predominant at a pH around 9 when Cl- and OH^- complexes are not significant	Negligible

TABLE 18. EFFECTS OF ADDITION OF CHEMICAL COMPOUNDS ON THE
SPECIATION OF FGD SLUDGE CONSTITUENTS

Constituent	Addition of Lime	Addition of Silicates	Addition of Hydrogen Sulfide	Addition of Phosphates	Addition of Magnesium
Al	Effect on total soluble Al is negligible	The soluble Al level can be greatly reduced when silicate addition is higher than 280 ppm as Si	Negligible	Effect on total soluble Al is negligible	Will not affect the total soluble Al
As	Lime addition can cause more $Ba_3(AsSO_4)_2(s)$ to form, so reduce the total soluble As slightly	Negligible	Negligible	Negligible	Will not affect the total soluble As
Cd	When the lime dosage is higher than 1,500 ppm, soluble Cd can be increased from 0.01 ppb to 1.45 ppb	Negligible	Cd can be reduced to trace levels when sulfide addition is higher than 0.2 ppm	When phosphate addition is higher than 310 ppm (as P), the soluble Cd can be increased about 2 times	Will not affect the total soluble Cd
Ca	When the dosage of lime is from 100 to 10,000 ppm, the total soluble Ca will increase from 200 ppm to 400 ppm	Negligible	Negligible	If phosphate addition is higher than 310 ppm (as P), soluble Ca can be reduced slightly	Magnesium addition may decrease the $Ca-SO_4$ and Ca-F complexes, but will not change the total soluble Ca
Cr	Lime addition tends to increase the total soluble Cr due to hydroxide complexes formation	Negligible	Negligible	Negligible	May affect the total soluble Cr through the CrF^{2+} reduction

TABLE 18 (continued)

Constituent	Addition of Lime	Addition of Silicates	Addition of Hydrogen Sulfide	Addition of Phosphates	Addition of Magnesium
Cu	Lime addition tends to increase soluble Cu, but will not raise the soluble Cu above the detectable level	Negligible	Cu can be reduced to trace levels by adding as little as 0.001 ppm of sulfide	Negligible	Will not affect the total soluble Cu
Fe	When the lime dosage is higher than 1,500 ppm, the soluble Fe level will be increased from 0.012 ppb to 22 ppb	Negligible	Negligible	Negligible	Will not affect the total soluble Fe
Pb	Lime addition tends to increase the total soluble Pb due to carbonate complex formation	Negligible	Pb can be reduced to trace levels by adding as little as 0.001 ppm of sulfide	Negligible	Will not affect the total soluble Pb
Mg	Lime addition will only affect the total soluble Mg slightly but will significantly transform $Mg-CO_3$ complexes	Negligible	Negligible	Soluble Mg will be reduced about 2.5 times as the phosphate level is increased from 0.3 to 3,100 ppm (as P)	Will cause the increase of soluble Mg
Mn	Lime addition tends to reduce the soluble Mn to the 20-36 ppb range	Negligible	Negligible	Negligible	Will not affect the total soluble Mn
Hg	Lime addition tends to increase the total soluble Hg slightly due to an increase in pH	Negligible	Hg can be reduced to trace levels by adding as little as 0.001 ppm of sulfide	Negligible	Will not affect the total soluble Hg

279

TABLE 18 (continued)

Constituent	Addition of Lime	Addition of Silicates	Addition of Hydrogen Sulfide	Addition of Phosphates	Addition of Magnesium
K	Negligible	Negligible	Negligible	Negligible	Magnesium addition may decrease the $K_2SO_4(aq)$ level, but will not affect the total soluble K
Se	Lime addition will increase the total soluble Se due to an increase in pH	Negligible	Negligible	Negligible	Will not affect the total soluble Se
Na	Negligible	Negligible	Negligible	Negligible	Magnesium addition may decrease the $Na_2SO_4(aq)$ level, but will not affect the total soluble Na
Zn	Lime addition may increase the total soluble Zn to ppm levels	The soluble Zn level is reduced when silicate addition exceeds 280 ppm as Si	Zn will be reduced to trace levels when sulfide addition is higher than 0.5 ppm	Negligible	Will not affect the total soluble Zn

280

The overall effects of pH on the total constituent concentration depend on the solubility constants of the new solids formed, the new ligand concentrations, and the formation constants of the complexes. For example, a high pH level can increase total soluble mercury and selenium, and yet decrease most of the other bivalent trace metals. For trivalent metals such as chromium and iron, the minimum soluble constituent concentrations occur in the neutral pH region.

Although a change in ionic strength in the FGD sludge can affect the stability constants, its effect on the soluble levels of constituents, or on the stability fields of various solids, are usually negligible if their related ligand levels are unchanged. The soluble chloride concentration of the FGD waste is a very important factor in determining the total soluble level of cadmium, copper, lead, mercury, and zinc. Variations in borate concentration have an impact primarily on total soluble copper and lead concentrations. The soluble sulfate concentration may affect the total soluble calcium, magnesium, cadmium, and zinc concentrations. In general, if the total soluble levels of the above-mentioned ligands (e.g., chloride, borate, and sulfate) are known, the total soluble metal concentrations in the aged FGD leachates can be approximated without extensive computation.

With regard to operational changes, sulfite oxidation may reduce the concentration of sulfite complexes and increase the concentration of sulfate complexes, but will have very little impact on the total soluble concentration of most metals. The most significant effect of sulfite oxidation is the transformation of $CaSO_3 \cdot 1/2H_2O(s)$ to $CaSO_4.2H_2O(s)$ or $CaCO_3(s)$, depending on pH levels. This transformation may affect the soluble levels of arsenic, mercury, and selenium if the redox potential is controlled by sulfate/sulfite species.

The addition of lime to the FGD sludge has been employed in pozzolanic fixation processes for the purpose of improving the engineering properties of the dewatered sludge. However, the model shows that lime addition may have an adverse effect on constituent solubility. The addition of lime to FGD wastes may reduce the total soluble levels of certain constituents such as arsenic and manganese. However,the total soluble levels of most other trace toxic metals, such as cadmium, chromium, copper, lead, mercury, selenium, and zinc, increase in aged FGD sludge following lime addition. This may actually increase the potential for environmental damage, should the concentration increase outweight the dilution factor decrease which results from permeability reduction.

The addition of silicates may reduce the total soluble aluminum and zinc concentrations, but other elements studied are virtually unaffected.

Phosphate addition will only reduce two soluble major ions (calcium and magnesium) while increasing the soluble cadmium level. Phosphate itself is also a water pollutant, so the addition of phosphates is not recommended for the treatment of FGD wastewater.

Hydrogen sulfide addition may reduce the soluble concentrations of trace metals substantially, as shown in Table 18. This operational change, however, may not be desirable for an FGD system for two reasons: (1) hydrogen sulfide itself is a pollutant, and (2) the diffusion of oxygen into the sludge, followed by the oxidation process, will eventually return the soluble metals to their original concentration.

Magnesium has been shown to improve the efficiency of wet FGD systems; the use of high magnesium reagents could therefore become commonplace. The model shows that, in general, the magnesium addition will not significantly affect the total soluble levels of most constituents.

SECTION 9

CONCLUSIONS AND RECOMMENDATIONS

1. Thermodynamic modeling of chemical speciation in FGD sludge has shown that sludge constituents can exist in a wide variety of chemical forms or species. The predominance and concentration of any particular chemical species are influenced by chemical factors such as pH, Eh, ionic strength, and total concentrations of ligands and metals in the system. Although the FGD chemical systems are extremely complex, the speciation of their elemental constituents can be quantified by calculation with reasonable accuracy.

2. The thermodynamic approach indicates that, in most FGD systems (ionic strength (I) of 0.05 to 0.8, and pH of 3 to 11), the major solid species for metals are usually sulfates, sulfites, carbonates, and hydroxides. Silicate, phosphate, elemental metal, and molybdate solids may also become the predominant solid species under certain conditions. Based on the pH, Eh, and various related ligand conditions, the predominant solid species of most elemental constituents in the FGD system can be derived. The solids which will predominate for the sludge constituents of concern are as follows:

Aluminum - $Al_2O_3 \cdot 3H_2O(s)$, $AlPO_4(s)$ and $Al(H_2PO_4)(OH)_2(s)$
Antimony - $Sb(OH)_3Cl_2(s)$
Arsenic - $As^o(s)$
Cadmium - $CdCO_3(s)$ and $Cd(OH)_2(s)$
Calcium - $CaSO_4 \cdot 2H_2O(s)$, $CaSO_3 \cdot 1/2H_2O(s)$, and $CaCO_3(s)$
Chromium - $Cr(OH)_3(s)$
Copper - $Cu_2CO_3(OH)_2(s)$ and $Cu(OH)_2(s)$
Iron - $Fe(OH)_3(s)$ and $FeCO_3(s)$
Lead - $PbCO_3(s)$, $Pb(OH)_2(s)$, $Pb_3(OH)_2(CO_3)(s)$, and $PbMoO_4(s)$
Mercury - $Hg^o(\ell)$
Manganese - $MnOOH(s)$, $MnCO_3(s)$, $Mn(OH)_2(s)$, $Mn_3O_4(s)$ and $MnO_2(s)$
Nickel - $NiCO_3(s)$ and $Ni(OH)_2(s)$
Selenium - $Se^o(s)$
Zinc - $ZnSiO_3(s)$, $ZnCO_3(s)$, and $Zn(OH)_2(s)$

3. The results of thermodynamics calculations also show that the relative distribution of various soluble species in fresh and aged FGD sludges are quite similar. Stated another way, although the aging process may reduce or increase the total soluble

283

concentration of constituents, the primary soluble species (species which predominate, or whose concentration may become significant in the leachate) is common to both conditions. For each constituent, only a few species may become predominant for a given FGD condition. These soluble species are as follows:

Calcium - Ca^{2+}; Ca-SO4 complexes
Magnesium - Mg^{2+}; Mg-SO4 complexes
Potassium - K^+
Sodium - Na^+
Cadmium - Cd^{2+}; Cd-Cl complexes; Cd-CO3 complexes; Cd-SO3 complexes; Cd-SO4 complexes
Chromium - Cr^{3+}; Cr-OH complexes
Copper - Cu^{2+}; Cu-B(OH)4 complexes; Cu-Cl complexes
Iron - Fe-OH complexes; Fe-SO3 complexes
Mercury - Hg-Cl complexes; Hg-OH complexes
Lead - Pb^{2+}; Pb-B(OH)4 complexes; Pb-Cl complexes; Pb-CO3 complexes
Zinc - Zn^{2+}; Zn-Cl complexes; Zn-OH complexes

4. Knowledge of the relative distribution of constituent species in the FGD system is useful for (1) the evaluation of general toxicity, and (2) predicting the migration of the constituent in the environment. Although it was impossible to consider all the possible FGD conditions in this study, the calculated results for the boundary conditions (ionic strength of 0.05 and 0.8) do provide a range of the possible species concentrations. Most FGD sludges are expected to fall within these boundary conditions. The boundary results can be viewed in Figures 1 through 81, in the main text of this report.

After the primary solid and the soluble species are identified by the methods of this study, the total soluble constituent concentrations in the aged sludge can be calculated without the aid of a computer. The concentrations of free ions can be approximated by solving the mass equation(s) of primary solid(s) solubilities. The concentrations of soluble primary species can then be solved by the mass equations which, including the free soluble ions and the complex formation constraints, are described in Section 2. The summation of the primary soluble species for each constituent, will provide its estimated total level in the sludge liquid phase. Equations 73 through 83 are examples of this type of calculation.

5. When assessing the potential impacts of FGD sludge leachate on groundwater, examination of data from aged FGD wastes is most appropriate. Most in situ FGD sludges have a low permeability (10^{-4} to 10^{-10} cm/sec) (Ref. 1, 46) which provides months to years of contact time between leachate and sludge. During this period, various chemical species in the FGD sludge (either in the solid or soluble phases) would gradually approach equilibrium. Unfortunately, there is a lack of documented

information relating to the chemical species present in aged
FGD waste, due to the similar lack of long-term FGD operations.
Therefore, the thermodynamic model can be useful for predicting
both the concentrations of various species, and the total solu-
ble concentrations of constituents in aged FGD sludge. The
background required for the calculation need include no more than
the total levels of the constituents in the fresh FGD waste. This
thermodynamic approach could provide a considerable cost saving
over the traditional field survey.

6. The thermodynamic model discussed here can also be used
to predict solid or soluble species changes, and changes in the
levels of total soluble constituents caused by operational or
chemical factors. Examples of these sensitivity calculations
are presented in Section 7, and are summarized in Section 8.
The soluble constituent concentrations at the boundary conditions
(ionic strength of 0.05 and 0.8) are displayed in Figures 157
through 167. The shaded areas indicate the ranges of possible
total constituent concentrations in the aged FGD wastes. These
values may be used for rough estimation of the total soluble
constituents in various aged FGD leachates. Only those elements
for which the model projections agree with the analytical results,
are shown.

7. The thermodynamic model employed in this study was found
to be inaccurate when predicting the speciation of calcium,
chromium, fluoride, lead, and magnesium. The disparity may have
been caused by several factors, including adsorption by various
solids or the kinetic constraints of the reactions. The specia-
tion of other constituents, such as aluminum, arsenic, cadmium,
boron, cobalt, copper, iron, manganese, mercury, potassium,
selenium, sodium, and zinc, showed very close correlation with
the analytical results. More study is therefore suggested to
(1) verify the model against different types of FGD wastes, or
(2) include more of the controlling factors in the model.
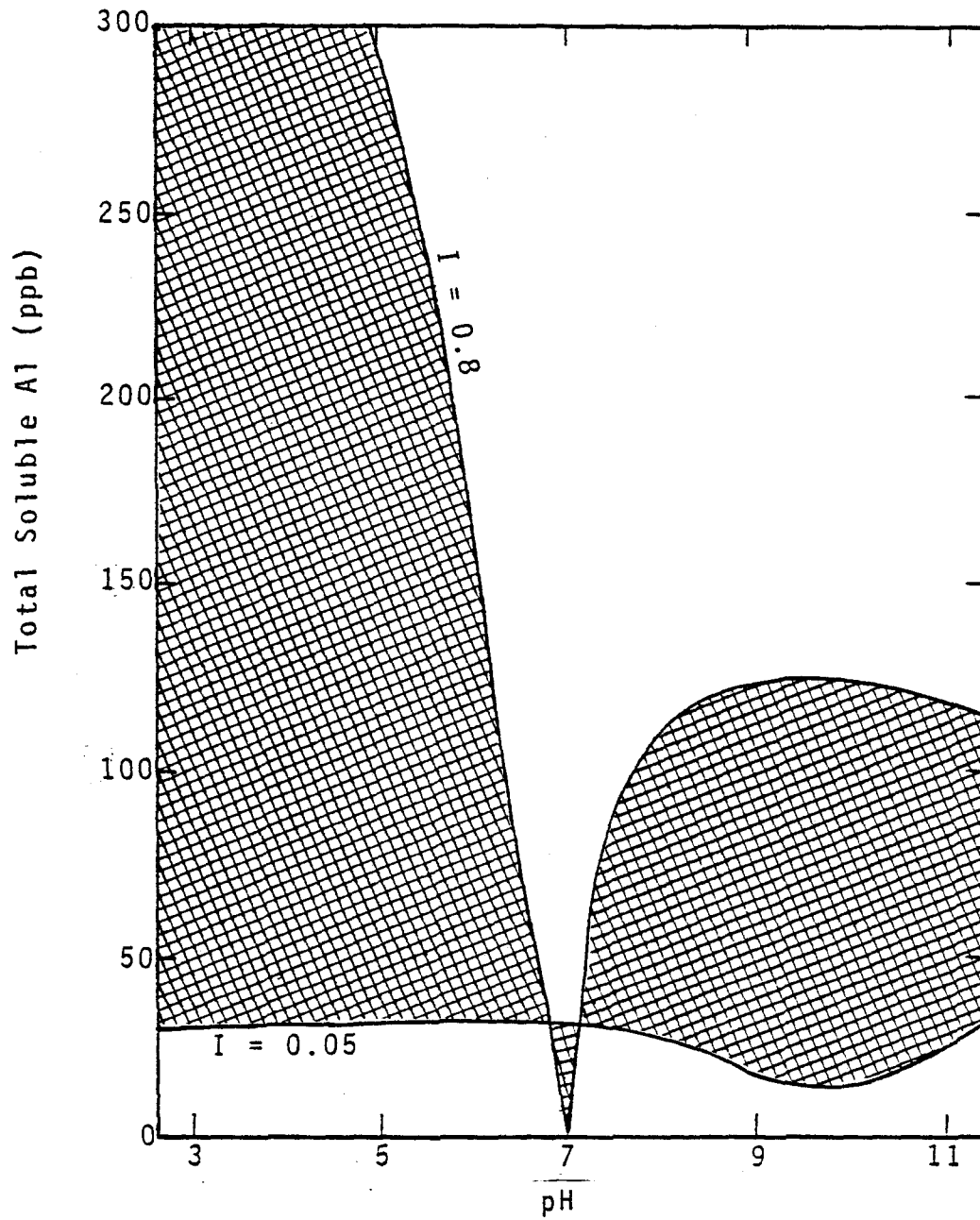
Figure 157. Range of aluminum concentrations in aged FGD sludge leachates by thermodynamic model calculation.
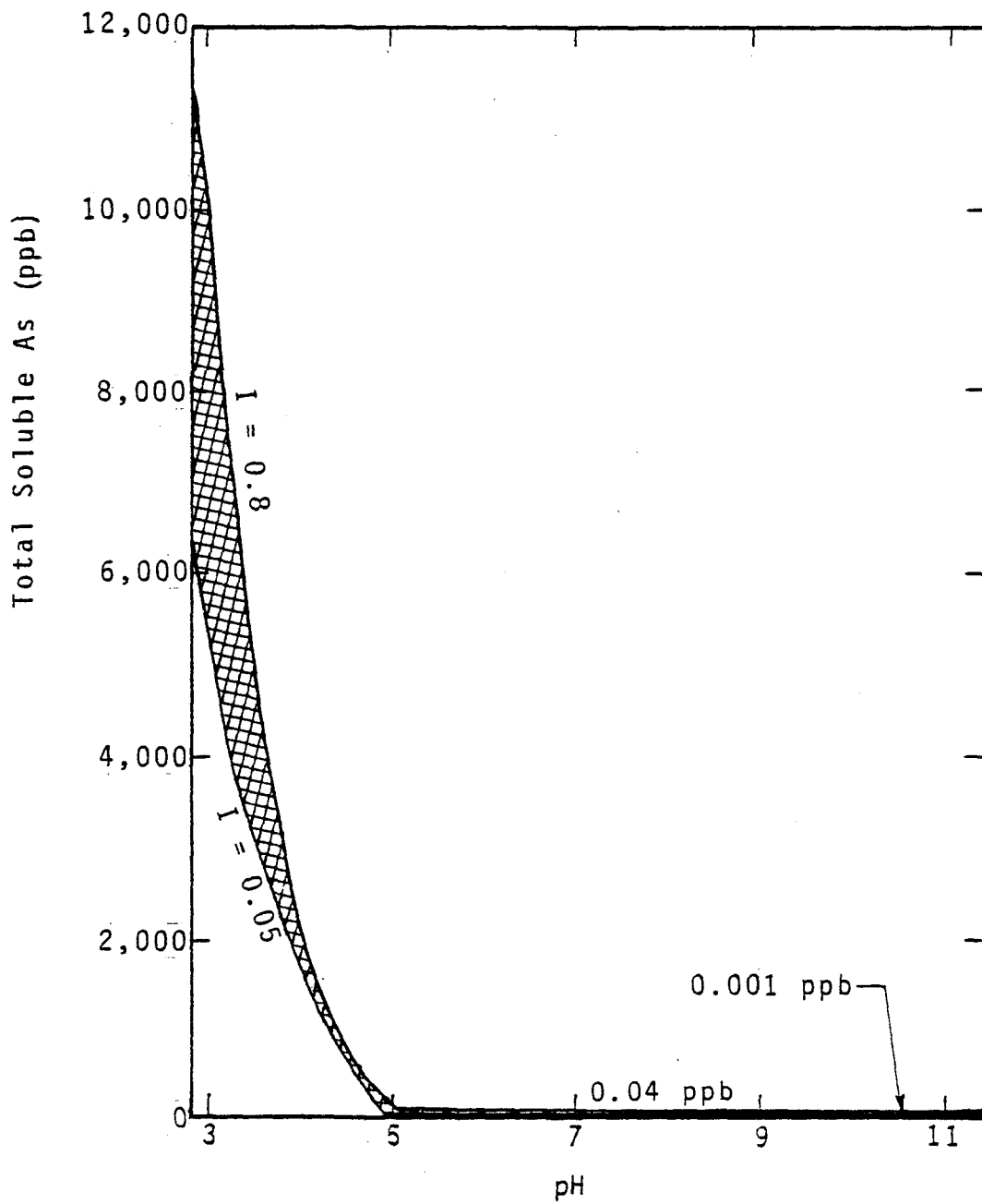
Figure 158. Range of arsenic concentrations in aged FGD
            sludge leachates by thermodynamic model calcu-
            lation.
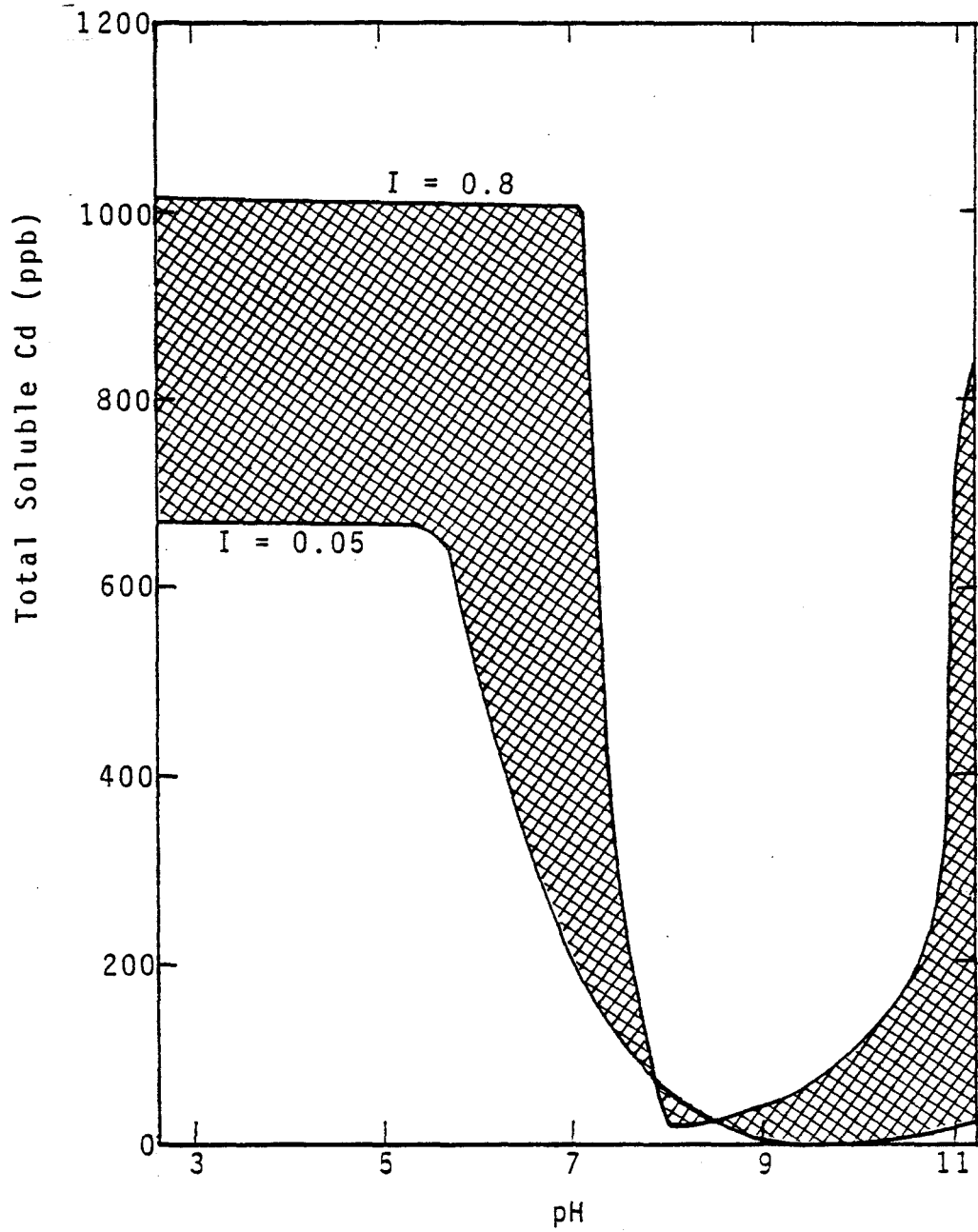
Figure 159. Range of cadmium concentrations in aged FGD sludge leachates by thermodynamic model calculation.
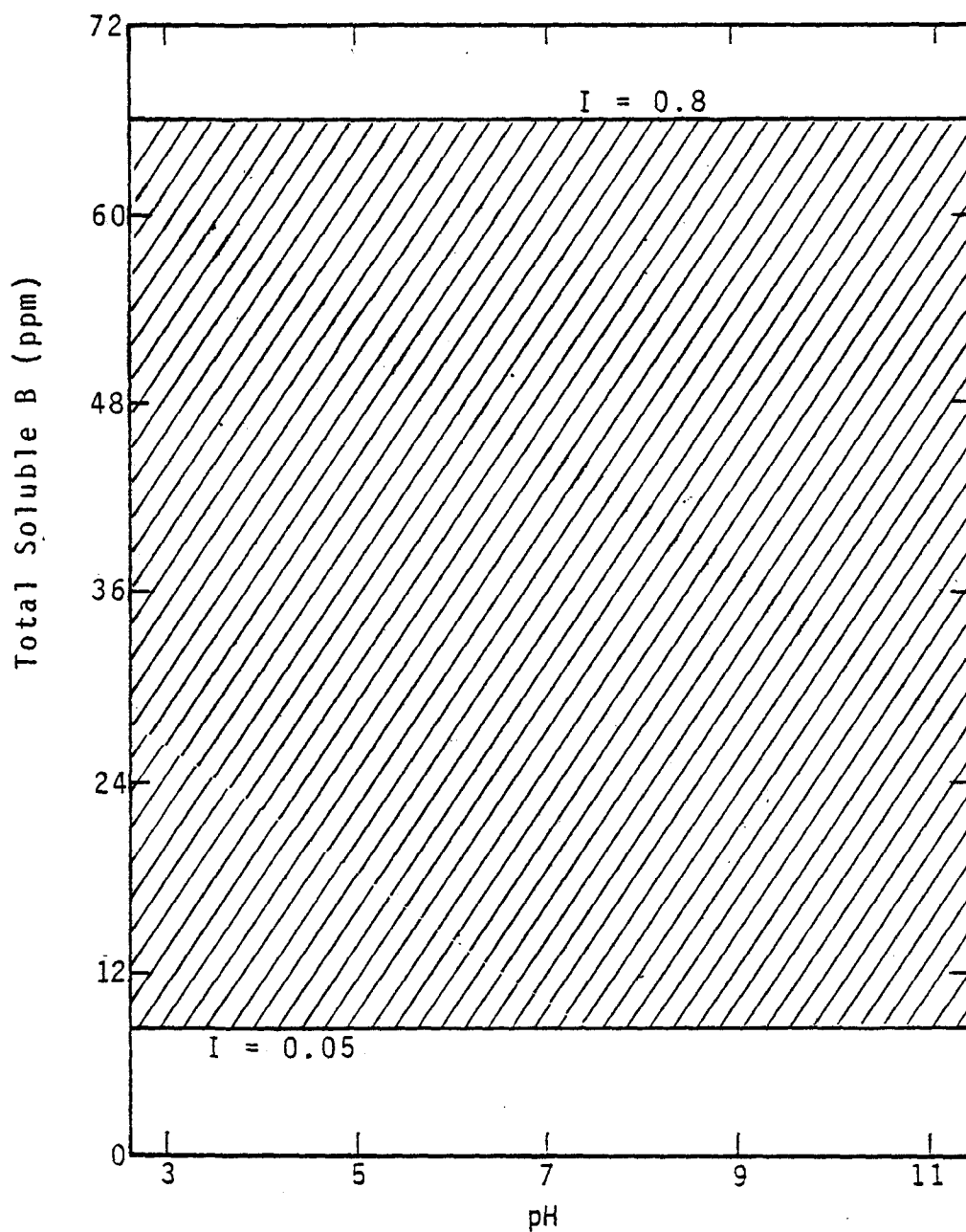
Figure 160.   Range of boron concentrations in aged FGD
             sludge leachates by thermodynamic model calcu-
             lation.
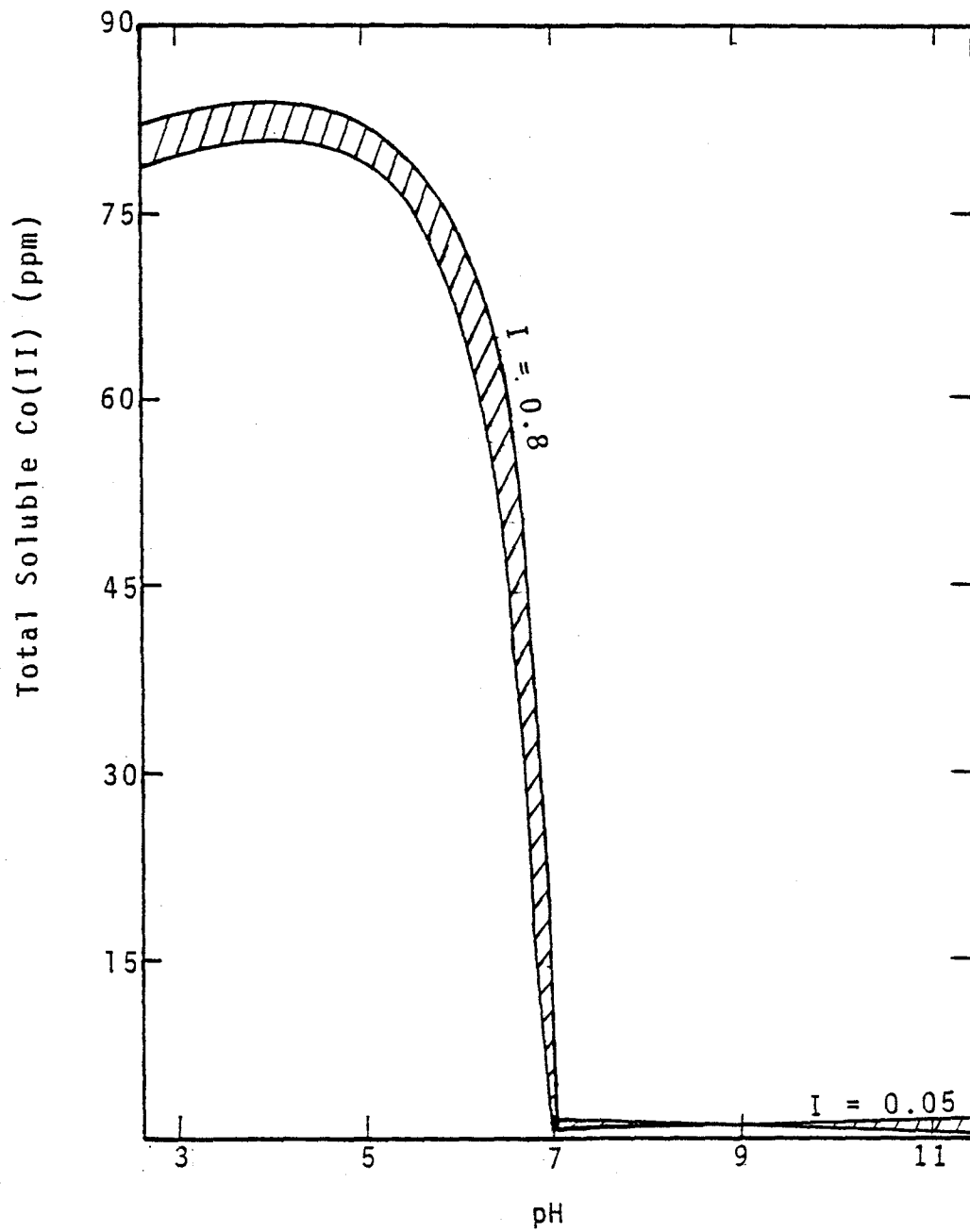
Figure 161. Range of cobalt concentrations in aged FGD
sludge leachates by thermodynamic model calcu-
lation.
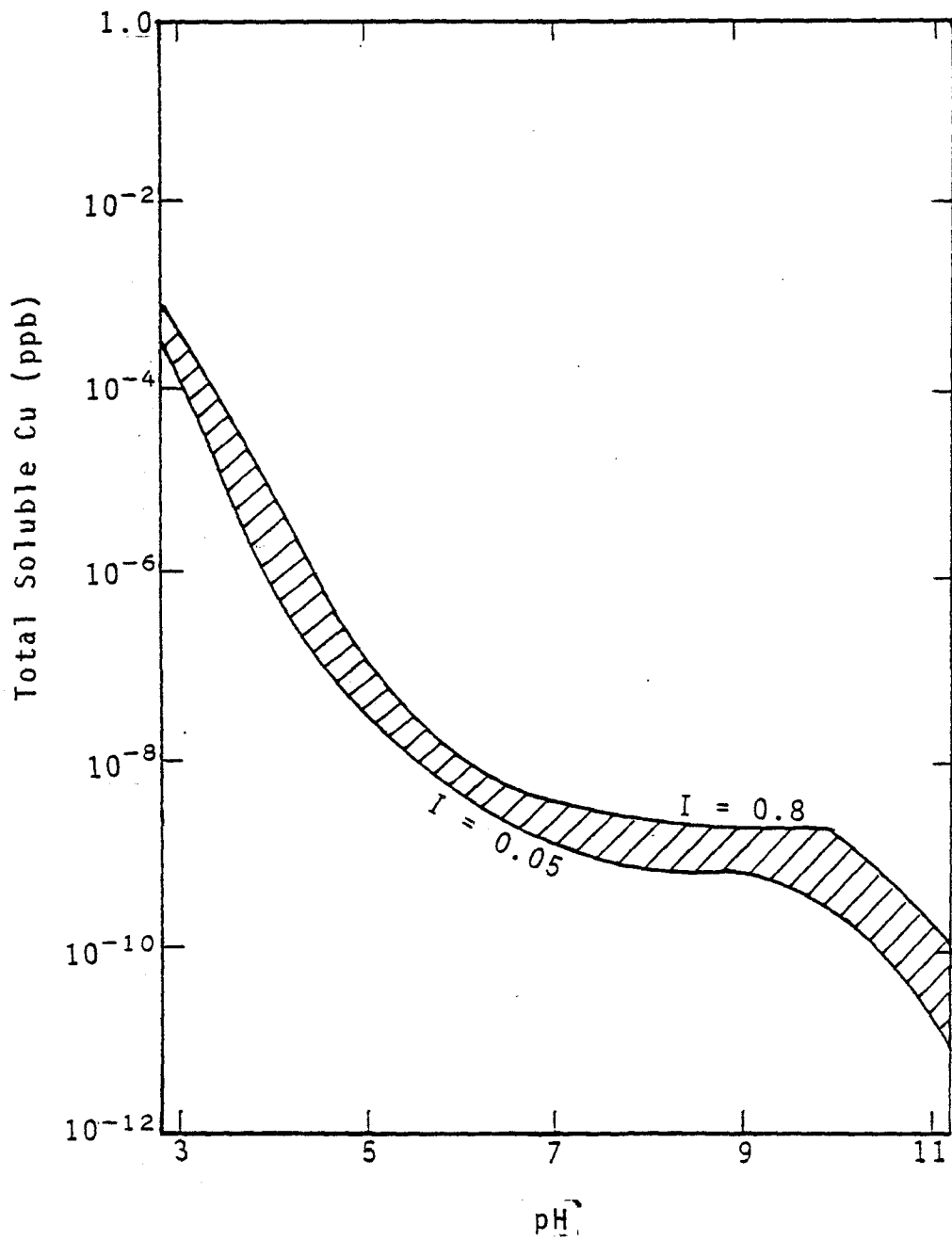
Figure 162. Range of copper concentrations in aged FGD sludge leachates by thermodynamic model calculation.
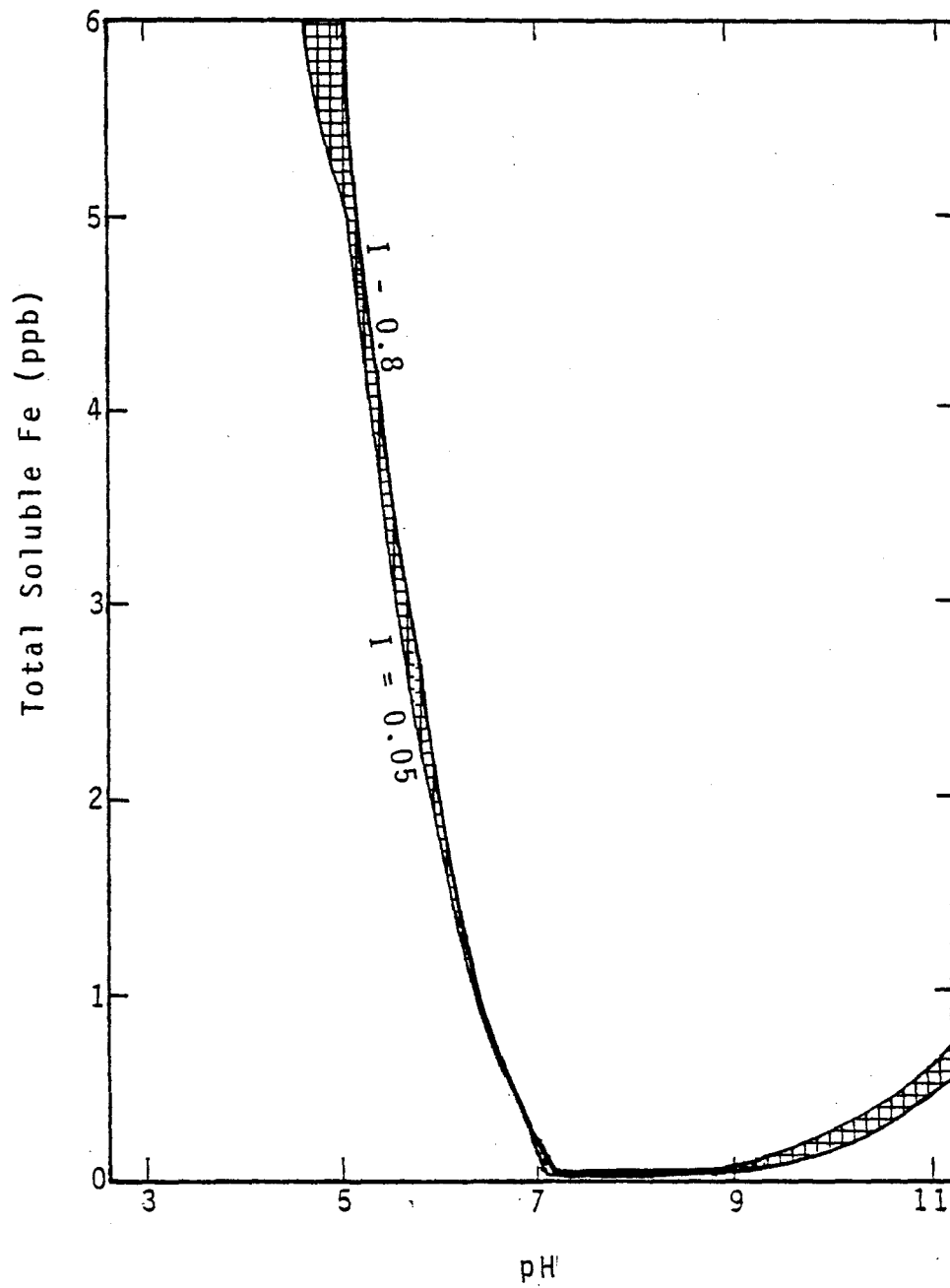
Figure 163. Range of iron concentrations in aged FGD sludge leachates by thermodynamic model calculation.
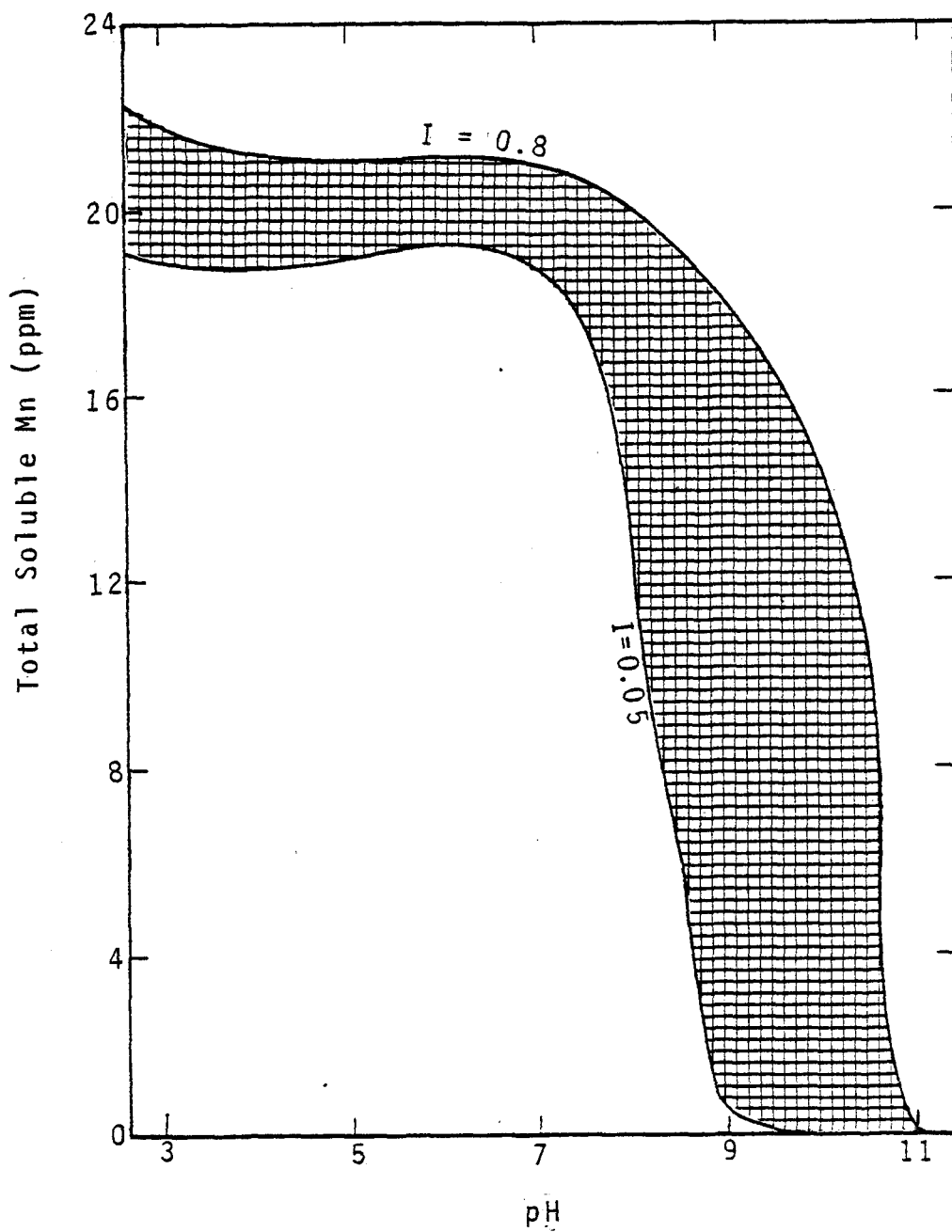
Figure 164. Range of manganese concentrations in aged FGD sludge leachates by thermodynamic model calculation.
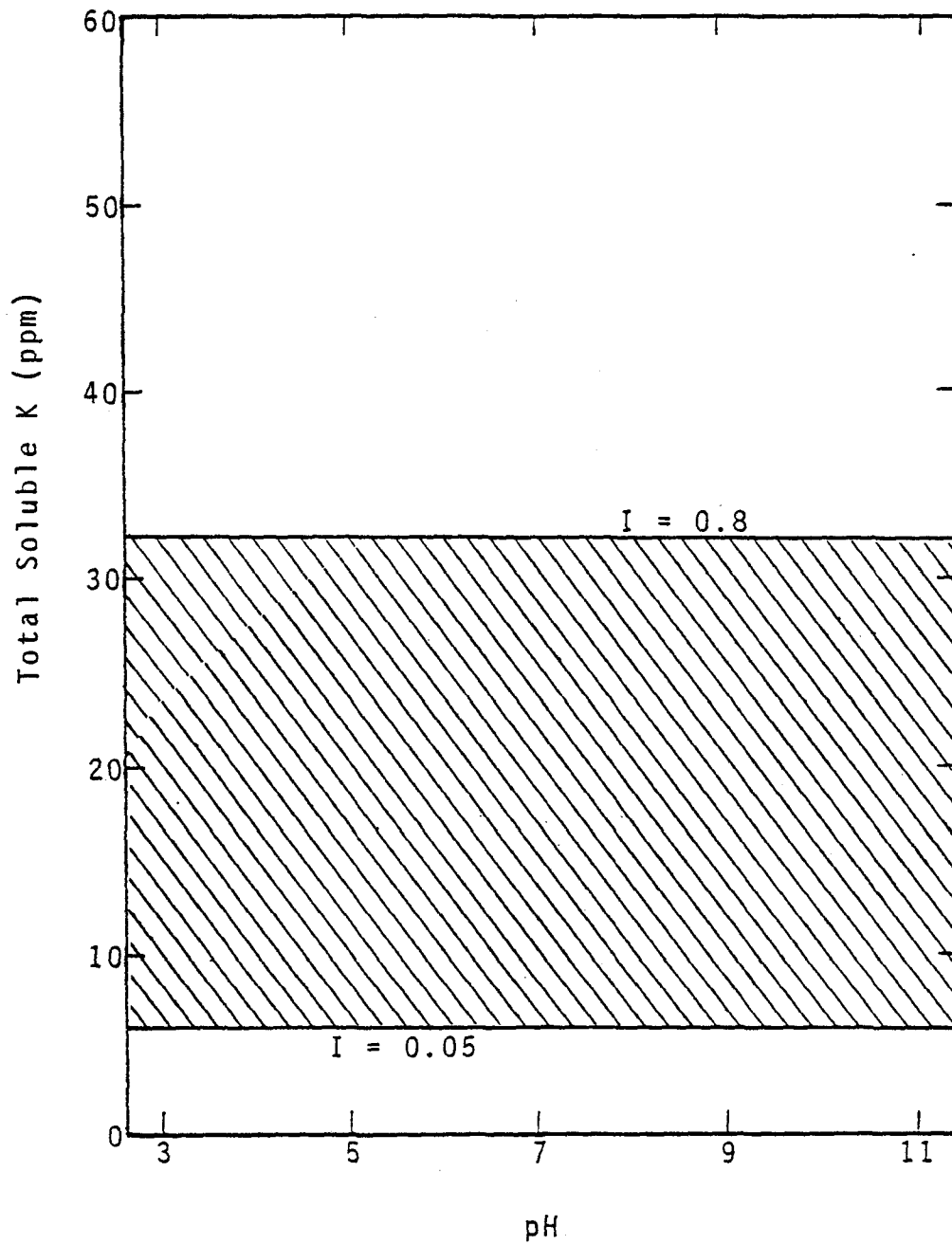
Figure 165. Range of potassium concentrations in aged FGD sludge leachates by thermodynamic model calculation.
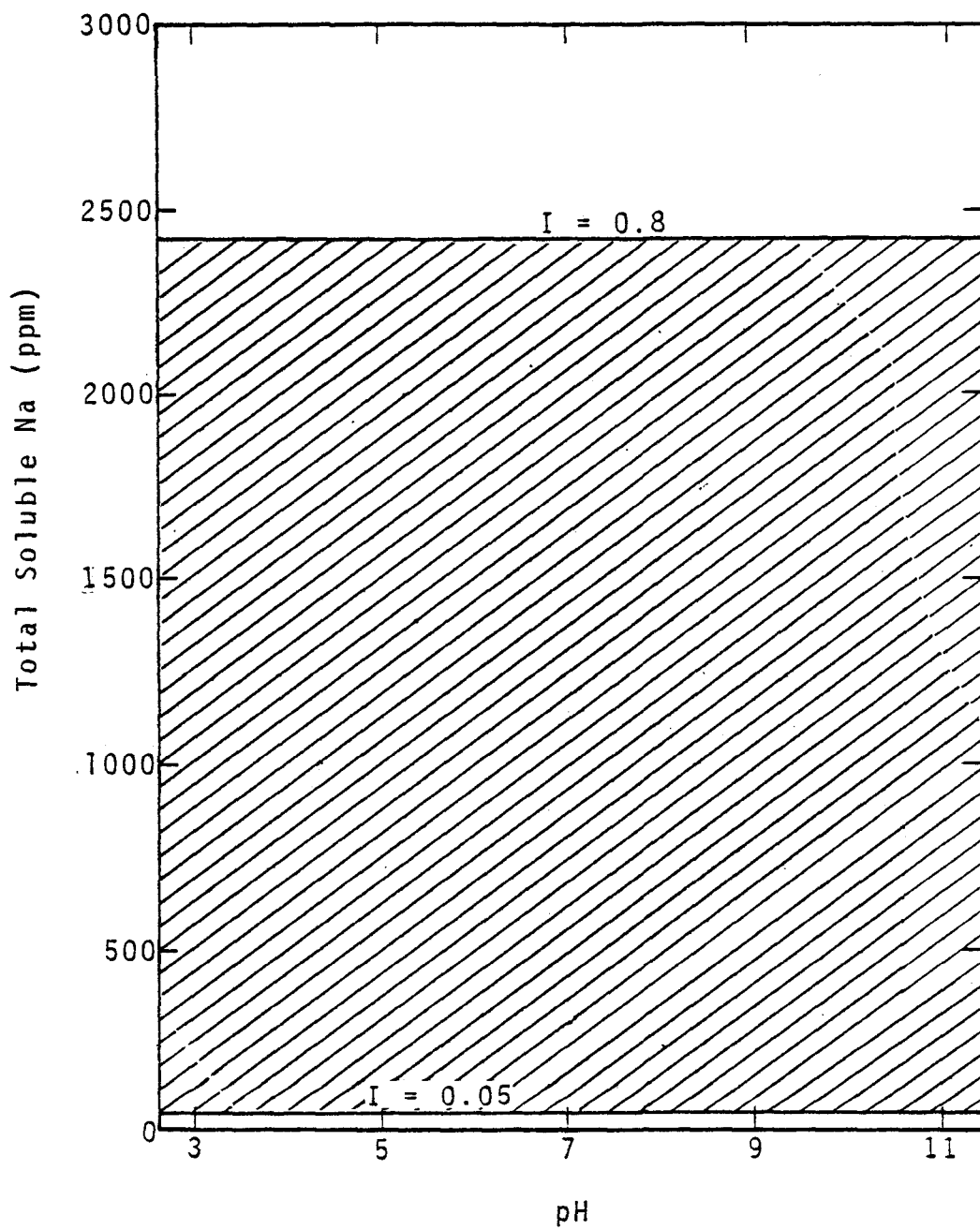
Figure 166.   Range of sodium concentrations in aged FGD
              sludge leachates by thermodynamic model calcu-
              lation.
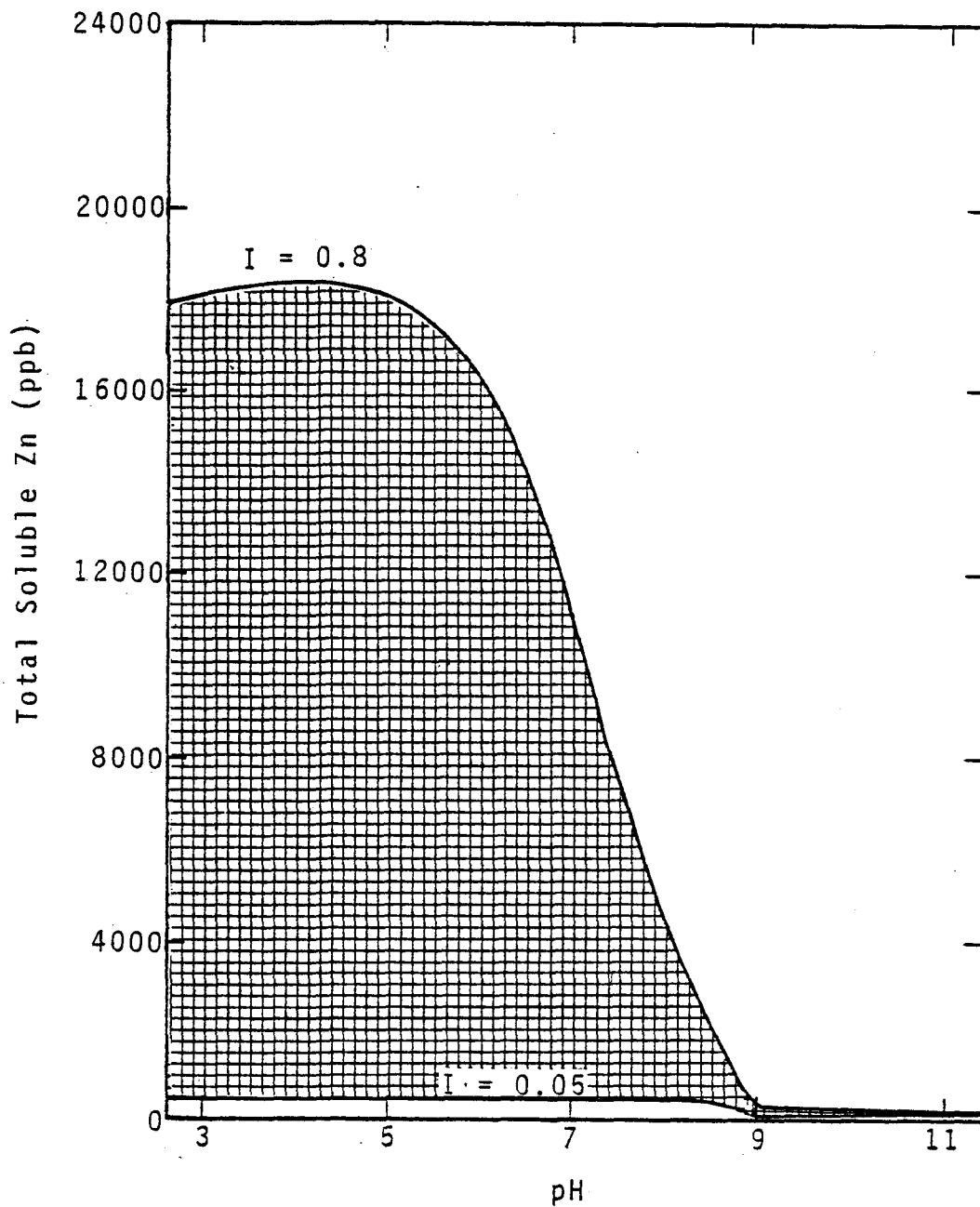
Figure 167. Range of zinc concentrations in aged FGD sludge
leachates by thermodynamic model calculation.

296

REFERENCES

1. Weaver, D.E., C.S. Schmidt, and J.P. Woodyard. Data Base for Standards/Regulations Development for Land Disposal of Flue Gas Cleaning Sludges. EPA-600/7-77-118, U.S. Environmental Protection Agency, December 1977.

2. Leo, P.P. and J. Rossoff. Control of Waste and Water Pollution from Power Plant Flue Gas Cleaning Systems: First Annual R and D Report. EPA-600/7-76-018, U.S. Environmental Protection Agency, October 1976.

3. Princiotta, F.T. Sulfur Oxide Throwaway Sludge Evaluation Panel (SOTSEP), Vol. II: Final Report - Technical Discussion, EPA-650/2-75-010-b, U.S. Environmental Protection Agency, April 1975.

4. Lunt, R.R., C.B. Cooper, S.L. Johnson, J.E. Oberholtzer, G.R. Schimke, and W.I. Watson. An Evaluation of the Disposal of Flue Gas Desulfurization Wastes in Mines and the Ocean: Initial Assessment. Prepared for U.S. Environmental Protection Agency, Office of Research and Development, Washington, D.D., 20460. Contract No. 68-03-2334, May 1977.

5. Bornstein, L.J., R.B. Fling, F.D. Hess, R.C. Rossi, and J. Rossoff. Reuse of Power Plant Desulfurization Waste Water. Prepared for Pacific Northwest Water Laboratory, National Environmental Research Center, U.S. Environmental Protection Agency, Corvallis, Oregon, Grant No. R802853-01-0, June 1975.

6. Stumm, W. and J.J. Morgan. Aquatic Chemistry. Wiley-Interscience, New York, 1970.

7. Leckie, J.O. and R.O. James. Control Mechanisms for Trace Metals in Natural Waters. In: Aqueous-Environmental Chemistry of Metals, ed. by A.J. Rubin, Ann Arbor Science Pub., Ann Arbor, Michigan, 1974. pp. 1-76.

8. Ringbom, A. Complexation in Analytical Chemistry, Interscience Publishers, New York, New York, 1963.

9. Brinkley, S.R., Jr. Note on the Conditions of Equilibrium for Systems of Many Constituents. J. Chem. Phys. 14, pp. 563-564, 1946.

10. Brinkley, S.R., Jr. Calculations of the Equilibrium Composition of Systems of Many Constituents. J. Chem. Phys. 15, pp. 107-110, 1947.

11. Feldman, H.F., W.H. Simons, and D. Bienstock. Calculating Equilibrium Compositions of Multiconstituent, Multiphase, Chemical Reaction System. U.S. Bureau of Mines, RI 7257, 22 pp. 1967.

12. Morel, F. and J. Morgan. A Numerical Method for Computing Equilibria in Aqueous Chemical Systems. Env. Sci. and Techn. 6, pp. 58-67, 1972.

13. Crerar, D.A. A Method for Computing Multicomponent Chemical Equilibria Based on Equilibrium Constants. Geochimica et Cosmochimica Acta, 39, pp. 1375-1384, 1975.

14. White, W.B., S.M. Johnson, and G.B. Dantzig. Chemical Equilibrium in Complex Mixture. J. Chem. Phys., 28, pp. 751-755, 1958.

15. Naphtali, L.M. Complex Chemical Equilibria by Minimizing Free Energy. J. Chem. Phys., 31, pp. 263-264, 1959.

16. Karpov, I.K., L.A. Kazmin. Calculation of Geochemical Equilibria in Heterogeneous Multicomponent Systems, Geochem. Int. 9, pp. 252-262, 1972.

17. Helgeson, H.C. Evaluation of Irreversible Reactions in Geochemical Processes Involving Minerals and Aqueous Solutions - I. Thermodynamic Relations. Geochem. Cosmochim. Acta, 32, pp. 853-877, 1968.

18. Helgeson, H.C. A Chemical and Thermodynamic Model of Ore Deposition in Hydrothermal Systems. Mineral, Soc. Amer. Spec. Paper, 3, pp. 155-186, 1970.

19. Helgeson, H.C., T.H. Brown, A. Nigrini, and T.A. Jones. Calculation of Mass Transfer in Geochemical Processes Involving Aqueous Solutions, Geochim. Cosmochim Acta, 34, pp. 569-592, 1970.

20. Butler, J.N. Ionic Equilibrium: A Mathematical Approach. Addison-Wesley, 1964. 547 pp.

21. Helgeson, H.C. Complexing and Hydrothermal Ore Deposition. Macmillan Co., New York, 1964. pp. 56-64.

22. Crerar, D.A. and G.M. Anderson. Solubility and Solvation Reactions of Quartz in Dilute Hydrothermal Solutions. Chem. Geol., 8, pp. 107-122, 1971.

23. Lu, J.C.S. Studies on the Long-Term Migration and Transformation of Trace Metals in the Polluted Marine Sediment-Seawater System. PhD. Thesis, University of Southern California, June 1976. pp. 184-233.

24. Sillen, L.G. and A.E. Martell. Stability Constants of the Metal-Ion Complexes. Spec. Pub. No. 17, The Chemical Society, London, 1964.

25. Sillen, L.G. and A.E. Martell. Stability Constants of the Metal-Ion Complexes. Spec. Pub. No. 25, The Chemical Society, London, 1971.

26. Ringbom, A. Complexation in Analytical Chemistry. Interscience Publishers, New York, New York, 1973.

27. Garrels, R.M. and C.L. Christ. Solutions, Minerals, and Equilibria. Harper, New York, New York, 1965.

28. Davies, C.W. Ion Association, Butterworth, New York, New York, 1962.

29. McDuff, R.E. and F.M. Morel. Description and Use of the Chemical Equilibrium Program REDEQL2. W.M. Keck Lab. of Environmental Engineering Science, California Institute of Technology, Pasadena, California, July 1975.

30. Wedepohl, K.H. Handbook of Geochemistry, Vol. II-2. Springer Pub., New York, New York, 1970

31. Energlyn, T.L. and L. Brealey. Analytical Geochemistry. Elsevier Pub. Co., New York, New York, 1971.

32. Garrels, R.M. Mineral Species as Functions of pH and Oxidation-Reduction Potentials, with Special Reference to the Zone of Oxidation and Secondary Enrichment of Sulphite Ore Deposits. Geochim. Cosmochim. Acta, 5, pp. 153-168, 1954.

33. Latimer, W.M. The Oxidation States of the Elements and their Potentials in Aqueous Solutions. Second edition, Prentice-Hall, Englewood Cliffs, New Jersey, 1964.

34. Krauskopf, K.B. Geochemistry of Micronutrients. In: Micronutrients in Agriculture, ed. by J.J. Mortvedt, P.M. Giordano, and W.L. Lindsay. Soil Sci. Soc. Amer., Inc., Madison, Wisconsin, 1972. pp. 7-40.

35. Weber, W.J., Jr. and H.S. Posselt. Equilibrium Models and Precipitation Reactions for Cadmium (II). In: Aqueous-Environmental Chemistry of Metals, ed. by A.J. Rubin, Ann Arbor Sci. Pub., Ann Arbor, Michigan, 1974.

36. Radian Corporation. The Environmental Effects of Trace Elements in the Pond Disposal of Ash and Flue Gas Desulfurization Sludge. Prepared for Electric Power Research Institute, Research Project 202, Palo Alto, California, 1975.

37. Mandel, L.N. Transformation of Iron and Manganese in Water-Logged Soils. Soil Science, 91(2):121-126, 1961.

38. Ponnamperuma, F.N., T.A. Loy, and E.M. Tianco. Redox Equilibrian in Flooded Soils - II. The Manganese Oxide Systems. Soil Science, 108(1):48-57, 1969.

39. Bricker, O. Some Stability Relations in the System $Mn-O_2-H_2O$ at 25°C and One Atmosphere Total Pressure. Amer. Mineral. 50:1296-1354, 1965.

40. Florence, T.M. and G.E. Batley. Determination of the Chemical Forms of Trace Metals in Natural Waters, with Special Reference to Copper, Lead, Cadmium and Zinc. Talanta, 24:151-158, 1977.

41. Smith, R.G., Jr. Evaluation of Combined Applications of Ultrafiltration and Complexation Capacity Techniques to Natural Waters. Anal. Chem. 48:74-76, 1976.

42. Florence, T.M. and G.E. Batley. Trace Metals Species in Seawater - I. Removal of Trace Metals from Seawater by a Chelating Resin. Talanta, 23:179-186, 1976.

43. Chan, Y.K. and K.L. Chan. Determination of Labile and Strongly Bound Metals in Lake Water. Water Res., 8:383-388, 1974.

44. Karger, B.L., L.R. Snyder, and C. Horvath. An Introduction to Separation Science. Wiley, New York, 1973.

45. Batley, G.E. and T.M. Florence. Determination of the Chemical Forms of Dissolved Cadmium, Lead and Copper in Seawater. Marine Chem., 4:347-363, 1976.

46. Radian Corporation. Evaluation of the Physical Stability and Leachability of Flue Gas Cleaning Wastes. Electric Power Research Institute, November 1977.

APPENDIX A.   STABILITY CONSTANTS OF SOLUBLE METAL SPECIES

Species	Ligand	Log β_1	Log β_2	Log β_3	Log β_4	Log β_5	Log β_6	Log K	K
Al^{3+}	$SO_4^=$	3.2	4.8						
	F^-	6.9	13.0	16.9	19.5	20.8	20.5		
	OH^-	9.5	18.5	27.0					
Ba^{2+}	OH	1.2							
Be^{2+}	SO_4^{2-}	1.9	3.0	2.0					
	Cl^-	1.6							
	F^-	5.6	9.7	12.7					
	OH^-	7.7							
Cd^{2+}	CO_3^{2-}	5.4						$\dfrac{[CdClH^{2+}]}{[Cd^{2+}][Cl^-][H^+]}$	12.2
	SO_4^{2-}	2.3							
	Cl^-	2.2	2.7	2.1	1.6			$\dfrac{[CdClOH(aq)]}{[Cd^{2+}][Cl^-][OH^-]}$	-6.7
	F^-	1.1	1.5	2.2					
	Br^-	2.1	2.9	3.2	3.7				
	I^-	2.4	3.5	5.2	6.1				
	PO_4^{3-}	3.9							
	NO_3^-	0.7							
	OH^-	4	7.6	8.7	8.5			$\dfrac{[Cd_2OH^{3+}]}{[Cd^{2+}]^2[OH^-]}$	54.6
	OH^-							$\dfrac{[Cd_4OH_4^{4+}]}{[Cd^{2+}]^4[OH^-]^4}$	23.1
Ca^{2+}	CO_3	3.0	11.6					$\dfrac{[CaCO_3H^+]}{[Ca^{2+}][CO_3^{2-}][H^+]}$	11.6
	SO_4^{2-}	2.3							
	F^-	1.1							
	PO_4^{3-}							$\dfrac{[Ca(PO_4)H(aq)]}{[Ca^{2+}][PO_4^{3-}][H^+]}$	14.6

Species	Ligand	Log β_1	Log β_2	Log β_3	Log β_4	Log β_5	Log β_6	Log K	K
Co^{2+}	CO_3^{2-}	5.4						$\dfrac{[CoCO_3H^+]}{[Co^{2+}][CO_3^{2-}][H^+]}$	12.3
	SO_4^{2-}	2.5						$\dfrac{[CoPO_4H(aq)]}{[Co^{2+}][PO_4^{3-}][H^+]}$	15.0
	Cl^-	1.4	1.7						
	Br^-	0.6							
	PO_4^{3-}								
	OH^-	4.8	9.7	10.8					
Cu^{2+}	CO_3^{2-}	6.7	9.9					$\dfrac{[CuCO_3H^+]}{[Cu^{2+}][CO_3^{2-}][H^+]}$	12.5
	SO_4^{2-}	2.3						$\dfrac{[CuCO_3(OH)_2^{-2}]}{[Cu^{2+}][CO_3^{2-}][OH^-]^2}$	-13.0
	Cl^-	1.6	2.2	1.9	1.4			$\dfrac{[CuClOH(aq)]}{[Cu^{2+}][Cl^-][OH^-]}$	-4.9
	F^-	1.3							
	Br^-	1.1	-0.3	-1.8	-4.0				
	I^-	9.7	9.5						
	PO_4^{3-}							$\dfrac{[CuPO_4H(aq)]}{[Cu^{2+}][PO_4^{3-}][H^+]}$	16.0
	PO_4^{3-}							$\dfrac{[CuPO_4H_2^+]}{[Cu^{2+}][PO_4^{3-}][H^+]^2}$	21.3
	$B(OH)_4^-$	7.1	12.4						
	OH^-	6.1	10.7	15.2	16.1			$\dfrac{[Cu_2(OH)_2^{2+}]}{[Cu^{2+}]^2[OH^-]^2}$	17.7
Cr^{3+}	SO_4^{2-}	2.7							
	Cl^-	0.8	1.9						
	F^-	4.5	9.1	11.3					
	Br^-	-1.9							
	PO_4^{3-}							$\dfrac{[CrPO_4H^+]}{[Cr^{3+}][PO_4^{3-}][H^+]}$	21.5
	OH^-	-10.7	19.2		18.2				

302

Species	Ligand	Log β_1	Log β_2	Log β_3	Log β_4	Log β_5	Log β_6	Log K	K
H^+	CO_3^{2-}	10.2						$\frac{[H_2CO_3(aq)]}{[H^+]^2[CO_3^{2-}]}$	16.5
	SO_4^{2-}	2.2							
	F^-	3.0							
	S^{2-}	14.0						$\frac{[H_2S(aq)]}{[H^+]^2[S^{-2}]}$	21.2
	PO_4^{3-}	12.5							
	PO_4^{3-}							$\frac{[H_2PO_4^-]}{[H^+]^2[PO_4^{3-}]}$	19.9
	PO_4^{-3}							$\frac{[H_3PO_4(aq)]}{[H^+]^3[PO_4^{3-}]}$	21.9
	$SiO_2(OH)_2^{2-}$	13.1						$\frac{[H_2SiO_2(OH)_2]}{[H^+]^2[SiO_2(OH)_2^{2-}]}$	22.7
	$B(OH)_4^-$	9.1							
	SO_3^{2-}	7.3							
	MoO_4^{2-}	4.3							
	AsO_4^{3-}	11.8						$\frac{[H_2AsO_4^-]}{[H^+]^2[AsO_4^{3-}]}$	18.8
	HVO_4^{2-}	8.2							
	SeO_3^{2-}	8.5						$\frac{[H_2SeO_3(aq)]}{[H^+]^2[SeO_3^{2-}]}$	11.2
Fe^{3+}	SO_4^{2-}	4.1	5.6						
	Cl^-	1.4	2.1	1.3					
	F^-	5.6	10.2	12.9					
	Br^-	0.7	0.5						
	I	3.5	2.4						
	PO_4^{3-}							$\frac{[FePO_4H^+]}{[Fe^{3+}][PO_4^{3-}][H^+]}$	20.7
	$SiO_2(OH)_2^{2-}$							$\frac{[FeSiO_2(OH)_2H^-]}{[Fe^{3+}][SiO_2(OH)_2^{2-}][H^+]}$	23.5

303

Species	Ligand	Log β_1	Log β_2	Log β_3	Log β_4	Log β_5	Log β_6	Log K	K
	B(OH)$_4^-$	8.9	15.8						
	OH$^-$	11.8	21.8		28.8			$\dfrac{[Fe_2(OH)_2^{4+}]}{[Fe^{3+}]^2[OH^-]^2}$	25.1
Fe^{2+}	SO$_4^{2-}$	2.3							
	Cl$^-$	0.9							
	PO$_4^{3-}$	21.6	23.9						
	OH$^-$	5.4	24.8						
Pb^{2+}	CO$_3^{2-}$	7.4	10.8					$\dfrac{[PbCO_3H^+]}{[Pb^{2+}][CO_3^{2-}][H^+]}$	13.2
	CO$_3^{2=}$							$\dfrac{[Pb(CO_3)_2H_2(aq)]}{[Pb^{2+}]^2[CO_3^{2-}]^2[H^+]}$	25.4
	SO$_4^{2-}$	2.7							
	Cl$^-$	1.7	2.6	2.8	2.0			$\dfrac{[PbClOH(aq)]}{[Pb^{2+}][Cl^-][OH^-]}$	-6.6
	Br$^-$	1.9	3.2	3.8	3.9				
	I$^-$	1.8	3.6	4.2	4.4				
	B(OH)$_4^-$	5.2	11.1						
	OH$^-$	6.3	10.9	13.0				$\dfrac{[Pb_2OH^{3+}]}{[Pb^{2+}]^2[OH^-]}$	7.7
		-7.7	-17.1	-28.1					
	OH$^-$							$\dfrac{[Pb_3(OH)_4^{2+}]}{[Pb^{2+}]^3[OH^-]^4}$	30.1
	OH$^-$							$\dfrac{[Pb_6(OH)_8^{4+}]}{[Pb^{2+}]^6[OH^-]^8}$	68.4
Mg^{2+}	CO$_3^{2-}$	3.2						$\dfrac{[MgCO_3H^+]}{[Mg^{2+}][CO_3^{2-}][H^+]}$	11.6
	SO$_4^{2-}$	2.4							
	F$^-$	1.8							
	PO$_4^{3-}$							$\dfrac{[Mg(PO_4)H(aq)]}{[Mg^{2+}][PO_4^{3-}][H^+]}$	15.1
	OH$^-$							$\dfrac{[MgOH^-]}{[Mg^{2+}][OH^-]}$	3.8

Species	Ligand	Log β_1	Log β_2	Log β_3	Log β_4	Log β_5	Log β_6	Log K	K
Mn^{2+}	CO_3^{2-}							$\dfrac{[MnCO_3H^+]}{[Mn^{2+}][CO_3^{2-}][H^+]}$	12.1
	SO_4^{2-}	2.3							
	Cl^-	1.1	1.1	0.6					
	Br^-	0.9	0.8						
	PO_4^{3-}							$\dfrac{[MnPO_4H(aq)]}{[Mn^{2+}][PO_4^{3-}][H^+]}$	15.6
	OH^-	3.9	9.8						
Hg^{2+}	CO_3^{2-}	11.3						$\dfrac{[HgCO_3H^+]}{[Hg^{2+}][CO_3^{2-}][H^+]}$	16.6
	SO_4^{2-}	2.4	3.5						
Hg^{2+}	Cl^-	7.2	14.0	15.1	15.4			$\dfrac{[HgClOH(aq)]}{[Hg^{2+}][Cl^-][H^+]}$	4.6
	F^-	1.6							
	Br^-	9.6	18.1	20.5	24.0				
	I^-	13.4	24.6	28.4	30.3				
	S^{2-}	54.2						$\dfrac{[HgS_2H_2(aq)]}{[Hg^{2+}][S^{2-}]^2[H^+]^2}$	68.0
	OH^-	10.6	21.8	20.9				$\dfrac{[(Hg_2OH)^{3+}]}{[Hg^{2+}]^2[OH^-]}$	10.7
	OH^-							$\dfrac{[Hg_3(OH)_3^{3+}]}{[Hg^{2+}]^3[OH^-]^3}$	35.6
Ni^{2+}	CO_3^{2-}	5.5						$\dfrac{[NiCO_3H^+]}{[Ni^{2+}][CO_3^{2-}][H^+]}$	12.4
	SO_4^{2-}	2.3							
	Cl^-	0.5	1.3						
	F^-	1.1							
	Br^-	0.6							
	PO_4^{3-}							$\dfrac{[NiPO_4H(aq)]}{[Ni^{2+}][PO_4^{3-}][H^+]}$	14.9
	OH^-	5.3							

Species	Ligand	Log β_1	Log β_2	Log β_3	Log β_4	Log β_5	Log β_6	Log K	K
K^+	F^-	1.1							
Ag^+	SO_4^{2-}	1.1							
	Cl^-	3.1	4.9	4.9	5.1				
	F^-	0.4							
	Br^-	4.3	7.3	8.0	8.7				
	I^-	14.0	13.9						
	S^{2-}			17.3				$\dfrac{[AgSH(aq)]}{[Ag^+][S^-][H^+]}$	14.0
	S^{2-}							$\dfrac{[AgS_2H_2^-]}{[Ag^+]^2[S^{2-}][H^+]^2}$	19.0
	SO_3^{2-}	5.6	7.9						
	OH^-	2.0	4.0						
Na^+	SO_4^-	0.7							
Sn^{2+}	F^-	6.9	9.7	10.2					
	Br^-	1.1	1.7	1.4					
	OH^-	10.8							
Zn^{2+}	SO_4^-	2.3							
	Cl^-	1.4	1.7	0.8	1.2			$\dfrac{[ZnClOH(aq)]}{[Zn^{2+}][Cl^-][OH^-]}$	-7.0
	F^-	1.3							
	Br^-	0.9	0.9	0.3	0				
	OH^-	4.5	11.1	13.6	14.8			$\dfrac{[ZnPO_4H(aq)]}{[Zn^{2+}][PO_4^{3-}][H^+]}$	15.2
	OH^-							$\dfrac{[Zn_2OH^{3+}]}{[Zn^{2+}]^2[OH^-]}$	5

306

APPENDIX B

CHEMICAL ANALYSIS OF FRESH AND
AGED FGD SLUDGE SAMPLES

In order to verify the thermodynamic model used in this study, chemical analysis of fresh and aged FGD wastes were performed. This section describes the sampling procedures and analytical methods used.

SAMPLING PROCEDURE

Samples of FGD sludges and wastewaters were collected on October 18-19, 1977, at the Kansas City Power and Light La Cygne Power Station. The following is a description of the methods used to collect, prepare, preserve, and transport the samples taken.

Sample Container Preparation

The sample containers (1- and 4-liter capacities), caps, and filtration syringes used were made of polypropylene material. This equipment was soaked in a solution of 5-percent nitric acid. The containers, cap, and syringes remained in the acid solution for 24 hours. Upon completion of the acid soak, the containers, caps, and syringes were immediately rinsed three times each with doubly distilled deionized water. Upon vigorous shaking off of excess water, the caps were placed on the containers and stored. The syringes were shaken of excess water and then wrapped in parafilm to prevent contamination.

Sample Collection

Approximately 125 ml of sludge were drawn from the sludge effluent lines of each of the eight scrubbers. The eight 125-ml aliquots of sludge were then placed into a 1-liter polypropylene bottle and allowed to settle for 4 hours. Upon settling, a 150-ml aliquot of the supernatant was then drawn from and filtered through a 0.45- m Millipore filter. Two 75-ml portions of the filtrate were then placed in a separate 600-ml polypropylene bottle. The sample container identified for metal determination was then acidified with ultra-pure nitric acid to a pH of 1. Both sample containers were then refrigerated at 5°C until the next sampling addition. The final volume of each subset sample was 600 ml.

Fresh Wastewater--

The composite sample was taken six times during a 24-hour period over two consecutive days. The sample consisted of two subset samples (refer to Table B1). The subset sample identified as 2876-KAN-RW-1 was designated for metal analysis only; sample 2876-KAN-RW-2 was used for all other analyses.

Fresh Sludge--

The fresh sludge composite sample was taken at the same time intervals and fashion as the fresh effluent. A 2.5-liter aliquot was taken from each of the sludge effluent lines and placed in a 20-liter polypropylene container. Upon settling (4 hours), the supernatant was discarded and approximately 500 ml of settled sludge was transferred to a 4-liter polypropylene container. The sludge composite sample was then refrigerated (4°C). Part of the sludge sample was aged for 20 days for the study of the aging effects on the FGD sludge.

Stabilized Wastewater--

The stabilized wastewater composite was sampled from the sludge lagoon. The samples were taken in an area of quiescence near the point to reentry to the power plant. Samples were taken once daily with a 600-ml aliquot, which was filtered (0.45 m) and split into two 300-ml subset samples. The sample marked 2876-KAN-SW-1 was then acidified with ultra-pure nitric acid to a pH of 1. Both subset samples were refrigerated (4°C).

Stabilized Sludge--

The stabilized sludge was also taken from the sludge lagoon. The plant engineer identified the areas of oldest deposition of lime sludge (about 5 years old). These areas had formed sills and were easily accessible.

A casing was needed to take samples from 180 to 270 cm below the surface of the sill. The casing was fabricated from eight-inch diameter PVC pipe. The original 360-cm casing was cut into two 180 cm sections and filled with a connector.

Once the casing was in place, the sample of stabilized sludge was augered from a depth of 180 to 270 cm and placed in a 4-liter container. The auger bucket was teflon-coated to prevent metal contamination.

Sample Shipment

All samples described above were placed in metal ice chests. Ample amounts of ice were included to ensure that the sample remained at 4°C. The sample was airfreighted from Kansas City to Los Angeles and delivered to the USC Department of Environmental Engineering within 10 hours.

TABLE B-1.   FGD SLUDGE SAMPLE IDENTIFICATION SCHEME

Label	Sample Description
2876-KAN-RS	Fresh sludge from scrubber mixing tank (all parameters)
2876-KAN-SS	Stabilized sludge from lagoon (all parameters)
2876-KAN-RW-1	Fresh wastewater - from scrubber mixing tank, filtered, fixed (acidified)(metals)
2876-KAN-RW-2	Fresh wastewater - from scrubber mixing tank, filtered - not fixed (all other parameters)
2876-KAN-SW-1	Stabilized wastewater - from lagoon, filtered, fixed (metals)
2876-KAN-SW-2	Stabilized wastewater - from lagoon, filtered, not fixed (all other parameters)

ANALYTICAL METHODS

Below is a discussion of the analytical procedures imple-
mented in the parameter determination on the samples of wastewater
and sludge taken at the La Cygne station.

General Parameters

The determination of pH, nitrogen compounds, alkalinity,
chloride, fluoride, redox potential, and total dissolved solids
follows the standard methods described in Ref. 1. The procedures
and instruments used are as follows:

- pH — Potentiometry (Orion 801A)

- NH_3-N — Brucine Method (Perkin-Elmer 124, light path 10 cm, 410 nm)

- Alkalinity — Potentiometric titration (Orion 801A)

- Chloride — Mercuric nitrate method

309

- Redox potential　　　　　Potentiometry (Pt electrode, Orion 810A)

- Total dissolved　　　　　Gravimetry
  solids

- Boron　　　　　　　　　Curcumin method

- Silica　　　　　　　　　Molybdosilicate

The determination of phosphorus was accomplished using the modified Ascorbic Method. The procedures of the method are outlined as follows:

(a)　Measure 1 ml of slurry sample and put in teflon beaker (if filtrate sample, use 50-100 ml).

(b)　Digest the sample at water boiler temperature using HF (1 ml) and HClO4 (2 ml) with teflon cover.

(c)　After solution is clear, remove the cover and heat to dryness.

(d)　Cool, add 2 ml of H_2O_2 and heat to dryness again.

(e)　Add 20 ml of H_2O and 5 ml of 10N H_2SO_4.

(f)　Filter the sample through the glass fiber and dilute to 100 ml.

(g)　Take 40 ml of sample and add 3 ml of 1.6 percent ammonium molybdate and 4 ml of mixed reagent. (Mixed reagent = 50 ml of tartrate + 50 ml of 10 percent ascorbic acid). (If dilution is required, the reagents to sample ratio should be kept constant. An appropriate amount of 10N H_2SO_4 should be used to keep the final pH value constant).

(h)　Measure the sample by spectrophotometer at 717 nm.

The measurement of orthosphate on filtrates was performed as above without the digestion procedures.

A refractometer (American Optical Corp. Goldberg T/C, Model 10419), was used for the measurement of salinity. The dry weight data of the total slurry samples were analyzed on both volume and weight basis.

A titrimetric method is used for dissolved sulfide determination. Total acid-soluble sulfide was determined by stripping and titrimetric processes:

(a) Measure 5 ml ZnAc and 95 ml distilled water into each
     of two absorption flasks. Connect the two absorption
     flasks with a 1-liter reaction flask and purge the
     system with N_2 gas for 5 minutes.

(b) Transfer 10 - 50 ml slurry sample into the reaction
     flask and add distilled water to 500 ml, then mix
     completely.

(c) Acidify the sample with 10 ml conc. H_2SO_4 and replace
     the prepared 2-hole stopper tightly. Pass N_2 through
     the sample for approximately one hour.

(d) Add 10 ml of iodine solution and 2.5 ml conc. HCl to
     each of the absorption flasks, shake and mix thoroughly.

(e) Transfer contents of both flasks to a 500 ml flask and
     back-titrate with 0.025N sodium thiosulfate titrant,
     using starch solution as indicator.

The analysis of FGD sludge for carbonate sulfite and sulfate followed the Palmrose Method as described below:

(a) Obtaining and preparing sample

     (1) Using a 2-1/2 ml syringe, exactly 2 ml of sludge
          sample are drawn. Care must be taken here, for if
          excess sample is taken and if the excess is dis-
          carded by drawing the plunger back to 2 ml, the
          solids may partially settle and what remains is
          no longer representative.

     (2) The sample is then injected into a beaker contain-
          ing 60 to 75 ml of demineralized water. The
          diluted sample is redrawn into the syringe several
          times to completely wash or purge the sample.

(b) $CaSO_3$ Titration

     (1) Add 5 ml of starch - KI solution to the sample.

     (2) Estimate the expected $CaCO_3$ concentration. Deter-
          mine the volume of H_2SO_4 needed to neutralize the
          $CaCO_3$. Add 5 ml to that volume and add the sum
          to the sample and record the volume added.

     (3) Titrate the sample with potassium iodate (KIO_3).
          Do not stir the sample until a blue color starts

311

to appear. Titrate until one drop produces an
intense blue color. Premature stirring would
aggravate the SO_2 stripping problem. Note the
volume of KIO_3 used.

(c) Excess Acid Titration

(1) To bring the sample back from the deep blue to a
clear color, add a couple drops of sodium thio-
sulfate. If more than a few drops are required
to effect the color change, the KIO_3 end point
was exceeded and the entire process should be
started over.

(2) A few drops (3 to 5) of methyl purple indicator
are added to the sample. This will turn the solu-
tion blue.

(3) Titrate the sample to a greenish yellow end point
with 1/8 normal NaOH. Record the volume of
hydroxide titrated. If the ml of NaOH is less
than 5 ml or greater than 10 ml, the entire
analysis should be redone by adjusting the amount
of H_2SO_4 added in step (b)(2).

(d) Calculations

If this procedure is followed exactly and all reagents
are of the specified normality, the composition is calculated
as follows:

$$gm\ CaCO_3/l = 3.125 \times (ml\ H_2SO_4 - ml\ NaOH)$$

$$gm\ CaSO_3 \cdot 1/2H_2O - 4.025 \times ml\ KIO_3$$

The concentration of $CaSO_4 \cdot 2H_2O$ was calcualted by subtract-
ing the amount of calcium in $CaCO_3$ and $CaSO_3 \cdot \frac{1}{2}H_2O$ from that of
total calcium concentration in sludge.

Metals

Sludge samples used in the determination of metals (except
mercury) in the lime slurry sludge, were digested by concen-
trated hydrofluoric acid (HF), nitric acid (HNO_3), and perchloric
acid ($HClO_3$) to clear the solution at 175°C in a teflon beaker
(with teflon cover). Atomic absorption spectrophotometers
(Perkin Elmer's 305B and 460) were used in the analyses of metals.
Both flame and heated graphite atomizers (HGA 2100) were employed
in total sample analysis. The choice of an atomizer is dependent
on the suitable linear range (concentration) of the element which
is being determined. The following table was the guide used in
choosing the atomizer:

Optimum Working Range

Element	Flame atomizer (mg/ℓ)		Heated graphite atomizer (pg)*	
Na	0.03	– 1	20	– 2000
K	0.1	– 2	10	– 2500
Ca	0.2	– 20	20	– 1000
Mg	0.02	– 2	1	– 40
As	0.002	– 0.02	50	– 1000
Cd	0.05	– 2	3	– 100
Cu	0.2	– 10	50	– 2000
Fe	0.3	– 10	30	– 1000
Hg	10	– 300	500	– 7000
Mn	0.1	– 10	10	– 500
Ni	0.3	– 10	200	– 5000
Pb	1	– 20	50	– 1500
Se	0.002	– 0.02	50	– 1000
Ti	5	– 100	1000	– 80000
V	2	– 100	400	– 20000
Zn	0.05	– 2	1	– 70

*Based on interrupt flow of argon gas

The fresh and stabilized wastewater needed no further digestion since the sample had been filtered (0.45 μm) and fixed pH=1) in the field. Analysis of the metals (except mercury) was accomplished by direct injection into the HGA furnace.

Mercury determination was accomplished by flameless atomic adsorption cold vapor method. Samples (raw and stabilize lime slurry sludges) for total mercury analysis were digested in teflon bombs (Parr No. 4745). The procedures are as follows:

(a) Weight triplicate 0.1 - 1g of sample and place in bottom of a teflon acid digestion bomb.

(b) Carefully add 10 ml conc. HNO_3, 3 ml 48% HF and 1 g $KMnO_4$ and close the digestion bomb tightly.

(c) Place the digestion bomb into an oven (or hot plate) and adjust the temperature to 70°C.

(d) Digest the sample until solution is clear.

(e) Determinations were accomplished by flameless atomic adsorption cold vapor method.

The pore water samples were withdrawn from various sludge samples (fresh, 20-day-old, and stabilized) by the centrifugation method at 5,000 g and 30 minutes of centrifugation. After centrifugation, the supernatants were filtered through a 0.45 m Millipore filter, and were immediately acidified to pH around 1 to preserve the sample. The procedures used for the analysis of pore water samples are the same as those used for the analysis of fresh and stabilized wastewaters, as described previously.

APPENDIX B

REFERENCES

1. APHA, AWWA, WPCF. Standard Methods for the Examination of Water and Wastewater, 14th ed., Washington, D.C. 1975.